The University of Jordan

Authorization Form

I, Ahmad Ghazi ALTarabsheh, authorize the University of Jordan to supply copies of my Thesis/ Dissertation to libraries or establishments or individuals on request, according to the University of Jordan regulations.

Signature:

Date: ٢٠/٨/١٨

الجامعة الأردنيـــــة
كلية الدراسات العليا

التاريـــخ: /   /

نموذج رقم (١٨)
اقرار والتزام بالمعايير الأخلاقية والأمانة العلمية وقوانين الجامعة الأردنية وأنظمتها وتعليماتها لطلبة الماجستير

أنا الطالب: احمد غازي الطرابشة   الرقم الجامعي: (٨٠٩٠١٩٠)

تخصص: الهندسة المدنية/انشاءات   الكليـــــــة: الهندسة

عنوان الرسالة:

Nonlinear Seismic Analysis Of High Rise Buildings with Semi Rigid Connection

اعلن بأنني قد التزمت بقوانين الجامعة الأردنية وأنظمتها وتعليماتها وقراراتها السارية المفعول المتعلقة باعداد رسائل الماجستير عندما قمت شخصيا" باعداد رسالتي وذلك بما ينسجم مع الأمانة العلمية وكافة المعايير الأخلاقية المتعارف عليها في كتابة الرسائل العلمية. كما أنني أعلن بأن رسالتي هذه غير منقولة أو مستلة من رسائل أو كتب أو أبحاث أو أي منشورات علمية تم نشرها أو تخزينها في أي وسيلة اعلامية، وتأسيسا" على ما تقدم فانني أتحمل المسؤولية بأنواعها كافة فيما لو تبين غير ذلك بما فيه حق مجلس العمداء في الجامعة الأردنية بالغاء قرار منحي الدرجة العلمية التي حصلت عليها وسحب شهادة التخرج مني بعد صدورها دون أن يكون لي أي حق في التظلم أو الاعتراض أو الطعن بأي صورة كانت في القرار الصادر عن مجلس العمداء بهذا الصدد.

توقيع الطالب:......................................   التاريخ: ١٨ / ٨ / ٢٠١١

تعتمد كلية الدراسات العليا
هذه النسخة من الرسالة
التوقيع..... التاريخ ١٨/...

NON-LINEAR SEISMIC ANALYSIS OF HIGH-RISE BUILDINGS WITH SEMI-RIGID CONNECTION

By

Ahmad Ghazi M.AL-Tarabsheh

Supervisor

Dr. Yasser M. Hunaiti

Co-Supervisor

Dr. Ghazi A. Abu-Farsakh

This Thesis was Submitted in Partial Fulfillment of the Requirements for the Master's Degree of Science in Civil Engineering

Faculty of Graduate Studies

The University of Jordan

August, 2011

COMMITTEE DECISION

This Thesis/Dissertation (Nonlinear Seismic Analysis of High Rise Buildings with Semi-Rigid connections) was Successfully Defended and Approved on ----------------------

Examination Committee	**Signature**
Dr. Yasser Mohammed Hunaiti, (Supervisor) Prof. of Civil Engineering	------------------------
Dr. Ghazi Abu Farsakh. (Co-Supervisor) Prof. of Civil Engineering	------------------------
Dr. Samih Shaker Qaqish (Member) Prof. of Civil Engineering	------------------------
Dr. Mutasim Soud Abdel-Jaber (Member) Assist. Prof. of Civil Engineering	------------------------
Dr. Hasan Nabil Katkhuda (Member) Assist. Prof. of Civil Engineering (Zarqa Hashemite university)	------------------------

DEDICATED TO MY PARENTS

ACKNOWLEDGEMENTS

My sincere appreciation and great respect goes to my advisor Dr. Yasser hunaiti and Co-Supervisor DR. Ghazi abu-farsakh for their guidance and support that has inspired me to pursue this research and higher education. I am very thankful for their patience and understanding through difficult times and for their continuous encouragement.

Special thanks also goes to Dr. Samih Qaqish, Dr. hasan Katkhuda , and Dr. Mutasim Abdel-Jaber for providing helpful suggestions and taking the time to serve on my thesis committee.

LIST OF CONTENT

LIST OF TABLES

LIST OF FIGURES

LIST OF APPENDICES

NONLINEAR SEISMIC ANALYSIS OF HIGH-RISE BUILDING WITH SEMI-RIGID CONNECTIONS

By
Ahmad G. AL-Tarabsheh

Supervisor
Dr. Yasser M. Hunaiti

Co-Supervisor
Dr. Ghazi A. Abu-Farsakh

ABSTRACT

In this study, four steel systems namely; fully rigid moment resisting frame system, partially restrained moment resisting frame system, buckling restrained braced frame system and eccentrically braced frame system, are subjected to a series of three dimensional nonlinear time history analysis and nonlinear static push over analysis in effort to evaluate their seismic performance and to propose a partially restrained moment resisting frame system with better ductility, better energy dissipation capacity and acceptable self centering capacity. This can be done by finding a pattern in placing semi-rigid connection that would optimize seismic response.

Two buildings geometries are presented to provide a range of buildings proportions. A six storey buildings is used to present mid-rise structures; while a 20-storey buildings is used to present high-rise buildings. However, energy dissipation capacity, self-centering capacity, inter-storey drift ratio, force distribution, ductility, and yielding mechanism are used to evaluate the seismic performance of the four systems that mentioned above.

Analysis start with the partially restrained moment resisting frame system, by taking multiple combinations of rigid and semi-rigid connections, these hybrid combination are next subjected to nonlinear time history analysis and nonlinear static pushover analysis, and at the end of these analysis process the partially restrained moment resisting frame cases are compared, after that buckling restrained braced frame system with different location of the bracing member, and eccentric braced frame system with different combination of bracing location and shear link length are considered. The results for these three systems are compared to that for the fully restrained moment resisting frame system.

The results of the research indicated that the proposed placement of partially restrained connections provide high energy dissipation capacity, acceptable capacity-demand ratio, good self centring capacity, good storey-drift ratio, and reduced the forces in both beams and columns, which allow designing these frame to smaller steel sections.On other hand, result for eccentric braced frame structure show that, this system is not suitable for both 6 and 20 storey buildings, since it become very difficult to limit yielding to the shear link only, however, buckling restrained braced frame (BRBF) system show very good behavior for 6-storey building., while it show less desired behavior for the 20-storey buildings, since it become very difficult to limit yielding to the buckling restrained bracing member only.

CHAPTER 1

Introduction

1.1 General**:**

The primary objective of the earthquake resistant design is to protect human life by preventing collapse of structures during strong and rare earthquakes, with keeping the economic losses within minimum range. Applying this concept especially in seismic design of high rise buildings has always been among the most challenging for researcher and professional, this is because of the high degree of uncertainty and the extreme randomness associated with earthquakes loads, which in turn make the structural seismic response so unpredictable. Some of the variables that cause this structural response under seismic excitation are the magnitude of ground shaking and its intensity on the site, underground depth of focus and distance from epicenter, period of the earthquake, on-site soil properties, building geometry and dynamic characteristics, quality of used materials and construction procedures as well as maintenance of the building. However, this nature of earthquakes required the utilization of the probability approach in analysis and design of structures under earthquake excitation with full understanding of the structural behavior under seismic loads.

For many years, the basic intent of the building code seismic provisions was to provide buildings with an ability to withstand intense ground shaking without collapse, but potentially with some significant structural damage. In order to accomplish this, modern seismic codes start to encourage the use of building configurations, structural systems, materials and details that are capable of ductile behavior, and thus, design buildings with strength less than their elastic strength demand. A structure is said to behave in a

ductile manner if it is capable of withstanding large inelastic deformations without significant reduction in strength, and without the development of instability and collapse. The amount of reduction in the design force of structures is related to the amount of ductility the system is deemed to possess. Generally, the building code allows structural systems with more ductility to be designed for lower forces than less ductile systems. In General, if structures designed with strength less than their elastic strength demand, it should have some desirable properties such as good ductility, good energy dissipation capacity, and good self centering capacity under earthquake excitation. Levels of the strength reduction and ductility are defined in the Seismic codes for different structural systems. Where, these seismic codes defined specific condition and detailing for these systems to achieve the defined strength reduction and ductility ratio.

Due to the extreme randomness and high uncertainties associated with the prediction of earthquake characteristics, it would be better to control the structural behavior rather than putting the effort in predicting extremely random events. Such a behavior can be decided by the designers by using capacity design concept. In this concept a weak element called "fuses" used to control local failure mechanism when design buildings to survive the ground shaking, examples of these elements is semi-rigid connection, shear link in eccentrically braced frame (EBF) system, and bracing in buckling restrained braced frame (BRBF), in all cases a properly designed fuses will be the first to fail during the earthquake, thus failure is controlled by easily repaired. However; fuses should have less yield strength than the other element in the building so that the maximum force that the building can take will be limited to the maximum capacity of the fuses. In other words, the strength of the building is limited by its weakest member, and therefore the other members will never be subjected to a force larger than the force

in the fuses. Also these weakest element should have a good ductility, so that the building can sustain the maximum forces and experience yielding whether the other element are ductile or not as long as their strength is larger than the yielding strength of the ductile weakest element. Consequently, structure behavior will be controlled by the designer, and not by the earthquake characteristics.

For many years, moment resisting frame (MRF) systems have been widely adopted in seismically active areas such as Taiwan, Japan and North America. However, the damage to steel welded beam-to-column connections observed in the 1994 Northridge earthquake (USA) and the 1995 Kobe earthquake (Japan) have raised serious concerns about the seismic reliability of steel moment frames. It has turned structural engineers' attention to partially restrained moment resisting frame (PRMRM), eccentrically braced frame (EBF) and buckling restrained braced frame (BRBF) systems. Compared to fully restrained moment resisting frame (FRMRF) systems, these systems have superior reparability and cost. The use of these three systems has grown rapidly in seismically active zones such as Taiwan, Japan and North America. However, only a few studies have been made of the comparative performance of these steel systems. To address this issue, the present study evaluates the seismic performance of PRMRF, EBF and BRBF systems in comparison with that of FRMRF systems. In detail, nonlinear inelastic time-history analyses and three dimensional static pushover analyses have been performed. Analysis starts with the PRMRF by taking multiple combinations of rigid and semi-rigid connections, one earthquake records reflecting strong ground motion is applied, and the redistribution patterns are compared. A pattern for semi rigid connection placement is sought as this might impose a building natural damper that would decouple the building lateral drift from the ground motion acceleration. Such behavior is highly desirable, since it would optimize the building design with minimal material and

construction cost. Finally, the pattern which shows the best seismic behavior is compared with EBF system, BRBF system, and FRMRF system in efforts to optimize seismic performance of the steel structures.

1.2 Literature review**:**

1.2.1 Moment resisting frame

In 1960s welded steel moment-frame buildings used by engineers as being among the most ductile systems contained in the building code (Fema 355F). The earliest group of Uniform Building Code (UBC) provisions covered the period from 1958 to 1973. These codes had no limitations on lateral drift for seismic design. They did provide a limit for wind load drifts of 0.0025 (Gary, et al., 2004). Moreover, ductility was assumed to develop in the beam ends only, and no consideration was given to the panel zone. Recent research has shown that this is a highly unrealistic expectation, and unless the panel zone strength is significantly increased, it may reach its ultimate capacity before the beam has yielded (FEMA- 355C). Other design concepts that adversely affect the performance of buildings from this time period include the low design base shear and the absence of restrictions for weak column formation. The effects of on-site soil conditions were also neglected (FEMA- 355C).

In the years between 1976 and 1985 the UBC integrated few improvements. A maximum seismic drift of 0.005rad was introduced (Gary, et al., 2004). The code began to consider the building location and occupancy by incorporating the design spectral acceleration, S_a and the importance factor, I. In 1978, the Applied Technology Council published ATC 3-06, where it defined seismic hazard exposure groups and acknowledged the importance of the soil-structure interaction. It also published national maps for seismic hazard and introduced the response reduction factor, R.

The time period from 1988 to 1994 provided additional development in the UBC provisions. The ductility of the lateral load resistant system was accounted by the response modification factor, Rw. In addition, the seismic zone factor, Z, accounted for the peak ground acceleration for the 10/50 hazard. Panel zone strength requirements and

special loading conditions for columns were also established. As a result of these efforts, the National Earthquake Hazard Reduction Program (NEHRP) was developed.

Despite the year at which a building was designed, a steel structure was always assumed to behave in a ductile matter if subjected to an earthquake. This expected ductile behavior allowed designers to account only for a portion of the strength required if the building were to stay in its elastic range. But, the Northridge earthquake in 1994 challenged this assumption when many beam-column connections failed in a brittle manner (Fema 355 F). Damage was spread over large distances from the epicenter and appeared to be independent of the buildings' age or geometric properties. Although a majority of the buildings did not collapse, the economic losses surpassed $20 billion (Fema 355 F). Soon after the earthquake, the SAC Joint Venture was formed to investigate structural seismic response. The venture is a partnership between Structural Engineers Association of California (SEAOC), Applied Technology Council (ATC), California Universities for Research in Earthquake Engineering (CUREE), Federal Emergency Management Association (FEMA), American Institute of Steel Construction (AISC), American Welding Society (AWS) and others. Their mutual efforts concentrated on producing altered guidelines for design of new buildings and for retrofitting existing buildings.

The large economic losses from Northridge and other moderate earthquakes showed a need for new performance criteria. Previously, the seismic design of buildings was governed by a collapse prevention philosophy without consideration of monetary damage. However, in September 2000, the SAC Joint Venture published FEMA-355F which explicitly defined the governing design factors – performance levels and seismic hazards.

The four performance levels are operational, immediate occupancy, life safety and collapse prevention. To meet the immediate occupational level, a building has minimal to no structural and non-structural damage, and utilities remain unaffected. The immediate occupancy level implies that minor nonstructural and even structural damage may be observed, but is repairable while the building remains occupied. This means the utilities and equipment may need repair, but no permanent drift is recorded. Under the life safety level, damage is extensive and repair may be economically unfeasible. The buildings will remain stable; however, permanent drifts of 2.5 percent or larger are observed. Life loss is not expected. Finally, the collapse prevention level precludes gross loss of life, but implies hazard to life safety. Permanent drifts exceed 5 percent, and the building is severely damaged.

The brittle failure of the connection under Northridge earthquake can be related to many factors, one of these factors can be due to the high degree of uncertainty and the extreme randomness associated with earthquakes loads which in turn make structural response under earthquake load largely unpredictable, other factor can be related to the absence of the “strong column” concept in earlier editions of the design codes also effected buildings from this time period. If the beam is not deliberately failed first, damaged columns may form a soft-story mechanism, where localized story failure replaces global collapse. This mechanism is highly undesirable as it may result in some loss of life and large fiscal damage. Also this brittle failure can be related to the detailing of Pre-Northridge connections, specify that the beam web is bolted to a steel plate, which in turn is connected to the column. Therefore, the beam web is perforated to accommodate placement of bolts, and the cross sectional area, A, and the moment of inertia, I, are decreased. As a result, the section of the beam experiencing the highest demands has reduced sectional properties and in turn imposed high demand on the

connections (Fema 355F). Also, in theory, pre-Northridge connections were to transfer shear from the beam to the column through the beam web, while moment and axial forces were carried by the beam flanges. However, the boundary conditions of the connection forced much of the shear demand to the flanges with development of triaxial stresses (Miller 1998). While steel elements maintain much desirable ductility under a uniaxial stress, no yielding and decking develops if they are subjected to multi-axial stresses. Instead, the material fractures in a brittle matter, which explains the sudden failure of beam flanges and their corresponding welds during the Northridge earthquake. Other connection details also contributed to the poor performance of the pre-Northridge connections. A backing bar is commonly used in welding practices, and leaving it in place after fulfilling its function was believed to have no consequences on the connection strength. According to Popov et al. (1998), however, leaving the weld backing bar in place created an artificial crack in the flange welds. Inspections of many damaged connections confirmed fracture began in the weld notch created by the backing bar. The failure usually initiated in the bottom flange, where the backing bar obstructed proper welding procedures and inspections (Popov et al. 1998).

Another performance factor was the size of access holes, which provide access for welders to deliver weld continuity across the thickness of the beam web (Lu et al. 2000). Small access holes obstruct weld installation and may cause dubious weld performance. Large access holes on the other hand, increase stress concentrations in the beam flange.

Structural redundancy and member sizes also affect building performance (Lee and Foutch 2002). In earlier code provisions the lateral load moment-resisting frames usually involved plethora of members. Thus, the member sizes were relatively small, and the overall design had considerable redundancy. However, over time engineers

began to use heavier members in order to minimize the construction cost of the now smaller lateral load moment resisting fames. As a result, not only did the redundancy of the structure reduce, but also the demand on the connections increased. Meanwhile, the connections' detailing remained similar as a ductile behavior of pre-Northridge connections was assumed. The Northridge earthquake proved this design assumption was not scientifically backed, and the connection details before 1994 have been widely studied since then. Multiple problems were discovered as a result of this intensive research (Miller 1998).

Also material properties proved to be influential in structural performance as well. As previously addressed, large stress concentrations developed in the connection welds; thus the weld stiffness is crucial for adequate seismic performance. However, a typical welded metal used in pre-Northridge connections is E70T-4, which has a Charpy V_{notch} toughness of only 7-14 J at 70°C (158°F) (Chi et al 2000). To compare the required range of Charpy V_{notch} toughness in current provisions is 27-54 J at -28°C (-18°F) (Mao et al.2001). This lack of weld stiffness contributed to the widespread brittle failure of Pre-Northridge connections.

In addition, the member yield strength is significantly modified due to alloys added in the rolling mills. Therefore, the average yield strength of the widely used A36 steel is increased to 48 ksi (331 MPa) and the average ultimate stress is 70 ksi (483 MPa) (Popov et al. 1998). Since the UBC provisions prior to the Northridge earthquake provided only minimum limits and no maximum strengths were cited, the designers were forced to use the minimum yield strength of 36 ksi (248 MPa) as the strength at which plastic hinges would develop in the beam. However, in reality the plastic hinges will not form until the actual yield strength of the steel is reached, and plastic hinges appear in the weaker beam-to-column connections instead.

The brittle fracture of connections observed after the Northridge earthquake is rarely a result of any one of the pointed weaknesses. Instead, a combination of several of these factors produced this unexpected structural performance (Fema 355C). Following the earthquake, the engineering community began modifying design requirements and retrofitting buildings designed based on previous UBC editions. One method to improve the performance of existing buildings is to increase the beam capacity at the column face by supplying cover plates. As a result, the panel zone is stiffer, and the beam is able to reach inelastic behavior before failure occurs. FEMA-355C suggests placing haunches or ribs as an alternative to the cover plates. The major disadvantage to this approach is the uncertainty associated with plastic hinge location. A seismic load could force an inelastic behavior in the beam, the connection or preferably in both, which would provide optimal structural response (FEMA- 355C).

Another method is to decrease the beam flanges at the locations where plastic hinges were initially assumed to develop. This approach is termed the Reduced Beam Section (RBS) method, and it successfully shifts the seismic demand from the connection to the beam, where damage can be controlled (FEAM-355C). However, reducing the beam section at the location of anticipated plastic deformations implies that the remaining portion of the beam as well as all other structural elements must be designed to carry seismic loads elastically. Therefore, the RBS method has shown to be predictable, thus safe, but rather costly (Miller 1998).

Overall, current provisions are based on lessons learned from the Northridge earthquake. Among the many changes instigated since 1994 are the removal of weld backing bar at the bottom beam flange, closely monitored workmanship and regulation of the weld stiffness. Moreover, the panel zone capacity is now given significant attention. Also, FEMA 1997 restricted plastic rotation to a minimum of 0.003 rad.

While these regulations are believed to provide for adequate seismic structural response, the seismic design of buildings has yet to offer an economic solution (Miller 1998). Recent research results indicate that the use of semi-rigid connections in moment-resisting frames may address this problem while meeting all other design objectives of the current codes.

1.2.2 Eccentrically braced frame:

While steel moment frames can exhibit stable inelastic and ductile behavior under cyclic seismic excitation, the concentrically braced frames usually possess greater lateral stiffness which can limit the damage due to drift. However, moment frames are relatively flexible and their design is usually governed by the drift limitations in order to control the damage. On the other hand, the ductility and energy dissipation capacity of concentrically braced frames can significantly deteriorate if braces buckle under seismic loading. Eccentrically braced frames (EBFs) successfully combine the advantages of the moment frames and concentrically braced frames, namely high ductility and lateral stiffness, while eliminating the shortcomings of those frames by limiting the inelastic activity to ductile shear links and keeping braces essentially elastic without buckling, thus maintaining high lateral stiffness during earthquake events.

EBFs are characterized by an isolated segment of beam, which is referred to as link. The diagonal brace, at least at one end, is connected to the end of the link rather than the beam-column joint. All inelastic activity is intended to be confined to the properly detailed links.

Links act as structural fuses which can dissipate seismic input energy without degradation of strength and stiffness, thereby limiting the forces transferred to the adjacent columns, braces, and beam segments.

Link plastic rotation angle γ_p can be easily estimated by frame geometry assuming rigid-plastic behavior of the frame members. Depending on the section properties of the link, link may yield either in shear extending over the full length of the link or in flexure at the link ends, or the combination of shear and flexural yielding. Note that link plastic rotation angle is the same whether the link yields in shear or in flexure. Yielding mechanism of links depends on material properties of links such as moment capacity, shear capacity, and strain hardening. Modeling of EBF system and the other systems (FRMRF, PRMRF, and BRBF) will be discussed in chapter 3.

As pointed out earlier, the reason that inelastic activity should be limited within links is to prevent other elements from yielding. Well-detailed links can sustain large inelastic deformation reversals without losing strength and stiffness (AISC 2005). Therefore global structural stability and performance will not be jeopardized if inelastic activity is confined only to links. Unintended yielding or buckling of braces or columns can result in undesirable response (AISC 2005).

1.2.3 Buckling restrained braced frame (BRBF):

As mentioned before, steel moment-resisting frames are susceptible to large lateral displacements during severe earthquake ground motions, and require special attention to limit damage to nonstructural elements as well as to avoid problems associated with P-Δ effects and brittle or ductile fracture of beam to column connections [FEMA, 2000]. As a consequence, engineers in the US have increasingly turned to concentrically braced steel frames as an economical means for resisting earthquake loads. However, damage to concentrically braced frames in past earthquakes, such as the 1985 Mexico, 1994 Northridge, and 1995 Hyogo-ken Nanbu earthquakes, raises concerns about the ultimate deformation capacity of this class of structure. Individual braces often possess only limited ductility capacity under cyclic loading. Brace hysteretic behavior is

unsymmetrical in tension and compression, and typically exhibits substantial strength deterioration when loaded monotonically in compression or cyclically. Because of this complex behavior, actual distributions of internal forces and deformations often differ substantially from those predicted using conventional design methods. Design simplifications and practical considerations often result in the braces selected for some stories being far stronger than required, while braces in other stories have capacities very close to design targets. This variation in story capacity, together with potential strength losses when some braces buckle prior to others, tend to concentrate earthquake damage a few “weak” stories. Such damage concentrations place even greater burdens on the limited ductility capacities of conventional braces and their connections. It has also been noted that lateral buckling of braces may cause substantial damage to adjacent nonstructural elements. Prompted by these observations and concerns, seismic design requirements for braced frames have changed considerably during the 1990s, The concept of eliminating the compression buckling failure mode in intermediate and slender compression elements has long been a subject of discussion. The theoretical solution for eliminating the buckling failure mode is very simple: laterally brace a compression element, at close regular intervals, so that the compression element’s un-braced length effectively approaches zero.

The BRBF system delivered ductile, stable and repeatable hysteretic behavior (AISC 2005). BRBF systems are unique due to the configuration of the brace elements. They consist of two major components: the steel core resists axial stresses and the outer concrete filled steel casing resists buckling stresses, and the casing restrains the steel core from buckling thereby developing almost uniform axial strains in tension and compression.

BRBF have full, balanced hysteresis loops with compression yielding similar to tension yielding behavior. Therefore, plastic hinges associated with buckling cannot form in a BRBF.

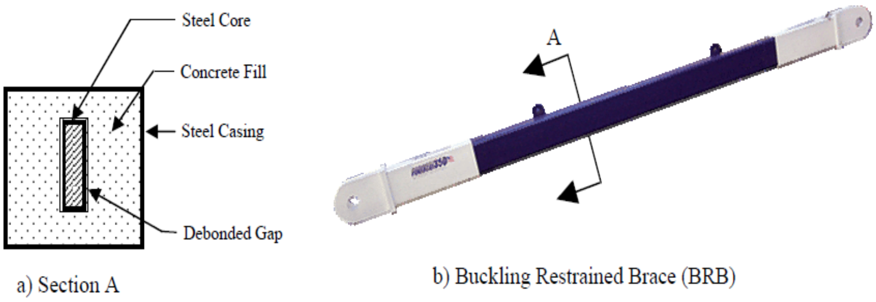


Fig 1.1 Buckling Restrained Bracing (BRB) (Saif Hussain, et al.)

1.3 Objectives

1. Find a pattern in placing partially restrained connections in MRF systems that would optimize global seismic response and reduce material, construction and potentially rehabilitation costs.
2. Study the behavior of PRMRF, EBF, and BRBF systems under seismic excitation, and compare their seismic performance with the seismic performance of the FRMRF system, in order, to find the characteristics of each systems and there suitability to different seismic excitation.
3. Expand knowledge about semi-rigid connections, the link elements in EBF systems, and bracing in BRBF system, their seismic performance, and their effect on the global behavior of steel buildings under seismic loads.
4. Explain the inelastic modeling of FRMRF, PRMRF, EBF, and BRBF systems using sap 2000 program, and in accordance to AISC seismic provision and FEMA codes.
5. Discuss the difference in the behavior of tall and short building under seismic excitation.
6. Create economic structural system that capable to withstand strong seismic excitation, without collapse, and with minimum rehabilitation cost.

CHAPTER 2

BACKGROUND ON NONLINEAR DYNAMIC ANALYSIS AND STEEL CONNECTIONS

2.1 First-Order Linear Elastic Analysis

In this approach the stress-strain or forces-displacement relation is assumed to be linear and elastic (reversible), so there will be no plastic deformation (which defined as permanent deformation after the removal of forces), and the redistribution of the internal force is not permitted during the life time of the structure, also the deflection of a structure is assumed to be very small so that geometrical and material nonlinearity are negligible.

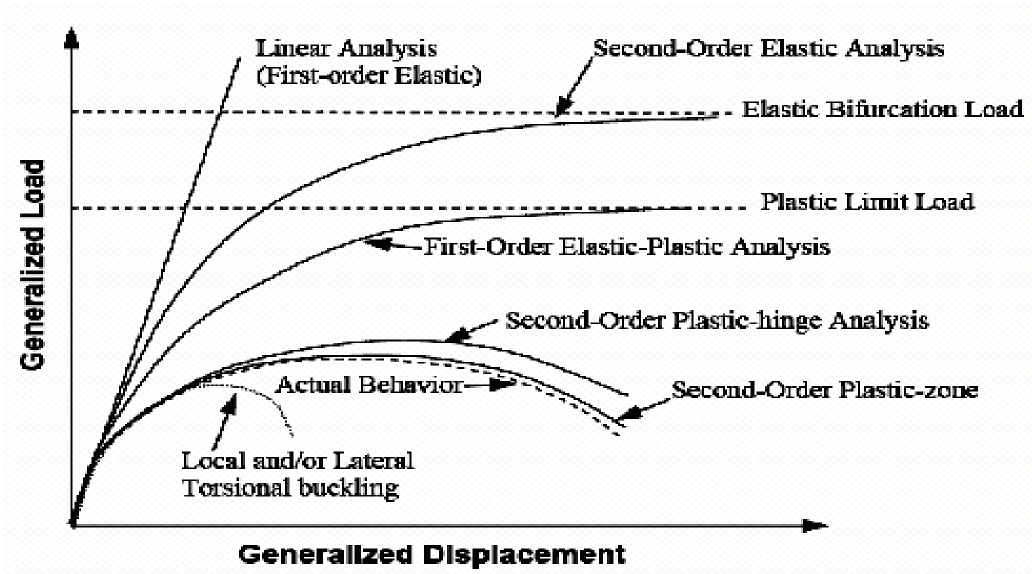


Fig 2.1 General analysis types for framed structures (Chan et al., 2000)

Linear elastic analysis is computationally simple, efficient, and the most important that the superposition principle is applicable. However, this linear approximation may not be accurate due to effects of the element and the structural deflections ($P - \delta$ and $P - \Delta$), respectively, also, design building to remain elastic during earthquake excitation require high strength and in turn extremely high cost which might not be economically feasible.

2.2 Second-order Non-linear Elastic Analysis

This approach takes into account the geometrical nonlinearity by considered P −δ and P − Δ effects in the analysis. The change in geometry is allowed by incorporating the variation of element stiffness in the presence of axial force, as a result, the calculated deflections, forces, and moments will be more accurate than the linear analysis.

However, the superimposition technique is not valid for in this method since the structural response is depending on the loads-deformations relation. Also, the effect of material yielding is not included in this method, which leads to over-predict the collapse load of a structure. As shown in Fig. 2.1. In addition, because the stiffness of structure is dependent on the axial force in the members, formation of stiffness matrix depends on the displaced configuration of the structure that is not known in advance. As a result, the second-order analysis method can only be performed by an iteration process.

2.2.1 The P –δ Effect:

This method occurs in members that subjected to axial load as shown in fig 2.2, so that after these members deform the axial force in these members will develop additional moment in the member, and thus reduce the stiffness of the deform member. Its magnitude is related to the axial load applied to the structural member. It affects the state of stress as well as the stiffness of the member. Its careful consideration is important for buckling analysis and design of slender skeletal structures.

2.2.2 The P −Δ Effect:

As shown in fig 2.2, this method reflects changes in the structural geometry. The transformation matrix, used to derive the stiffness matrix, requires updates to reflect changes to frame coordinates. This is done by modifying the lagrangian transformation at each iterative step by adding the horizontal and vertical displacement to the

corresponding proceeding coordinates. The updated transformation matrix is used to include effects from global displacements.

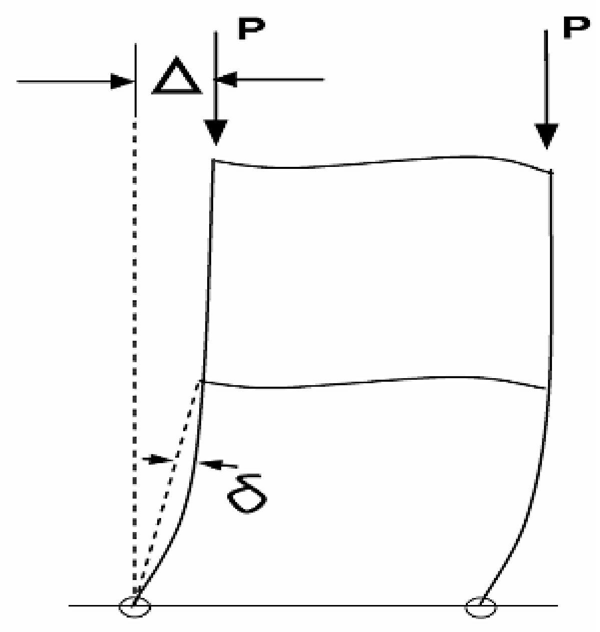


Fig.2.2 P –δ and P –Δ effects (Chan et al., 2000)

2.3 Second-Order Non-linear Inelastic Analysis:

In this method, nonlinearities in structures exist in two forms: geometrical nonlinearity and material nonlinearity. If the effect of material nonlinearity or material yielding is included in the analysis, the stress-strain or forces-displacement relation will not be reversible, and a plastic deformation will take place, result in hysteresis loop and thus dissipation of energy, also redistribution of the internal forces are permitted, and the ultimate load capacity of most structures will considerably affected as shown in fig 2.1.

For steel frame structures, material yielding starts in the cross-section at the outermost fiber, where moment equal the yielding moment (My), As additional load is applied yielding spreads through the member cross-section (plastification) and along the member length (plastic zone) while the moment in the cross-section increases gradually from My to the fully plastic moment (Mp) . Material non-linearity can be conducted by two approaches, concentrated plasticity (plastic hinge) approach and distributed plasticity (plastic zone) approach. In the first approach cross-section yielding at the member ends. While the latter approach models the spreading of plasticity within the whole volume of the structure. Furthermore, to obtain a more accurate full-yield strength surface of I- or H-sections under moment and axial load, the “section assemblage approach” is established, in this concept the central cored web taking axial force and the remaining area taking moment is established, namely. The brief detail of these two inelastic models and the concept of section assemblage method are introduced in the following sections.

2.3.1 Concentrated Plasticity Approach

This method is widely used in the computer modeling, where plastic hinge is denoted by a zero-length spring, while the structural element remains elastic. Therefore, this method lump the effects of material non-linearity into the member end nodes. This assumption simplifies the actual behavior of the member, but allows for significant savings in computational time. The concentrated plasticity approach has proven to be satisfactory in producing a good approximation of the real behavior of beams and columns. Popular methods to model plastic hinges are elastic-plastic hinge method, column tangent modulus method, beam-column stiffness degradation method, and end-spring method.

2.3.2 Distributed Plasticity Approach

In this method the structural element is divided into sections containing either elastic or plastic characteristics, so that plastic zone region (which defined as a segment of an element that experiences a demand larger than the yield moment) can be considered. As a result this method is more accurate than the plastic hinge method and it can effectively approximates real-world material nonlinear behavior, while providing the means to account for other factors, which influence member performance such as residual stresses and fabrication imperfections. However, this method requires a considerable amount of computational time, and it becomes exponentially impractical as the complexity of tested frames increases.

2.3.3 Plastic hinge function:

In most elastic-plastic analysis, a simplified linear interaction equation is applied to monitor the yielding of a section; in other word, to control the formation of a plastic hinge. However, this linear function is based on the simple combined stress equation for elastic analysis. Thus the function is correct for first yield analysis and can only give an approximation when used in plastic analysis

Researchers adopted various equations to model the ultimate section capacity (AISC-LRFD, 1986) as follows:

$$\begin{aligned} &\frac{P}{P_y} + \frac{8}{9}\frac{M}{M_p} = 1.0 \qquad for\ \frac{P}{Py} \geq 0.2, \\ &\frac{P}{2P_y} + \frac{M}{M_p} = 1.0 \qquad for\ \frac{P}{Py} < 0.2, \end{aligned} \qquad \ldots\ldots\ldots\ldots\ldots\ldots\ (2.1)$$

Each term in the above equations is defined as follows:

$P_y = \sigma_y * A$: is the squash load of the cross section,

$M_p = \sigma_y * Z_p$: is the plastic moment capacity of the member,

σ_y: is the yield stress of material,

A: is the cross-sectional area,

Z_p: is the plastic modulus,

M_p, P_y: Are the plastic bending moment and yield axial force at cross section.

This empirical formula can be considered as uneconomical for many sections, since it's considered as a lower bound capacity for a general section. Furthermore, these two discrete functions are discontinuous and lead to an abrupt change of yield function at P = 0.2 Py. It, therefore, represents an inconsistency between high and low axial loads and contains a discontinuity or kink in the axial force-moment curve (Chan et al., 2000).

A more accurate method to find plastic hinge function is to divide a section into a large number of finite sub-areas. The initial stress for the sub-areas in the section assumed to be the axial and residual stress in the member. The curvature is then gradually increased and the final strain is calculated. A set of moment versus curvature $M-\phi-P$ curves can then be generated and mathematical functions can be employed to curve fit the relationship and stored in a data bank for elastic-plastic analysis. The described method is accurate, but its use for practical design may be complicated as these moment-curvatures relationship are not generally available for routine uses (Chan et al., 2000).

A Section Assemblage Approach method is developed by Chan and Chui as an alternative approach to find the section capacity of a member subjected to a combination of compressive and flexural loading. This method only uses the basic sectional parameters, the depth, breadth, and web and flange thickness in the assessment of ultimate section strength by a simple concept of the central cored web taking axial force and the remaining web and flange taking moments. This idea can be applied to many typical sections including rectangular hollows, channel and I-sections.

2.4 Connections

2.4.1 Connection Classification:

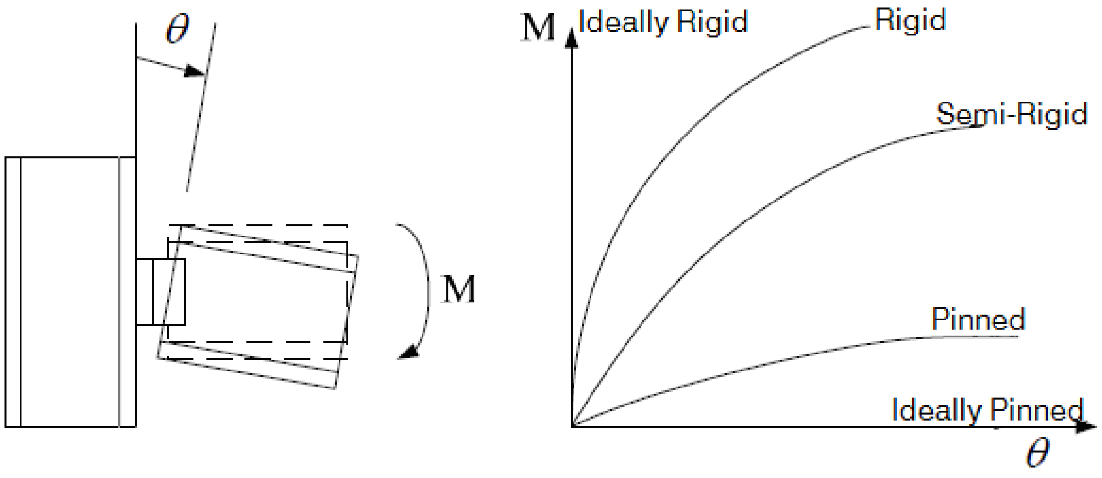


Figure 2.3: moment connections curves (Chan et al., 2000)

The Load and Resistance Factor Design (LRFD) Specifications (AISC, 2005) designated two types of construction in their provisions: Type FR (Fully Restrained) and Type PR (Partially- Restrained). Type FR corresponds to rigid connections. Type PR includes semi-rigid and pinned connections. If Type PR construction is used the effect of connection flexibility must be taken into account in the analysis and design procedures.

The influence of partially restrained connections on structural analysis is not only in changing the moment distribution among beams and columns, but also in the increase of frame drift and accordingly the increase of the P-Δ effect in the frame analysis. However, AISC-LRFD classifies Connections to FR or PR connections according to the following joint characteristics:

1. Strength

The most important aspect of the strength of a connection is its relationship to the strength of the beam it connects. If the beam strength exceeds the connection strength then the ductility of the connection is important. let M_u be the capacity of the connection and M_P^{beam} be the plastic moment capacity of the beam, the strength of a connection can be classified as follows:

A connection is full strength (FR) if $Mu \geq M_P^{beam}$; otherwise it is partial strength (PR). A (FR) connection can develop the full plastic moment capacity M_P, of the beam framing into it, while a (PR) connection can only develop a portion of it.

For design purposes, an (FR) connection can be designed elastically using appropriate resistance factors for the connection components. A (PR) connection must be designed to force ductile yielding as the primary failure mode in the connection components and to avoid any brittle failure modes.

For designs controlled by gravity and wind loads it is also useful to define a lower limit on strength below which the connection can be treated as a simple connection. Connections incapable of transmitting at least 0.2 M_P^{beam} at a rotation of 0.02 radians can be considered to have no flexural strength for design.

2. Ductility

Connection ductility is a key parameter when the deformations are concentrated in the connection elements, as the typical case in (PR) connections. Let θ_u represents the value of connection rotation at the maximum moment and θ_u^* represents the value of rotation at the point where the moment has dropped to 80% of its maximum value. The ductility of a connection can be classified as follows:

In general; a connection is ductile if $\theta_u^* \geq 0.03$ radians, otherwise it is brittle.

Although special rotation limits have only been proposed in seismic design applications, it should be recognized that connection ductility is the key to moment redistribution and safe design.

3. Stiffness

Because the nonlinear behavior of the connection manifests at low levels of load, the initial stiffness of the connection (R_{ki}) does not adequately characterize connection response at service levels. The secant stiffness (R_{ks}) is more indicative of low-level, nearly linear, response. Let the ratio of connection stiffness to beam stiffness be;

$$\alpha = EI / R_{ki} L \text{ ……… (2.2)}$$

Where L and EI are the length and the bending rigidity, respectively, of the beam that is being connected. The rigidity of the connection can be classified as follows:

If $\alpha > 20$: the connection is fully restrained (FR)

If $2 \leq \alpha \leq 20$: the connection is partially restrained (PR)

And if $\alpha < 2$: the connection is simple.

The term α, the general term for the effective characteristic length factor, is also useful in calculating member forces and column stability, since it provides a way to quantify the effective connection flexibility at various degrees of connection loading.

Because the reduction in buckling capacity due to joint flexibility depends upon whether the frame is braced or unbraced, the value of 20 has been suggested for unbraced frames, while a value of 8 has been suggested for braced frames.

2.4.2 Types of Semi-Rigid Connections:

In this section, common type of connections is discussed these connections are illustrated in Figure 2.4 as follow:

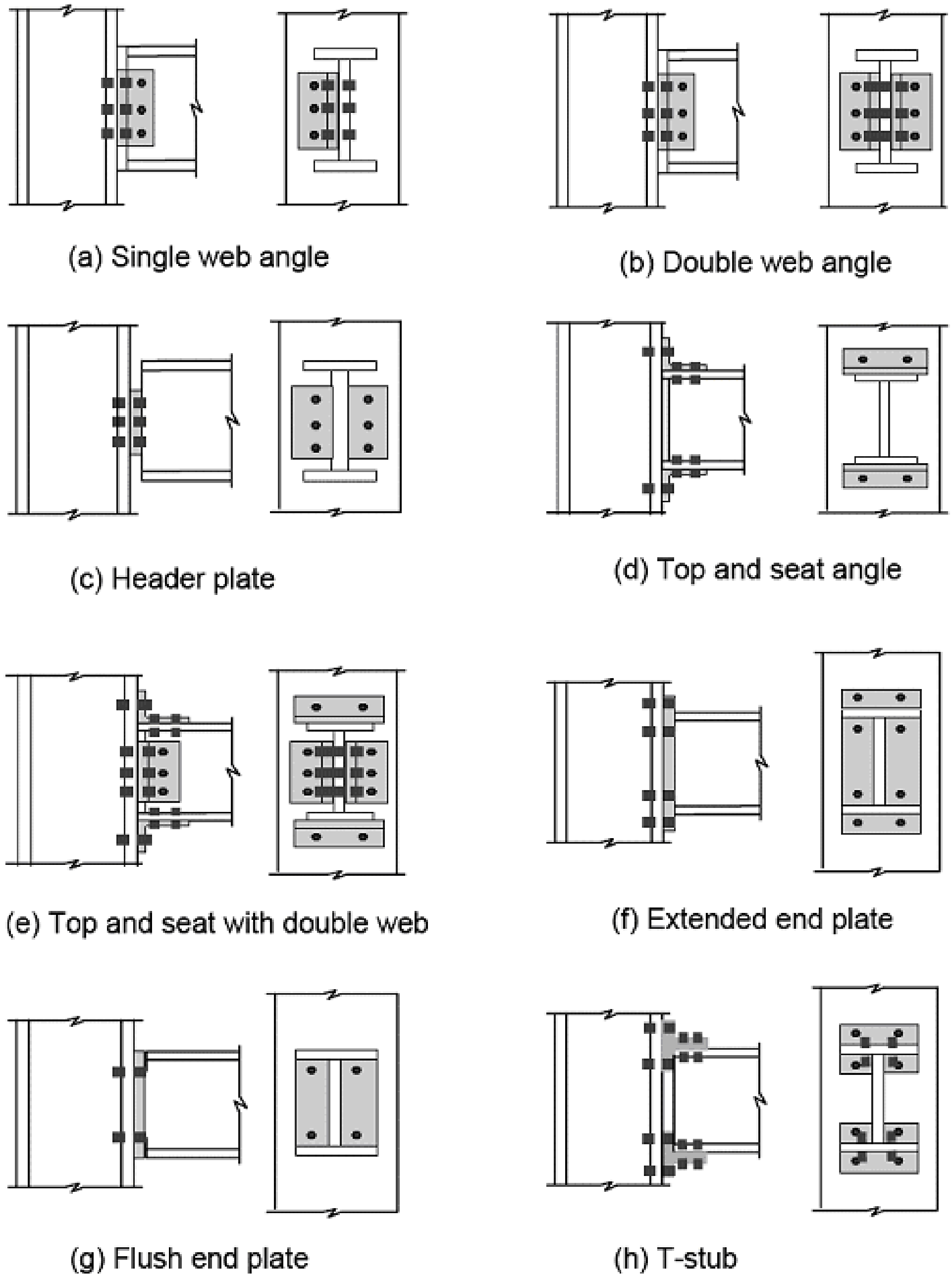


Fig. 2.4: Common type of beam-column connections (Chan et al., 2000)

2.4.2.1 Single Web Angle:

A single web angle connection consists of an angle either bolted or welded to both column and beam web (refer to Figure 2.4a). These connections have little moment rotation rigidity and are very flexible. They would be classified by Fema 355d as pinned connection.

2.4.2.2 Double Web Angle Connections:

Double web angle connection consists of two angles either bolted or welded to both column and beam web (refer to Figure 2.4b). fema-355d classify this type of connection as pinned connection.

2.4.2.3 Header Plate Connections:

A header plate connection consists of an end plate which its length is less than the depth of beam, welded to the beam and bolted to the column (refer to Figure 2.4c).

The M-θ behaviors of these connections are similar to that of double web angle connection. Also these connections are classified as pinned connection.

2.4.2.4 Top and Seat Angle Connections:

As shown in (Figure 2.4d), the AISC-ASD Specifications define the top and seat angle connection as follow: the seat angle transfers only vertical reaction and should not give significant restraining moment on the end of beam, the top angle is merely for lateral stability and is not considered to carry any gravity loads.

2.4.2.5 Top and Seat Angle Connections with Double Web Angle:

This connection is a combination of top and seat angle and double web angle connection as shown in (Figure 2.4e). By fema-355d these connections are considered as flexible partially restrained connection.

2.4.2.6 Extended/flush end-plate connections:

The extended end-plate connections are classified into two types as extended end-plate connection either on the tension side only or both the tension and compression sides (refer to Figures 2.4 f, 2.4g). These connections are built up by welding the endplate to the beam end along both flange and web in the fabricator's shop and then bolting end-plate to the column in the field. Both extended and flush end-plate connections are classified as stiff partially restrained connection. End-plate connections are often categorized in terms of thick end-plates or thin end-plates. Thin end-plates are those where the plate is thin enough to have yielding of the plate, and thick end-plates are those that develop yielding in the members. While thin end-plates may provide good ductility and inelastic deformation capacity, they do not develop the full plastic capacity of the beam and will act like fuses in the building.

2.4.2.7 T-stub Connections:

A T-stub connection consists of two T-stubs bolted to beam and column at the top and the bottom of beam flange as shown in (Figure 2.4h). This type of connections is considered as partially restrained connection with intermediate stiffness.

2.4.3 Finite element analysis of semi-rigid frames

The stiffness matrix of a beam, k_{beam} with rotational springs at the ends is shown by the following matrix (Chan et al., 2000):

$$k_{beam} = \frac{EI}{L}\begin{bmatrix} \frac{A}{I} & 0 & 0 & \frac{A}{I} & 0 & 0 \\ & \frac{(S_{ii}+S_{ij}+S_{jj})}{L^2} & \frac{(S_{ii}+S_{jj})}{L} & 0 & \frac{-(S_{ii}+S_{ij}+S_{jj})}{L^2} & \frac{(S_{ii}+S_{jj})}{L} \\ & & S_{ii} & 0 & \frac{-(S_{ii}+S_{jj})}{L} & S_{ij} \\ & & & \frac{A}{I} & 0 & 0 \\ & & & & \frac{(S_{ii}+S_{ij}+S_{jj})}{L^2} & \frac{-(S_{ii}+S_{jj})}{L} \\ Sym & & & & & S_{ii} \end{bmatrix} \quad .(2.9)$$

Where:

$$S_{ii} = \left(4 + \frac{12EI}{LR_j}\right) / R^*$$

$$S_{jj} = \left(4 + \frac{12EI}{LR_i}\right) / R^*$$

$$S_{ij} = S_{ji} = 2 / R^*$$

$$R^* = \left(4 + \frac{12EI}{LR_i}\right) * \left(4 + \frac{12EI}{LR_j}\right) - \left(\frac{EI}{L}\right)^2 * \frac{4}{R_i R_j}$$

R_i : Stiffness of rotational spring at ends i.

R_j : Stiffness of rotational spring at ends j.

E: is the modulus of elasticity and A, I, L, is the cross-sectional area, moment of inertia and the length of the member respectively.

The beam stiffness matrix can be assembled in the usual manner to form the structure stiffness matrix K for a given structure. Then the general equilibrium at the nodes is formed:

KU =F…….. (2.10)

This equation can be solved by the Gauss elimination or other well-known methods and consequently the nodes displacement vector U can be calculated. F is a vector representing external forces acting at the nodes.

For the beam with rotational springs at the ends, it must be considered that the fixed end forces are different from the quantities given in conventional beam elements. These new fixed end forces can be calculated by using slope deflection relations and superposition techniques.

At the end of the structural analysis, after the internal forces in members are calculated, then the resistance of each member in bending, tension and compression are compared with internal forces, and the formation of plastic hinges within the structure are checked. When a plastic hinge forms at the left-hand end of a beam, the original stiffness matrix of the beam, Eq. (2.9), is replaced by a reduced matrix k_{Lbeam}. This matrix can be obtained from Eq. (2.9) by replacing R_i=0 as shown by Eq. 2.11 (Chan et al., 2000):

$$k_{beam} = \frac{EI}{L}\begin{bmatrix} \frac{A}{I} & 0 & 0 & \frac{A}{I} & 0 & 0 \\ & \frac{S_{jj}^*}{L^2} & 0 & 0 & \frac{-S_{jj}^*}{L^2} & \frac{S_{jj}^*}{L} \\ & & 0 & 0 & 0 & 0 \\ & & & \frac{A}{I} & 0 & 0 \\ & & & & \frac{S_{jj}^*}{L^2} & \frac{-S_{jj}^*}{L} \\ Sym & & & & & S_{jj}^* \end{bmatrix} \quad .....(2.11)$$

Where

$$S_{jj}^* = \frac{3}{1+\frac{3EI}{LR_j}}$$

Similarly when the right-hand end is turned into a plastic hinge, the beam stiffness matrix can be obtained from Eq. (2.9) by replacing Rj=0 in a similar manner as was shown above.

Finally, when both ends are transformed into plastic hinges, the reduced stiffness matrix of the beam reduces to Eq. (2.12) (Chan et al., 2000):

$$k_{beam} = \begin{bmatrix} \frac{EA}{L} & 0 & 0 & \frac{EA}{L} & 0 & 0 \\ & 0 & 0 & 0 & 0 & 0 \\ & & 0 & 0 & 0 & 0 \\ & & & \frac{EA}{L} & 0 & 0 \\ & & & & 0 & 0 \\ Sym & & & & & 0 \end{bmatrix} \text{........(2.12)}$$

2.5 Linear and nonlinear dynamic analysis method

The equation of motion for multi-degree of freedom system under earthquake load can be written as:

$[M]\{\ddot{U}\}+[C]\{\dot{U}\}+[K]\{U\}=-[M]\{R\}\ddot{u}_g$ ……. (2.13)

Where:

$[M]$: Mass matrix (square matrix)

$[C]$: damping matrix (square matrix)

$[K]$: Stiffness matrix (square matrix)

$\{U\}$, $\{\dot{U}\}$, $\{\ddot{U}\}$: displacement, velocity, acceleration matrices (column matrices).

$\{R\}$: Earthquake loading vector (vector of rigid body displacement resulting from unit support displacement in direction of ground motion.

More information about this equation and its derivative can be found in [1], however, by solving the above equation, the deflection of the building under seismic excitation can be known, and as a result the stress in the members can be computed.

This equation is used for linear and nonlinear structure, and can be solved by many methods like: modal analysis, central difference method, Newmark-β method, and Wilson-θ method, two method will be discussed: modal analysis and Newmark-β method:

2.5.1 Modal analysis:

This method is used for linear analysis where the stiffness of the structure will remain constant under the excitation. There is two different type of modal analysis

2.5.1.1 Eigenvector analysis:

Eigen vector analysis determines the undamped free-vibration mode shapes and frequencies of the system. These natural Modes provide an excellent insight into the behavior of the structure. They can also be used as the basis for response-spectrum or time- history analyses, although Ritz vectors are recommended for this purpose. Eigen vector analysis involves the solution of the generalized Eigen value problem:

$$\left[K-\omega^2 M\right]\Phi = 0 \ldots\ldots (2.14)$$

Where K is the stiffness matrix, M is the diagonal mass matrix, ω^2 is the diagonal matrix of Eigen values, and Φ is the matrix of corresponding Eigen vectors (mode shapes).

Each Eigen value-eigenvector pair is called a natural Vibration Mode of the structure. The Eigen value is the square of the circular frequency, ω for that Mode. The cyclic frequency, ω and period, T, of the Mode are related by:

$$T = \frac{2\pi}{\omega} \ldots\ldots (2.15)$$

2.5.1.2 Ritz-Vector

Analysis Research has indicated that the natural free-vibration mode shapes are not the best basis for a mode-superposition analysis of structures subjected to dynamic loads. It has been demonstrated that dynamic analyses based on a special set of load- dependent Ritz vectors yield more accurate results than the use of the same number of natural mode shapes. The reason the Ritz vectors yield excellent results is that they are generated by taking into account the spatial distribution of the dynamic loading, whereas the direct use of the natural mode shapes neglects this very important information.

In sap 2000 program the spatial distribution of the dynamic load vector serves as a starting load vector to initiate the procedure. The first Ritz vector is the static displacement vector corresponding to the starting load vector. The remaining vectors are generated from a recurrence relationship in which the mass matrix is multiplied by the previously obtained Ritz vector, and used as the load vector for the next static solution. Each static solution is called a generation cycle.

When the dynamic load is made up of several independent spatial distributions, each of these may serve as a starting load vector to generate a set of Ritz vectors. Each generation cycle creates as many Ritz vectors as there are starting load vectors. If a generated Ritz vector is redundant or does not excite any mass degrees of freedom, it is discarded and the corresponding starting load vector is removed from all subsequent generation cycles. Standard Eigen-solution techniques are used to orthogonalize the set of generated Ritz vectors, resulting in a final set of Ritz vector Modes. Each Ritz-vector Mode consists of a mode shape and frequency. The full set of Ritz-vector Modes can be used as a basis to represent the dynamic displacement of the structure. When a sufficient number of Ritz- vector Modes have been found, some of them may closely approximate natural mode shapes and frequencies. In general, Ritz- vectors Modes do not represent the intrinsic characteristics of the structure in the same way the natural Modes do. The Ritz- vector modes are biased by the starting load vectors.

2.5.2 Newmark- β method

This method is popular in dynamic analysis, although it lacks the mathematical evidence, as name implies this method is created by Newmark who proposed the following system of equations (Nazzal 2000):

$$m\ddot{u}_{i+1} + c\dot{u}_{i+1} + ku_{i+1} = p_{i+1} ......(2.16)$$

$$\dot{u}_{i+1} = \dot{u}_i + \frac{\Delta t}{2}\ddot{u}_i + \frac{\Delta t}{2}\ddot{u}_{i+1} ....(2.17)$$

$$u_{i+1} = u_i + \Delta t * \dot{u}_i + \left(\frac{1}{2} - \beta\right) * \Delta t^2 * \ddot{u}_i + \beta * \Delta t^2 * \ddot{u}_{i+1} ...(2.18)$$

To solve the above three equation $\ddot{u}_i$, $\dot{u}_i$ and u_i should be known in advanced, so that $\ddot{u}_{i+1}$, $\dot{u}_{i+1}$ and u_{i+1} at step $i+1$ can be determined.

The value of parameter, β are limited to range from (0-0.25) this variation offers a group of sub methods some of these method is shown below:

$\beta = \frac{1}{4} \rightarrow$ Known as constant acceleration method

$\beta = \frac{1}{6} \rightarrow$ Known as linear acceleration method

$\beta = 0 \rightarrow$ Known as explicit Newmark method

As shown above, for $\beta = 0.25$ the method is known as constant acceleration method, this method is unconditionally stable method , so it will not collapse under any value of the time interval Δt, however, the stability of the other method with different value of β will depends mainly on the value of the time interval Δt .

Chapter 3

Analysis Procedure

In practical life, buildings design is covered by two design philosophy, the first approach is elastic design approach in which the stress-strain or forces-displacement relation is assumed to be elastic (reversible), so there will be no plastic deformation, and the redistribution of the internal force is not permitted during the life time of the structure, the other approach is the inelastic design approach, in which the stress-strain or forces-displacement relation will not be reversible, and a plastic deformation will take place, result in hysteresis loop and thus dissipation of energy, also redistribution of the internal forces are permitted, design building to remain elastic during strong and rare earthquake will require high strength and in turn high cost which may not be economically visible, so that elastic analysis is done only for very important facility like nuclear reactor which should remain elastic under different load condition, the less important facility like office buildings and other less important structures are usually designed according to inelastic design approach, which is more economy, but at the same time should be safe.

However, design building to behave inelastic during seismic excitation, mean that buildings will be designed with strength less than their elastic strength demand, so that building shall have additional properties such as ductility, energy dissipation capacity, and self centering capacity, and other properties so that these properties will compensate the reduction in the design strength.

In this study, ductility, energy dissipation capacity, self-centering capacity, force distribution in the structural member, and the distribution pattern of plastic hinges in the four modeled systems will be compared

A series of three-dimensional nonlinear inelastic time history analysis and three-dimensional nonlinear inelastic static analysis (Pushover analysis) was done using sap 2000 version 14.2.2 (the newest version), in effort to evaluate the actual behavior of the PRMRF, EBF, BRBF systems under seismic excitation compared to the seismic behavior of FRMRF.

1.1 Material nonlinearity in sap 2000

In this study, material nonlinearity is considered in sap 2000 program by using concentrated plastic hinge concept, in which plastic hinges are denoted by a zero-length spring at the end of the structural element, while the structural element between its ends remains elastic. Therefore, this method lump the effects of material non-linearity into the member end nodes. This assumption simplifies the actual behavior of the member, but allows for significant savings in computational time. The concentrated plasticity approach has proven to be satisfactory in producing a good approximation of the real behavior of beams and columns.

In sap 2000 hinges can be defined for each degree of freedom, by defined a force-displacement (moment-rotation) curve that gives the yield value and the plastic deformation following yield. This is done in terms of a curve with values at five points, A-B-C-D-E, as shown in Figure 3.1.

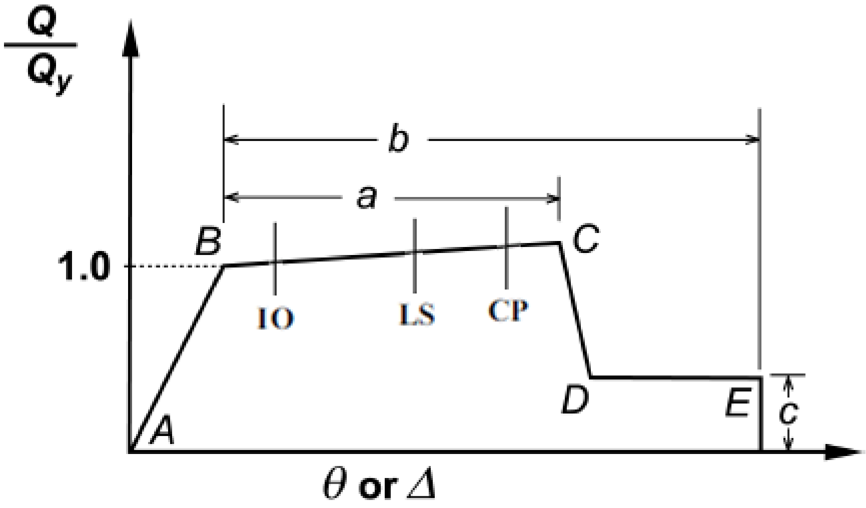


Fig 3.1: force-displacement (moment-rotation) curve used to define hinge in sap 2000 (Fema 356)

The curve is symmetric for positive and the negative direction. The values on the curve have the following meaning:

- Point A is always the origin.
- Point B represents yielding. No deformation occurs in the hinge up to point B, regard less of the deformation value specified for point B. The displacement (rotation) at point B will be subtracted from the deformations at points C, D, and E. Only the plastic deformation beyond point B will be exhibited by the hinge.
- Point C represents the ultimate capacity for the hinge.
- Point D represents a residual strength for the hinge.
- Point E represents total failure. Beyond point E the hinge will drop load down to point F (not shown) directly be low point E on the horizontal axis.

Parameters a, b, c, is defined in Tables 3.1 and table3.2 for different frame system members.

Table 3.1 Modeling Parameters for Nonlinear Hinge for Beams and Columns (Fema 356)

Component/action	Modeling Parameter			Acceptance Criteria		
	Plastic Rotation Angle, Radians		Residual Strength Ratio	Plastic Rotation Angle, Radian		
	a	b	c	IO	LS	CP
Beam-Flexure						
$\frac{b_f}{2t_f} \le \frac{52}{\sqrt{F_{ye}}}$ *and* $\frac{h}{t_w} \le \frac{418}{\sqrt{F_{ye}}}$	$9\theta_y$	$11\theta_y$	0.6	$1\theta_y$	$6\theta_y$	$8\theta_y$
$\frac{b_f}{2t_f} \ge \frac{65}{\sqrt{F_{ye}}}$ *or* $\frac{h}{t_w} \ge \frac{640}{\sqrt{F_{ye}}}$	$4\theta_y$	$6\theta_y$	0.2	$0.25\theta_y$	$2\theta_y$	$3\theta_y$
Column-Flexure						
For $P/P_{cl} < 0.2$						
$\frac{b_f}{2t_f} \le \frac{52}{\sqrt{F_{ye}}}$ *and* $\frac{h}{t_w} \le \frac{300}{\sqrt{F_{ye}}}$	$9\theta_y$	$11\theta_y$	0.6	$1\theta_y$	$6\theta_y$	$8\theta_y$
$\frac{b_f}{2t_f} \ge \frac{65}{\sqrt{F_{ye}}}$ *or* $\frac{h}{t_w} \ge \frac{460}{\sqrt{F_{ye}}}$	$4\theta_y$	$6\theta_y$	0.2	$0.25\theta_y$	$2\theta_y$	$3\theta_y$

Table 3.2 Modeling Parameters for Nonlinear Hinge for EBF link, semi rigid connection and bracing member (Fema 356)

EBF Link Beam						
a. $e \leq \frac{1.6M_P}{V_Y}$	0.15	0.17	0.8	0.005	0.11	0.14
b. $e \geq \frac{2.6M_P}{V_Y}$	Same as for beams					
c. $\frac{1.6M_P}{V_Y} < e < \frac{2.6M_P}{V_Y}$	Linear interpolation shall be used					
Bolted end plate						
Yield of end plate	0.042	0.042	0.8	0.01	0.028	0.035
Component/action	Modeling Parameter			Acceptance Criteria		
	Plastic deformation		Plastic Rotation Angle, Radian	Plastic deformation		
	a	b	c	IO	LS	CP
Braces in Tension	$11\Delta_T$	$14\Delta_T$	0.8	$0.25\Delta_T$	$7\Delta_T$	$9\Delta_T$
Braces in compression	$0.5\Delta_c$	$8\Delta_c$	0.2	$0.25\Delta_c$	$5\Delta_c$	$7\Delta_c$

1.1.1 Nonlinear hinges in beams and columns:

Hinges in beams and columns are defined according to the limit in table 3.1 above, θ_y is the rotation at yield, which defined in equation 3.1 and 3.2 for beams and columns respectively (Fema 356):

$$\theta_y = \frac{Zf_{ye}l_b}{6EI_b} \text{ …….. (3.1)}$$

$$\theta_y = \frac{Zf_{ye}l_c}{6EI_c}\left(1 - \frac{P}{P_{ye}}\right) \text{…….. (3.2)}$$

Where

Z: Plastic section modulus

f_{ye}: expected yield strength of the material

l_b: beam length

l_c: column length

I: moment of inertia

E: modulus of elasticity

P_{ye}: expected axial yield force of the member = $A_g * f_{ye}$

The slope of (bc) region is taken as 3%, also the yielding moment (M_p) is equal to $Z * f_{ye}$

1.1.2 Nonlinear hinges for Shear link element:

Three cases are defined the nonlinear behavior for the shear link member depending on the length of the link (e) the first case is when $e \le \frac{1.6M_P}{V_y}$, in which the link will yield in shear, or $e \ge \frac{2.6M_P}{V_y}$, in which the link will yield in flexure, or a combination of shear and flexure when the length of the link is lies between these two limits, link shear

behavior is recommended than the other two behavior, however, plastic moment (M_P) and yield shear force (V_y) is computed according to equations 3.3 and 3.4 respectively

$$M_p = Z * f_{ye} ......(3.3)$$

$$V_y = 0.6 * f_{ye} * A_w ......(3.4)$$

Where

A_w is: the area of the web.

f_{ye}: expected yield strength of the material

1.1.3 Nonlinear hinges for BRBF bracing member:

As mentioned before BRBF bracing member consist of two major components: the steel core resists axial stresses and the outer concrete filled steel casing resists buckling stresses, and the casing restrains the steel core from buckling thereby developing almost uniform axial strains in tension and compression, therefore the nonlinear hinges for these bracing members are modeled by symmetric curve (fig 3.1) in tension and compression with (a, b, c) value as in table 3.2 (tension bracing), connection between the bracing member and beams assumed to be hinge so that nonlinear hinges are defined only for the axial load at the end of BRBF bracing members.

1.1.4 Nonlinear hinges for EBF bracing members:

Connection of EBF bracing to the beam is assumed to be rigid in this study, which is suggested by AISC 2005, seismic provision, and improved to accurately simulate the actual behavior of beam-bracing connection by many researcher like in (extended-link), therefore, two type of nonlinear hinges is defined at each end of the bracing, the first one is present the axial deformation of the bracing, in which the curve will not be symmetric like in BRBF bracing since compression buckling is allowed, so the positive side of the link will be in tension with deformation value as in table 3.2 above for

tension bracing and the negative side will be in compression with deformation value as in table 3.2 compression bracing.

The hinge type is present the flexural deformation of the bracing, these hinges is defined as for beams.

1.1.5 Nonlinear modeling of semi rigid connection:

A thin plate extended end plate connection is used in this study, end plate of this connection is thin enough to have yielding of the plate, this connection may provide good ductility and inelastic deformation capacity, also these connections do not develop the full plastic capacity of the beam, so they will act like fuses in the building.

According to Fema 355d these connections can develop less than 80% of the full plastic capacity of the beam, in this study the moment capacity of these connection (M_{pc}) are assumed to be 70% of moment capacity of the beam (($M_{Pb} = Z_b * f_{ye}$)), the rotational spring stiffness (K_θ) is equal the connection moment capacity (M_{pc}) divided by constant factor as shown in equation 3.5 below:

$(K_\theta = M_{pc}/0.003)$…… (3.5)

the rotational spring stiffness is equal to the connection moment capacity divided by 0.003, this formula is suggested by fema 356 based on many experimental result, also this formula give acceptable result when compared to the experimental value of the connection spring stiffness that is obtained by (Abolmaali, et al. 2009) . Plastic rotation (θ_p) and maximum rotation for supporting gravity load (θ_g) (which are defined as the value of a and b in fig 3.1 respectively), are as defined in table 3.2 which have a constant value of 0.042 radians.

1.2 Nonlinear inelastic time history analysis:

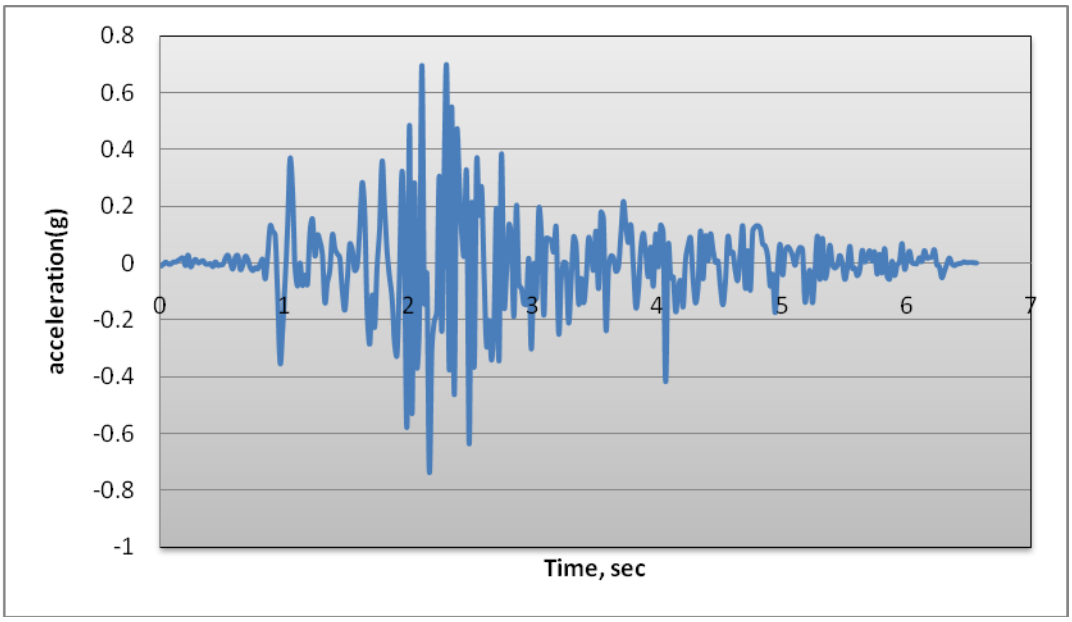
In this method two time history loads were used in the analysis the first load is an earthquake record, and the second time history load is a cyclic load.

1.2.1 Earthquake records:

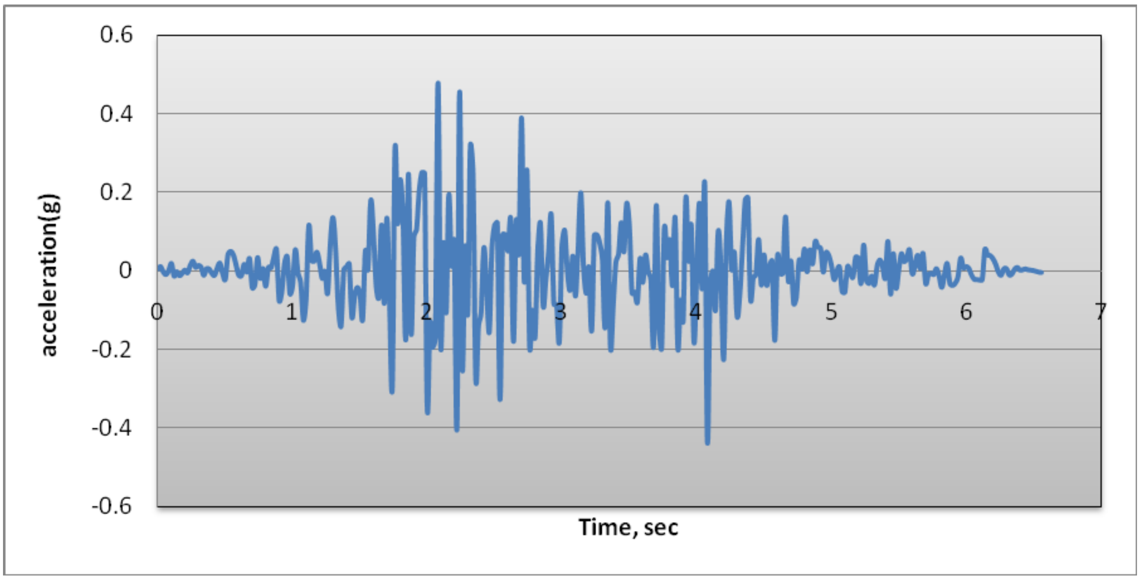
Analysis with actual earthquake records is carried out to simulate the nonlinear inelastic behavior of the PRMRF, EBF, BRBF, frame systems, compared to that of the FRMRF, the properties that obtained from this analysis are demand ductility, self centering capacity, member forces, and plastic hinge formation pattern.

One earthquake records which is Tabas earthquake is used in this study to present a comprehensive evaluation of the proposed modeled buildings; this record is obtained from the Pacific Earthquake Engineering Research (PEER) center database. In which it provides the actual acceleration values recorded during an earthquake. Thus, it allows the evaluation of buildings' relevant performance.

However, this earthquake has an epicenter in tabas, Iran. It occurred on September 16, 1978, this earthquake is chosen because it was huge earthquake with a magnitude of 7.35 on the Richter scale, and with peak ground acceleration (PGA) of 0.8128g, forty villages within a 30 miles (48 km) radius were damaged, with the worst damage was to the Tabas town, which was at the epicenter of the quake and completely flattened, this earthquake last about (33) second making it extremely dangerous compared to the normal earthquake duration of 10 – 20 seconds. However, fig3.2a and fig3.2b present the horizontal and vertical acceleration time history of tabas earthquake respectively in term of gravitational acceleration, g.

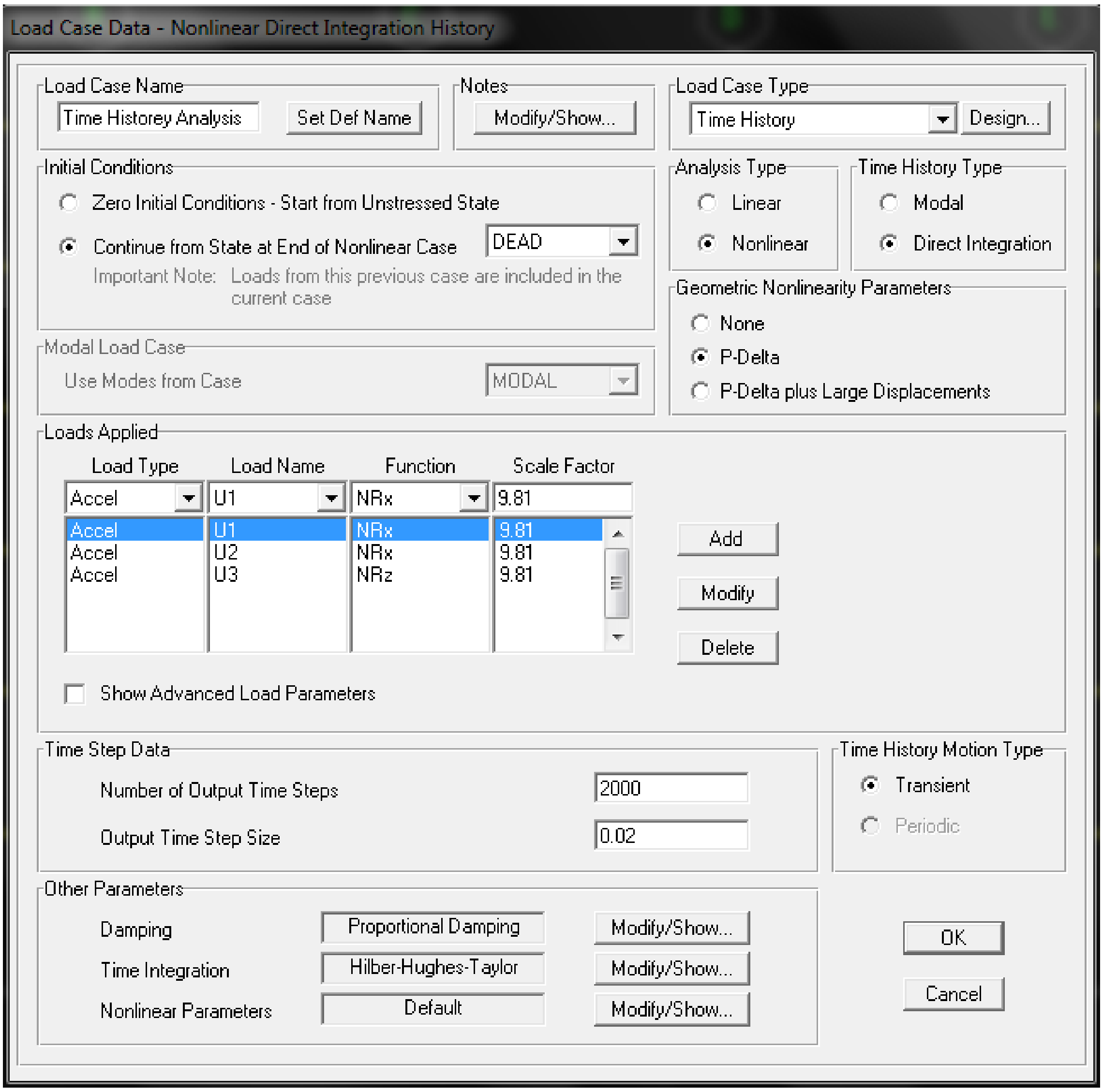


a)



b)

Fig 3.2 a) Tabas horizontal acceleration time history analysis b) Tabas vertical acceleration time history analysis



— **Fig 3.3 Non-linear time history analysis case using tabas earthquake as defined in sap 200**

1.2.2 Cyclic load:

The second time history load is a cyclic load, cyclic sine function load is applied for the six storey buildings, while cyclic cosine function load was applied to the twenty storey building, this load is applied to get hysteretic behaviour and the energy dissipation capacity for the different modelled system, both sine and cosine functions have 5 cycle with amplitude of 5 and duration of 1 second fig 3.4 and 3.5 show the defined sine and cosine functions respectively in sap 2000 that used in the analysis.

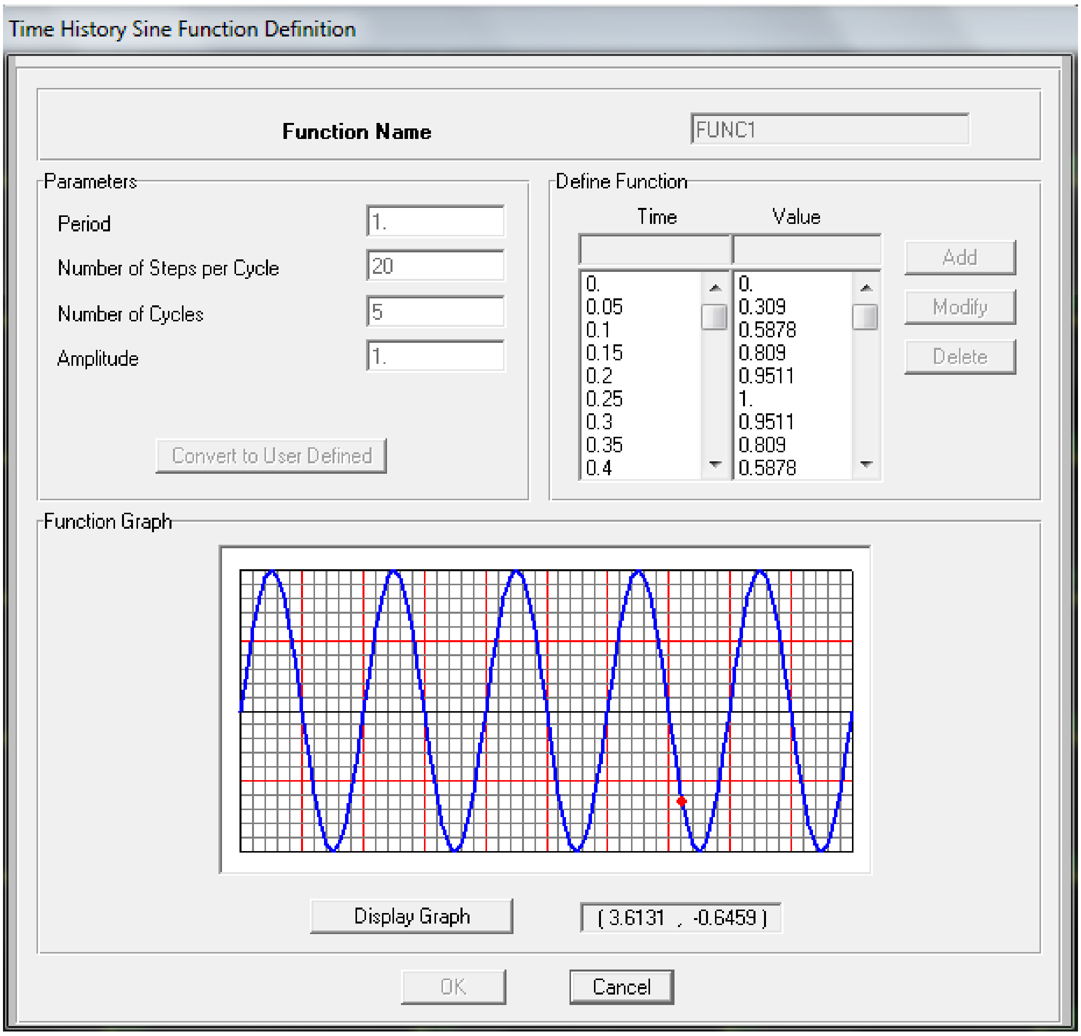
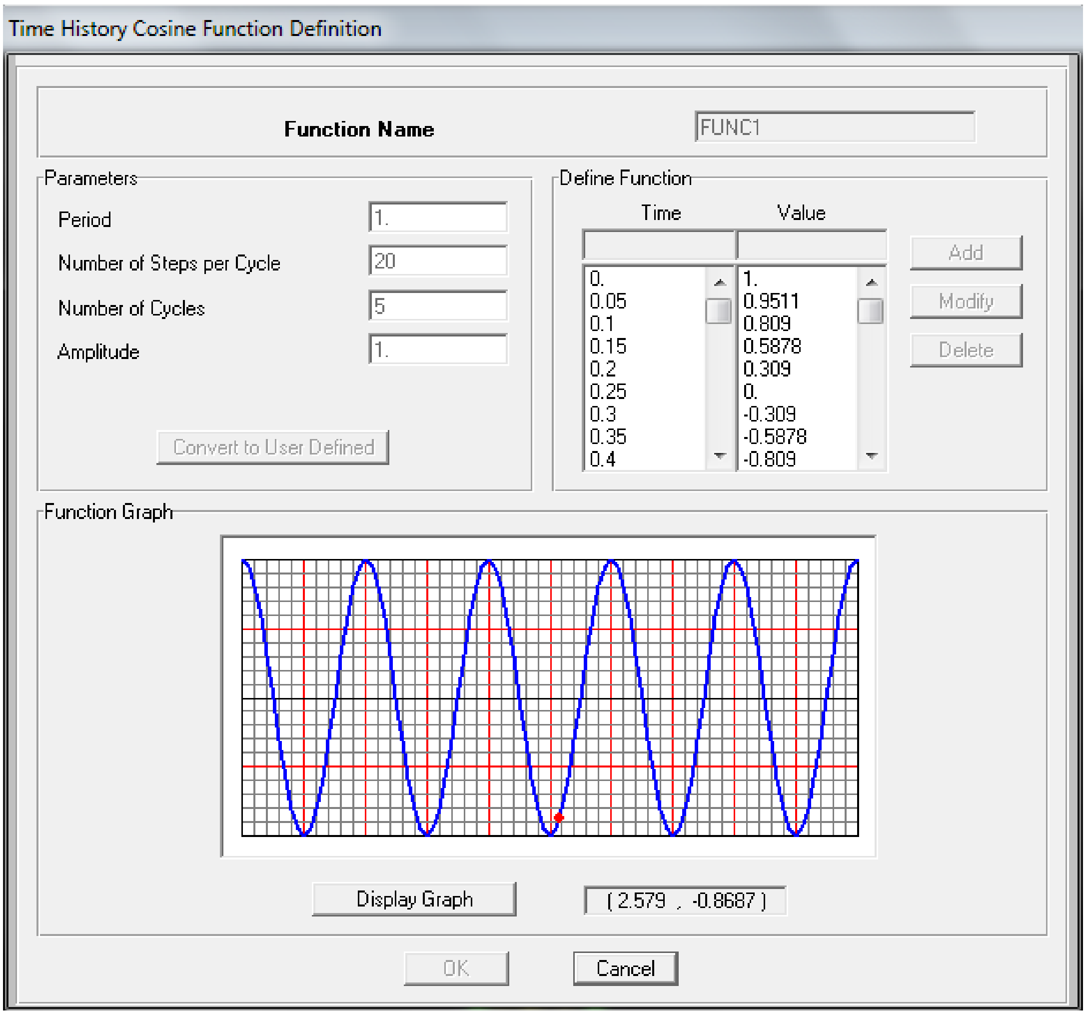
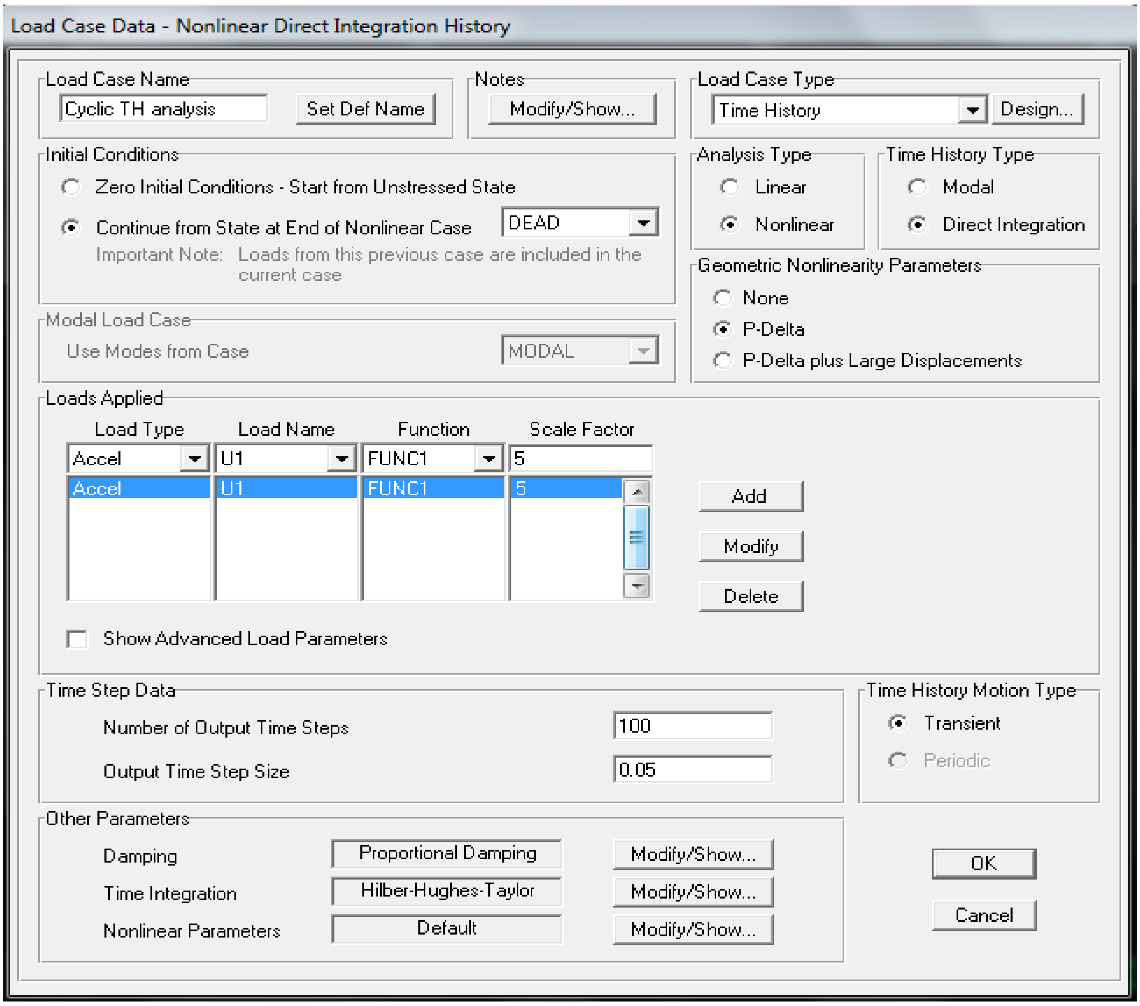


Fig 3.4 sine function as defined in sap 2000 used for cyclic analysis for 6-storey systems



b)

Fig 3.5 cosine function as defined in sap 2000 used for cyclic analysis for 20-storey systems.



— **fig 3.6 Non-linear time history analysis case using cyclic function as defined in sap 2000**

Newmark constant acceleration method (which is discussed in chapter 2) is used for dynamic analysis, geometrical and material nonlinearity was included in the analysis by accounting for P-delta effect and material yielding, concentrated plastic hinge approach used to simulate material nonlinearity as discussed before, also its worth to mention that a nonlinear analysis under the dead load with p-delta effect was carry out first, so that the building stiffness at the end of this case was used as the start stiffness for the nonlinear time history analysis, so that this will simulate the actual behavior of the structure.

1.3 Pushover analysis:

The pushover analysis of a structure is a static non-linear analysis under permanent vertical loads and gradually increasing lateral loads. The equivalent static lateral loads approximately represent earthquake induced forces. A plot of the total base shear versus top displacement in a structure is obtained by this analysis that would indicate any premature failure or weakness. The analysis is carried out up to failure, thus it enables determination of collapse load and ductility capacity.

The purpose of pushover analysis is to evaluate the expected performance of structural systems by estimating performance of a structural system by estimating its strength and deformation demands in design earthquakes by means of static inelastic analysis, and comparing these demands to available capacities at the performance levels of interest. The inelastic static pushover analysis can be viewed as a method for predicting seismic force and deformation demands, which accounts in an approximate manner for the redistribution of internal forces that no longer can be resisted within the elastic range of structural behavior.

In this study a series of nonlinear pushover analysis was done to get the capacity of each modeled building, while seismic demand was taken from nonlinear time history analysis as mentioned in the previous section, cyclic displacement-controlled analysis is used in which the modeled buildings were pushed to a relatively high displacement, in effort to get the capacity displacement of the building (which is defined as the displacement at the top of the building at failure), geometric and material nonlinearity was included in the analysis as mentioned in the previous section, also building stiffness is the stiffness at the end of nonlinear static analysis under dead load as discussed before.

It should be mentioned that pushover analysis is approximate in nature and is based on static loading; as such it cannot represent dynamic phenomena with a large degree of

accuracy. It may not detect some important deformation modes that occur in a structure subjected to severe earthquakes, and it may significantly from predictions based on invariant or adaptive static load patterns, particularly if higher mode effects become important, because of this pushover analysis is used in this study to obtain the capacity of the modeled structures only, and nonlinear time history analysis is used to obtain the demand of the modeled building under earthquake excitation.

CHAPTER 4

Modeling details

4.1 Brief Description of the buildings

Six and twenty story steel office buildings designed by (Chun, et al. 2010) are chosen for this research, the two buildings have the same floor plan (5 * 3 bays) with 9-m bay spacing, whereas the height is 4.5 m at the first story and 4.0 m at the remaining floors. Each building has four different lateral load-resisting systems, including FRMRF, PRMRF, EBF and BRBF systems.

Tables 4.1 and 4.2 summarize the member sizes and steel grades for the example buildings. As can be seen, the buildings used built up box columns and H-shaped beams and braces. The columns and braces were made of A572 Grade 50 steel, and the beams, EBF links were made of A36 steel.

Load and Resistance Factored Design (LRFD) was adopted for moment frames, and a capacity design was used in braced frames, Beams, columns and bracing member were modeled by three dimensional frame elements with six (6) degree of freedom at each node. Floor diaphragms and the roof were assumed to be rigid in their own planes.

Dead and live loads that act on the roof and on the other floors diaphragms are calculated in table 4.3, where the dead load include the self weight and ceiling, mechanical, and partition load in the floor system, while the live load is computed according to UBC code, these loads are then distributed to the beams by using tributary area concept, the own weight of each beam is calculated by the program. Also since the concrete floor slabs were not directly modeled in the FE model, the composite action between concrete slabs and steel beams was considered by increasing the modulus of elasticity of the floor beams by 12.5%.

Table 4.1 member size and steel grades for 6-storey buildings

(1) 6-storey FRMRF and PRMRF			
Storey	Column (A572)	Girder_X (A36)	Girder_Z (A36)
1F-2F	Box 500*500*25	H588*300*12*22	H582*301*12*17
3F-4F	Box 500*500*22	H494*302*13*22	H500*304*15*24
5F-6F	Box 500*500*19	H488*300*11*16	H386*299*9*14
(2) 6-storey EBF			
Storey	Column (A572)	Girder_X (A36)	Girder_Z (A36)
1F-2F	Box 450*450*25	H582*300*12*17	H582*300*12*17
3F-4F	Box 450*450*22	H488*300*11*18	H482*300*11*15
5F-6F	Box 450*450*19	H488*300*11*18	H482*300*11*15
Storey	Link_X (A36)		Link_Z (A36)
1F-2F	H582*300*12*17		H582*300*12*17
3F-4F	H488*300*11*18		H482*300*11*15
5F-6F	H488*300*11*18		H482*300*11*15
Storey	Brace_X (A572)		Brace_Z (A572)
1F-2F	H440*300*11*18		H440*300*11*18
3F-4F	H300*300*10*15		H300*300*10*15
5F-6F	H300*300*10*15		H300*300*10*15
(3) 6-storey BRBF			
Storey	Column (A572)	Girder_X (A36)	Girder_Z (A36)
1F-2F	Box 450*450*25	H582*300*12*17	H582*300*12*17
3F-4F	Box 450*450*22	H488*300*11*18	H440*300*11*18
5F-6F	Box 450*450*19	H488*300*11*18	H386*299*9*14
Storey	BRB_X		BRB_Y
1F	Ac=60m2		Ac=35m2
2F	Ac=50m2		Ac=35m2
3F	Ac=50m2		Ac=55m2
4F	Ac=50m2		Ac=55m2
5F	Ac=25m2		Ac=55m2
6F	Ac=25m2		Ac=70m2

Table 4.2 member size and steel grades for 20-storey buildings

(1) 20-storey FRMRF and PRMRF			
Storey	Column (A572)	Girder_X (A36)	Girder_Z (A36)
1F-3F	Box 750*750*32	H800*300*15*26	H800*300*15*26
4F-6F	Box 750*750*28	H800*300*15*26	H800*300*15*26
7F-9F	Box 750*750*25	H708*302*15*28	H712*306*19*30
10F-12F	Box 700*700*28	H708*302*15*28	H708*302*15*28
13F-15F	Box 700*700*25	H700*300*13*24	H700*300*13*24
16F-18F	Box 600*600*28	H594*302*14*23	H594*302*14*23
19F-20F	Box 500*500*19	H588*300*12*22	H582*300*12*17
(2) 20-storey EBF			
Storey	Column (A572)	Girder_X (A36)	Girder_Z (A36)
1F-3F	Box 650*650*32	H792*302*14*22	H700*300*15*24
4F-6F	Box 650*650*28	H792*302*13*22	H700*300*15*24
7F-9F	Box 650*650*25	H708*302*15*28	H700*300*15*24
10F-12F	Box 550*550*28	H708*302*15*28	H700*300*15*24
13F-15F	Box 550*550*25	H700*300*13*24	H692*300*13*20
16F-18F	Box 550*550*28	H594*302*14*23	H582*300*12*17
19F-20F	Box 500*500*19	H588*300*12*22	H482*300*11*15
Storey	Link_X (A36)	Link_Z (A36)	
1F-3F	H792*302*14*22	H700*300*15*24	
4F-6F	H792*302*13*22	H700*300*15*24	
7F-9F	H708*302*15*28	H700*300*15*24	
10F-12F	H708*302*15*28	H700*300*15*24	
13F-15F	H700*300*13*24	H692*300*13*20	
16F-18F	H594*302*14*23	H582*300*12*17	
19F-20F	H588*300*12*22	H482*300*11*15	
Storey	Brace_X (A572)	Brace_Z (A572)	
1F-3F	H588*300*12*20	H488*300*11*18	
4F-15F	H488*300*11*18	H488*300*11*18	
16F-18F	H440*300*11*18	H440*300*11*18	
19F-20F	H440*300*11*18	H300*300*10*15	
(3) 6-storey BRBF			
Storey	Column (A572)	Girder_X (A36)	Girder_Z (A36)
1F-3F	Box 700*700*32	H792*300*14*22	H700*300*13*24
4F-6F	Box 650*650*25	H792*300*14*22	H700*300*13*24
7F-9F	Box 650*650*222	H708*302*15*28	H700*300*13*24
10F-12F	Box 550*550*25	H708*302*15*28	H700*300*13*24
13F-15F	Box 550*550*22	H700*300*13*24	H692*300*13*20
16F-18F	Box 550*550*19	H594*302*14*23	H582*300*12*17
19F-20F	Box 500*500*19	H588*300*12*20	H482*300*11*15
Storey	BRB_X	BRB_Y	
1F-3F	Ac=60m2	Ac=75m2	
4F-6F	Ac=55m2	Ac=70m2	
7F-9F	Ac=50m2	Ac=60m2	
10F-12F	Ac=45m2	Ac=55m2	
13F-15F	Ac=35m2	Ac=45m2	
16F-18F	Ac=25m2	Ac=30m2	
19F-20F	Ac=15m2	Ac=20m2	

Table 4.3 dead and live load on the slab for both 6 and 20- storey buildings

Roof Diaphragm Load	
Dead load (KN/m^2)	2.825
Live load (KN/m^2)	1.0
Floors Diaphragm Load	
Dead load (KN/m^2)	3.45
Live load (KN/m^2)	2.4

4.2 FRMRF system:

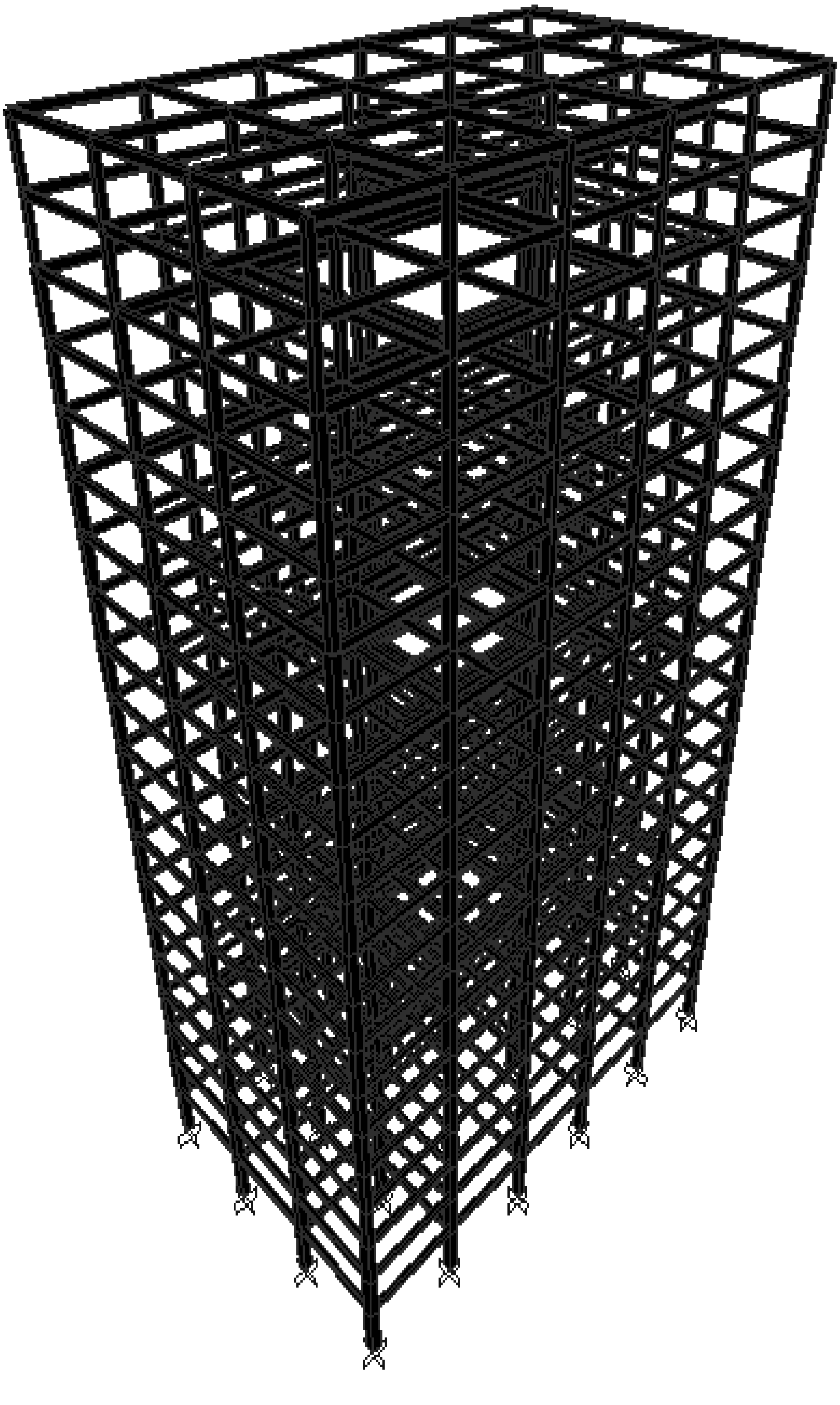
the members size are as defined in table 4.1 for six storey building and 4.2 for twenty storey building, beams and columns are assumed to yield in flexure only, therefore nonlinear flexural plastic hinges were defined at the both end of each members which are defined according to table 3.1, the value of the hinge rotation, the acceptance criteria, and strain hardening ratio for each storey for FRMRF beams and columns in both directions for 20-storey and 6-storey buildings are as shown in table 4.5 and table 4.5 respectively, also fig 4.1 and fig 4.2 show 3-D view, side and plane view for 20 and 6-storey buildings respectively, fig 4.3 and fig 4.4 show the two type of plastic flexural hinge that defined in sap 2000 for both 6 and 20-storey building.

Table 4.4 values of hinge rotation, acceptance criteria, and strain hardening ratio for 20-storey FRMRF members

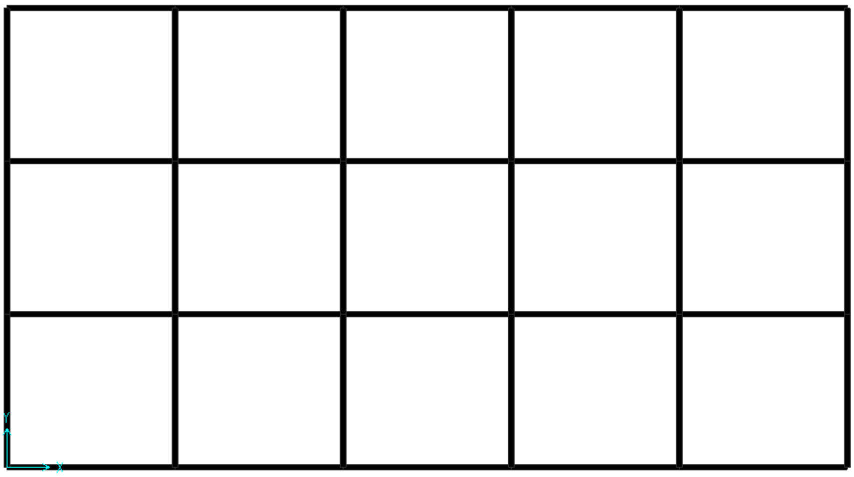
Storey	Modeling Parameter			Acceptance Criteria			Strain hardening ratio
	Plastic Rotation Angle, Radians		Residual Strength Ratio	Plastic Rotation Angle, Radian			
	a	b	c	IO	LS	CP	
Beam-Flexure							
All beams	$9\theta_y$	$11\theta_y$	0.6	$1\theta_y$	$6\theta_y$	$8\theta_y$	1.27
Columns-Flexure							
All columns	$4\theta_y$	$6\theta_y$	0.2	$0.25\theta_y$	$2\theta_y$	$3\theta_y$	1.12

Table 4.5 values of hinge rotation, acceptance criteria, and strain hardening ratio for 6-storey FRMRF members

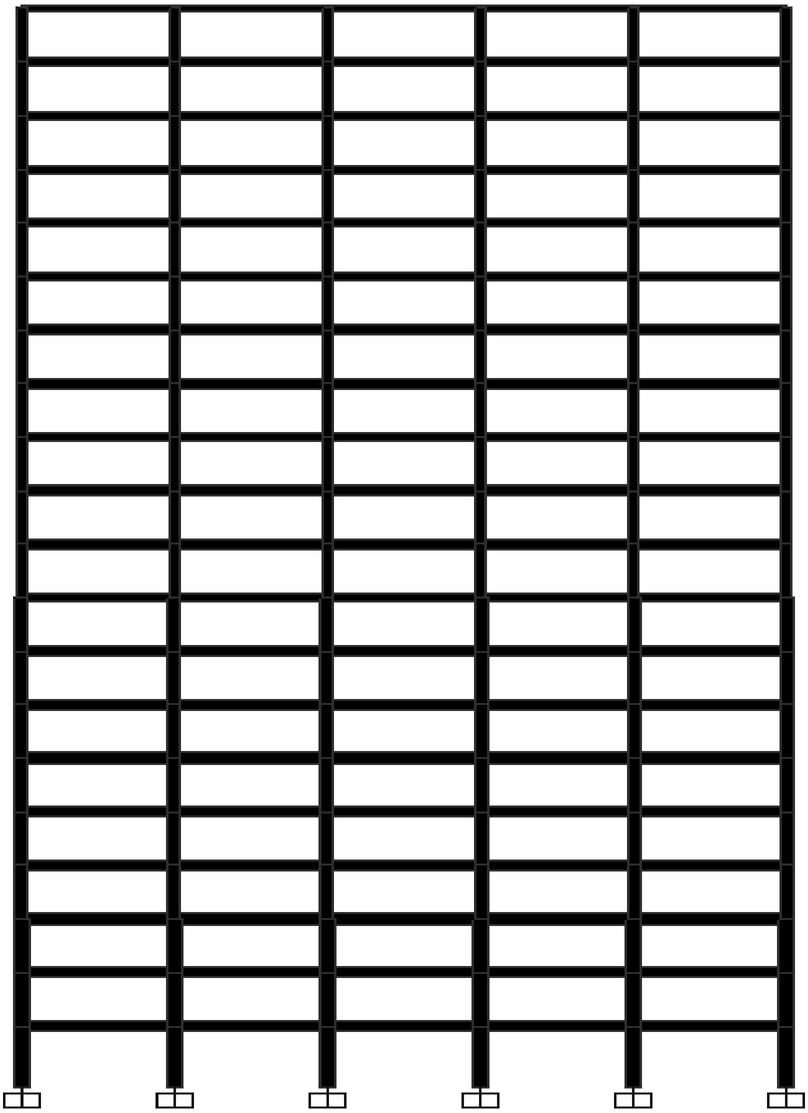
Storey	Modeling Parameter			Acceptance Criteria			Strain hardening ratio
	Plastic Rotation Angle, Radians		Residual Strength Ratio	Plastic Rotation Angle, Radian			
	a	b	c	IO	LS	CP	
Beam-Flexure							
1-2x	$9\theta_y$	$11\theta_y$	0.6	$1\theta_y$	$6\theta_y$	$8\theta_y$	1.27
1-2y	$4\theta_y$	$6\theta_y$	0.2	$0.25\theta_y$	$2\theta_y$	$3\theta_y$	1.12
3-4x	$9\theta_y$	$11\theta_y$	0.6	$1\theta_y$	$6\theta_y$	$8\theta_y$	1.27
3-4y	$9\theta_y$	$11\theta_y$	0.6	$1\theta_y$	$6\theta_y$	$8\theta_y$	1.27
5-6x	$4\theta_y$	$6\theta_y$	0.2	$0.25\theta_y$	$2\theta_y$	$3\theta_y$	1.12
5-6y	$4\theta_y$	$6\theta_y$	0.2	$0.25\theta_y$	$2\theta_y$	$3\theta_y$	1.12
Columns-Flexure							
All columns	$4\theta_y$	$6\theta_y$	0.2	$0.25\theta_y$	$2\theta_y$	$3\theta_y$	1.12



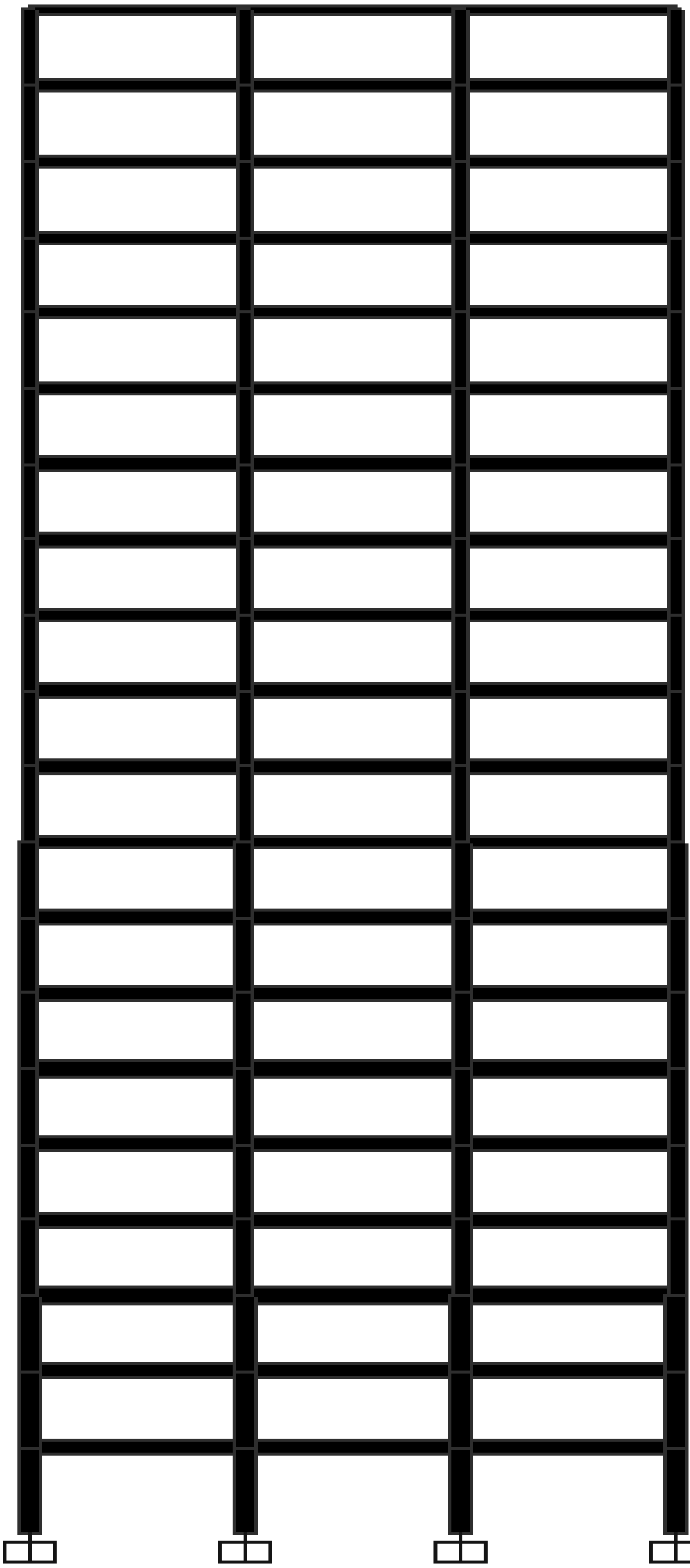
a)



b)

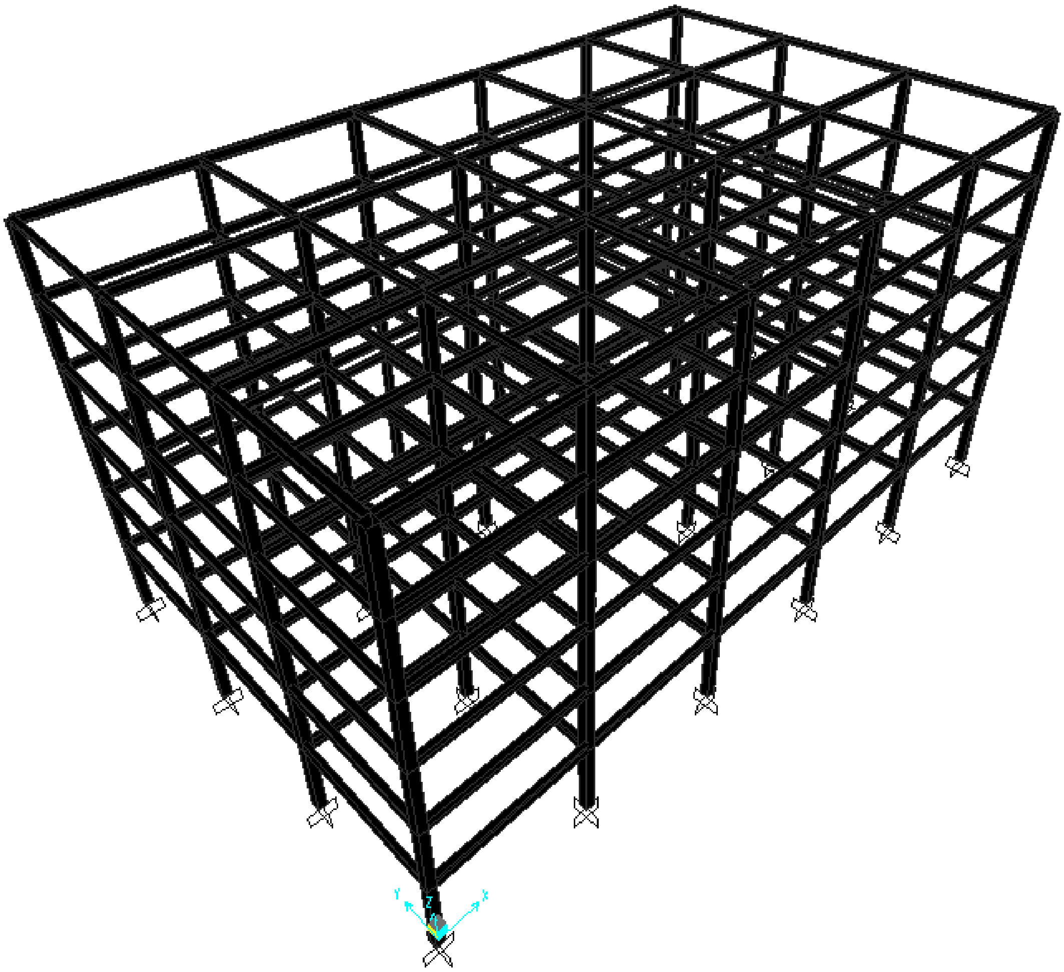


c)

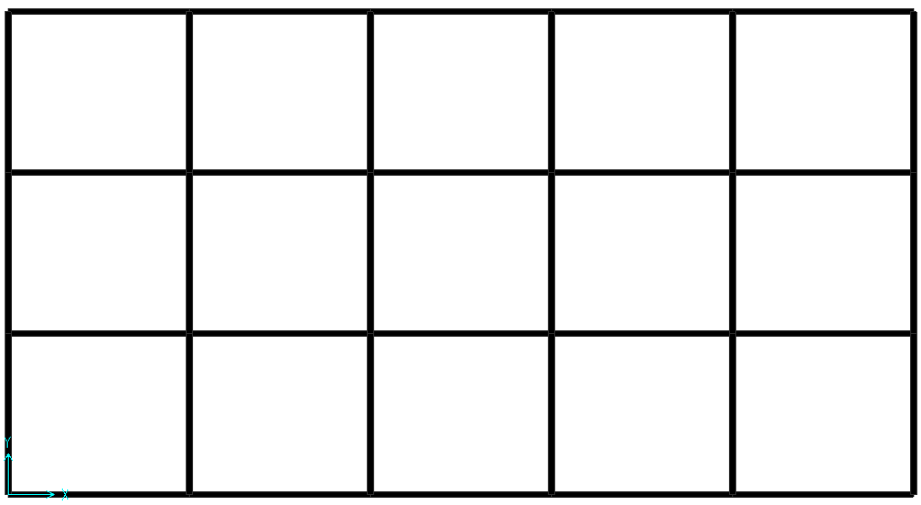


d)

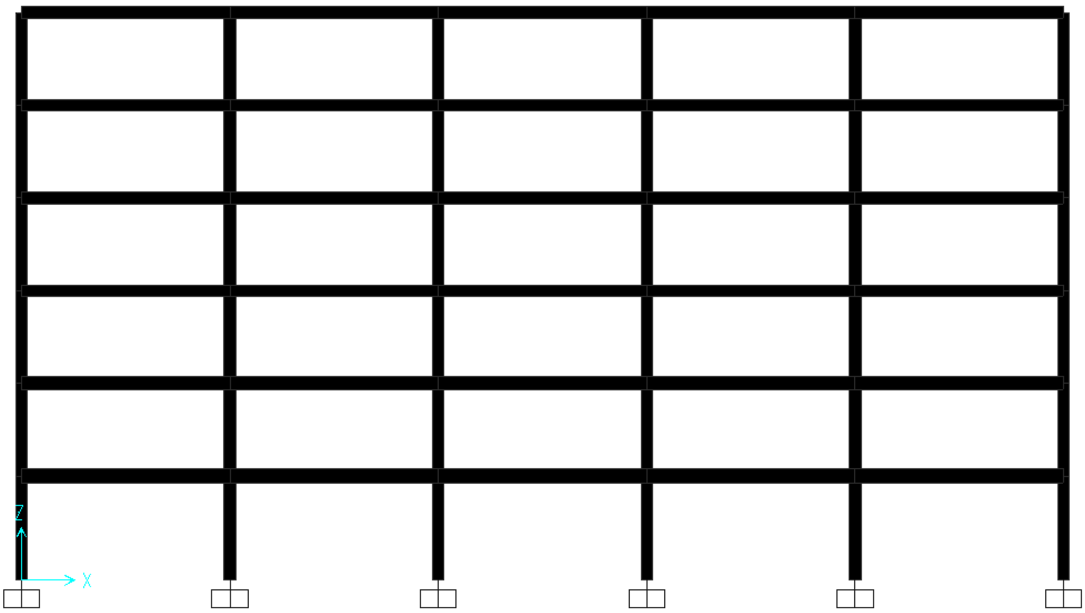
Fig 4.1 building view a) 3D view b) top view c) side view for frame in x-direction d) side view for frame in y-direction



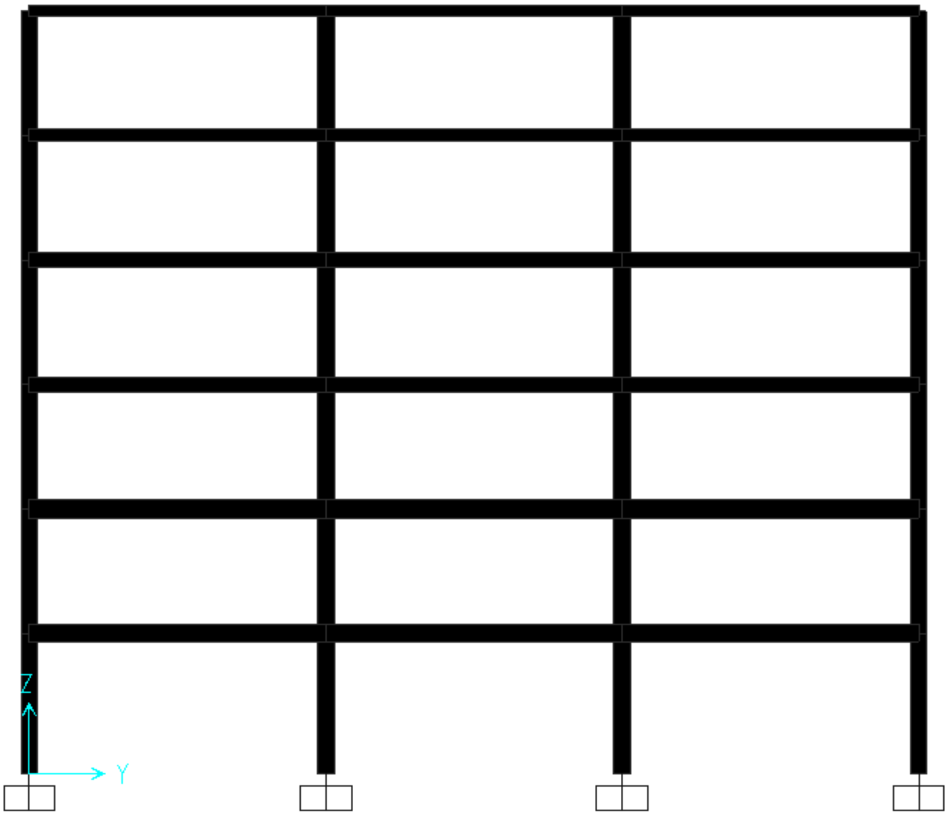
a)



b)

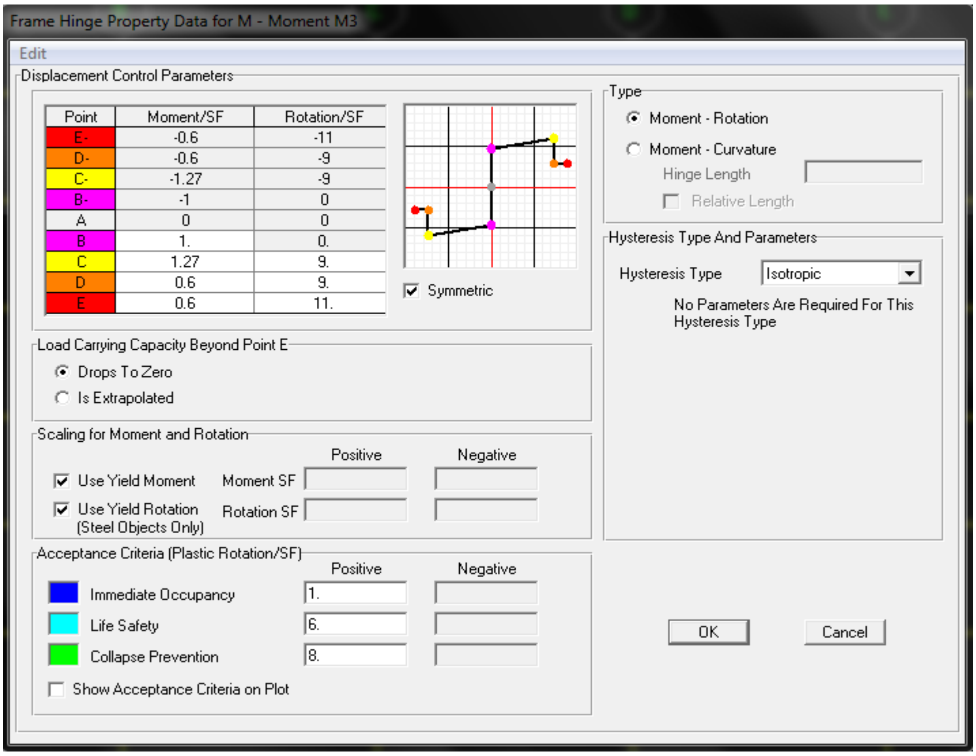


c)

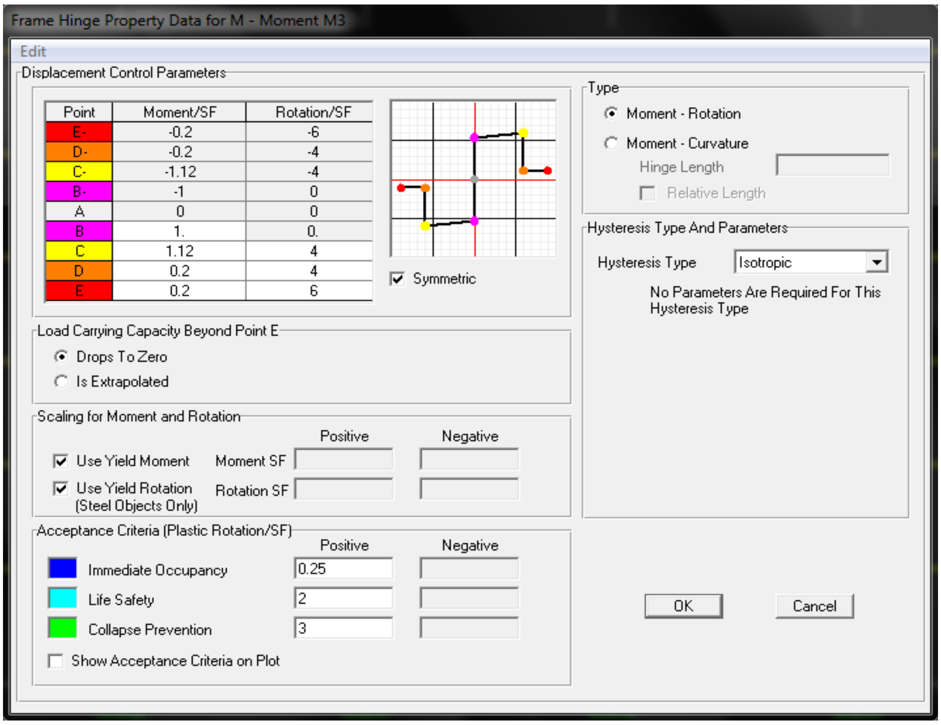


d)

Fig 4.2 building view a) 3D view b) top view c) side view for frame in x-direction d) side view for frame in y-direction



a)



b)

Fig 4.3 flexural hinge defined in sap 2000 for both 6 and 20 storey buildings

4.3 PRMRF system:

This system has the same members size as for FRMRF system, also as in FRMRF system the beams and columns assume to yield in flexure only, and the flexural plastic hinge for beams and columns are as defined in table 4.3 for 20-storey building and in table 4.4 for 6-storey building , a thin plate extended end plate is used in this study to present the effect of semi-rigid connections on the behavior of steel buildings, as mentioned before the plate of this connection is thin enough to have yielding of the plate, this connection may provide good ductility and inelastic deformation capacity, also these connections do not develop the full plastic capacity of the beam, so they will act like fuses in the building. According to Fema 355d these connections can develop less than 80% of the full plastic capacity of the beam, therefore the moment capacity of these connection are assumed to be 70% of moment capacity of the beam, this ratio is suggested by Fema 355d for T-Stub connection, which its behavior is very close to thin plate extended end plate connection, and also this ratio is used by [long span].

In this study the nonlinear behavior of semi-rigid connection is modeled in sap 2000 using two steps as follow:

1. The first step is to assign connection rotational spring stiffness at the end of the beam where the semi-rigid connection will be placed, this stiffness will be used to simulate the linear behavior of the semi-rigid connection. The rotational spring stiffness can be assigned to the beam in sap 2000 by using partial fixity command.
2. The second step to model semi rigid connection in sap 2000 is to define plastic hinge at the end of the beam where the semi-rigid connection will be placed, this hinge will represent the nonlinear behavior of the extended end plate connection. These hinges are defined according to sec 3.1.5 with constant rotation equal to 0.042 radians and with moment capacity of 70% of the moment capacity of the beam.

Spring rotational stiffness and Moment capacity values are shown in table 4.6 and table 4.7 for 6 and 20-storey buildings respectively, also fig 4.4 and fig 4.5 show hinge definition for extended end plate connection in sap 2000 program for 6SR1-2x and 20SR1-6x.

Table 4.6: rotational spring stiffness and plastic moment values for six storey PRMRF systems

Storey	Spring rotational Stiffness (K_θ) (KN.m/radian)	Moment (KN.m)
1-2x	401619	1205
1-2y	329427	989
3-4x	329600	989
3-4y	368259	1105
5-6x	246462	740
5-6y	160370	482

Table 4.7: rotational spring stiffness and moment capacity value for twenty storey PRMRF systems

Storey	Spring rotational Stiffness (K_θ) (KN.m/radian)	Moment (KN.m)
1-3x	706720	2120
1-3y	706720	2120
4-6x	706720	2120
4-6y	706720	2120
7-9x	638002	1914
7-9y	719316	2158
10-12x	638002	1914
10-12y	638002	1914
13-15x	542875	1629
13-15y	542875	1629
16-18x	435847	1308
16-18y	435847	1308
19-20x	401618	1205
19-20y	396493	1189

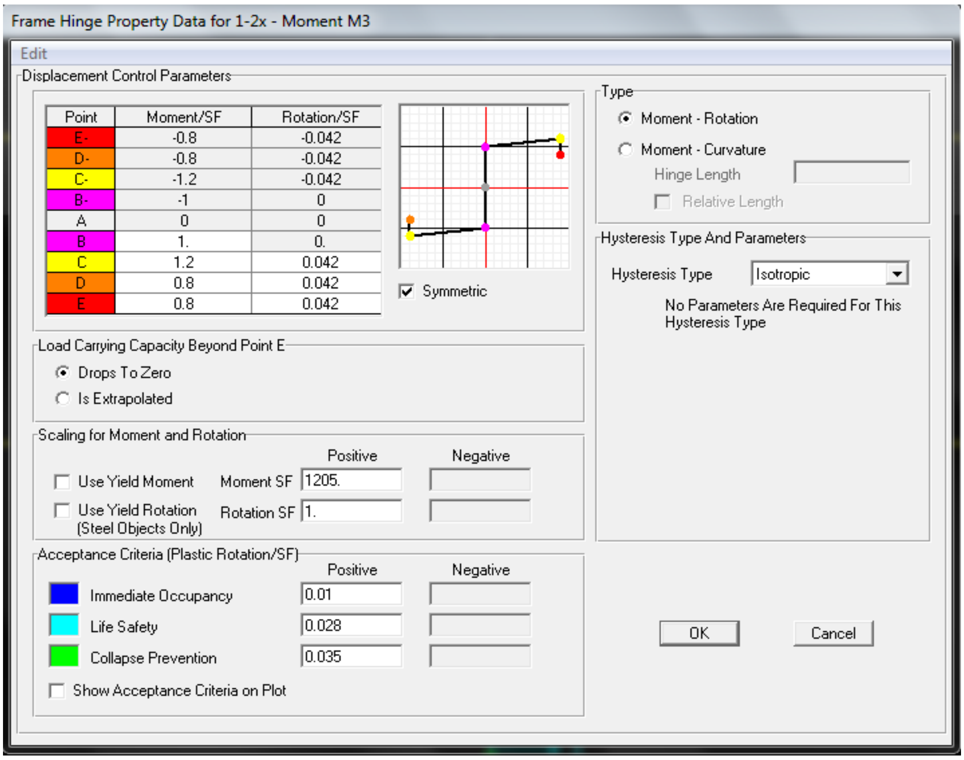


Fig 4.4 hinge definitions in sap 2000 for extended end plate connection for storey 12 in 6SR1-2x case

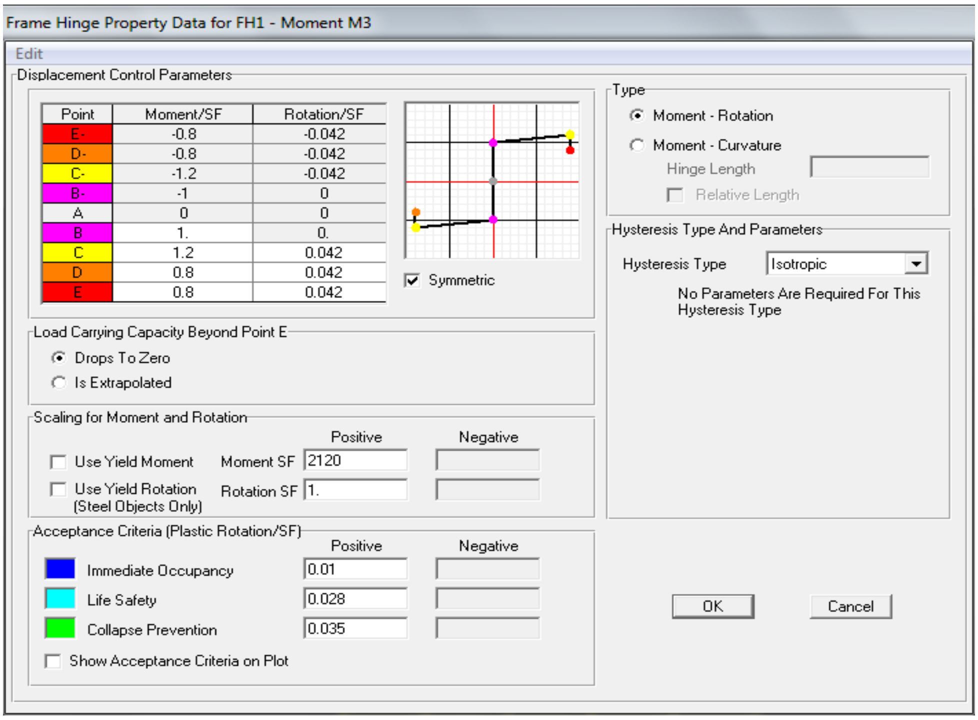


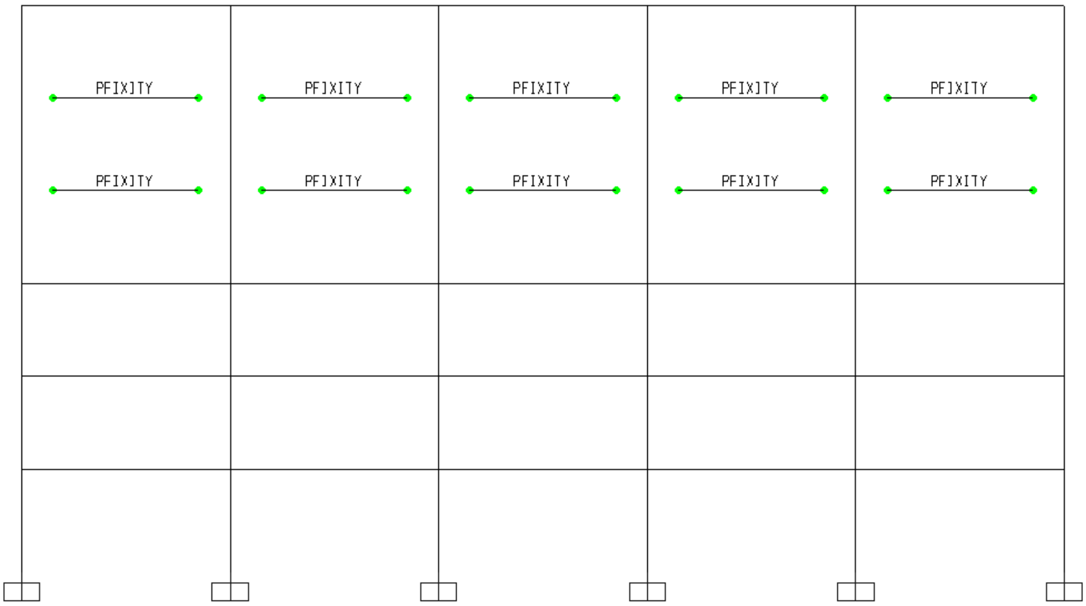
Fig 4.5 hinge definitions in sap 2000 for extended end plate for storey 1-3 in 6SR1-6x case

4.1.1 six storey PRMRF system:

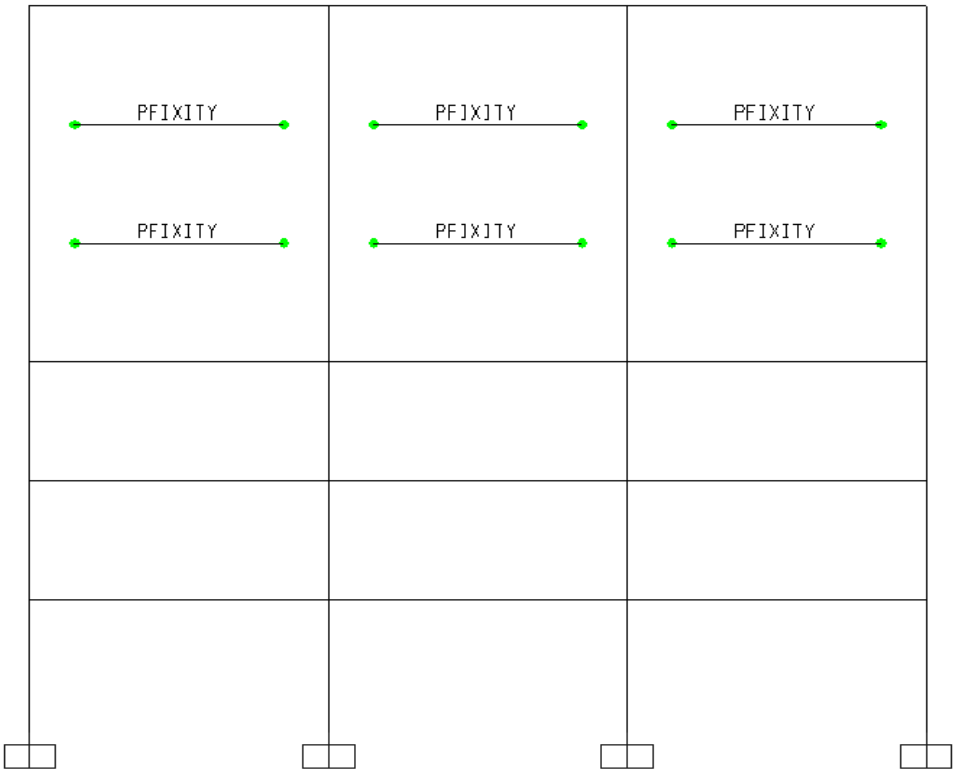
Total fourteen hybrids building with different combinations of rigid and semi-rigid connection were modeled in sap 2000, in effort to optimize the seismic performance of steel building by finding a pattern in replacing rigid connection with semi-rigid connection. The adopted building designation for these 14 combinations is

6SR storey numbers in which extended end plate is placed in direction of frame

For example (6SR 12 x) mean that semi-rigid connection is placed in the first and second storey for the frame in the x-direction). These fourteen models and their corresponding notation are presented in fig 4.6 through fig 4.19 for 6-storey PRMRF system.

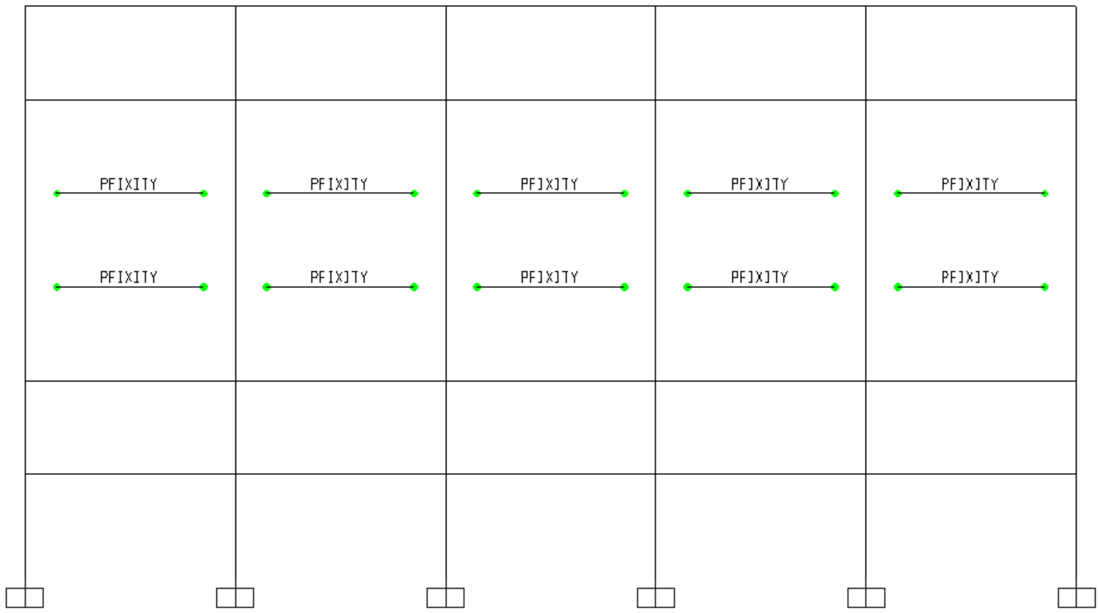


a)

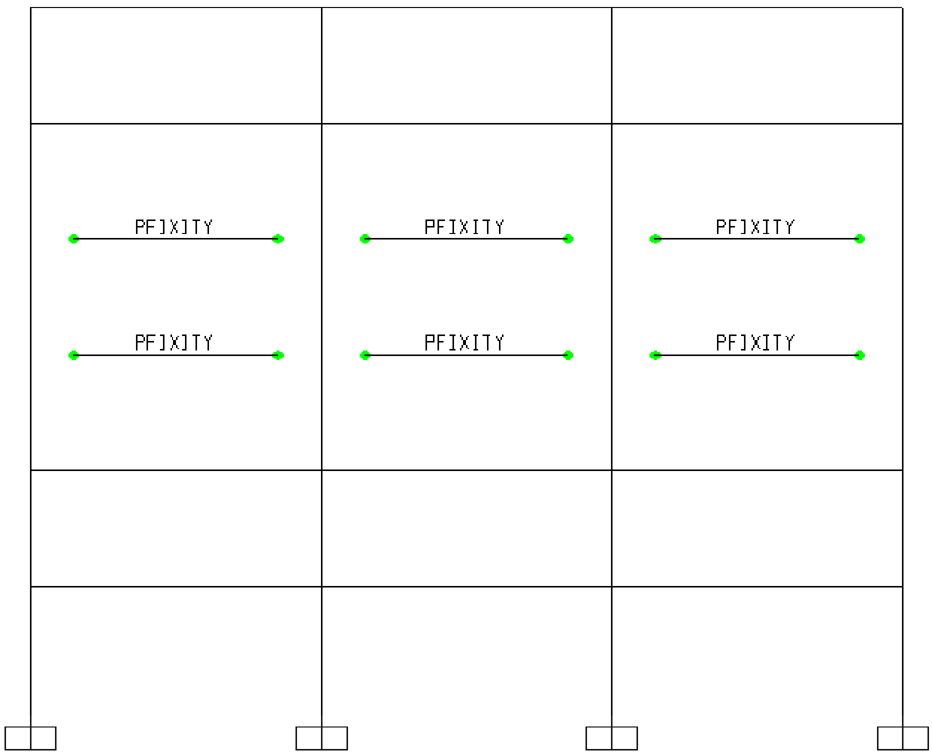


b)

Fig 4.6 connection location a) SR45x b) SR45y

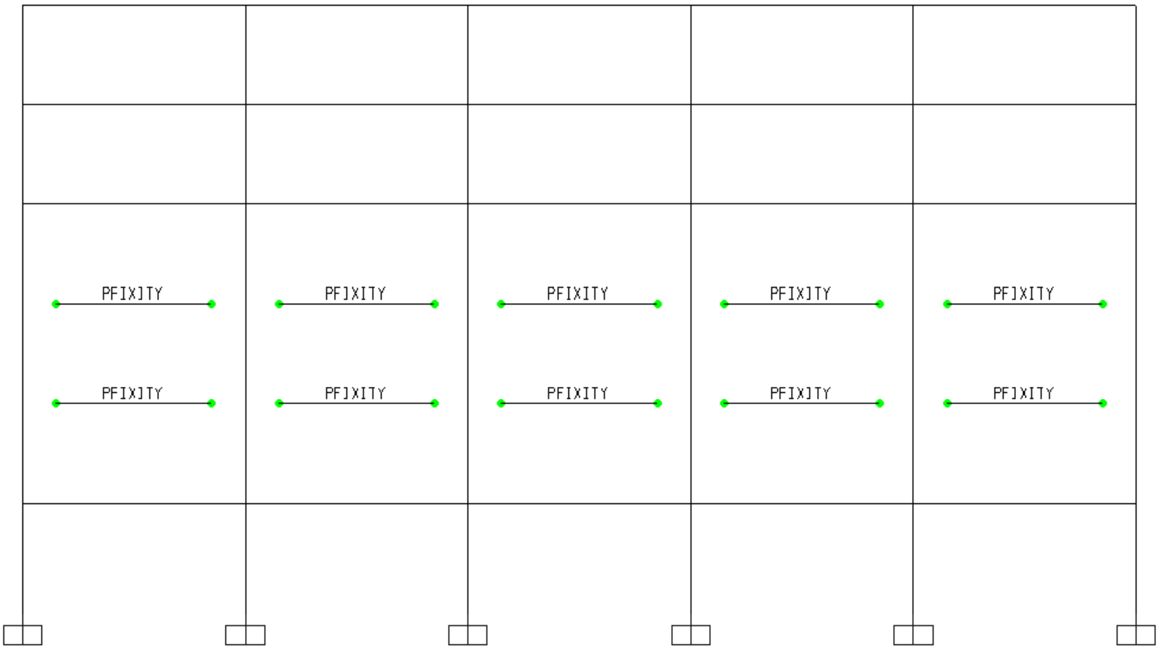


a)

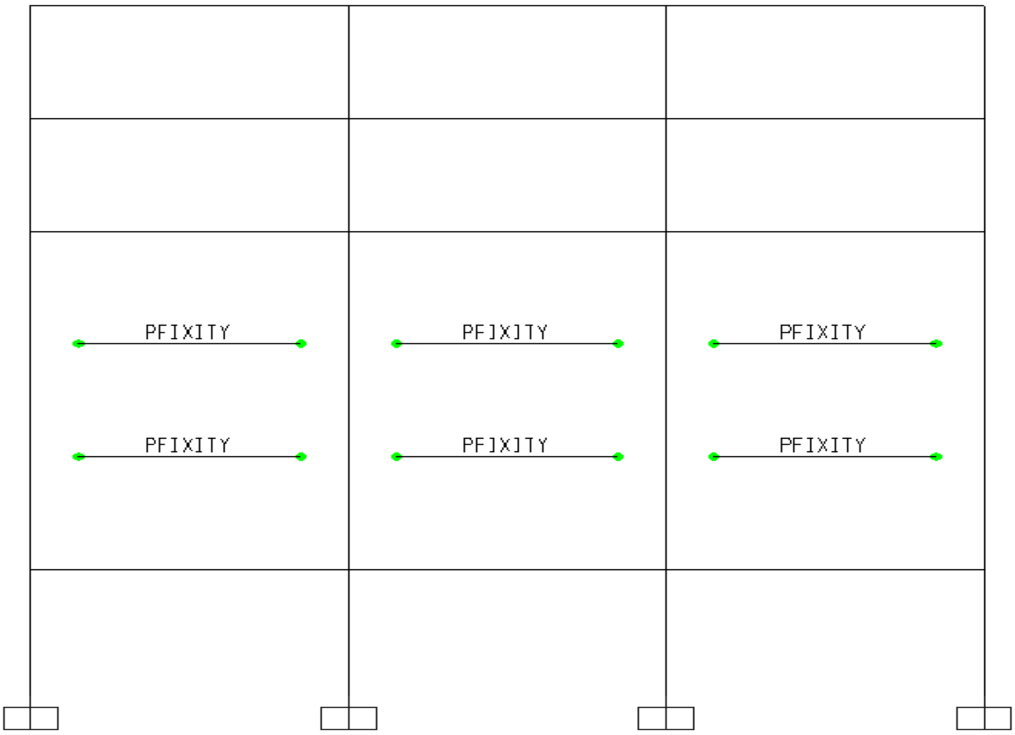


b)

Fig 4.7 connection location a) SR34x b) SR34y

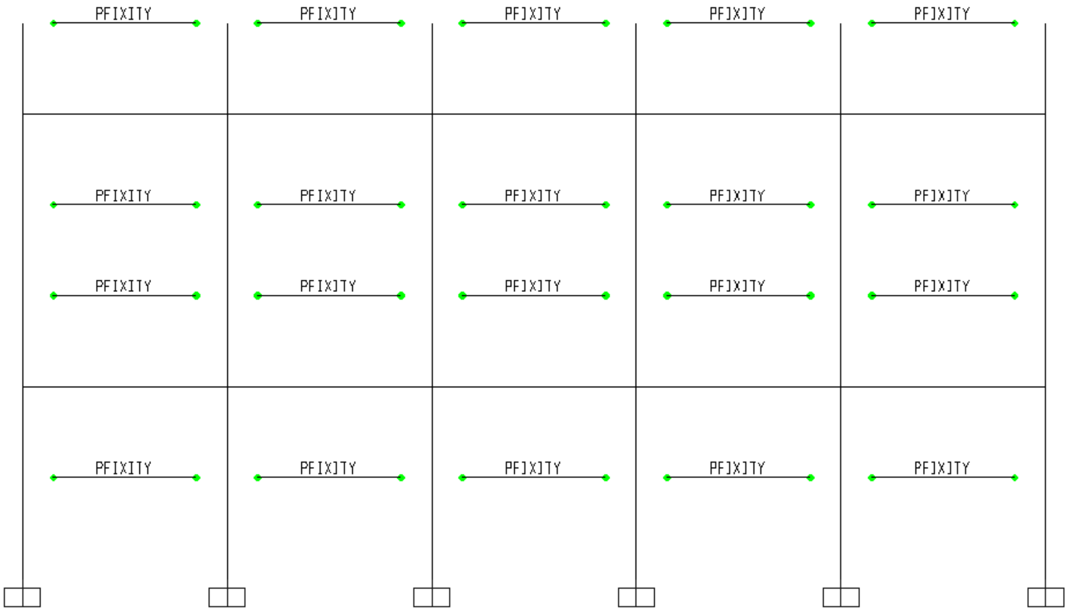


a)

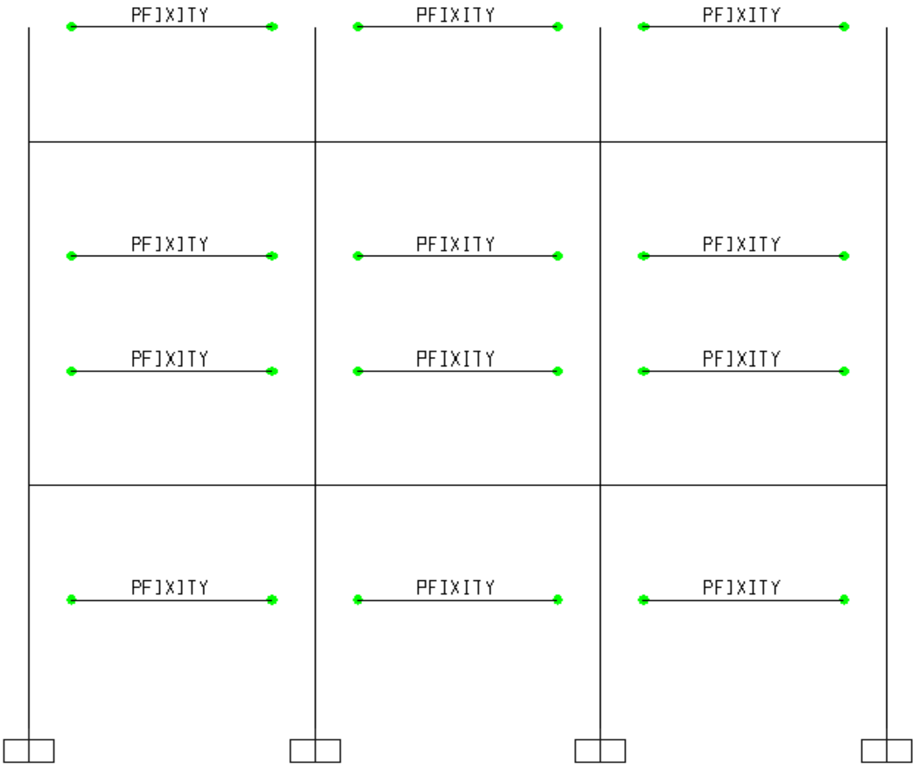


b)

Fig 4.8 connection location a) SR23x b) SR23y

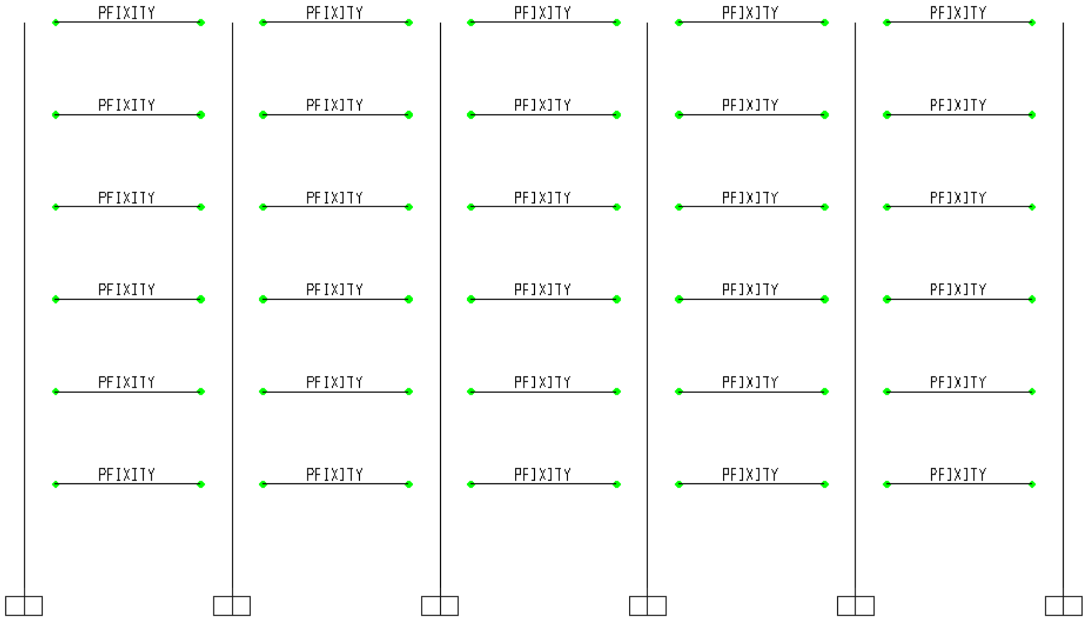


a)

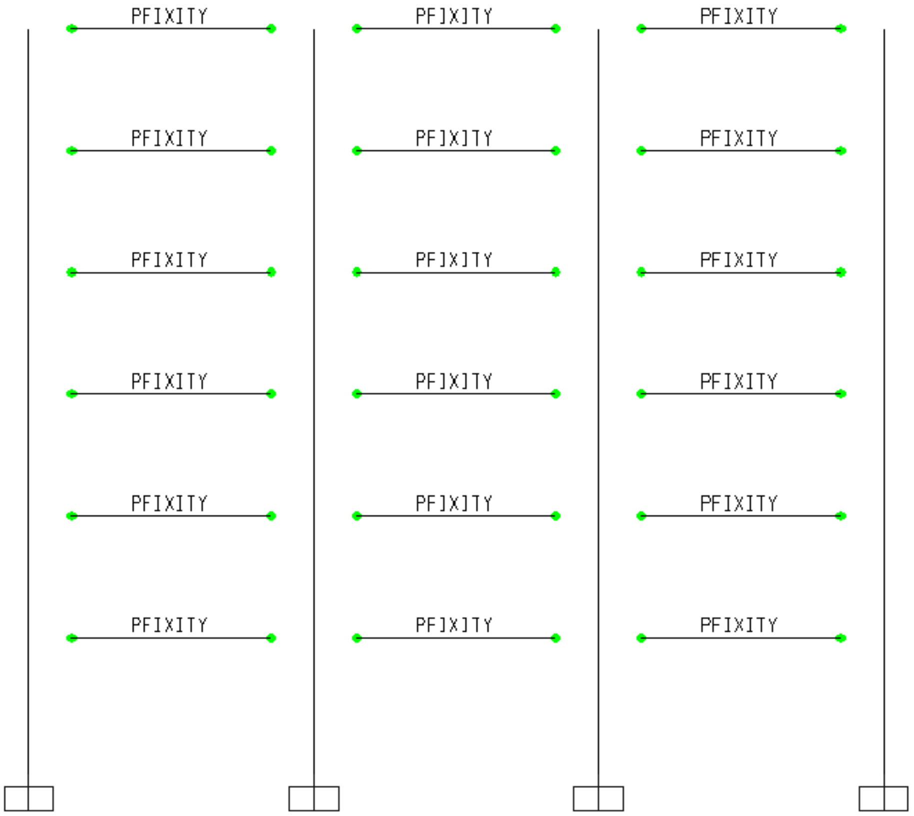


b)

Fig 4.9 connection location a) SR1346x b) SR1346y

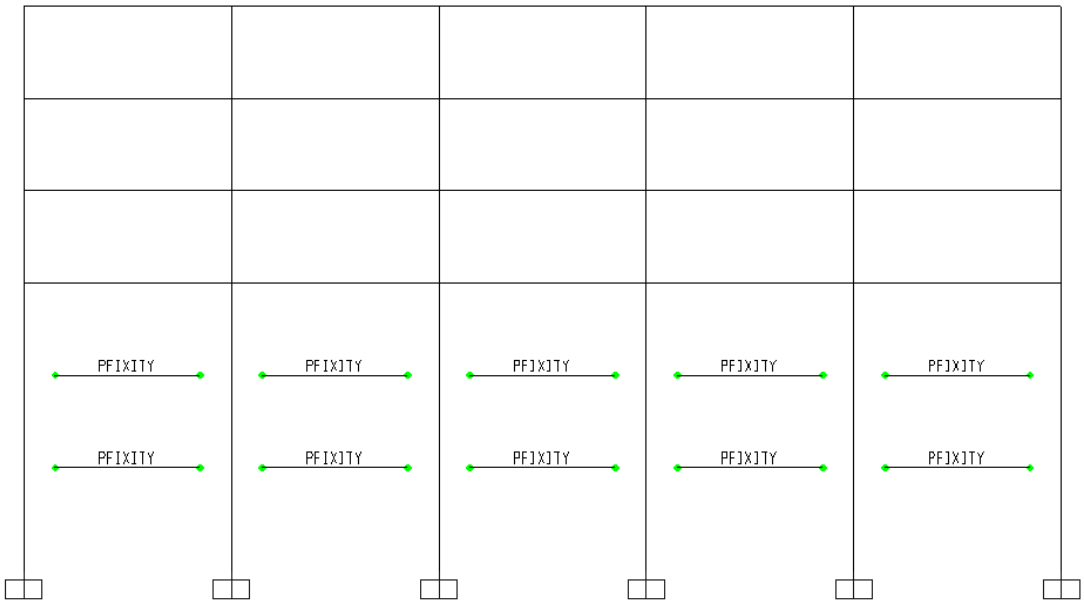


a)

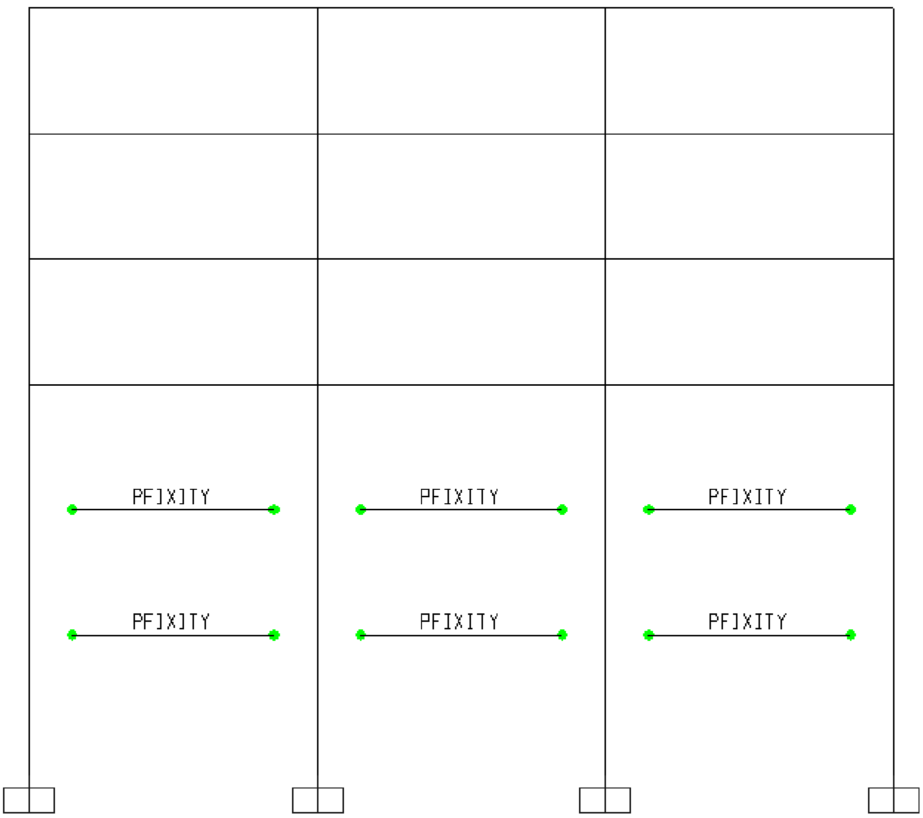


b)

Fig 4.10 connection location a) SRallx b) SRall6y

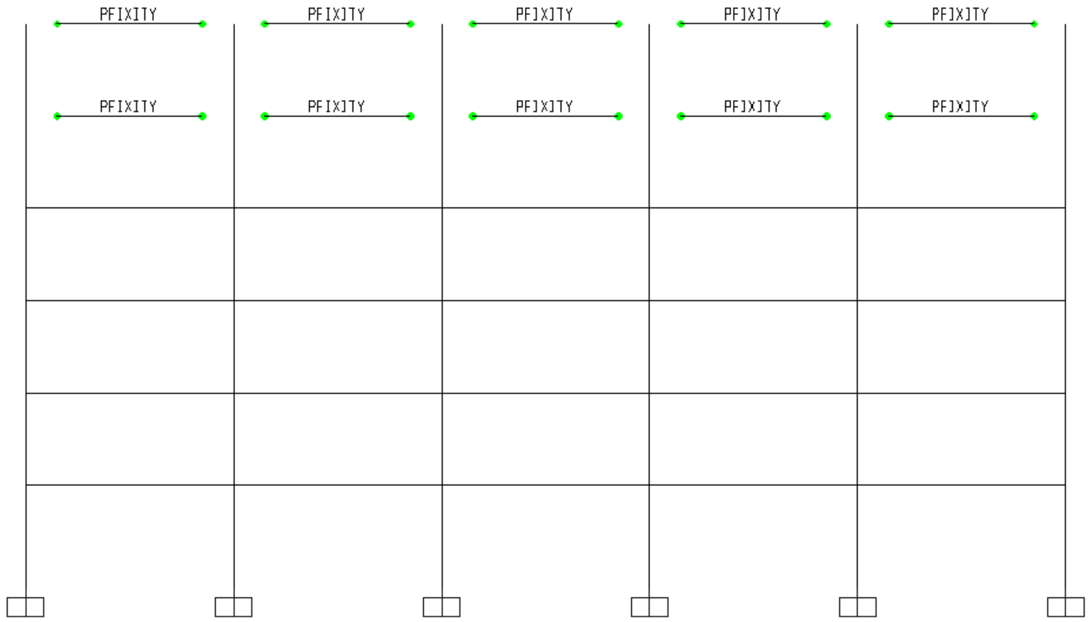


a)

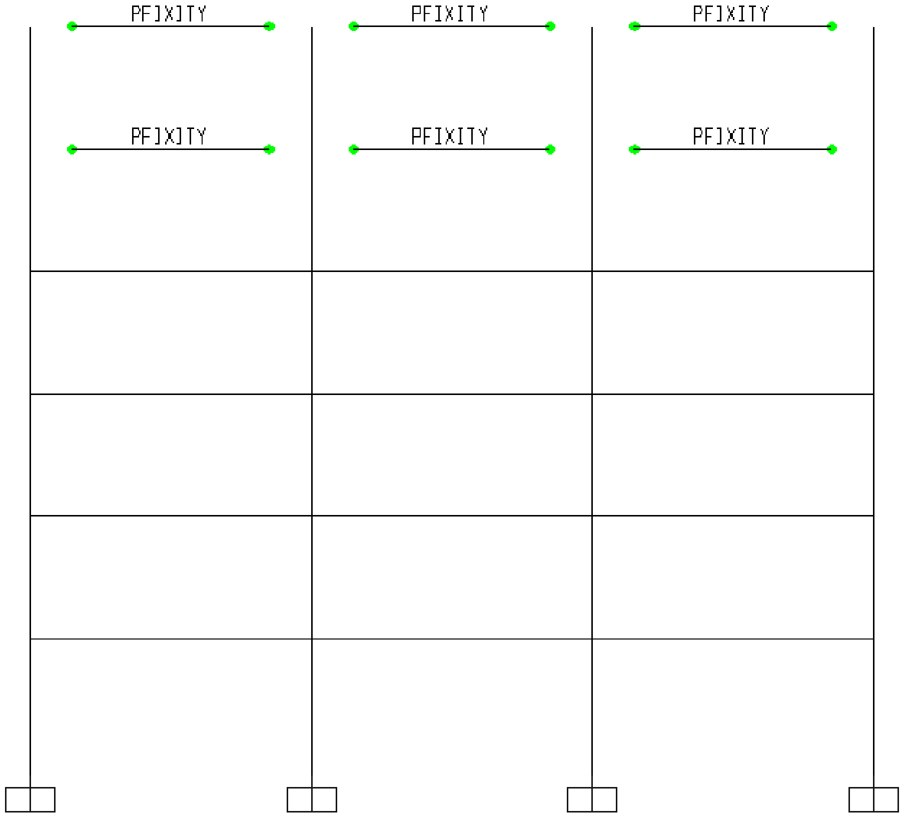


b)

Fig 4.11 connection location a) SR12x b) SR12y

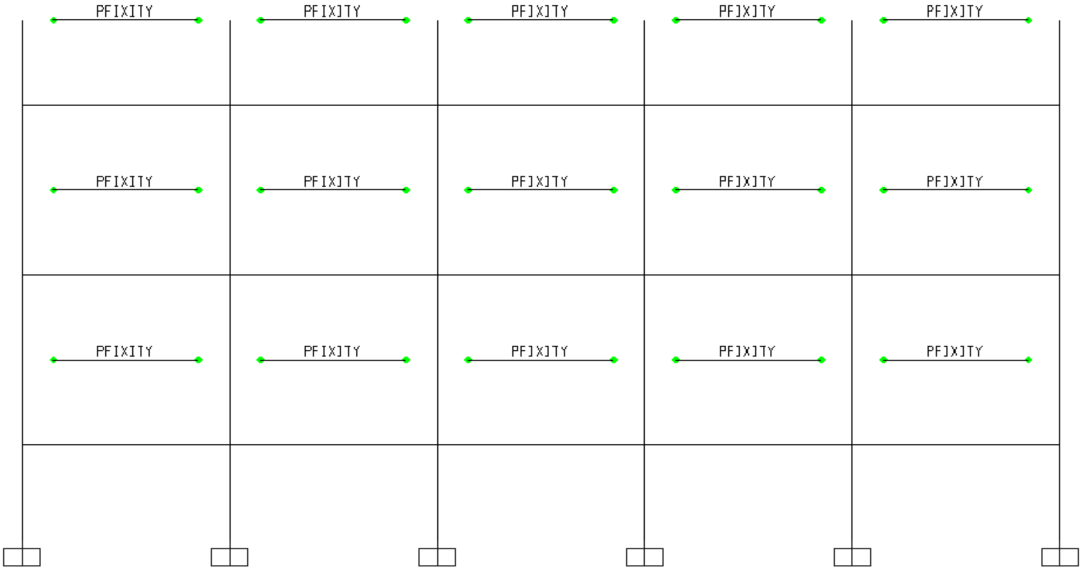


a)

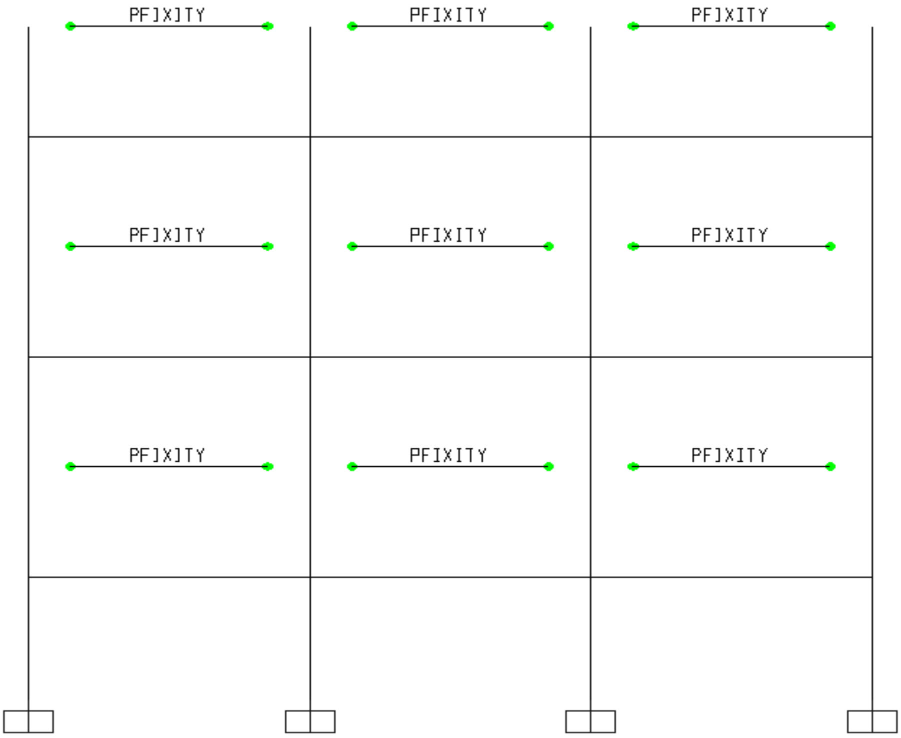


b)

Fig 4.12 connection location a) SR56x b) SR56y

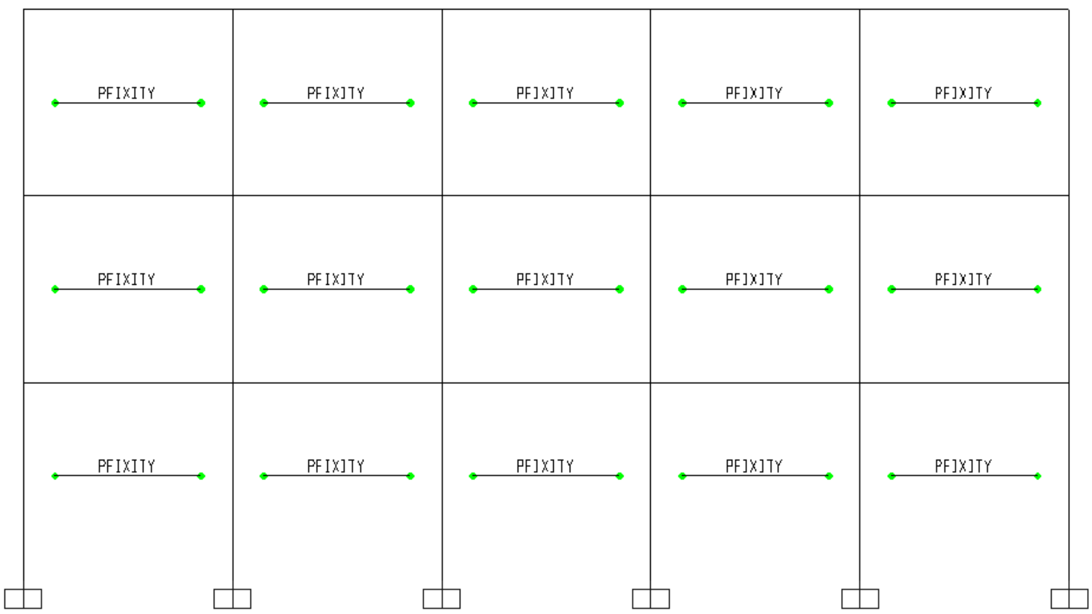


a)

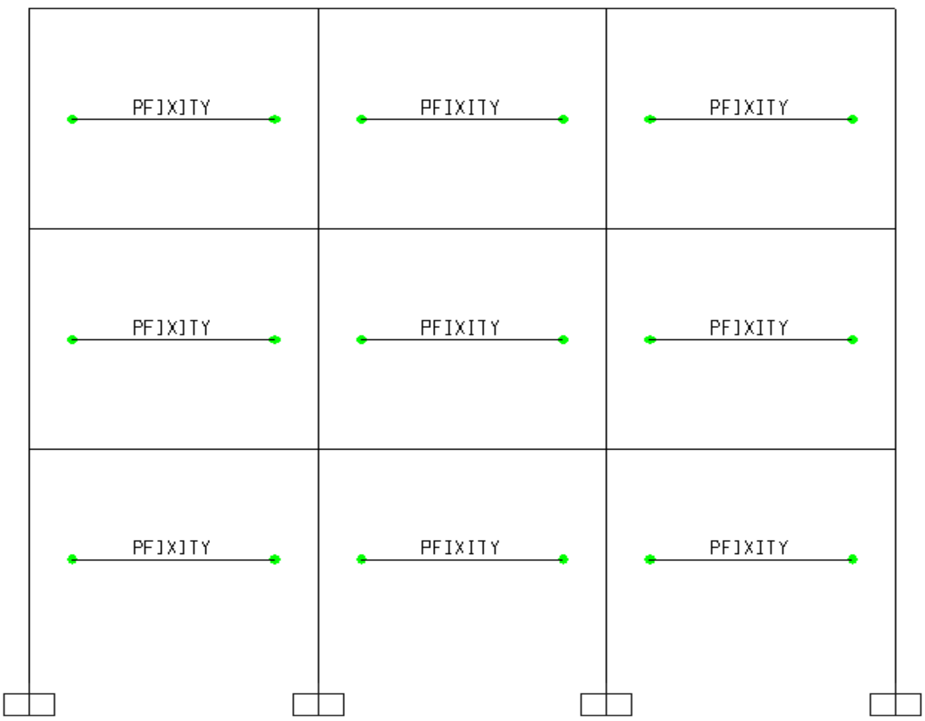


b)

Fig 4.13 connection location a) SR246x b) SR246y

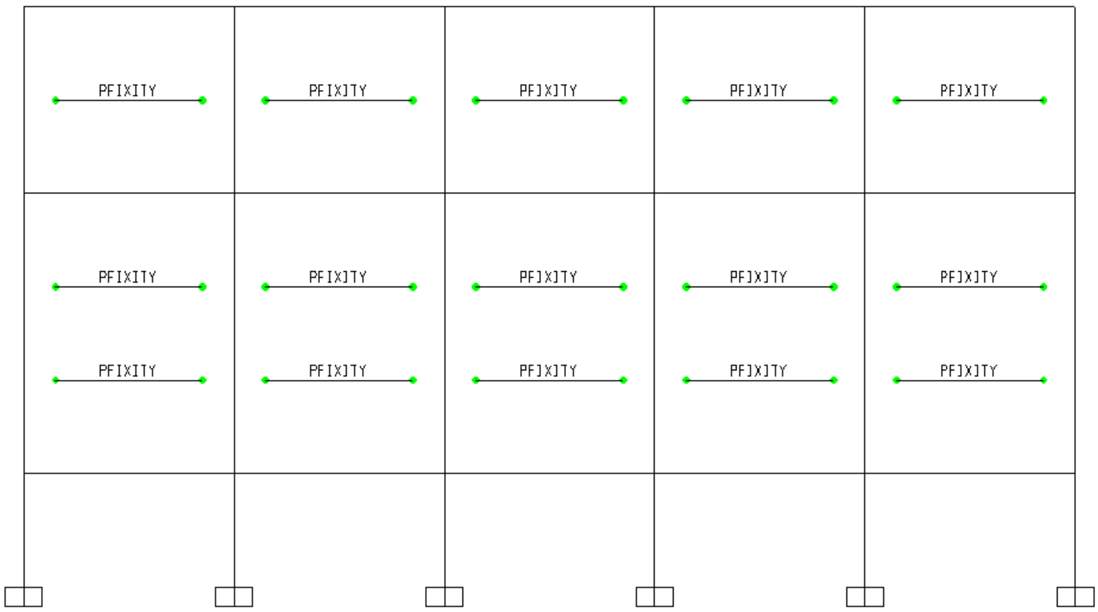


a)

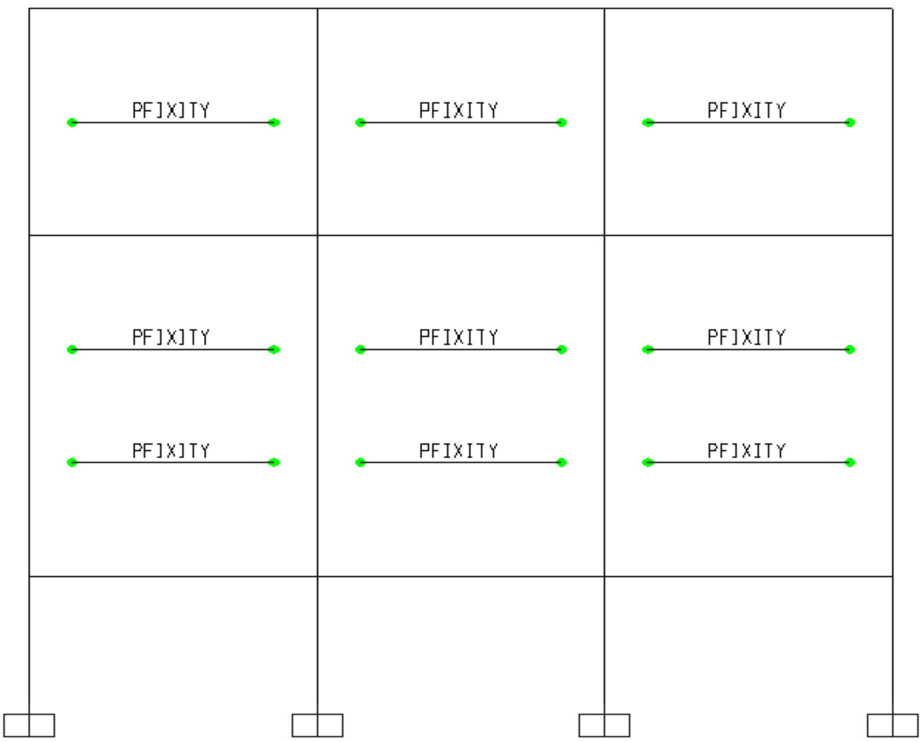


b)

Fig 4.14 connection location a) SR135x b) SR135y

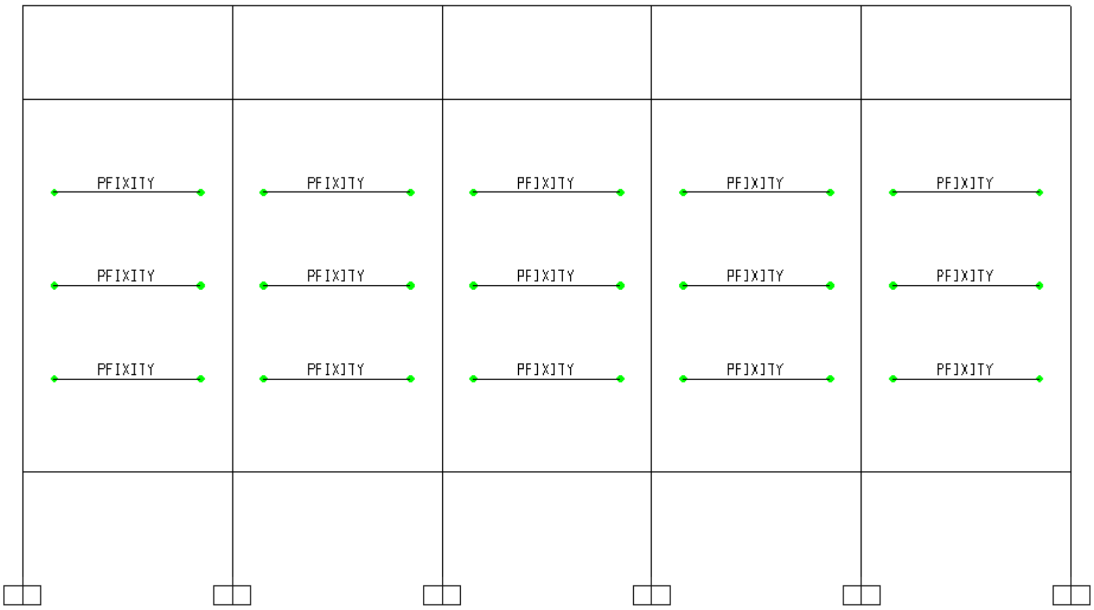


a)

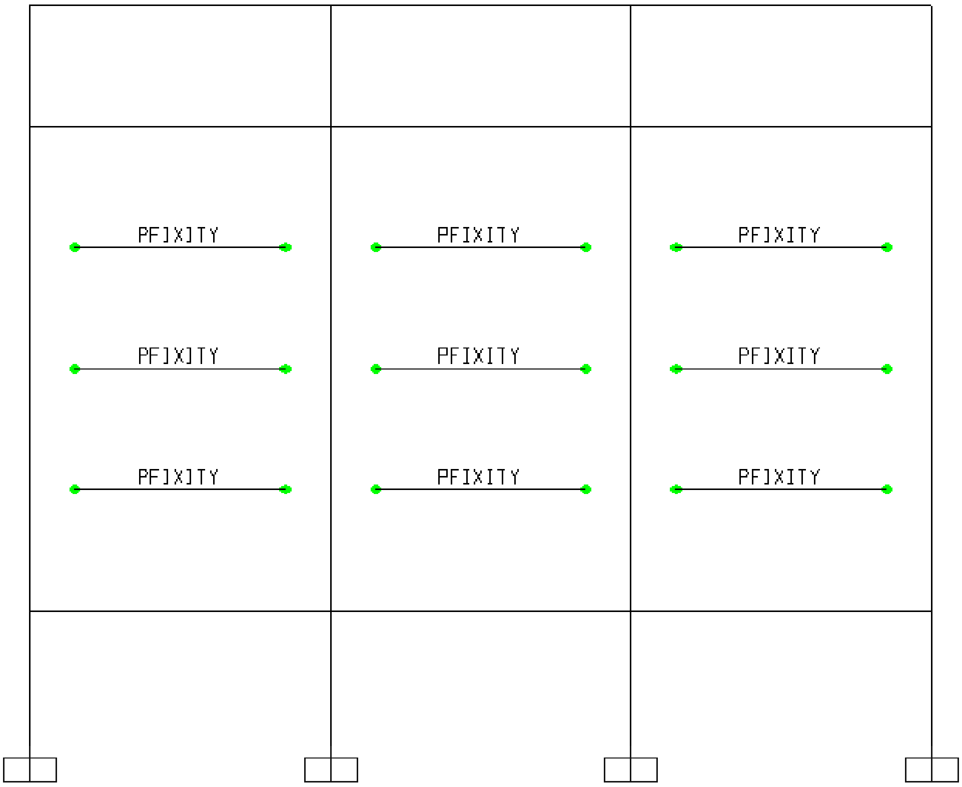


b)

Fig 4.15 connection location a) SR235x b) SR235y

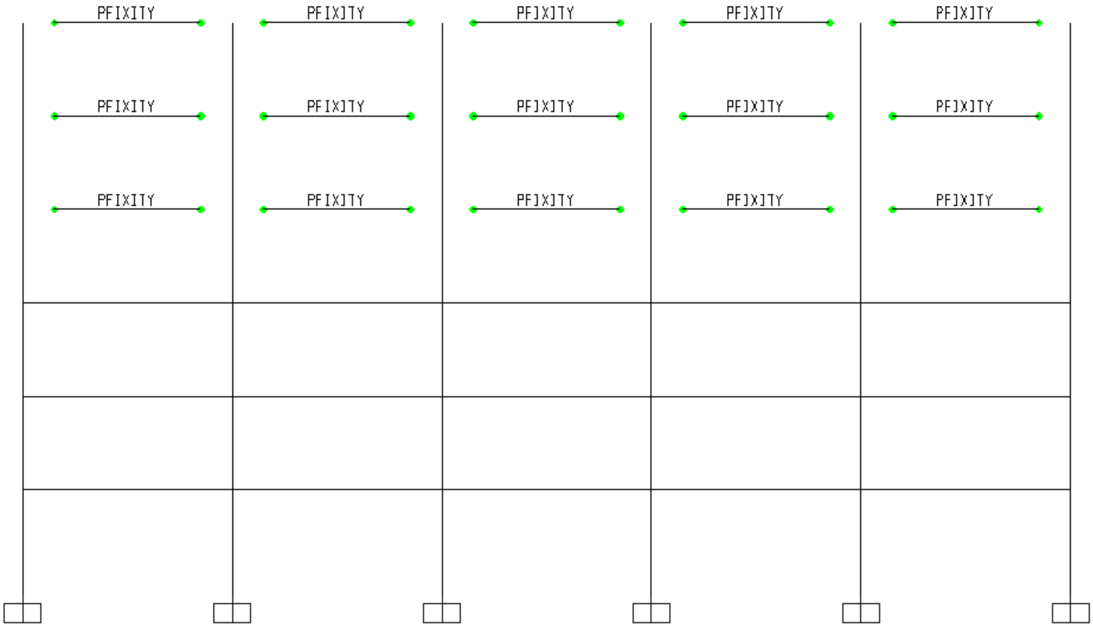


a)

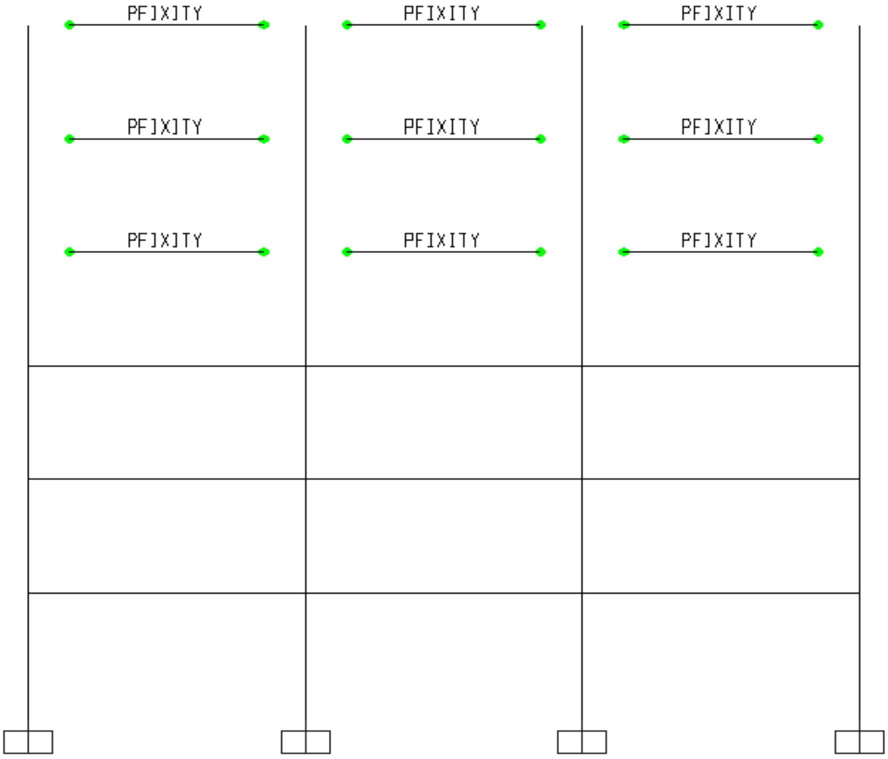


b)

Fig 4.16 connection location a) SR234x b) SR234y

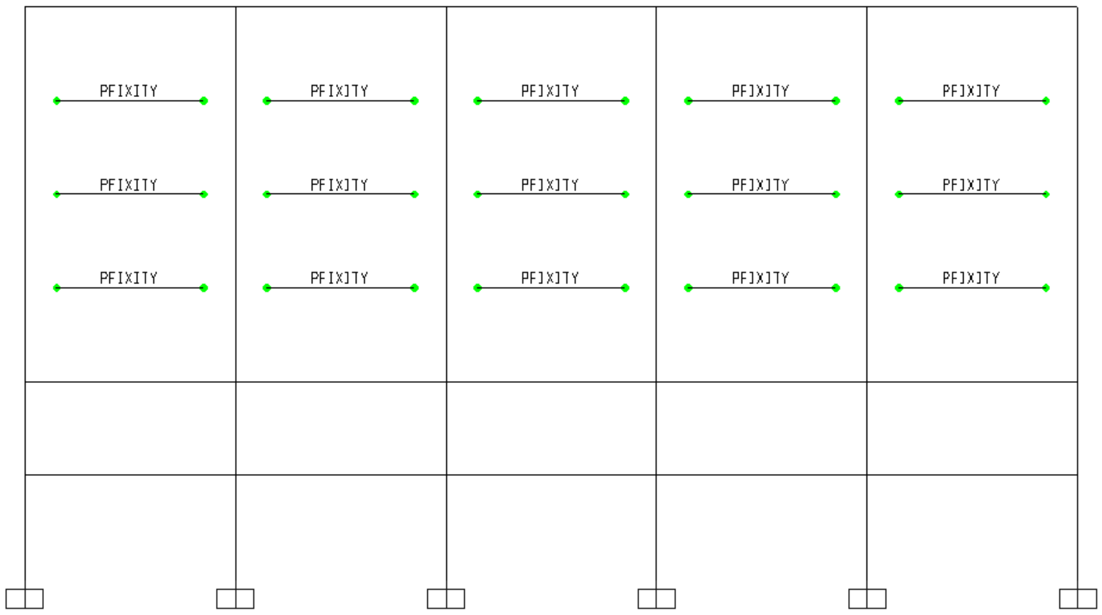


a)

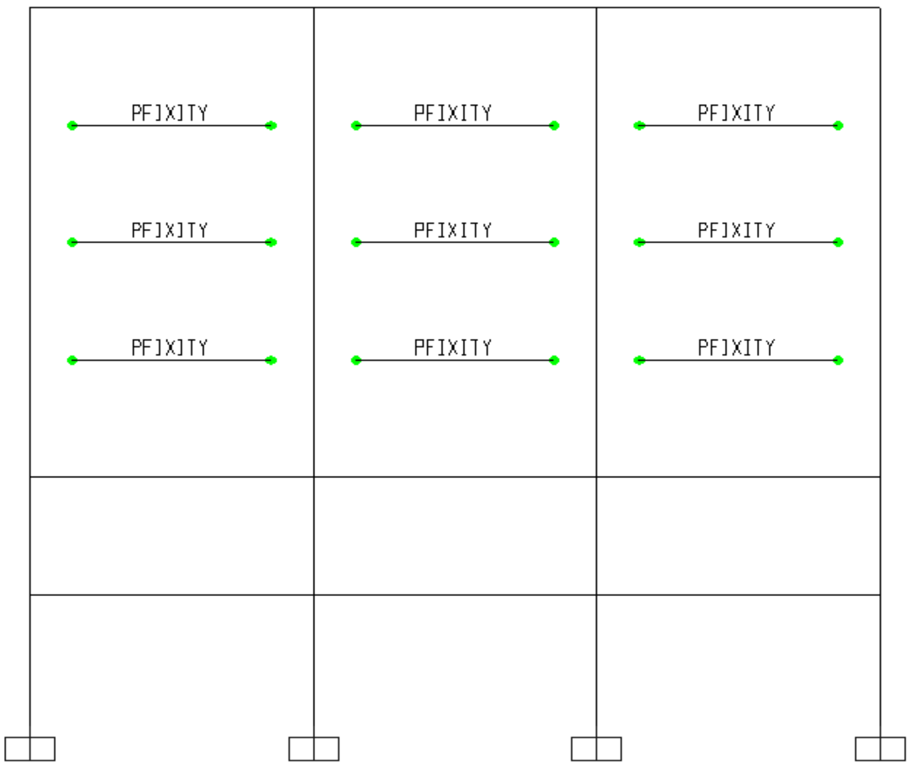


b)

Fig 4.17 connection location a) SR456x b) SR456y

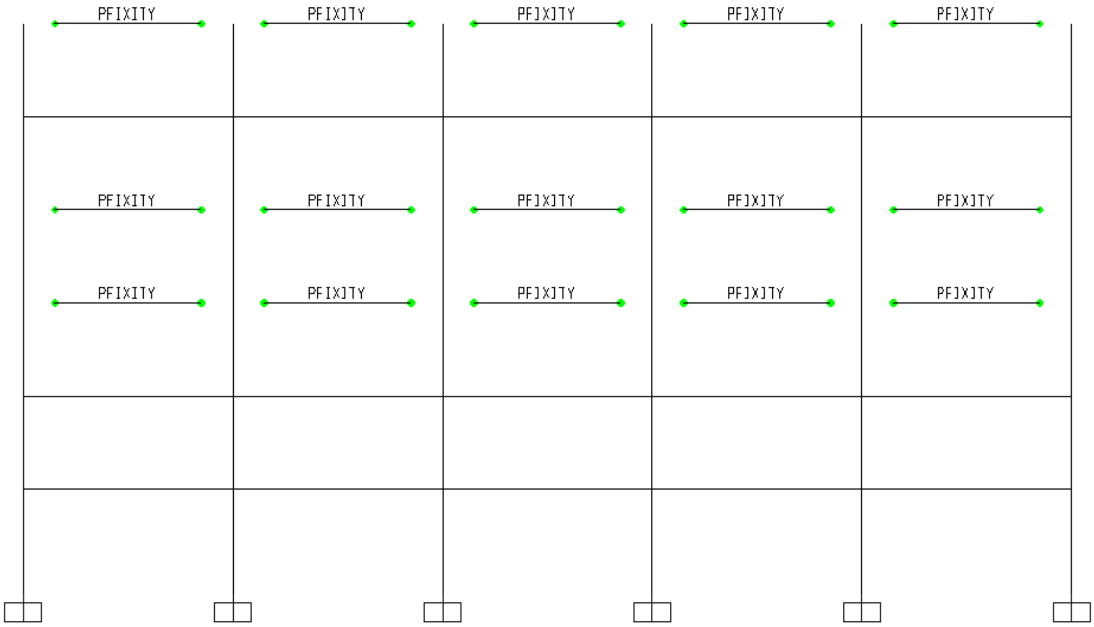


a)

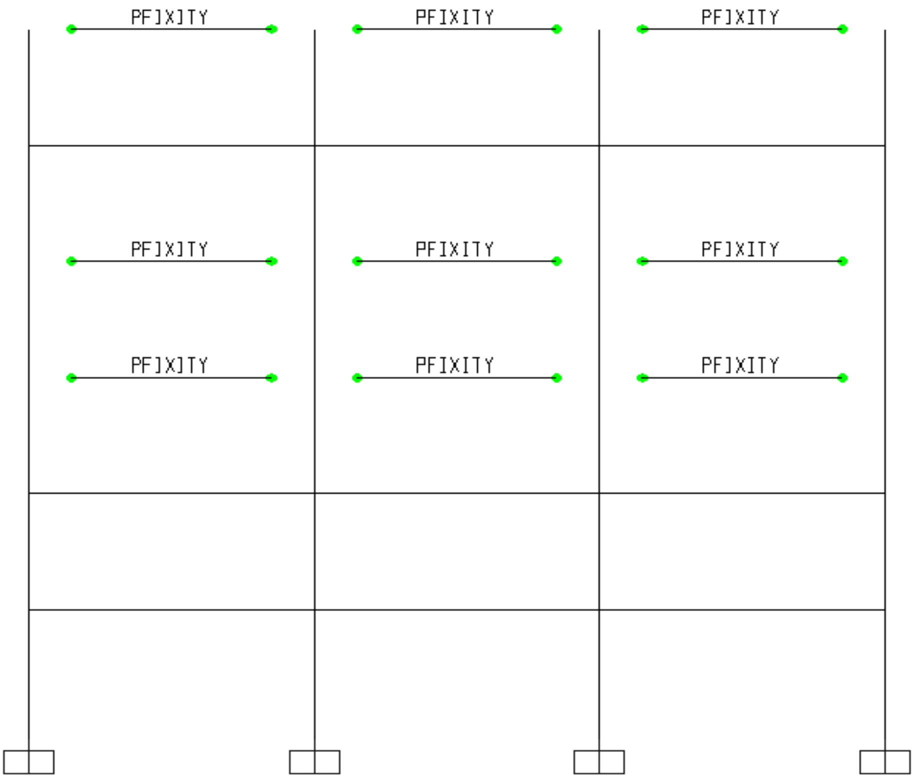


b)

Fig 4.18 connection location a) SR456x b) SR456y



a)

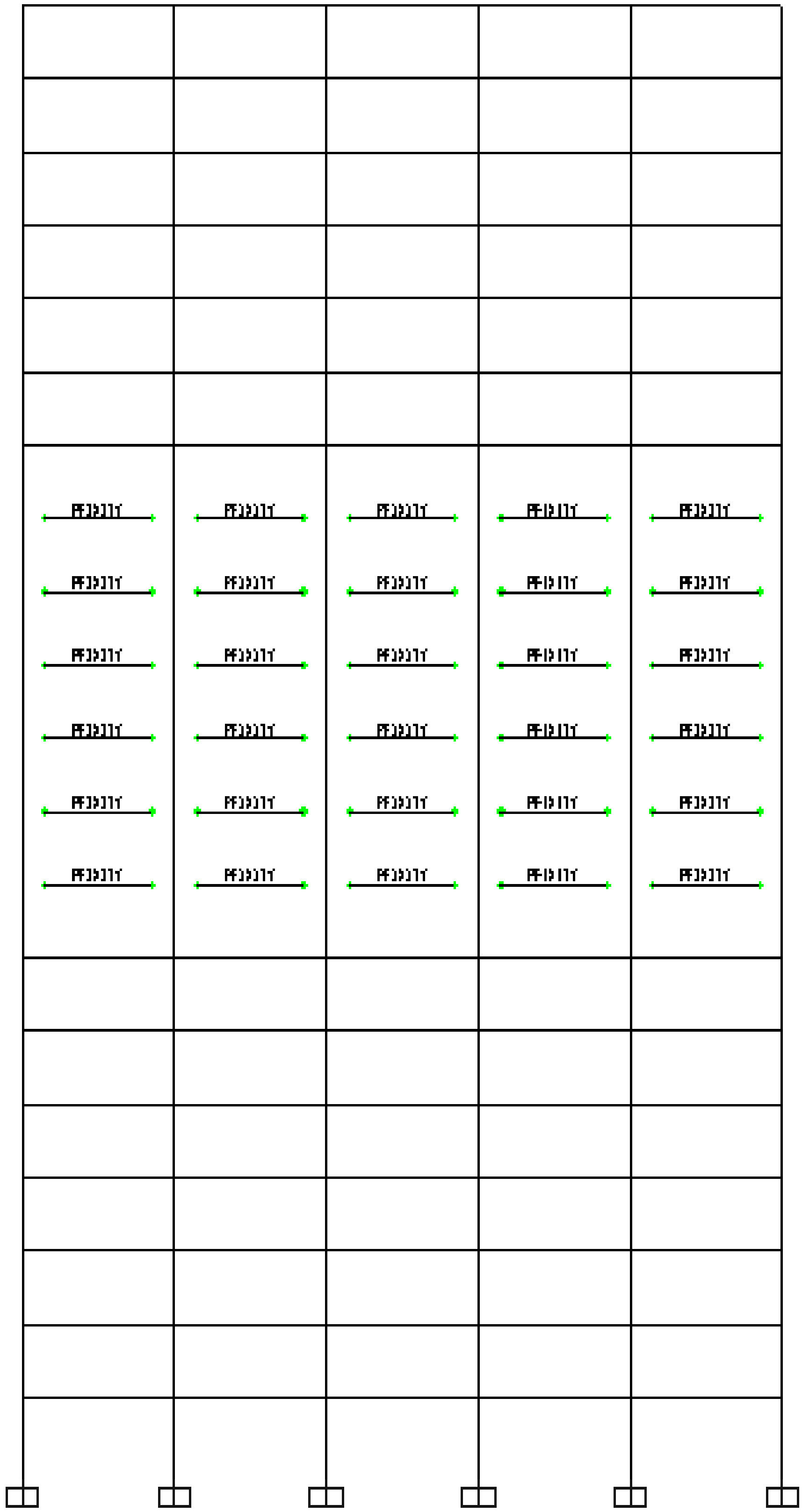


b)

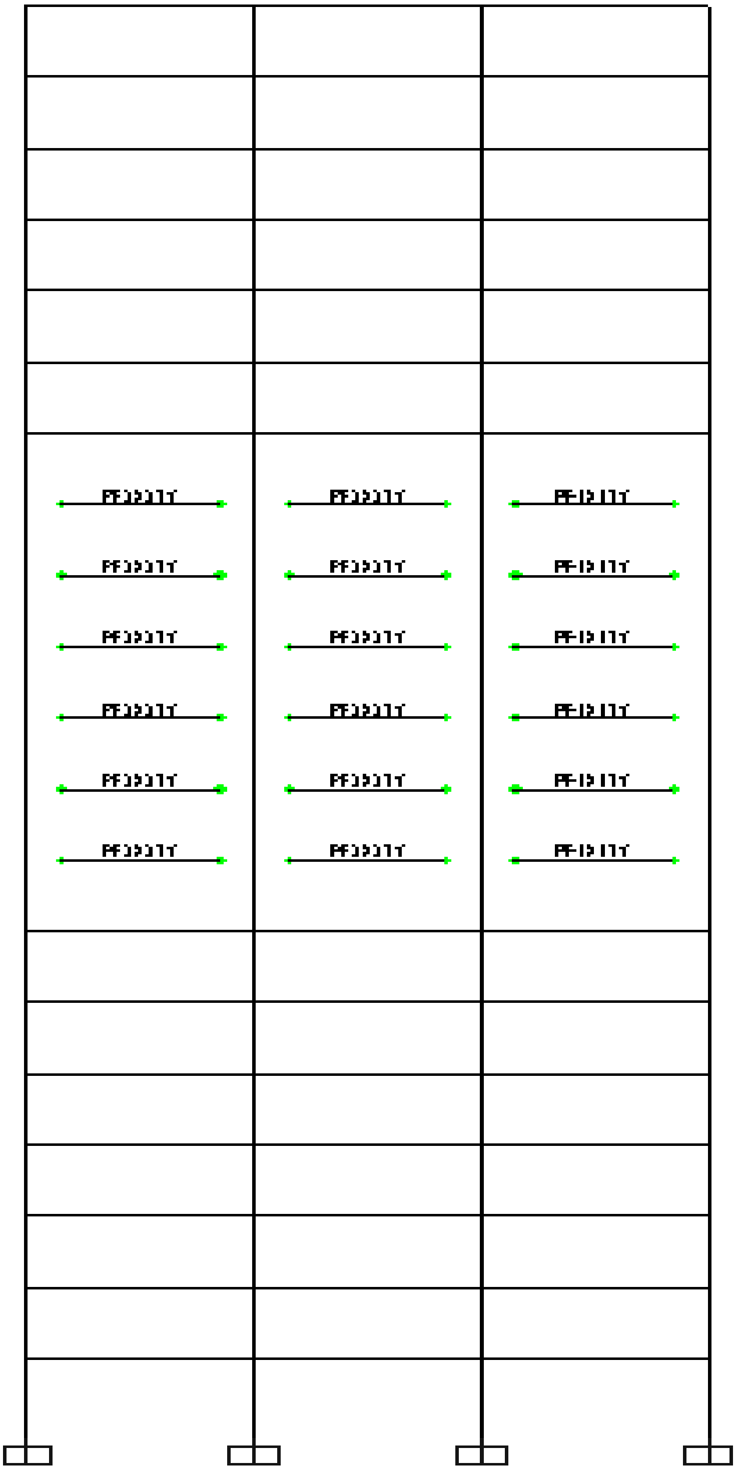
Fig 4.19 connection location a) SR346x b) SR346y

4.1.2 twenty storey PRMRF system

A total four hybrid building with different combinations of rigid and semi-rigid connection were modeled in sap 2000, the adopted building designation of these five building is the same that adopted for the six storey PRMRF system which is 20SR storey number in which extended end plate is placed in direction of frame For example (20SR 12 x) mean that semi-rigid connection is placed in the first and second storey for the 20storey building in the x-direction frames, these five models and their corresponding notation are presented in fig 4.20 through fig 4.23.

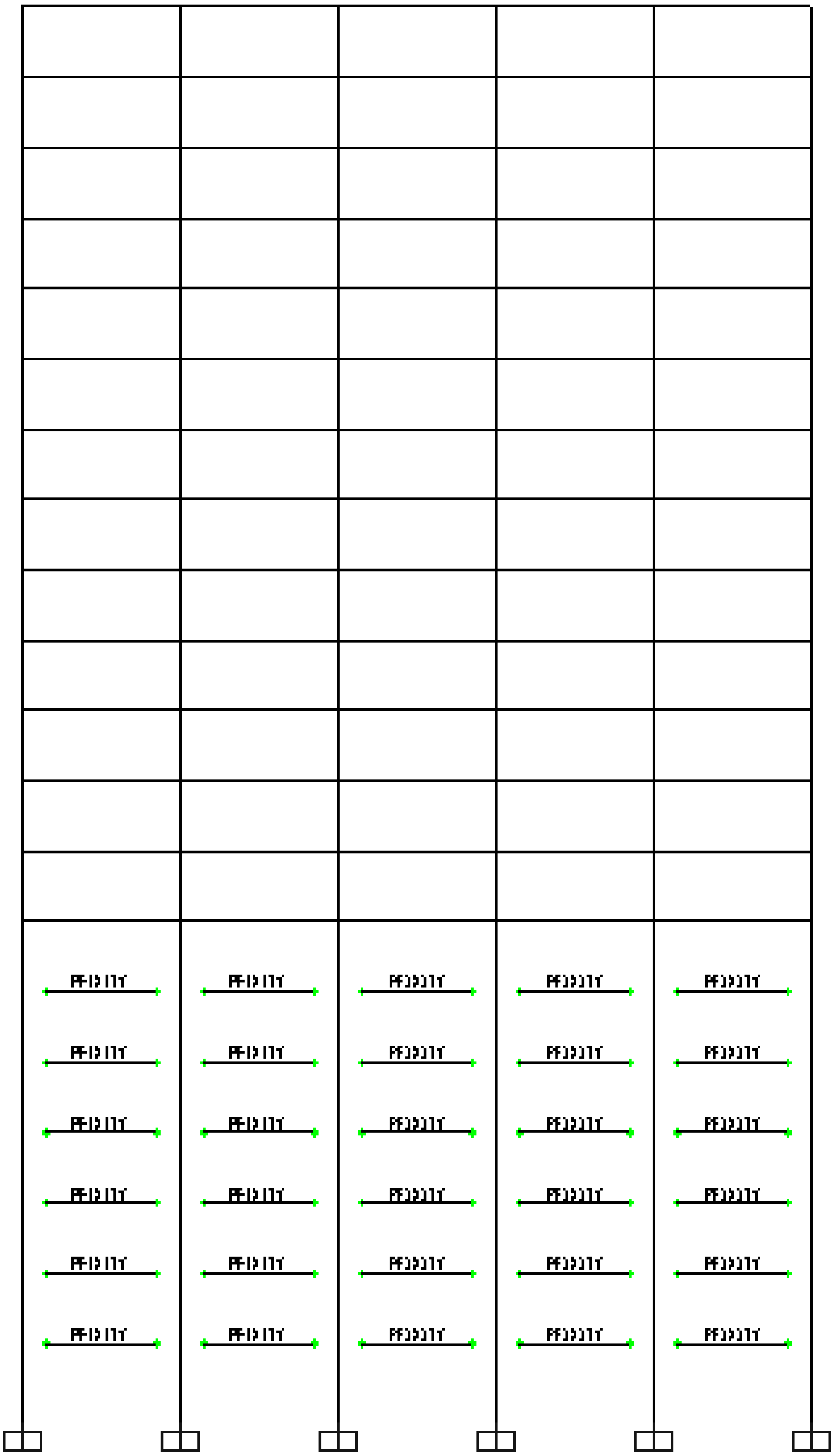


a)

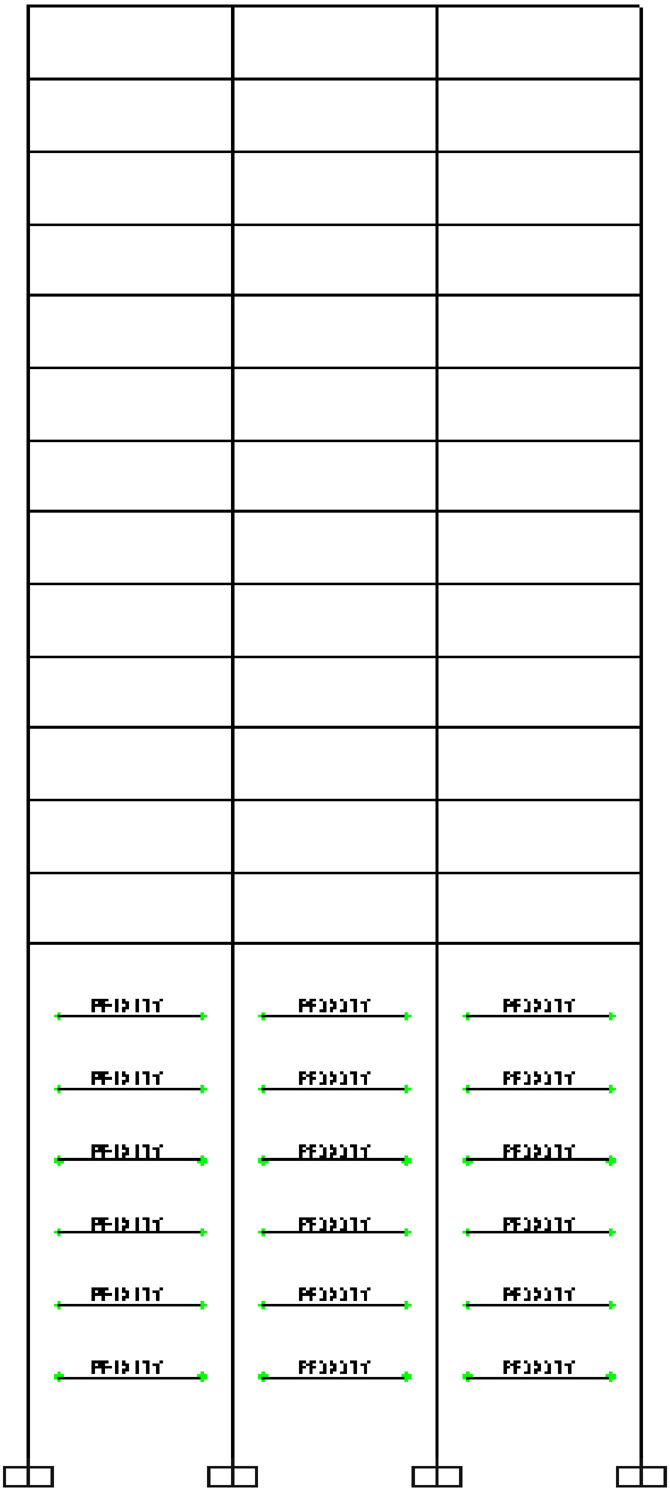


b)

Fig 4.20 connection location a) 20SR8-13x b) 20SR8-13y

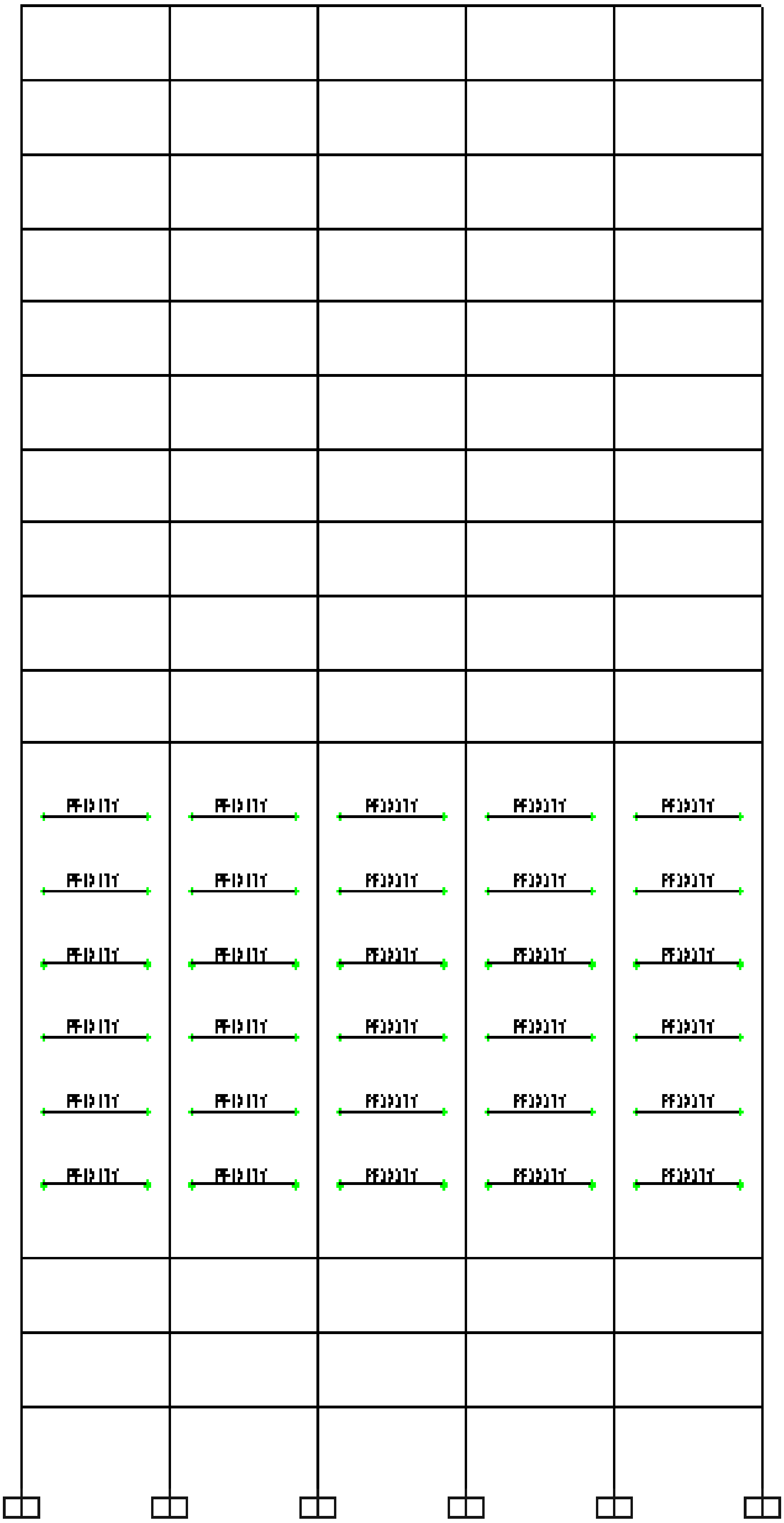


a)

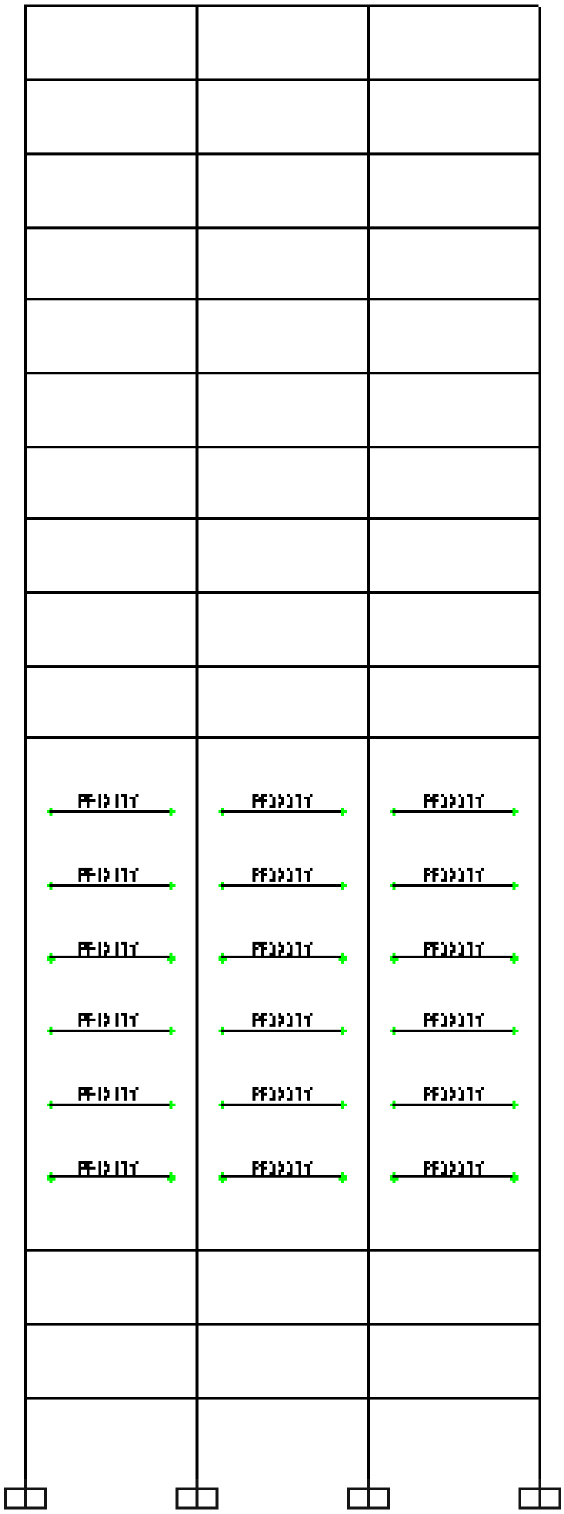


b)

Fig 4.21 connection location a) 20SR1-6x b) 20SR1-6y

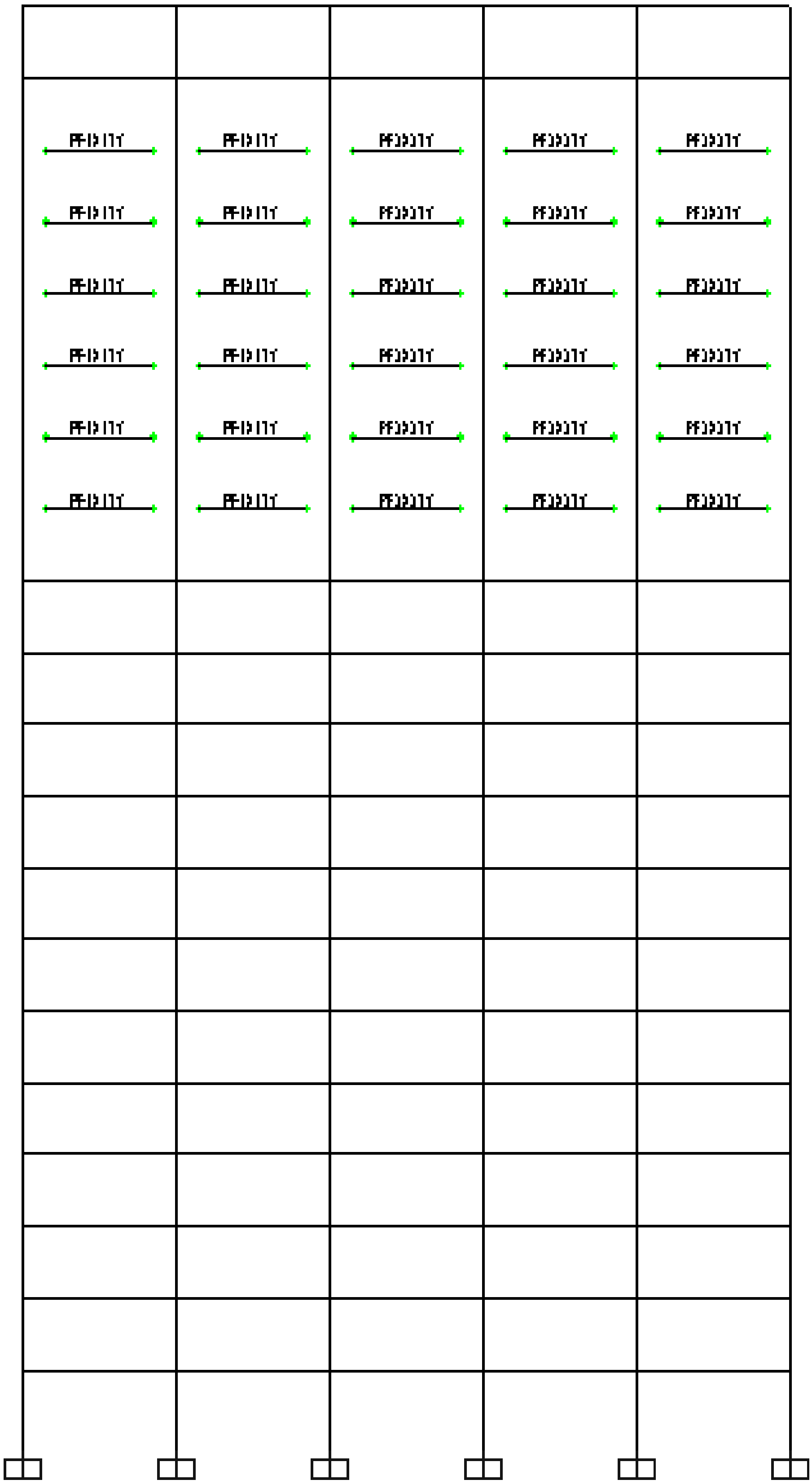


a)

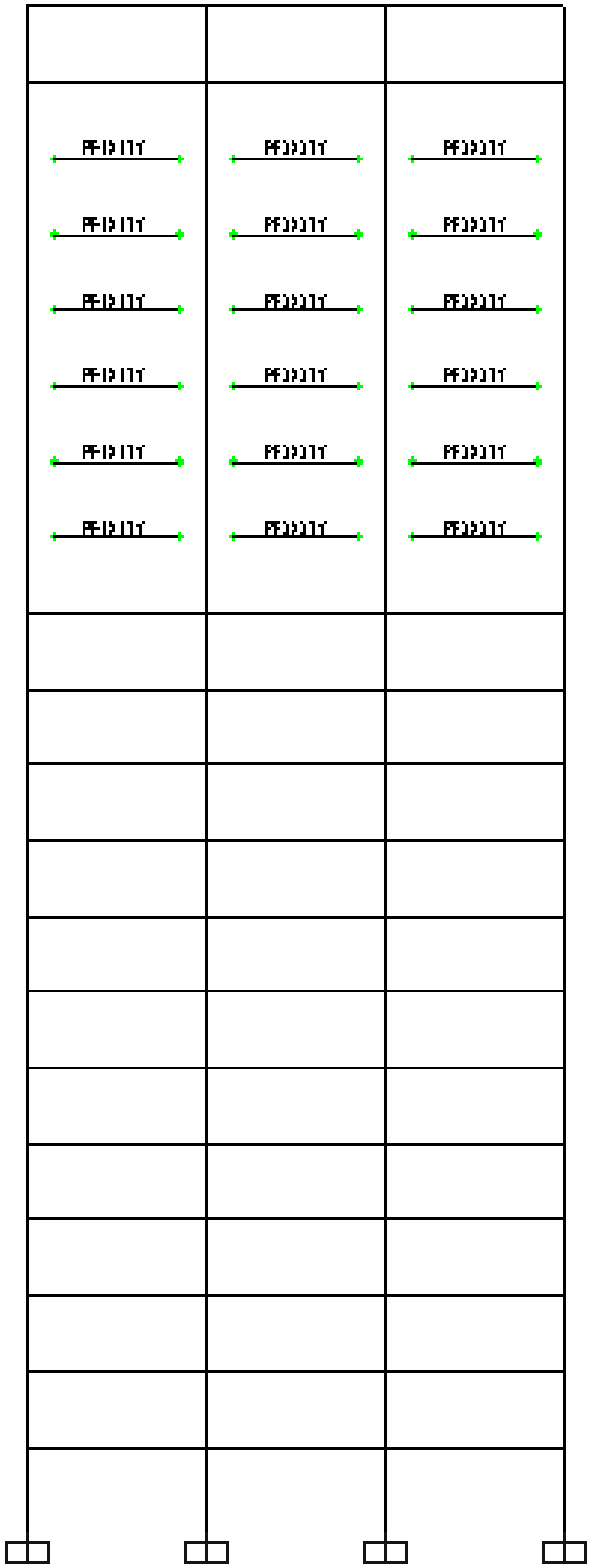


b)

Fig 4.22 connection location a) 20SR4-9x b) SR4-9y



a)



b)

Fig 4.23 connection location a) 20SR13-18x b) 20SR13-18y

4.2 BRBF System:

Members sections of this system are shown in table 4.1 and table 4.2 for six and twenty storey buildings, as for the two previous systems, beams and columns are assumed to yield in flexure only, therefore flexural hinges are defined at the end of each beam and column, these hinges are defined according to table 3.2, the value of the hinge rotation, the acceptance criteria, and strain hardening ratio for each storey in BRBF beams and columns in both directions for six and twenty storey buildings are as shown in table 4.3. As the name of this system implies the bracing members are restrained against buckling, in other word compression buckling is not allowed in the bracing, therefore bracing members will yield in compression as in tension, and the axial hinge curve (fig 3.1) will be symmetric for both tension and compression side, also the beam-bracing connections are assumed to be hinge connection, therefore the bracing member in this system will yield in tension and compression only without any moment transfer from beams. This system should be designed so that bracing members should be the weakest members in the building, and it will act like fuses (the first to yield), therefore the bracing members in this system is like semi-rigid connection in PRMRF.

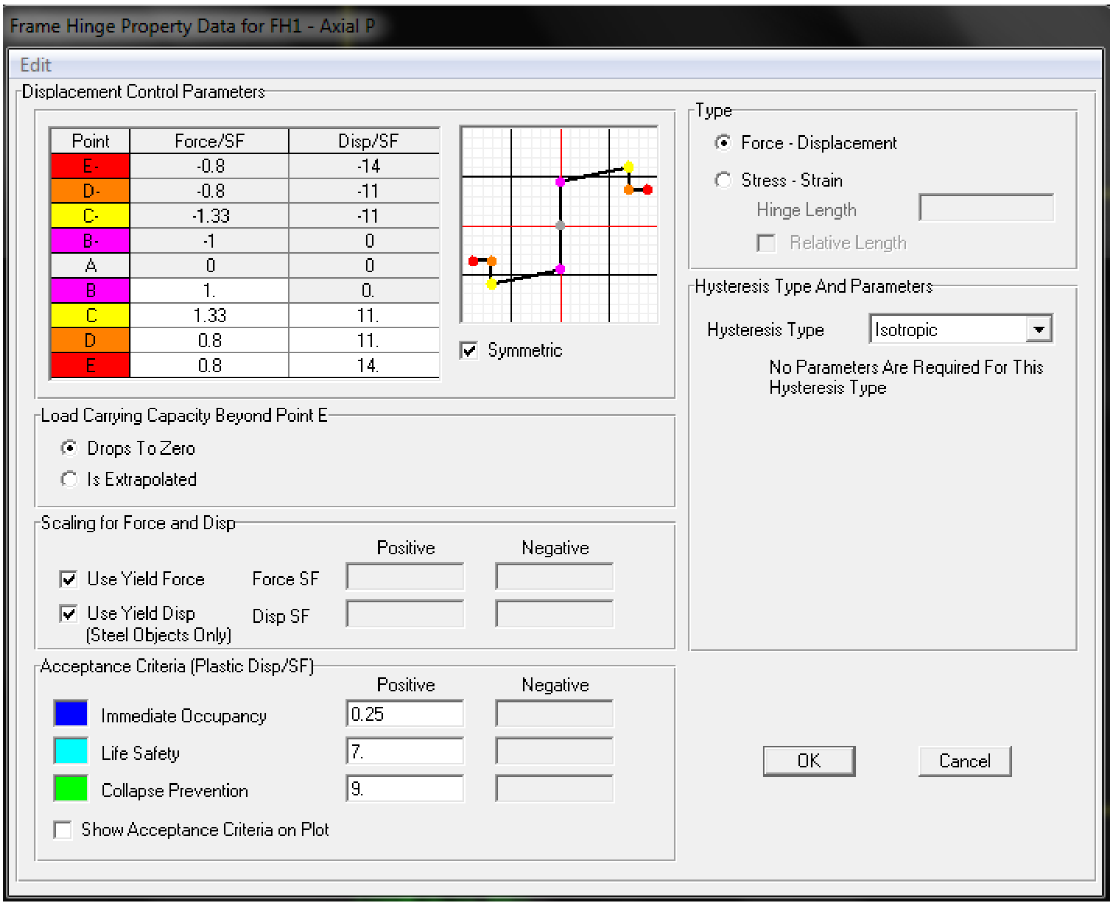
Axial hinge parameter are shown in table 4.9 for both 6 and 20-storey buildings, also fig 4.24 show BRBF bracing axial hinge curve as defined in sap 2000.

Table 4.8: values of hinge rotation, acceptance criteria, and strain hardening ratio for beams and columns for both 6 and 20-storey BRBF system

Component	Modeling Parameter			Acceptance Criteria			Strain hardening ratio
	Plastic Rotation Angle, Radians		Residual Strength Ratio	Plastic Rotation Angle, Radian			
	a	b	c	IO	LS	CP	
All beams and columns	$4\theta_y$	$6\theta_y$	0.2	$0.25\theta_y$	$2\theta_y$	$3\theta_y$	1.12

Table 4.9: values of axial hinge deformation, acceptance criteria, and strain hardening ratio for beams and columns for both 6 and 20-storey BRBF system

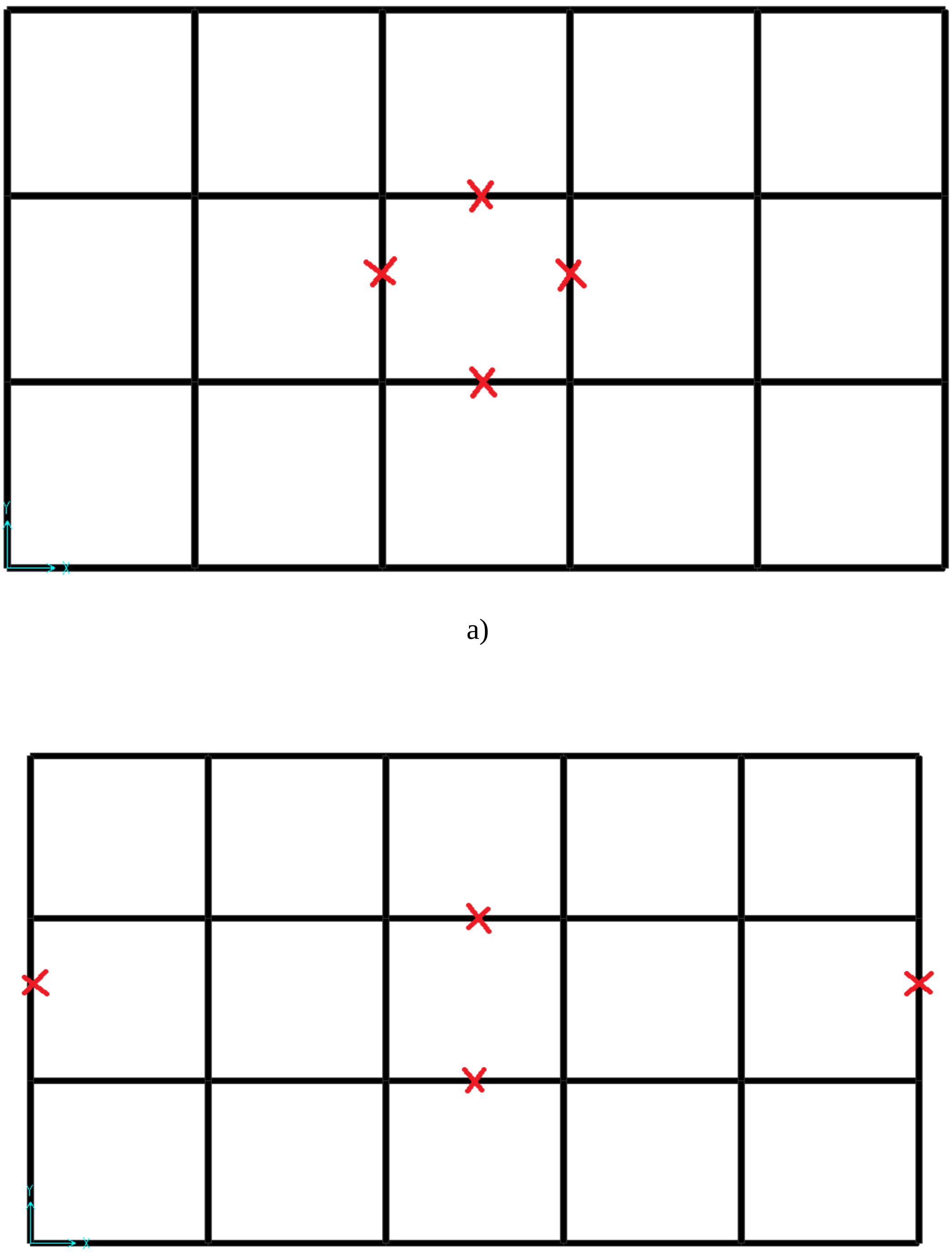
Component	Modeling Parameter			Acceptance Criteria			Strain hardening ratio
	Plastic deformation		Residual Strength Ratio	Plastic deformation			
	a	b	c	IO	LS	CP	
Braces in Tension	$11\Delta_T$	$14\Delta_T$	0.8	$0.25\Delta_T$	$7\Delta_T$	$9\Delta_T$	1.33



4.24 axial hinge curve for BRBF bracing members defined in sap 2000

4.2.1 6-story BRBF system:

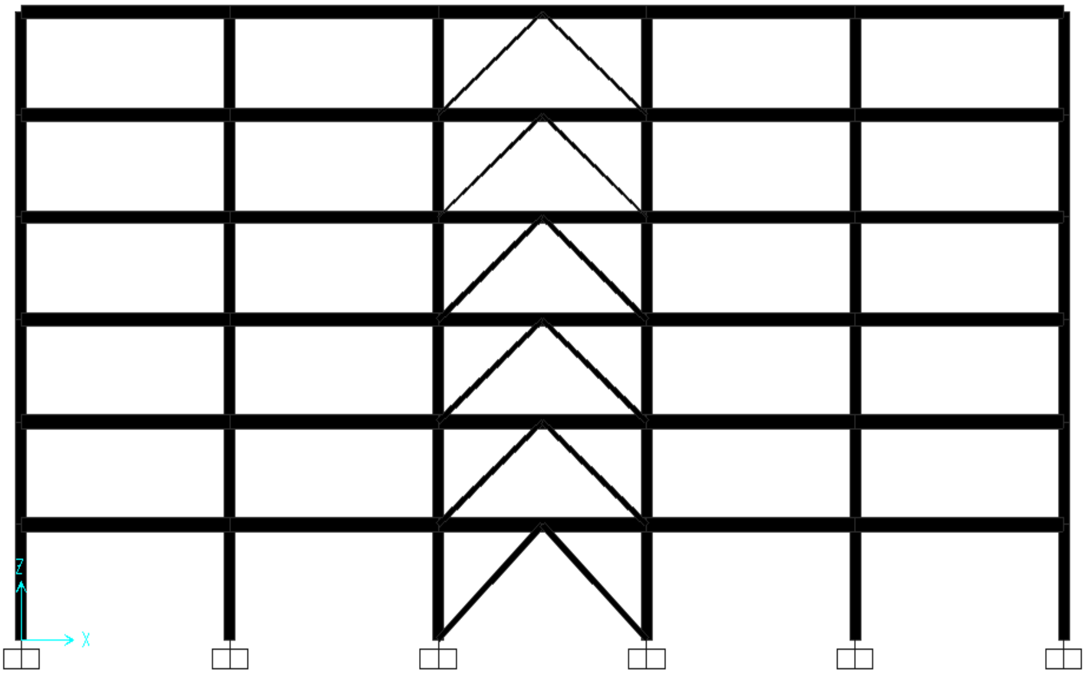
Two models with different bracing location were taken for this system, the adopted building designation for this system is 6BRBF csx csy, where the characters x and y indicate that bracing exist in x-frame and y-frame respectively, also c, and s (which means core, and side frame respectively) indicate the location of bracing in the x or y frame, the absence of any of these two characters means that bracing members are not exist at its location. For example (6 BRBF csx csy) means that the six storey building is braced at its core, and at its external side in the middle of x and y frame, while (20BRBF cx cy) indicates that the six storey building is braced at its core only. These two bracing models and their notations are shown in fig 4.25, While fig 4.26 show the bracing frame in x and y direction.



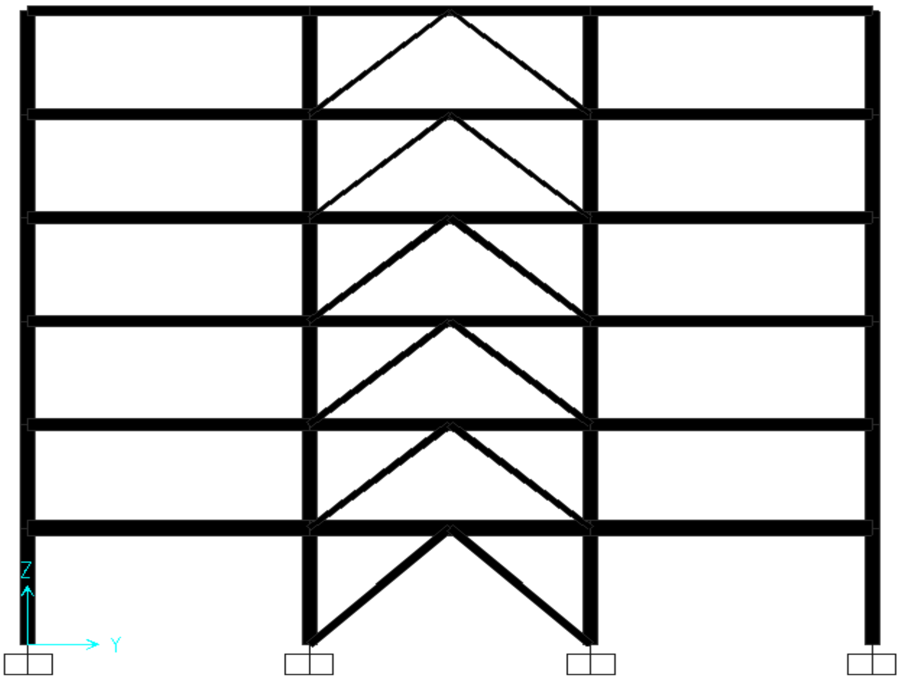
a)

b)

Fig 4.25 two 6-storey BRBF model a) 6BRBF cx cy b) 6BRBF cx sy



a)

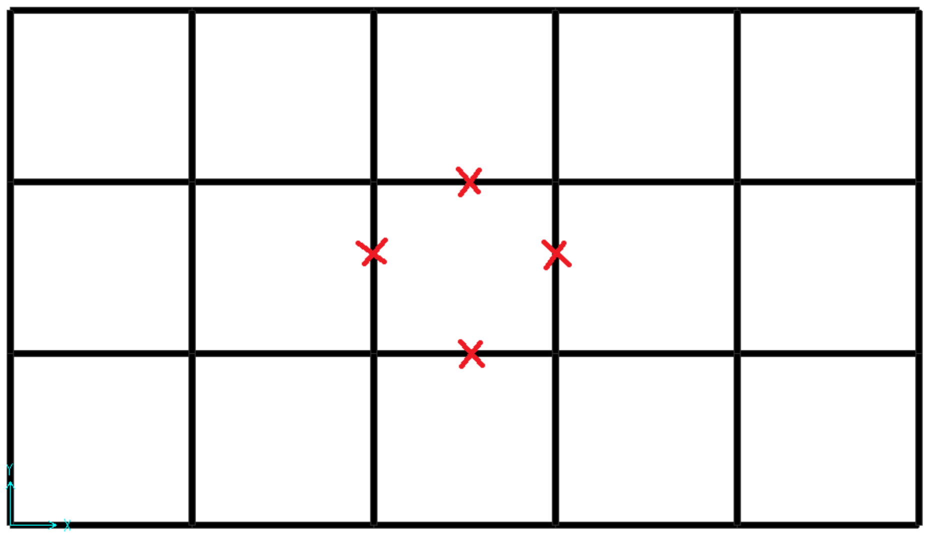


b)

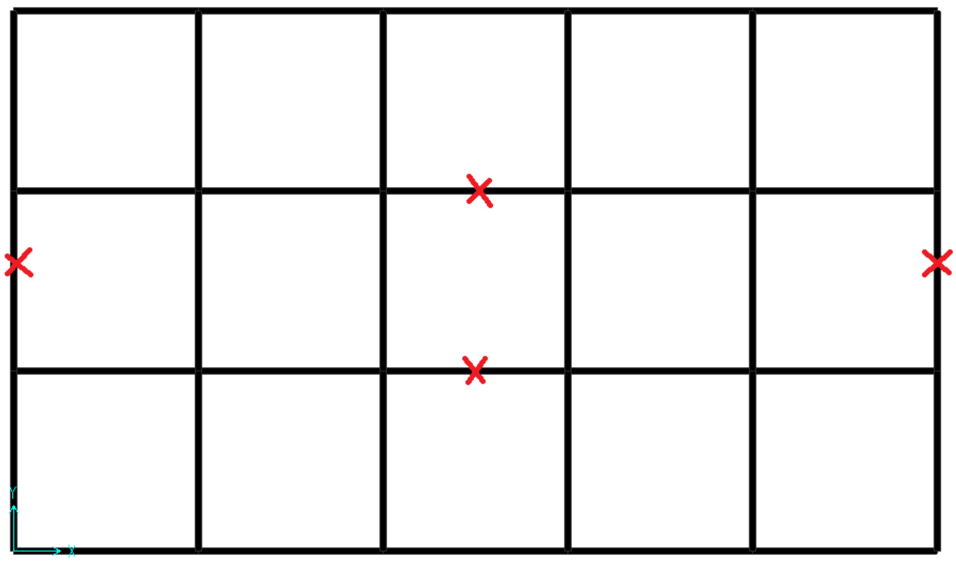
Fig 4.26 6BRBF Bracing frames a) bracing location for X-frame b) bracing location for Y-frame

4.2.2 Twenty storey BRBF system

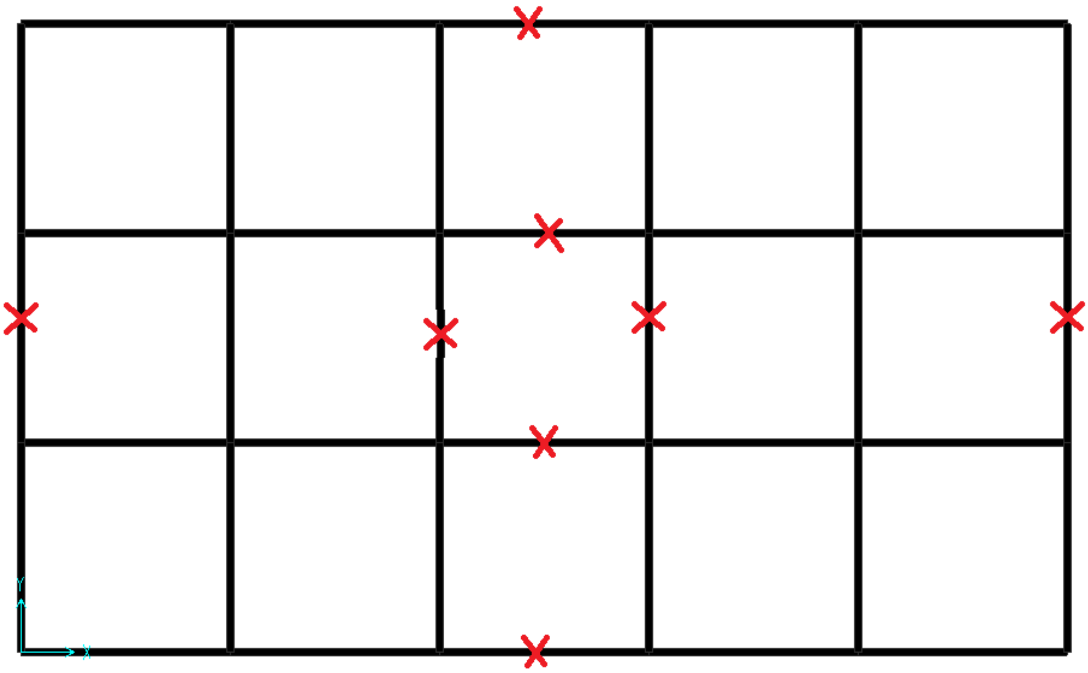
Three models with different bracing location were taken for this system, the adopted building designation for this system is 20BRBF csx csy, where the characters x, y c, and s are as defined in the previous section, these four cases and their notation are shown in Fig 4.27, while fig 4.28 show the bracing frame in x and y direction.



a)

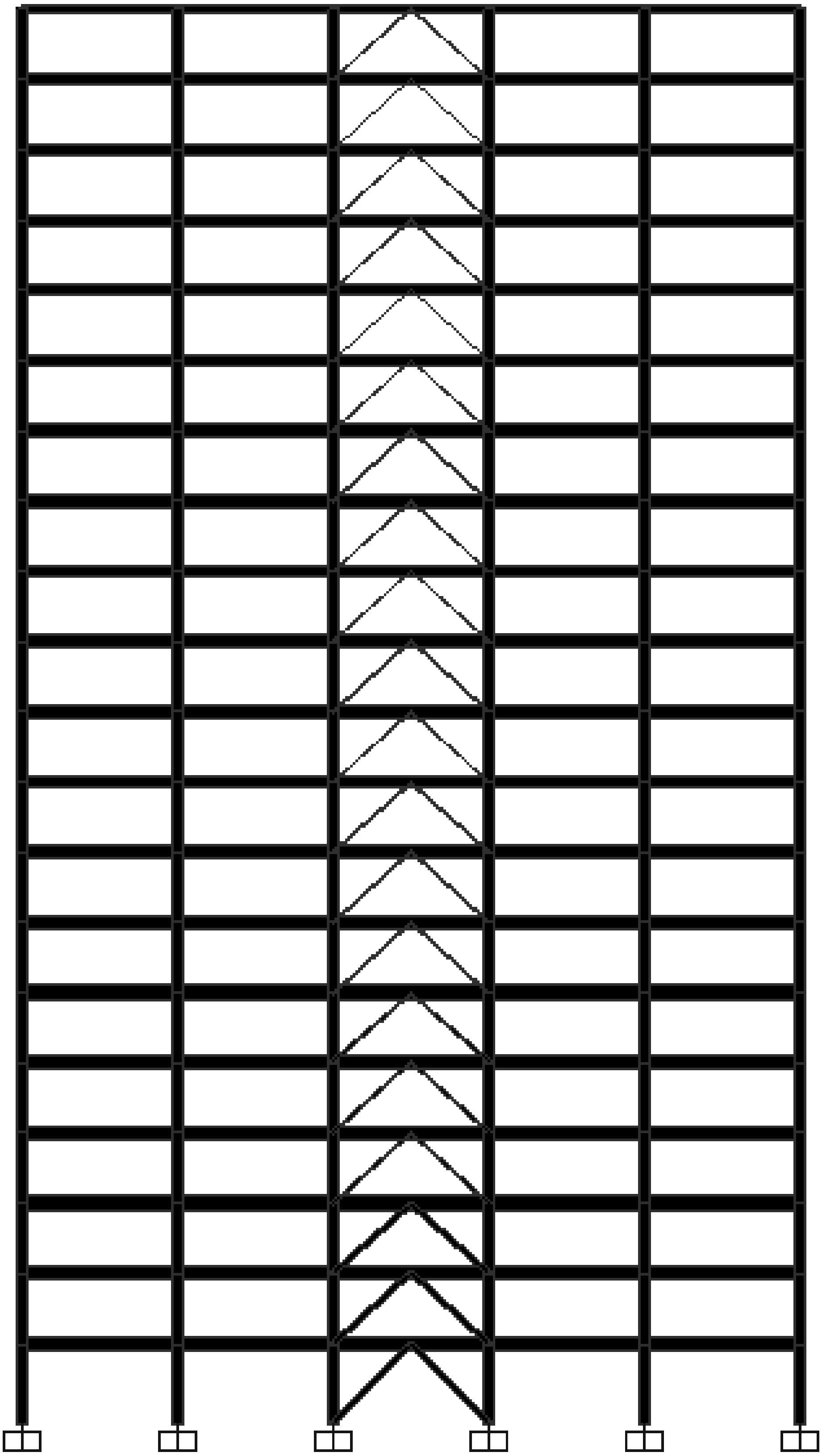


b)

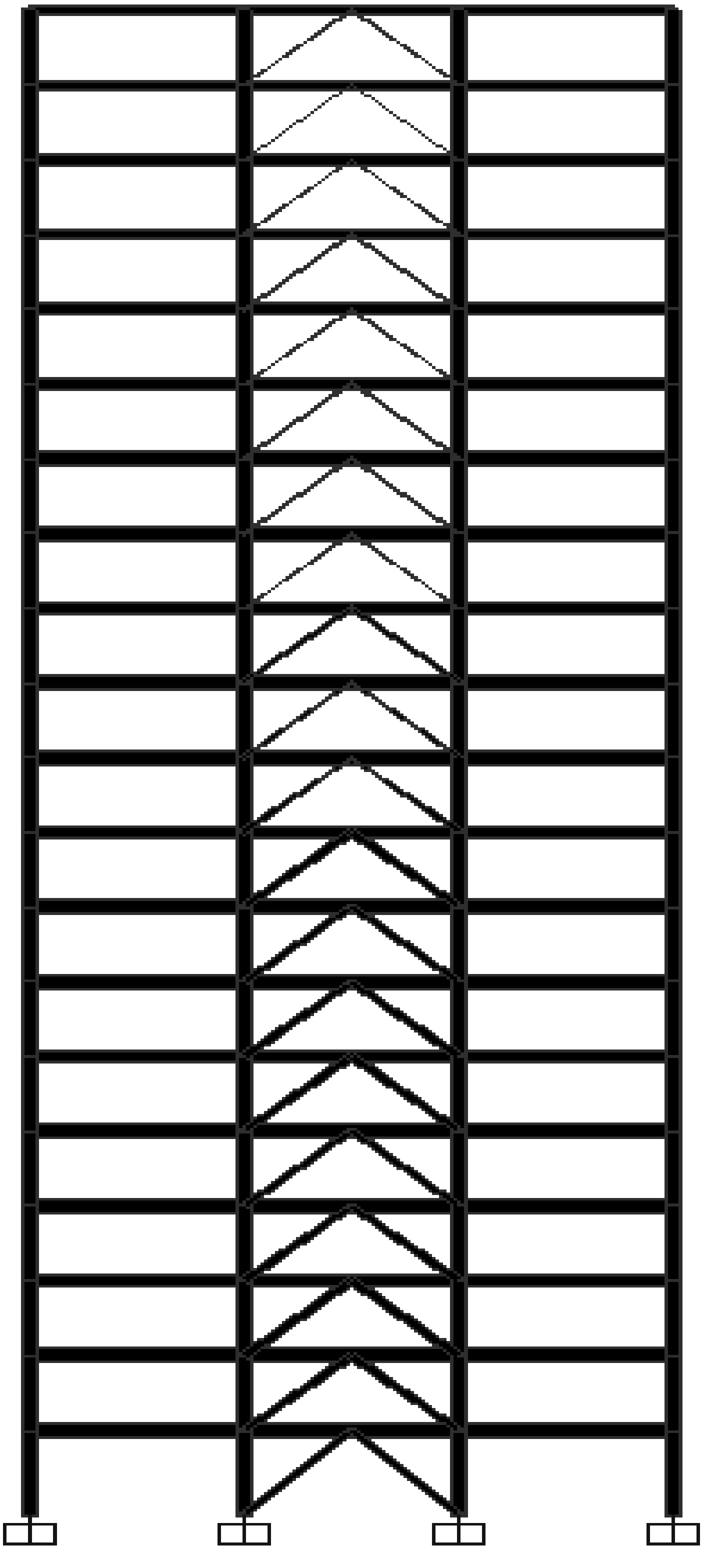


c)

Fig 4.27 two 20-storey BRBF model a) 20BRBF cx cy b) 20BRBF cx sy c) 20BRBF csx csy



a)



b)

4.28 20-storey bracing frames a) bracing location for X-frame b) bracing location for Y-frame

4.3 EBF Systems:

Members sections for this system are presented in table 4.1 and 4.2 for six and twenty storey building respectively, as for previous systems beams and columns are assumed to yield in flexure only, therefore flexural hinges are defined at the end of each beam and column, these hinges are defined according to table 3.1, the value of the hinge rotation, the acceptance criteria, and strain hardening ratio for beams and columns in each storey in both six and twenty storey EBF systems are presented in table 4.6. As the name of this system implies the bracing members are eccentric, and will not meet in the same point on the beam as in the BRBF system, the element between the bracing is called link, this link should designed to be the weakest element in the building and thus act like fuses in the building, the yielding behavior of the link will depend on its length as discussed before in sec3.1.2, other element outside the link should remain elastic during seismic excitation, therefore any yielding outside the link should be prevented.

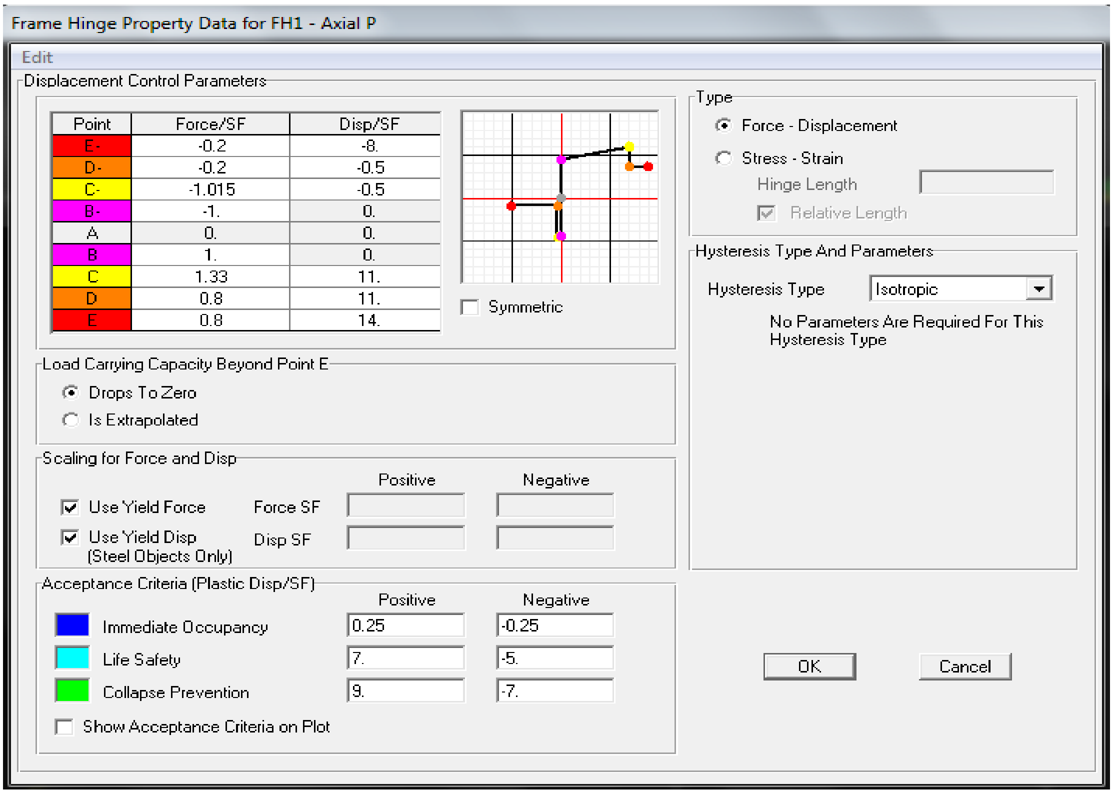
Beam-bracing connections are assumed to be fixed, so that bracing members can yield either in axial or in flexure, therefore yielding behavior of bracing members was presented by define two type of hinges at the end of each bracing member, the first hinge is flexural hinge defined according to table 3.1 in which bracing members will be treated as a column member. The second hinge is axial hinge, unlike the axial hinges that defined for BRBF bracing members, for this hinge the tension side will be different from the compression side, this is because compression buckling is not prevented in EBF bracing members like in BRBF bracing members. These axial hinges were defined according to table 3.1 for bracing in tension for tension side and bracing in compression for compression side, these parameters shown in table 4.10 with the strain hardening ratio, also fig 4.29 shows EBF bracing axial hinge as defined in sap 2000.

In this study, the shear link length (e) is taken smaller than $1.6M_p/V_y$, so that the link will yield in shear only according to (AISC seismic provision 2005), for this reason the nonlinear behavior of the shear link is presented by define a shear hinge at the two end of the shear link, these shear hinges were defined according to table 3.1, the value of the plastic deformation, the acceptance criteria, and strain hardening ratio for EBF links in both directions are as shown in table 4.10, while fig 4.30 show shear plastic hinge as defined in sap 2000 for shear link in storey 1-2x.

Table 4.10 hinge parameter for shear link, bracing in tension, and bracing in compression

Component	Modeling Parameter			Acceptance Criteria			Strain hardening ration
	Plastic deformation		Residual Strength Ratio	Plastic deformation			
	a	b	c	IO	LS	CP	
Shear Link	0.15	0.17	0.8	0.005	0.11	0.14	1.25
Braces in Tension	$11\Delta_T$	$14\Delta_T$	0.8	$0.25\Delta_T$	$7\Delta_T$	$9\Delta_T$	1.33
Braces in compression	$0.5\Delta_c$	$8\Delta_c$	0.2	$0.25\Delta_c$	$5\Delta_c$	$7\Delta_c$	1.015

.


Frame Hinge Property Data for FH1 - Axial P

Edit

Displacement Control Parameters

Point	Force/SF	Disp/SF
E-	-0.2	-8.
D-	-0.2	-0.5
C-	-1.015	-0.5
B-	-1.	0.
A	0.	0.
B	1.	0.
C	1.33	11.
D	0.8	11.
E	0.8	14.

Symmetric

Type: Force - Displacement; Stress - Strain; Hinge Length; Relative Length

Hysteresis Type And Parameters: Hysteresis Type: Isotropic. No Parameters Are Required For This Hysteresis Type

Load Carrying Capacity Beyond Point E: Drops To Zero; Is Extrapolated

Scaling for Force and Disp (Positive / Negative): Use Yield Force, Force SF; Use Yield Disp (Steel Objects Only), Disp SF

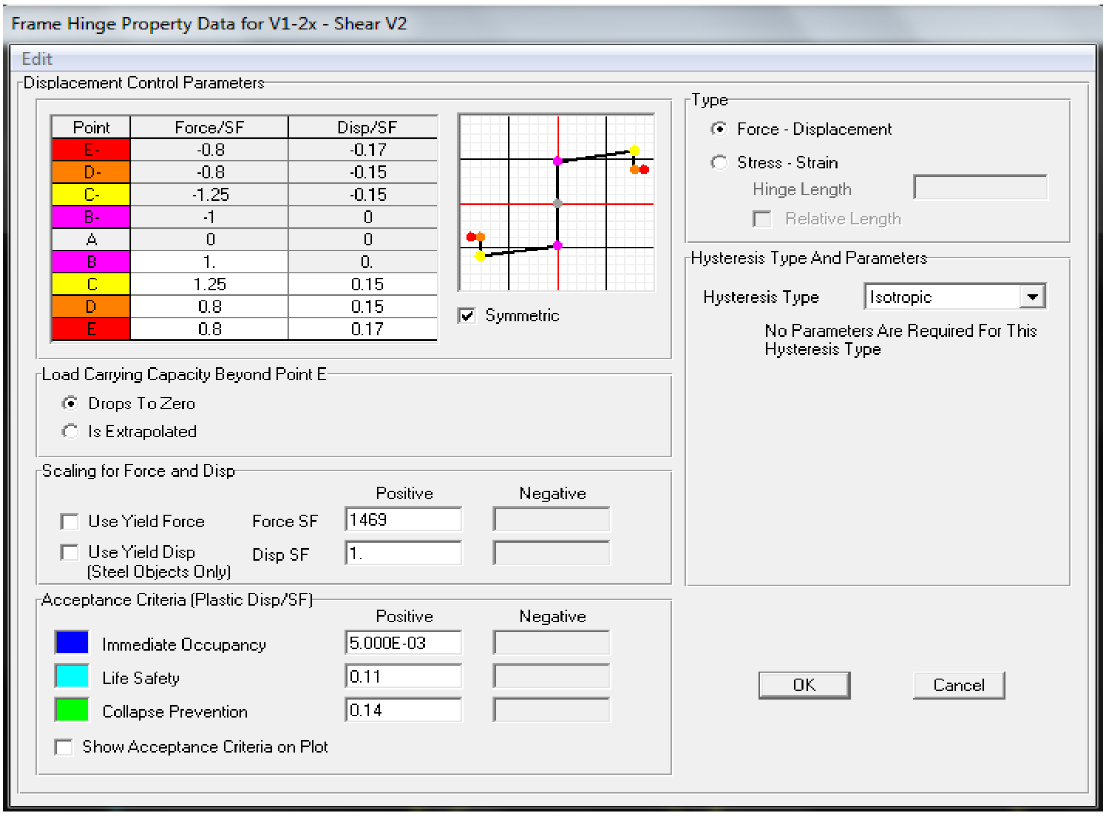
Acceptance Criteria (Plastic Disp/SF)

	Positive	Negative
Immediate Occupancy	0.25	-0.25
Life Safety	7.	-5.
Collapse Prevention	9.	-7.

Show Acceptance Criteria on Plot

OK Cancel

4.29 axial hinge curve for EBF bracing members defined in sap 2000


Frame Hinge Property Data for V1-2x - Shear V2

Edit

Displacement Control Parameters

Point	Force/SF	Disp/SF
E-	-0.8	-0.17
D-	-0.8	-0.15
C-	-1.25	-0.15
B-	-1	0
A	0	0
B	1.	0.
C	1.25	0.15
D	0.8	0.15
E	0.8	0.17

Symmetric

Type: Force - Displacement; Stress - Strain; Hinge Length; Relative Length

Hysteresis Type And Parameters: Hysteresis Type: Isotropic. No Parameters Are Required For This Hysteresis Type

Load Carrying Capacity Beyond Point E: Drops To Zero; Is Extrapolated

Scaling for Force and Disp

		Positive	Negative
Use Yield Force	Force SF	1469	
Use Yield Disp (Steel Objects Only)	Disp SF	1.	

Acceptance Criteria (Plastic Disp/SF)

	Positive	Negative
Immediate Occupancy	5.000E-03	
Life Safety	0.11	
Collapse Prevention	0.14	

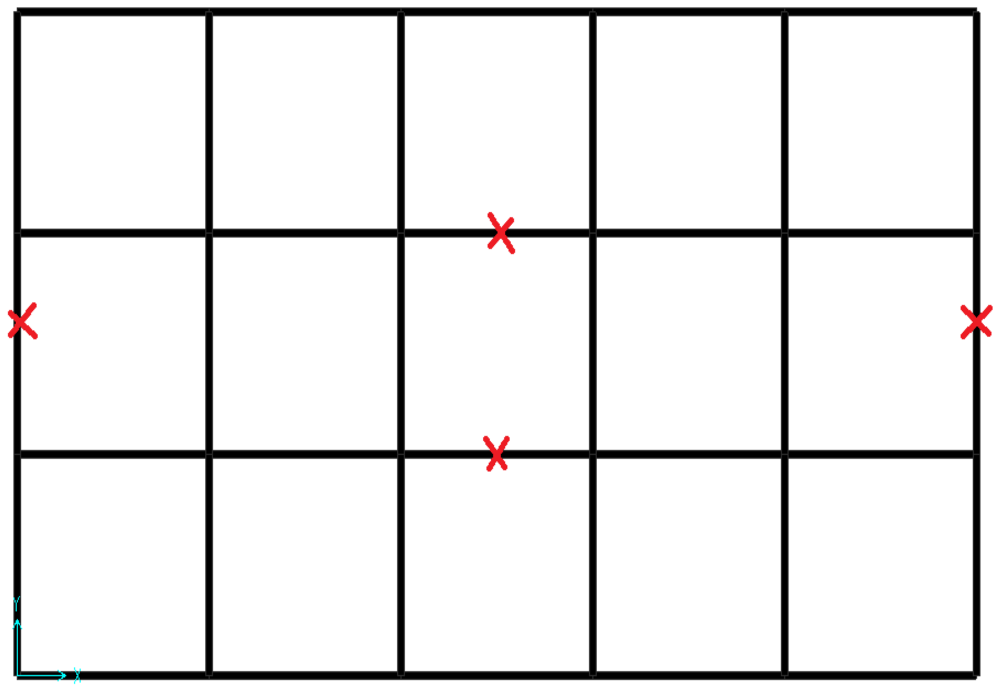
Show Acceptance Criteria on Plot

OK Cancel

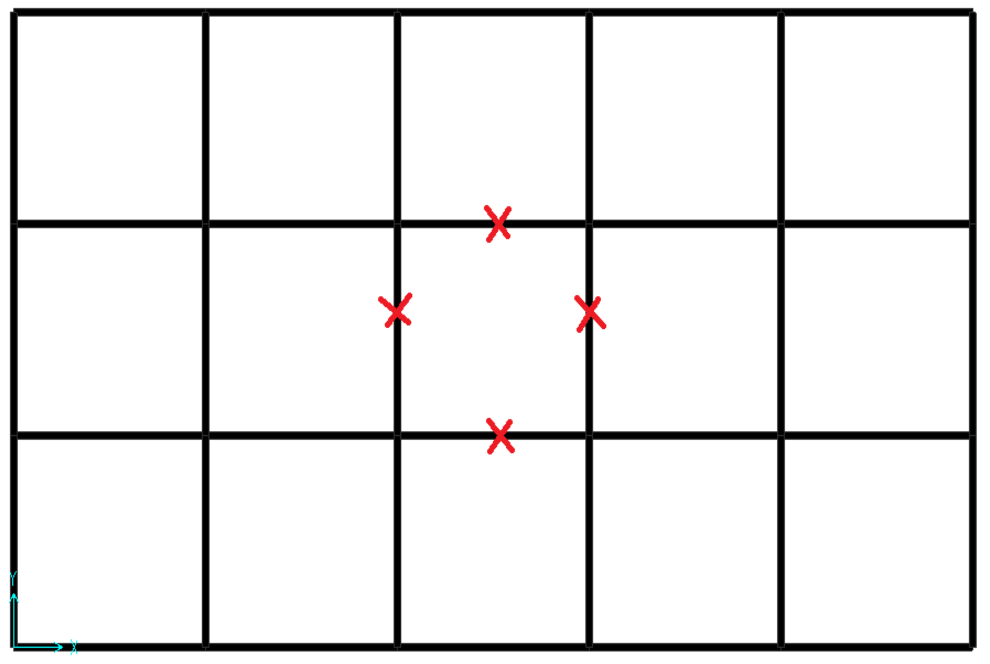
Fig 4.30 hinge properties as defined in sap 2000 for shear link in story 1-2x

4.3.1 6-storey EBF systems

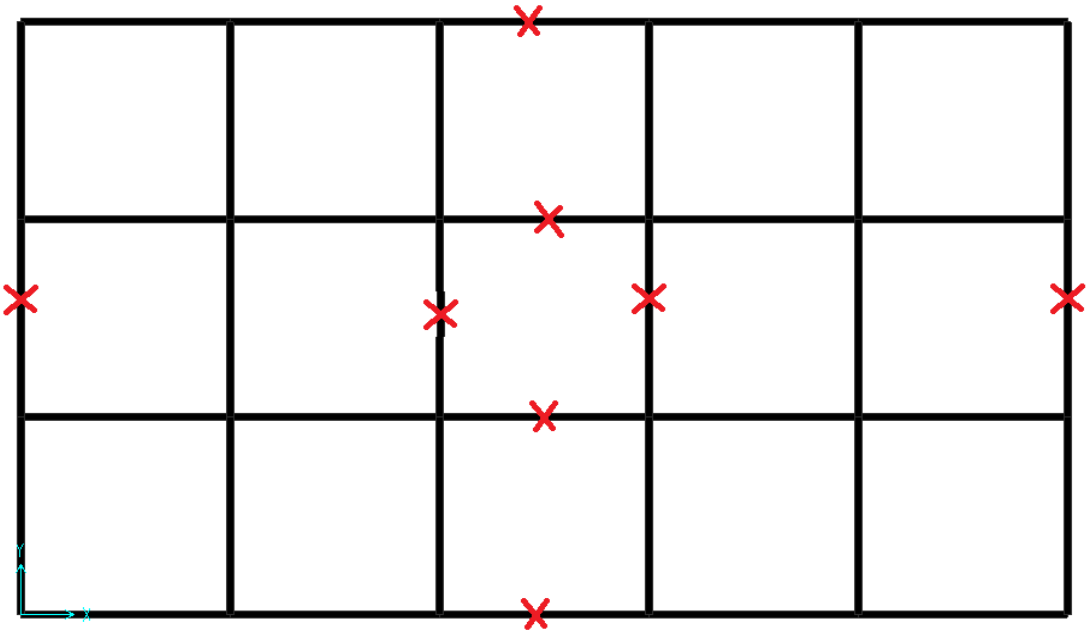
Four building with different bracing location were modeled to evaluate the seismic performance of this system, two of these four building have different link length to present the effect of the link length on the behavior of the 6- storey EBF system, the adopted building designation for these modeling is (6EBF cscox cscoy), where the characters x and y indicate that bracing exist in x-frame and y-frame respectively, also c, s and co (which means core, side, and corner respectively) indicate the location of bracing in the x or y frame, the absence of any of these three character means that bracing members are not exist at its location. For example (6EBF cscox cscoy) means that the building is braced at its core, and at its external side in the middle span of x and y frames and at the external corner of x and y frame, while (6EBF cx cy) indicates that the building is braced at its core only, these modeled buildings and their corresponding notation are shown in fig 4.31, also the value of max length of shear link to yield in shear $\left(e_{\max} \leq 1.6 M_p / V_y\right)$, the selected shear link length used in this study, and yield shear force at each storey level in the four modeled building are presented in table 4.11.



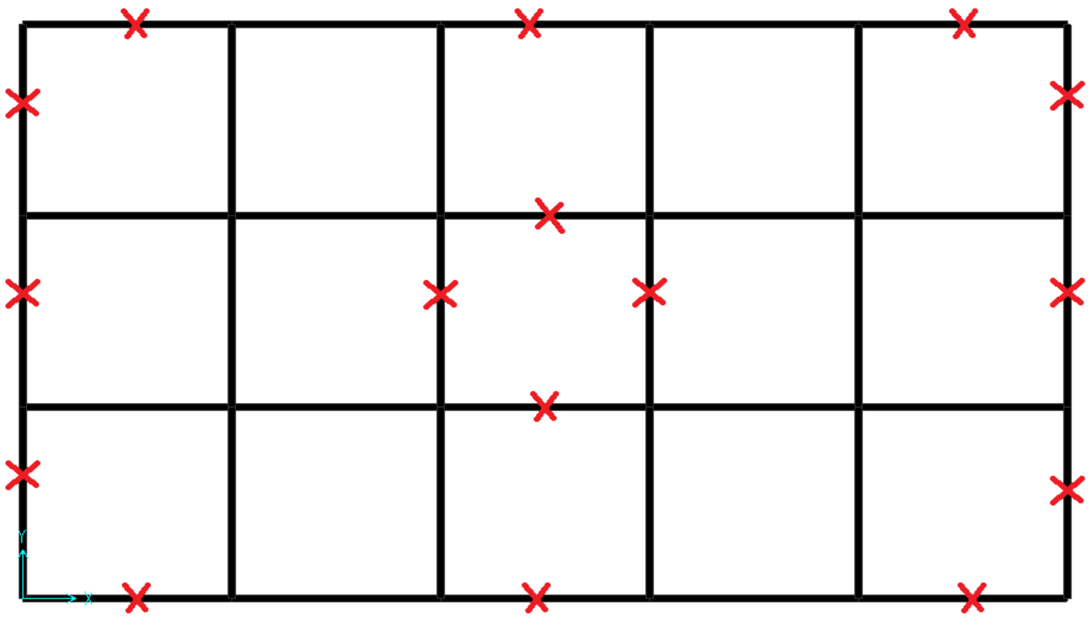
a)



b)



c)



d)

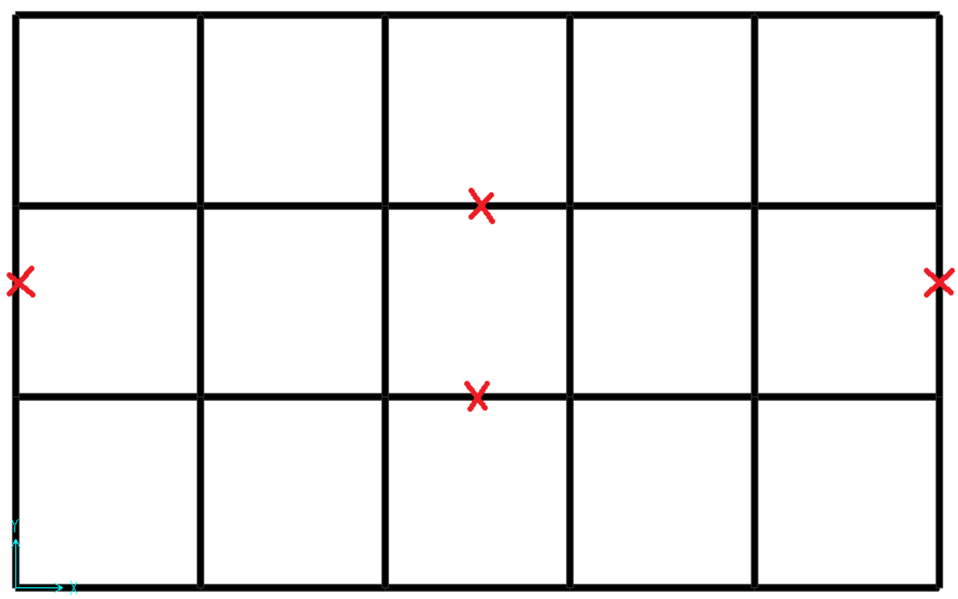
Fig 4.31 6-storey EBF models a) 6EBF sx cy b) 6EBF cx cy c) 6EBF csx csy d) 6EBFcscox cscoy

Table 4.11 yield shear force, link max length to yield in shear (e_{max}), and used length for different for 6-storey EBF systems

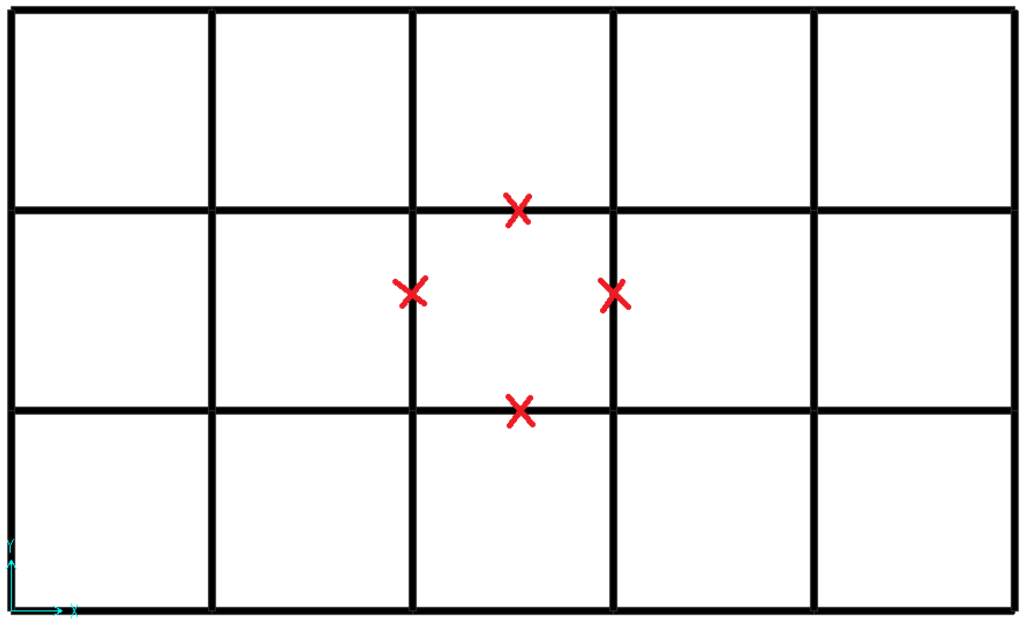
Storey	Yield shear force (KN)	$1.6M_p$ $/V_y$ (m)	6EBF sx cy	6EBF 1 cx cy	6EBF 2 cx cy	6EBF1 csx csy	6EBF 2 csx csy	6EBF 3 csx csy	6EBF cscox cscoy
1-2x	1469	1.53	1.25	1.25	1.25	1.25	1.25	1.0	1.25
1-2y	1469	1.53	1.25	1.4	1.25	1.4	1.25	1.0	1.25
3-4x	1110	1.66	1.4	1.4	1.4	1.4	1.4	1.0	1.4
3-4y	1110	1.42	1.4	1.25	1.4	1.25	1.4	1.0	1.4
5-6x	1110	1.66	1.4	1.4	1.4	1.4	1.4	1.0	1.4
5-6y	1110.	1.42	1.4	1.25	1.4	1.25	1.4	1.0	1.4

4.3.2 20-storey EBF systems

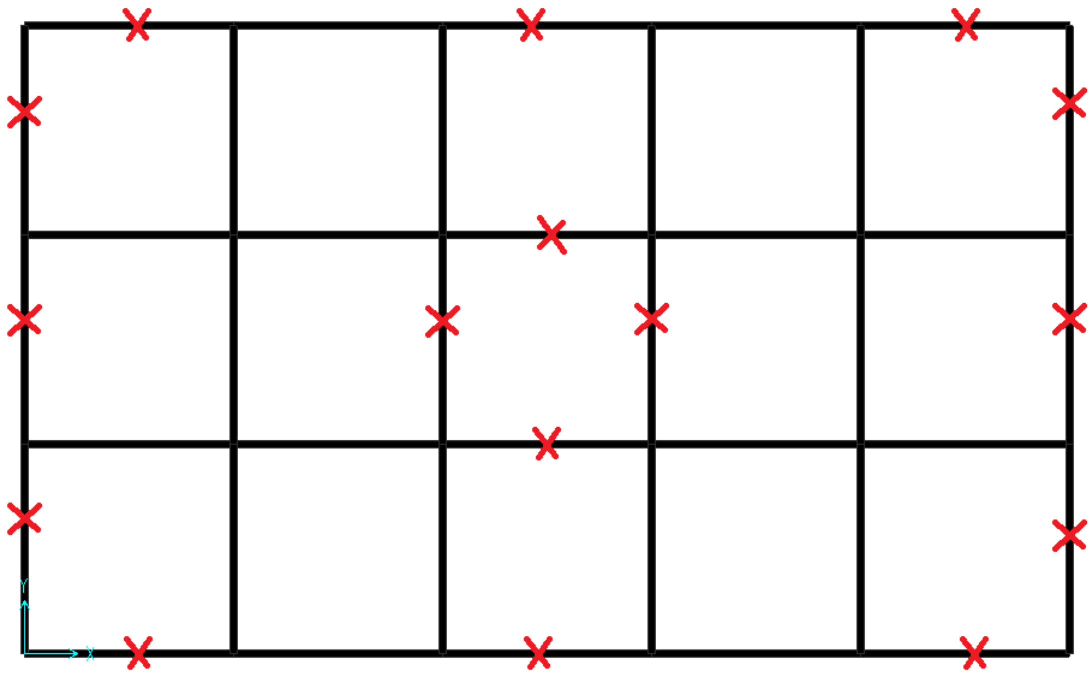
Three buildings with different bracing location were modeled to evaluate the seismic performance of this system, one of these three buildings has different link length to present the effect of the link length on the behavior of the 20-storey EBF systems, the adopted building designation for these modeling is (20EBF cscox cscoy), where the characters x, y c, s and co are defined in Sec 4.5.1, For example (20EBF cscox cscoy) means that the building is braced at its core, and at its external side in the middle span of x and y frames and at the external corner of x and y frame, while (20EBF cx cy) indicates that the building is braced at its core only, these modeled buildings and their corresponding notation are shown in fig 4.32, also the value of max length of shear link to yield in shear $\left(e_{\max} \leq 1.6 M_p / V_y\right)$, the selected shear link length used in this study, and yield shear force at each storey level in the three modeled building are presented in table 4.12.



a)



b)



d)

Fig 4.32 20-storey EBF models a) 20EBF sx cy b) 20EBF cx cy c) 20EBFcscox cscoy

Table 4.12 yield shear force, link max length to yield in shear (e_{max}), and used length for different 20-storey EBF systems

Storey	Yield shear force (KN)	$1.6M_p/V_y$ (m)	20EBF cx cy	20EBF1 cx sy	20EBF2 cx sy	20EBF 3 cx sy	20EBF cscox cscoy
1-3x	2339	1.80	1.55	1.55	1.0	1.8	1.55
1-3y	1893	1.96	1.7	1.7	1.0	1.9	1.7
4-6x	2339	1.80	1.55	1.55	1.0	1.8	1.55
4-6y	1893	1.9	1.7	1.7	1.0	1.9	1.7
7-9x	2184	2.00	1.7	1.7	1.0	2	1.7
7-9y	1893	1.96	1.7	1.7	1.0	1.9	1.7
10-12x	2184	2.	1.7	1.7	1.0	2	1.7
10-12y	1893	1.966	1.7	1.7	1.0	1.9	1.7
13-15x	1893	1.966	1.7	1.7	1.0	1.9	1.7
13-15y	1893	1.703	1.5	1.5	1.0	1.7	1.5
16-18x	1707	1.750	1.5	1.5	1.0	1.7	1.5
16-18y	1469.014	1.533	1.25	1.25	1.0	1.5	1.25
19-20x	1469	1.747	1.5	1.5	1.0	1.7	1.5
19-20y	1110	1.428	1.25	1.25	1.0	1.4	1.25

Chapter 5

Analysis Result

The four systems (FRMRF, PRMRF, BRBF, and EBF systems) introduced in chapter 4 are subjected to a series of nonlinear static pushover analysis, and nonlinear time-history analysis, in effort to evaluate their seismic performance, and to introduce PRMRF system with better ductility, energy dissipation capacity, and acceptable self centering capacity compared to the other three systems.

These four systems was subjected first to tabas earthquake to evaluate their performance under strong earthquake excitation, properties that obtained from this analysis are self centering capacity, ductility demand, storey-drift ratio, frequencies and periods of the modeled systems, and the plastic hinge formation pattern, these systems are next subjected to a cyclic time history load (sine function for the 6-storey buildings and cosine function for the 20-storey buildings) hysteresis behavior and energy dissipation capacity for the different systems are obtained from this analysis, finally, these systems are subjected to nonlinear static pushover analysis to obtain their capacity, systems that appears to have desirable properties at the end of these analysis process are subjected to Northridge earthquake, to evaluate their seismic performance under different ground shaking. All the analysis result for PRMRF, BRBF, and EBF systems are compared to that of FRMRF system. As mentioned before energy dissipation capacity, self centering capacity, capacity-demand ductility ratio, inter-storey drift ratio, force distribution in the systems members, and plastic hinge formation pattern for the different systems, will be used to evaluate the seismic performance of the modeled systems.

5.1 Hysteresis Behaviour and Energy dissipation capacity

In this study the hysteresis behavior for the different modeled buildings are obtained by applying nonlinear time history analysis using cyclic sine function load for the 6-storey buildings and cyclic cosine function load for the 20-storey buildings, these two functions are defined in chapter 3. However, the base shear and the top storey displacement result from this analysis are drawn against each other, where the base shear is drawn on the y-axis, and the top storey displacement drawn on the x-axis. The resultant drawing present the hysteresis loop of the building and the total area under these loops will present the dissipated energy by the structure.

In this study the area under the hysteresis loops are computed by program that has been created by the author for this purpose, the program is written on excel 2007, and has input capacity as the capacity for excel 2007, this program contain two sheet: the first sheet is the user sheet and the second sheet is the calculation sheet (invisible from the user), the user sheet contain base shear and top storey displacement values, and the value of the total area (energy dissipation by the structure), in this program the total area under each cycle is divided to sub-areas between two successive points to rectangle and triangle and then the total area is the sum of all subareas between all points, this method is clarified in fig 5.1, which present hysteresis loop behavior for one of the modeled buildings, in this figure the area is divided to rectangle and triangle between three points just to clarify the idea, but in the generated program the area is divided between all points to rectangles and triangles and then the total area (which is the sum of all these subareas) will present the energy dissipated by the structure , as can be seen in fig 5.1, each loop is presented by large number of points with small interval between these points, therefore the result that obtained by this method will be accurate with small percentage of error. However, the accuracy of the program is verified by computing the

area under simple hysteresis loop with known dissipated energy value, presented in (Nazzal, 2000) this hysteresis loop is shown in fig 5.2, and the computed area by the program was exactly the same as computed by (Nazzal, 2000).

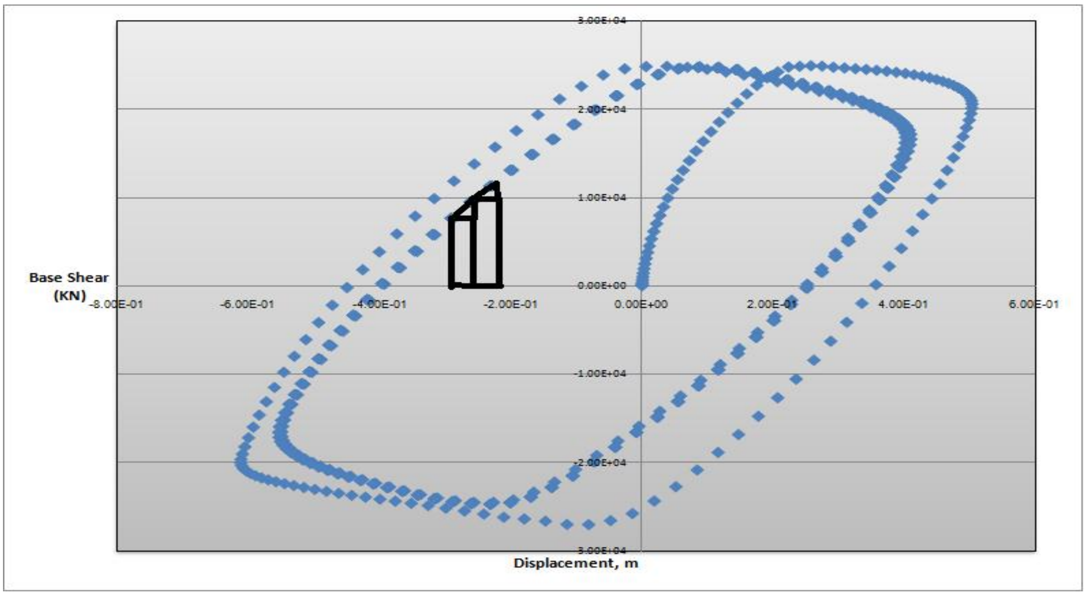


Fig 5.1 the method to compute the area under the hysteresis loop

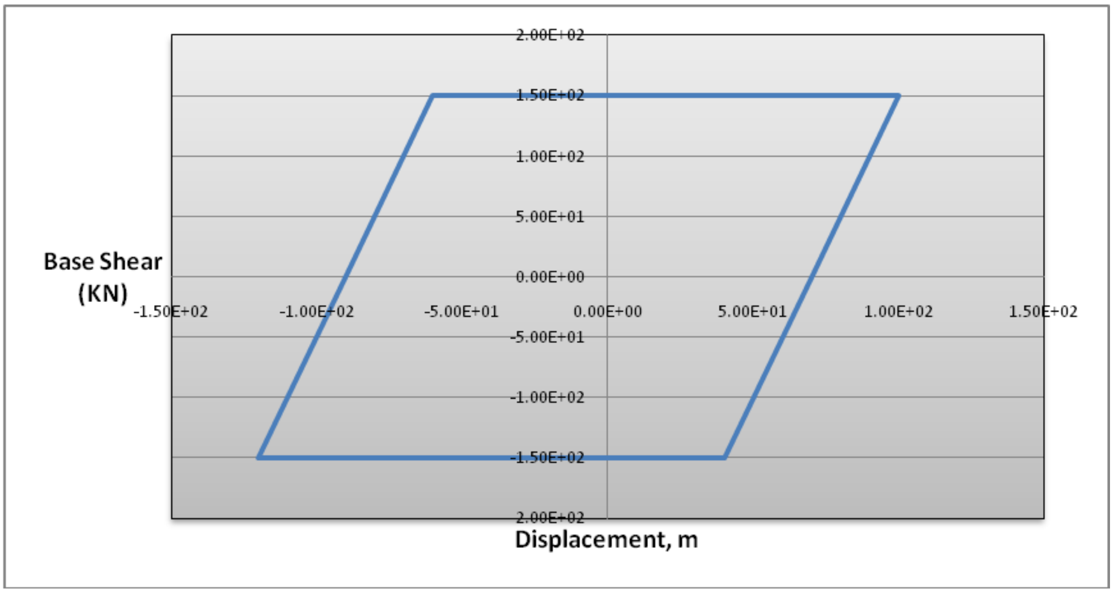


Fig 5.2 hysteresis loop used to verify the created program accuracy

5.1.1 6-storey systems

Hysteresis behavior for the four 6-storey systems are shown in appendix A, also the amount of energy dissipated by PRMRF, BRBF, and EBF systems as a ratio of the dissipated energy by the FRMRF system in both x and y directions are presented in table 5.1.

As can be seen from the table, PRMRF system has the highest energy dissipation capacity ratio compared to the other two systems (BRBF and EBF systems), while EBF system has the lowest energy dissipation ratio, and the BRBF system has ratios between these two systems, the reason of this behavior is that the EBF system is very rigid system, therefore this system will provide a very small top displacement compared to the other systems, and thus low energy dissipation capacity.

This behavior can be seen also from the hysteresis loop of these systems presented in appendix A, in which figure A18 through figure A23 show that the top displacement for 6EBF system has a range (0.015-0.15m), while figure A1 to figure A15 show that the top displacement for 6FRMRF and 6PRMRF systems exceed 0.4m, also figure A16 and figure A17 show that the top displacement for 6BRBF system has a range (0.2-0.3m), therefore the top displacement for FRMRF and PRMRF system exceed 3 times the top displacement for 6EBF system and 1.5 times the top displacement for 6BRBF system.

Also it should be remember that both BRBF and EBF systems are dissipate energy by yielding of the buckling restrained bracing and the yielding of the shear link respectively, so they don’t need to go through high displacement to dissipate energy as the case for FRMRF and PRMRF systems.

Energy dissipation values in table 5.1 for the PRMRF system indicate that the higher dissipated energy ratio occurred by 6SR45, 6SR56, and 6SR456 systems, as can be seen from the table these three systems have energy dissipated ratios more than one which

means that these system dissipate energy more than FRMRF system, also it can be seen that 6SR45 has the highest dissipate energy in the x-direction, while 6SR 456 has the highest dissipated energy in the y-direction. Also 6SR34 and 6SR345 have energy dissipation ratios higher than one in the x-direction and almost one in the y-direction; the other partially restrained systems have low energy dissipation capacity.

also as shown in chapter 4 frames in the x-direction are stiffer than frames in the y-direction, and by comparing the energy dissipation ratios for both frames, it can be seen that frames in the x-direction have higher energy dissipation ratio than frames in the y-direction, therefore it can be concluded that placing semi-rigid connection in stiff frame can give higher dissipated energy than from placing semi-rigid connection in low-stiffness frame.

In summary, placing semi-rigid connection in the 6PRMRF system can be controlled by the frame stiffness, in which placing semi-rigid connection at the middle or at the top of frames in the x-direction which is stiff frame and at the top of frames in y-direction which is low-stiffness frame can improve the energy dissipation capacity of that frames, while placing semi-rigid connection at first floors in the stiff frames and at the middle or at the first floors in the low-stiff frames will adversely affect the energy dissipated capacity of that frame, however, both 6SR45 and 6SR456 case has high energy dissipating capacity in both directions comparing to other 6PRMRF cases.

Table 5.1 energy dissipation capacity for 6-storey systems compared to 6FRMRF

system	Energy Dissipation Capacity Ratio	
	X-Direction	Y-Direction
6SR45	1.119293	1.049734
6SR34	1.025037	0.957371
6SR23	0.893962	0.779751
6SR1346	0.932253	0.865009
6SR all	0.765832	0.687389
6SR12	0.786451	0.701599
6SR56	1.10162	1.044405
6SR246	0.955817	0.852575
6SR135	0.89838	0.809947
6SR235	0.849779	0.78508
6SR234	0.87187	0.82238
6SR456	1.132548	1.080266
6SR345	1.036819	0.968313
6SR346	1.032401	0.967407
6BRBF cx cy	0.726068	0.927176
6BRBF cx sy	0.723122	0.854352
6EBF cx sy	0.412371	0.21492
6EBF1 cx cy	0.259205	0.216696
6EBF2 cx cy	0.259205	0.342806
6EBF cscox cscoy	0.022091	0.023623
6EBF1 csx csy	0.038586	0.057016
6EBF2 csx csy	0.117378	0.15968
6EBF3 csx csy	0.050663	0.067673

5.1.2 20-storey system

Hysteresis behavior for the four 20-storey systems are shown in appendix B, also the amount of energy dissipated by PRMRF, BRBF, and EBF systems as a ratio of the dissipated energy by the FRMRF system in both x and y directions are presented in table 5.2.

As can be seen from the table, and as for 6-storey system, PRMRF system has the highest energy dissipation capacity ratio compared to the other two systems (BRBF and EBF systems), while both 20BRBF and 20EBF systems have the lowest energy dissipation ratio, with approximate equal ratios, the same conclusion for 6-storey systems can be applied to these three system, in which both EBF and BRBF systems is very rigid system, and therefore they will provide a very small top displacement compared to the FRMRF and PRMRF systems, and thus low energy dissipation capacity.

Also as for 6-storey frame this behavior of 20-storeys system can be seen from the hysteresis loop of these systems presented in appendix B, in which figure B6 through figure B12 show that the top displacement for 20EBF and 20BRBF systems doesn’t exceed 0.25m, while figure B1 to figure B5 show that the top displacement for 20FRMRF and 20PRMRF systems exceed 0.9m for the most 20-storey hybrid buildings, therefore the top displacement for FRMRF and PRMRF system exceed 3 times the top displacement for both the 20EBF and 20BRBF systems.

Also as for the 6-storey buildings, the reason for the low top displacement value for both BRBF and EBF systems is that these two systems dissipate energy by the yielding of the buckling restrained bracing and the yielding of the shear link respectively, so they don’t need to go through high displacement to dissipate energy as the case for FRMRF and PRMRF systems.

Energy dissipation values in table 5.2 for the PRMRF system indicate that all the 20-storey partially restrained buildings have energy dissipation ratios bigger than one, which mean that all these building dissipate energy more than the 20FRMRF system, however, 20SR13-18 system has the highest energy dissipation ratio for both directions. Considering these results it can be conclude that placing semi-rigid connection in the 20-storey buildings improve its energy dissipation capacity regardless of the location of these connections, however, 20SR13-18 case has the highest energy dissipation capacity among all 20PRMRF cases, also at the contrary of the 6-storey buildings, for 20-storey buildings frames in y-direction provide higher energy dissipation ratio than frames in the x-direction.

Table 5.2 energy dissipation capacity for 20-storey system compared to 20FRMRF

system	Energy Dissipation Capacity Ratio	
	X-Direction	y-Direction
20SR8-13	1.207675	1.284031
20SR1-6	1.230248	1.082461
20SR4-9	1.128668	1.240838
20SR13-18	1.275395	1.387435
20BRBF cx cy	0.537246	0.513089
20BRBF cx sy	0.537246	0.514398
20BRBF csx csy	0.586907	0.918848
20EBF cx cy	0.792	0.549
20EBF1 cx sy	0.565	0.525
20EBF2 cx sy	0.626	0.551
20EBF3 cx sy	0.786	0.546

5.2 Self-Centring Capacity

Building self-centering capacity mean the ability of the building to return to its original position (zero top displacement) at the end of earthquake excitation, however, if building doesn’t have this property it's become important to do $P-\Delta$ analysis for large top displacement, to make sure that the building is stable and will not collapse.

5.2.1 6-storey systems

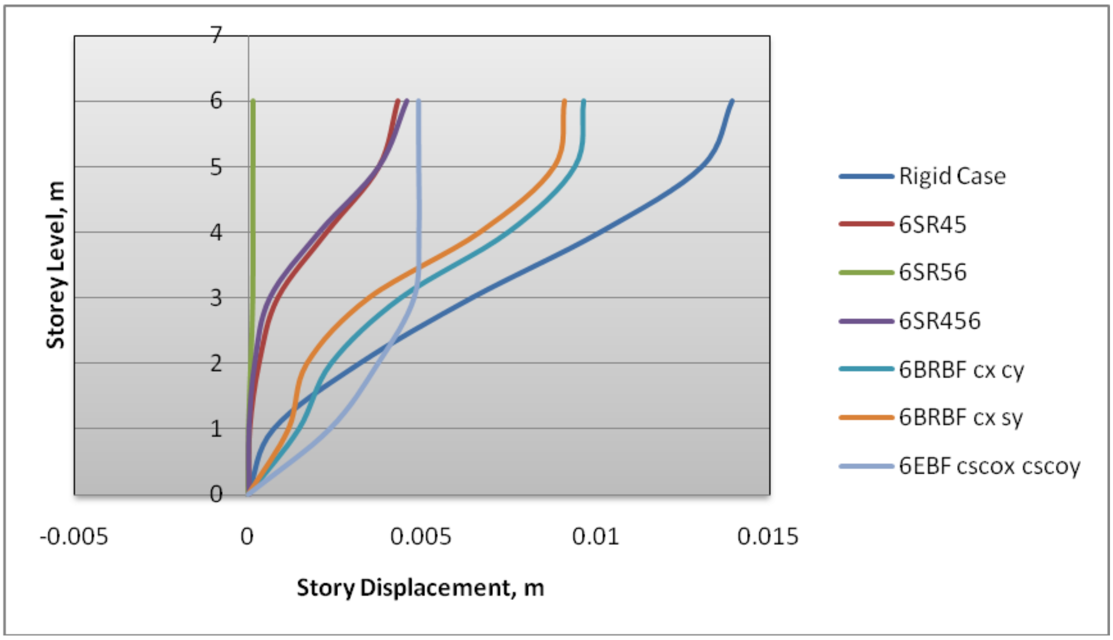
Top displacements for these systems are presented in table 5.3, while the top displacement time-history relations are presented in appendix C. As can be seen from fig C1 6FRMRF system doesn’t have self-centering capacity in both directions, however, top displacement values in table 5.3 for this frame is small and doesn’t requires $P-\Delta$ analysis.

For PRMRF system the top displacement value in table 5.3 and displacement time-history relation in appendix c show that FRMRF system doesn’t have self-centering capacity in both direction, while placing semi-rigid connection can improve its self-centering capacity, in which placing semi-rigid connection at the last three floors can provide self-cantering capacity for frames in x-direction, while placing semi-rigid connection at first floors will provide self-cantering capacity for frames in y-direction, except for 6SR12 system, applying this rule it can be seen that 6SR45, 6SR56, 6SR456 systems have self centering capacity in for frames in x-direction, and 6SR23, 6SR234, 6SR135, 6SR246, 6SR235 systems have self centering capacity for frames in y-direction. However, it should be remember that building with semi-rigid connection placed at the first floors will adversely affect the energy dissipation capacity of that building, therefore only 6SR45, 6SR56, 6SR456 systems which have self-centering capacity in x-direction will be discussed, these three systems have also the highest energy dissipation capacity as discussed in sec 5.1.1, however, 6SR56 system have

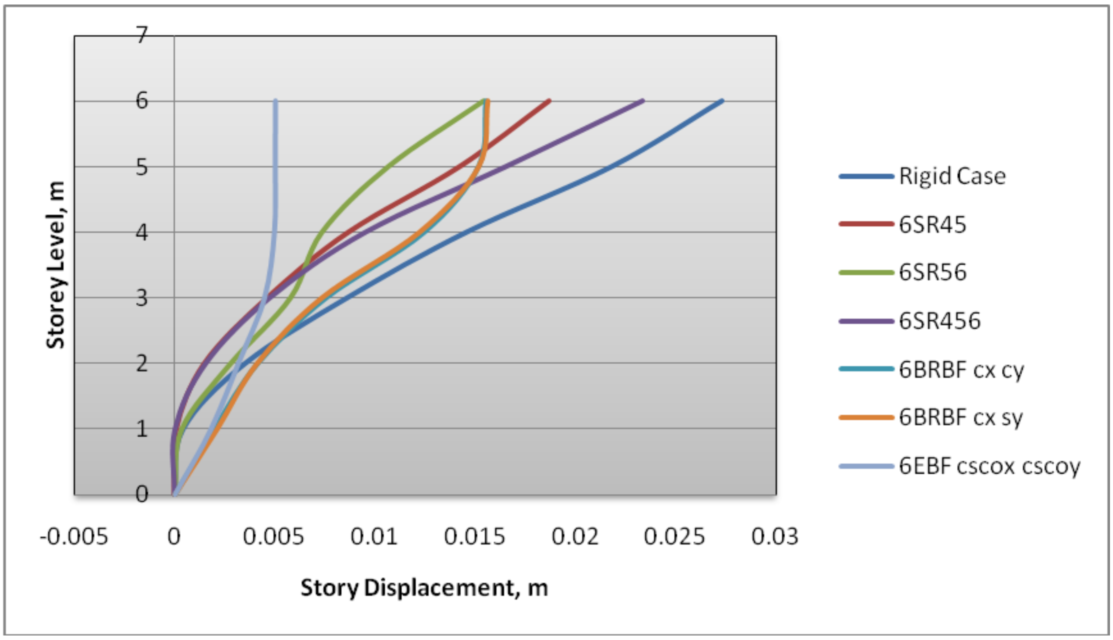
lowest value of top displacement in the x-direction compared to all partially restrained system, and also has the lowest top displacement value in the y-direction compared to 6SR45, and 6SR456 systems, also 6SR45 frame have lower top displacement values in both x and y directions than the 6SR456 building.

Also values in table 5.3 show that the two 6BRBF systems have self-centering capacity in the x-direction only, while 6EBF cscox cscoy system provide self-centering capacity in both directions, this is because 6EBFcscox cscoy is very stiff, the other 6EBF system cases didn't present because they didn't survive tabas earthquake excitation.

Finally, storey displacement at storey level for 6SR45, 6SR56, 6SR456, 6BRBF cx cy, 6BRBF cx sy, and 6EBF cscox cscoy, in x and y directions are presented in fig 5.3, this figure shows that partially restrained building have better self-centering capacity than the braced systems in x-direction, with 6SR56 building show the best self-centering capacity among all modeled buildings, while for y-direction 6EBF cscox cscoy show the lowest storey displacement in the last three storey, while 6SR 45 show the lowest displacement in the first three storey.



a)



b)

Fig 5.3 Storey displacement at each storey level a) x-direction b)y-direction

Table 5.3 top displacement for 6-storey system

System	System Top displacement in X-direction (m)	System Top displacement in Y-direction (m)
Rigid Case	0.013915	0.027282
6SR45	0.004293	0.018645
6SR34	0.016909	0.012345
6SR23	0.023128	0.004781
6SR1346	0.021563	0.010387
6SR all	0.011618	0.011059
6SR12	0.016977	0.011826
6SR56	0.000122	0.015407
6SR246	0.015242	0.007984
6SR135	0.016116	0.008708
6SR235	0.022297	0.005567
6SR234	0.02527	0.004514
6SR456	0.004622	0.023501
6SR345	0.020557	0.018365
6SR346	0.017207	0.014733
6BRBF cx cy	0.009647	0.015542
6BRBF cx sy	0.009089	0.015588
6EBF cscox cscoy	0.004914	0.005019

5.2.2 20-storey systems

The top displacement time-history relations are presented in appendix D. As can be seen from fig D1and 20FRMRF system doesn't have self-centering capacity in both directions.

For 20PRMRF system displacement time-history relation in appendix d show that the 20SR1-6, 20SR13-18, and 20SR4-9 systems have self-centering capacity in both direction, however, 20SR13-18 building have the highest energy dissipation capacity as discussed in the previous section, while 20SR1-6 provide the lowest energy dissipation ratio in y-direction, and 20SR4-9 building has low energy dissipating ratio in x-direction

Also fig D6 through fig D8 show that the 20BRBF cx sy system and 20BRBF cx cy systems have self-centering capacity in both direction, while 20BRBF csx csy doesn't provide self-centering capacity in both direction.

It should be noted from the graphs in appendix D that all the 20-storey systems are still vibrating so the value of the top displacement will be useless for this system, and thus it doesn't present in this section.

5.3 inter-storey drift ratio

This is a very important parameter since the structural damage is directly related to this parameter, however the present study adopted the suggestion by FEMA 356 and used drift limits of 0.7%, 2.5% and 5.0% for defining the limit states of immediate occupancy, life-safety and near-collapse for FRMRF and PRMRF systems. On the other hand, the drift limits of 0.5%, 1.5% and 2.0% were used for defining the limit states for EBF and BRBF systems

5.3.1 6-storey system

Inter-story drift ratio for the 6-storey systems compared to that of 6FRMRF system are shown in appendix E, from these figures it can be seen that the inter-storey drift ratio for these systems cannot exceed 0.25%, which is very small percentage compared to Fema 365 drift limitations.

However, inter-storey drift ratio for the partially restrained building cases are shown in fig E1 through fig E14, it can be seen from these figures that, 6SR45, 6SR56, and 6SR456 give the lowest drift for both direction, also it should be noted that these cases also gives the highest energy dissipation capacity, and good self-centering capacity as discussed before, also 6SR56 give the lowest inter-story drift ratio in both direction compared to 6FRMRF system, and 6SR45 give the second lowest drift ratio, and SR 456 gives the highest drift ratio comparing to 6SR56 and 6SR45 buildings, also it can be seen that the other partially restrained buildings have in general low drift in y-direction comparing to the 6FRMRF systems, while their drift in the x-direction is larger than 6FRMRF system.

Considering the above observations it can be conclude that, 6PRMRF system have acceptable inter-storey drift ratio (doesn’t exceed Fema 356 drift limitation) for all modeled cases, however, it can be noted that frames in y-direction show better ratio

than frames in x-direction for almost all 6PRMRF cases, also placing semi-rigid connection at the top floors will give low inter-storey drift ratio in both direction compared to the FRMRF system, since 6SR45, 6SR56 and 6SR456 cases show the lowest inter-storey drift ratio.

5.3.2 20-storey system

Inter-story drift ratio for the 20-storey systems compared to that of 6FRMRF system are shown in appendix F, from these figures it can be seen that the inter-storey drift ratios for FRMRF and PRMRF systems don't exceed 0.7%, and the inter-storey drift ratios for BRBF system don't exceed 0.5% so there will be no damage from the inter-storey drift ratio.

However, inter-storey drift ratio for the partially restrained building cases are shown in figF1 through figF5, it can be seen from these figures that, 20SR1-6, and 20SR13-18 give the lowest drift for x-direction, but for y-direction they provide lower drift ratio for the first 10 storey then their drift ratio become bigger than that for 20FRMRF system, also it should be noted that these two cases have self-centering capacity in both direction, while 20SR13-18 gives the highest energy dissipation capacity, also it can be seen that the other partially restrained buildings have in general low drift ratio in both direction comparing to 20FRMRF system.

Considering the above observations it can be conclude that, as for 6PRMRF system, 20PRMRF systems have acceptable inter-storey drift ratio (doesn't exceed fema 356 drift limitation), however, placing semi-rigid connection at (13-18) floors or (1-6) floors will give low inter-storey drift ratio in x-direction and lower inter-storey drift ratio up to tenth floor in y-direction compared to the 20FRMRF system.

Finally, both 6BRBF and 6EBF systems have low inter-storey drift ratio in both direction compared to 20FRMRF system, however, 20BRBF cases have low inter-

storey drift ratio for frames in x-direction, while these cases have low inter-storey drift ratio for frames in y-direction up to the thirteenth floors and after that storey drift ratio is increased compared to the 20FRMRF system.

5.4 Force Distribution Ratio

The effect of semi-rigid connection on the force distribution in the PRMRF members as a ratio of the force in the FRMRF members are presented in appendix G for 6PRMRF system and in appendix H for 20PRMRF system, in which shear, moment and axial forces in columns, also shear and moment in beams are presented for 6SR45, 6SR56, 6SR12, 6SR34, and 6SR23, building for 6PRMRF systems, and for 20SR8-13, 20SR1-6, 20SR4-9, 20SR13-18 buildings for 20PRMRF system, these buildings are chosen to reflect the effect of semi-rigid connection at different storey level

5.4.1 6PRMRF system

5.4.1.1 Shear Force ratio in columns

shear force ratio in columns for both x and y directions are presented in figure G1 through figure G5, shear force ratio acting in x-direction in columns has notation of (Vcx), while shear force ratio acting in y-direction in columns has notation of (Vcy), however, figure G1 through figure G5 show that placing semi-rigid connection at a certain floor level will result in increasing Vcx in some column at that storey level, also may result in increasing Vcx for floors level above or below the semi-rigid floors level or both, for example, as shown in fig G1 for 6SR45 case Vcx is increased in some columns at third, fourth, and fifth floors, with average Vcx at these three floors as shown in table 5.4, so there is a slight increasing in the Vcx for the third floor, while Vcx is decrease for all other floors. Also from table 5.4 and by considering fig G1 through fig G5, it can be seen that 6SR45 has lowest values of Vcx at all floors level comparing to the other five cases at all floors level.

Table 5.4 Average Vcx for 6PRMRF system at each floor level

Floor level	6SR45	6SR34	6SR23	6SR12	6SR56
1	0.989846	1.025377	1.024944	1.000822	0.997822
2	0.987757	1.030503	1.007401	0.980157	1.001044
3	1.014992	1.065488	1.040545	1.007244	1.018119
4	0.947277	1.011692	0.984925	0.973683	0.99873
5	0.929776	1.015002	0.995295	0.988841	1.022302
6	0.885227	1.004092	0.994104	0.979679	1.044605

Table 5.5 Average Vcy for 6PRMRF system at each floor level

Floor level	6SR45	6SR34	6SR23	6SR12	6SR56
1	0.933799	0.964876	0.939003	0.923057	0.981156
2	0.932822	0.947582	0.89829	0.882742	0.984927
3	0.910566	0.934716	0.895611	0.859005	0.989206
4	0.943782	0.962255	0.88365	0.896277	1.01894
5	0.775017	0.893869	0.8029	0.779362	0.963134
6	0.745816	0.920018	0.846092	0.819264	0.978889

On the other hand, the average value of Vcy for the five 6PRMRF cases are present in table 5.5, from this table and by considering fig G1 through fig G5, it can be seen that almost all cases have Vcy values smaller than one, however, as can be seen from table 5.5, 6SR12 case has the lowest values of Vcy, followed by 6SR23 and 6SR45 cases respectively, while 6SR56 case show the highest Vcy values at all storey followed by 6SR56 case which shows the second highest Vcy value in all storey compared to the other cases.

5.4.1.2 Axial Force Ratio in Columns

Axial force ratio in columns are presented in figure G6 through figure G10, however, the above figures show that almost all five cases show increasing in the axial ratio values for some columns in all storey, except for 6SR45 case in which axial force ratio are reduced in the fourth and fifth floors while very small increasing occur in the other floors, this result can be shown also from table 5.6 in which the average of axial force ratio at each floors for the five 6PRMRF are presented. Values in this table indicate that the average axial force ratio in all five cases at all floors are less than one, with lowest ratios obtained by 6SR45 case, and the highest ratios are obtained by 6SR56 case, while the ratios for the remaining cases are lie between the ratios for these two cases.

Table 5.6 axial force ratio at each floor for the five 6PRMRF cases

Floor level	6SR45	6SR34	6SR23	6SR12	6SR56
1	0.925403	0.981434	0.966049	0.961048	0.995814
2	0.920137	0.976182	0.957723	0.965807	0.996864
3	0.913699	0.964824	0.963553	0.973771	0.995664
4	0.899246	0.974609	0.972483	0.960324	0.994563
5	0.924029	0.997216	0.970541	0.963765	0.9825
6	0.957434	0.990226	0.968435	0.963219	0.99558

5.4.1.3 Moment Force Ratio in Columns

moment force ratio at both end of columns about x and y directions are presented in figure G11 through figure G15, moment force ratio acting at the start and at the end of the columns about x direction have notations of Mcsx and Mcex respectively, while , moment force ratio acting at the start and at the end of the columns about y direction have notation of Mcsy and Mcey respectively, however, figure G11 through figure G15 show that placing semi-rigid connection at a certain floor level result in decreasing Mcx either at the start or at the end of the columns or at both ends of the column for some cases, for example, as shown in fig G11 which present columns moment ratio in both x and y direction for 6SR45 case, both Mcsx and Mcex is less than one at the fourth floor, also, Mcsx is less than one at the fifth floor, while Mcex is bigger than one in the fifth floor, therefore, moment demand in the x-direction for the column between the fourth and the fifth floor will probably remain the same, According to the current design practice only the higher value of the two end moments in a member is used to determine its size. Therefore, an observed increase in moments on one side of an element does not always result in a larger section for the column, since the other end of the member may experience the controlling design moment., however, the same behavior are observe in other 6SR45 columns and in the columns for the remaining four cases, in which decreasing in the moment ratio at one end is faced by increasing in the moment ratio at the other end.

On the other hand, almost all five cases have Mcy ratio larger than one either at the start or at the end of the columns at the semi-rigid floor level, while this moment ratio become less than one for columns in the other floor level below the semi-rigid floors level, and in some columns above the semi rigid floor level.

For example, as shown in fig G11b the moment ratio for 6SR45 cases are increased at the fourth floor, while this ratio are decrease at the first and the second floors, also this ratio is decreased for some column in the remaining floors, however, the lowest value of Mcy are obtained from both 6SR56 and 6SR12 cases, in which moment ratio for 6SR56 are less than one at the first second and at the fourth floor, while moment ratio at the fifth floor have value larger than one, and the moment ratio for some columns at the third and sixth floors are less than one, on the other hand, moment ratio for 6SR12 are less than one at the fourth fifth and at the sixth floors, while moment ratio at the first and third floor have value larger than one, and the moment ratio for some columns at the second floors are less than one

Considering the above result, it can be conclude that placing semi-rigid connection at a certain floor level result in decrease the moment ratio at that floor level either at the start or at the end or at both end as discussed before, but, this decrease on one end will be faced by increasing in the moment ratio at the other end, which will not necessary lead to bigger column section, on the other hand, frames in y-direction have lowest moment ratio than frames in x-direction, in which, two or three floors away form the semi-rigid floors in the y-direction frames have moment ratio at both columns end for all columns in the floors less than one, which mean that these columns will be designed to have smaller section, while moment ratio for frames in x-direction are larger than one for all cases.

5.4.1.4 Shear Force Ratio in Beams

Shear force ratio at both end of beams are presented in figure G16 through figure G20 in which, shear force ratio at the left and at the right end of beam in the x-direction has a notation of V_{bsx} and V_{bex} respectively, and shear force ratio at the left and at the right end of beams in the y-direction has a notation of V_{bsy} and V_{bey} respectively, however, figure G16 through figure G20 show that placing semi-rigid connection at a certain floor level result in decreasing V_{bx} at the start and at the end of the beam, for example, as shown in fig G16a, which present beam shear ratio in both x and y direction for 6SR45 case, both V_{bsx} and V_{bex} is less than one at the fourth and at the fifth floors, while V_{bx} is bigger than one at the third and at the sixth floors, and for some beams at the first and at the second floors, therefore, beams in the fourth and fifth floors in the x-direction will be designed for smaller shear value and thus small section. On the other hand, all beams at the third and at the sixth floor, and some beams at the first and second floors will be designed to larger shear value and thus bigger section. Also, The same behavior are observe for the other cases, however, 6SR12 case show the best distribution of the shear force in the x-direction beams in which V_{bx} are decreased in the beams at all floors except at the third floor where both V_{bsx} and V_{bex} are increased.

On the other hand, almost all five cases have V_{by} ratio smaller than one at the semi rigid floor level, while this ratio is approximately equal one at the start and at the remaining floors level. For example, as shown in fig G16b the shear ratio for 6SR45 cases are decreased at the fourth and at the fifth floors, while this ratio are less than or equal approximately one at the remaining floors, however, the lowest value of V_{by} are obtained from 6SR23 case, in which shear ratio are between (0.7-0.9) at almost all floors level except for the first floor where shear force ratios are approximately one as shown in fig G20.

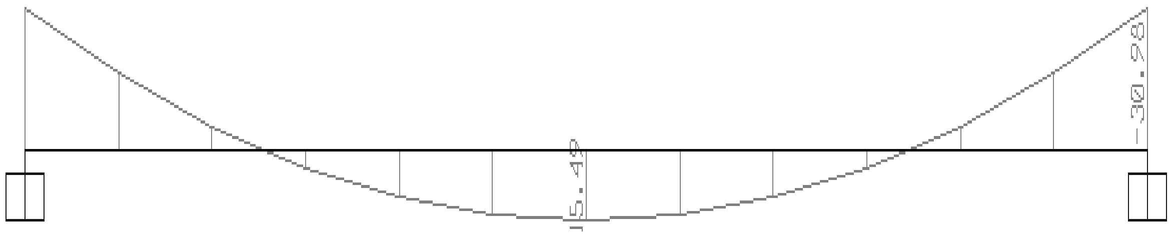
5.4.1.5 Moment Force Ratio in Beams

Moment force ratio at both end of beams are presented in figure G21 through figure G21 in which, moment force ratio at the left and at the right end of beam in the x-direction has a notation of M_{bsx} and M_{bex} respectively, and moment force ratio at the left and at the right end of beams in the y-direction has a notation of M_{bsy} and M_{bey} respectively, however, the effect of semi-rigid connection on the distribution of the moment in beams are shown in fig 5.4, in which fig5.4a represent moment for fixed end beam, while fig5.4b show the same beam with semi-rigid connection at its end, however, this figure show that the negative moment is twice the positive moment for the fixed end beam, this variation between positive and negative moment will lead to uneconomic design of this beam, because this beam will be designed to resist the max moment at its end, while the middle of the beam will be subjected to lower moment, but by placing semi-rigid connection at the two end of the beam the difference between the positive and the negative moment will minimize, and thus design the beam to resist lower moment with more economic section.

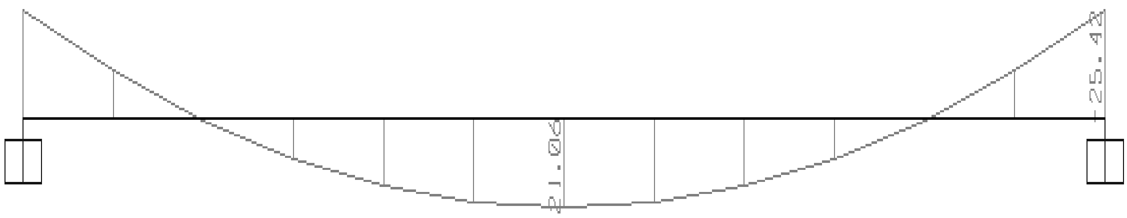
The same concept can be applied in this study, as can be seen in fig G21 through fig G25, placing the semi-rigid connection in the beams at certain floor will reduce the moment at the two ends of that beams and increase the moment at the middle of that beams. However, 6SR56, 6SR12, and 6SR23 cases show the best moment distribution in the x-direction in all floors, since their moment ratio in their rigid floor are equal approximately one, while the other cases show that moment ratio at the rigid floors are larger than one.

On the other hand for beam in y-direction moment distribution in all cases show the same behavior, in which moment ratio for the rigid floors have value of one while,

moment ratio for the semi-rigid floors is increased at the middle of the beam and decreased at the end of the beam.



a)



b)

Fig 5.4 effect of semi-rigid connection on the moment distribution in the beam a) fixed connection b) semi-rigid connection at both end of the beam

5.4.2 20PRMRF system

5.4.2.1 Shear Force ratio in columns

shear force ratio in columns for both x and y directions are presented in figure H1 through figure H4, also, the average shear value act in the x and y direction are presented in table 5.7 and table 5.8 respectively, in which shear force ratio acting in x-direction in columns has notation of (Vcx), while shear force ratio acting in y-direction in columns has notation of (Vcy), however, figure H1a through figure H4a show that almost all cases have Vcx ratio smaller than one for the majority of the columns at all floors level , except for 20SR13-18 in which Vcx have values bigger than one at the first floor and from the seventh to the twelfth floors, this result can be seen also in table 5.7 in which the average value of all cases at all floors level are less than one except for 20SR13-18 case as mention. However, lowest values are obtained by 20SR4-9 case.

On the other hand, both table 5.8 and figure H1b through figure H4b show that 20SR4-9 and 20SR8-13 cases have average Vcy ratio smaller than one at all floors, with minimum ratio obtained by 20SR4-9 case, while Vcy ratio is larger than one at the ninety and at the twenty floors for 20SR1-6 and equal one at the tenth floor for 20SR13-18 cases, also, value at the remaining floors for these two cases are close to one.

Table 5.7 Average Vcx for 6PRMRF system at each floor level

Floor level/PRMRF case	20SR8-13	20SR1-6	20SR4-9	20SR13-18
1	0.94526	0.965739	0.914263	0.994713
2	0.927053	0.965032	0.889995	0.961545
3	0.930692	0.968202	0.891465	0.953869
4	0.933392	0.968893	0.892199	0.951553
5	0.931539	0.972654	0.891449	0.936246
6	0.917948	0.976403	0.889194	0.942594
7	0.914818	0.981019	0.882482	0.98007
8	0.903788	0.979624	0.867416	0.982968
9	0.889476	0.969167	0.843489	0.990119
10	0.895164	0.96369	0.819949	1.00192
11	0.898144	0.960426	0.810198	0.997342
12	0.903193	0.955471	0.819564	0.990452
13	0.889649	0.947209	0.806973	0.979804
14	0.895248	0.941116	0.796356	0.964777
15	0.910043	0.937938	0.793475	0.947461
16	0.910237	0.911188	0.796589	0.932236
17	0.900047	0.882155	0.79122	0.917296
18	0.882511	0.85261	0.786256	0.902292
19	0.86439	0.850995	0.804101	0.923704
20	0.851192	0.880749	0.842052	0.974166

Table 5.8 Average Vcy for 6PRMRF system at each floor level

Floor level/PRMRF case	20SR8-13	20SR1-6	20SR4-9	20SR13-18
1	0.951348	0.966886	0.925483	0.994713
2	0.911657	0.957996	0.893155	0.961545
3	0.915057	0.958609	0.893464	0.953869
4	0.912846	0.952088	0.883168	0.951553
5	0.908849	0.948838	0.879054	0.936246
6	0.900204	0.946933	0.877648	0.942594
7	0.879151	0.948953	0.87098	0.98007
8	0.881752	0.946544	0.858334	0.982968
9	0.867478	0.937588	0.83987	0.990119
10	0.85847	0.917068	0.803406	1.00192
11	0.860507	0.912772	0.788819	0.997342
12	0.872883	0.909996	0.796023	0.990452
13	0.867647	0.900611	0.787448	0.979804
14	0.873179	0.903374	0.78677	0.964777
15	0.878975	0.893291	0.78561	0.947461
16	0.868565	0.888049	0.80898	0.932236
17	0.853932	0.923378	0.823893	0.917296
18	0.863081	0.973131	0.847628	0.902292
19	0.899446	1.012541	0.907514	0.923704
20	0.94076	1.059817	0.963346	0.974166

5.4.2.2 Axial Force Ratio in Columns

Axial force ratio in columns are presented in figure H5 through figure H8, however, the above figures show that almost all four cases have axial force ratio less than one for the majority of the columns at all storey level, this result can be seen also from table 5.9 in which the average of axial force ratio at each floors for the four 20PRMRF are presented. Values in this table indicate that the average axial force ratio in all almost four cases at all floors are less than one, except for 20SR13-18 case where the axial force ratio are bigger than one from the first to the fifth floors, however, 20SR4-9 has the lowest average axial force ratio, followed by 20SR5-13 and then by 20SR1-6 respectively, and finally 20SR13-18 case has the highest ratio among the three cases.

Table 5.9 axial force ratio at each floor for the four 20PRMRF cases

Floor level/PRMRF case	20SR8-13	20SR1-6	20SR4-9	20SR13-18
1	0.983919	0.982834	0.974336	1.006256
2	0.979178	0.980957	0.969997	1.015825
3	0.976748	0.980684	0.964618	1.007127
4	0.974924	0.981939	0.960846	1.004227
5	0.974711	0.982261	0.957873	1.003152
6	0.977689	0.981703	0.954119	0.998661
7	0.986381	0.981091	0.951643	0.991675
8	0.975959	0.979613	0.948977	0.981055
9	0.969192	0.977157	0.945876	0.9877
10	0.962347	0.975242	0.945125	0.98964
11	0.956527	0.974656	0.950762	0.991775
12	0.951175	0.97517	0.944243	0.993003
13	0.942502	0.974866	0.936825	0.992801
14	0.948172	0.97906	0.938006	0.990506
15	0.944702	0.972919	0.928889	0.989661
16	0.937859	0.967334	0.919348	0.987385
17	0.935396	0.965665	0.916174	0.983003
18	0.927603	0.961123	0.912267	0.982378
19	0.927876	0.961564	0.914904	0.980164
20	0.926217	0.959333	0.913561	0.980572

5.4.2.3 Moment Force Ratio in Columns

moment force ratio at both end of columns about x and y directions are presented in figure H9 through figure H12, moment force ratio acting at the start and at the end of the columns about x direction have notations of Mcsx and Mcex respectively, while , moment force ratio acting at the start and at the end of the columns about y direction have notation of Mcsy and Mcey respectively, however, figure H9 through figure H12 show that 20SR4-9 case have the lowest moment force ratio among all other cases for both x and y-direction, in which moment force ratio about x and y axes are large than one at the eleventh and at the seventeenth floors, and also this ratio are larger than one for few columns at the tenth and twelfth floors, while moment ratio for columns at other floors have ratio less than one, however, it should be remembered from the previous discussion in section 5.4.1.3 that increasing in the moment ratio at one end of the columns will not necessary lead to design column for larger section.

5.4.2.4 Shear Force Ratio in Beams

Shear force ratio at both end of beams are presented in figure H13 through figure H17 in which, shear force ratio at the left and at the right end of beam in the x-direction has a notation of V_{bsx} and V_{bex} respectively, and shear force ratio at the left and at the right end of beams in the y-direction has a notation of V_{bsy} and V_{bey} respectively, however, figure H13 through figure H17 show that placing semi-rigid connection at a certain floor level will result in decreasing shear force ratio at the start and at the end of the beam in both direction. However, 20SR4-9 case has the lowest moment ratio at both end of the beam in both directions, while 20SR13-18 case has the highest moment ratio among all cases.

5.4.2.5 Moment Force Ratio in Beams

Moment force ratio at both end of beams are presented in figure H18 through figure H21 in which, moment force ratio at the left and at the right end of beam in the x-direction has a notation of M_{bsx} and M_{bex} respectively, and moment force ratio at the left and at the right end of beams in the y-direction has a notation of M_{bsy} and M_{bey} respectively, however, the effect of semi-rigid connection on the distribution of the moment in beams are discussed in section 5.4.1.5 for 6PRMRF system.

Applying that concept, fig H18 through fig H21 show that 20SR4-9 has the best moment distribution among all other cases in which, moment ratio at the semi-rigid floors at the two end of the beam has value smaller than one, while the moment at the middle of the semi-rigid beams have values larger than one, also the moment at the other floor are smaller than one.

Considering the above result it can be conclude that, force distribution results for 20PRMRF system show that all cases have almost the same force distribution ratio in columns and beams for both direction, with lowest force ratio obtained with 20SR4-9 case, however, it should be remembered that this case doesn't have self-centering capacity in both direction, and it has high inter-storey drift ratio, and also low energy dissipation capacity comparing to other 20PRMRF cases.

However, weight for the 6 and 20 braced systems are presented in table 5.10 and table 5.11 respectively, as a ratio of the weight of FRMRF system, from these two tables it can be seen that BRBF system is most economic than the other three system for both 6 and 20- storey buildings.

Table 5.10 weight ratio for 6BRBF and 6EBF system

System	Weight ratio
6BRBF cx cy and 6BRBF cx sy	0.924489
6EBF cx cy and 6EBF cx sy	0.975289
6EBF csx csy	1.052006
6EBF cscox cscoy	1.094314

Table 5.11 weight ratio for 20BRBF and 20EBF system

System	Weight ratio
20BRBF cx cy and 20BRBF cx sy	0.828271
20BRBF csx csy	0.842623
20EBF cx cy and 20EBF cx sy	0.885048
20EBF cscox cscoy	1.040667

5.5 Ductility

Structural ductility defined as the ability of structure to undergo large deformation without significant reduction in its strength, in other word it’s the ratio between maximum displacement and yield displacement, however, maximum displacement could be from earthquake excitation or could present the maximum displacement that can be obtained by the structure before it fail, these two type of displacement define ductility demand and ductility capacity respectively, in which ductility demand is defined as the ratio between the maximum top displacement under earthquake excitation to the yield top displacement, while ductility capacity defined as the ratio between the maximum top displacement that the structure can go before failure to the yield top displacement, where yield top displacement is defined as the top displacement at the first formation of plastic hinge, also it should be noted that these two type of ductility present the global ductility of the structure.

In this study ductility demand is obtained by applying nonlinear time history analysis using tabas earthquake for all system , on the other hand ductility capacity are obtained by applying static pushover analysis, in which all structures are pushed to failure to obtain the maximum displacement that the structure can go before failure, however, structure with low ductility demand and with high ductility capacity are the most desire, therefore capacity-demand ductility ratio are used in this study to evaluate the ductility of the different system.

5.5.1 6-storey system

In this section Ductility demand, ductility capacity, yield displacement ratio, and capacity-demand ratio for 6PRMRF, 6BRBF, 6EBF systems as are presented in table 5.12 for frame in x-direction and in table 5.13 for frame in y-direction as a ratio of that for 6FRMRF system, however, ratios in table 5.12 show that ductility-demand ratio for 6SR34, 6SR235, and 6SR346 cases are bigger than one, but it must be noted that these three buildings will go to large top displacement under earthquake excitation, such behavior may not be desired in practice due to many factors like pounding effect and other factors, also these three buildings have ductility demand ratio bigger than one which means that plastic hinge will form in beams at an early stage, and thus more damage to these buildings.

On the other hand, ratios in table 5.13 show that many 6PRMRF cases have capacity-demand ratio bigger than one, but the higher ratio are obtained by 6SR45 cases, also, this case have the lowest ductility demand ratio among all other cases with value close to one, which means that no further damage will occur to this case due to placing semi-rigid connections, also, this case has a slight increase in the lateral top displacement ratio (5%) which is very small. However, other cases have higher ductility demand ratio which will lead to more damage to the buildings as discussed before.

Also table 5.12 and table 5.13 show that both 6BRBF and 6EBF systems have high ductility demand ratio, this is because that the yield displacement ratio for these systems are very small, also it can be seen that capacity-demand ratio for 6EBF system is smaller than one in both direction this can be due to the reason that the global behavior of this system is similar to linear behavior, while the nonlinear behavior shall be restricted to the shear links only, so that the global top displacement for this system will

be small, also, 6BRBF have capacity-demand ratio less than one for frames in x-direction, and ratio bigger than one for frames in y-direction.

Table 5.12 ductility ratio for 6-storey systems in x-direction under tabas earthquake

system	Max Top Displacement Ratio	Ductility Demand ratio	Ductility Capacity ratio	Capacity/Demand
6SR45	1.134562	1.134562	0.971343	0.85614
6SR34	1.190174	1.276772	1.300151	1.018311
6SR23	1.164337	1.381824	1.084335	0.784712
6SR1346	1.241	1.292708	0.730001	0.564707
6SR all	1.173232	1.318882	1.177753	0.892994
6SR12	1.120712	1.346024	1.342115	0.997095
6SR56	1.063532	0.996385	0.724109	0.726736
6SR246	1.18382	1.27531	1.188853	0.932207
6SR135	1.213045	1.315419	0.847342	0.644161
6SR235	1.185515	1.307135	1.518506	1.161705
6SR234	1.176197	1.336587	0.966058	0.72278
6SR456	1.153748	1.141834	0.988451	0.86567
6SR345	1.241	1.319602	0.944515	0.715757
6SR346	1.210928	1.290609	1.330264	1.030726
6BRBF cx cy	0.755078	1.980251	1.44683	0.733096
6BRBF cx sy	0.757205	1.965655	1.434106	0.731323
6EBF cscox cscoy	0.377582	1.24955	0.410668	0.328653

Table 5.13 ductility ratio for 6-storey systems in y-direction under tabas earthquake

system	Max Top Displacement Ratio	Ductility Demand Ratio	Ductility Capacity Ratio	Capacity/Demand
6SR45	1.054966	1.001267	1.371356	1.369621
6SR34	0.973064	0.992768	0.826767	0.832789
6SR23	0.973401	1.180847	1.227673	1.039655
6SR1346	1	0.983797	1.531883	1.557113
6SR all	0.996633	1.051237	2.722334	2.589649
6SR12	0.969697	1.187916	1.119452	0.942366
6SR56	1.059259	1.01634	1.045866	1.029052
6SR246	0.978114	1.107688	1.333715	1.204053
6SR135	0.983838	0.987592	1.095379	1.109141
6SR235	0.986195	1.148702	1.278326	1.112844
6SR234	0.999663	1.159257	1.719865	1.483592
6SR456	1.090572	1.088275	1.275741	1.17226
6SR345	1	0.975288	0.558675	0.57283
6SR346	0.989562	0.97759	0.560469	0.573317
6BRBF cx cy	0.615269	1.44683	1.846101	1.275963
6BRBF cx sy	0.614098	1.434106	1.825328	1.272799
6EBF cscox cscoy	0.283953	1.050626	0.524619	0.499339

5.5.2 20-storey system

As for 6-storey systems, ductility demand, ductility capacity, yield displacement ratio, and capacity-demand ratio for 20PRMRF and 20BRBF systems as are presented in table 5.14 for frame in x-direction and in table 5.15 for frame in y-direction as a ratio of that for 6FRMRF system, however, ratios in the table 5.14 show that 20SR8-13 case show the most desired behavior among all cases in which capacity-demand ratio for 20SR8-13 are bigger than one, also it must be noted that this case has a slight increased in both ductility demand and the maximum displacement ratio.

On the other hand, ratios in table 5.15 show that 20SR8-15 has the highest capacity-demand ratio among all other cases, also this case has ductility demand and max top displacement ratio less than one.

Also table 5.14 and table 5.15 show that ductility demand ratio for 20BRBF system are bigger than three which is a high ratio, the reason for this is that the yield displacement for this system are very small and thus high ductility demand ratios.

Table 5.14 Ductility ratio for 20-storey systems in x-direction

system	Max Top Displacement Ratio	Ductility Demand Ratio	Ductility Capacity Ratio	Capacity/Demand
20SR8-13	1.008866	1.021561	1.086546	1.063613
20SR1-6	1.029219	0.907806	0.751338	0.827641
20SR4-9	0.957493	1.504137	1.444892	0.960612
20SR13-18	1.055657	1.121745	1.099385	0.980067
20BRBF cx sy	0.881775	3.68311	3.842809	1.04336
20BRBF cx cy	0.881901	3.683563	3.275627	0.889255
20BRBF csx csy	0.850921	3.025276	2.857009	0.94438

Table 5.15 Ductility ratio for 20-storey systems in y-direction

system	Max Top Displacement Ratio	Ductility Demand Ratio	Ductility Capacity Ratio	Capacity/Demand
20SR8-13	0.96873	0.825745	0.875835	1.060661
20SR1-6	1.000526	0.757539	0.762518	1.006573
20SR4-9	0.920495	1.268397	1.071156	0.844496
20SR13-18	1.034591	0.840462	0.705821	0.839802
20BRBF cx sy	0.910738	4.741985	6.880732	1.451024
20BRBF cx cy	0.90399	3.697595	4.080825	1.103643
20BRBF csx csy	0.875668	4.15569	4.301514	1.03509

5.6 Plastic Hinge Formation Pattern

One of the benefits of using semi-rigid connection in building is to control failure location, where the semi-rigid connection will act like fuses (weakest element) in the building, and will be the first to fail, the same behavior can be obtained by the buckling restrained bracing members in BRBF system and by the shear link element in EBF system, however, AISC code allow additional yielding outside the fuses element in the PRMRF system and in the BRBF system, but for EBF system AISC code limit yielding in the EBF system to the shear link only, therefore, the global behavior of this system will be very close to the behavior of the linear system as shown in the previous section. Yielding mechanism for the 6-storey buildings are presented in appendix I for tabas earthquake and in appendix J for other earthquake which is Northridge earthquake, the record for this earthquake is obtained from the PEER database this earthquake has an epicentre in Northridge, California. It occurred on January 17, 1994, the earthquake magnitude is 6.7 on the Richter scale, with peak ground acceleration of 1.6615 g, which is very high and the total duration of the record is 40 seconds making it extremely dangerous compared to the normal earthquake duration of 10 – 20 seconds. While yielding mechanism for the 20-storey systems are presented in appendix K. Figures in these appendices, show that yielding will start in the fuses element and will spread to the other fuses since they are the weakest element in the buildings.

Buildings under seismic excitation can be considered as a cantilever fixed at its base and having triangular load present the distribution of the seismic force along the height of the buildings as shown in fig 5.5, therefore, the maximum force will be at the bottom of the building, so the plastic hinges will form first at the low floors level and then spread to the higher floors under strong earthquake loads. This behavior can be shown in fig I1 and fig I2 in which yielding in 6FRMRF system is start in the first floors for

frames in the x-direction, and in the second floor for frames in the y-direction. also, the same behavior are presented in fig K1 and fig K2 in which the plastic hinge start at the third and at the fourth floors for 20FRMRF systems for frames in the x and y direction. However, results for 6PRMRF system presented in fig I3 through fig I12, and results for 20PRMRF system presented in fig J3 through fig J10 show that plastic hinge will start at the location of the semi-rigid joints, however, for all cases it can be seen that plastic hinge are formed only in the beams, while the columns are remain elastic in all cases, such behavior is very desired under earthquake excitation.

On the other hand, yielding of 6BRBF system are shown in fig I13, while yielding of 20BRBF system are shown in fig K11 and fig K12, these figures show that the buckling restrained bracing members will be the weakest element and the plastic hinges will start in these elements, however, fig I13 show that yielding in the 6BRBF system are limited to the bracing element only, while fig K11 and fig K12 show that additional yielding are spread to the beams after the yield of all bracing members, such a behavior is allowed by AISC code since it will not have a significant effect on the behavior of this system as shown in the previous chapters.

Finally, yielding mechanism of 6EBF system are presented in fig I14 through fig I19, while yielding mechanism for 20EBF system are presented in fig K13 through fig K18, however, these figures show that EBF system are in general unsuitable to use in high seismic region, this is because it's become very difficult to limit yielding to the shear link only especially in high rise building, this result is shown in the above figures, in which the 6EBF cscox cscoy are the only case that survive the earthquake excitation among all 6EBF cases, but this case has a lot of bracing members which may not be economically feasible, on the other hand, all 20EBF cases are fail during earthquake excitation. However, the length of the shear link element may have a significant effect

on the behavior of the EBF system under seismic excitation, for example, fig I14 show that failure start for 6EBF1 csx csy case in the shear link at the first storey for both x and y direction, while failure for 6EBf2 csx csy is start in the shear link at the third floor, by referring to table 4.10 it can be seen that the length of the first two floors in 6EBF1 csx csy case is 1.4 m in the y-direction and the length of the third and the fourth floors in this case are 1.25, on the other hand, the length of the first two floors in 6EBF2 csx csy case is 1.25 m in the y-direction and the length of the third and the fourth floors in this case are 1.4 m in the y-direction two floors in 6EBF1 csx csy case is 1.4 m in the y-direction, and the length of the shear link in x-direction are the same for the two cases, also, fig I18 and fig I19 show that using very short shear link (1.0 m in this case) will put additional demand on the bracing, beams, and columns member which may yield to use bigger section for these members, on the other hand fig J13 through fig J20 show that it's very difficult to limit yielding to the shear link only disregard of its length.

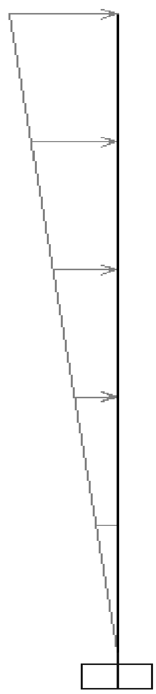


Fig 5.5 seismic force distribution along the height of buildings

5.7 Fundamental period

In this section fundamental period for both 6-storey system and 20-storey system are presented to reflect the effect of semi-rigid connection on the stiffness of the PRMRF, BRBF, and EBF systems, however, these results are presented in table5.16 for 20-storey systems and in table 5.17 for 6-storey systems. From these two tables it can be noted that fames in the x-direction are stiffer than frames in the y-direction, also it can be noted that both 6SR45 and 20SR13-18 cases, which show desired behaviour in the previous section, have high stiffness compared to the other cases.

On the other hand, and as expected both 6EBF cscox cscoy and 20BRBF csx csy have the highest stiffness among all cases.

Table 5.16 fundamental period for 20-storey systems

Case	Period for Frame in x-direction	Period for Frame in y-direction
Rigid Case	2.51953	2.64972
20SR8-13	2.67885	2.81052
20SR1-6	2.74063	2.87465
20SR4-9	2.74574	2.87678
20SR13-18	2.58258	2.71686
20BRBF cx sy	2.35105	2.55606
20BRBF cx cy	2.45903	2.55503
20BRBF csx csy	2.12234	2.24134
20EBF cx cy	2.20368	2.44989
20EBF1 cx sy	2.20501	2.4519
20EBF2 cs sy	2.16908	2.3967
20EBF3 cx sy	2.21773	2.47083

Table 5.17 fundamental period for 6-storey systems

Case	Period for Frame in x-direction	Period for Frame in y-direction
Rigid Case	1.10852	1.200656
SR45	1.13664	1.231564
SR34	1.157069	1.254547
SR23	1.176664	1.27362
SR1346	1.190723	1.291854
SR all	1.24302	1.347221
SR12	1.181703	1.278621
SR56	1.119481	1.212931
SR246	1.168267	1.267765
SR135	1.175741	1.27149
SR235	1.184462	1.281087
SR234	1.197442	1.297789
SR456	1.139995	1.236824
SR345	1.166425	1.263589
SR346	1.159738	1.259038
6BRBF cx cy	0.88185	1.07818
6BRBF cx sy	0.85985	0.88224
6EBF cx sy	0.7772	0.78685
6EBF1 cx cy	0.76344	0.78453
6EBF2 cx cy	0.76342	0.78579
6EBF1 csx csy	0.62422	0.6349
6EBF2 csx csy	0.65444	0.66226
6EBF3 csx csy	0.62181	0.62935
6EBF cscox cscoy	0.5183	0.51483

Chapter 6

SUMMARY, CONCLUSIONS AND RECOMMENDATIONS

6.1 Summary

In this study four steel systems namely; FRMRF, PRMRF, BRBF and EBF systems are subjected to a series of nonlinear inelastic time history analysis and nonlinear static push over analysis in effort to evaluate their seismic performance and to introduce PRMRF system with better ductility, better energy dissipation capacity and acceptable self centering capacity, by finding a pattern in placing semi-rigid connection that would optimize seismic response, two buildings geometries are presented to provide a range of buildings proportions. A six storey buildings is used to present mid-rise structures; while a 20-storey buildings is used to present high-rise buildings. However, energy dissipation capacity, self-centering capacity, inter-storey drift ratio, force distribution, ductility, and yielding mechanism are use to evaluate the seismic performance of the four system that mentioned above, in this section results of these properties will be discussed separately in detail

6.1.1 energy dissipation result

analysis result in chapter 5 show that placing semi-rigid connection in the 6PRMRF system can be controlled by the frame stiffness, in which placing semi-rigid connection at the middle or at the top of frames in the x-direction which is stiff frame and at the top of frames in y-direction which is low-stiffness frame can improve the energy dissipation capacity of that frames, while placing semi-rigid connection at first floors in the stiff frames and at the middle or at the first floors in the low-stiff frames will adversely affect the energy dissipated capacity of that frame, however, both 6SR45 and 6SR456 case has high energy dissipating capacity in both directions comparing to other 6PRMRF cases.

On the other hand, placing semi-rigid connection in the 20-storey buildings improve its energy dissipation capacity regardless of the location of these connections, however, 20SR13-18 case has the highest energy dissipation capacity among all 20PRMRF cases, also at the contrary of the 6-storey buildings, for 20-storey buildings frames in y-direction provide higher energy dissipation ratio than frames in the x-direction.

However, 6EBF system show low energy dissipation under earthquake excitation, such behaviour was expected by the researcher, since the global behaviour of this frame should be as a linear system with nonlinear deformation limited to the shear link element only, on the other hand 20EBF system show energy dissipation ratio close to that for 20BRBF system, this probably means that yielding in this system will not be limited to the shear link only, this result will be discussed later.

Finally, both 6BRBF and 20 BRBF systems have energy dissipation ratio between that for the PRMRF and EBF systems, this is because this system is less rigid than EBF system and more stiff than PRMRF system, in which AISC code allow some yielding outside the buckling restrained bracing members.

6.1.2 Self-Cantering Capacity Result

Analysis result in chapter five show that FRMRF system doesn't have self-centring capacity in both direction, while placing semi-rigid connection can improve its self-centring capacity, in which placing semi-rigid connection at the last three floors can provide self-cantering capacity for frames in x-direction, while placing semi-rigid connection at first floors will provide self-cantering capacity for frames in y-direction, except for 6SR12 system, applying this rule it can be seen that 6SR45, 6SR56, 6SR456 systems have self centring capacity in for frames in x-direction, and 6SR23, 6SR234, 6SR135, 6SR246, 6SR235 systems have self centring capacity for frames in y-direction.

On the other hand, For 20PRMRF system, the 20SR1-6, 20SR13-18, and 20SR4-9 systems have self-centring capacity in both direction, however, it should be remember that 20SR13-18 building have the highest energy dissipation capacity as discussed in the previous section, while 20SR1-6 provide the lowest energy dissipation ratio in y-direction, and 20SR4-9 building has the lowest energy dissipating ratio in x-direction.

Finally, 6BRBF systems have self-centering capacity in the x-direction only, while 6EBF cscox cscoy system provide self-centering capacity in both directions, this is because 6EBFcscox cscoy is very stiff, on the other hand, 20BRBF cx sy system and 20BRBF cx cy systems have self-centering capacity in both direction, while 20BRBF csx csy doesn’t provide self-centering capacity in any direction.

6.1.3 Inter-Storey Drift Ratio

Result in chapter 5 show that the 6PRMRF system have acceptable inter-storey drift ratio (doesn’t exceed fema 356 drift limitation) for all modelled cases, however, it can be noted that frames in y-direction show better ratio than frames in x-direction for almost all 6PRMRF cases, also placing semi-rigid connection at the top floors will give low inter-storey drift ratio in both direction compared to the FRMRF system, since 6SR45, 6SR56 and 6SR456 cases show the lowest inter-storey drift ratio.

On the other hand, as for 6PRMRF system, 20PRMRF systems have acceptable inter-storey drift ratio (doesn't exceed fema 356 drift limitation), however, placing semi-rigid connection at (13-18) floors or (1-6) floors will give low inter-storey drift ratio in x-direction and lower inter-storey drift ratio up to tenth floor in y-direction compared to the 20FRMRF system.

Finally, both 6BRBF and 6EBF systems have low inter-storey drift ratio in both direction compared to 20FRMRF system, however, 20BRBF cases have low inter-storey drift ratio for frames in x-direction, while these cases have low inter-storey drift

ratio for frames in y-direction up to the thirteenth floors and after that storey drift ratio is increased compared to the 20FRMRF system.

6.1.4 Force Distribution Ratio

Results in Chapter 5 for 6PRMRF system show that 6SR45 case show good result for force distribution ratio in columns, however, this case show high shear force and bending moment ratio for beams in the x-direction, while 6SR12 case show less force ratios in beams in both directions.

On the other hand, force distribution results for 20PRMRF system show that all cases have almost the same force distribution ratio in columns and beams for both direction, with lowest force ratio obtained with 20SR4-9 case, however, it should be remembered that this case doesn’t have self-centring capacity in both direction, and it has high inter-storey drift ratio, and also low energy dissipation capacity comparing to other 20PRMRF cases.

6.1.5 Ductility

Results in chapter 5 for 6PRMRF system show that no desired behaviour are obtained from all 6PRMRF system with respect to their ductility ratio for frames in x-direction compared to the ductility of 6FRMRF system. However, for frames in y-direction 6SR45 case has the most desired ductility among all other 6PRMRF cases.

On the other hand, results for 20PRMRF system show that 20SR8-13 case has the most desired properties among all other 20PRMRF cases.

Finally, results in chapter 5 for both 6BRBF and 6EBF systems show that these two system have high ductility demand ratio, this is because that the yield displacement ratio for these systems are very small, also it can be seen that capacity-demand ratio for 6EBF system is smaller than one in both direction this can be due to the reason that the global behaviour of this system is similar to linear behaviour, while the nonlinear

behaviour shall be restricted to the shear links only, so that the global top displacement for this system will be small, also 6BRBF have capacity-demand ratio less than one for frames in x-direction, and ratio bigger than one for frames in y-direction.

On the other hand, ductility demand ratio for 20BRBF system are bigger than three which is a high and undesired ratio, because it will lead to more damage to the buildings as discussed before, however the reason for this high ratio is that the yield displacement for this system are very small and thus high ductility demand ratios.

6.1.6 Plastic hinge formation pattern

As discussed in sec 5.6, semi-rigid connection, buckling restrained bracing member, and shear link element shall be designed to be the weakest element in the building, so it will act like fuses, and will be the first to fail, considering this behaviour and the result in appendix I for 6-storey systems subjected to tabas earthquake, and in appendix J for 6-storey systems subjected to Northridge earthquake, and in appendix K for 20-storey systems, it can be conclude that EBF system are not suitable for the high seismic region since it become very difficult to limit yielding to the shear link only especially for high-rise building, since it was shown that for 6EBFsystem only 6EBF cscox cscoy case survive tabas earthquake, however, this case has too much bracing members and its very expensive to construct, on the other hand, for 20EBF system it was shown that no case survive the tabas earthquake excitation and also it shown that it was very difficult to limit yielding to the shear link only.

On the other hand, 6BRBF system was able to limit yielding to the buckling restrained bracing members only, while beams and columns member still elastic under tabas earthquake excitation, such behaviour is much desired since this system will be economic with high ductility and high energy dissipation capacity provided by the buckling restrained bracing member, and not by its global behaviour as discussed

before, however, in 20BRBF system it become very difficult to limit yielding in the buckling restrained bracing member only, although few yielding outside the bracing member was allowed by AISC code, but this yielding may affect its behaviour under seismic excitation, therefore PRMRF system is the most suitable system for high rise buildings under strong earthquake excitation with semi rigid connection, since it show improvement in the properties of the FRMRF system as shown before.

6.2 Conclusion

The major conclusions drawn from this research are summarized in the following list:

- Using fuses element in building will enable the designer to control the structural behaviour rather than putting the effort in predicting extremely random events, where the fuses element should be the weakest element in the building and thus the first to fail.
- Using fuses in the buildings will make the building pick less force from earthquake excitation, where this force will be limited to the capacity of these fuses, and because these fuses should be ductile element, the capacity of the building should be improved.
- Energy dissipation improvement will results in less lateral deformations and less member demands.
- Energy dissipation result for 6PRMRF systems show that placing semi-rigid connections in floors level above the mid-floor level (third floor) will result in better energy dissipation capacity compared to the 6FRMRF system and compared to other 6PRMRF system (6SR456, 6SR45 and 6SR56 cases have the highest energy dissipation ratio).
- Placing semi-rigid connection in 20PRMRF cases show energy dissipation ratio bigger than one for all cases regardless of the location of semi-rigid connection.
- All 6-and 20PRMRF systems show acceptable inter-storey drift ratio where this ratios don’t exceed the limit ratios that given by fema 356 code.
- placing semi-rigid connections in floors level above the mid-floor level for both 6PRMRF and 20PRMRF systems will result in better inter-storey drift ratio compared to the FRMRF system and compared to other PRMRF system

- Placing semi at a certain floor level will result in reducing shear force in the beams and will result also in moment redistribution between the negative and the positive moment in beams so that it will reduce the high value of the negative moment and increase the low value of the positive moment so that these two values will be close to each other and thus the beam will be designed to more economical section.
- Almost all 6PRMRF system show high ductility demand ratio which means that plastic hinges will probably form in more location in the building and thus more damage to the building, however, the location of the most of these plastic hinges will be in the semi-rigid connection rather than in the beams which will remain elastic therefore such failure will be easy and cheap to repair.
- Placing semi-rigid connection at the fourth and the fifth floors level in 6PRMRF system (6SR45 case) show the most desired properties comparing to other 6PRMRF cases, while Placing semi-rigid connection at the fourth to the ninth floors level in 20PRMRF system (20SR4-9 case) show the most desired properties comparing to the other 20PRMRF cases. This desired behaviour of both 6SR45 case and 20SR4-9 case can be related to their yielding behaviour, where the most plastic hinges in these two cases was formed in the semi-rigid connection and few plastic hinges was formed in the beams, which will result in more economical section, better ductility and higher energy dissipation capacity.
- From the result for both 6PRMRF system and 20PRMRF system it would be recommended to place the semi rigid connection at a number of floors equal to (1/3) of the total number of floors for both high and mid-rise buildings.
- Semi-rigid connections increase the fundamental period of the structure and thus decrease its stiffness.

- Result for 20PRMRF system was better than the result for 6PRMRF system, including energy dissipation capacity, yielding mechanism and all other properties, therefore it would be recommended to use PRMRF system for high-rise building rather than for mid-rise buildings in the high seismic region.
- Results for BRBF system show that this system has low energy dissipation capacity compared to the FRMRF system and PRMRF system, this is because this system will provide high lateral stiffness larger than the FRMRF and PRMRF system and therefore will go to smaller top displacement and thus low energy dissipation, however, this system will dissipate energy through the yielding of the buckling restrained bracing member and not by its global behaviour.
- 6BRBF system show better energy dissipation capacity and better ductility demand ratio than the 20BRBF system, this is because in the 20BRBF cases yielding is not limited to the bracing members only, therefore, the stiffness of this system will be reduced, while in the 6BRBF system yielding is limited only to the bracing member only and all element outside the bracing member will remain elastic.
- BRBF system is more economical than the FRMRF and the EBF systems since it have the lowest weight ratio compared to both 6 and 20-storey buildings.
- Analysis result for BRBF system show that this system is the most suitable to use for mid-rise buildings in high seismic region among the other systems that studied in this research, since it can provide high lateral stiffness and limit yielding to the fuses element (RBR bracing member), which will result in high capacity and acceptable energy dissipation capacity.

- Analysis result for 6EBF system show lower energy dissipation capacity, and lower ductility capacity and capacity-demand ductility ratio compared to the other 6-storey systems, and this is in spite of that the shear link element are properly detailed and yielding is limited to it. This indicates that this system has low capacity and it's not suitable for use in high seismic region for the mid-rise building. Also results for 20EBF system indicates that it become very difficult to limit yielding to the shear link regardless of the link of the shear, therefore, it will be recommended to use this system in low seismic region for mid-rise buildings.
- For the length of the shear link element it would be recommended to use length less than the limit given in the AISC code which is $1.6M_p/V_p$, on the other hand using a very short or even using length equal to the AISC limit will put additional requirement on the bracing member and thus yielding will not be limited to the shear link only.

As a result it would be recommended for high seismic region to use PRMRF system for high-rise buildings, BRBF system for mid-rise buildings and EBF system for low-rise buildings.

6.3 Recommendation

Since this study covers a relatively new and unfamiliar subject, the following recommendations that may become beneficial in design for earthquake response are made:

1. Additional earthquake record needs to be applied to the recommended PRMRF cases and to both BRBF and EBF systems to evaluate their seismic performance under different earthquake excitation.
2. The concept in this study needs to be applied to additional building geometries with different height, where it's recommended to use 2-storey building to present low rise buildings, and 10-and 40-storey buildings to apply the conclusion in this study to more high-and mid-rise buildings geometries.
3. The length of the shear link need to be taken bigger than $1.6Mp/Vp$, to evaluate its effect on the behavior of the EBF system especially in high-rise buildings.
4. Frames with different stiffness need to be modeled in the four systems discussed in this study to evaluate the effect of frame stiffness on the behavior of these four systems

REFRENCES

Ali Abolmaali, Anant Kukreti, Ardavan Motahari, Mehdi Ghassemieh (2009), **Energy dissipation characteristics of semi-rigid connections**. Journal of Constructional Steel Research, 65, 1187-1197.

American Institute of Steel Contruction, (2005), **AISC Seismic Provisions for Structural Steel Buildings**.

ATC, 1978, Tentative Provisions for Development of Seismic Regulations for Buildings, **ATC 3-06**, Applied Technology Council, Redwood City, California.

Chopra, Anil K, (2007), **Dynamics of structures theory and applications to earthquake engineering.** (3rd ed) Ed. Prentice Hall. Upper Saddle River, N.J: Pearson/Prentice Hall.

Chi, Wei M., Gregory G. Deierlein, and Anthony Ingraffea (2000), **Fracture Toughness Demands in Welded Beam-Column Moment Connections.** Structural Engineering, 126, 88-97.

Federal Emergency Management Agency (1997), FEMA-273, **NEHRP Guidelines for the Seismic Rehabilitation of Buildings**, Washington, DC.

Saif Hussain, Paul Van Benschoten, Mohamed Al Satari, Silian Lin, **Buckling Restrained Braced Frame (BRBF) Structures: Analysis, Design and Approvals Issues**. Coffman Engineers, Inc. Los Angeles, CA.

Gary R. Searer and Sigmund A. Freeman (2004), Design drift requirements for long-period structures, **13th World Conference on Earthquake Engineering**, Vancouver, B.C., Canada, Paper No. 3292.

Ker-Chun Lin, Chu-Chieh J. Lin, Jung-Yu Chen, and Heui-Yung Chang (2010), **Seismic reliability of steel framed buildings**. Structural Safety, 32, 174–182.

Lu W.Le, James M. Ricles, Changshi Mao, and John W. Fisher (2000), **Critical Issues in Achieving Ductile Behavior of Welded Moment 306 Connections.** Constructional Steel Research 55, 325- 41.

Miller, Duane K. (1998), **Lessons Learned from the Northridge Earthquake.** Engineering Structures, 4-6 20, 249-60.

Mao, Changshi, James Ricles, Le W. Lu, and John Fisher. (2001), **Effect of Local Details on Ductility of Welded Moment Connections.** Journal of Structural Engineering, 127, 1036-044.

Nihan Dogramac Aksoylar, Amr S. Elnashai, Hussam Mahmoud (2011), **The design and seismic performance of low-rise long-span frames with semi-rigid connections**. Journal of Constructional Steel Research, 67, 114-126.

PEER Strong Motion Database: Introduction." Welcome to Pacific Earthquake Engineering Research Center - PEER. Web. 15 Mar. 2011. peer.berkeley.edu/nga/search.html.

Popov, Egor P, Tzong S. Yang, and Shih P. Chang. (1998), **Design of Steel MRF Connections Before and After 1994 northridge Earthquake.** Engineering Structures, 20, 1030-1038.

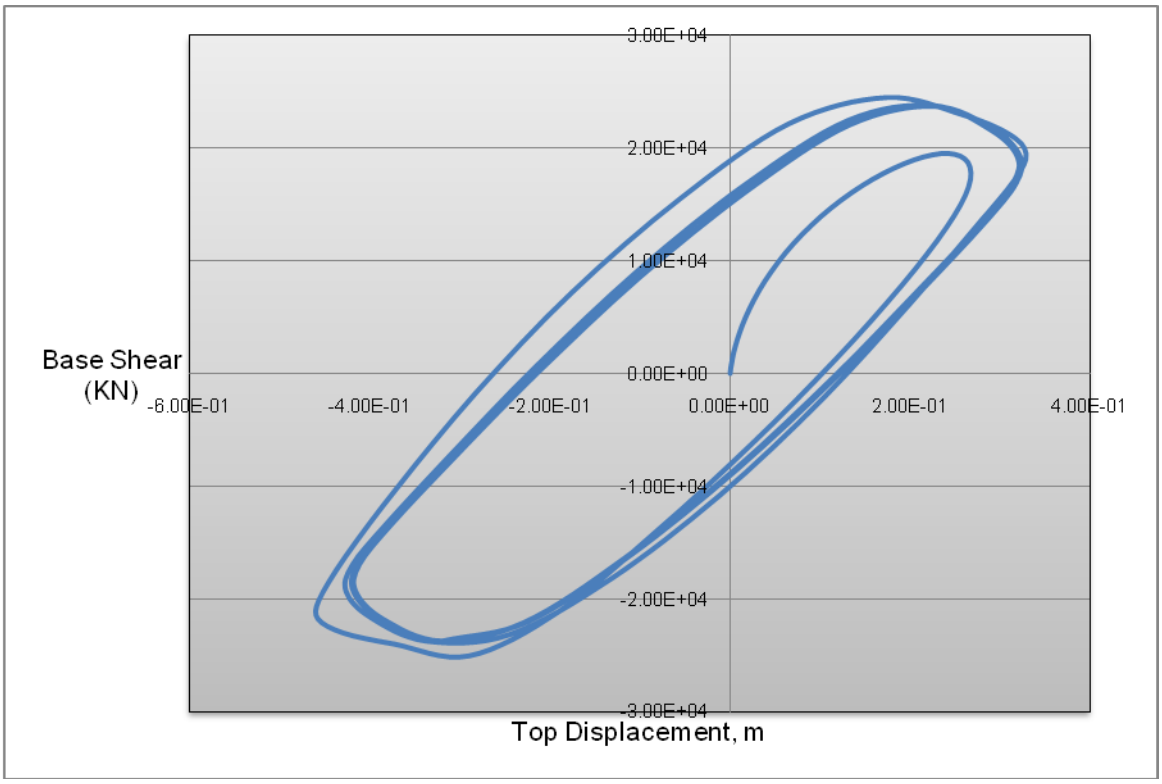
RayW. Clough, Joseph Penzien (1995), **Dynamics of structures.** (3rd ed) Ed. Computers & Structures, Inc.

SAC Joint Venture, (2000), **FEMA-355C**, State of the Art Report on Systems Performance of Steel Moment Frames Subject to Earthquake Ground Shaking, prepared by the SAC Joint Venture for the Federal Emergency Management Agency, Washington, DC.

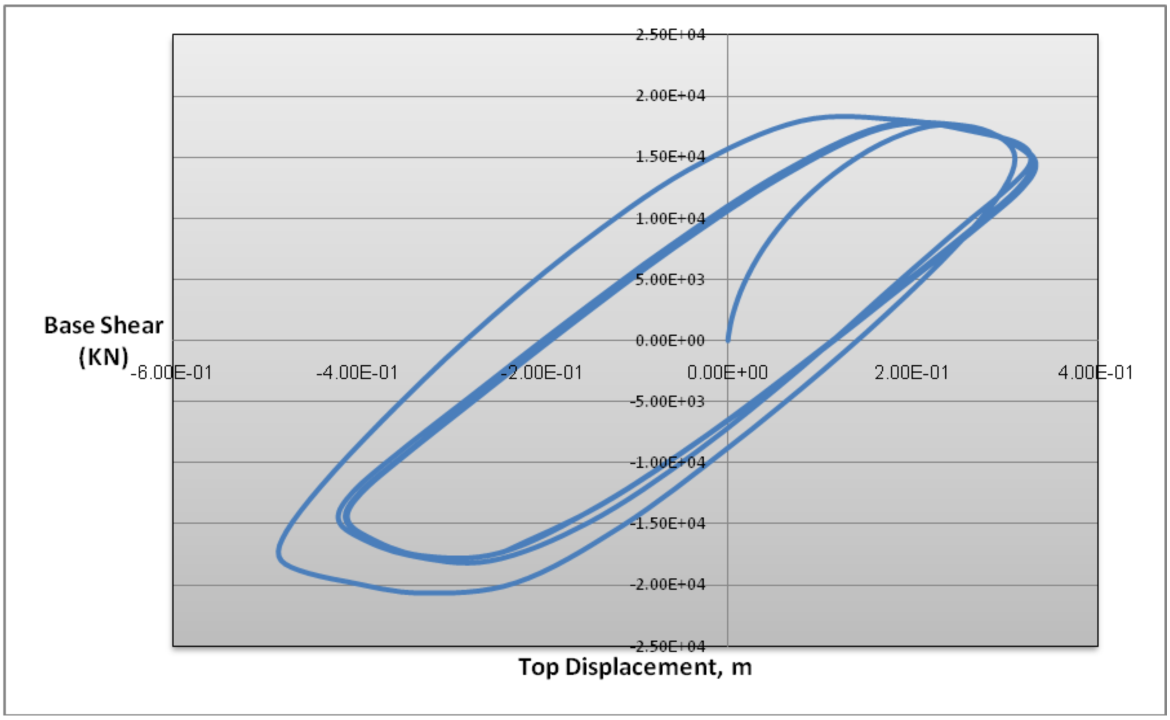
SAC Joint Venture, (2000), **FEMA-355F**, State of the Art Report on Systems Performance of Steel Moment Frames Subject to Earthquake Ground Shaking, prepared by the SAC Joint Venture for the Federal Emergency Management Agency, Washington, DC.

APPENDIX A

HYSTERESIS LOOP FOR 6-STOREY SYSTEMS

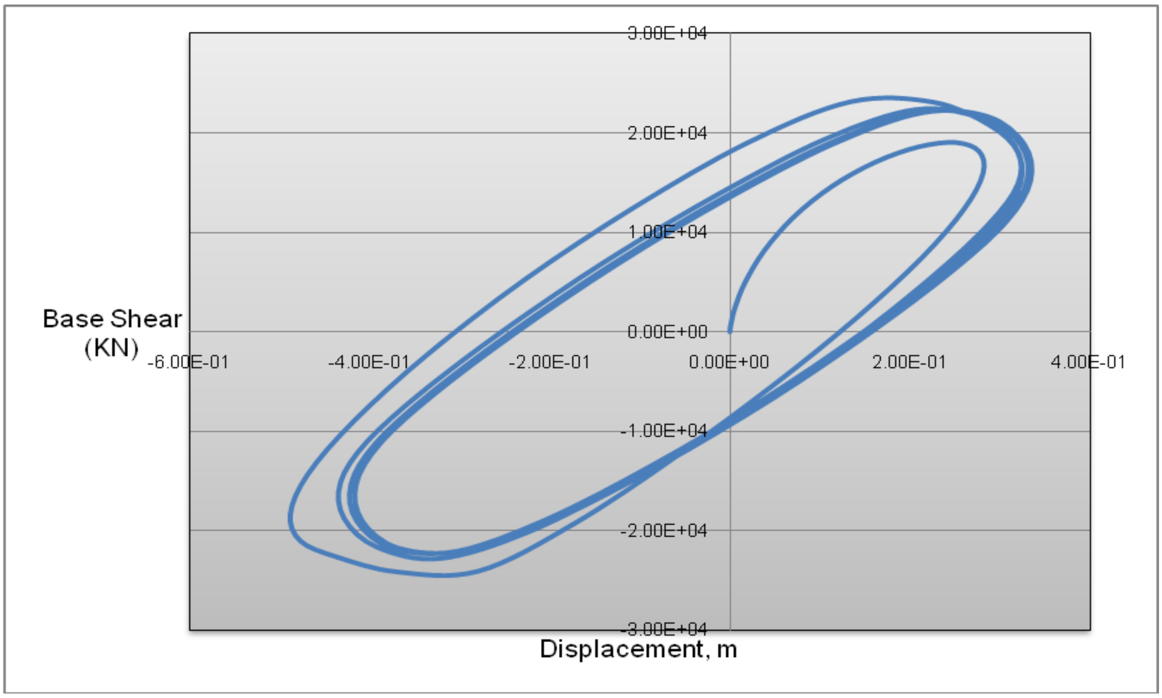


a)

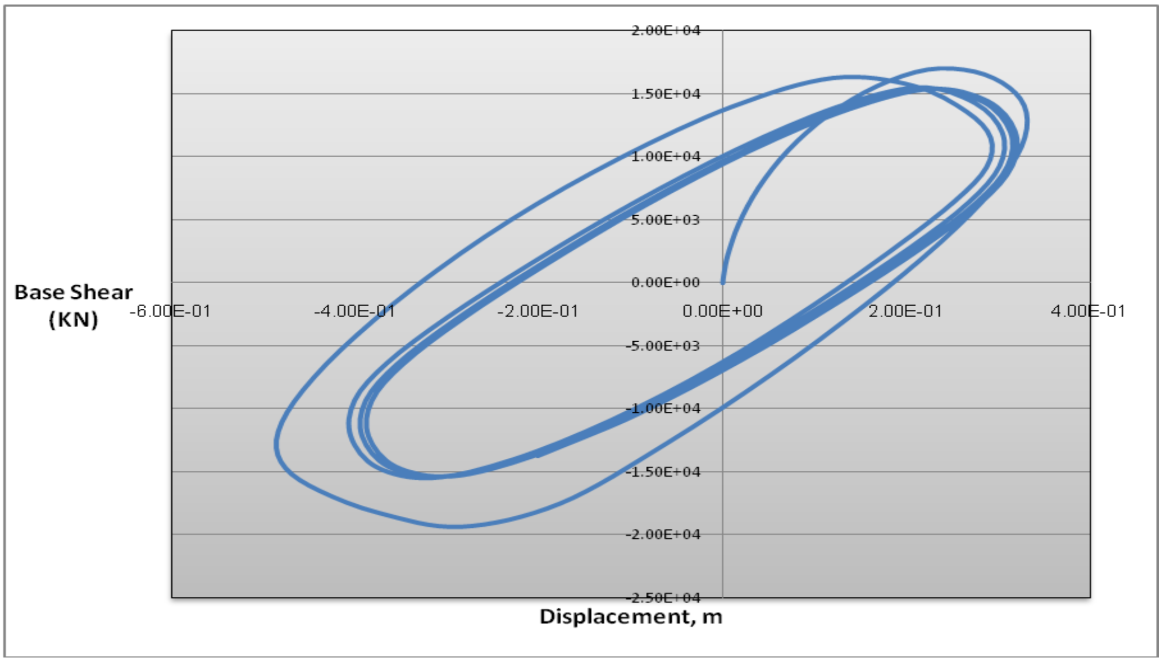


b)

Fig A.1 hysteresis loop behaviour for 6-storey Rigid Case building a) x-direction frames b) y-direction frames

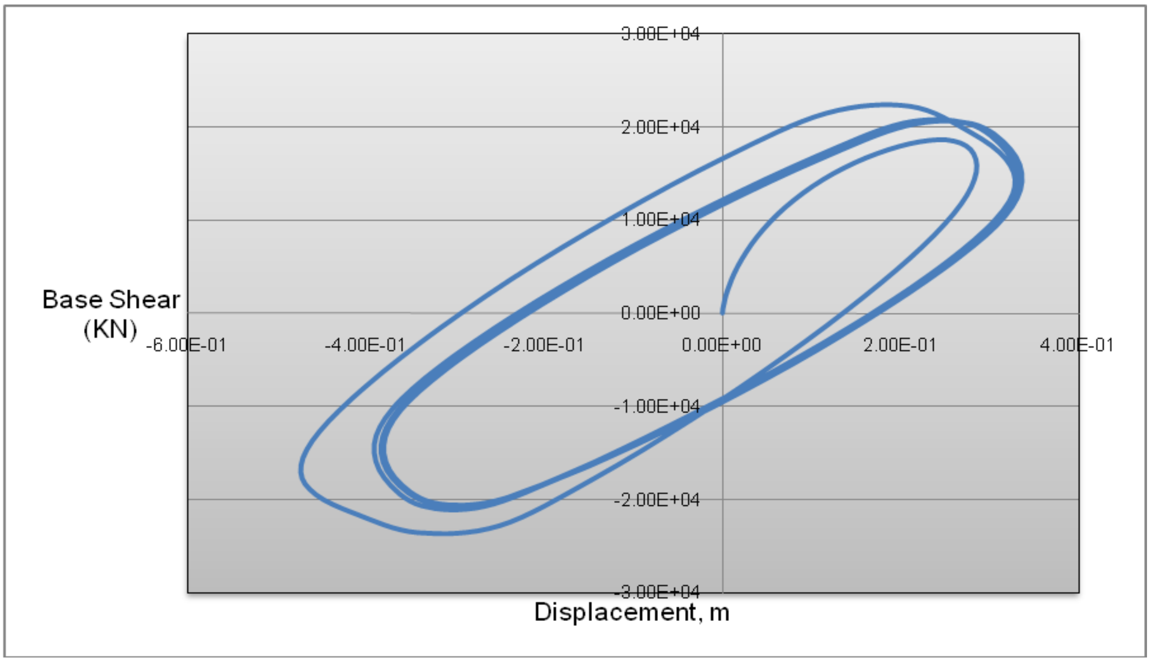


a)

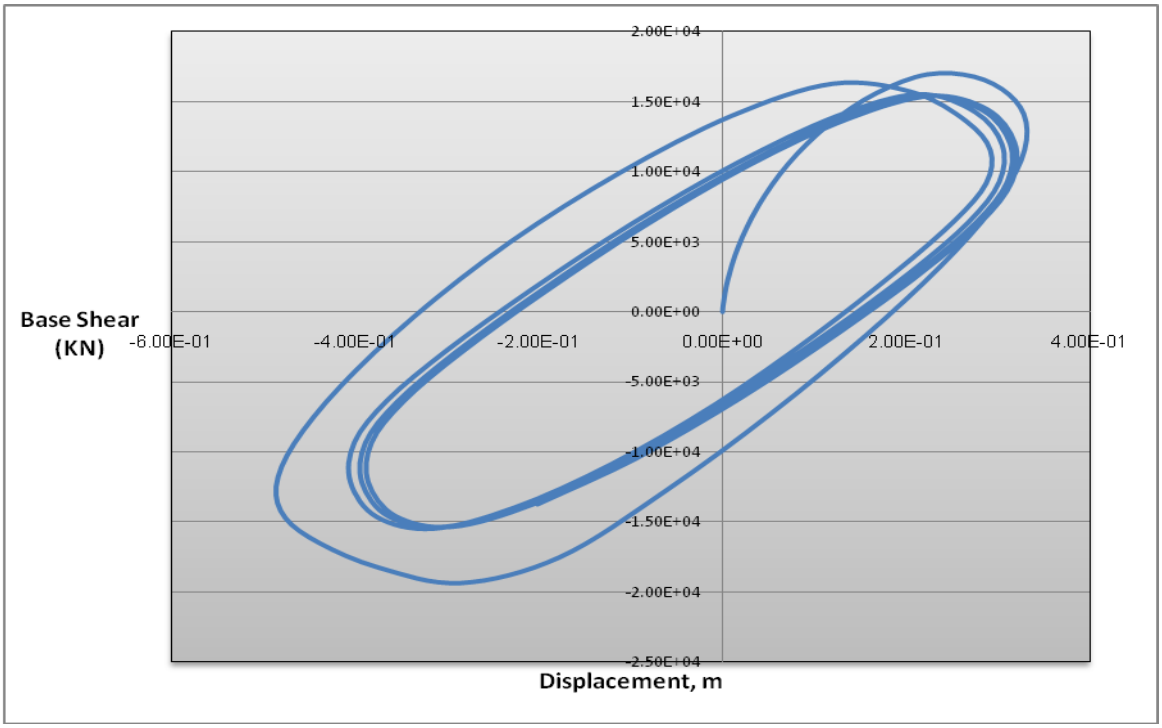


b)

Fig A.2 hysteresis loop behavior for 6SR45 building a) x-direction frames b) y-direction frames

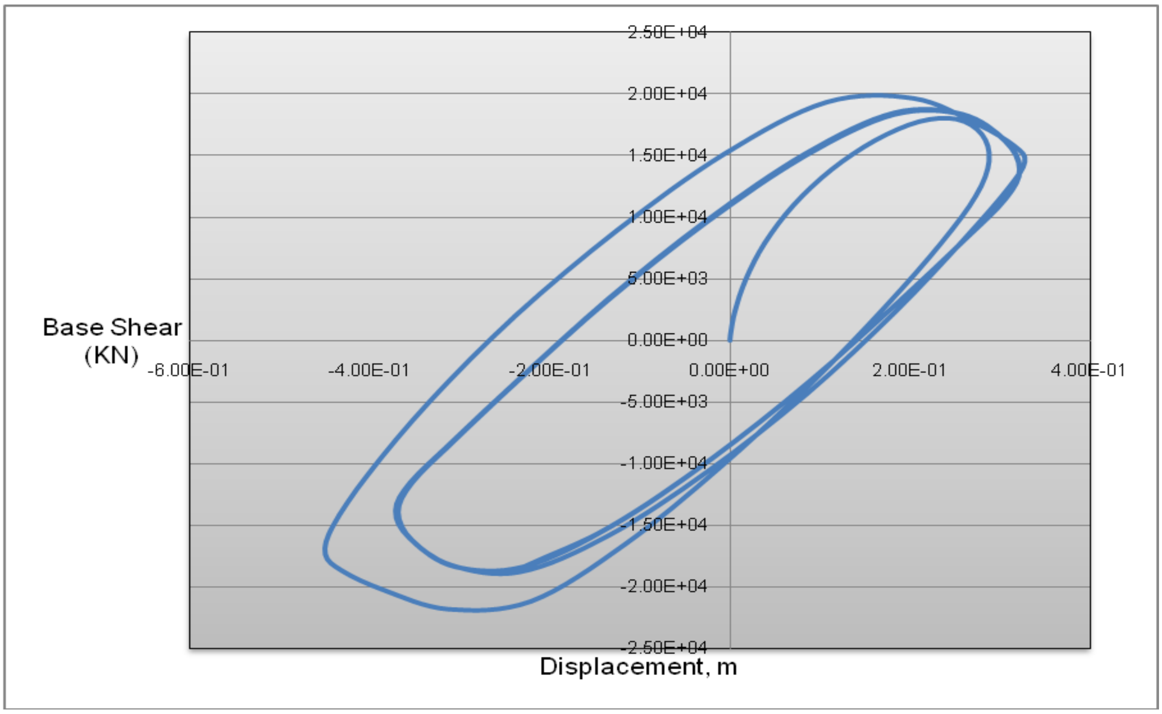


a)

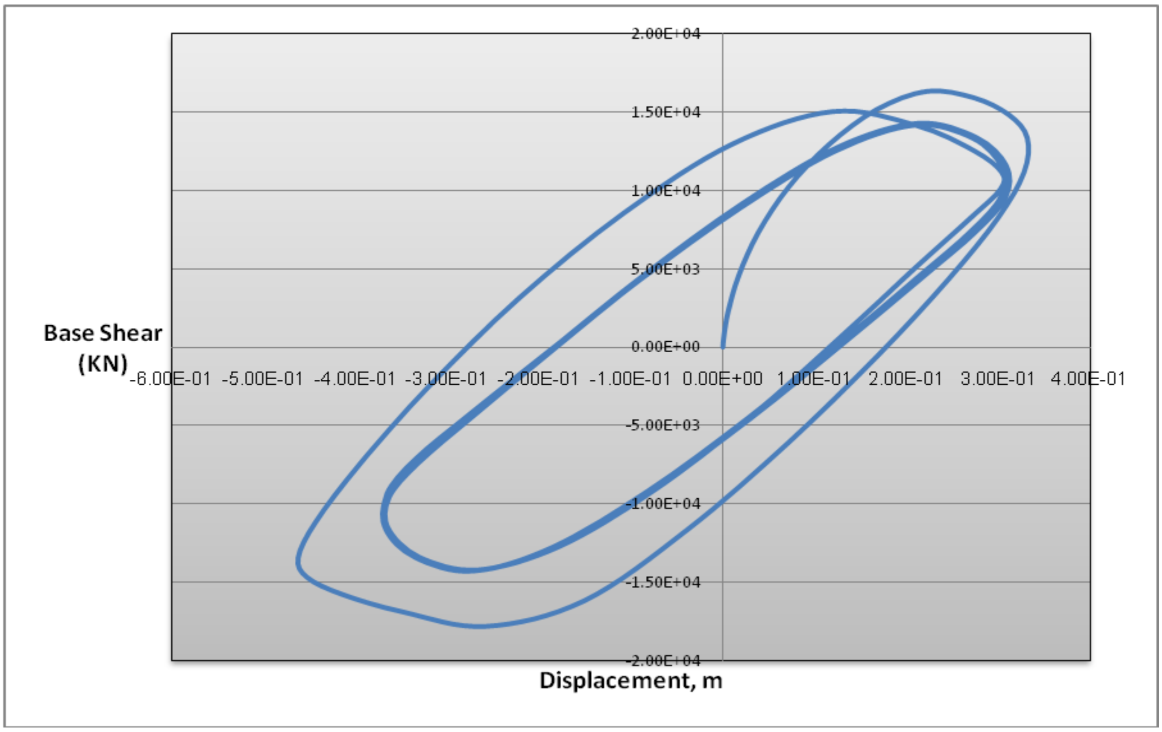


b)

Fig A.3 hysteresis loop behavior for 6SR34 building a) x-direction frames
b) y-direction frames

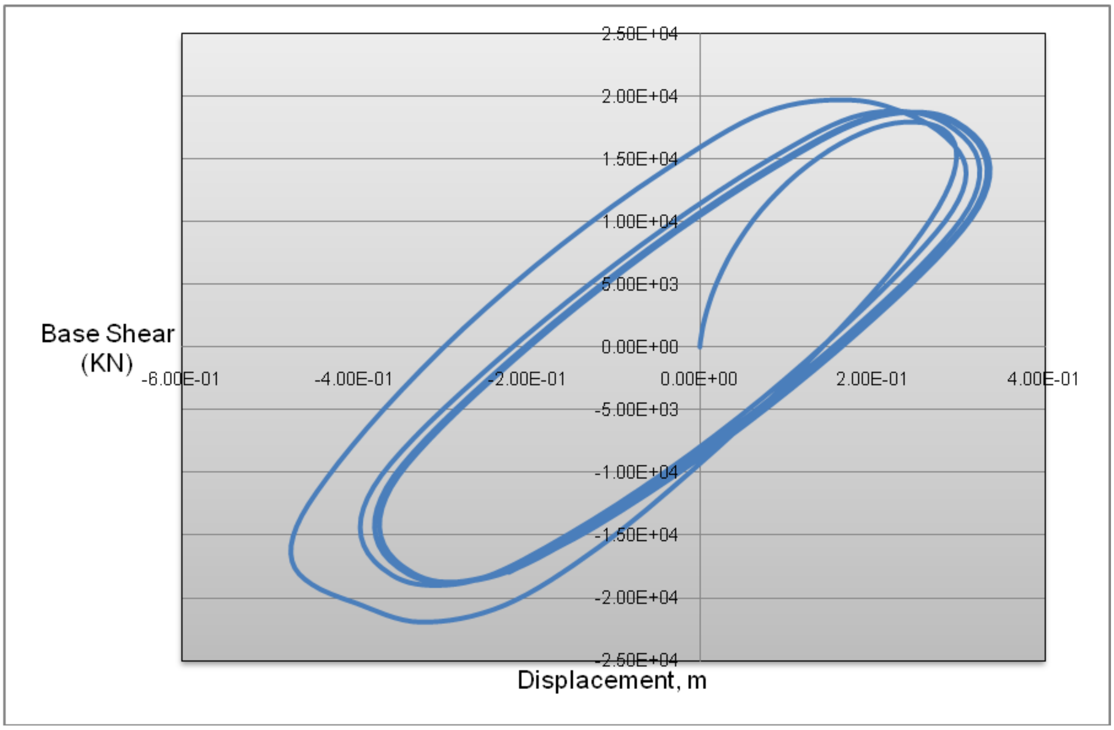


a)

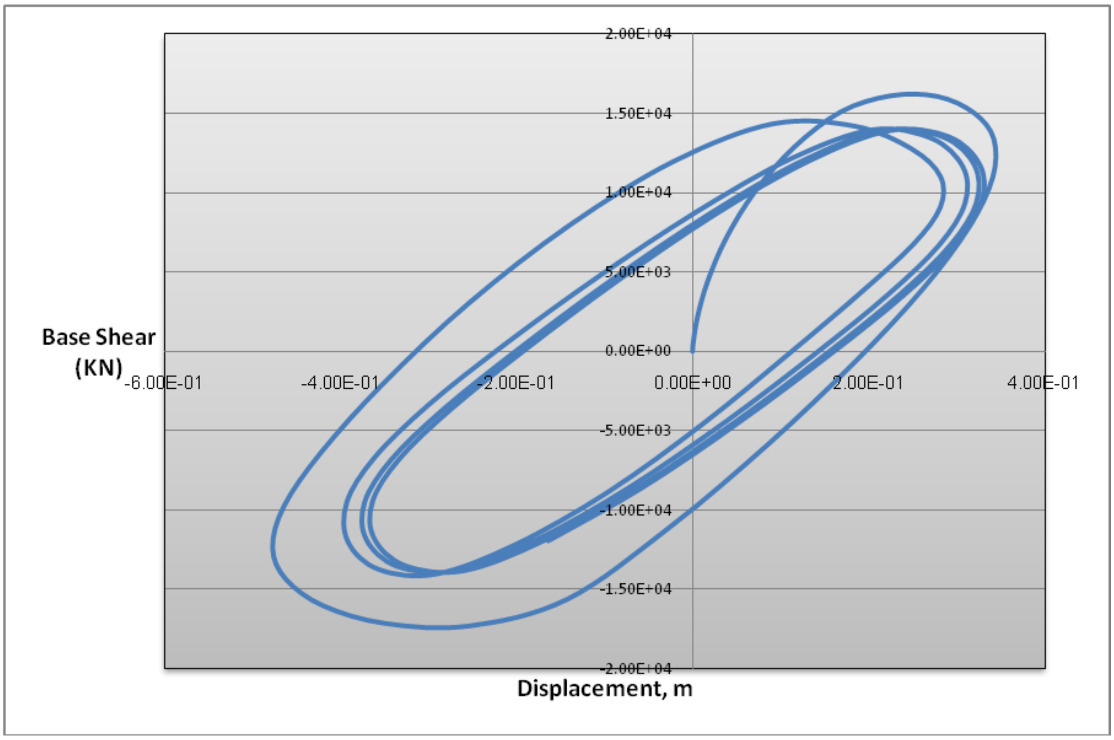


b)

Fig A.4 hysteresis loop behavior for 6SR23 building a) x-direction frames b) y-direction frames

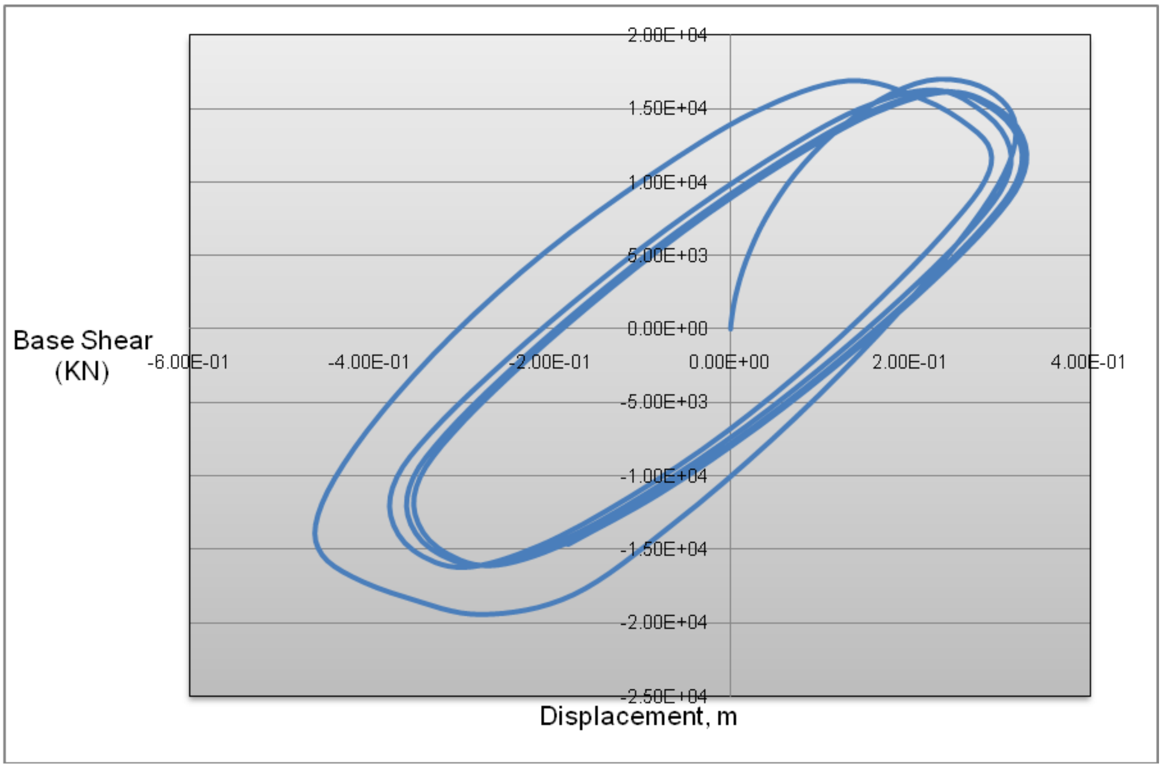


a)

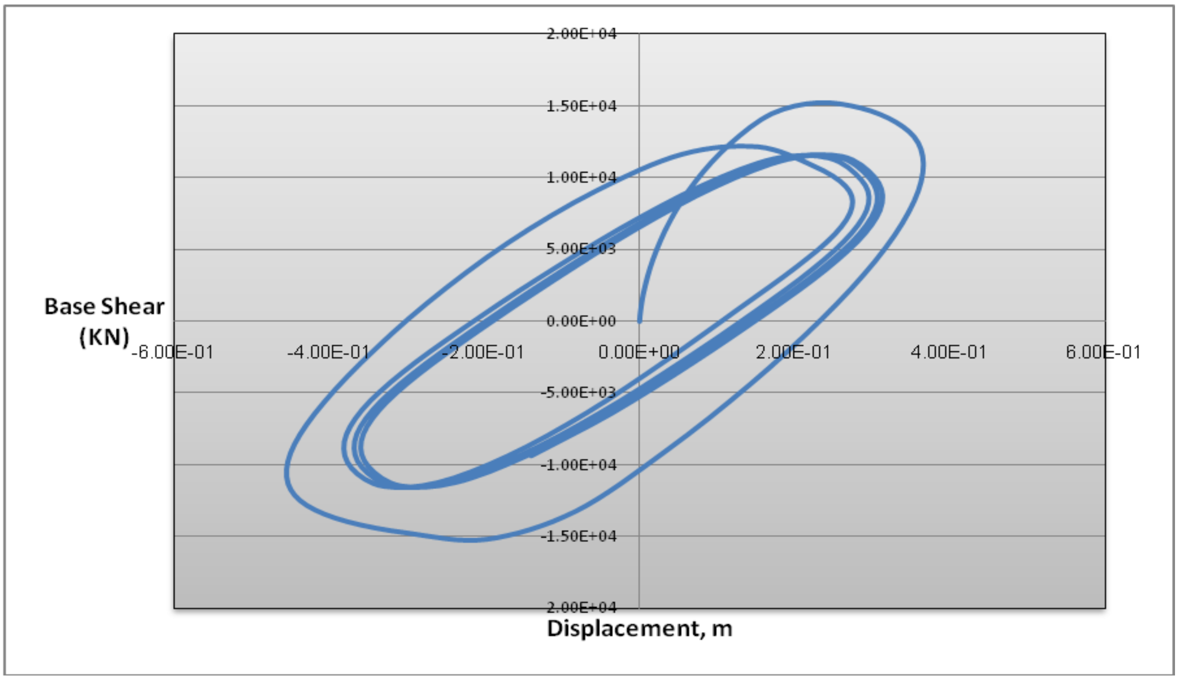


b)

Fig A.5 hysteresis loop behavior for 6SR1346 building a) x-direction frames
b) y-direction frames

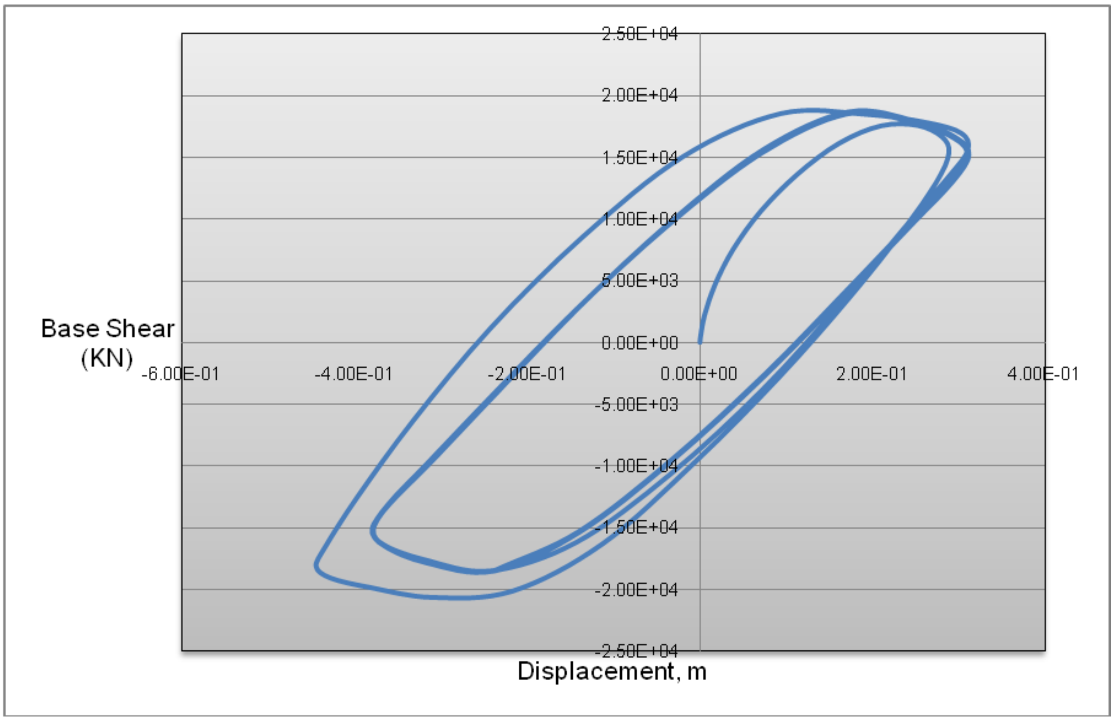


a)

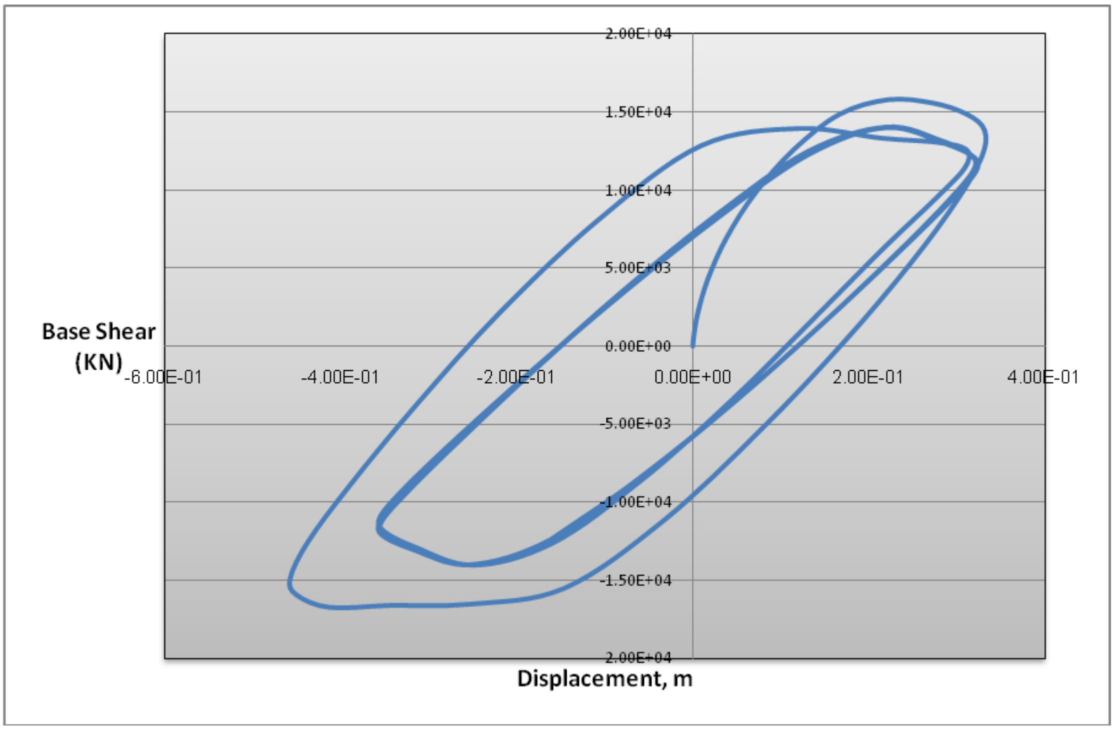


b)

Fig A.6 hysteresis loop behavior for 6SRall building a) x-direction frames
b) y-direction frames

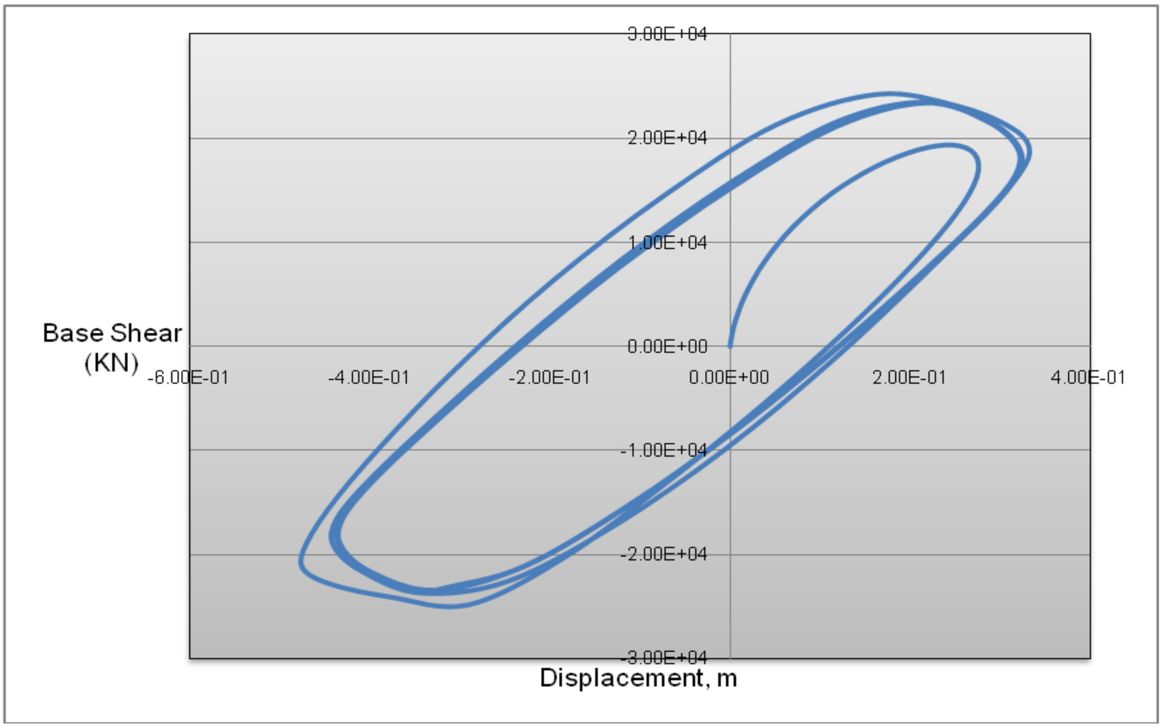


a)

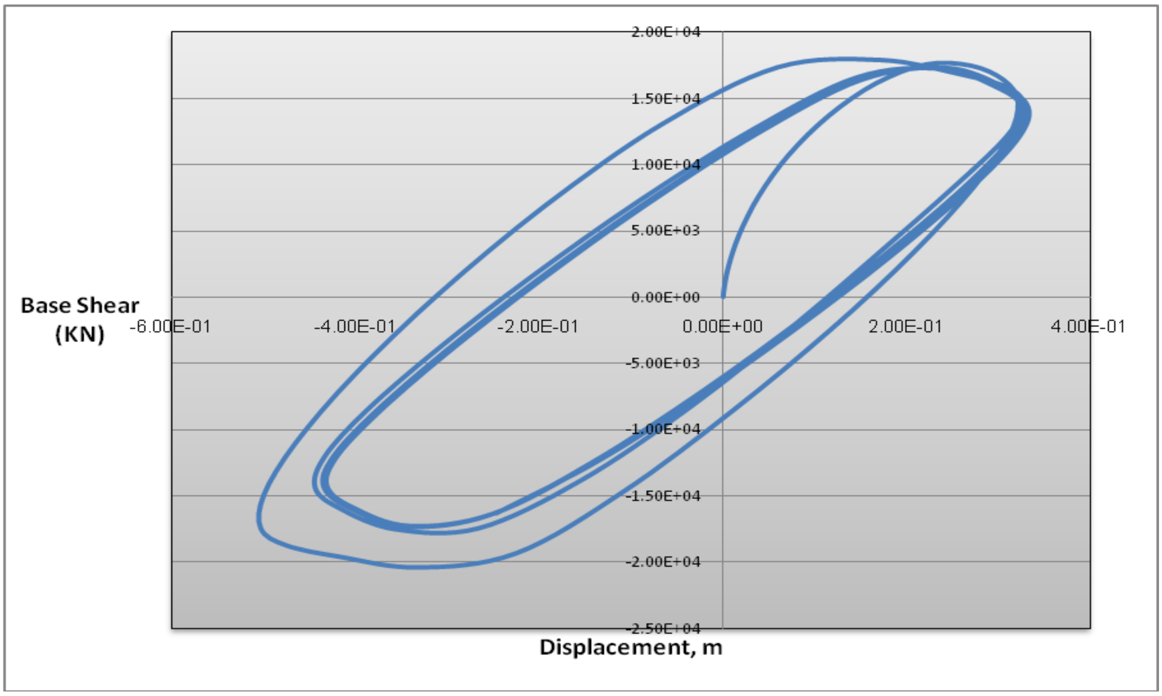


b)

Fig A.7 hysteresis loop behavior for 6SR12 building a) x-direction frames
b) y-direction frames

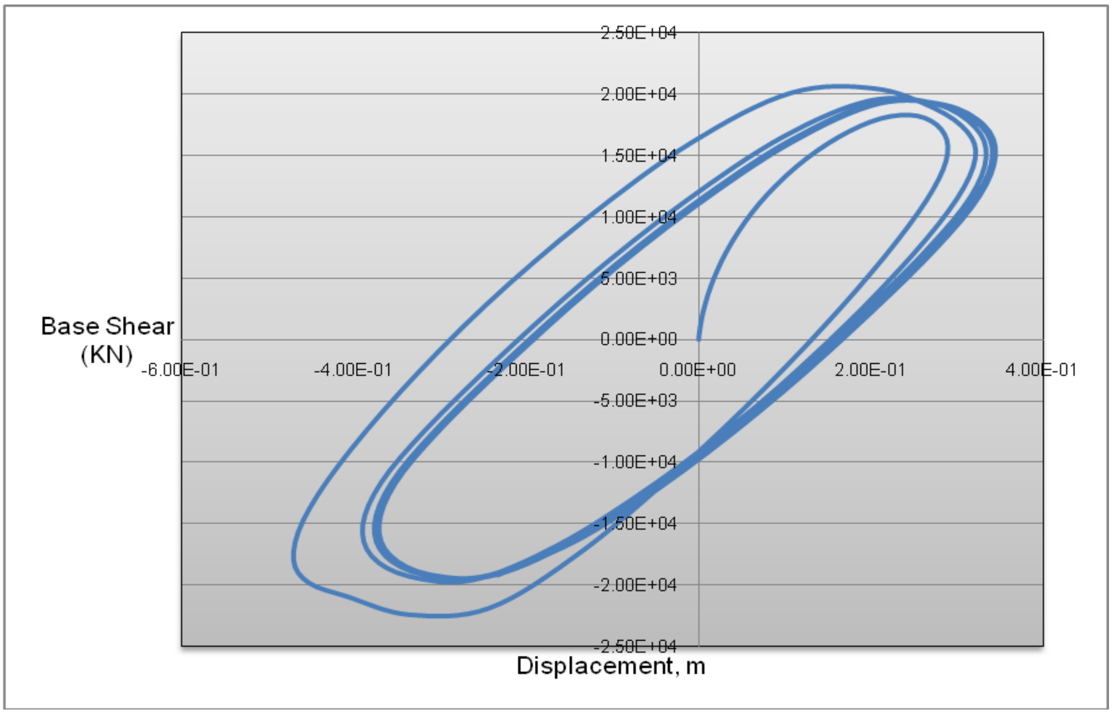


a)

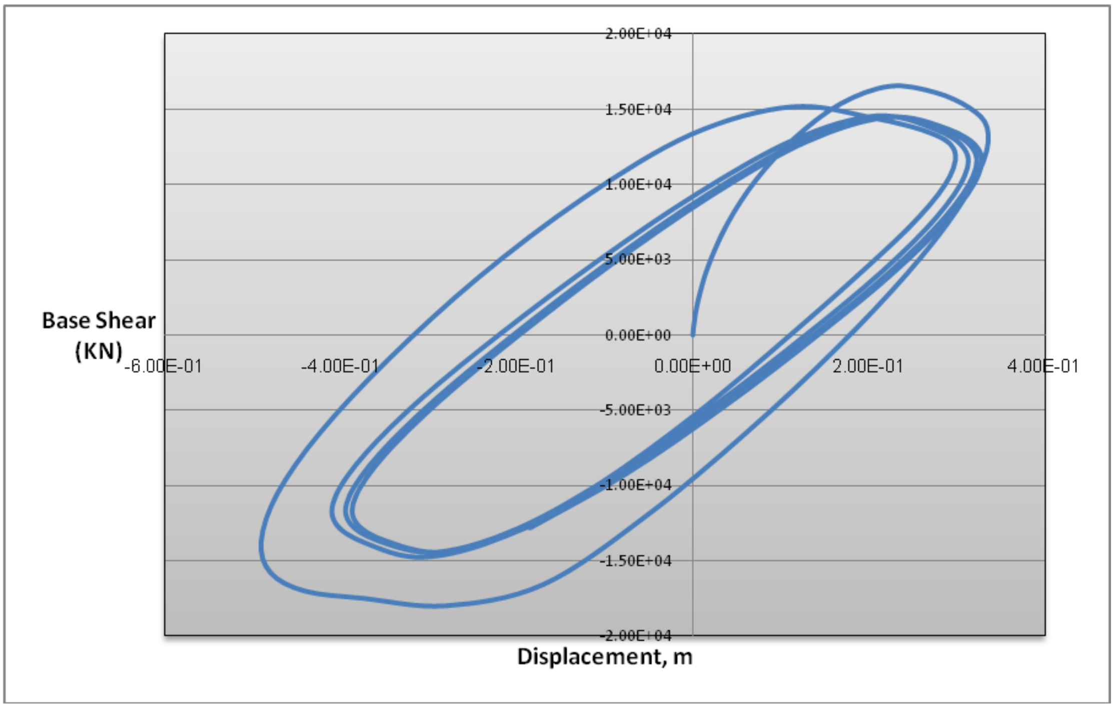


b)

Fig A.8 hysteresis loop behavior for 6SR56 building a) x-direction frames b) y-direction frames

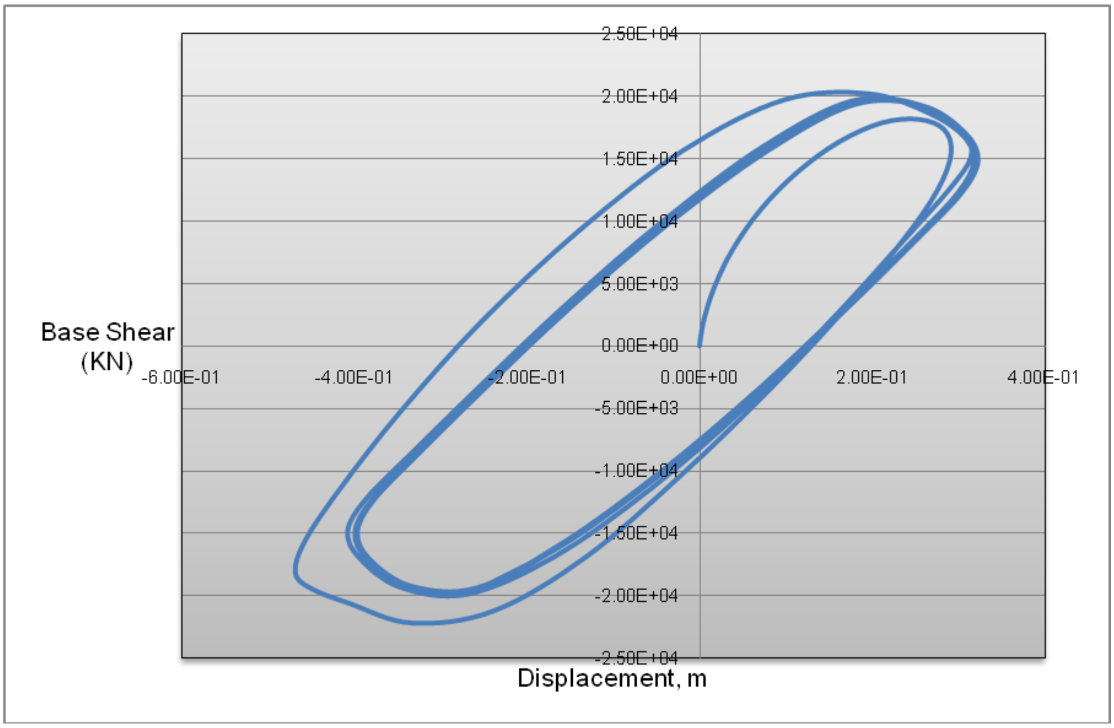


a)

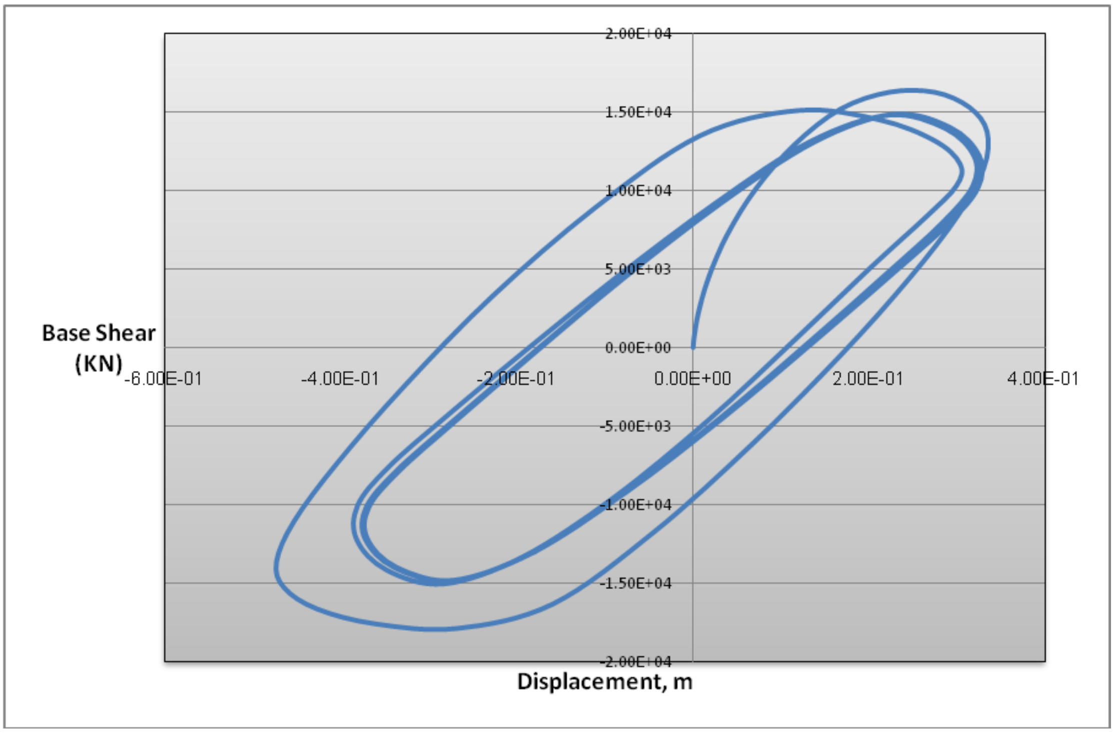


b)

Fig A.9 hysteresis loop behavior for 6SR246 building a) x-direction frames
b) y-direction frames

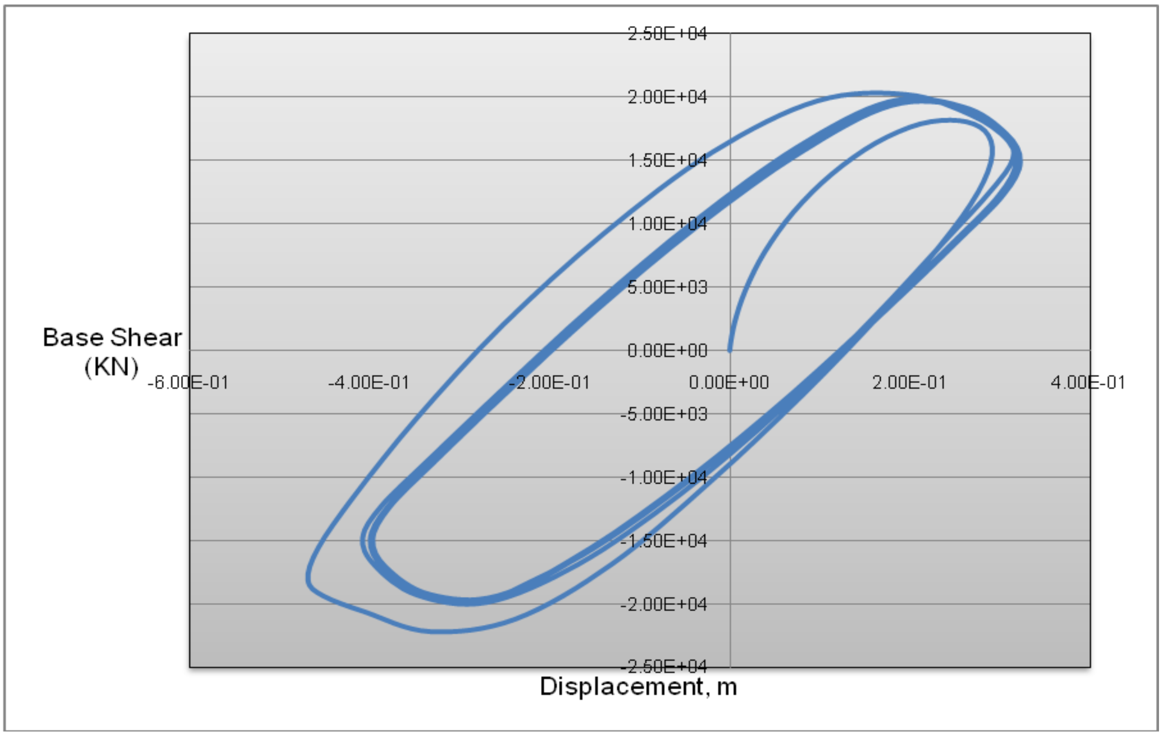


a)

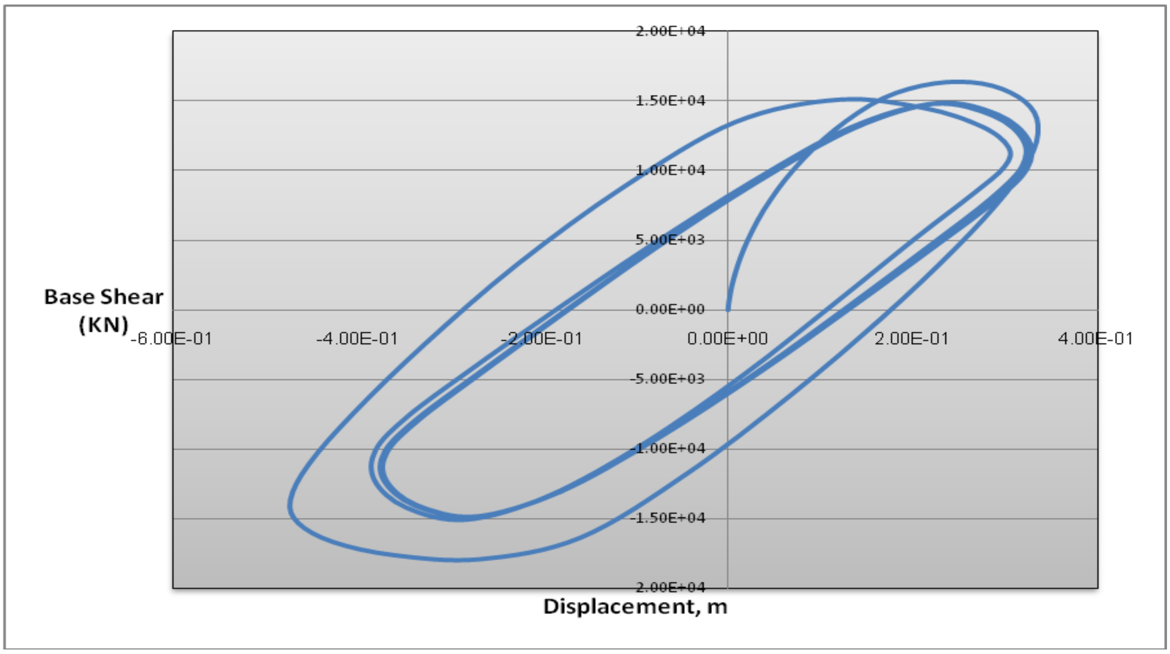


b)

Fig A.10 hysteresis loop behavior for 6SR135 building a) x-direction frames
b) y-direction frames

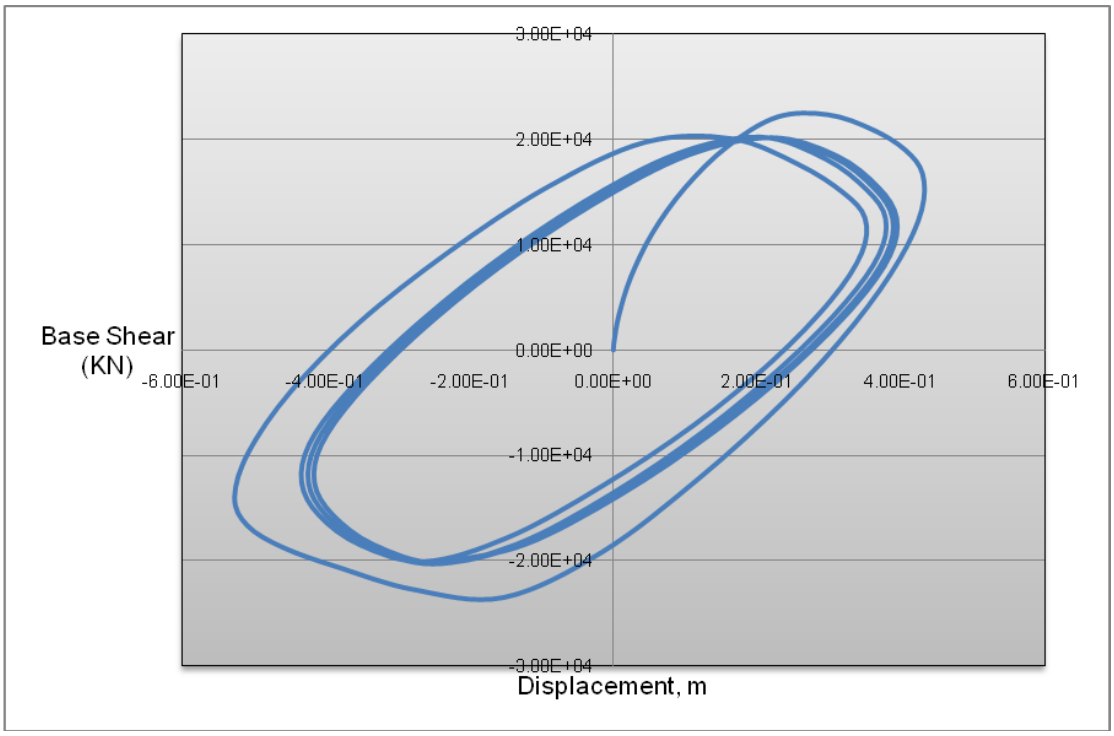


a)

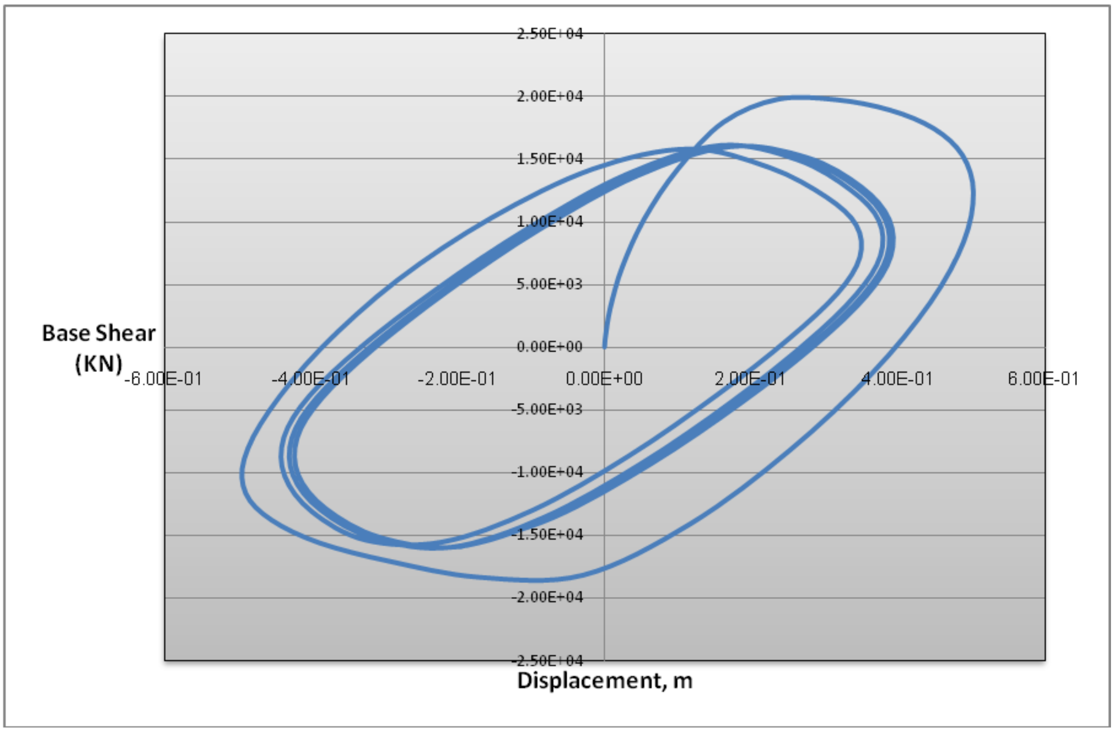


b)

Fig A.11 hysteresis loop behavior for 6SR235 building a) x-direction frames
b) y-direction frames

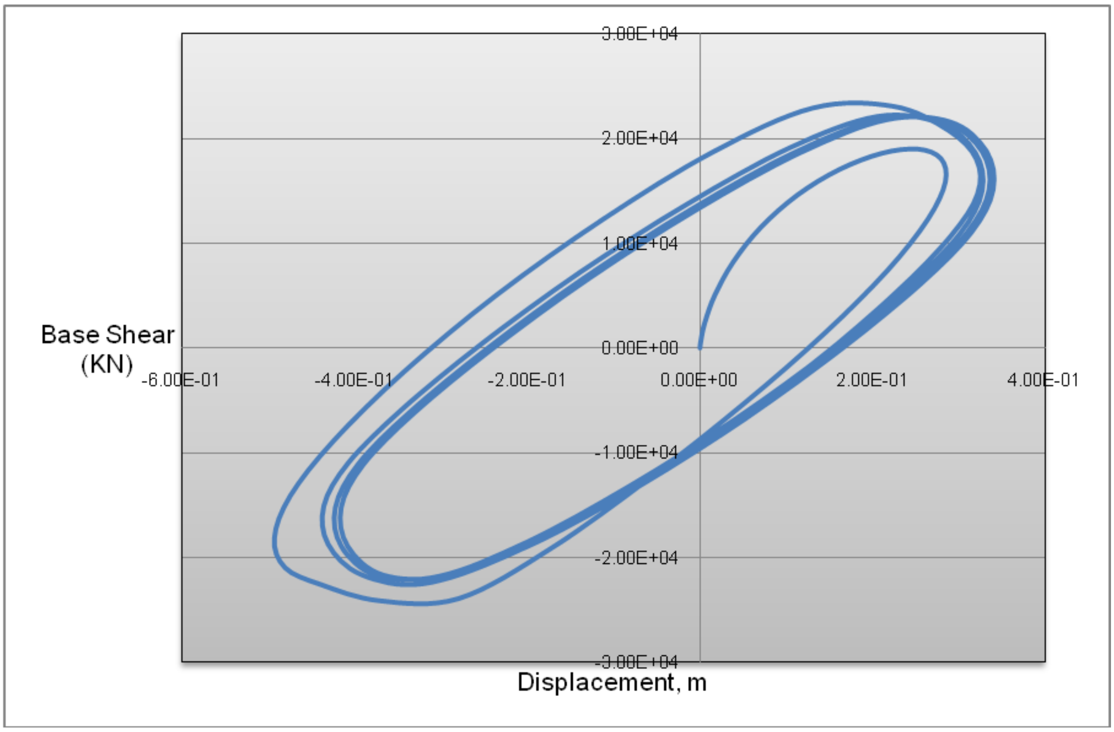


a)

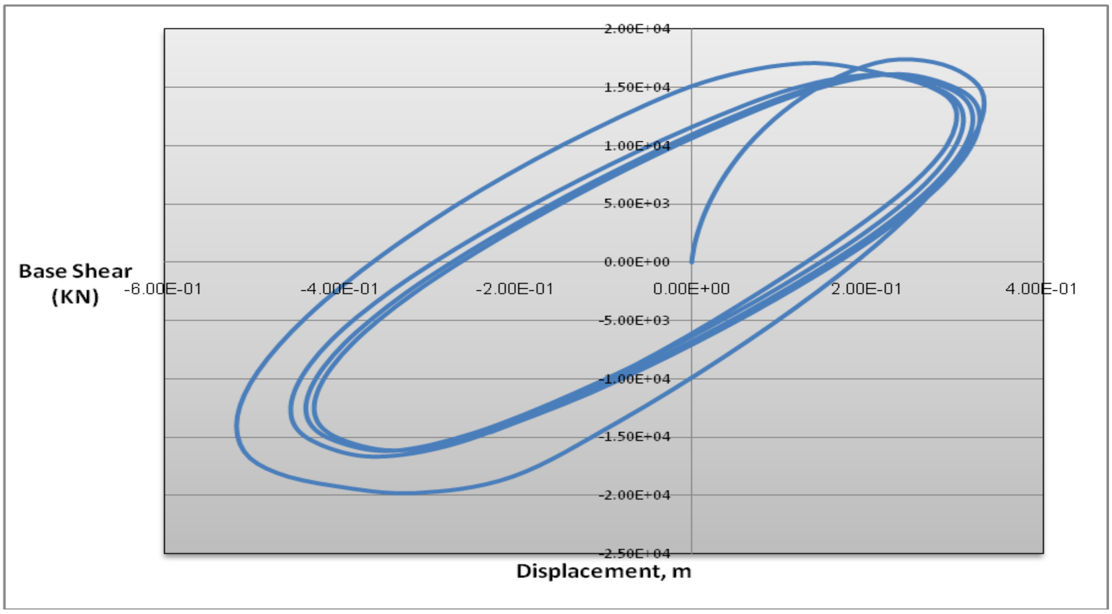


b)

Fig A.12 hysteresis loop behavior for 6SR234 building a) x-direction frames b) y-direction frames

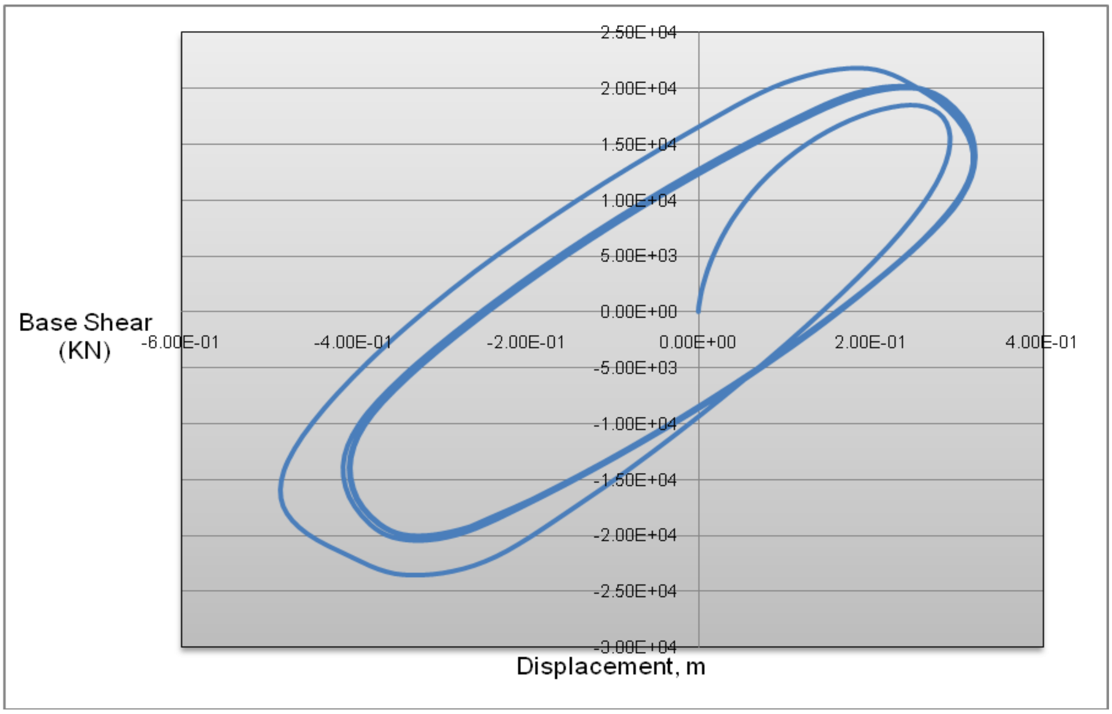


a)

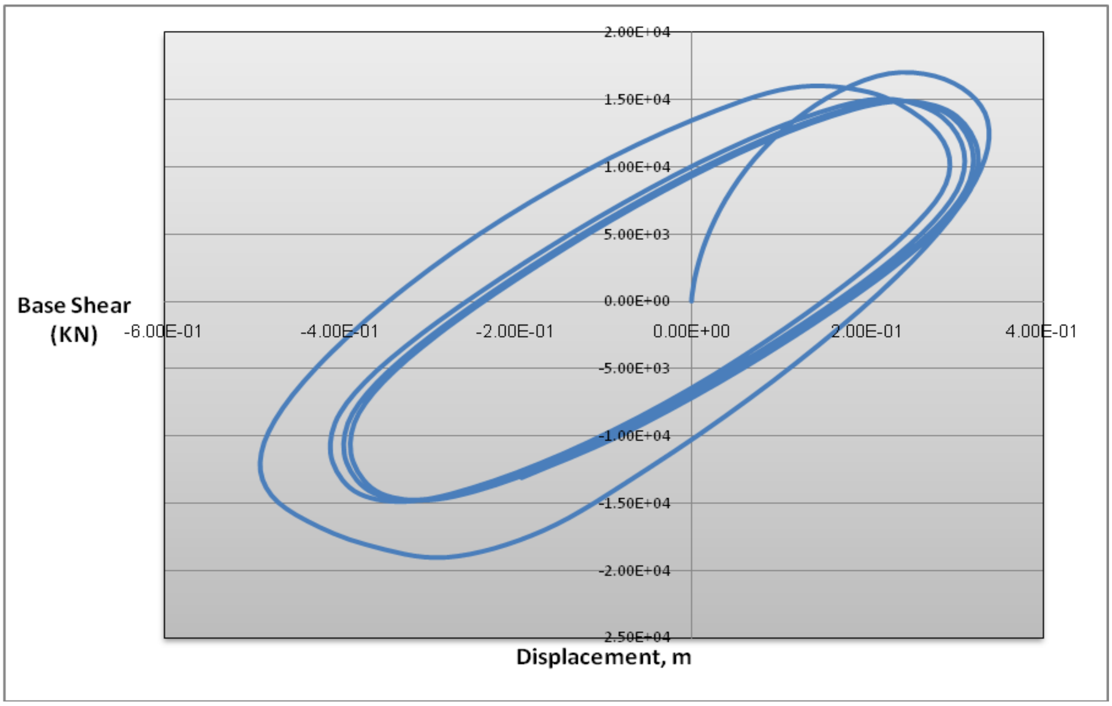


b)

Fig A.13 hysteresis loop behavior for 6SR456 building a) x-direction frames
b) y-direction frames

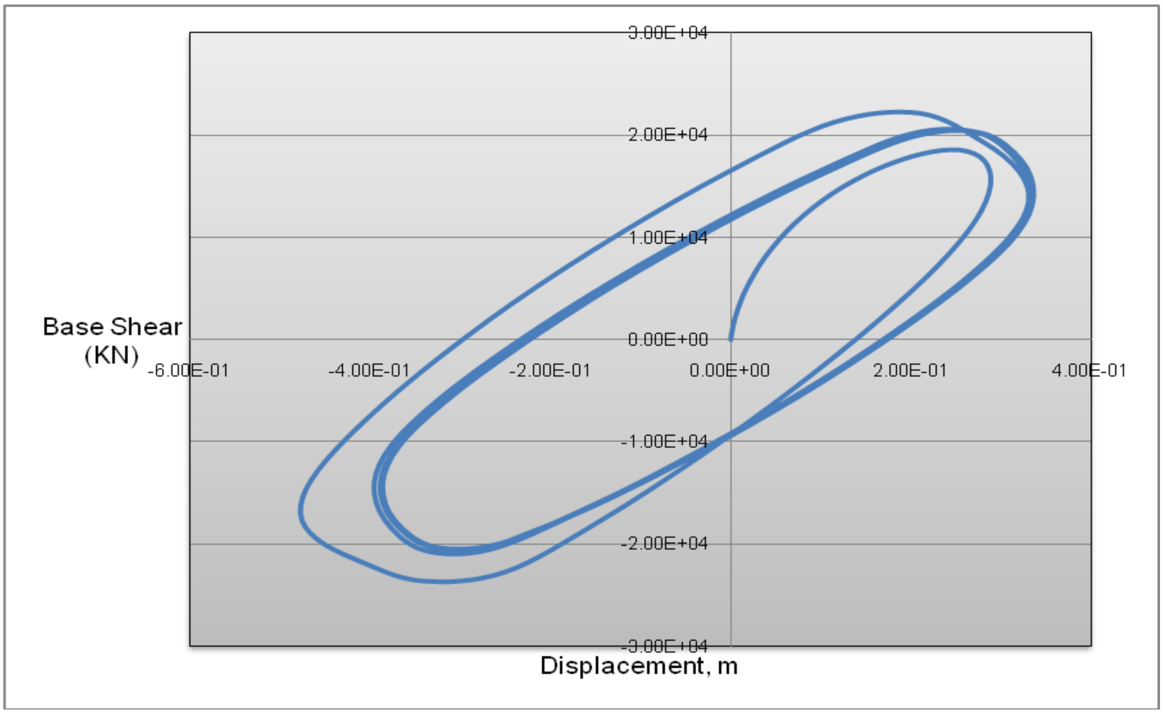


a)

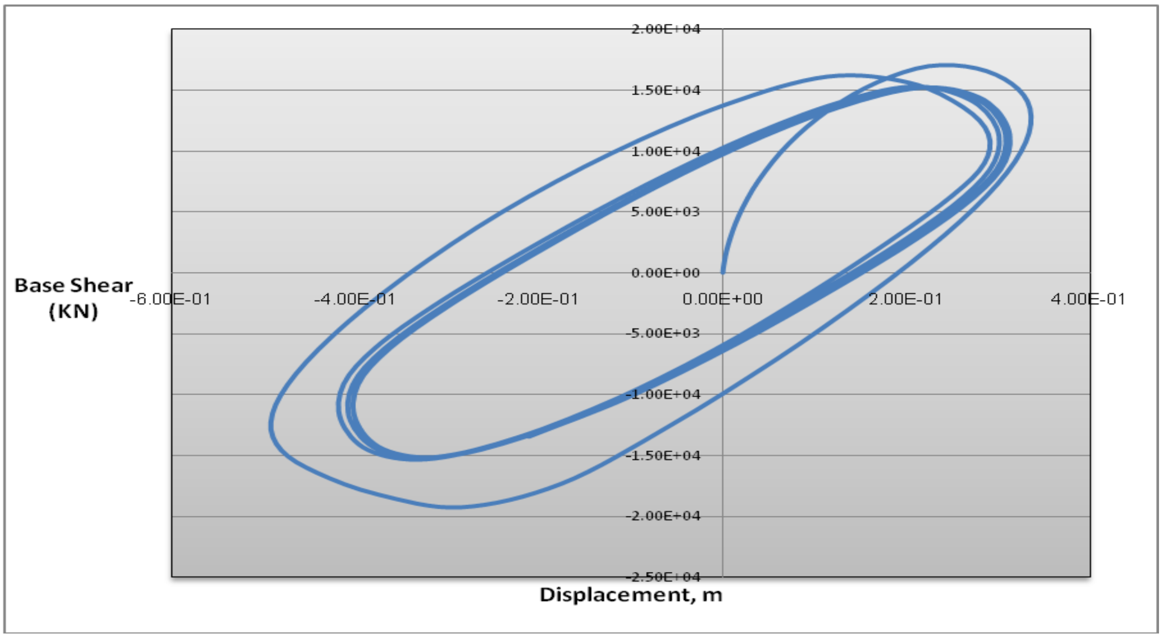


b)

Fig A.14 hysteresis loop behavior for 6SR345 building a) x-direction frames
b) y-direction frames

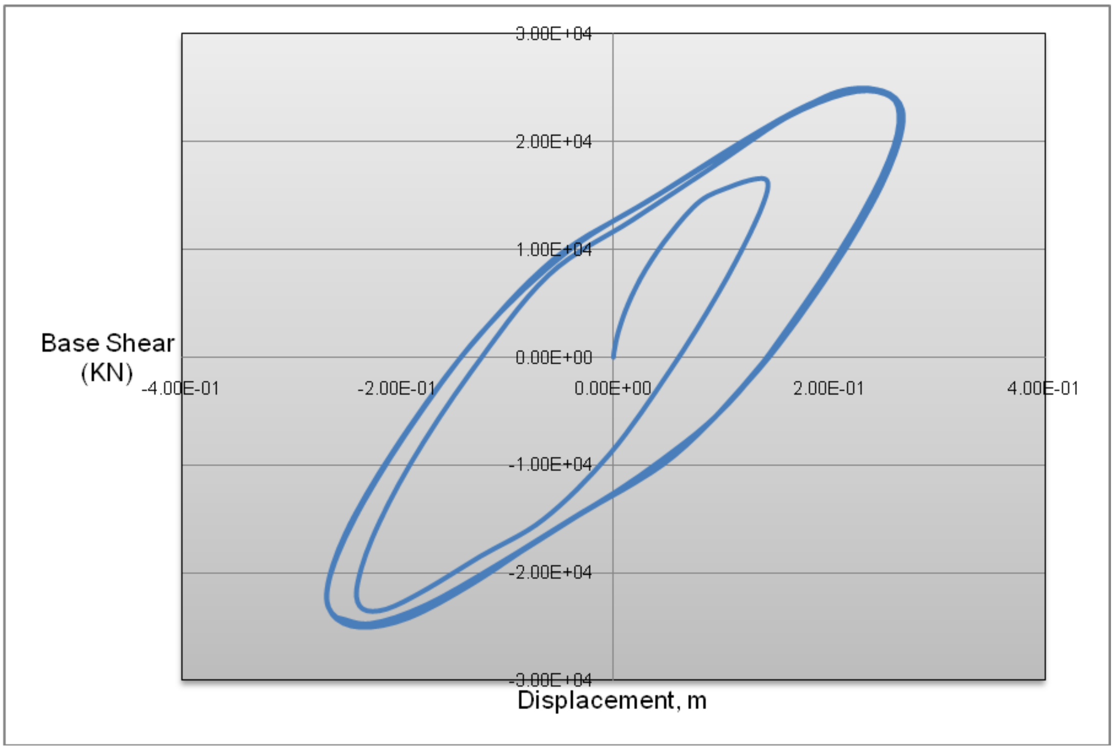


a)

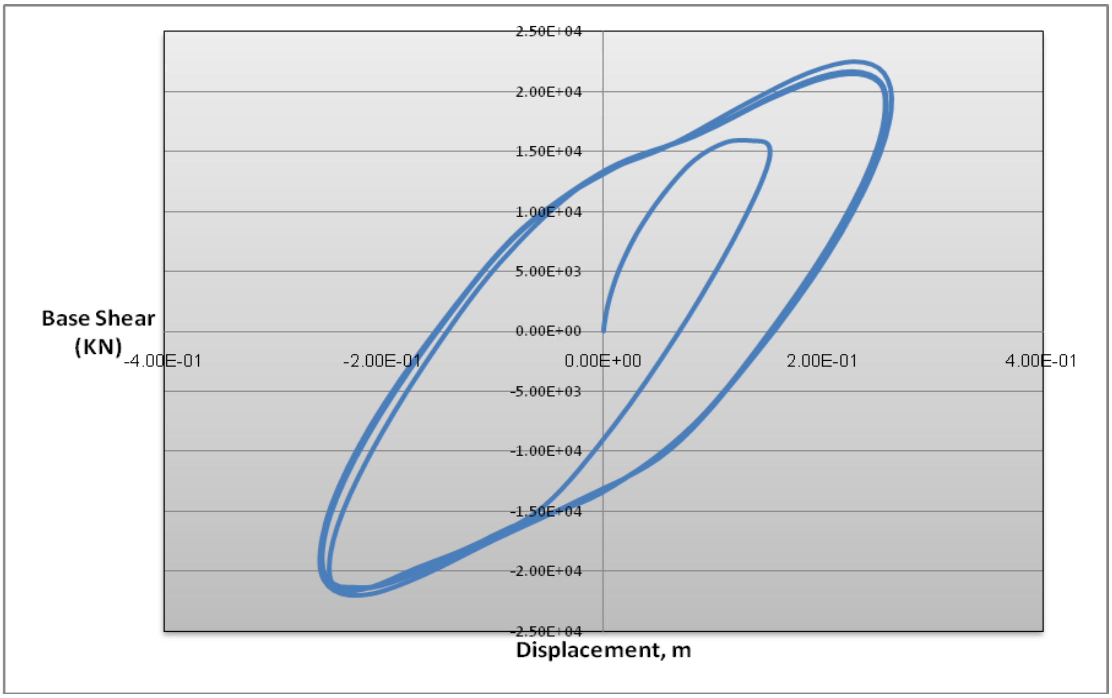


b)

Fig A.15 hysteresis loop behavior for 6SR346 building a) x-direction frames
b) y-direction frames

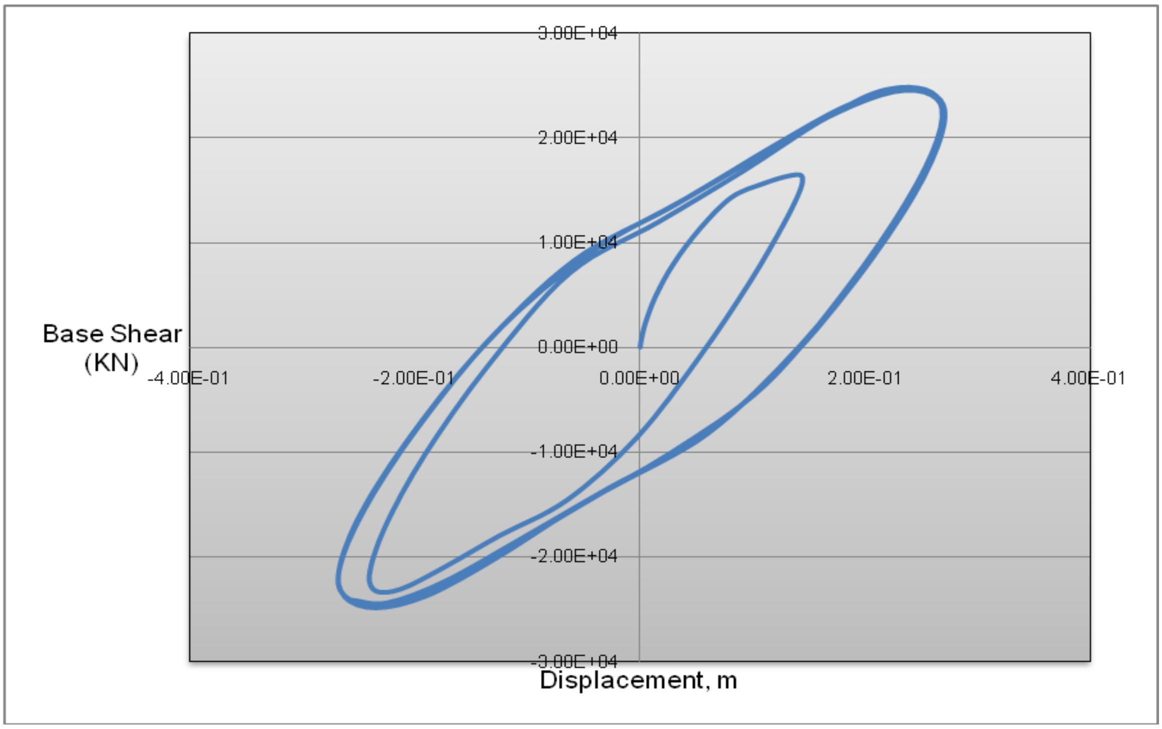


a)

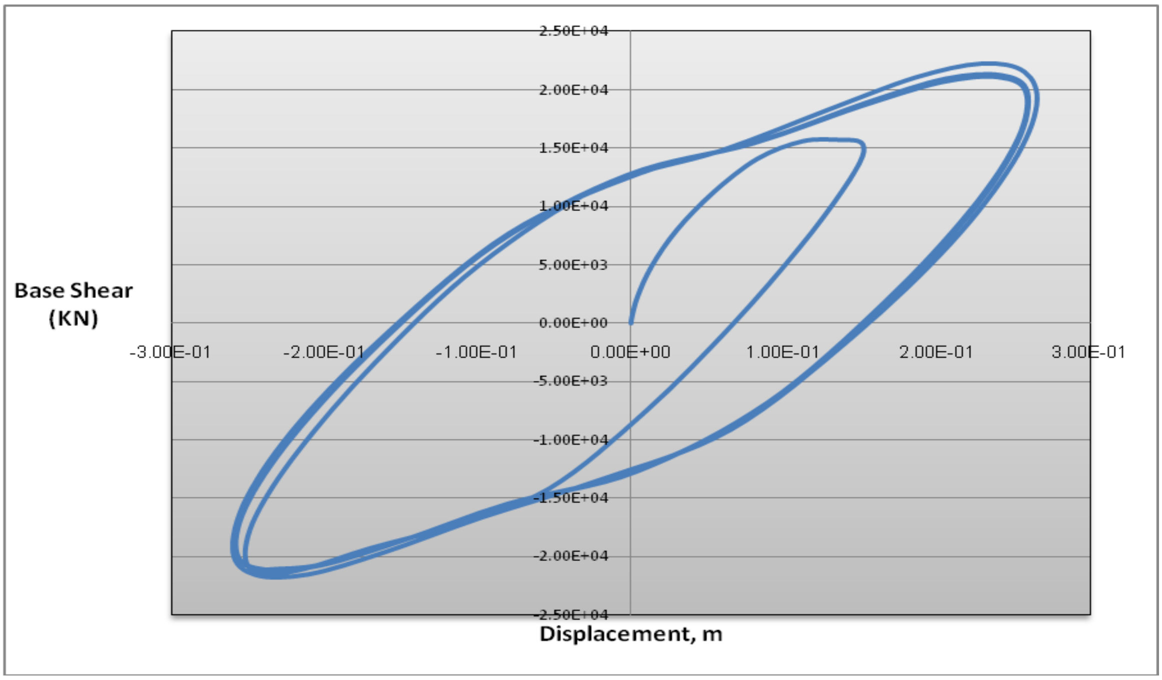


b)

Fig A.16 hysteresis loop behavior for 6BRBF cx cy building a) x-direction frames b) y-direction frames

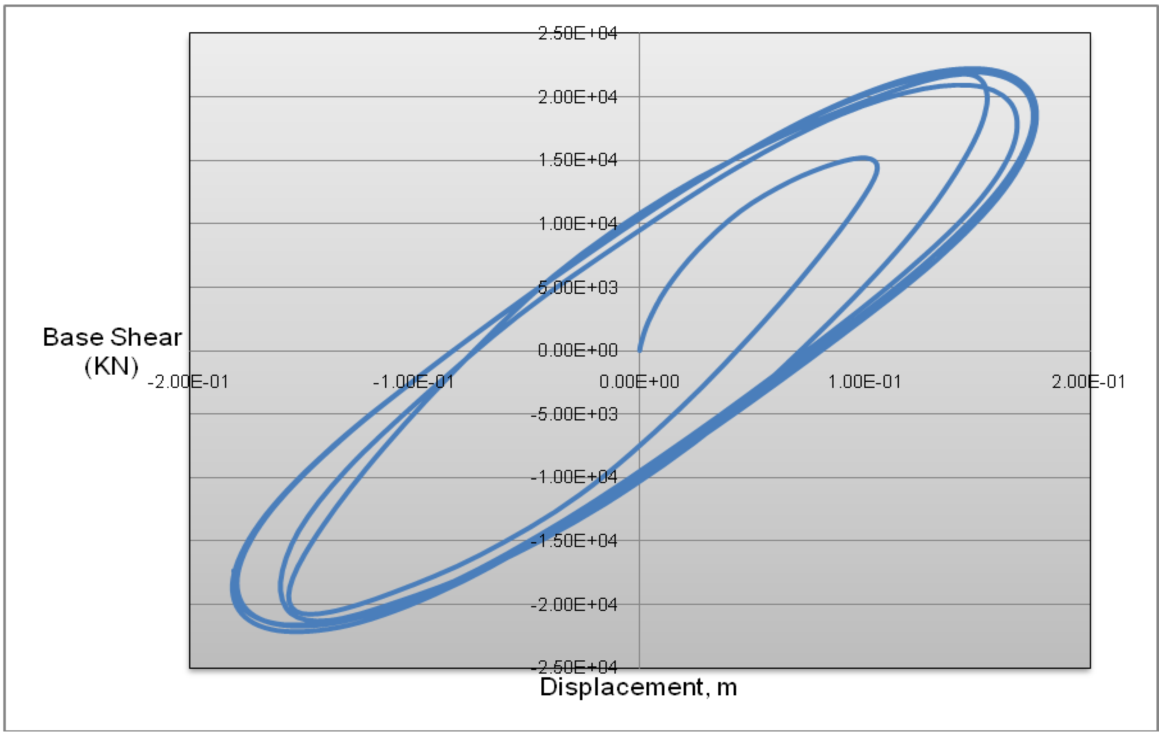


a)

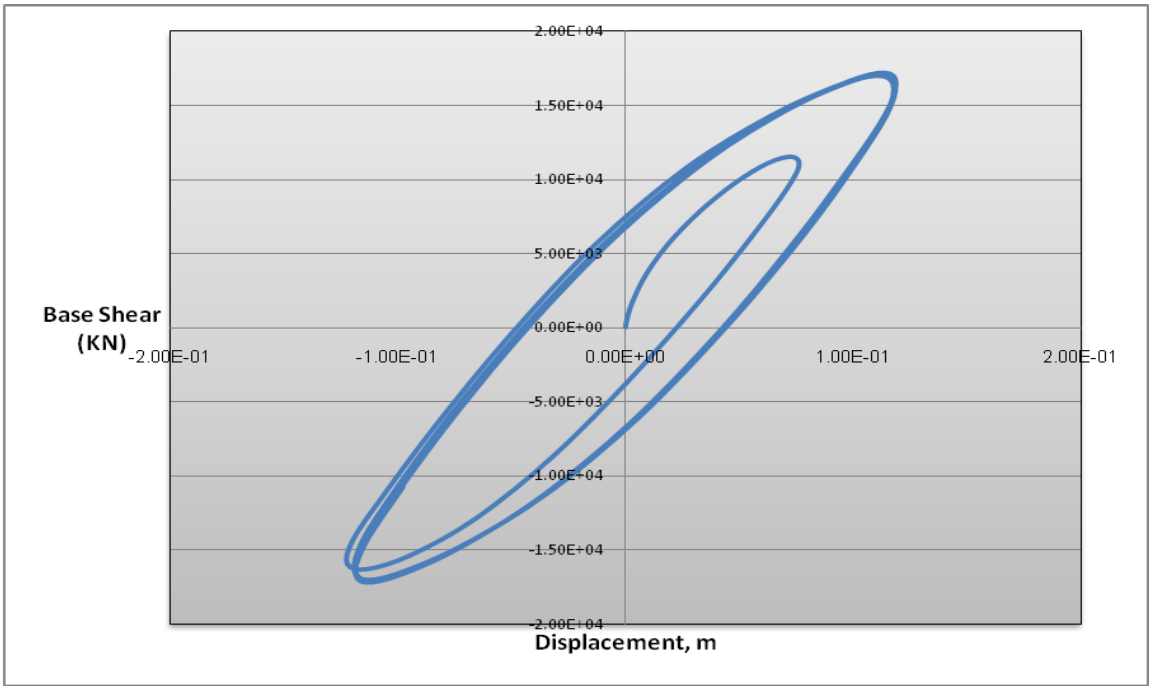


b)

Fig A.17 hysteresis loop behavior for 6BRBF cx sy building a) x-direction frames b) y-direction frames

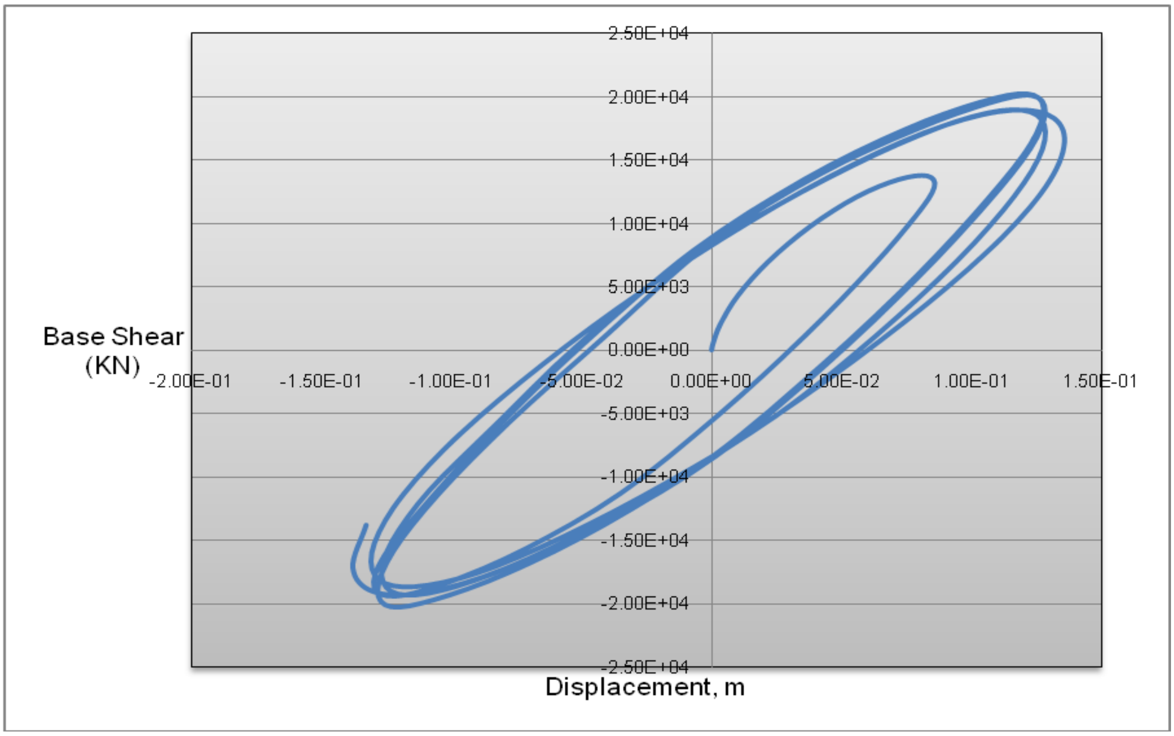


a)

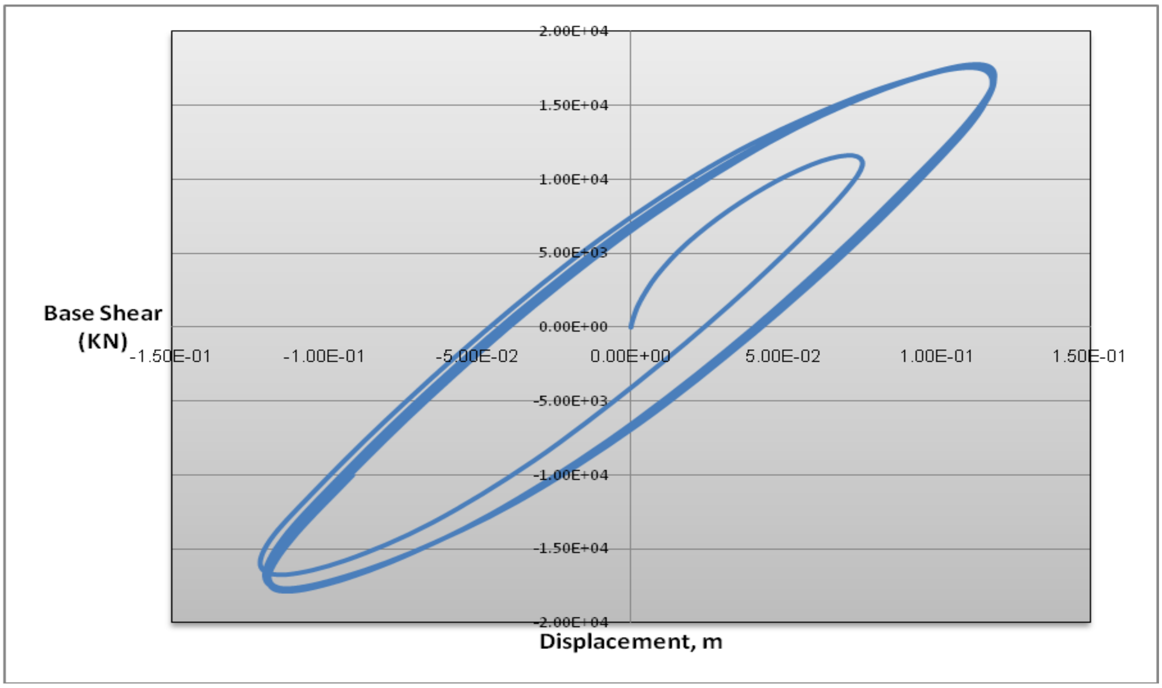


b)

Fig A.18 hysteresis loop behavior for 6EBF cx sy building a) x-direction frames
b) y-direction frames

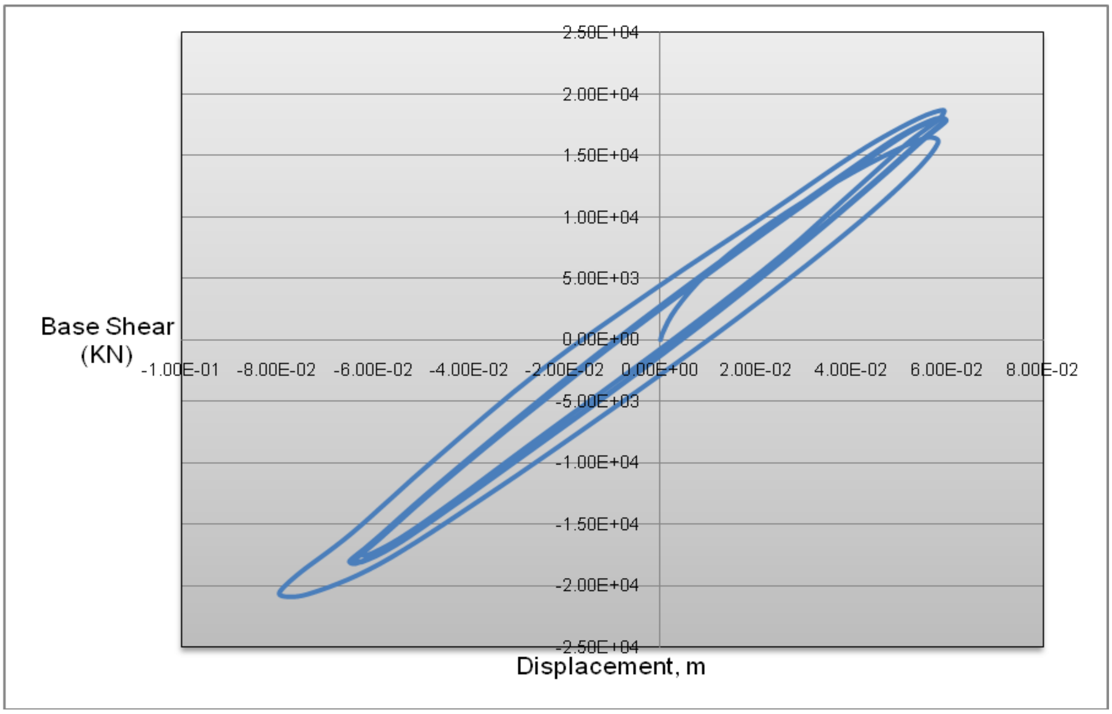


a)

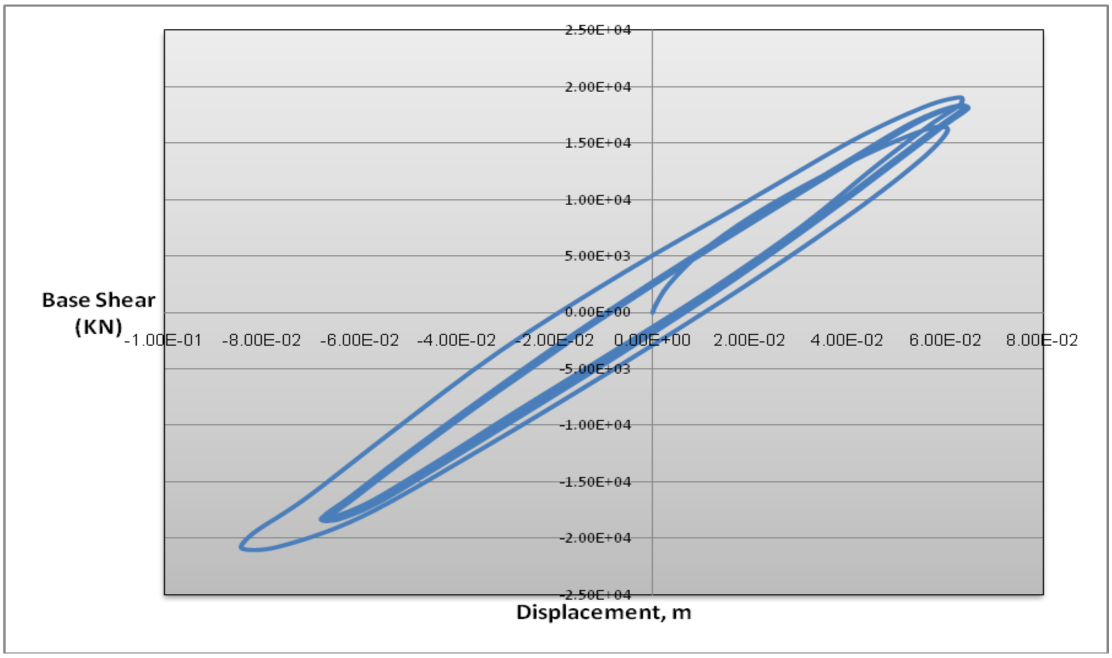


b)

Fig A.23 hysteresis loop behavior for 6EBF cx cy building a) x-direction frames b) y-direction frames

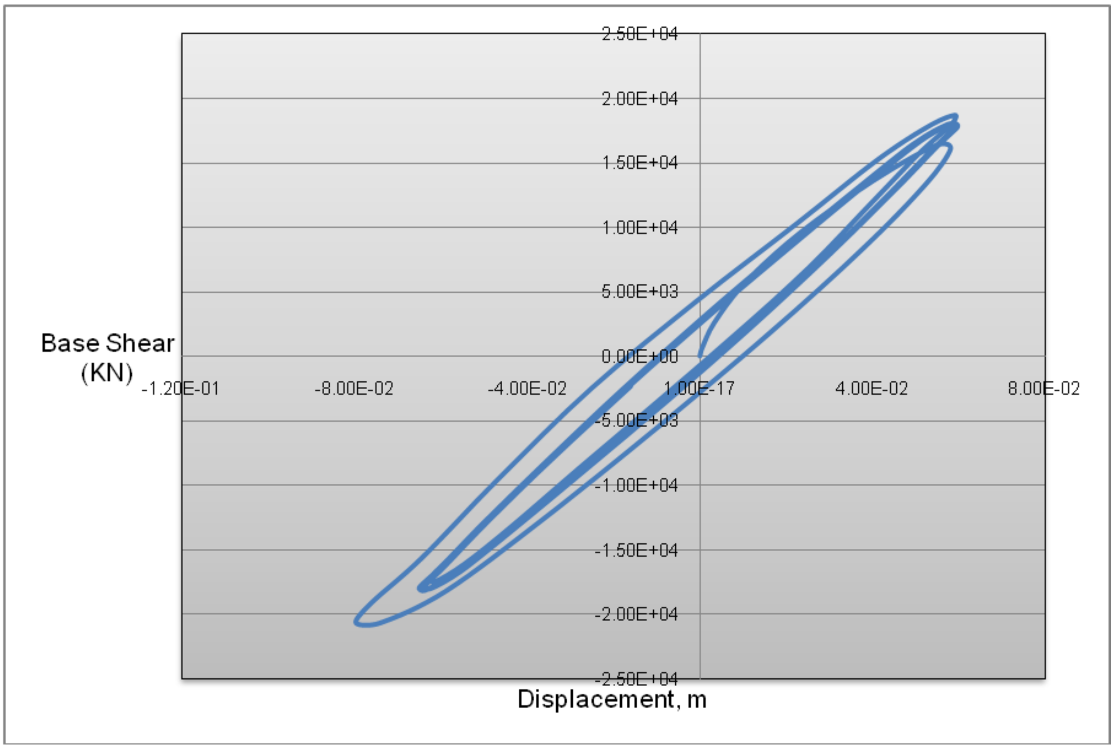


a)

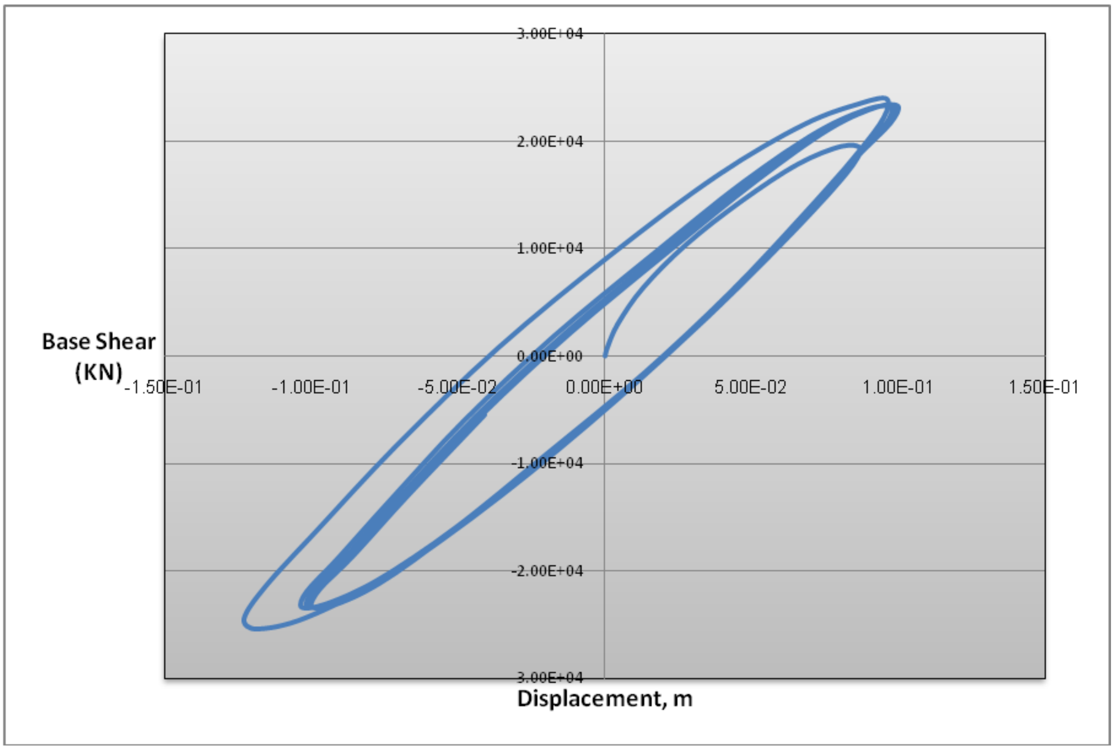


b)

Fig A.20 hysteresis loop behaviour for 6EBF1 csx csy building a) x-direction frames b) y-direction frames

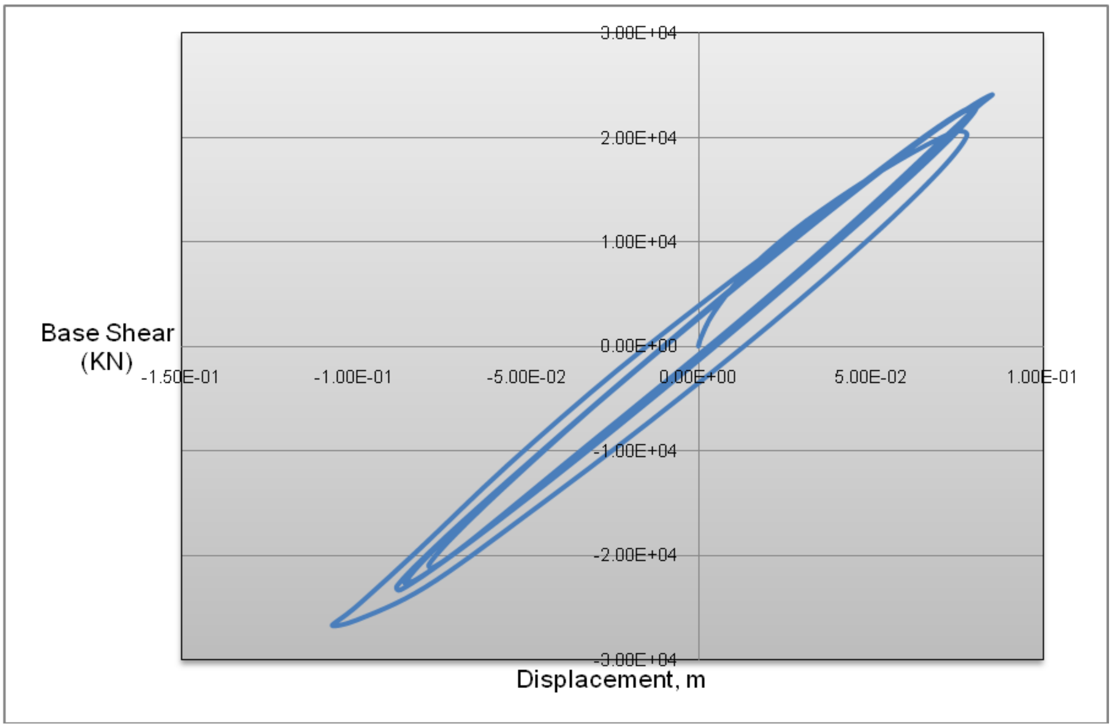


a)

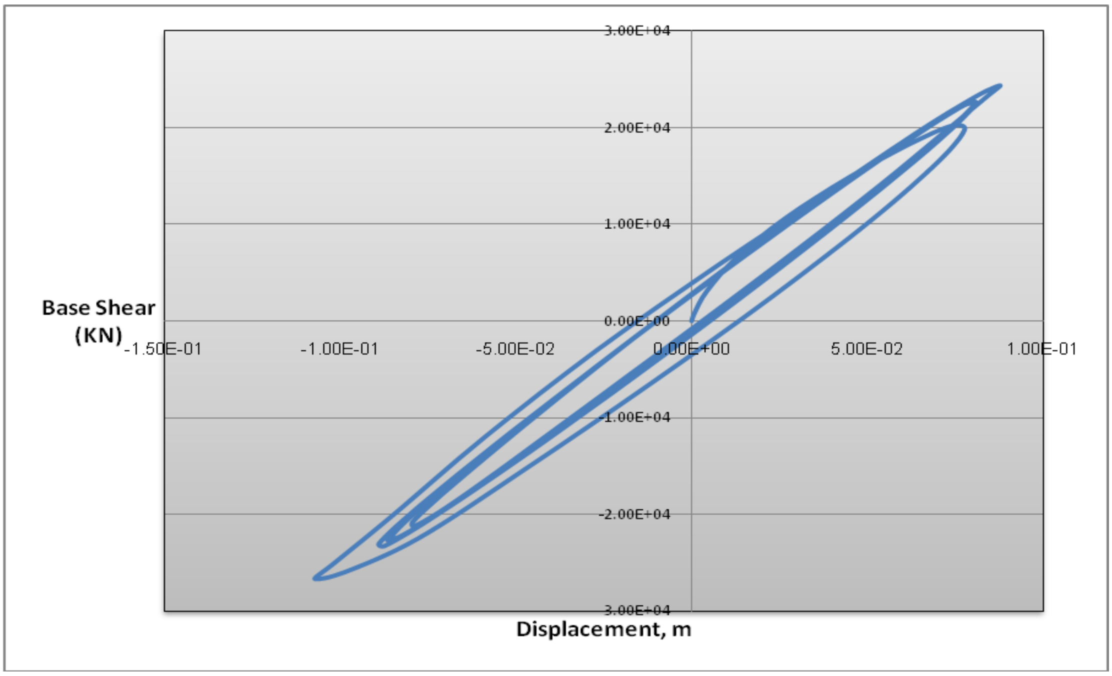


b)

Fig A.21 hysteresis loop behavior for 6EBF2 csx csy building a) x-direction frames b) y-direction frames

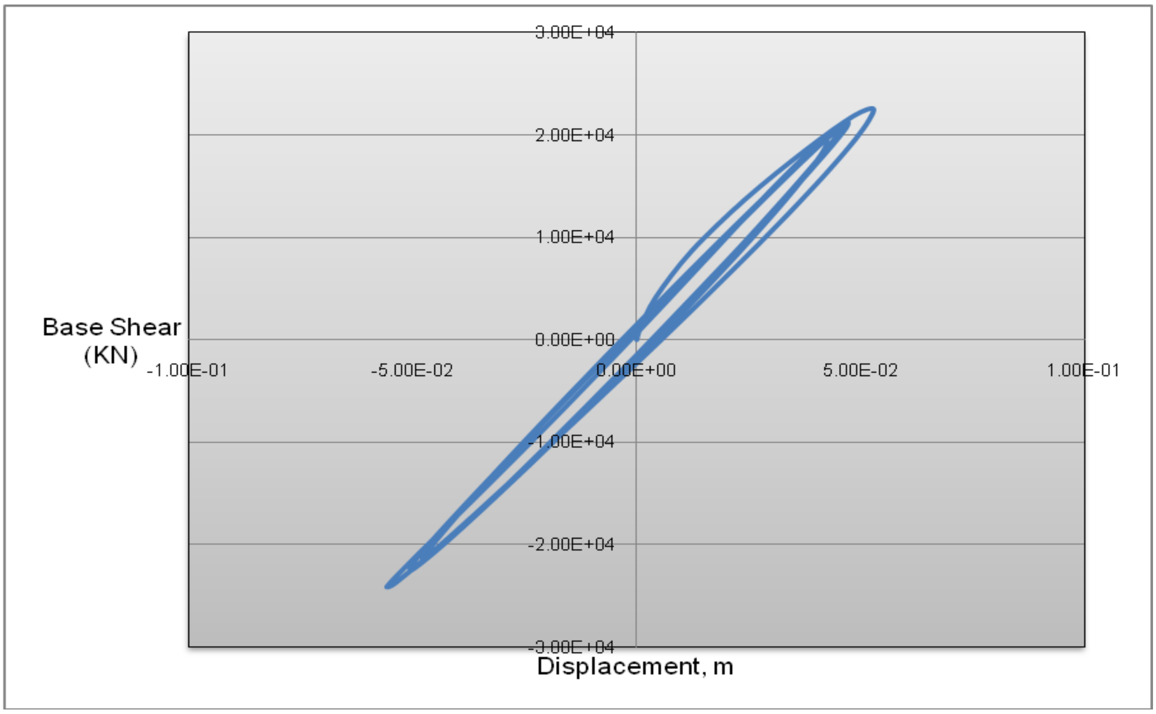


a)

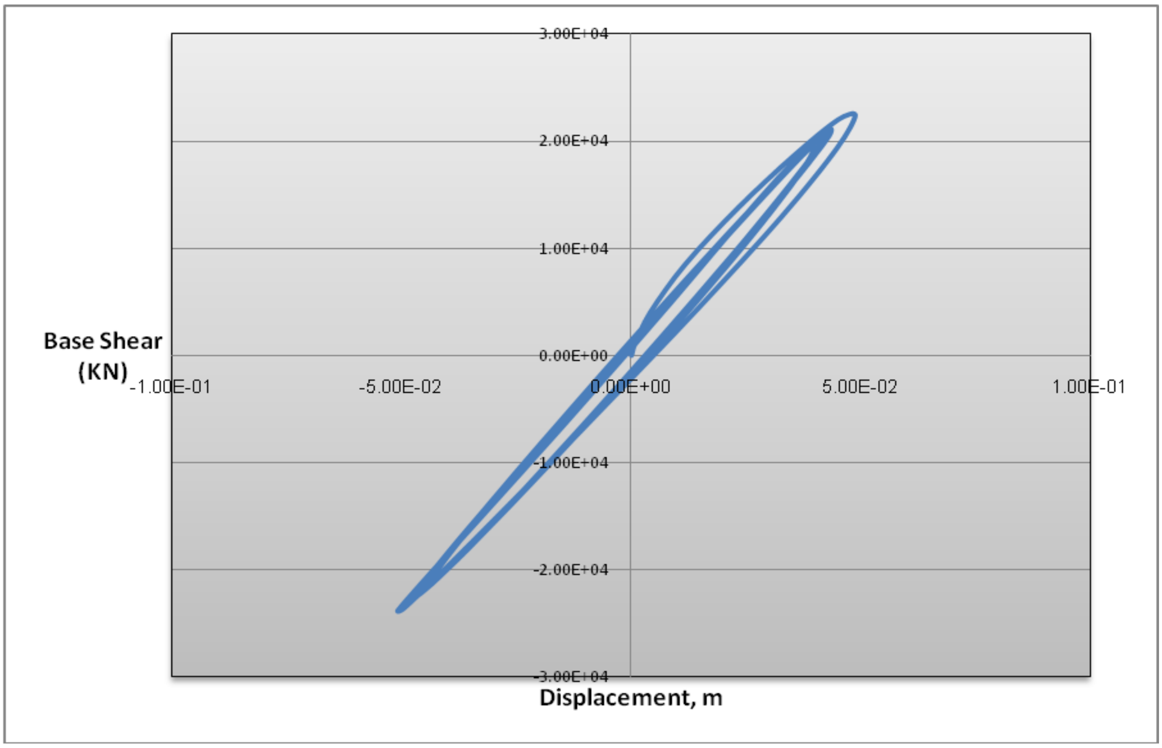


b)

Fig A.22 hysteresis loop behavior for 6EBF3 csx csy building a) x-direction frames b) y-direction frames



a)

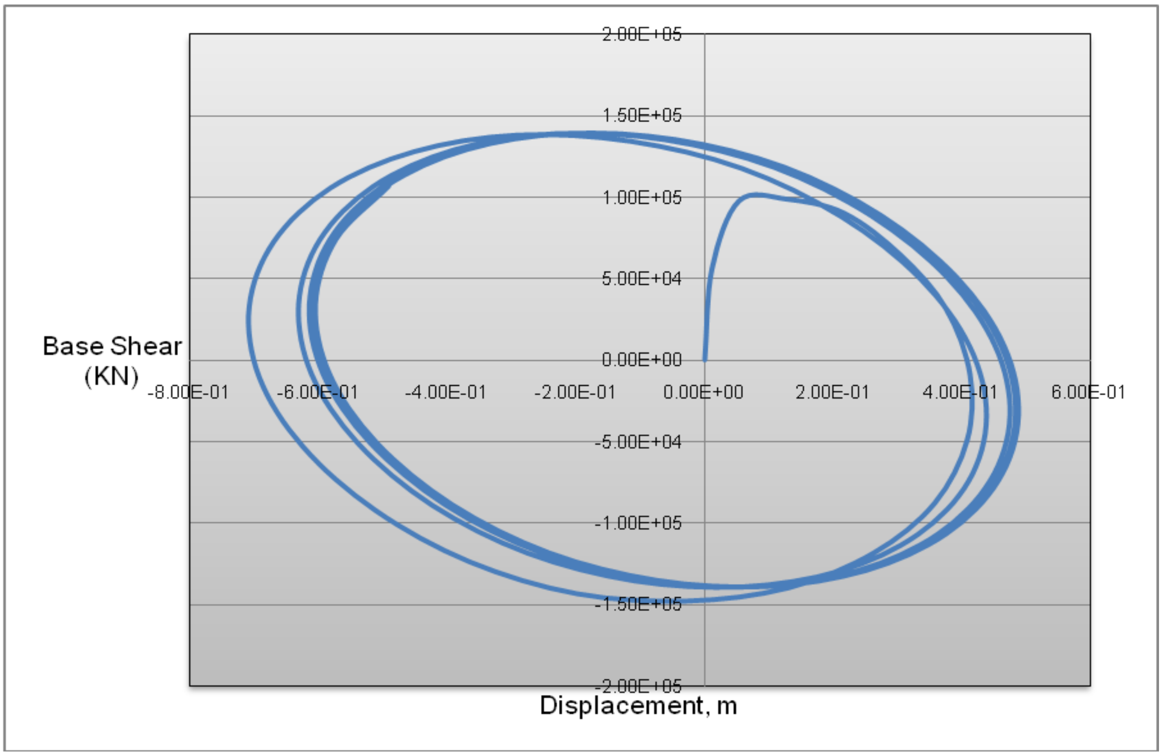


b)

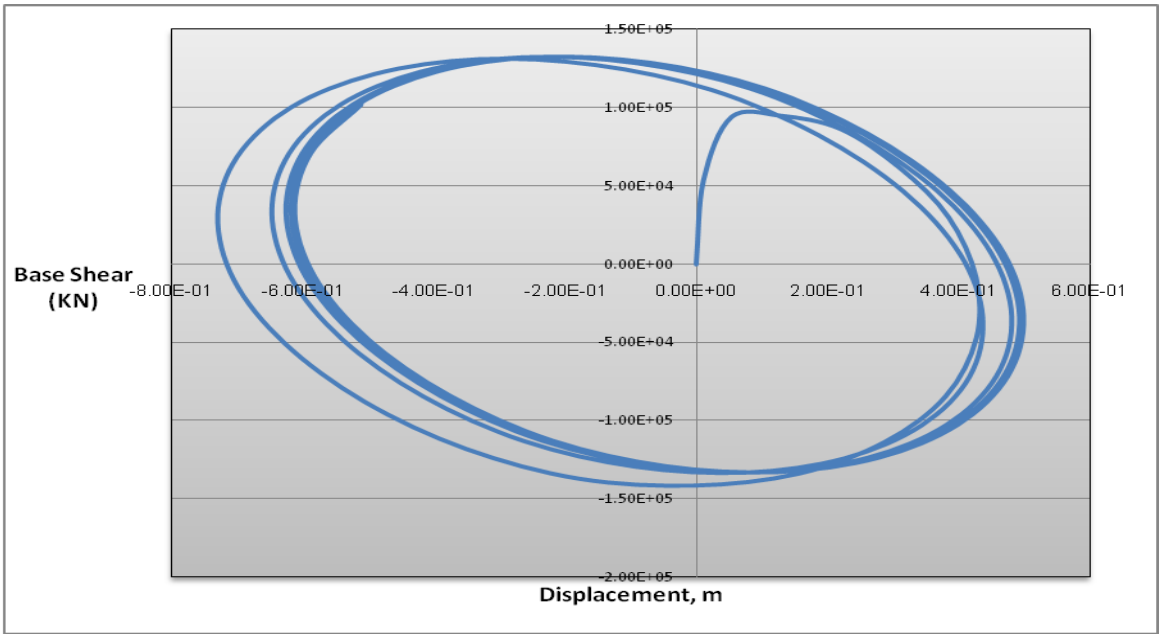
Fig A.19 hysteresis loop behavior for 6EBF cscox cscoy building a) x-direction frames b) y-direction frames

APPENDIX B

HYSTERESIS BEHAVIOR OF 20-STOREY SYSTEMS

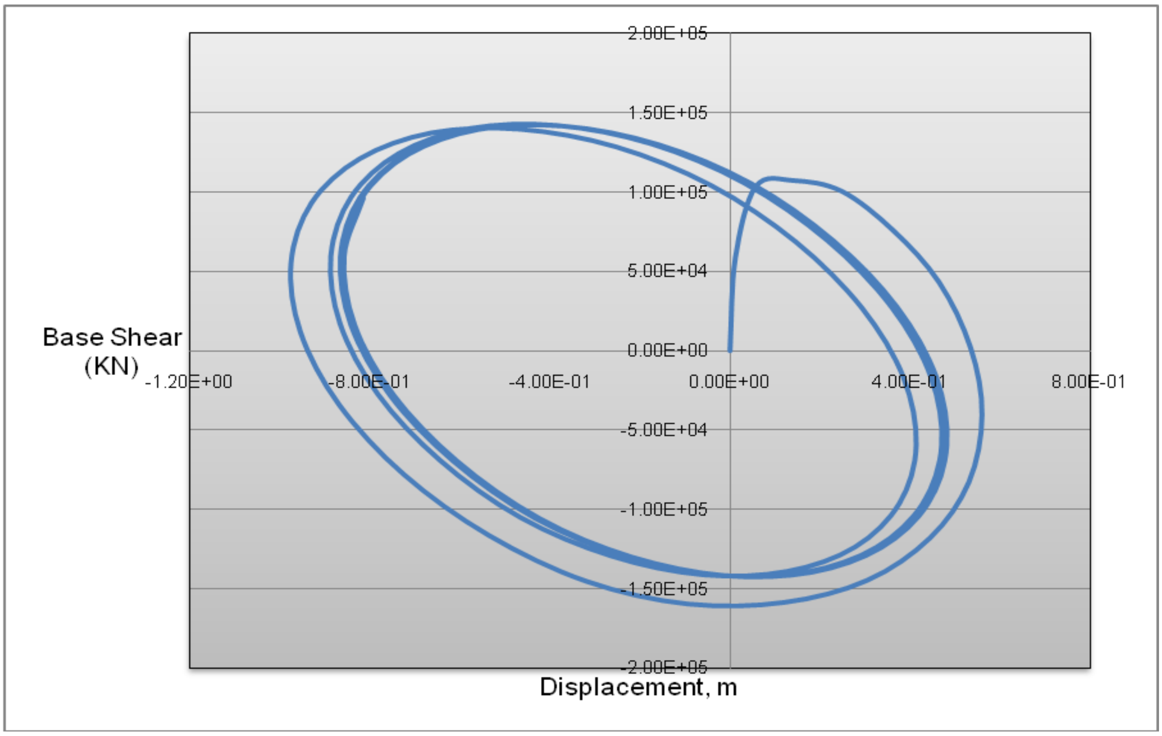


a)

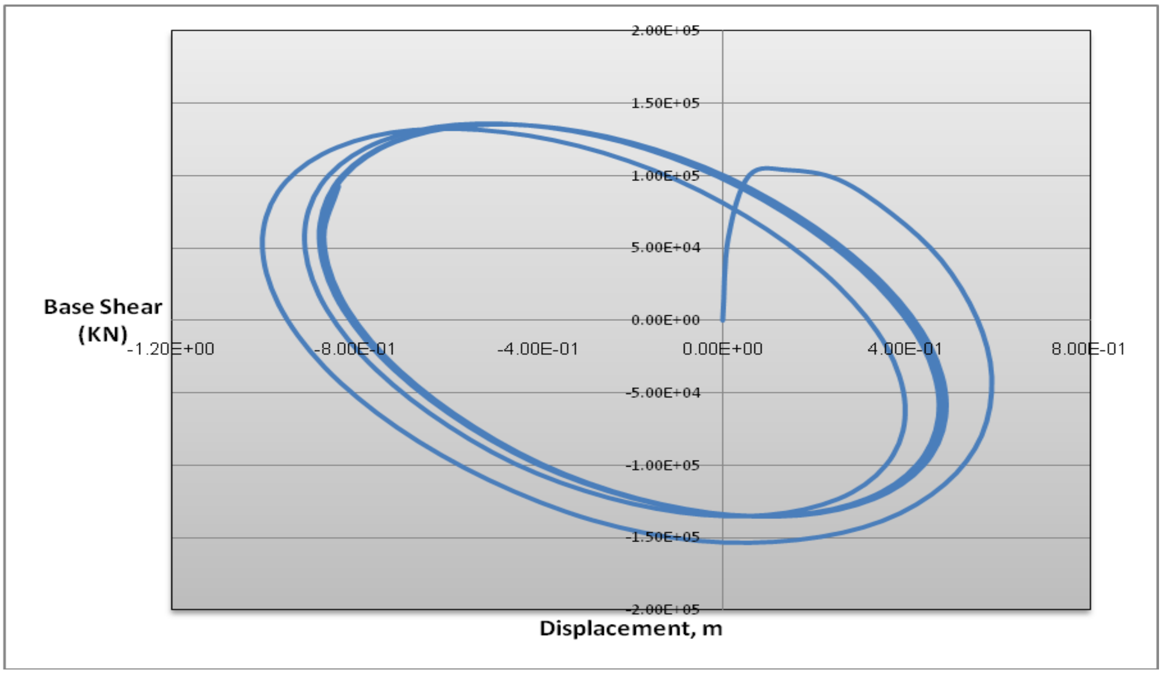


b)

Fig B.1 hysteresis loop behavior for 20FRMRF building a) x-direction frames b) y-direction frames

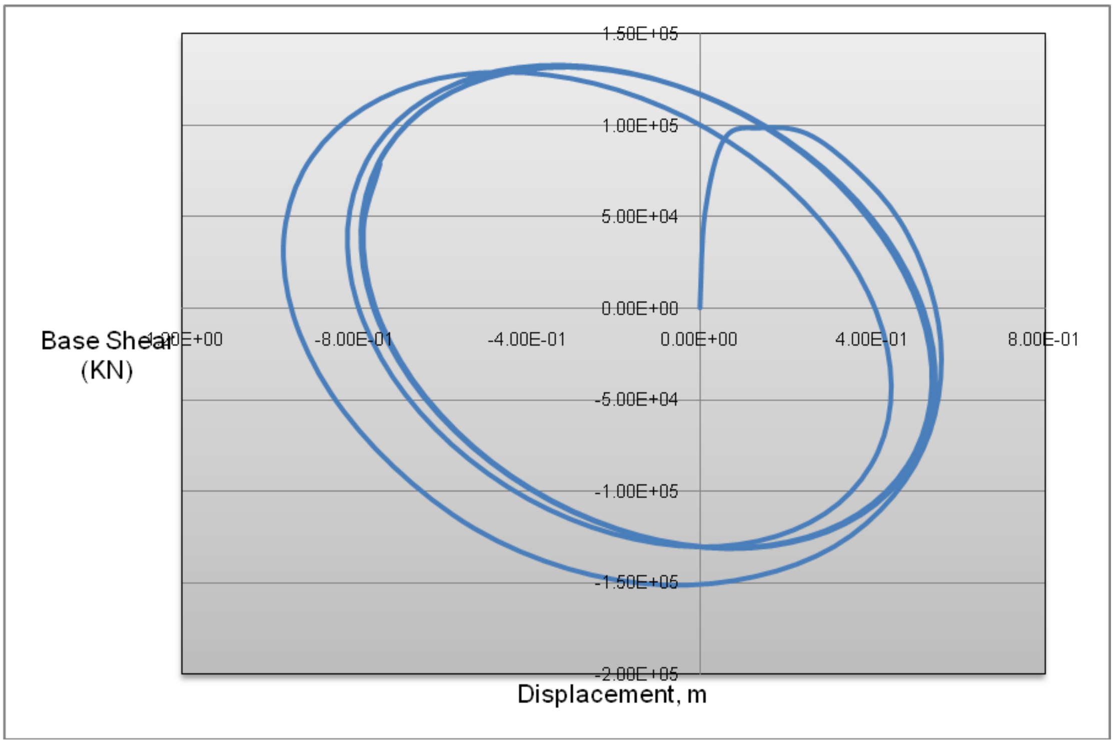


a)

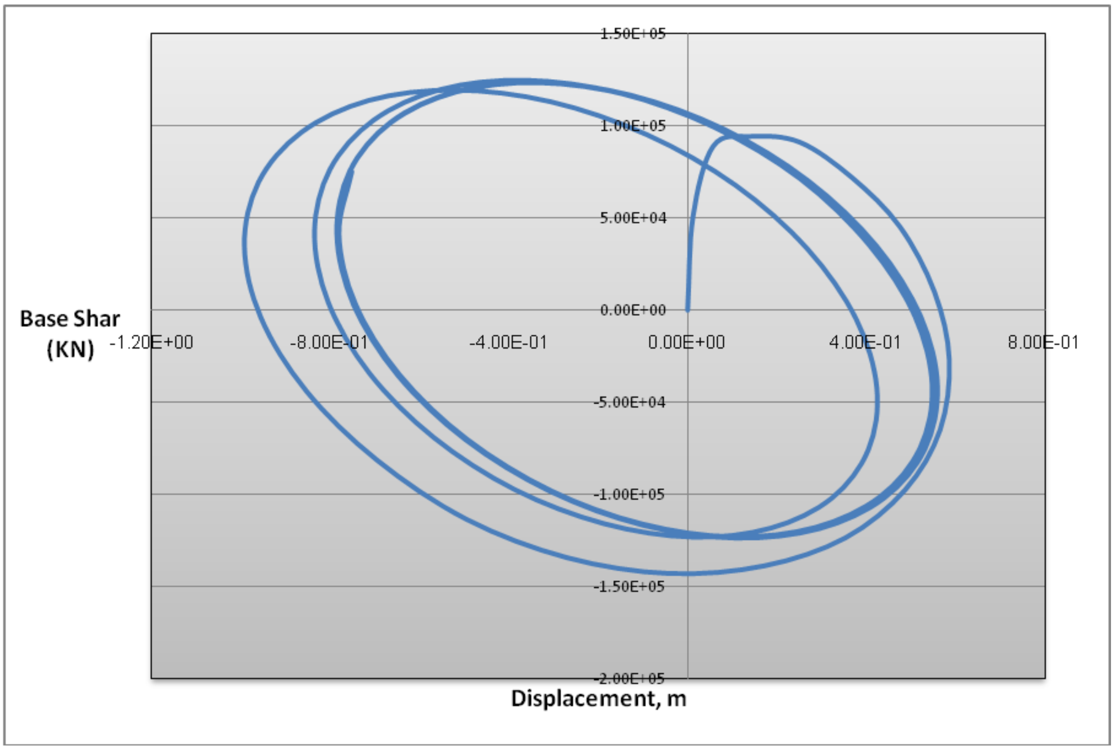


b)

Fig B.2 hysteresis loop behaviour for 20SR8-13 building a) x-direction frames b) y-direction frames

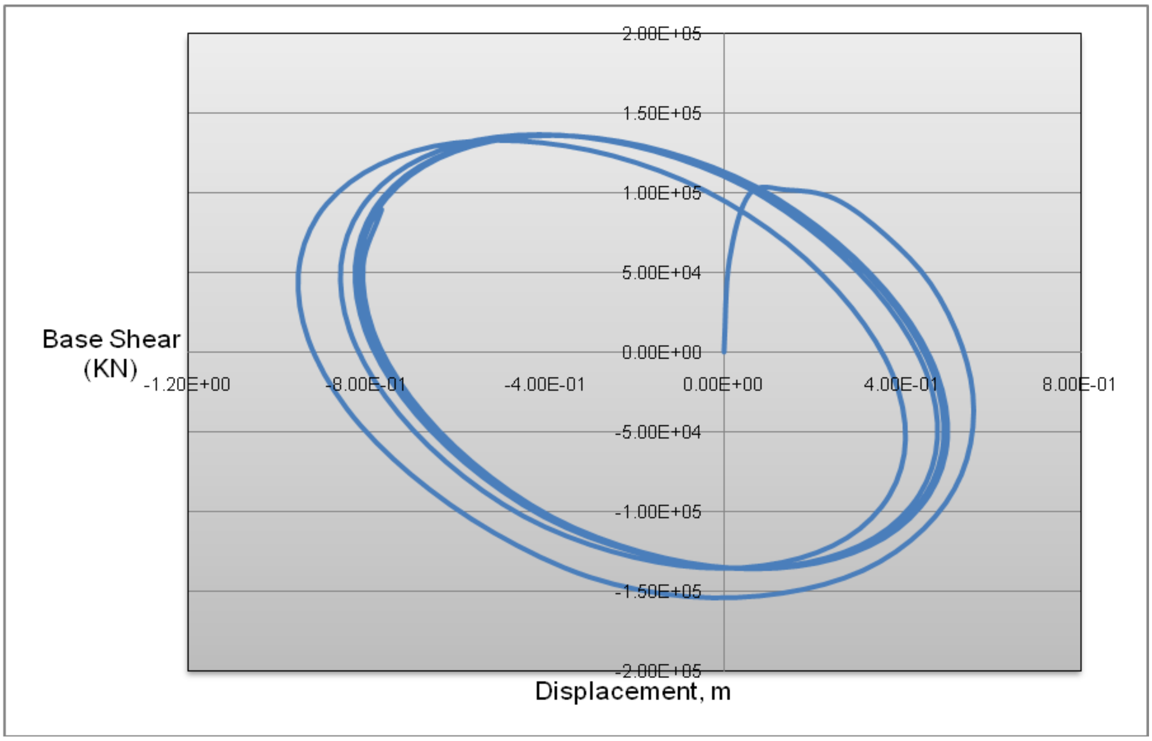


a)

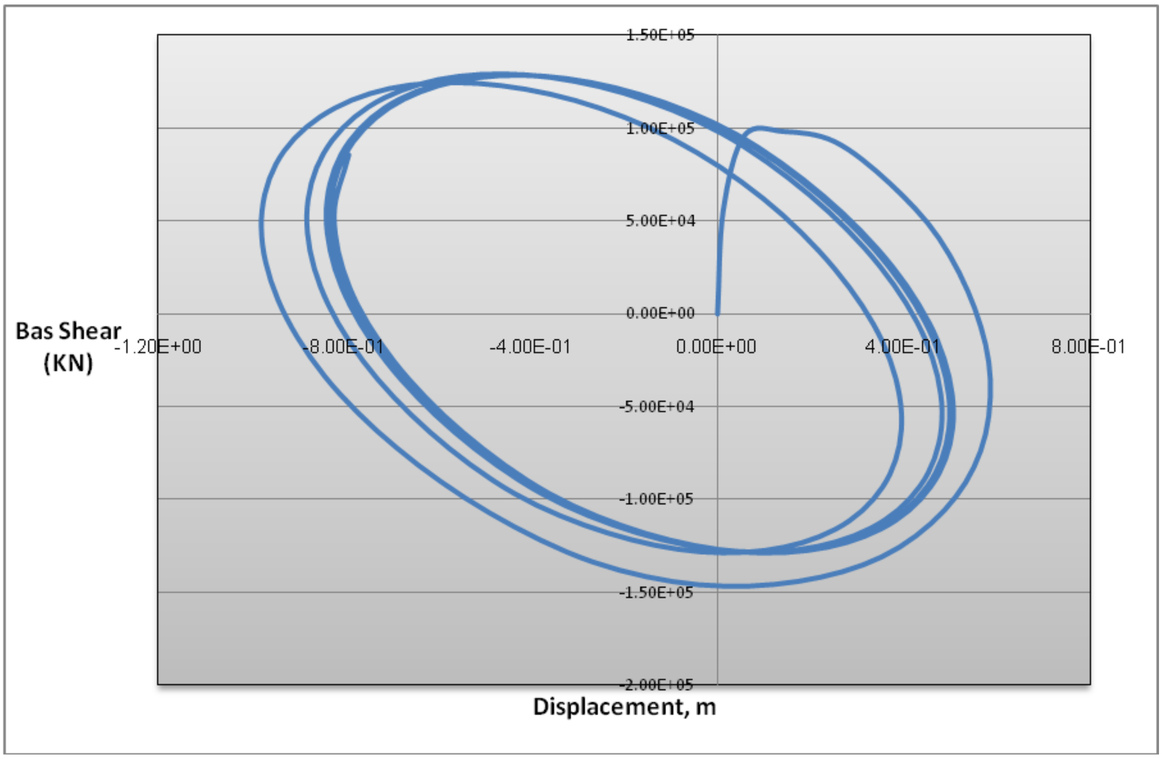


b)

Fig B.3 hysteresis loop behavior for 20SR1-6 building a) x-direction frames
b) y-direction frames

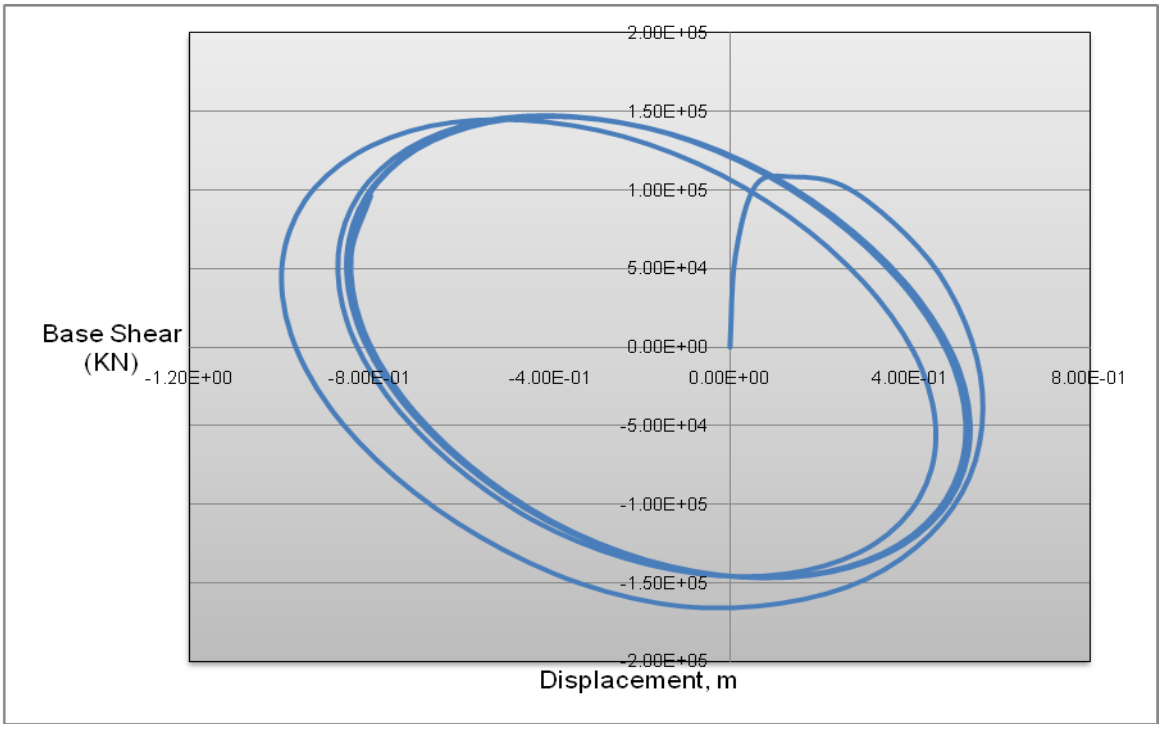


a)

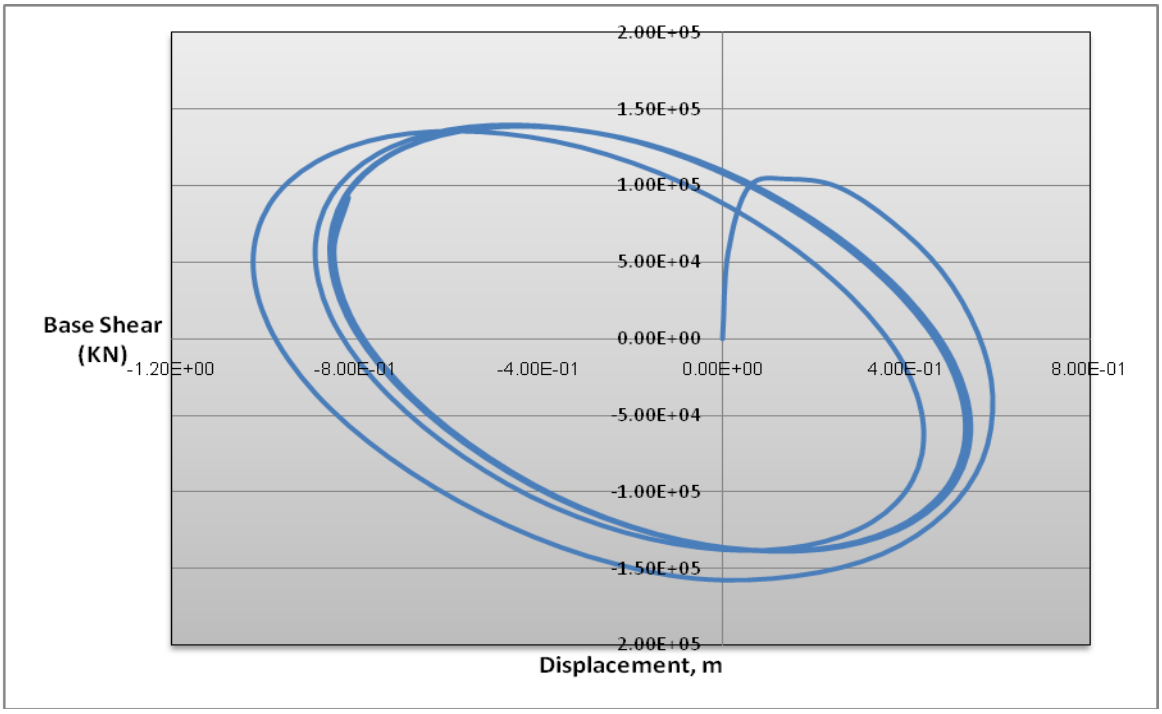


b)

Fig B.4 hysteresis loop behavior for 20SR4-9 building a) x-direction frames
b) y-direction frames

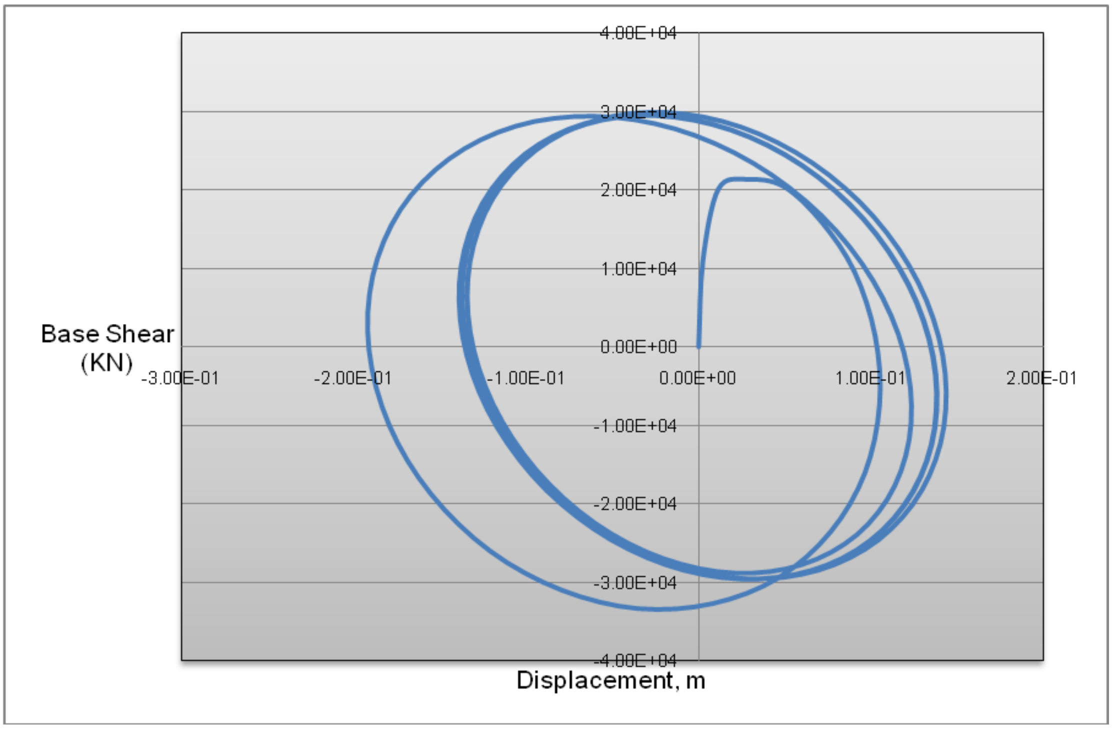


a)

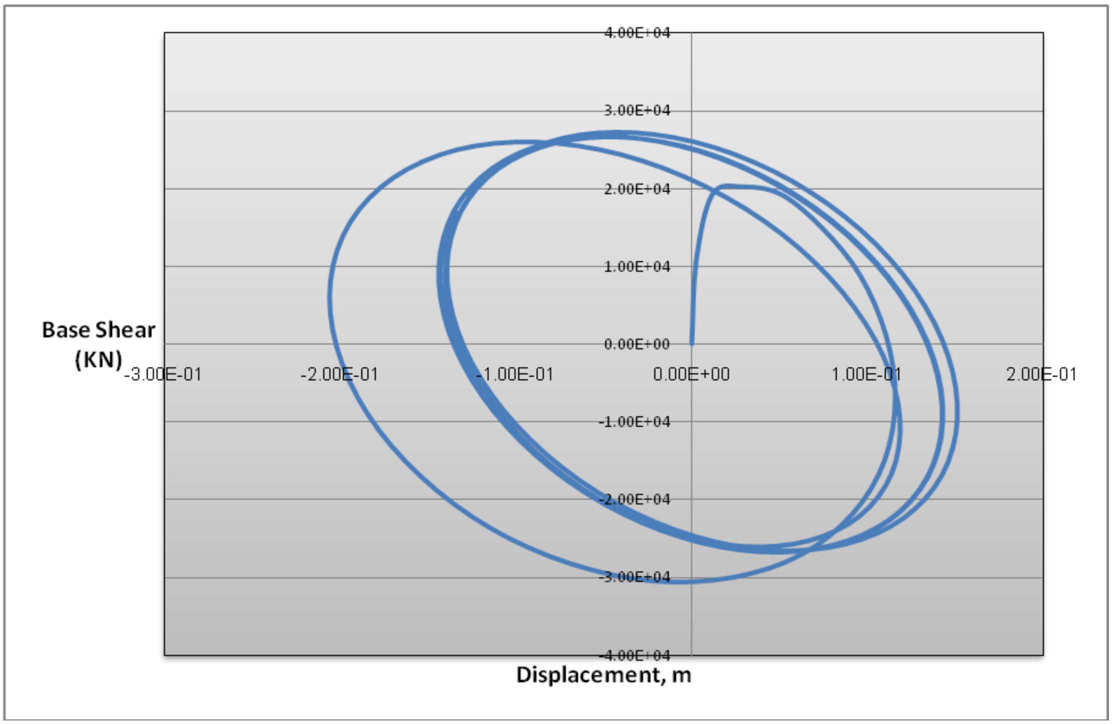


b)

Fig B.5 hysteresis loop behavior for 20SR13-18 building a) x-direction frames
b) y-direction frames

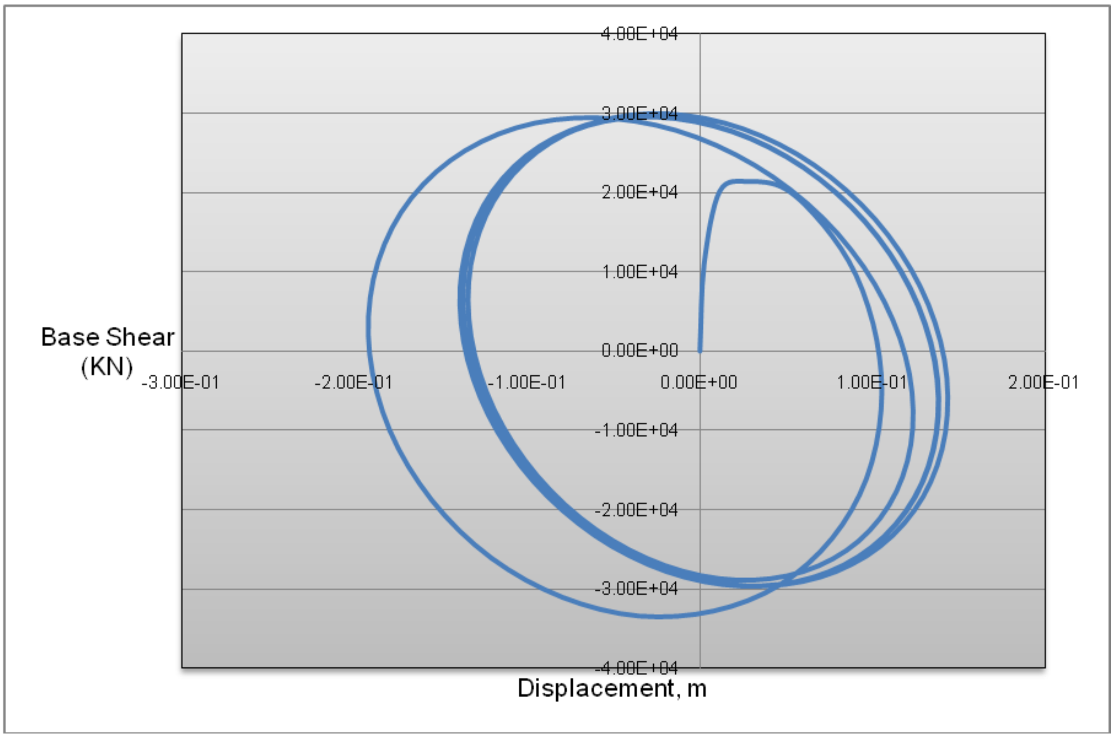


a)

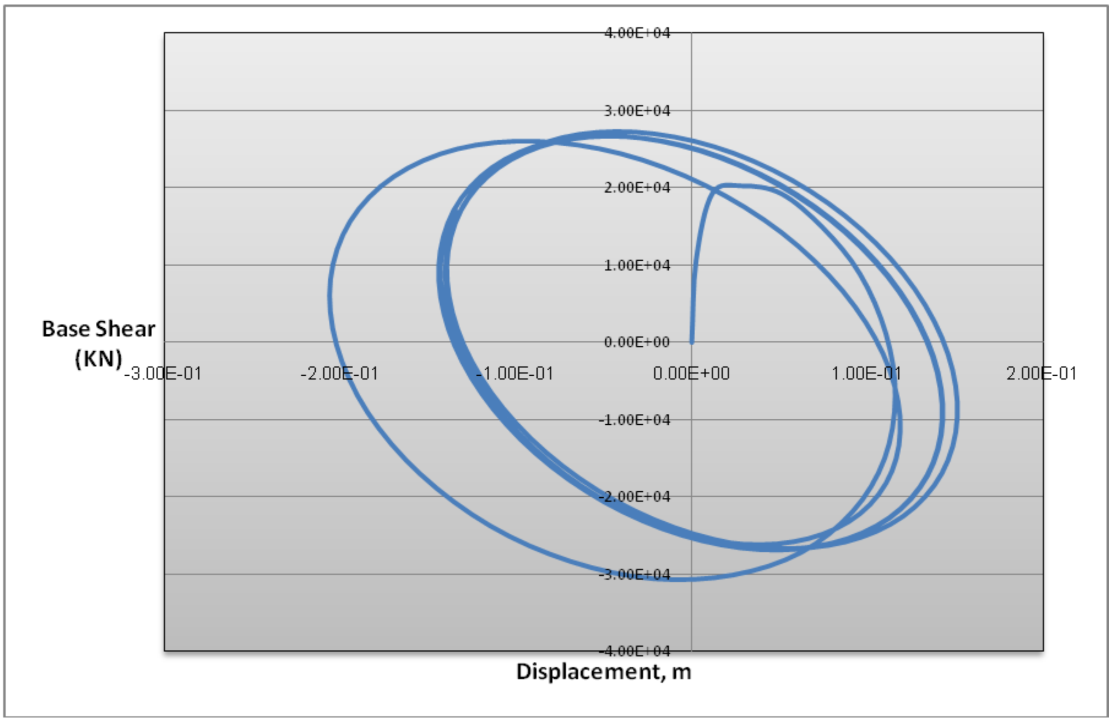


b)

Fig B.6 hysteresis loop behavior for 20BRBF cx sy building a) x-direction frames b) y-direction frames

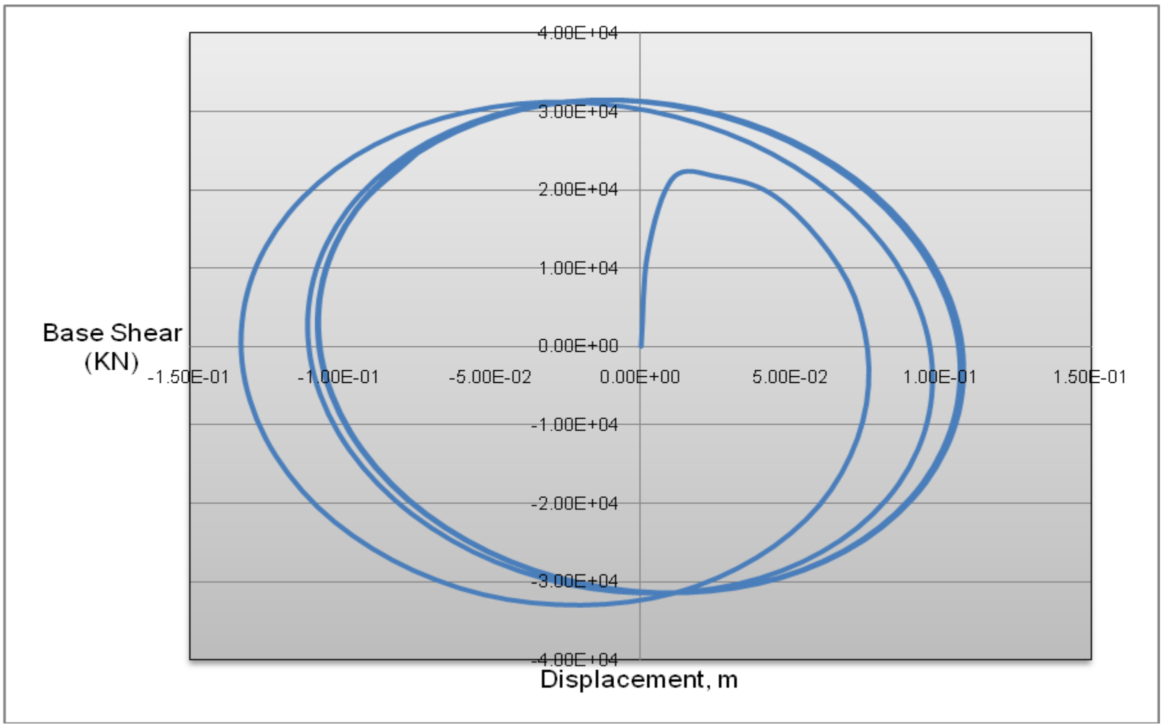


a)

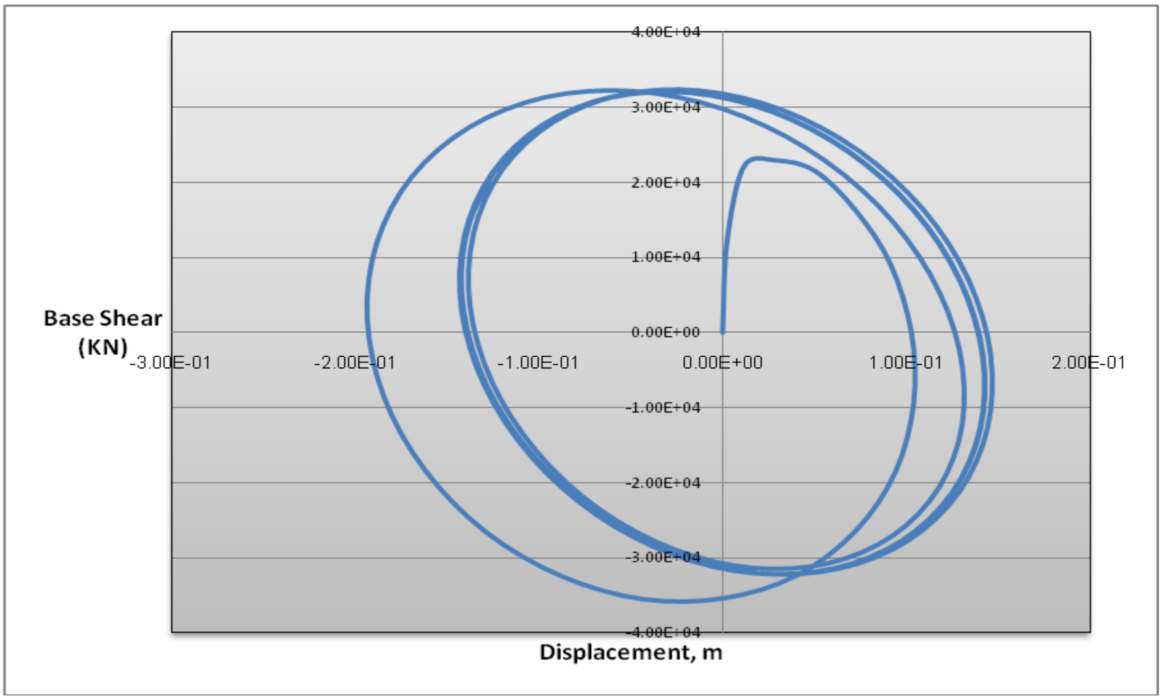


b)

Fig B.7 hysteresis loop behavior for 20BRBF cx cy building a) x-direction frames b) y-direction frames

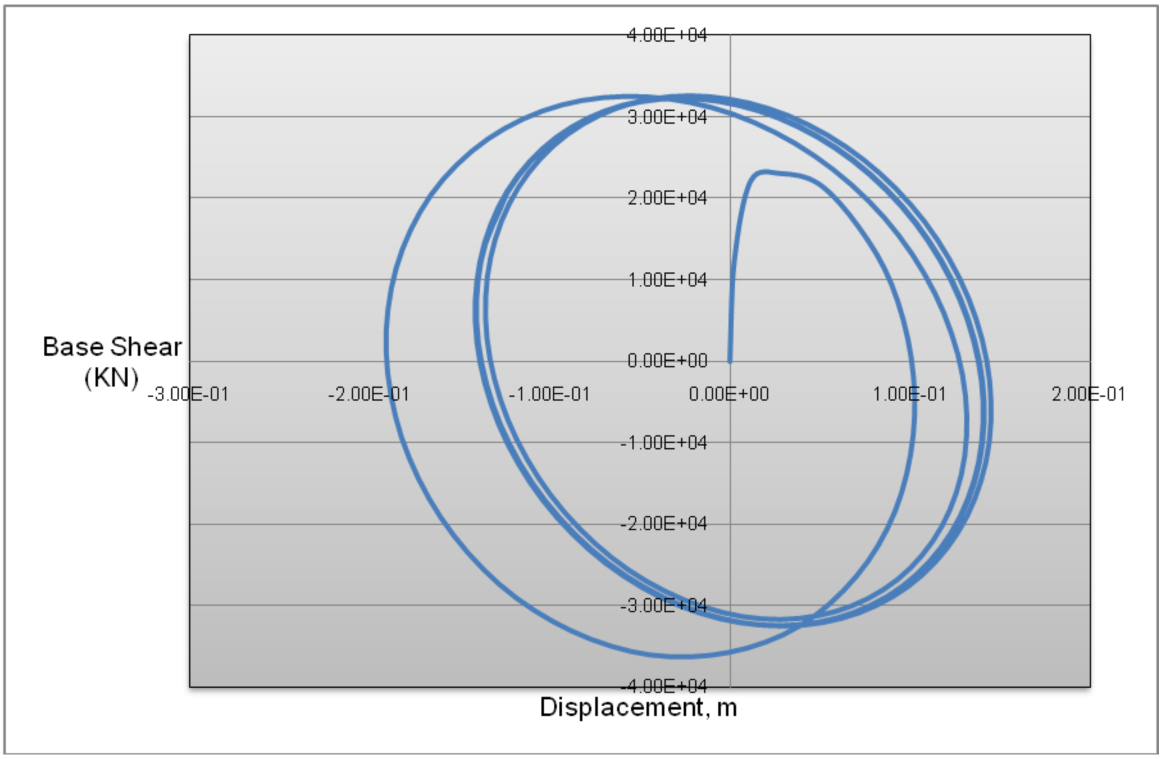


a)

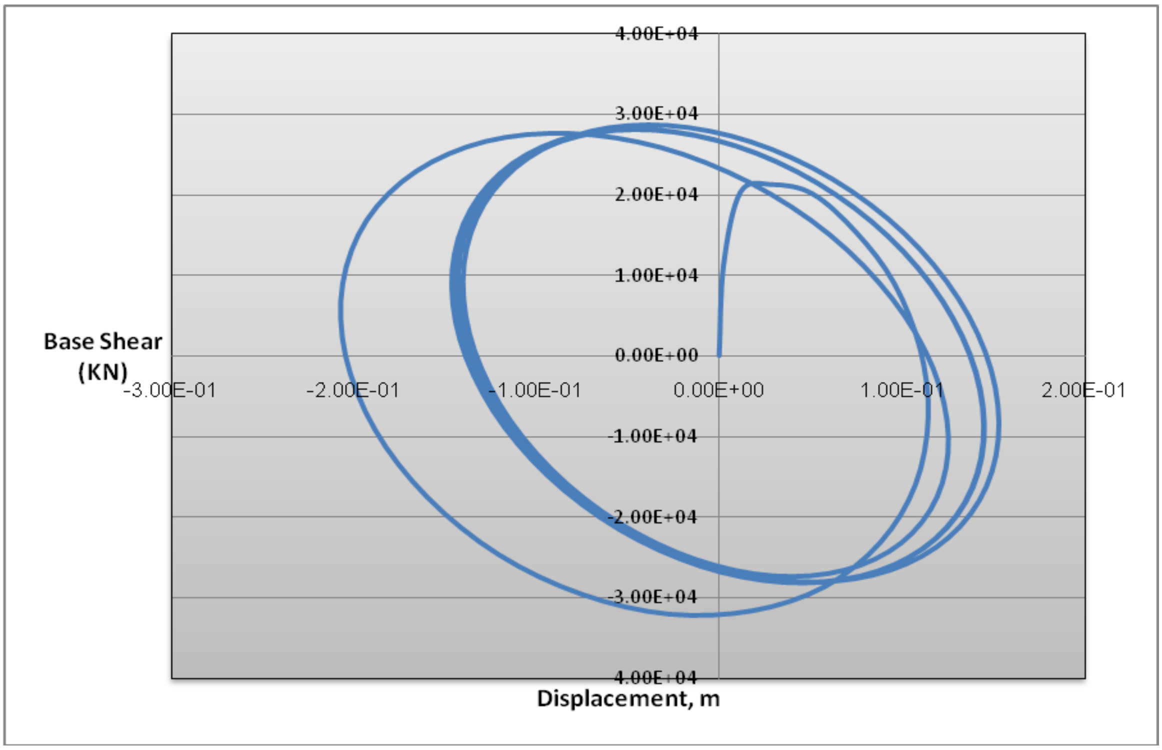


b)

Fig B.8 hysteresis loop behavior for 20BRBF csx csy building a) x-direction frames b) y-direction frames

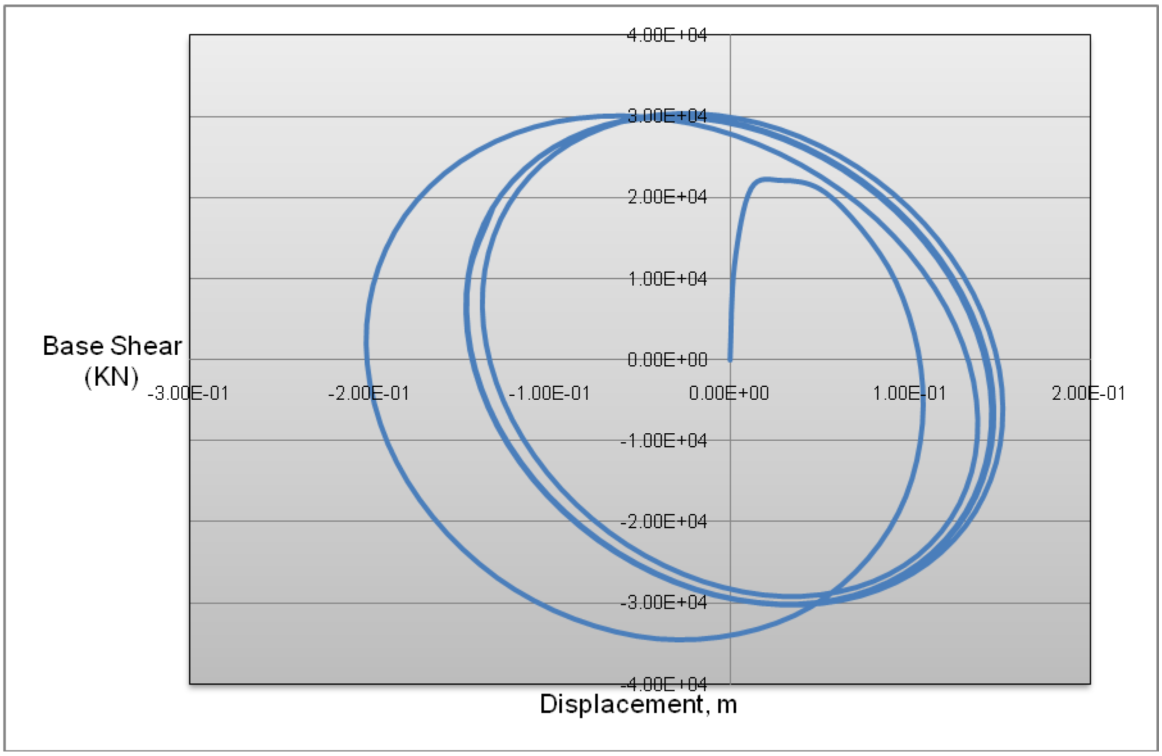


a)

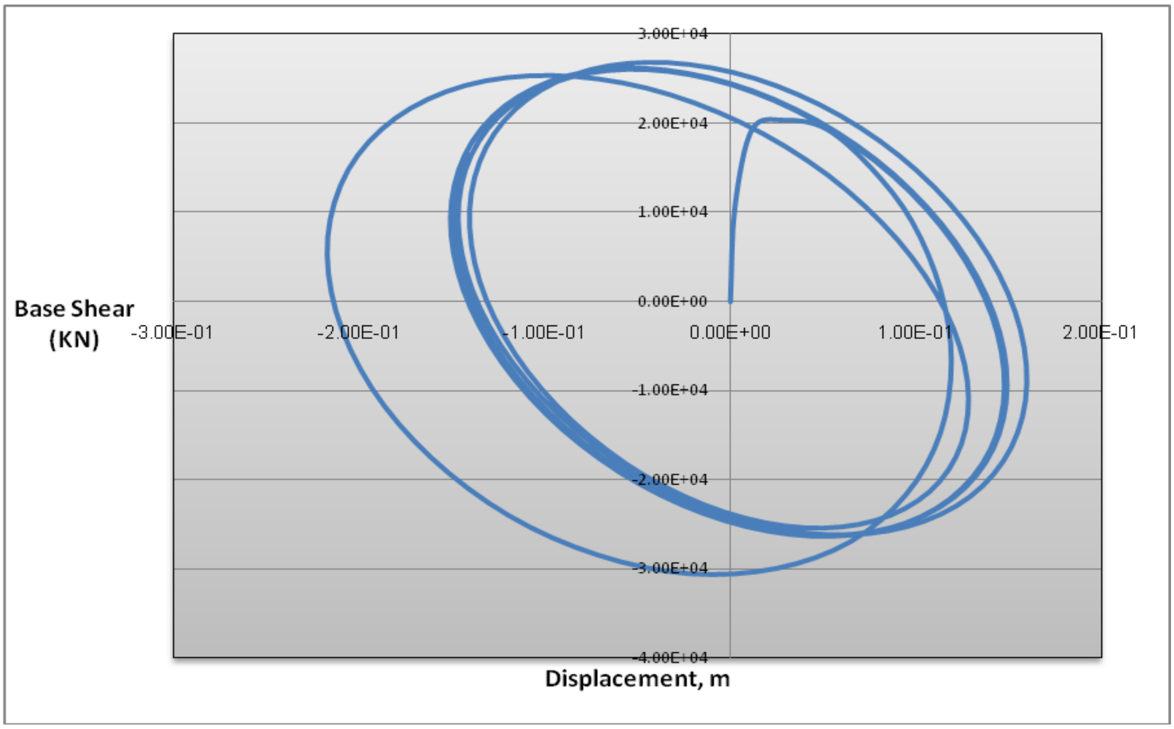


b)

Fig B.9 hysteresis loop behavior for 20EBF cx cy building a) x-direction frames b) y-direction frames

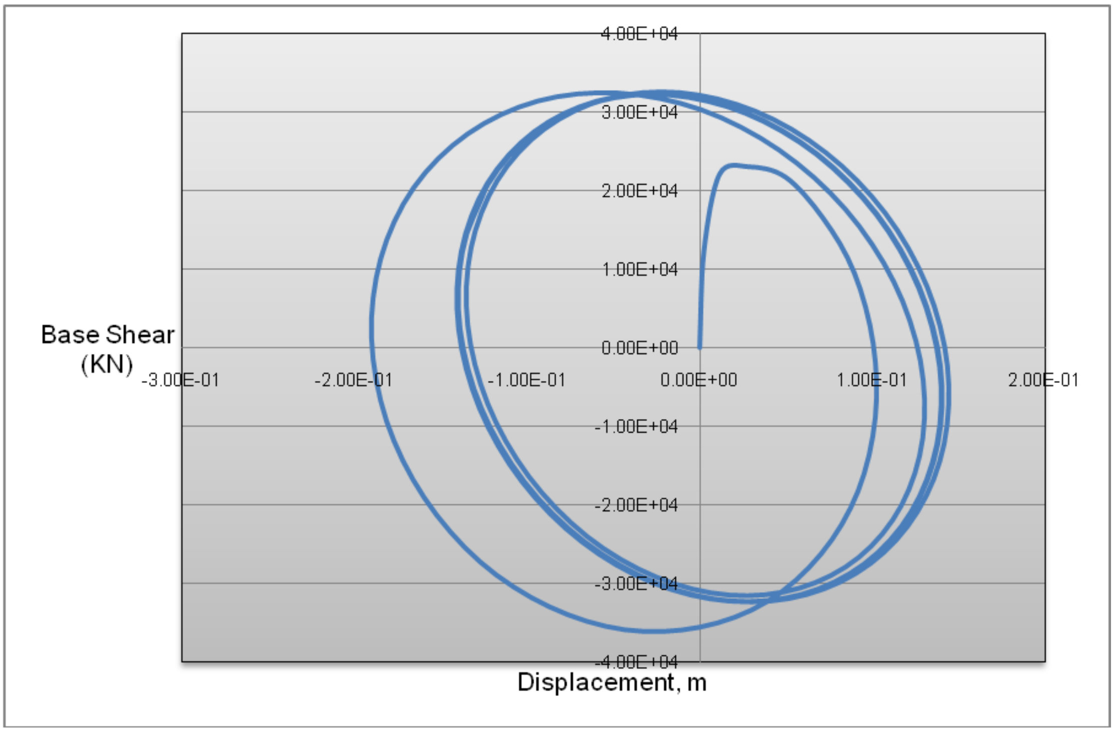


a)

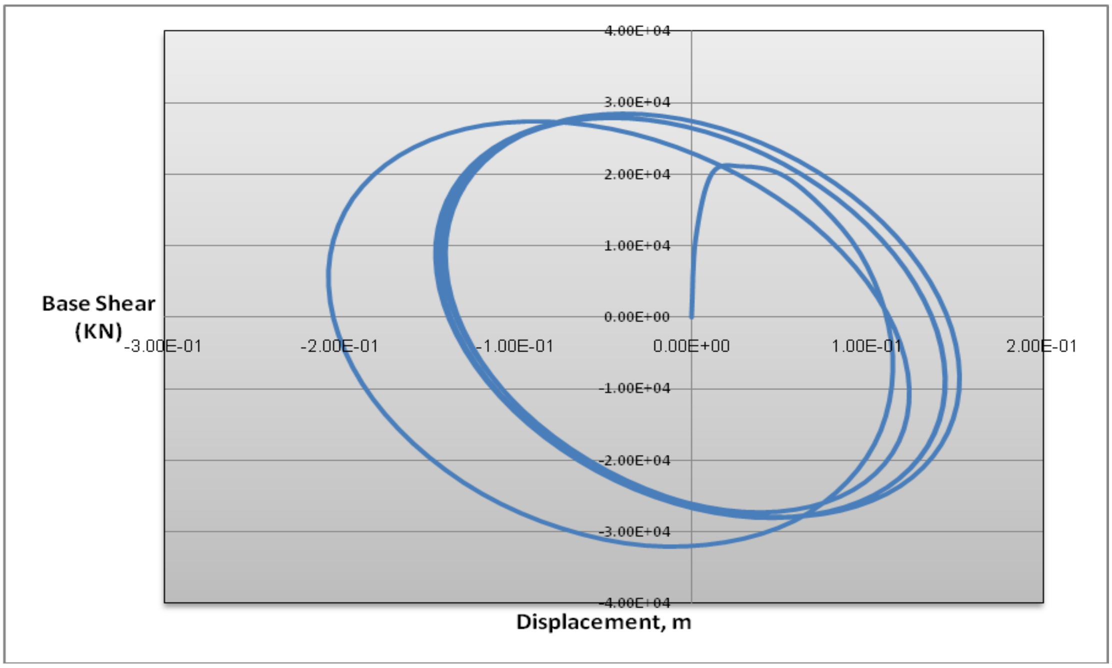


b)

Fig B.10 hysteresis loop behavior for 20EBF1 cx sy building a) x-direction frames
b) y-direction frames

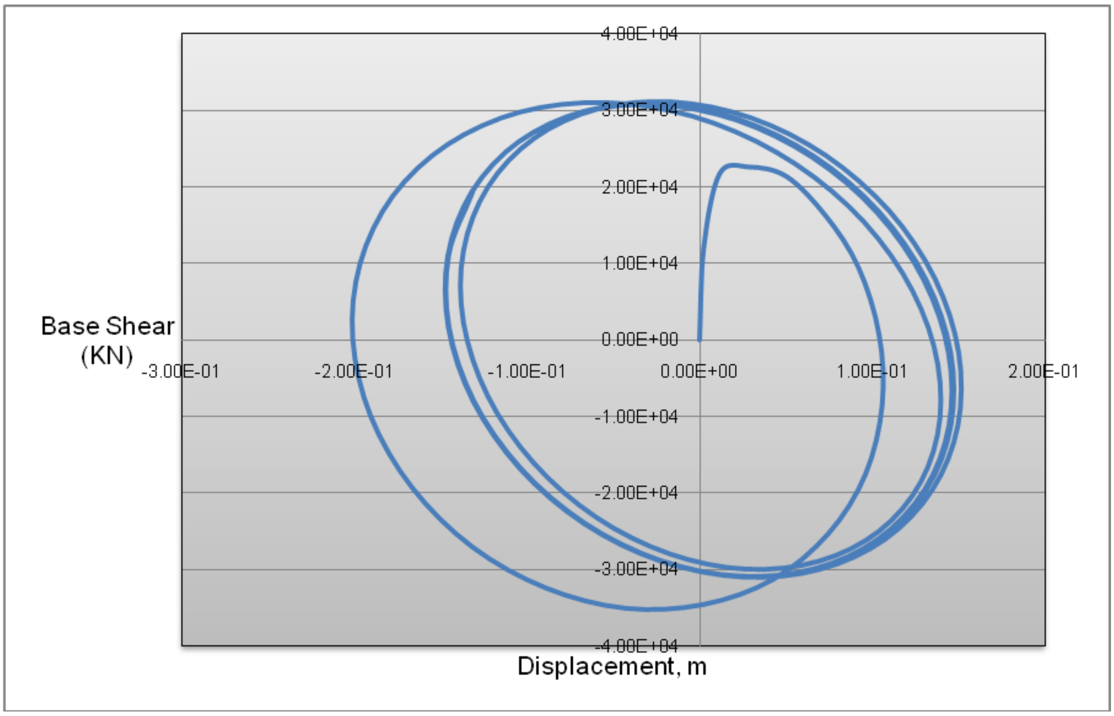


a)

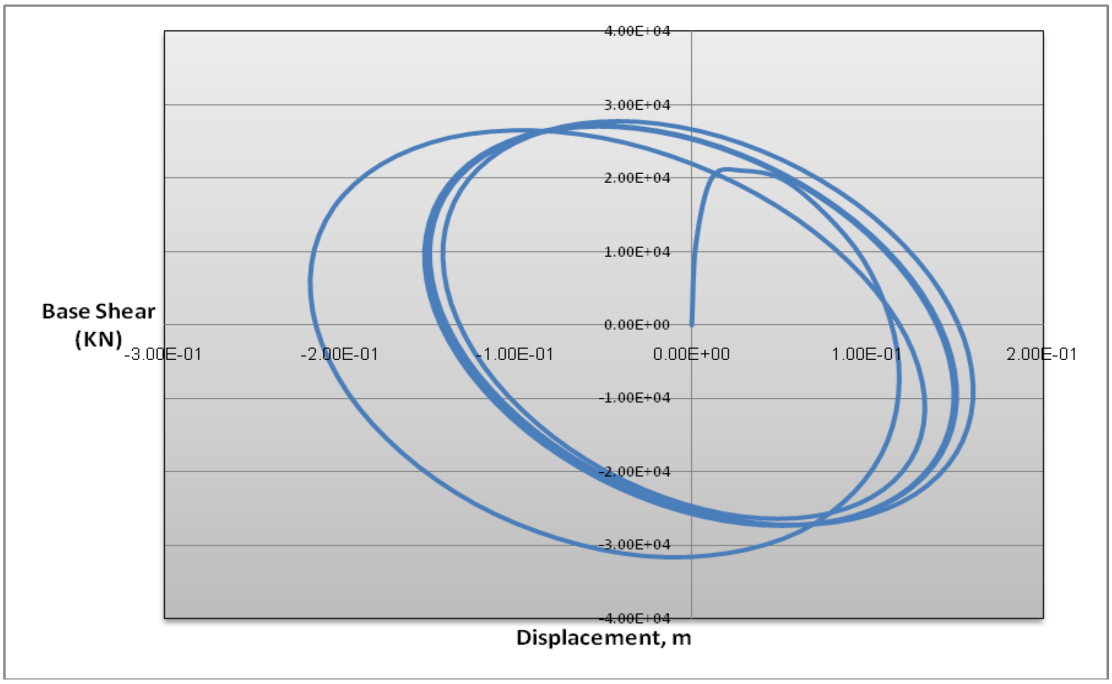


b)

Fig B.11 hysteresis loop behavior for 20EBF2 cx sy building a) x-direction frames
b) y-direction frames



a)

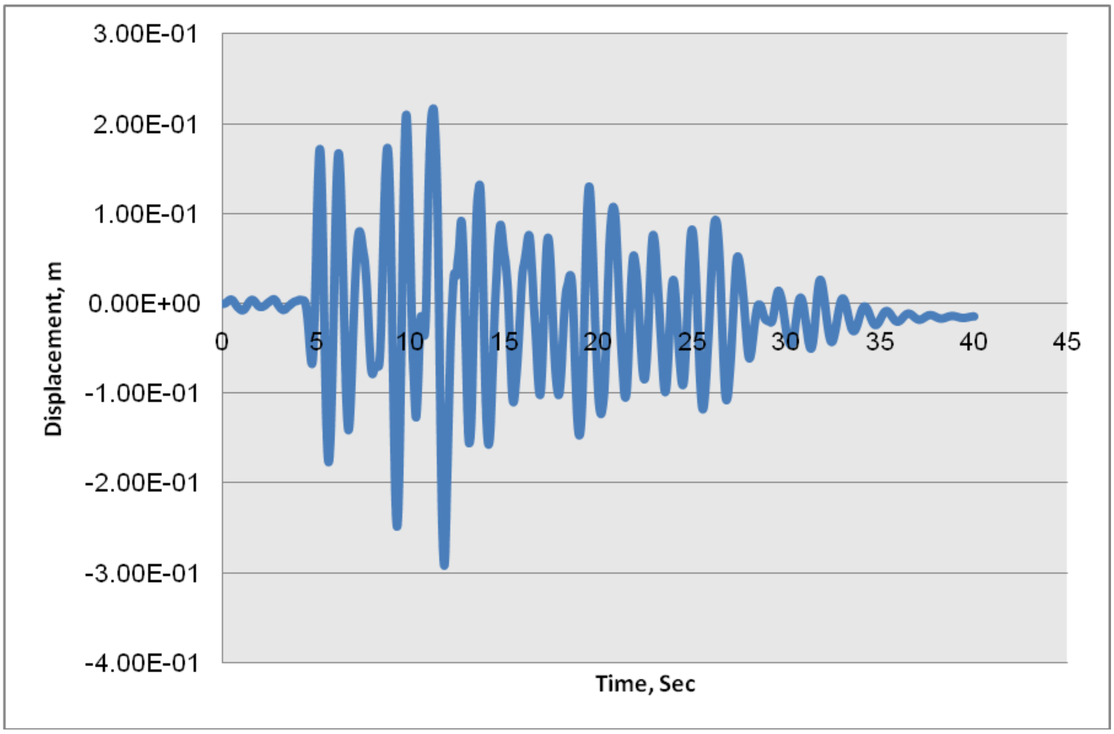


b)

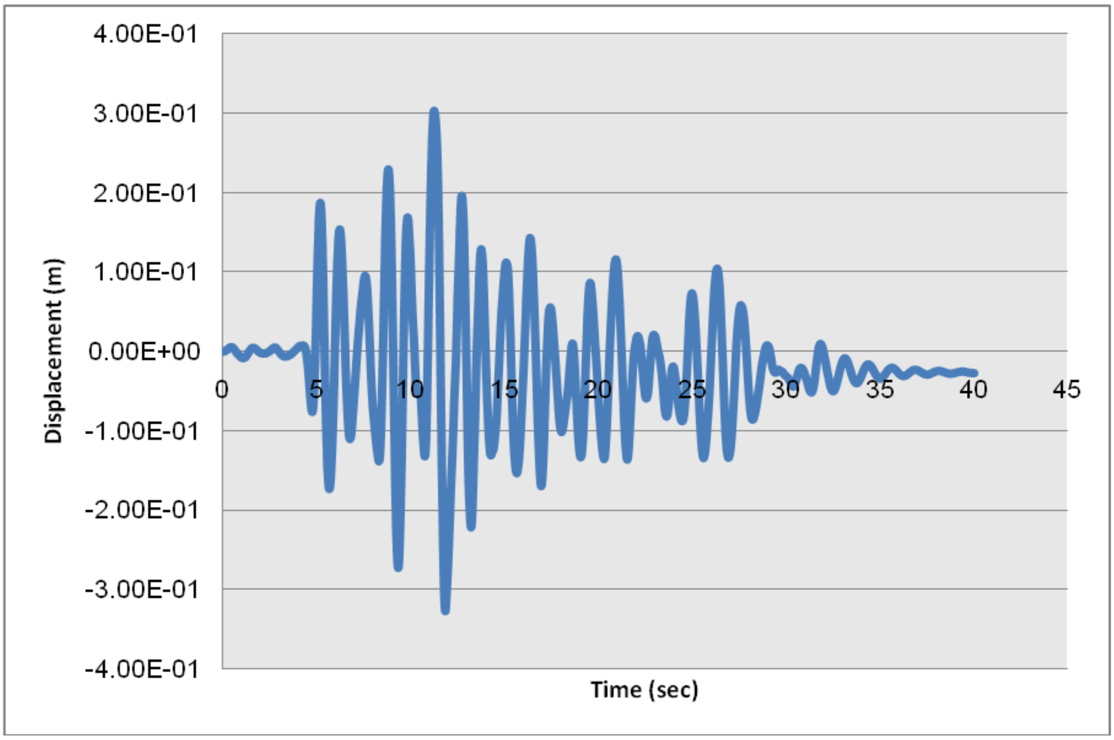
Fig B.12 hysteresis loop behavior for 20EBF3 cx sy building a) x-direction frames b) y-direction frames

APPENDIX C

6-STOREY DISPLACEMENT TIME-HISTORY RELATIONS

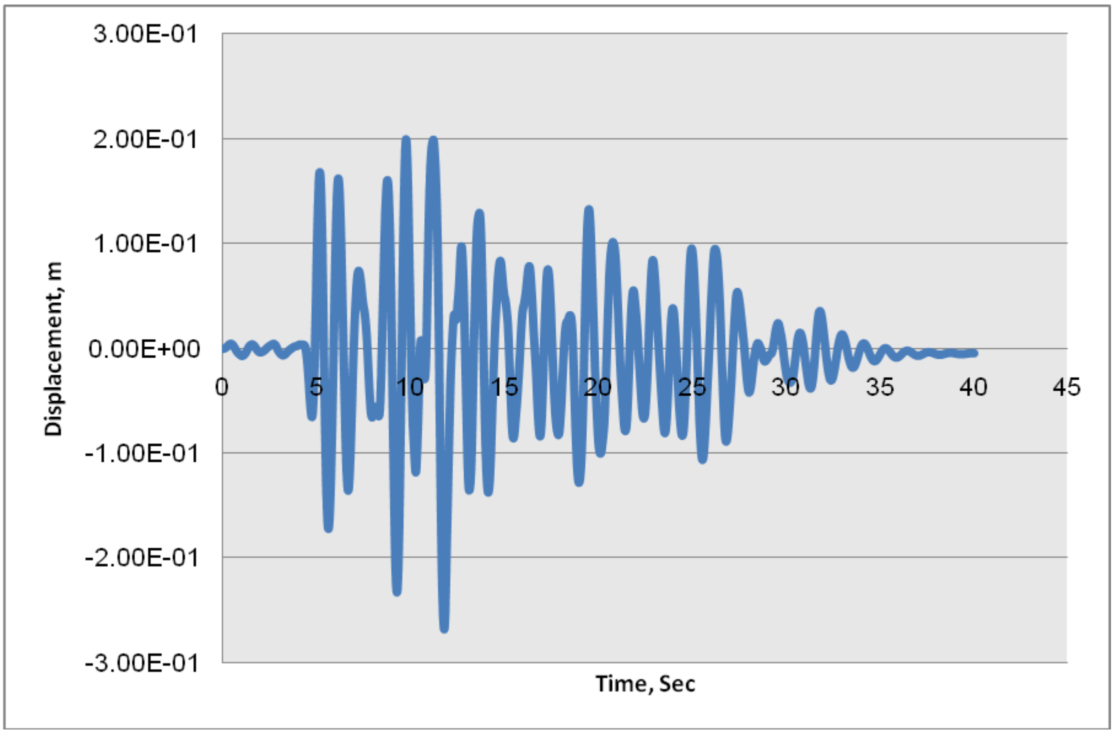


a)

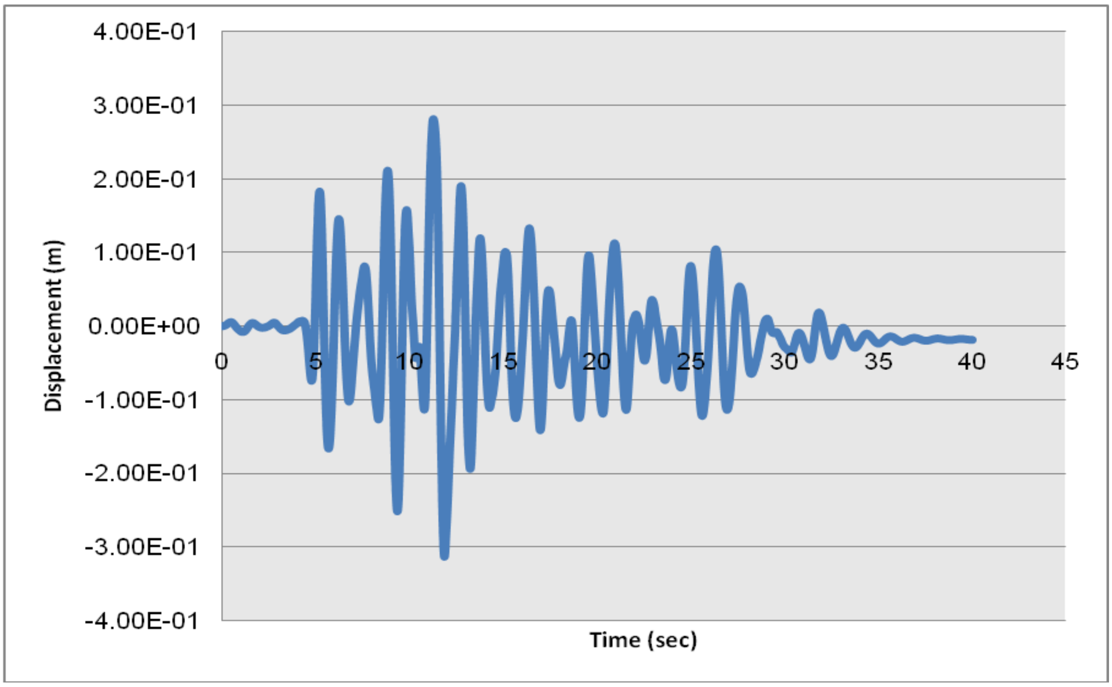


b)

Fig C1 Displacement time-hitory relation for 6FRMRF a) x-direction
b) y-direction

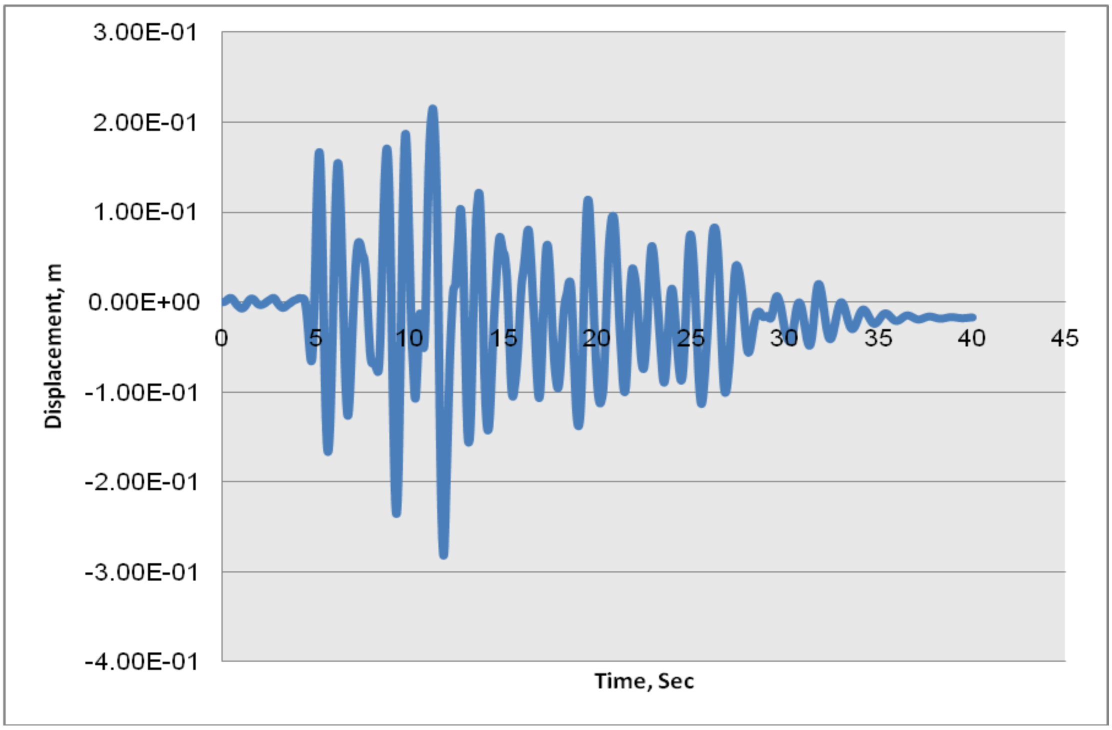


a)

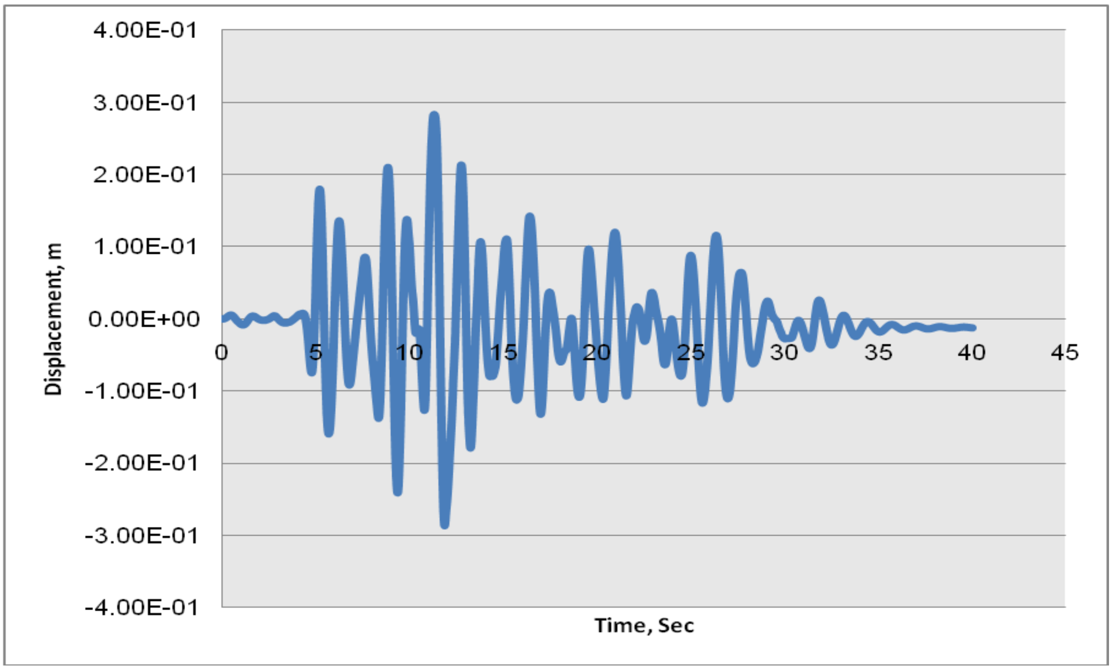


b)

Fig C2 Displacement time-hitory relation for 6SR45 a) x-direction
b) y-direction

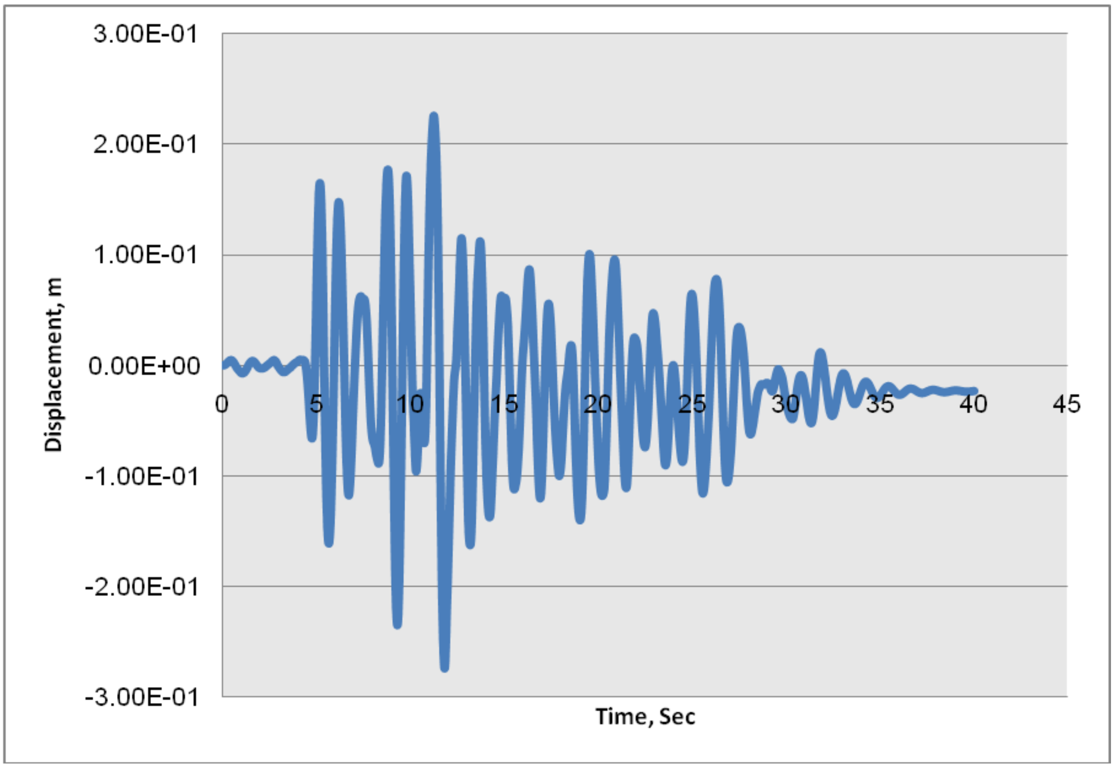


a)

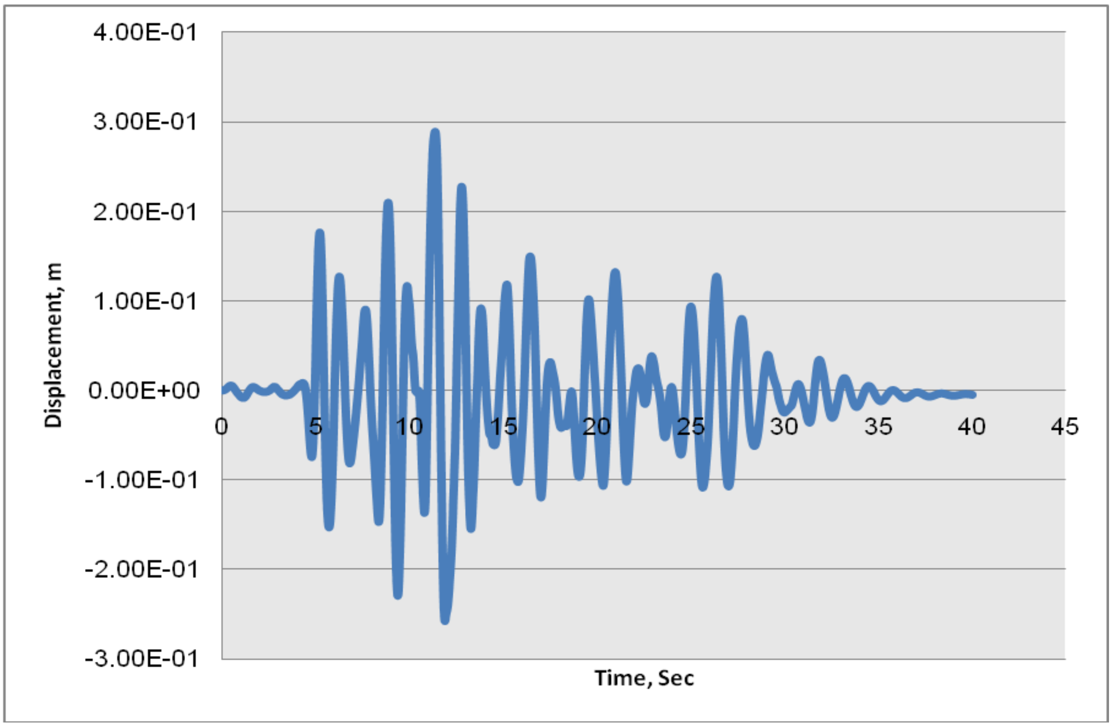


b)

Fig C3 Displacement time-hitory relation for 6SR34 a) x-direction
b) y-direction

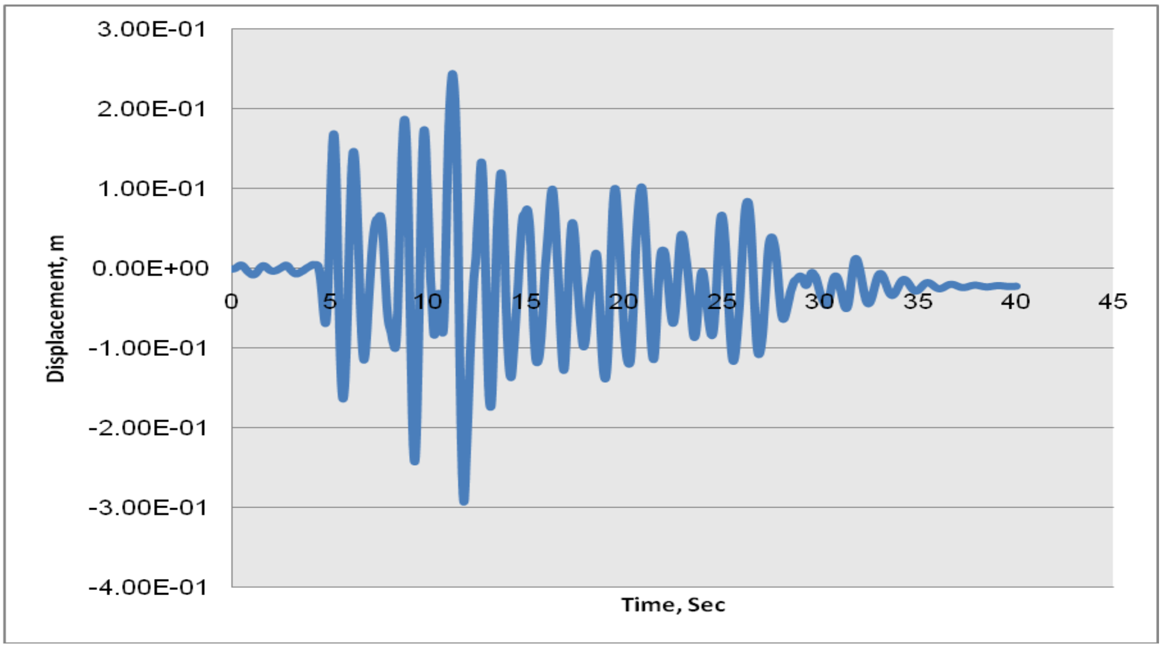


a)

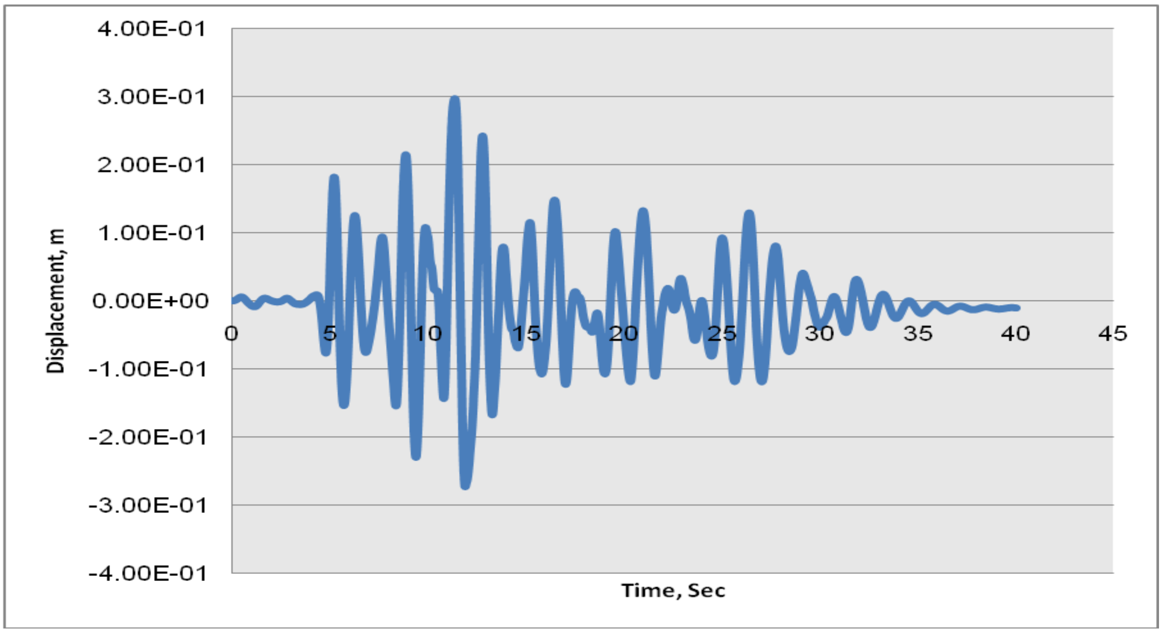


b)

Fig C4 Displacement time-hitory relation for 6SR23 a) x-direction
b) y-direction

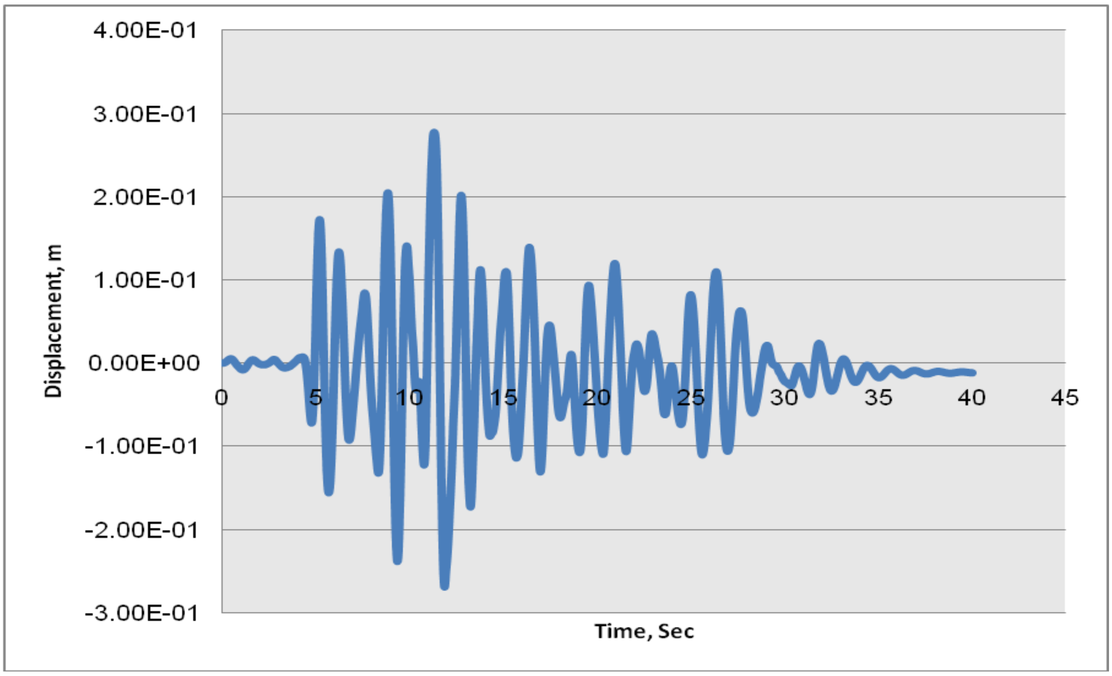


a)

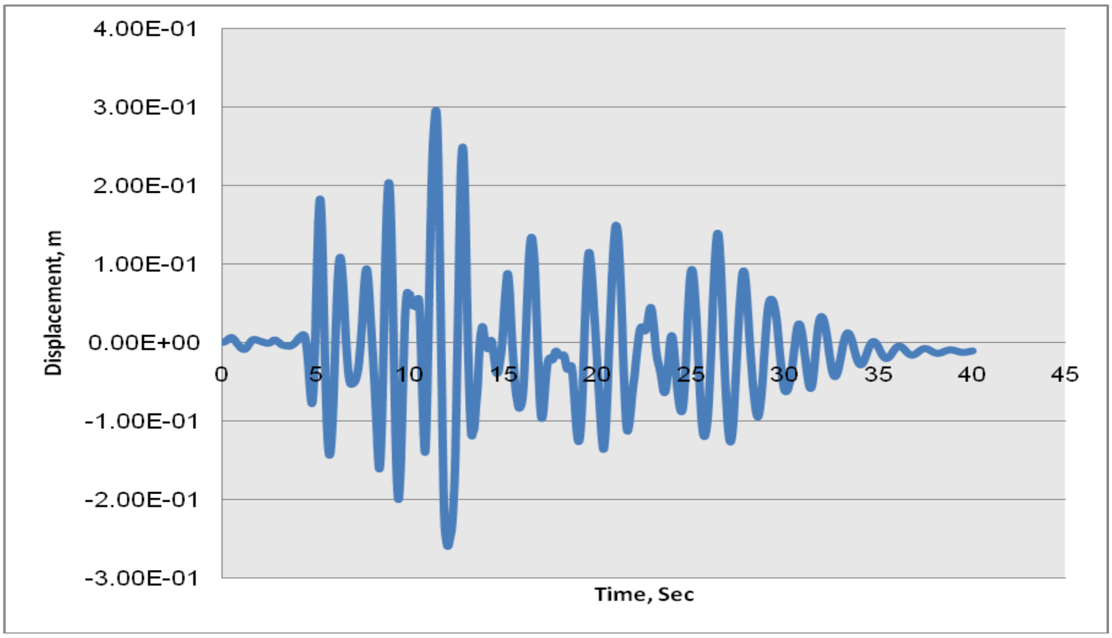


b)

Fig C5 Displacement time-hitory relation for 6SR1346 a) x-direction
b) y-direction

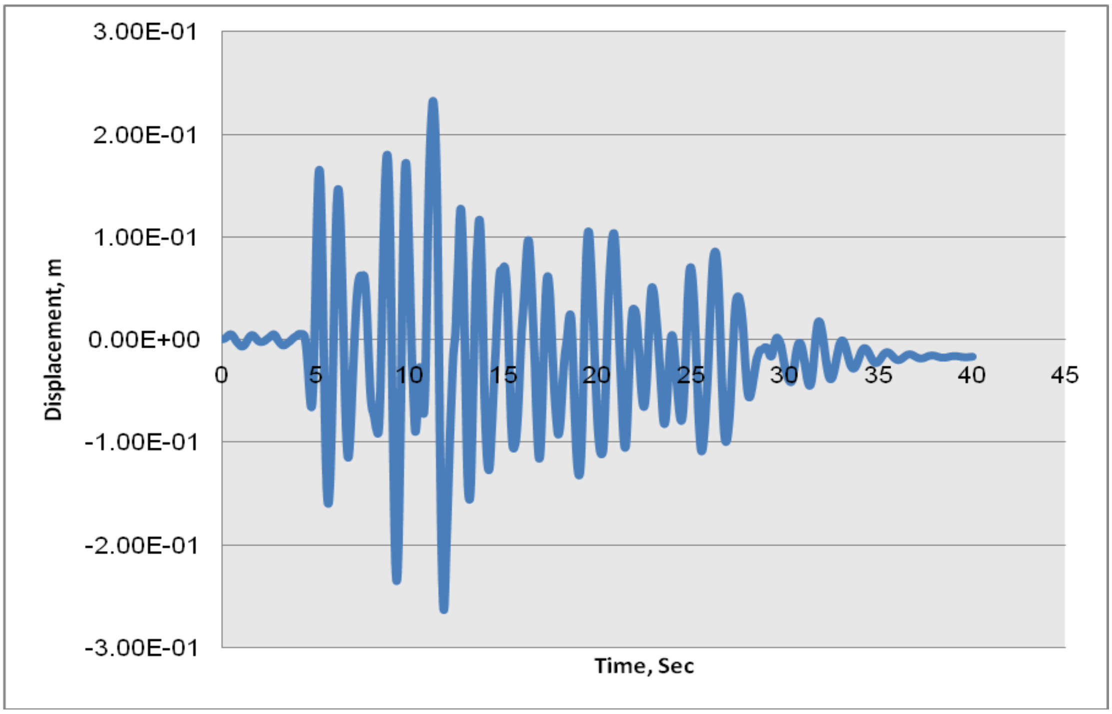


a)

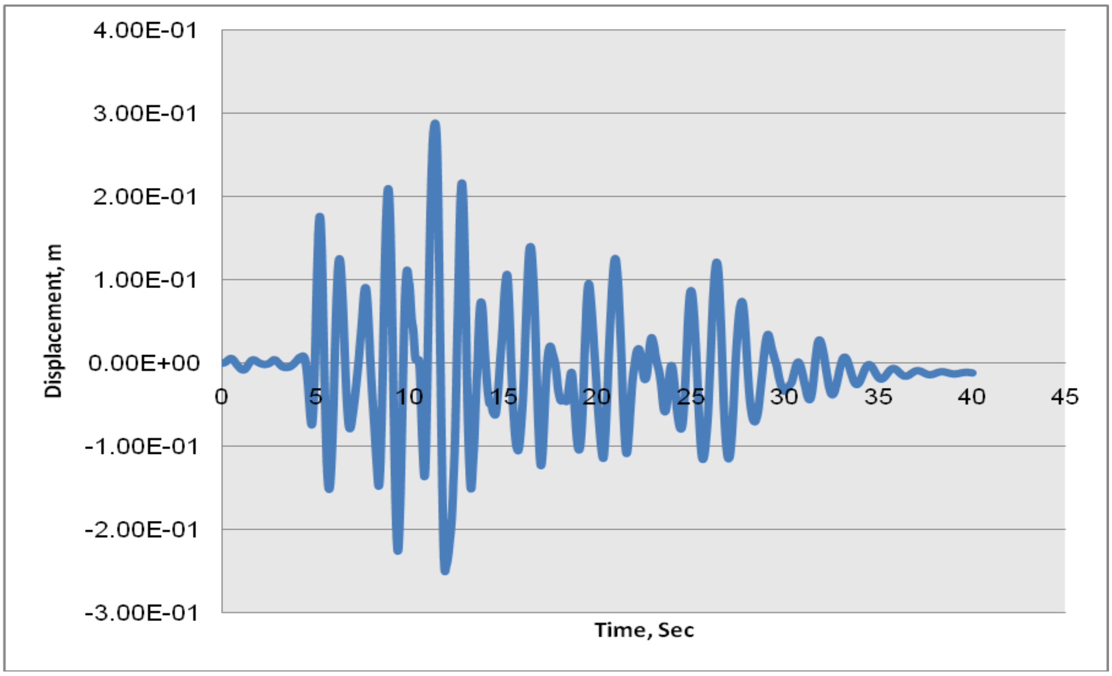


b)

Fig C6 Displacement time-hitory relation for 6SRall a) x-direction
b) y-direction

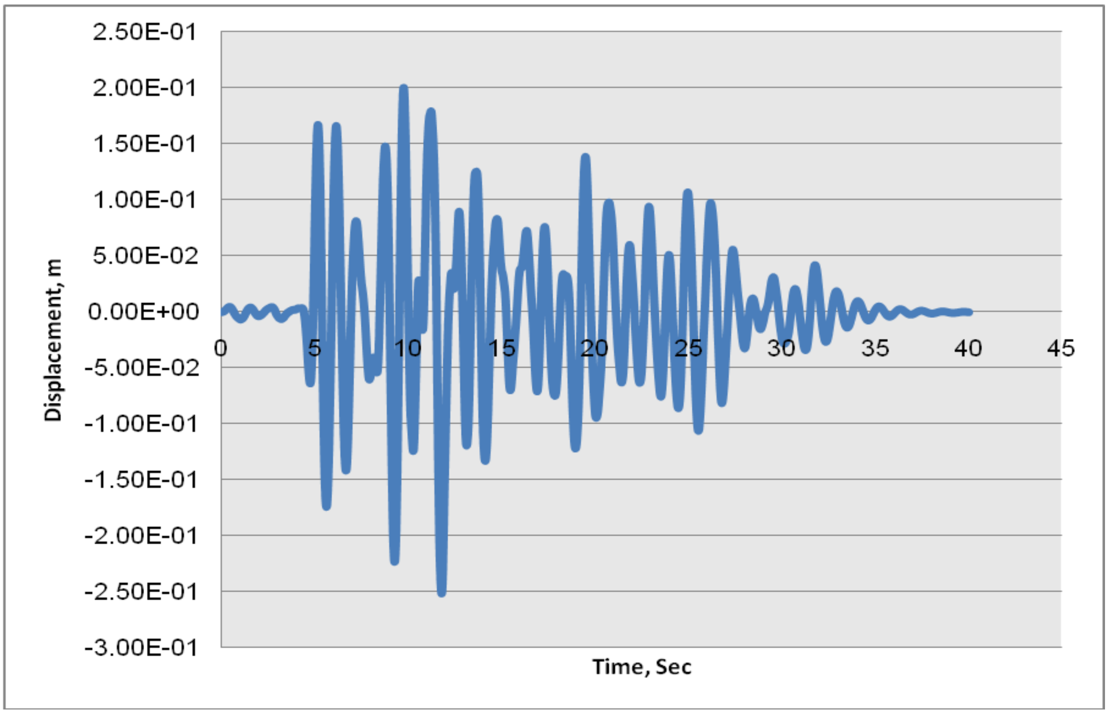


a)

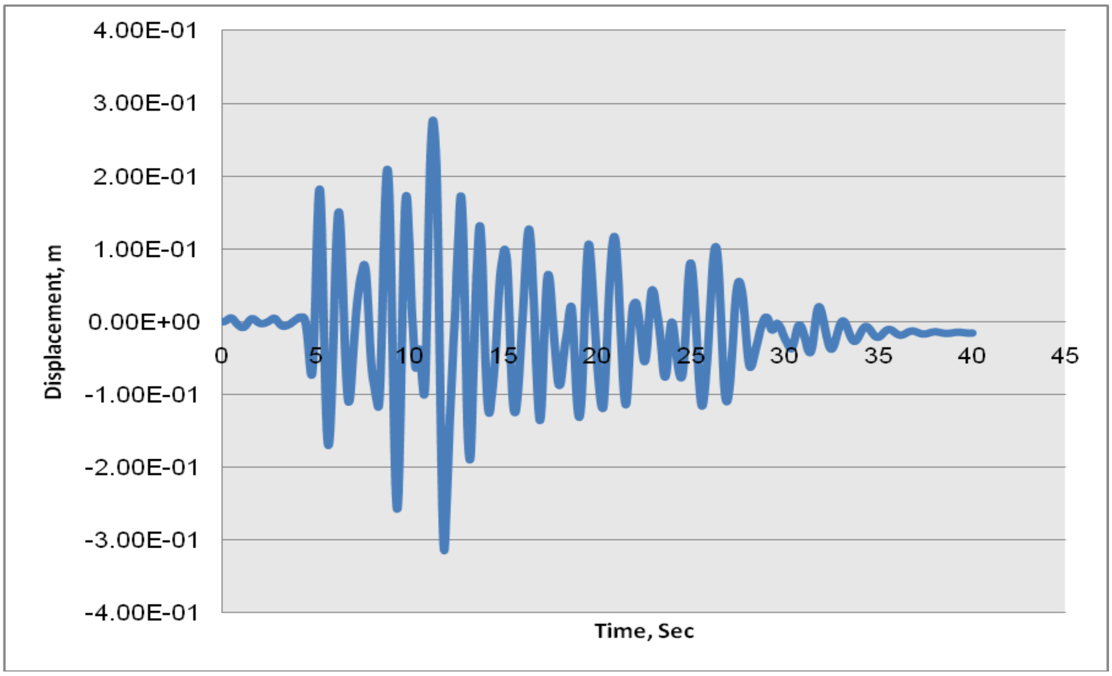


b)

Fig C7 Displacement time-hitory relation for 6SR12 a) x-direction
b) y-direction

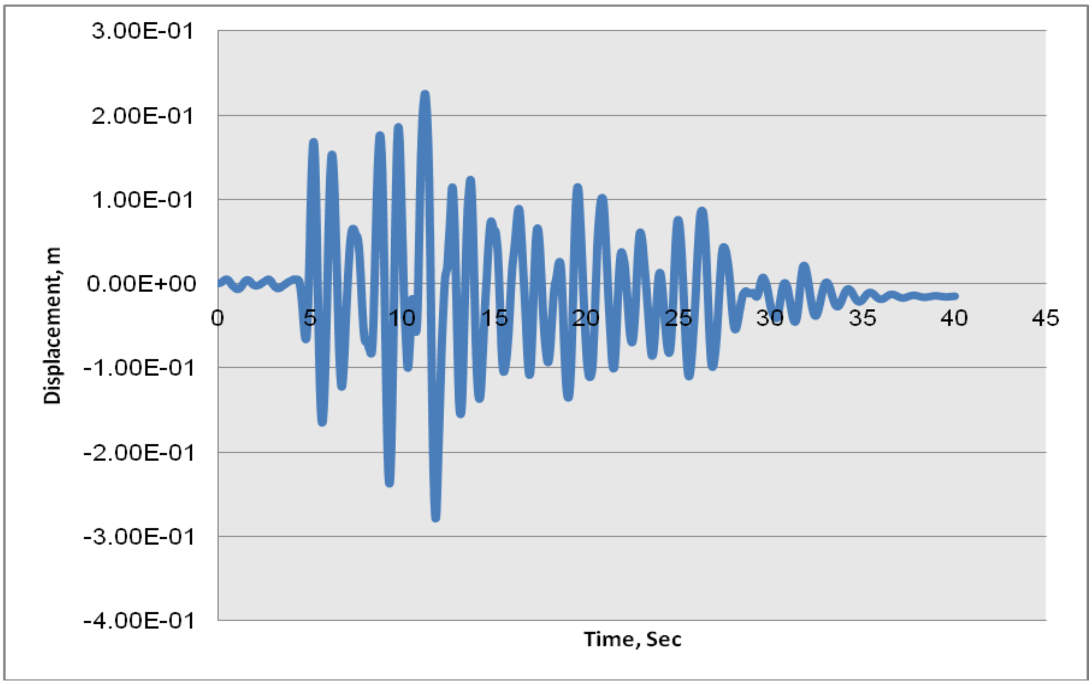


a)

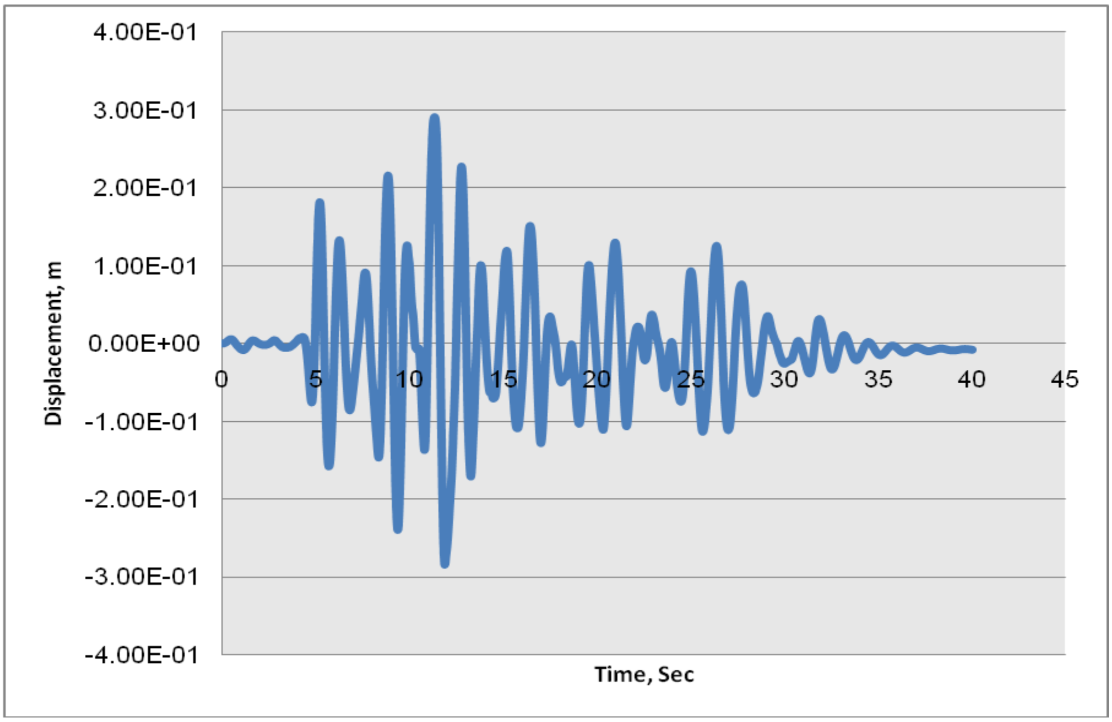


b)

Fig C8 Displacement time-hitory relation for 6SR56 a) x-direction
b) y-direction

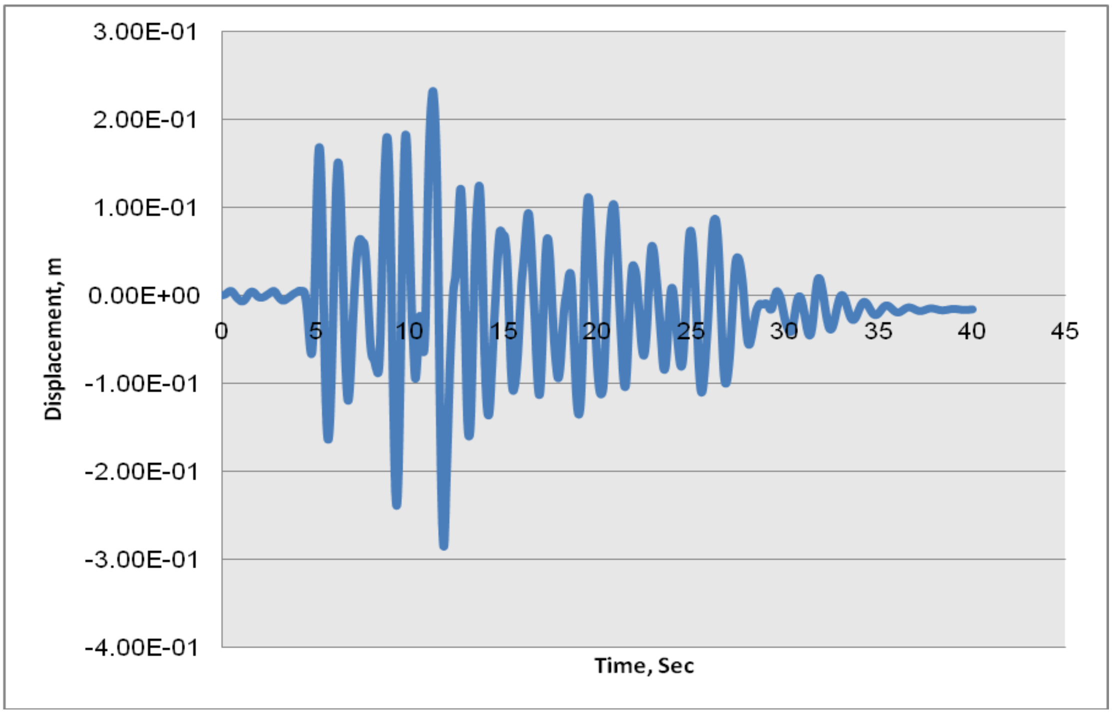


a)

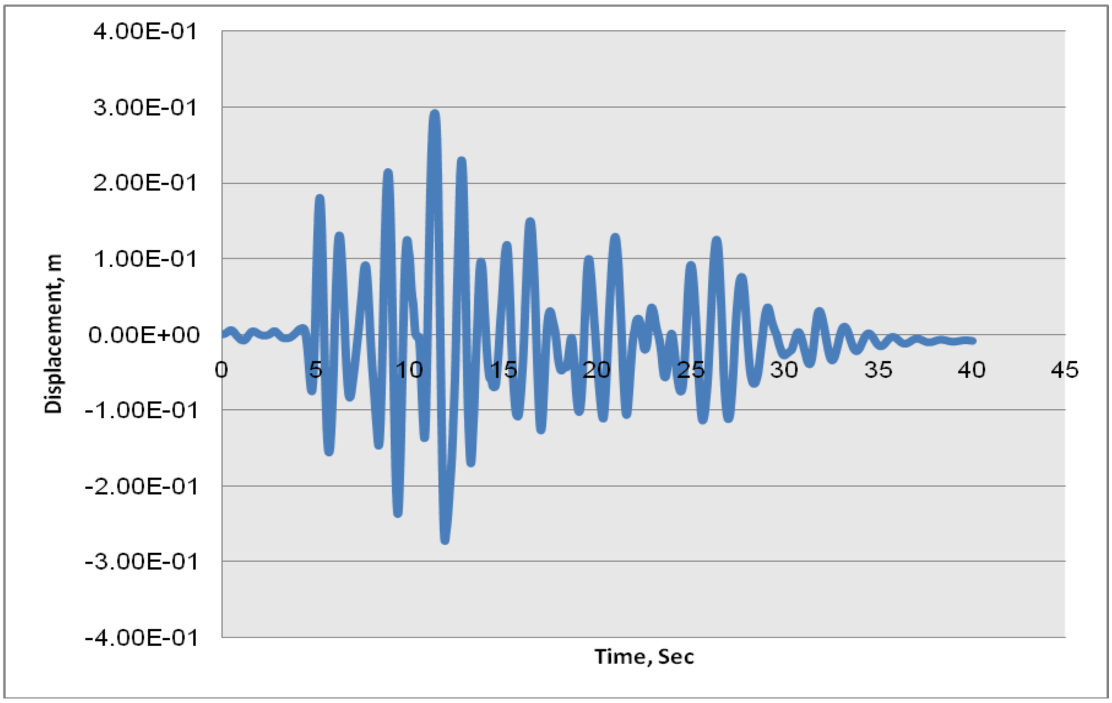


b)

Fig C9 Displacement time-hitory relation for 6SR246 a) x-direction
b) y-direction

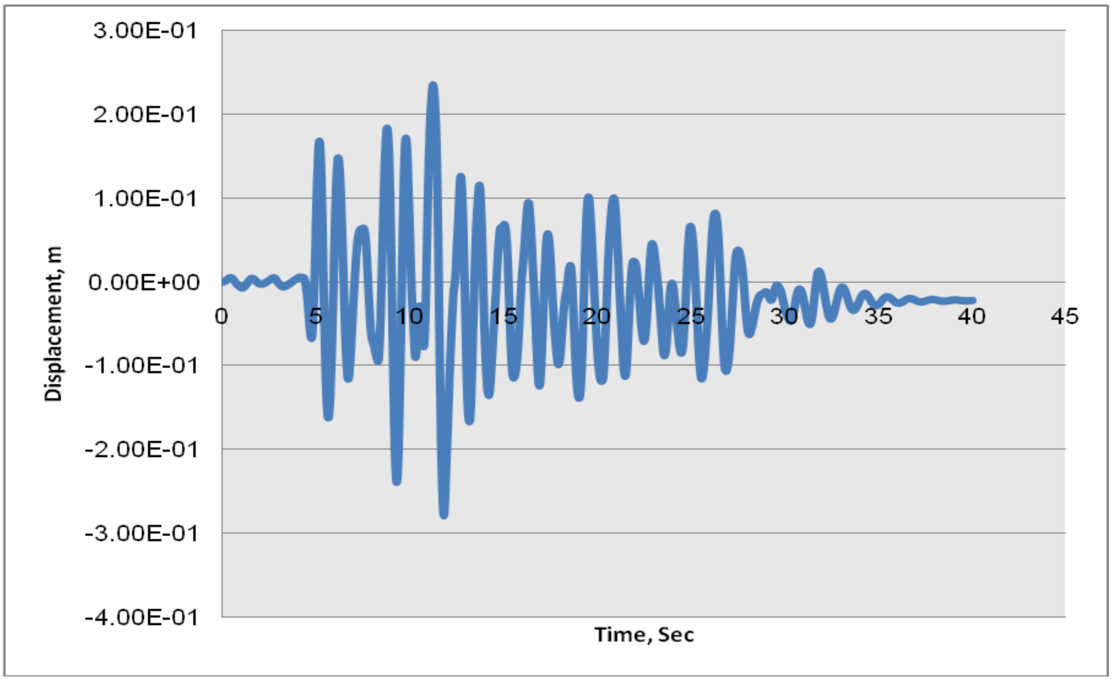


a)

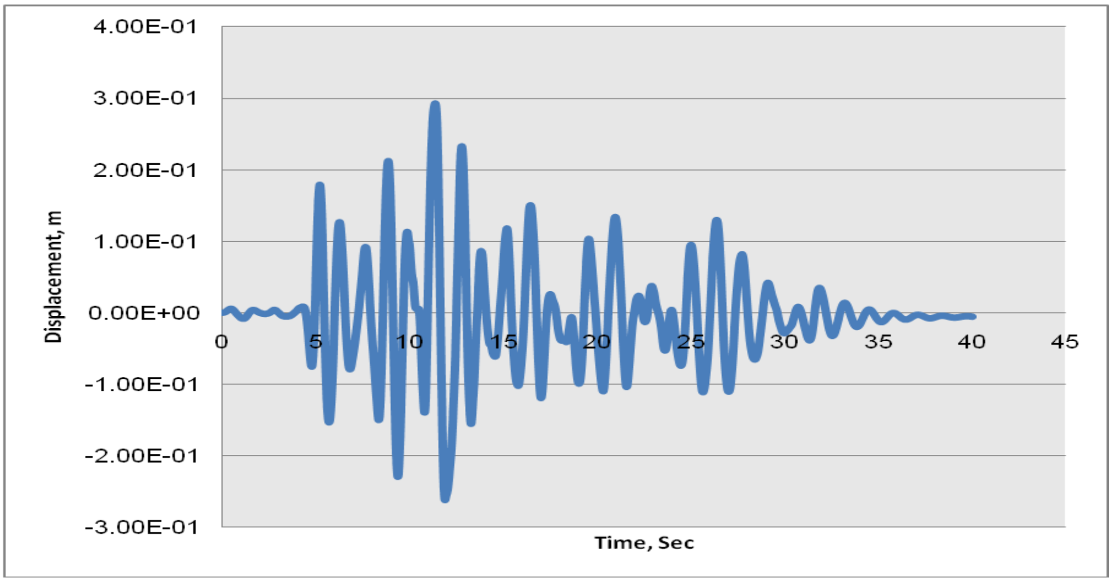


b)

Fig C10 Displacement time-hitory relation for 6SR135 a) x-direction
b) y-direction

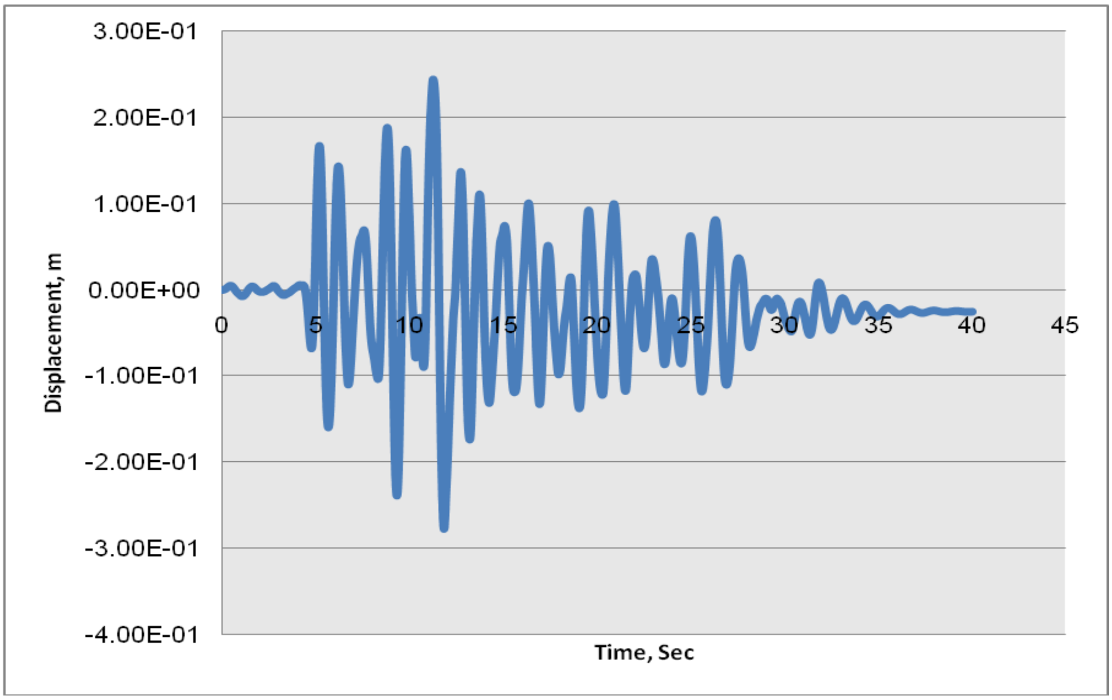


a)

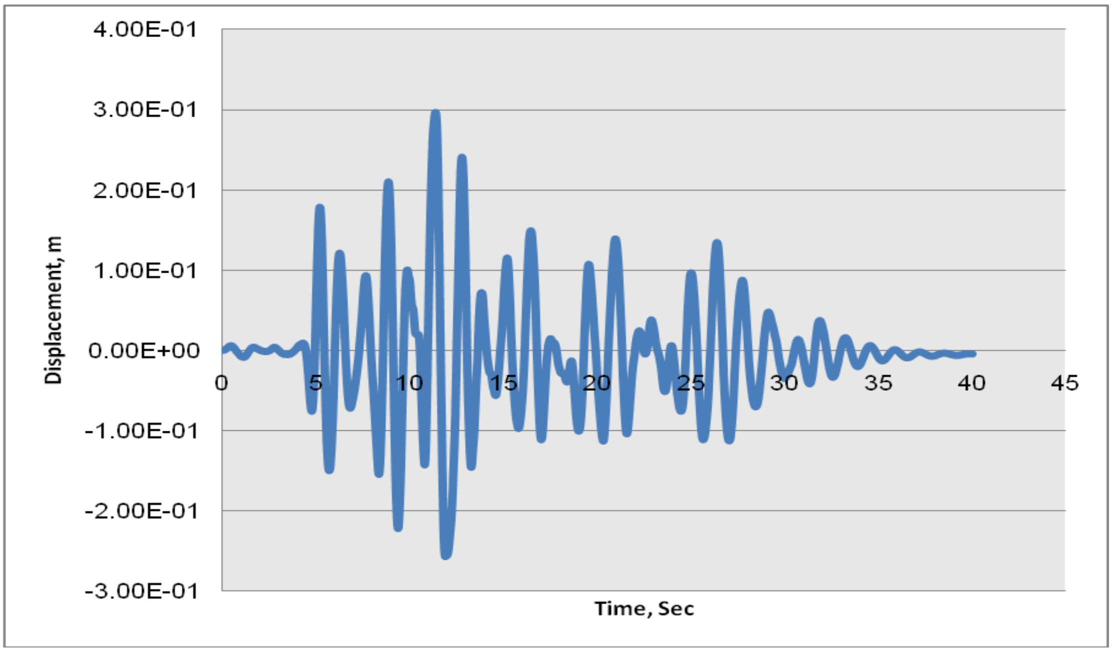


b)

Fig C11 Displacement time-hitory relation for 6SR235 a) x-direction
b) y-direction

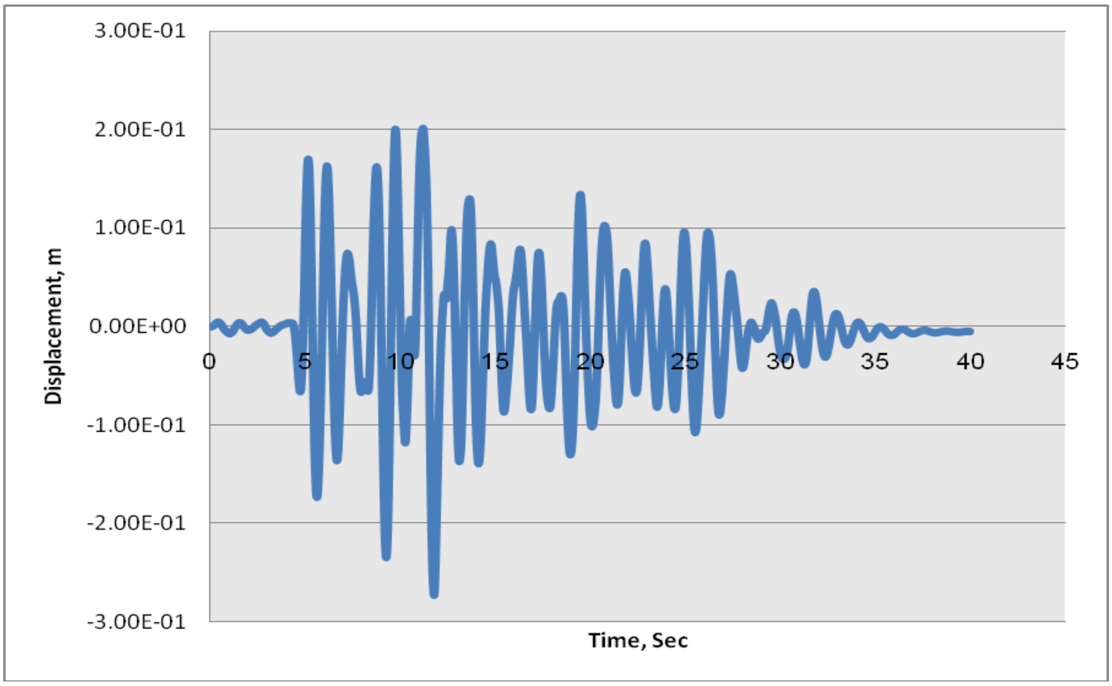


a)

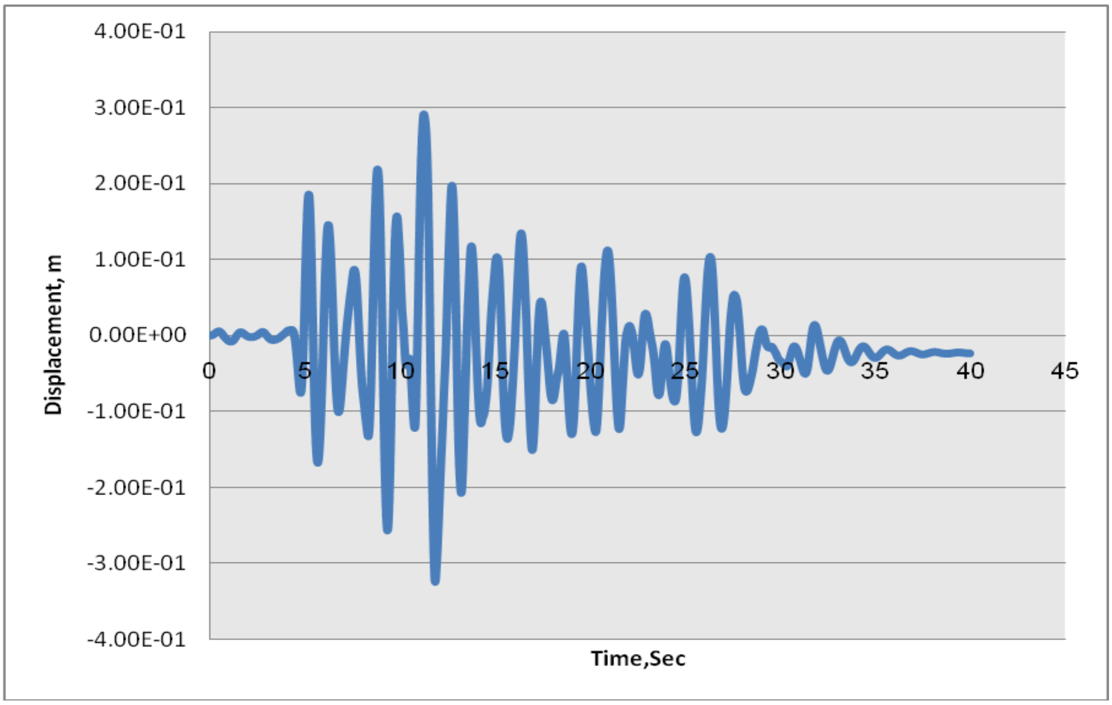


b)

Fig C12 Displacement time-hitory relation for 6SR234 a) x-direction
b) y-direction

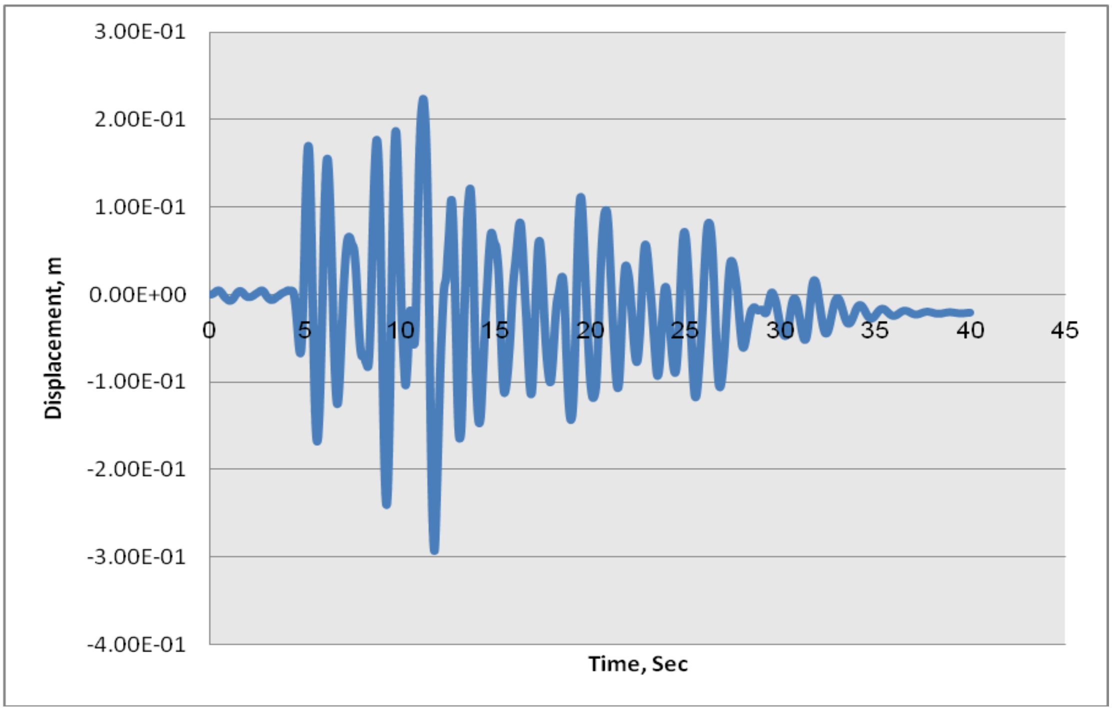


a)

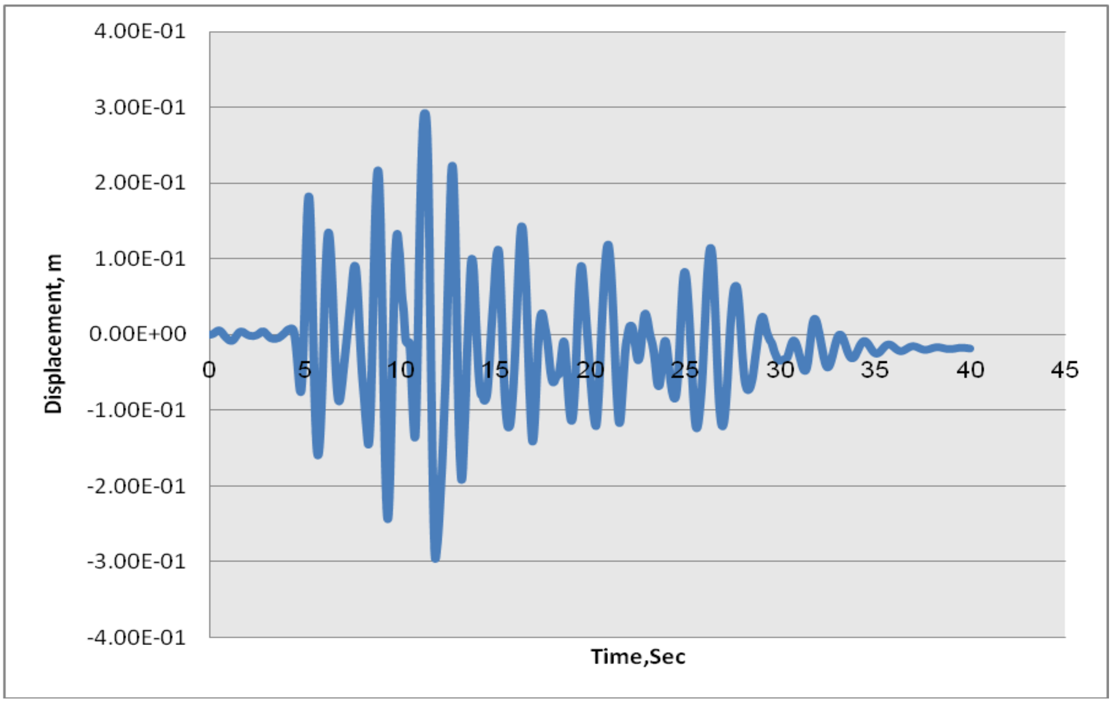


b)

Fig C13 Displacement time-hitory relation for 6SR456 a) x-direction
b) y-direction

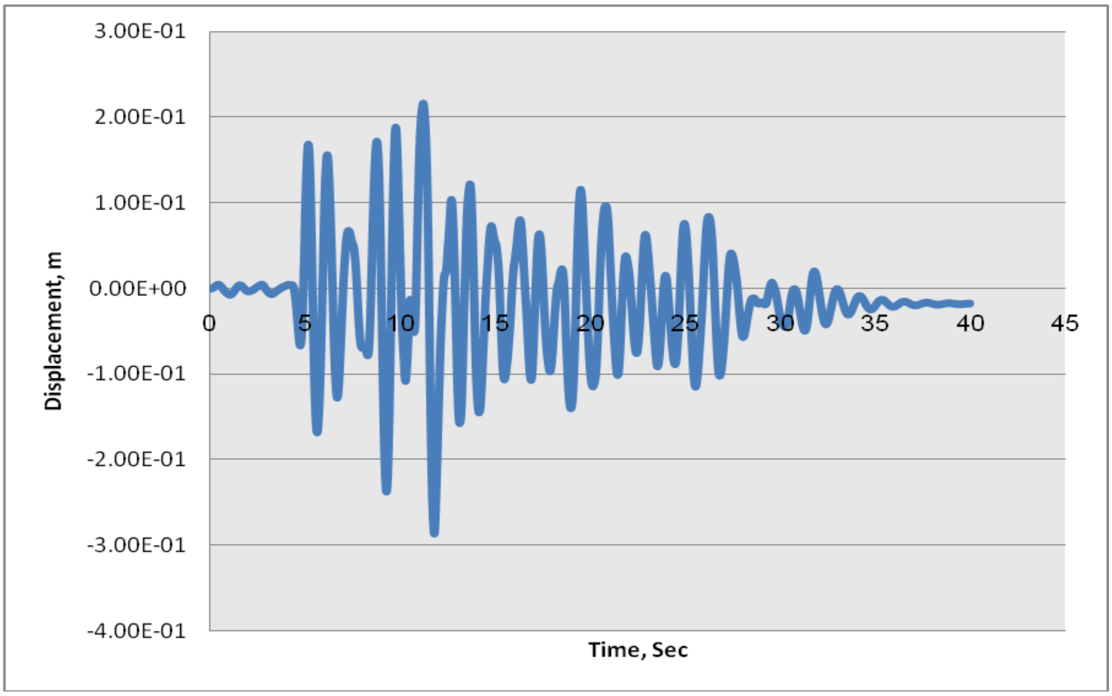


a)

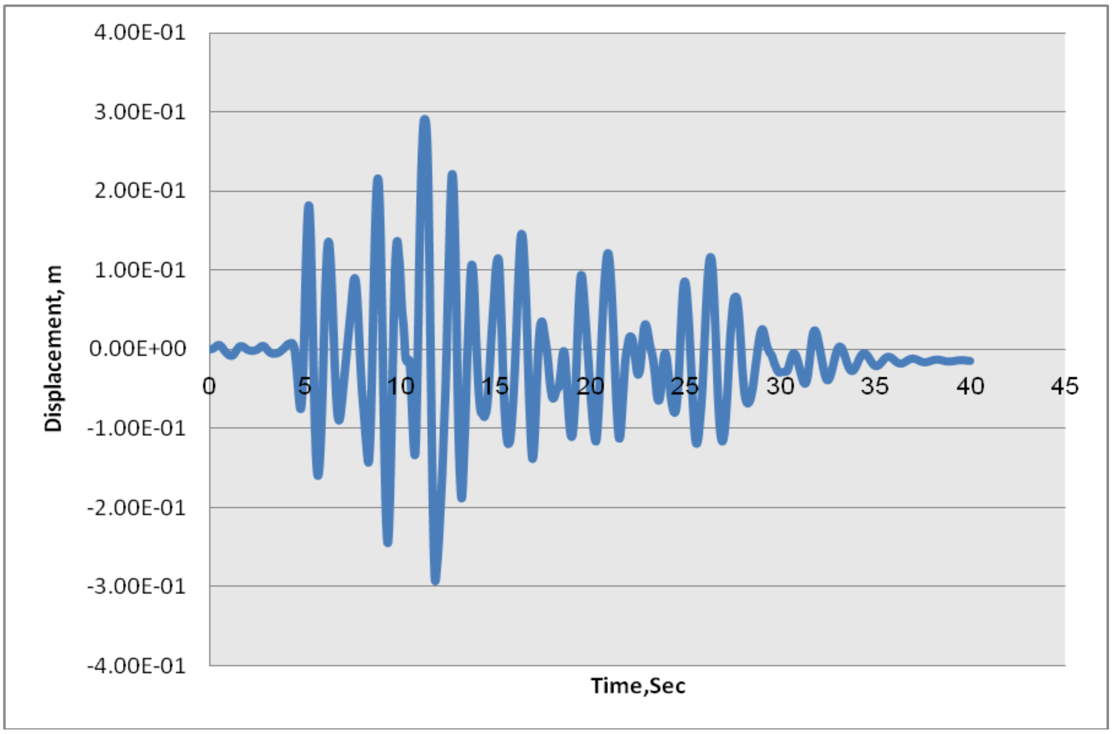


b)

Fig C14 Displacement time-hitory relation for 6SR345 a) x-direction
b) y-direction

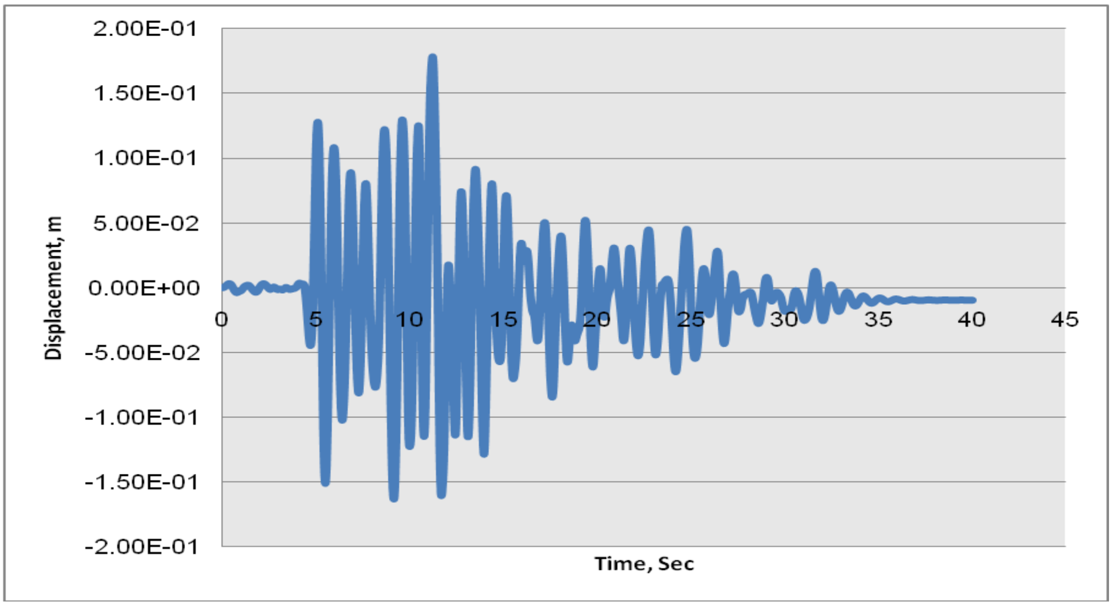


a)

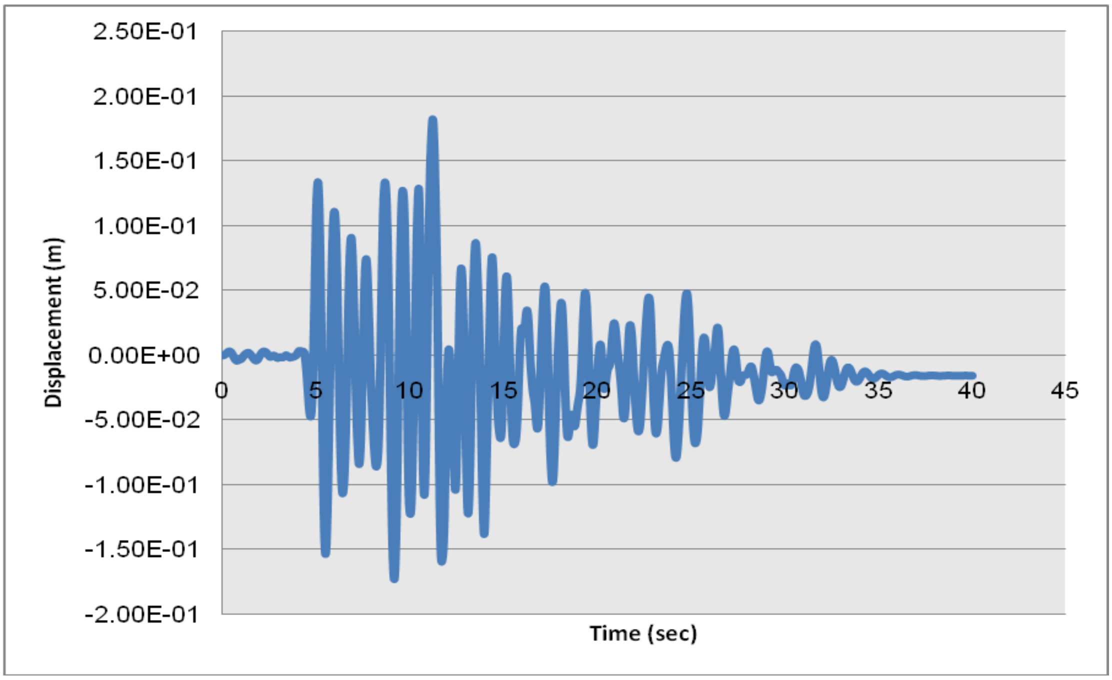


b)

Fig C15 Displacement time-hitory relation for 6SR346 a) x-direction
b) y-direction

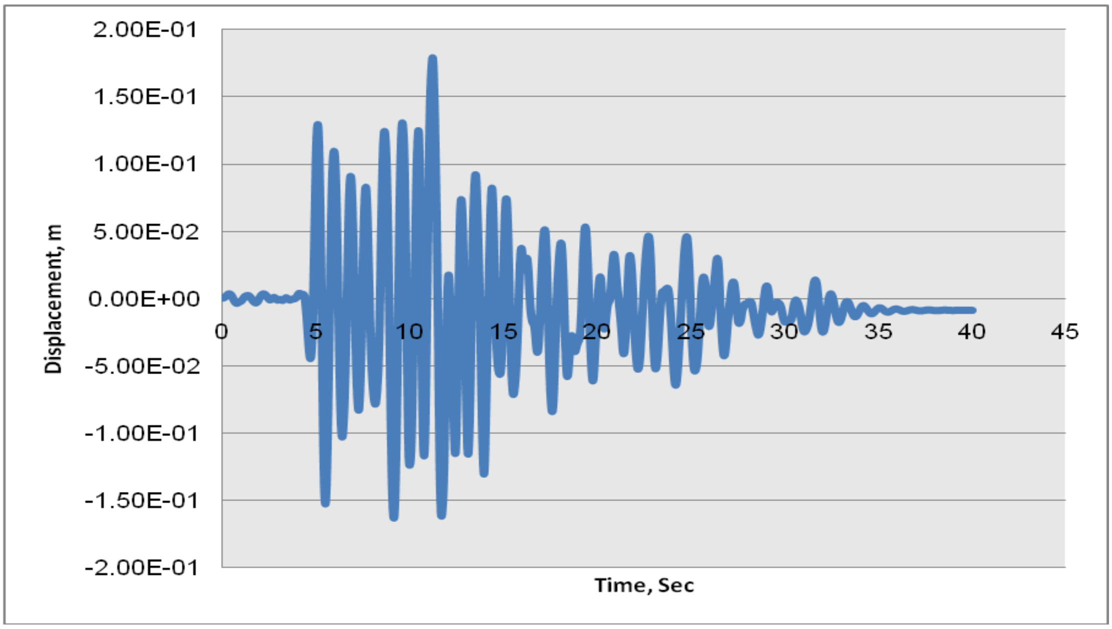


a)

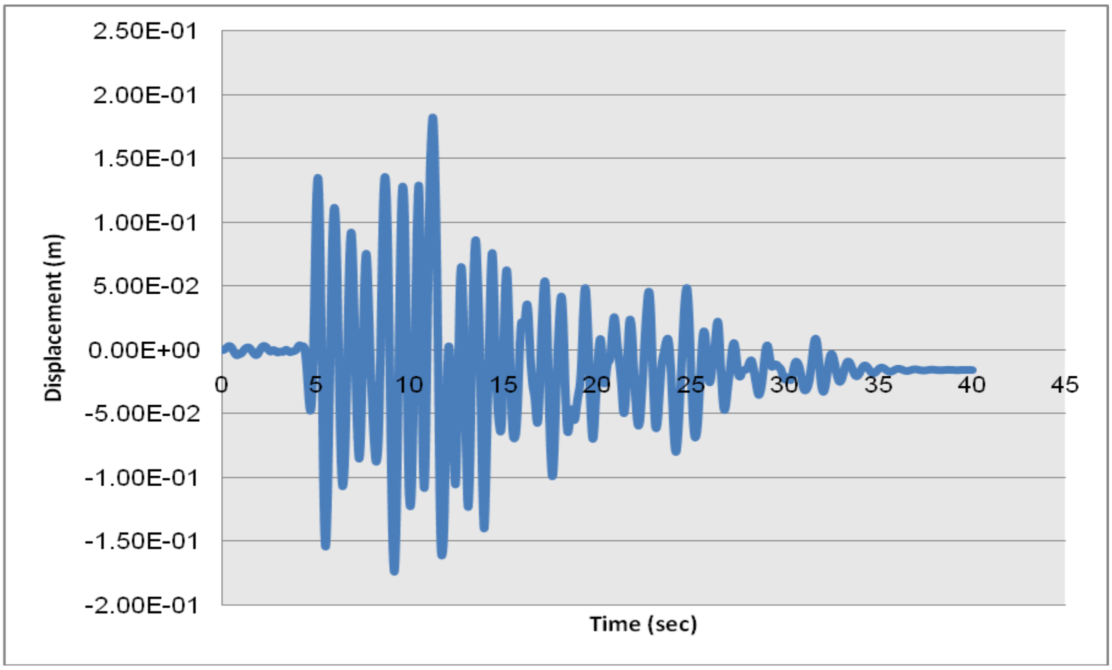


b)

Fig C16 Displacement time-hitory relation for 6BRBF cx CY a) x-direction
b) y-direction

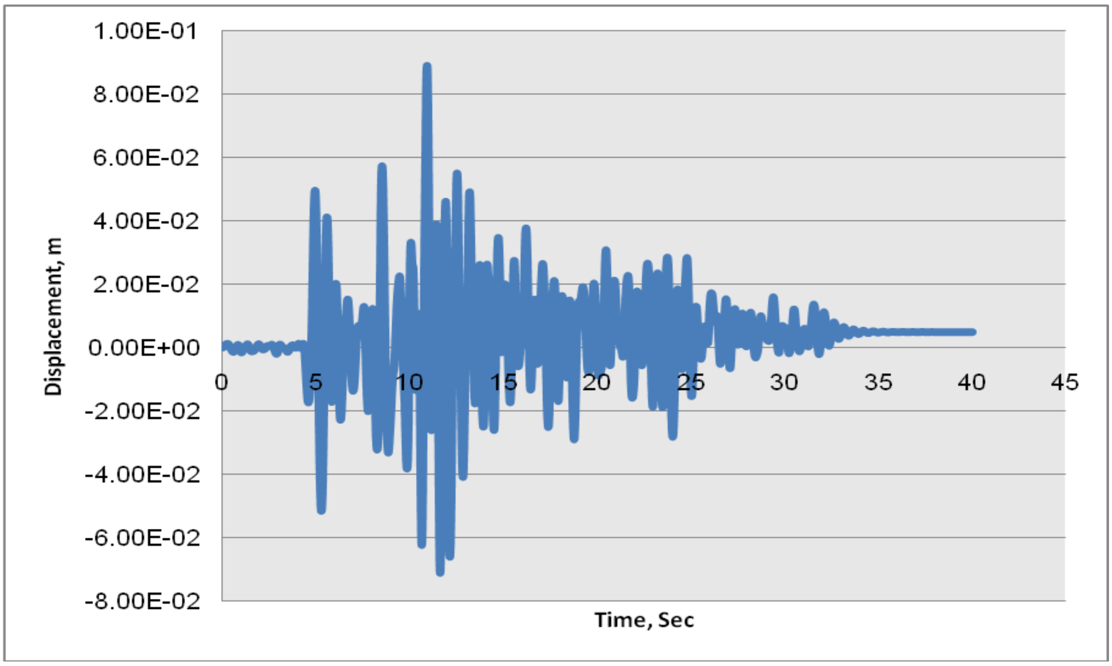


a)

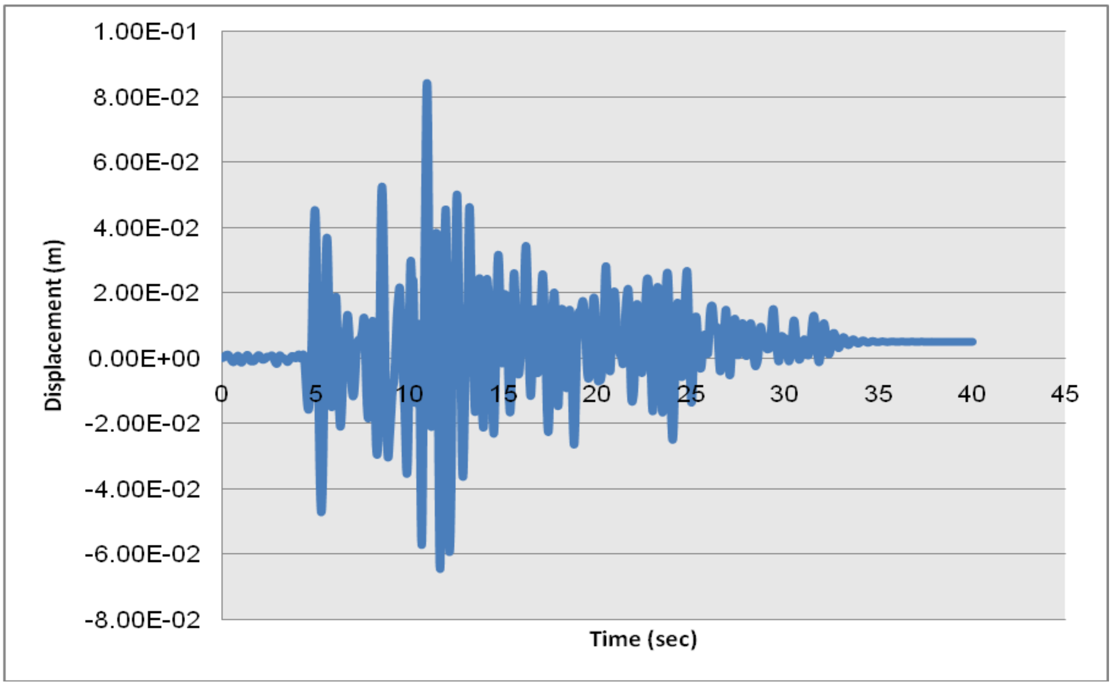


b)

Fig C17 Displacement time-hitory relation for 6BRBF cx sy a) x-direction
b) y-direction



a)

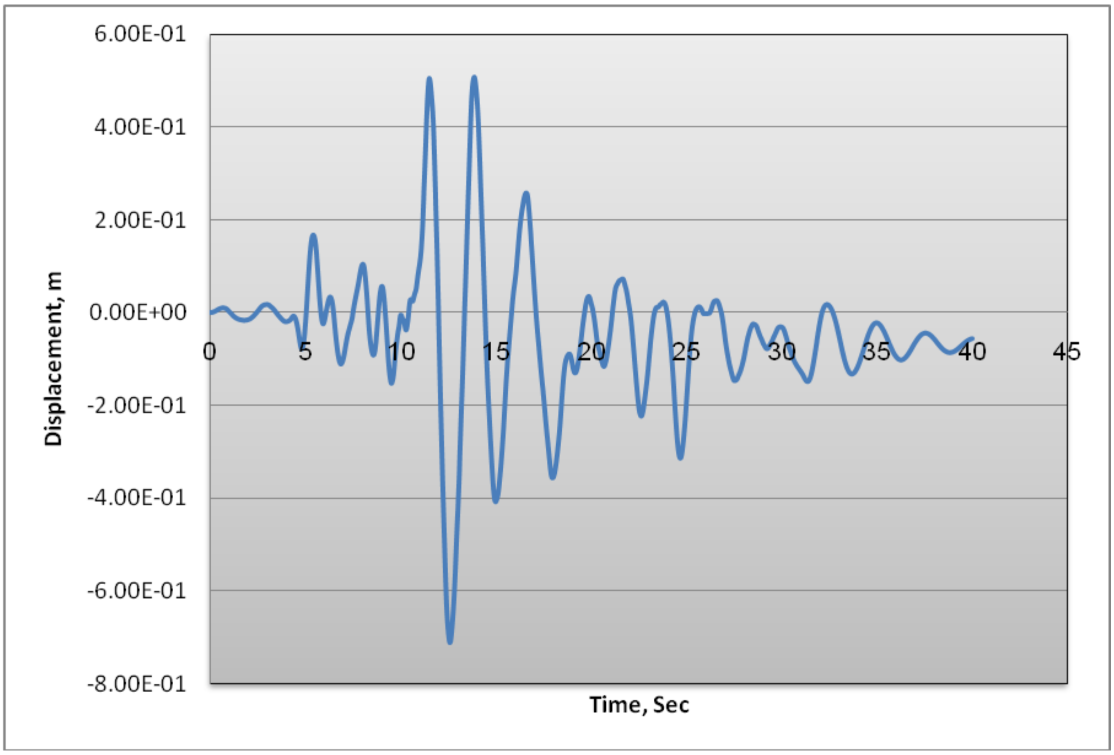


b)

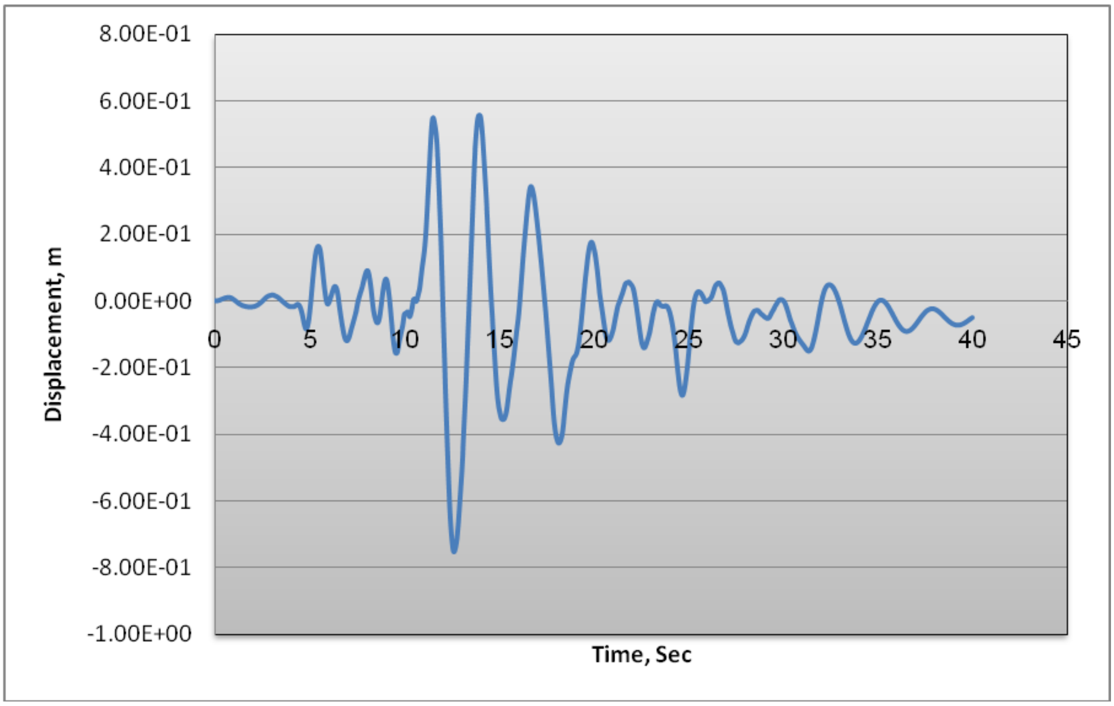
Fig C18 Displacement time-hitory relation for 6EBF cscox cscoy a) x-direction b) y-direction

APPENDIX D

20-STOREY DISPLACEMENT TIME-HISTORY RELATION

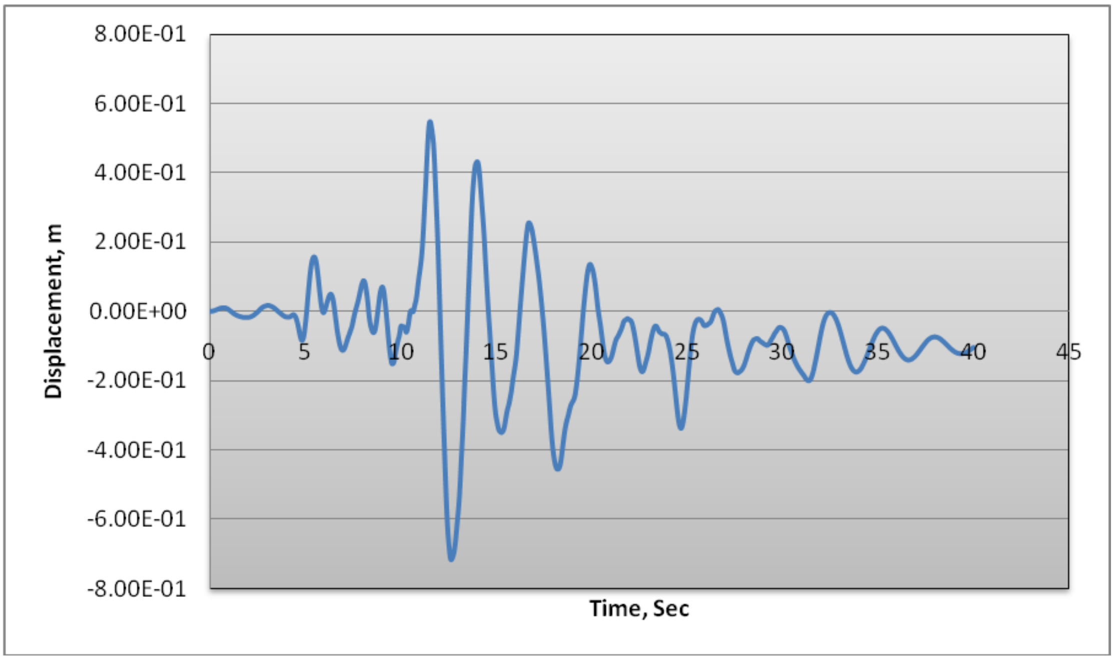


a)

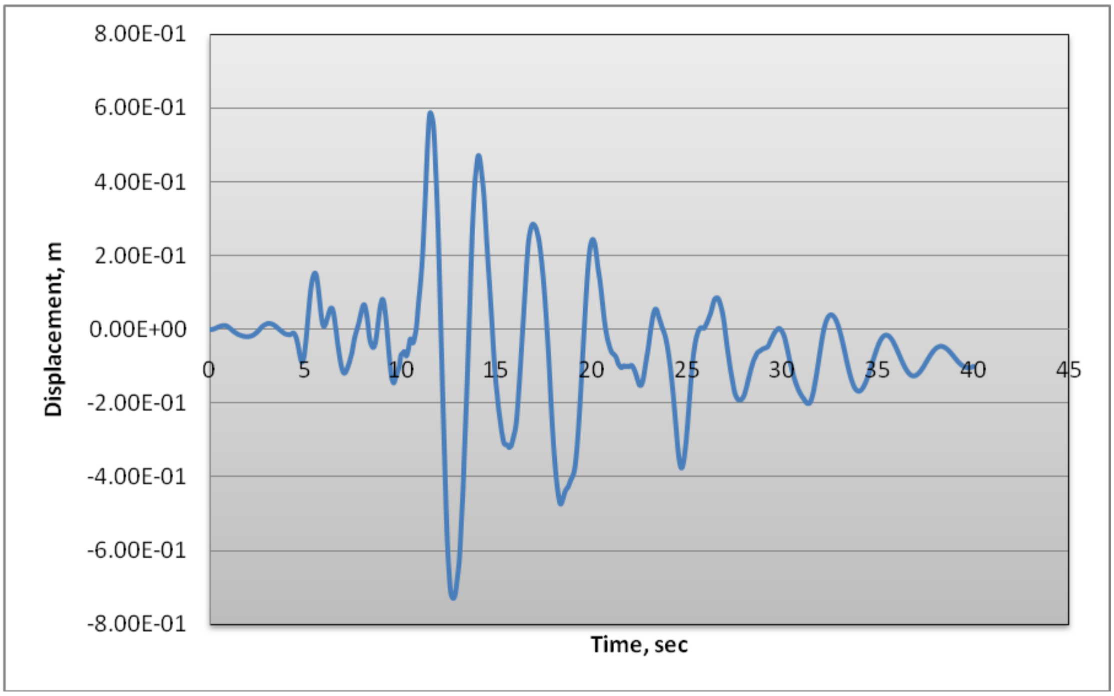


b)

Fig D1 Displacement time-history relation for 20FRMRF a) x-direction b) y-direction

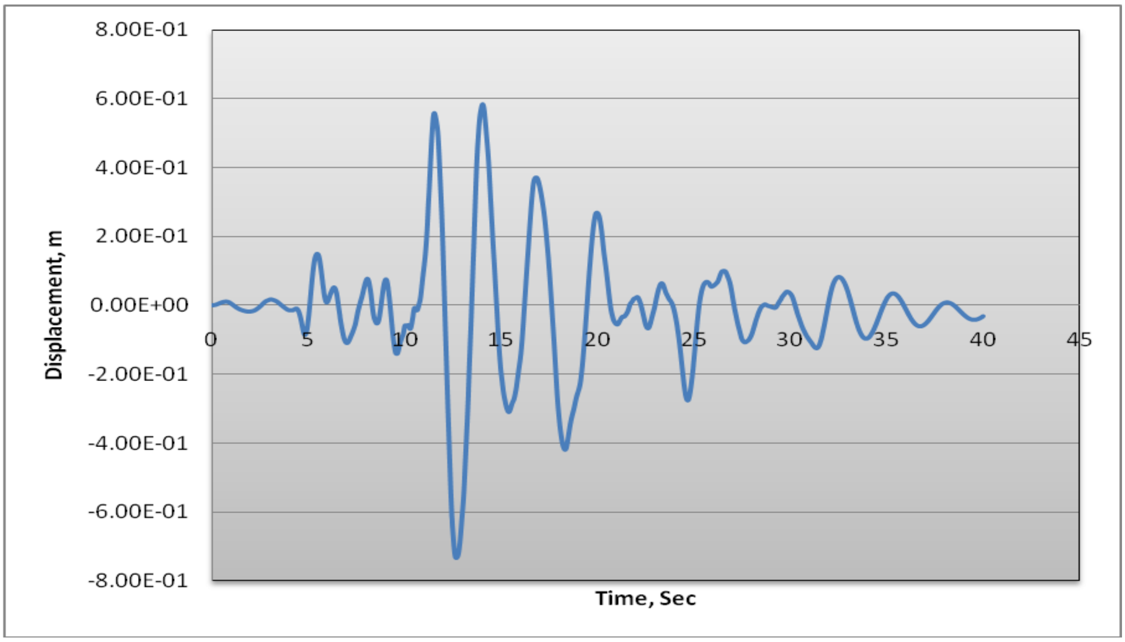


a)

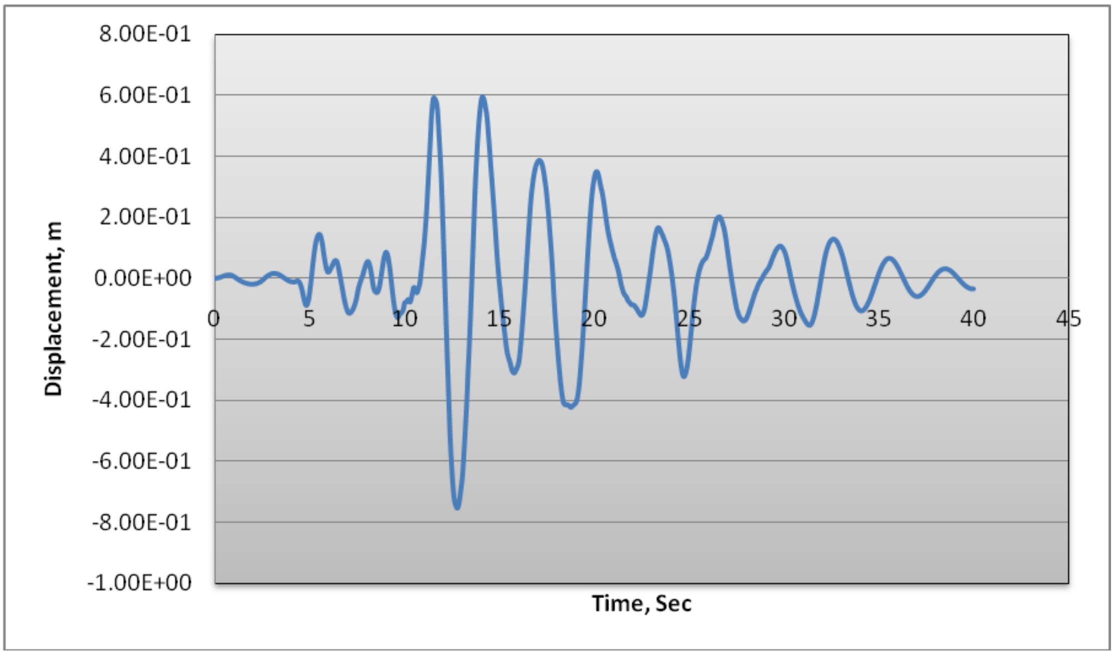


b)

Fig D2 Displacement time-hitory relation for 20SR8-13 a) x-direction
b) y-direction

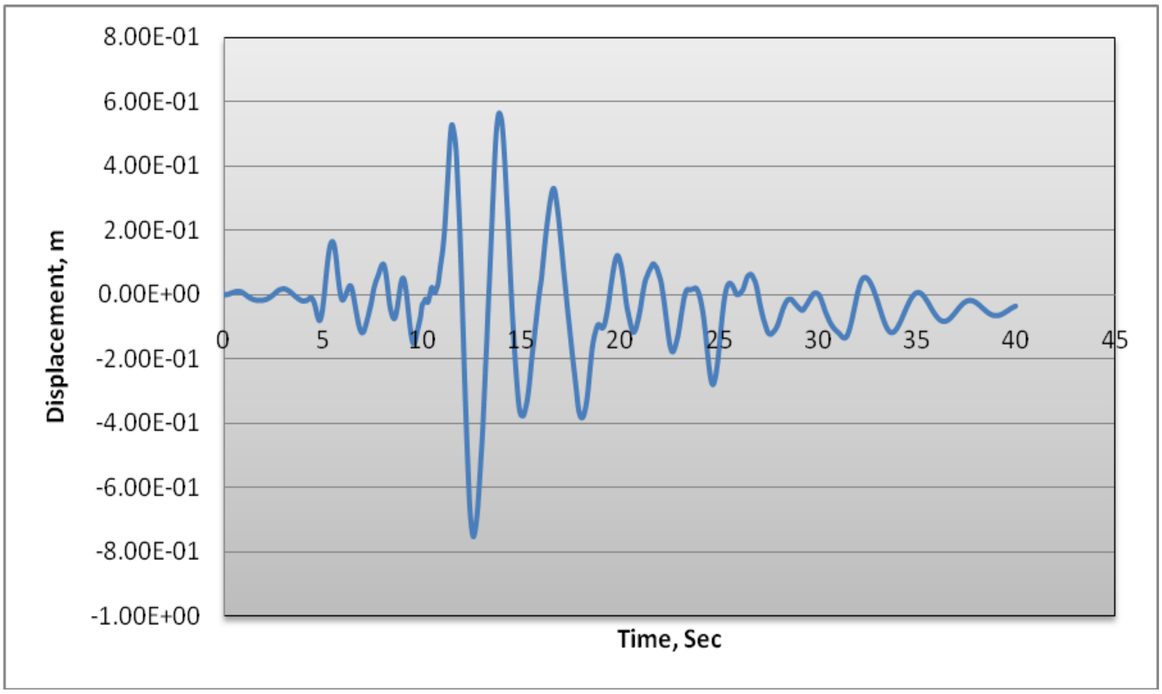


a)

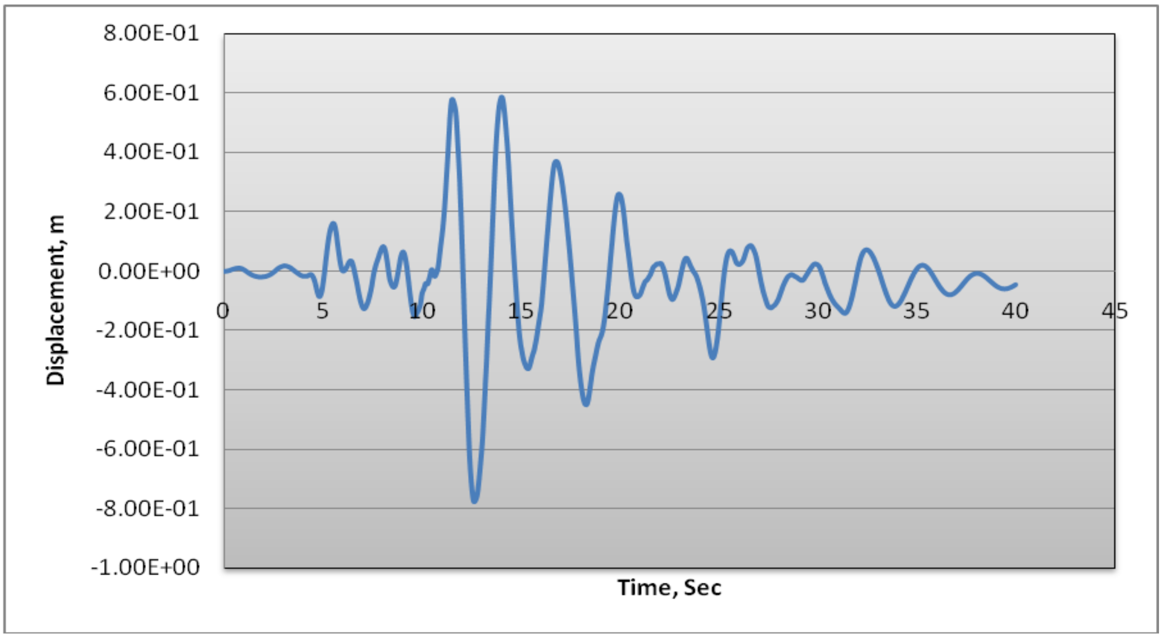


b)

Fig D3 Displacement time-hitory relation for 20SR1-6 a) x-direction
b) y-direction

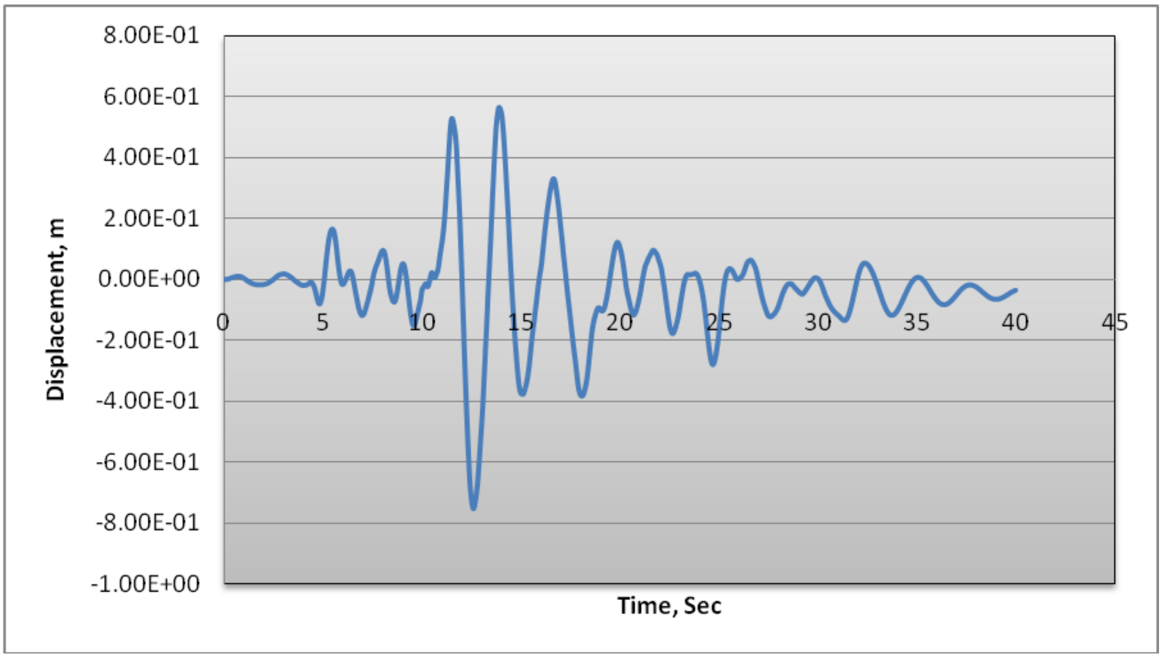


a)

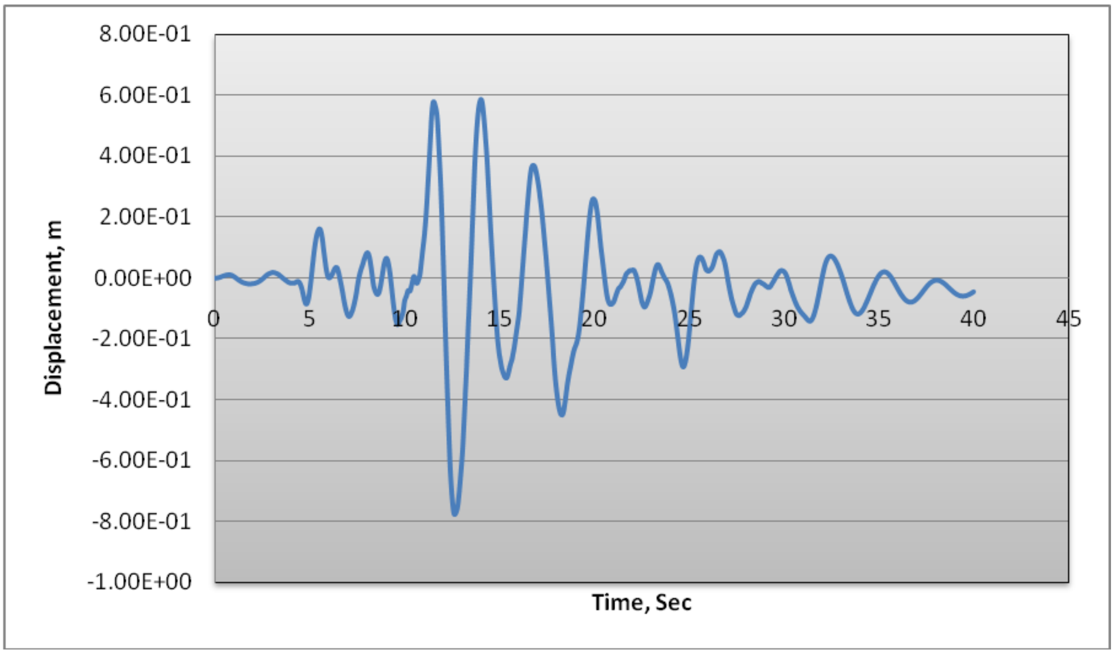


b)

Fig D4 Displacement time-hitory relation for 20SR4-9 a) x-direction
b) y-direction

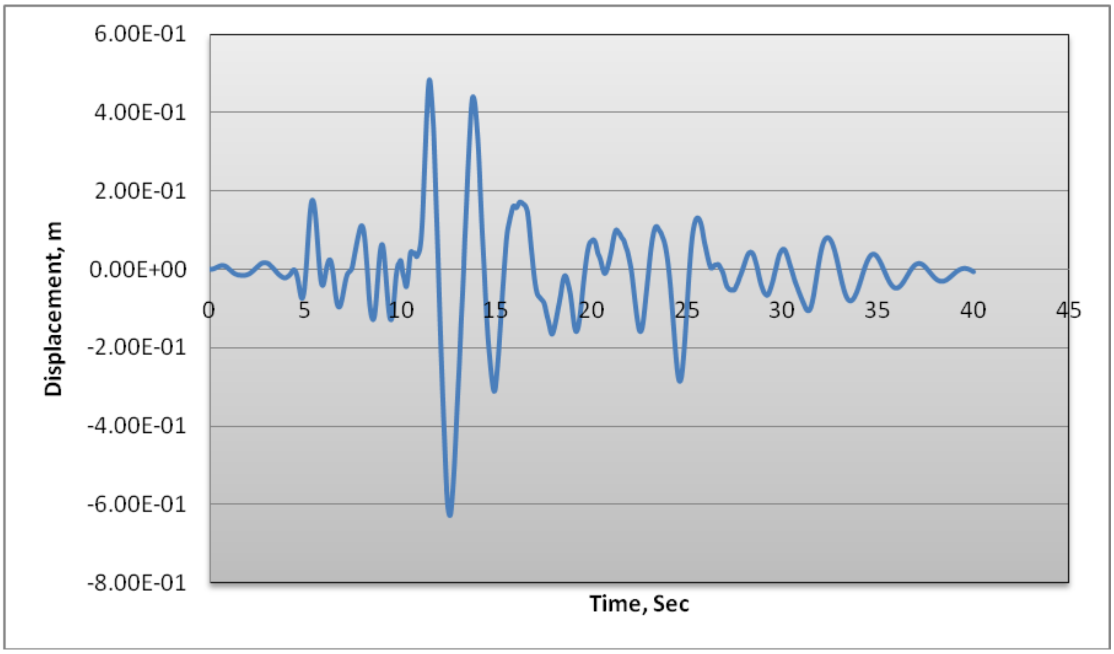


a)

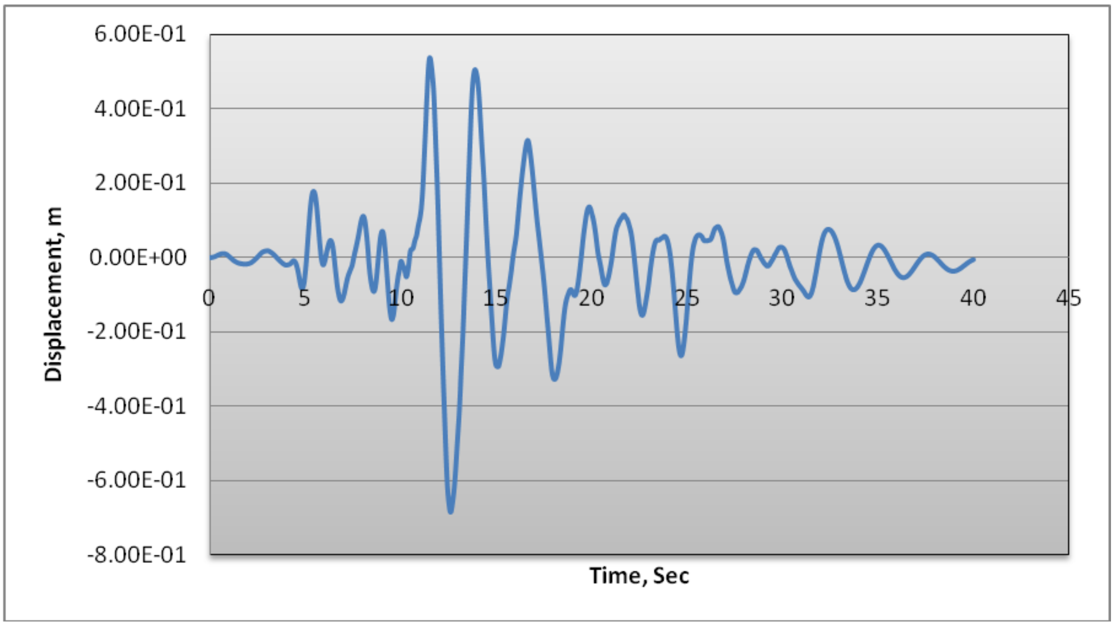


b)

Fig D5 Displacement time-hitory relation for 20SR13-18 a) x-direction
b) y-direction

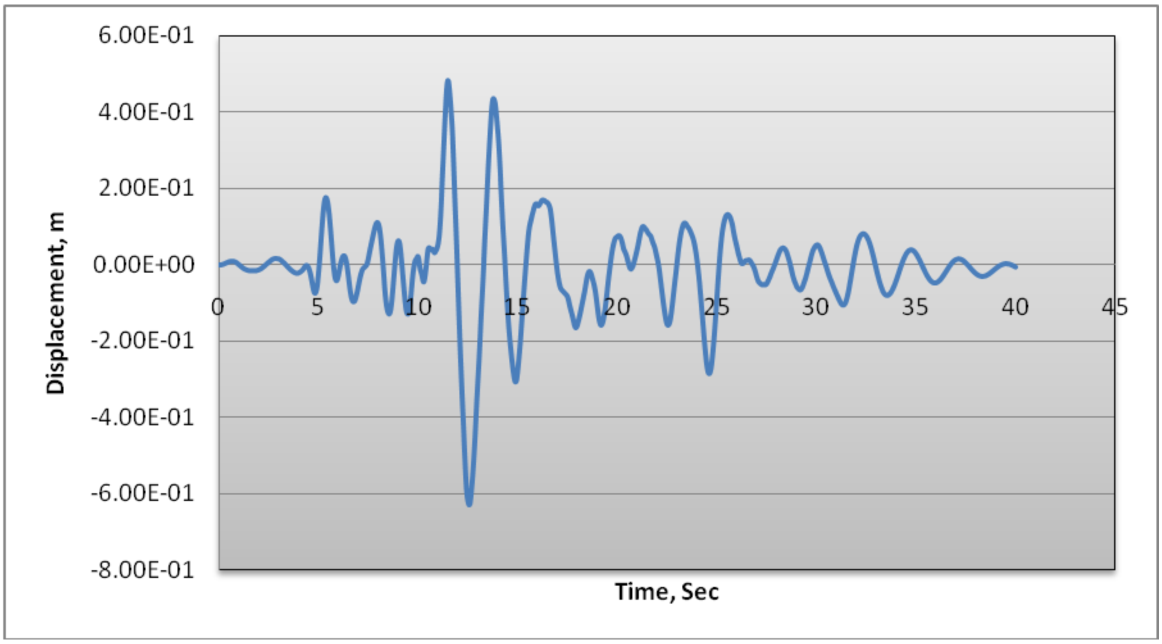


a)

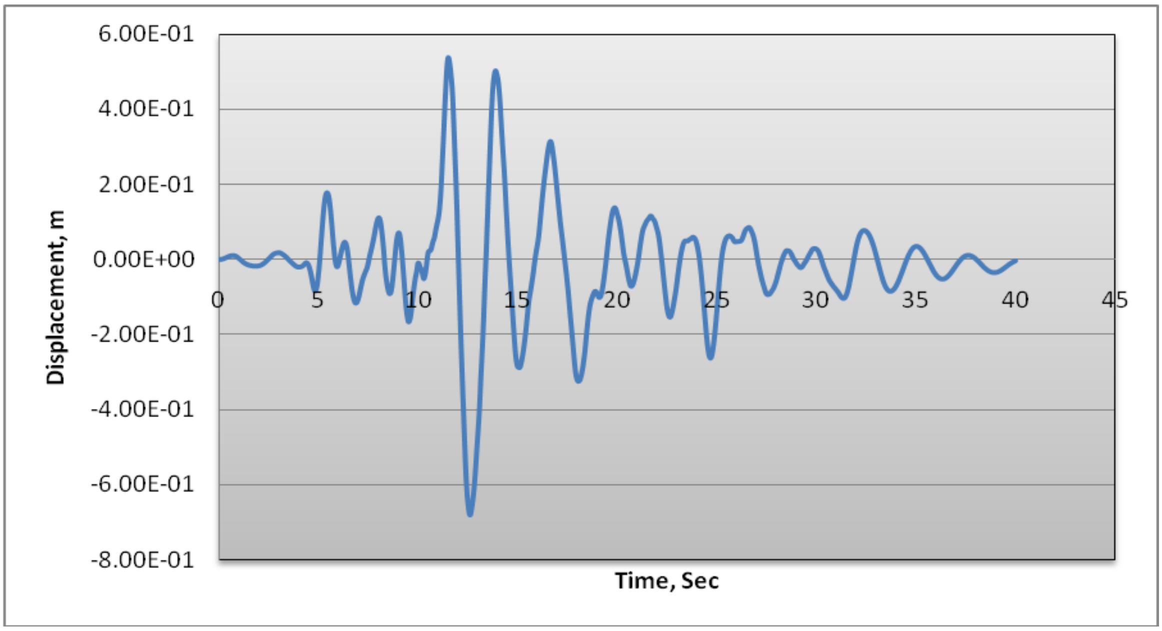


b)

Fig D6 Displacement time-hitory relation for 20BRBF cx sy a) x-direction
b) y-direction

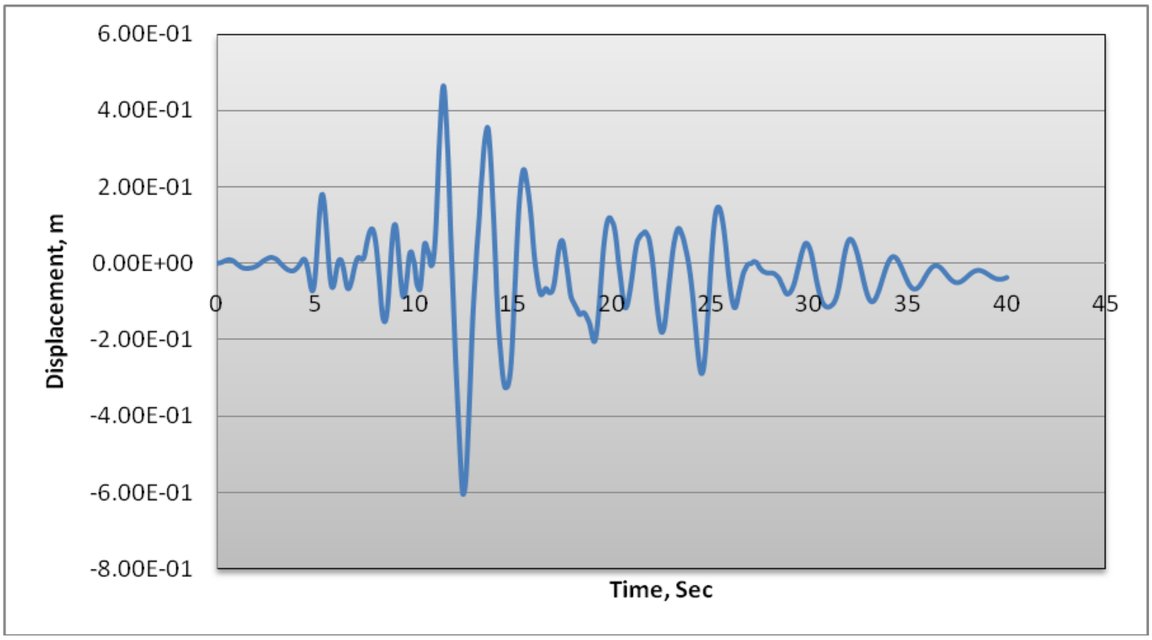


a)

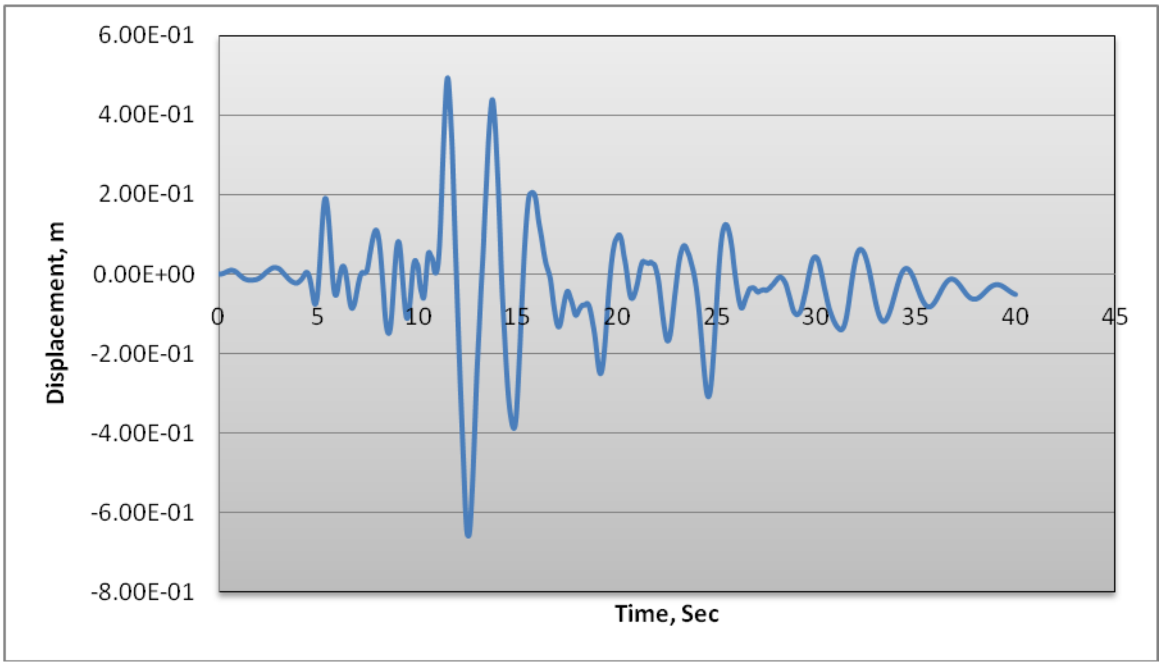


b)

Fig D7 Displacement time-hitory relation for 20BRBF cx cy a) x-direction
b) y-direction



a)

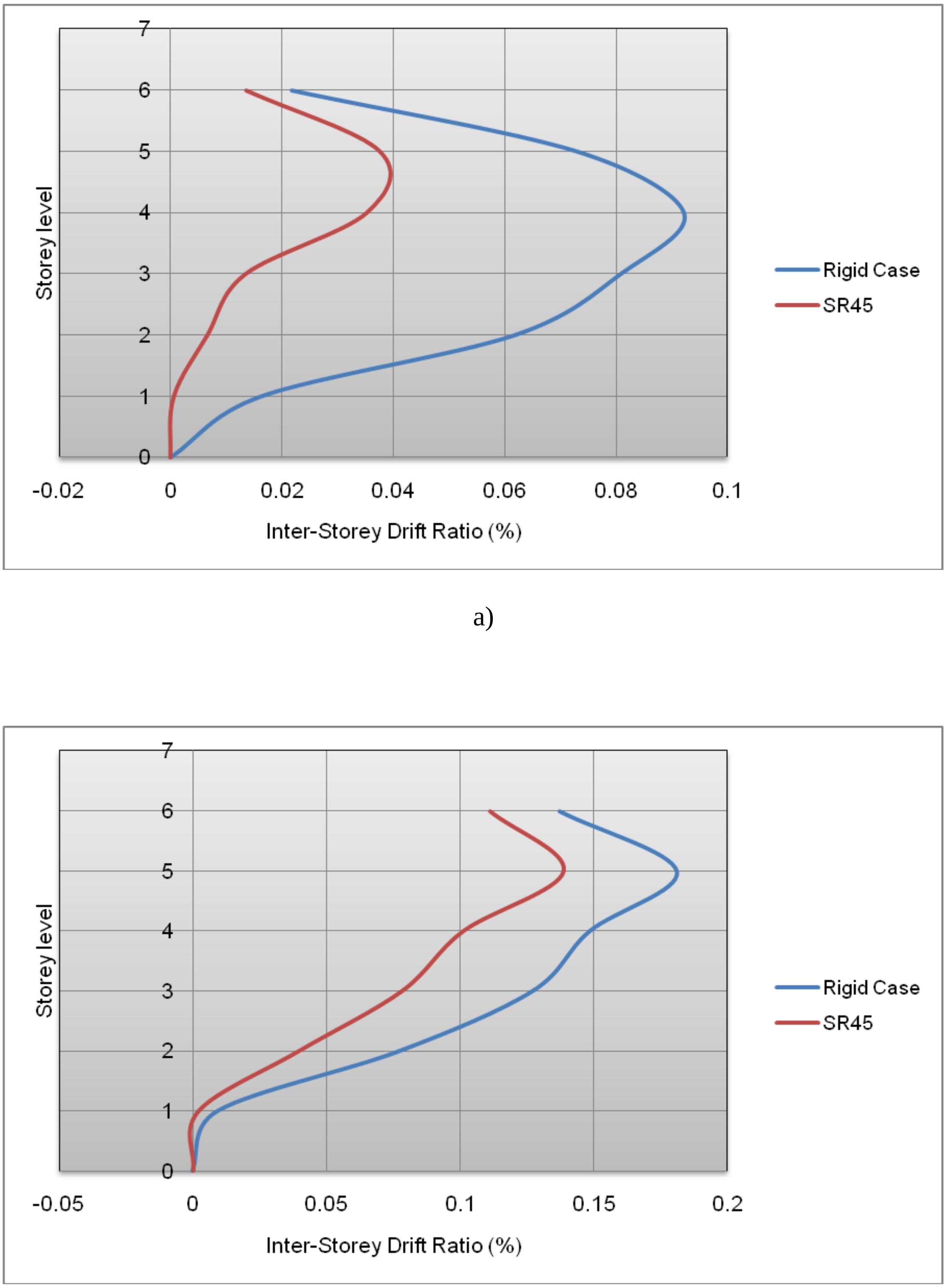


b)

Fig D8 Displacement time-hitory relation for 20BRBF csx csy a) x-direction
b) y-direction

APPENDIX E

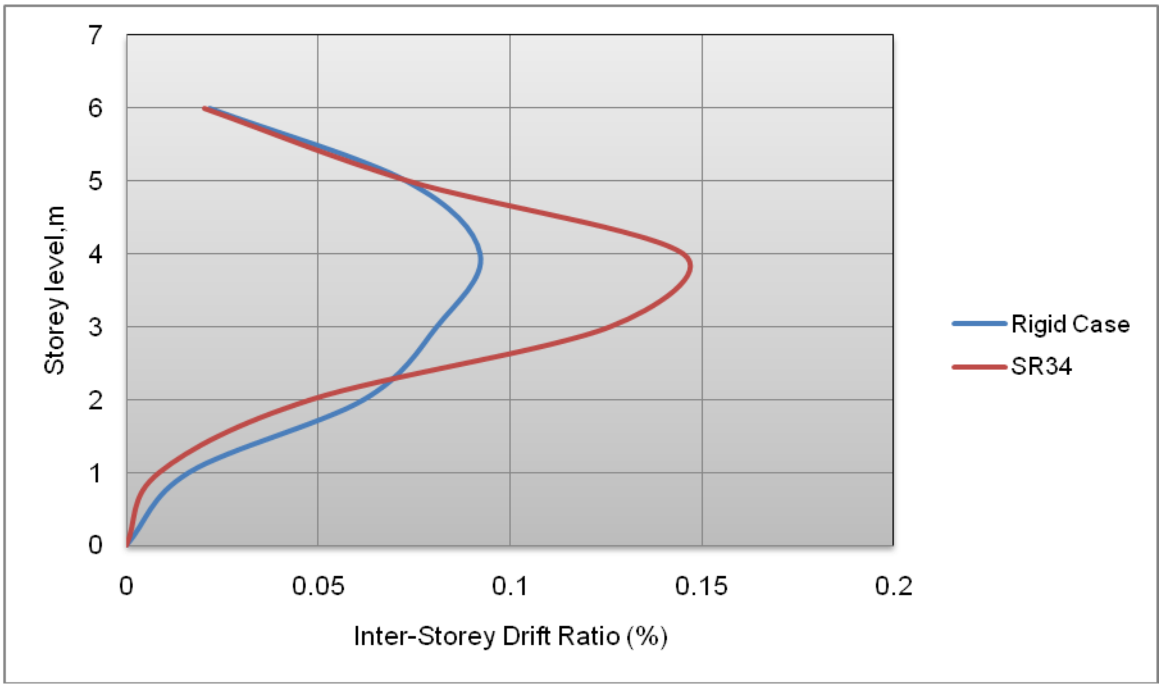
6-STOREY SYSTEMS INTER-STOREY DRIFT RATIO



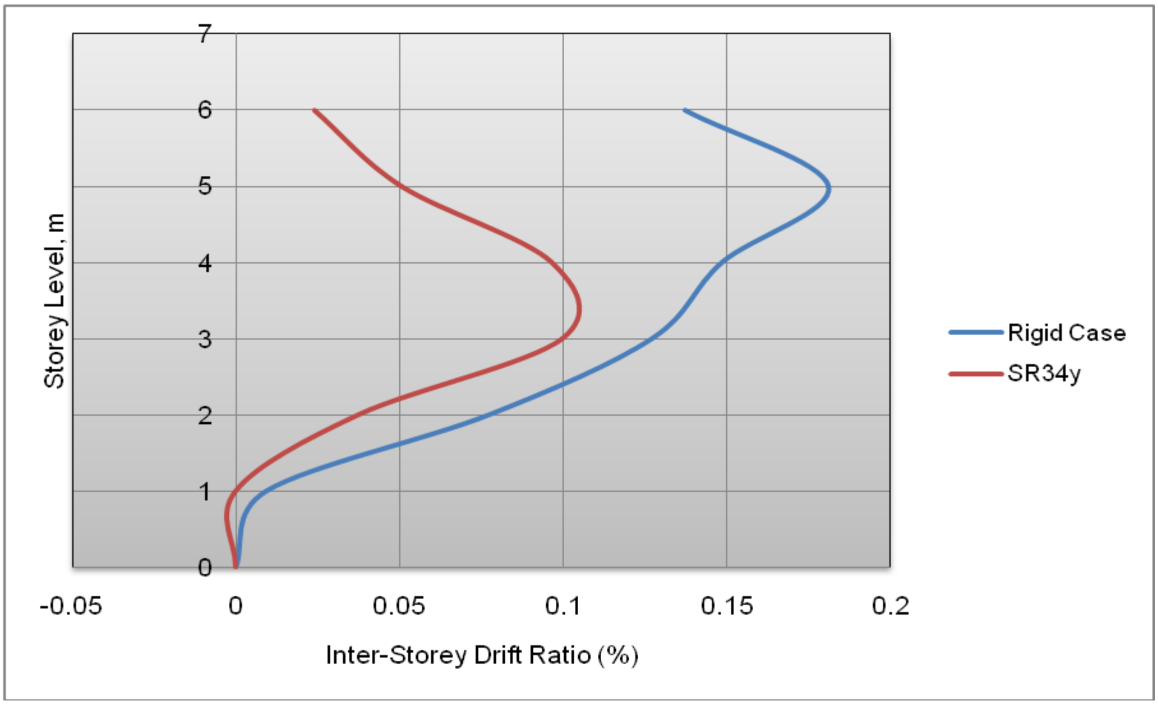
a)

b)

Fig E1 Inter-storey drift ratio a) x-direction b) y-direction

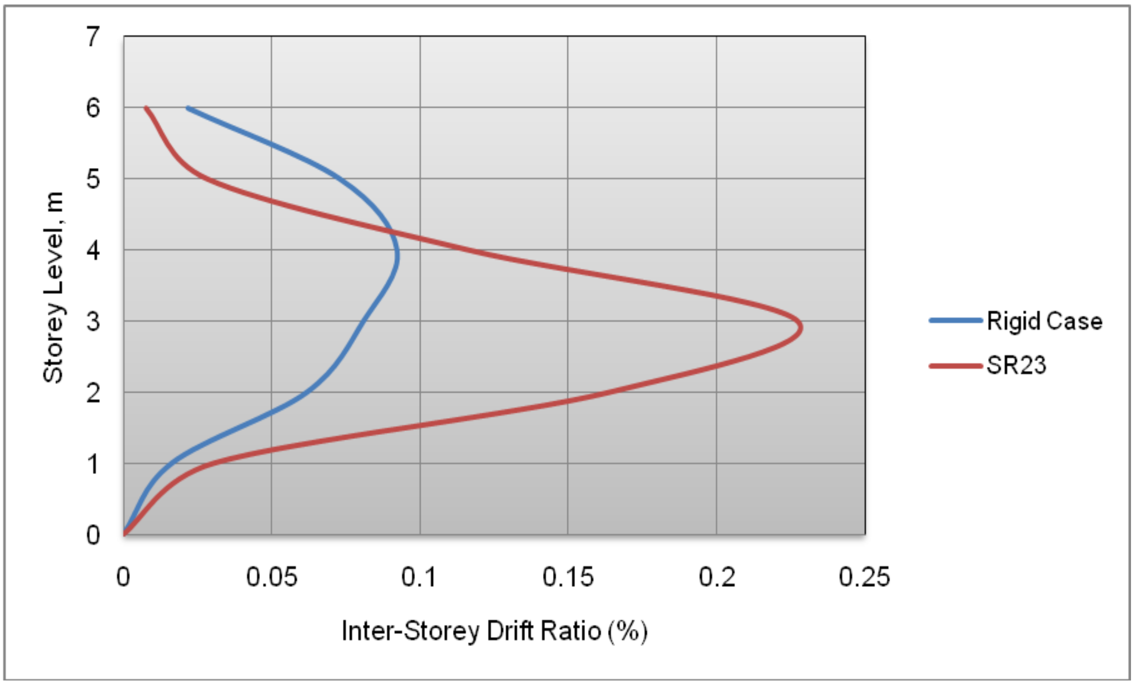


a)

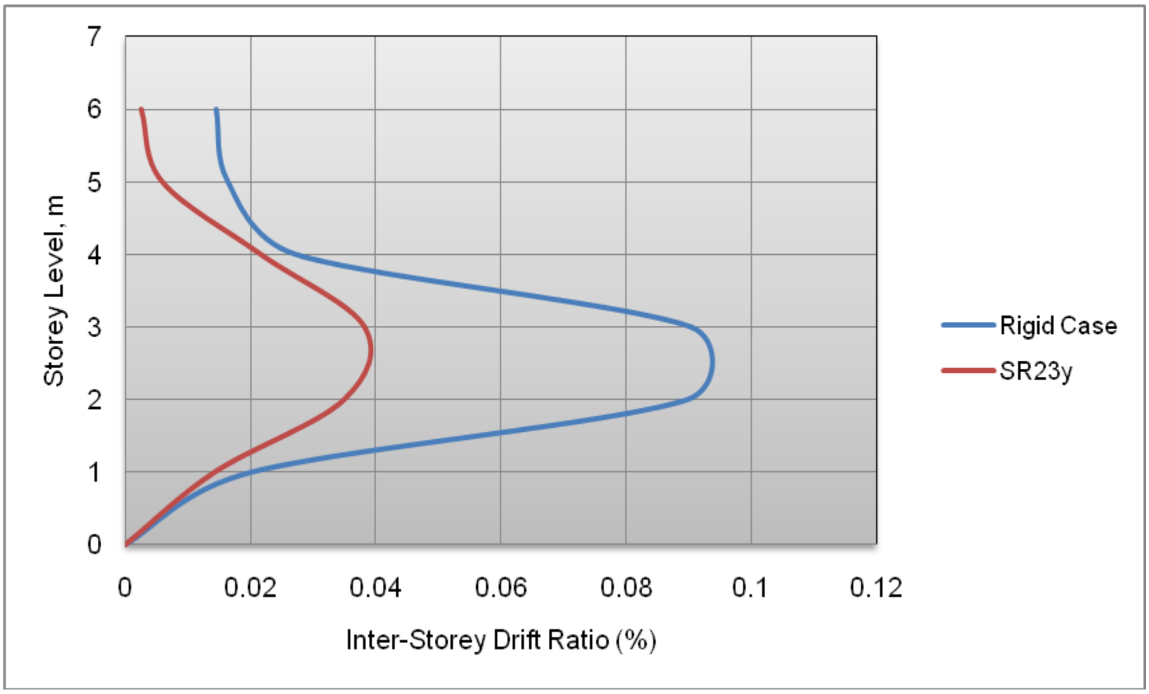


b)

Fig E2 Inter-storey drift ratio a) x-direction b) y-direction

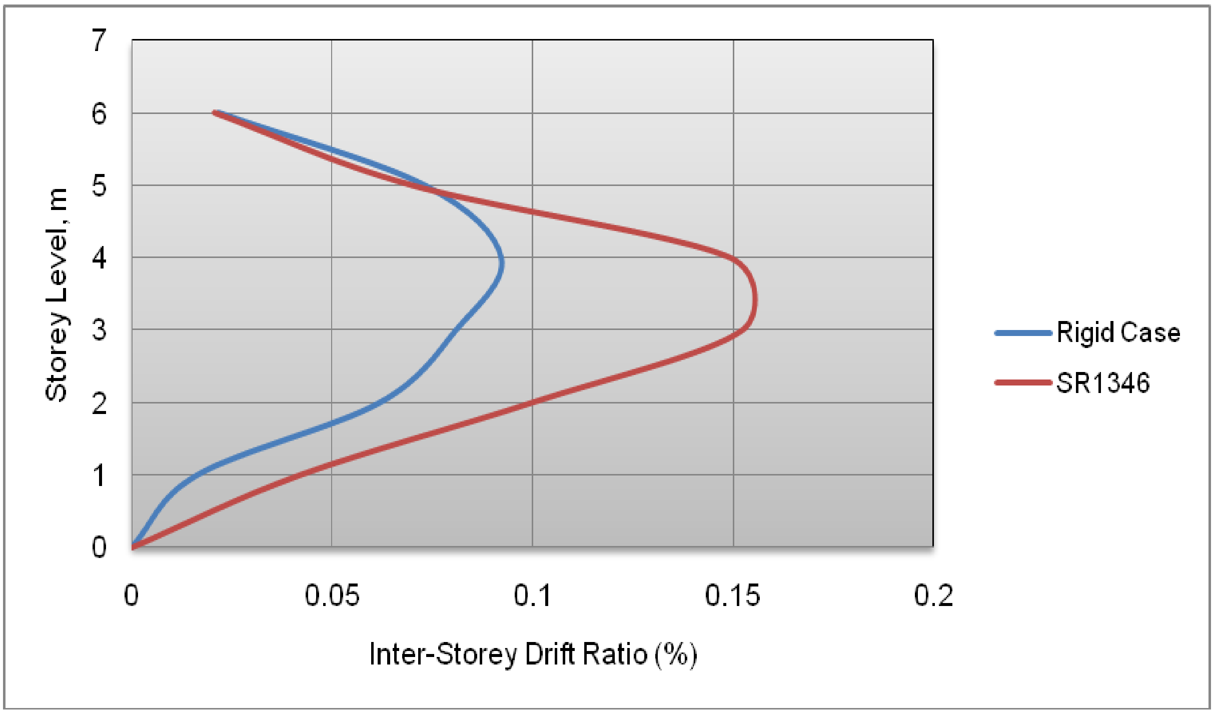


a)

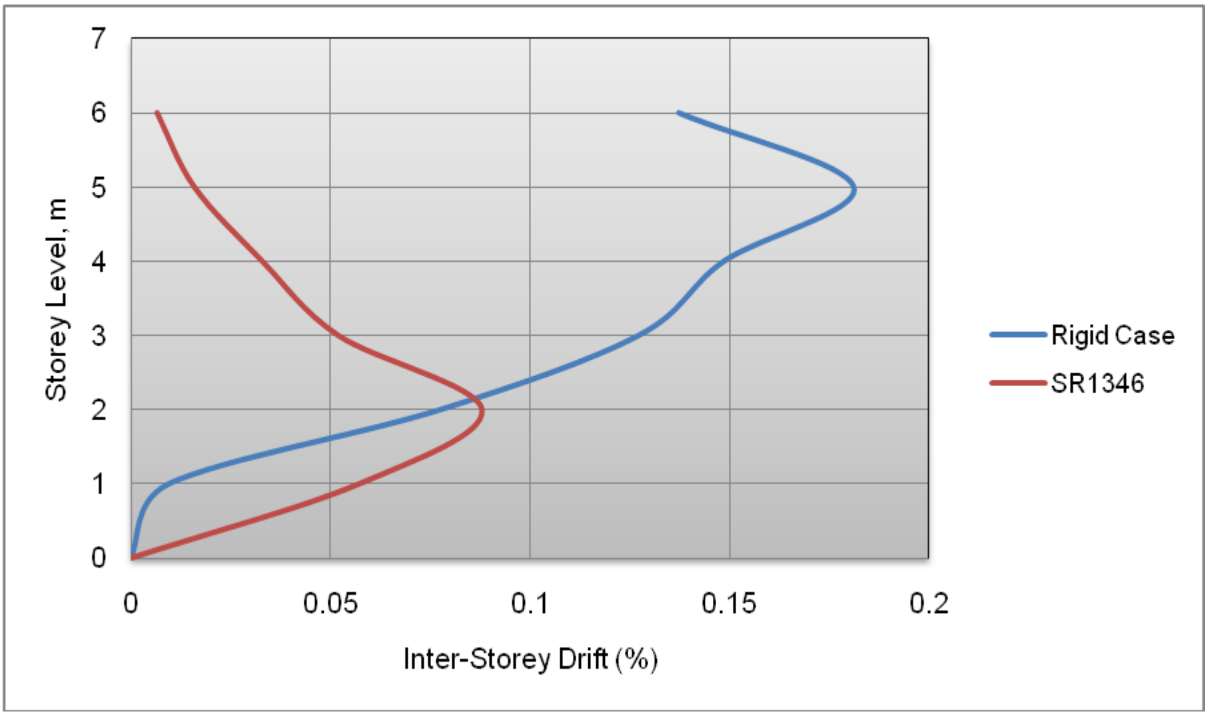


b)

Fig E3 Inter-storey drift ratio a) x-direction b) y-direction

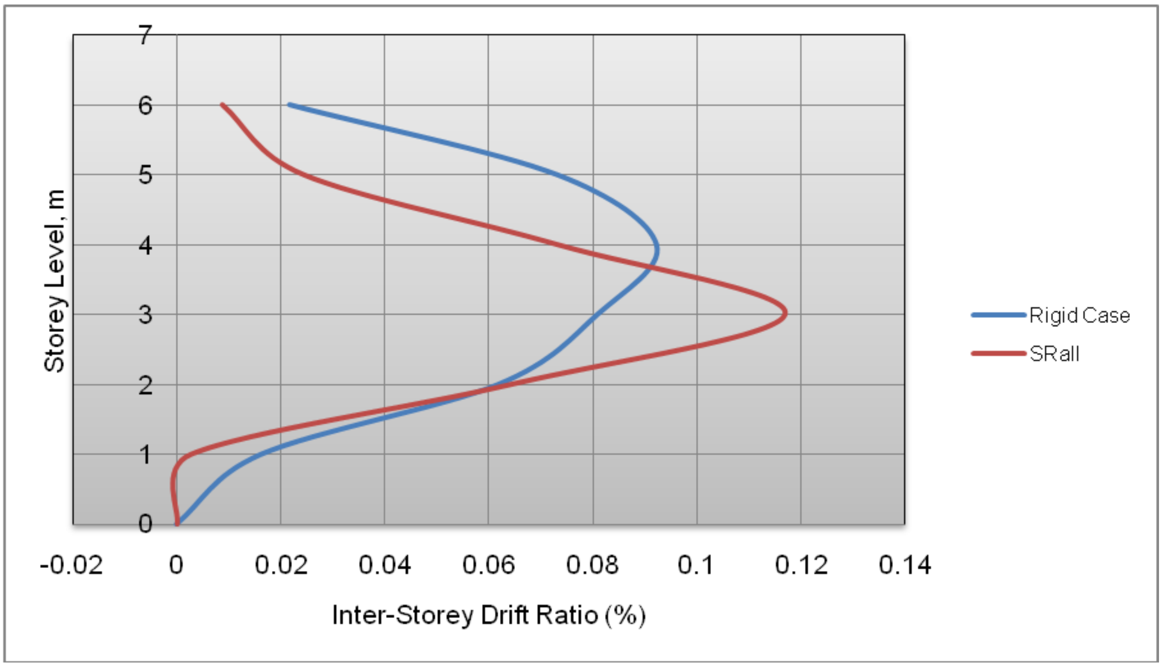


a)

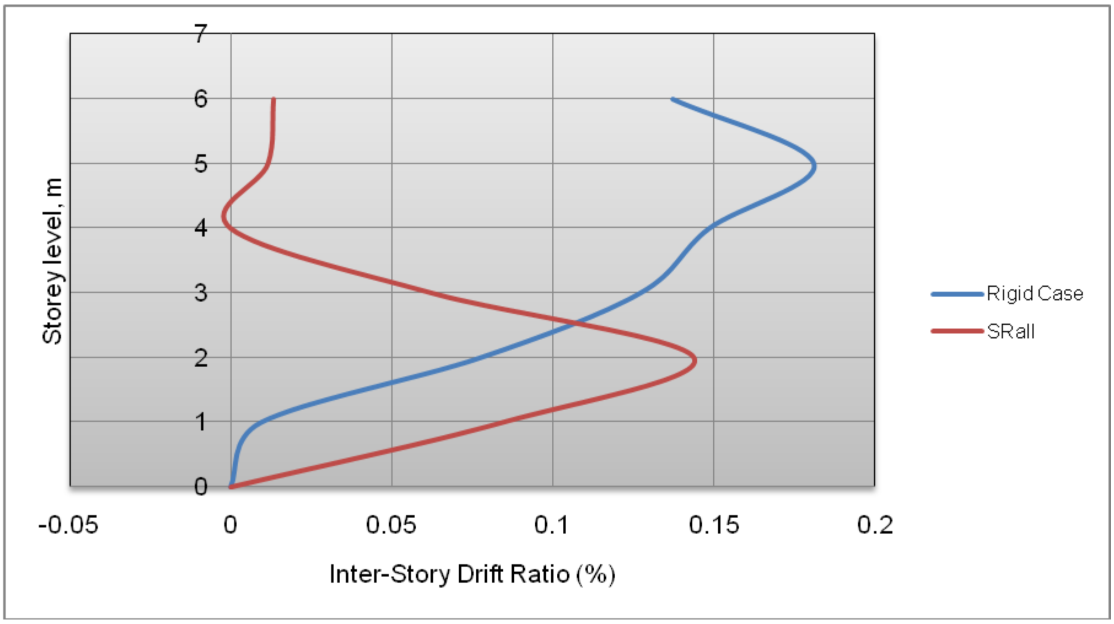


b)

Fig E4 Inter-storey drift ratio a) x-direction b) y-direction

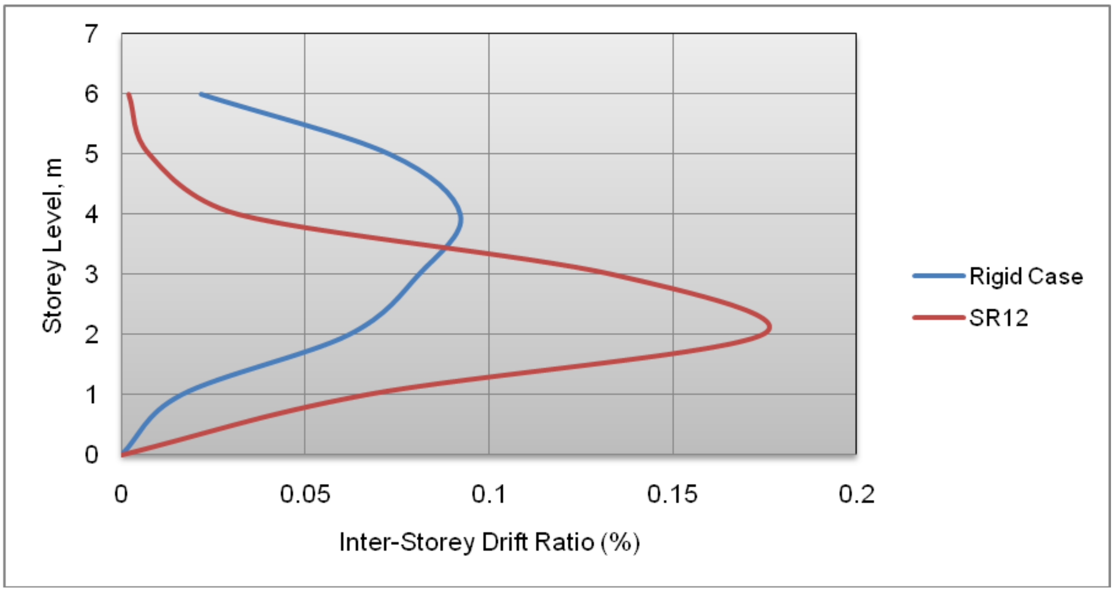


a)

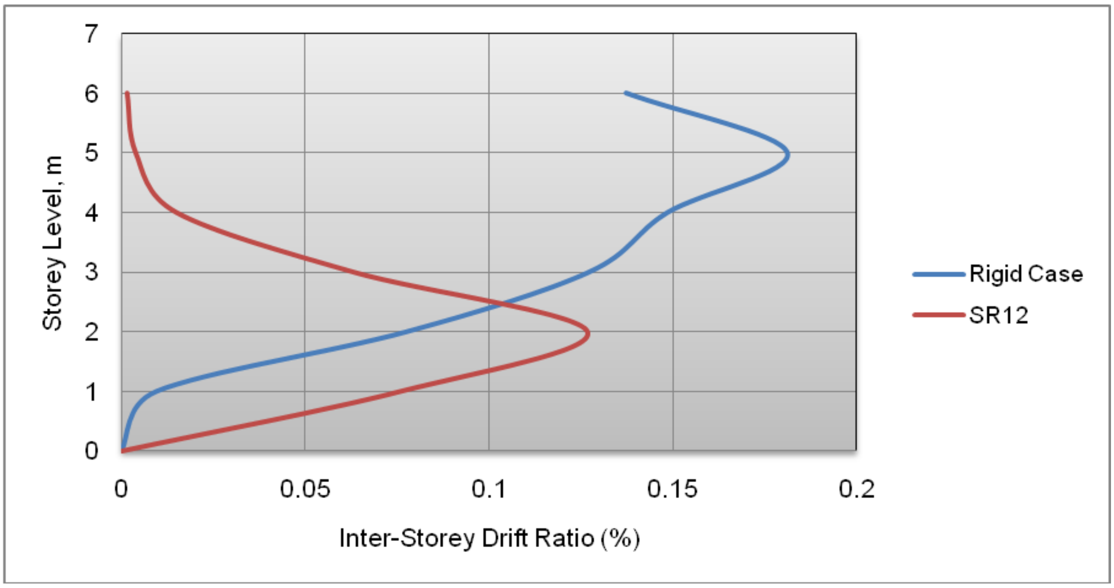


b)

Fig E5 Inter-storey drift ratio a) x-direction b) y-direction

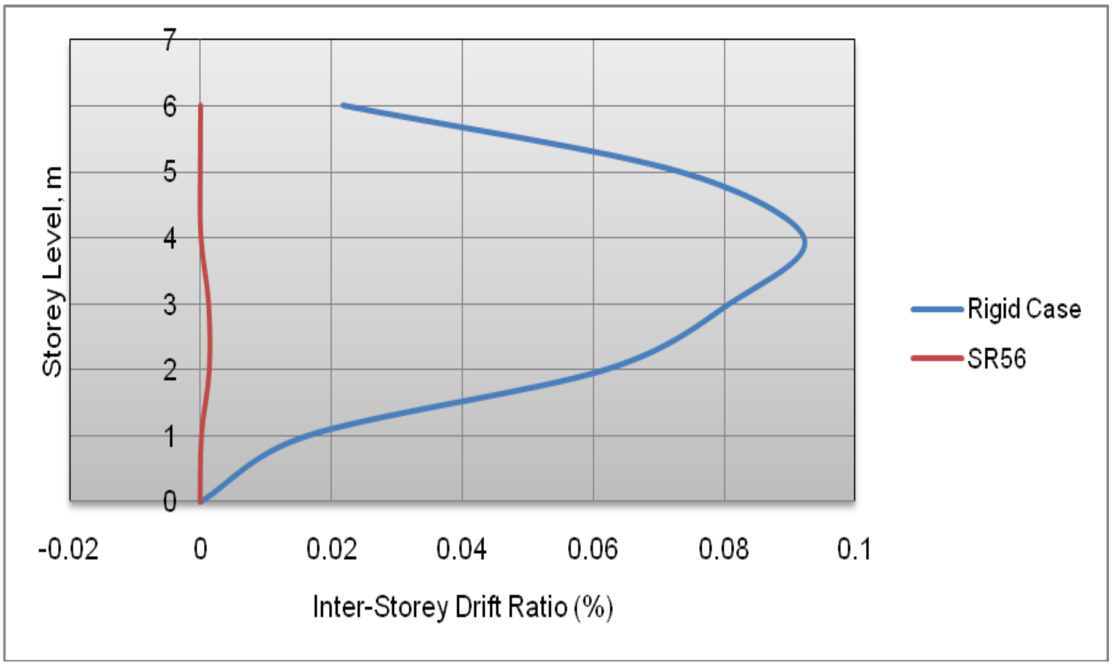


a)

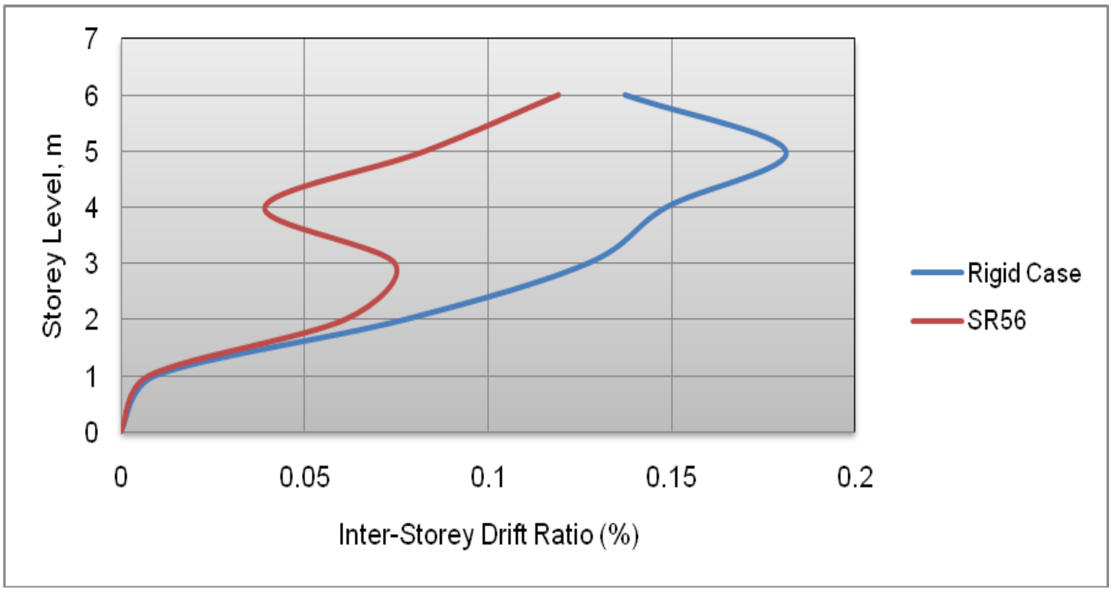


b)

Fig E6 Inter-storey drift ratio a) x-direction b) y-direction

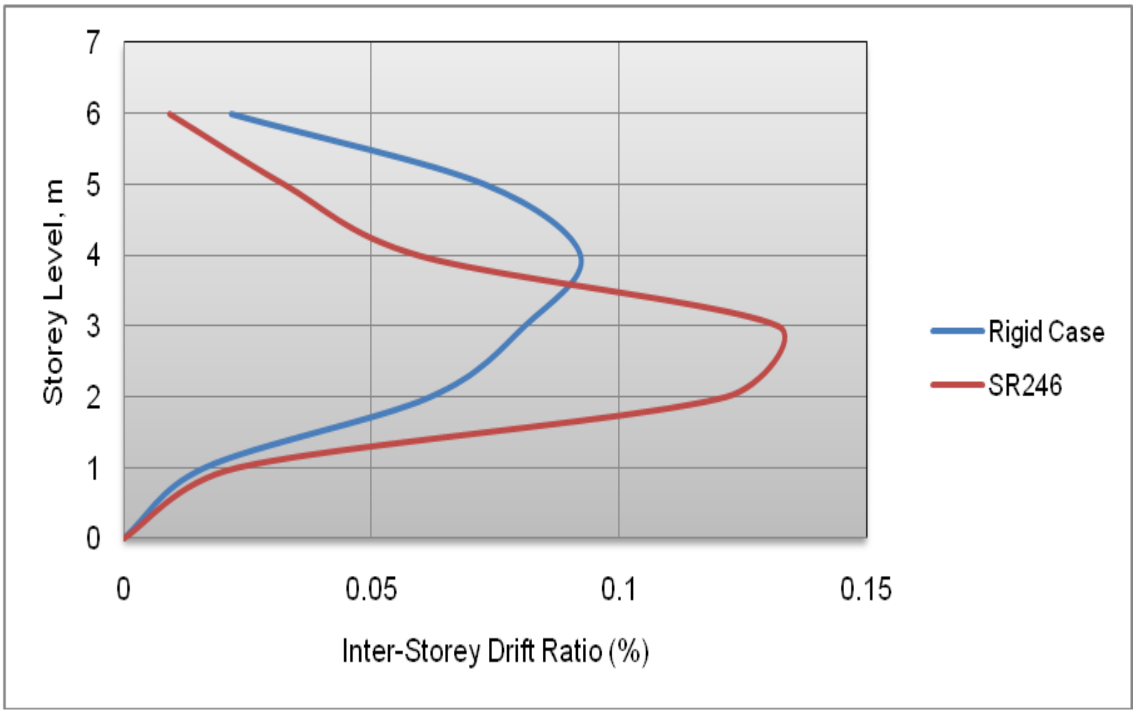


a)

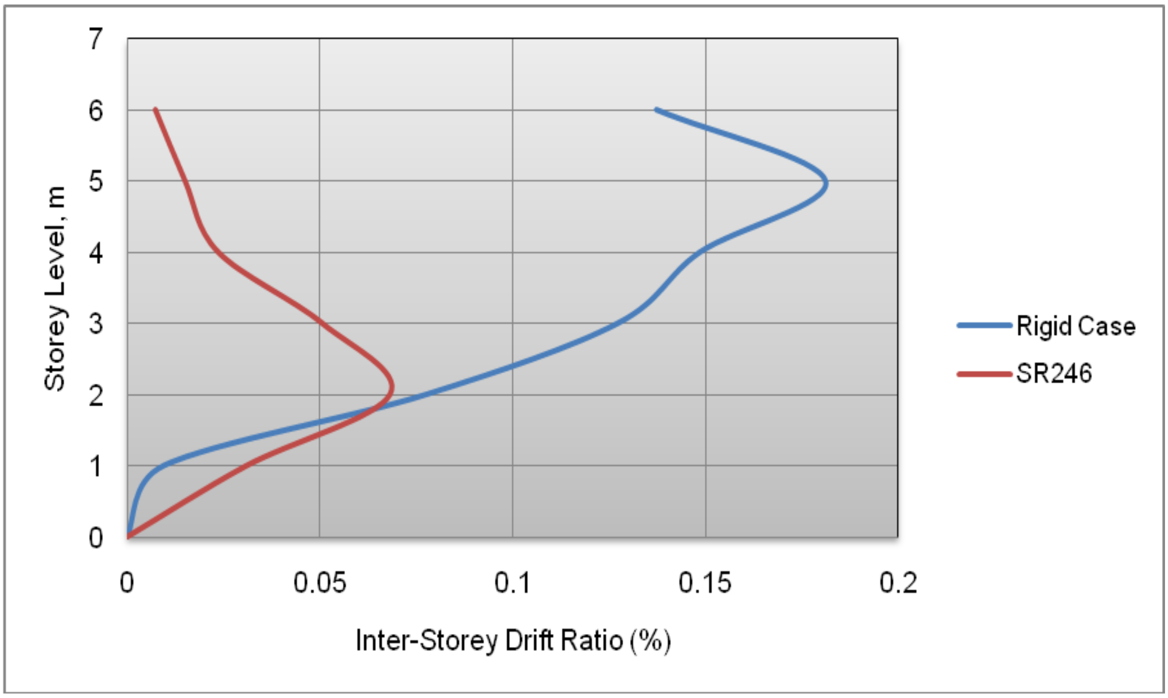


b)

Fig E7 Inter-storey drift ratio a) x-direction b) y-direction

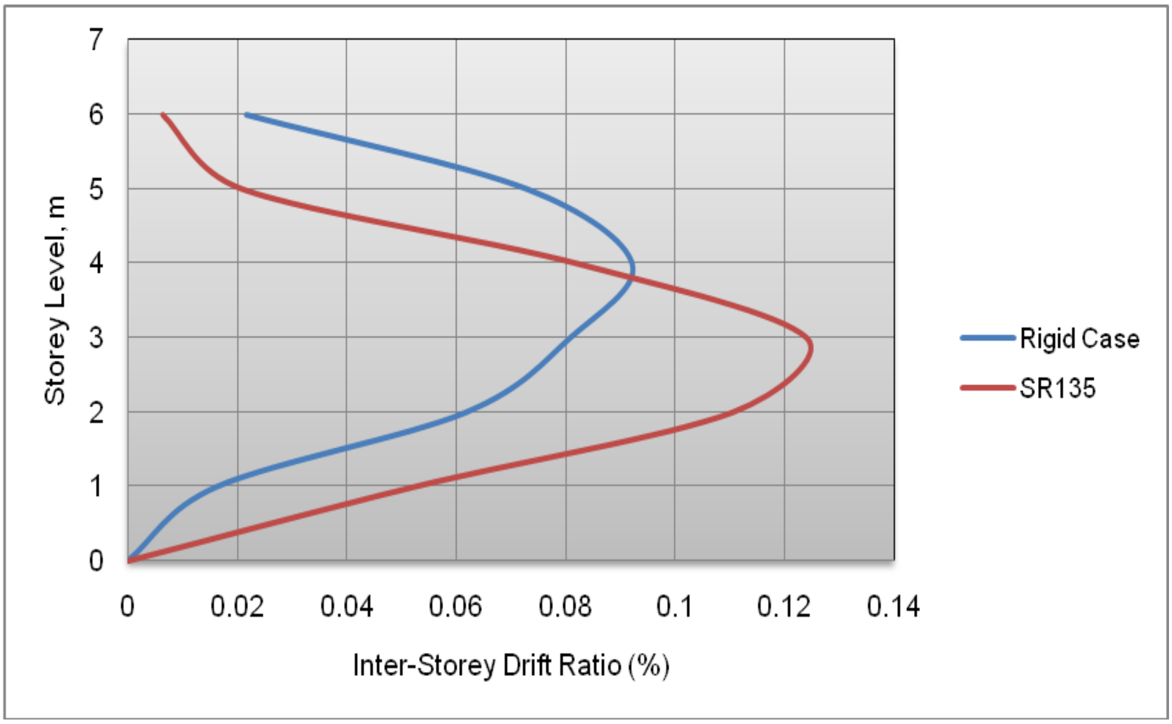


a)

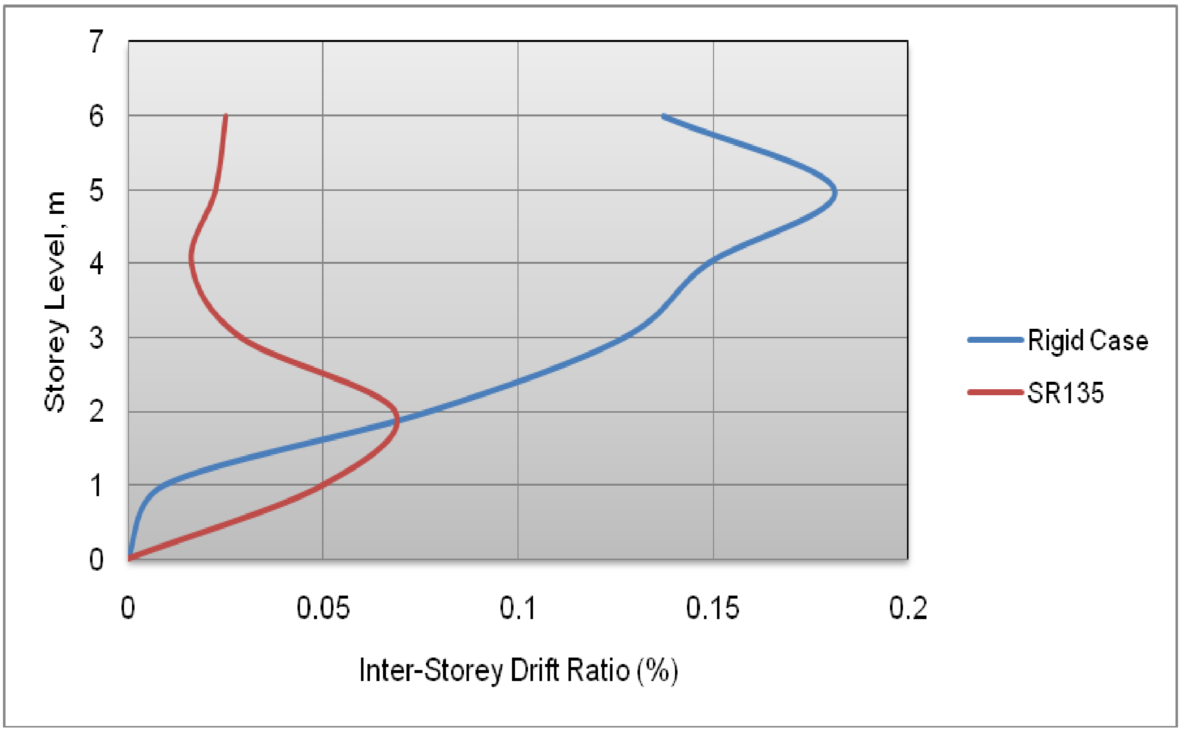


b)

Fig E8 Inter-storey drift ratio a) x-direction b) y-direction

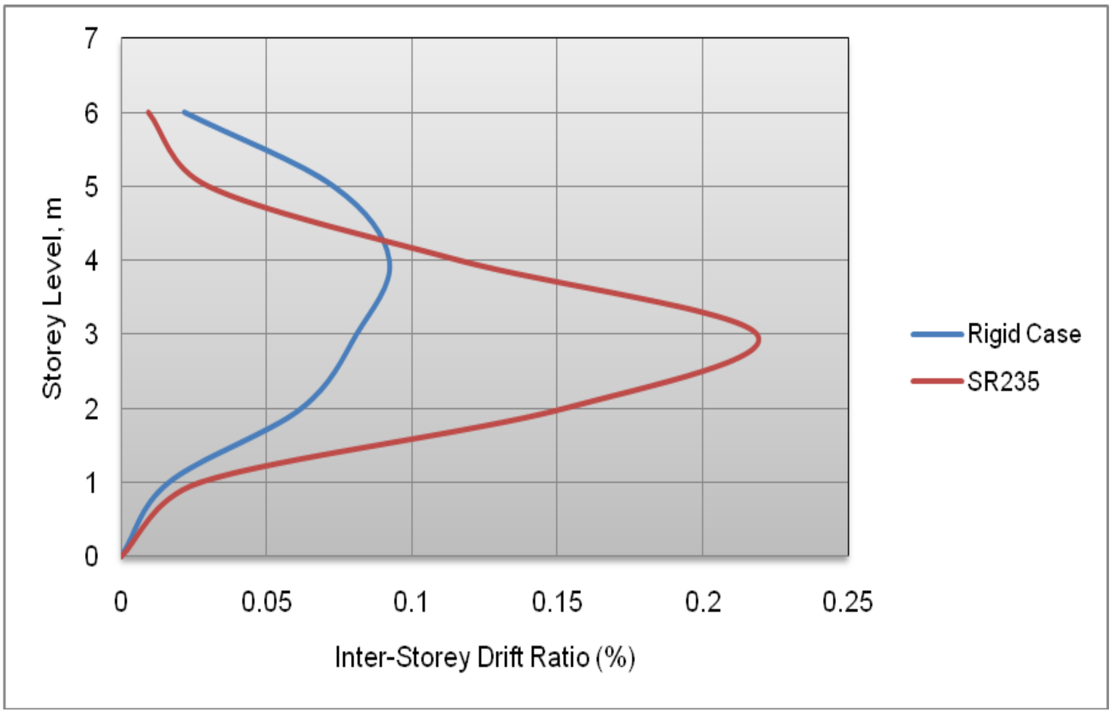


a)

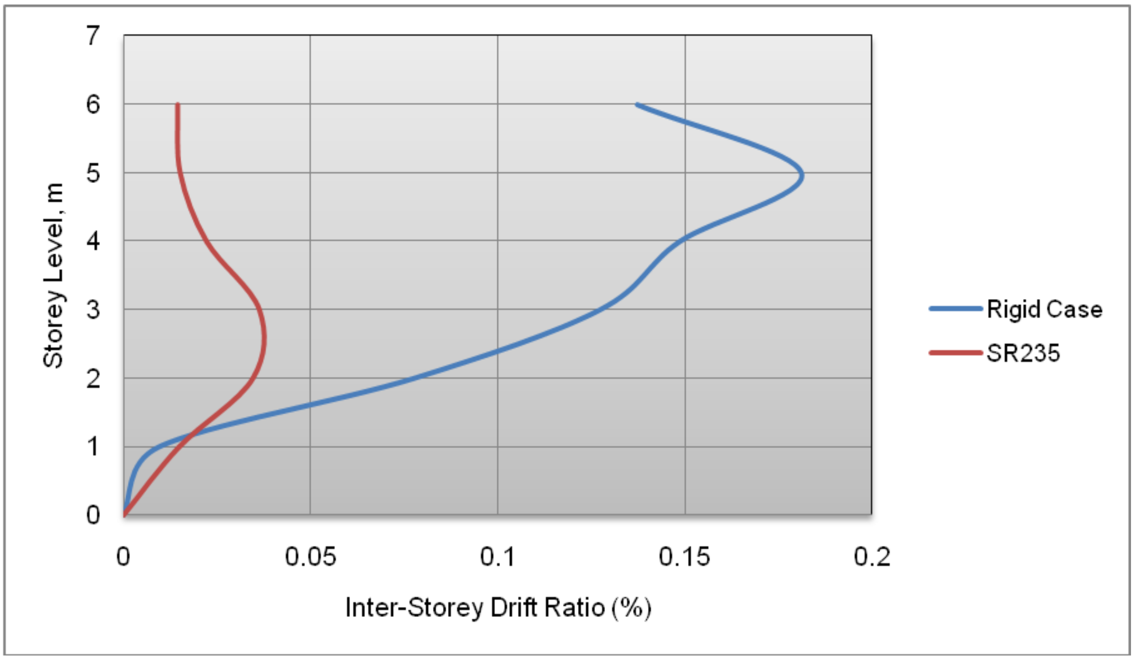


b)

Fig E9 Inter-storey drift ratio a) x-direction b) y-direction

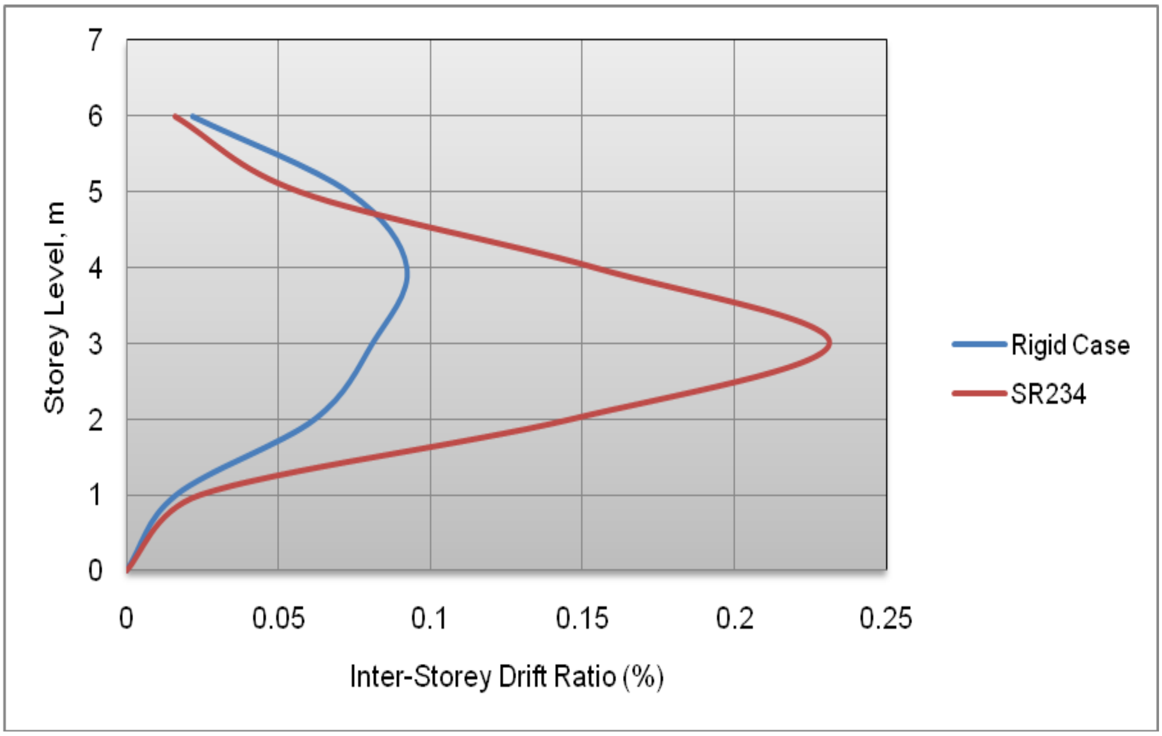


a)

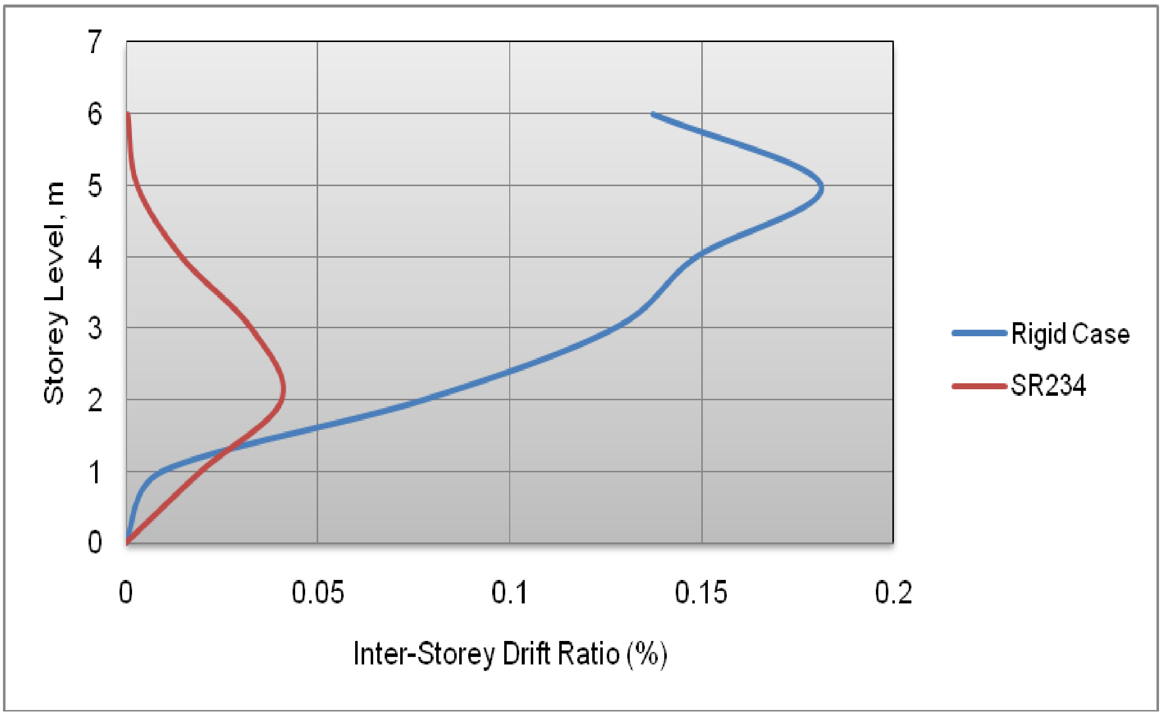


b)

Fig E10 Inter-storey drift ratio a) x-direction b) y-direction

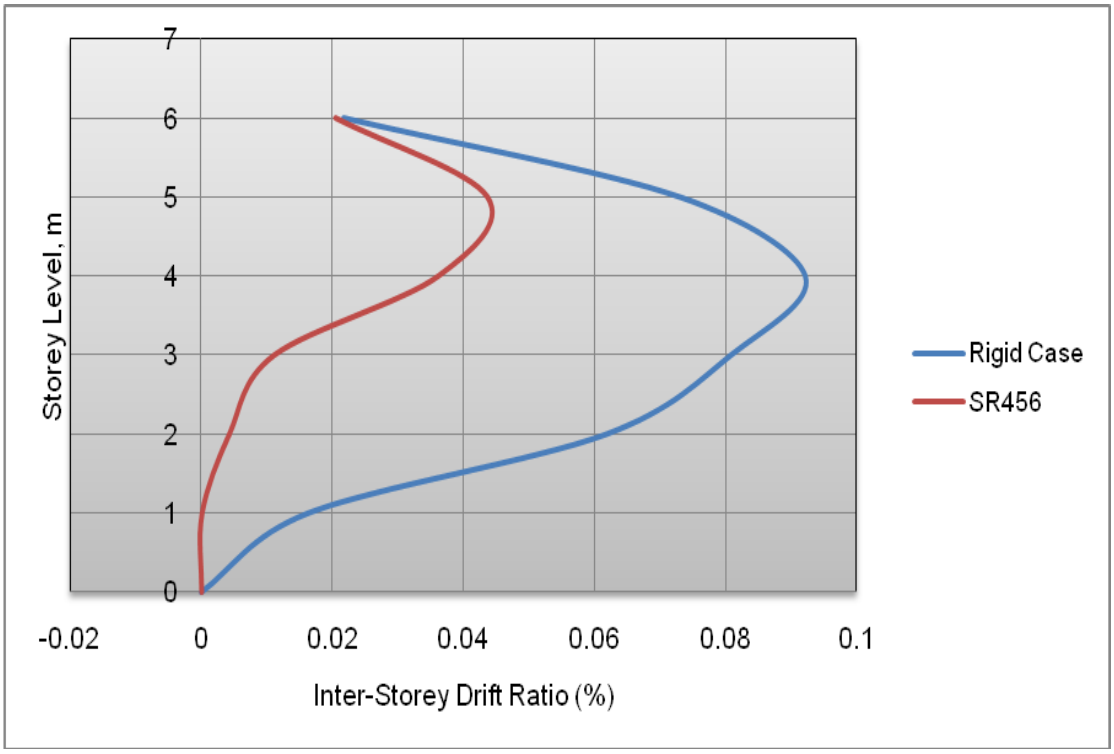


a)

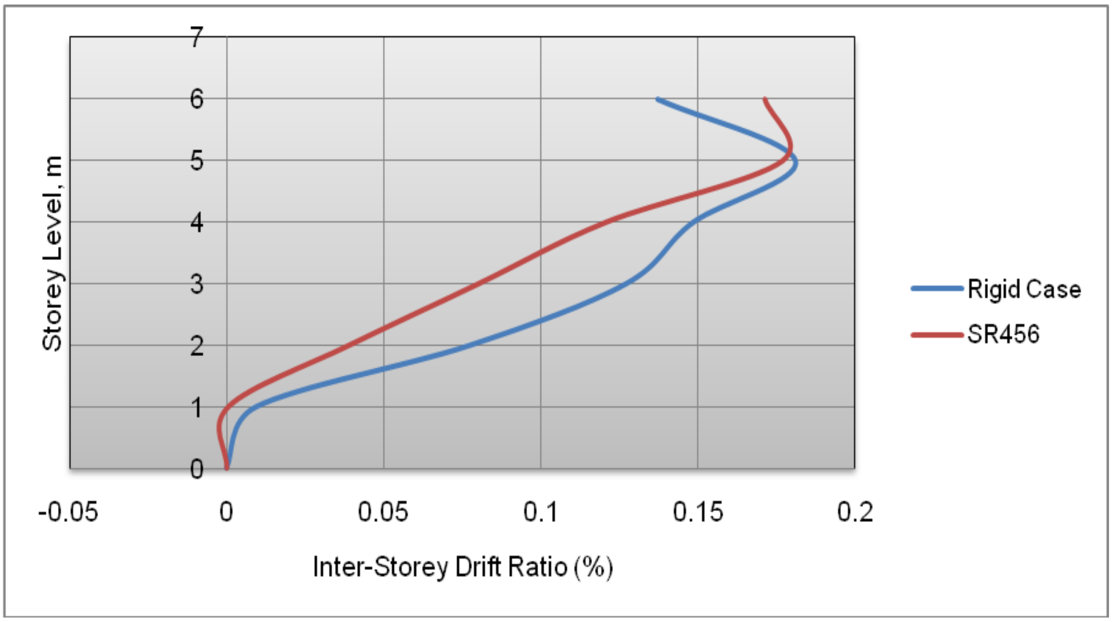


b)

Fig E11 Inter-storey drift ratio a) x-direction b) y-direction

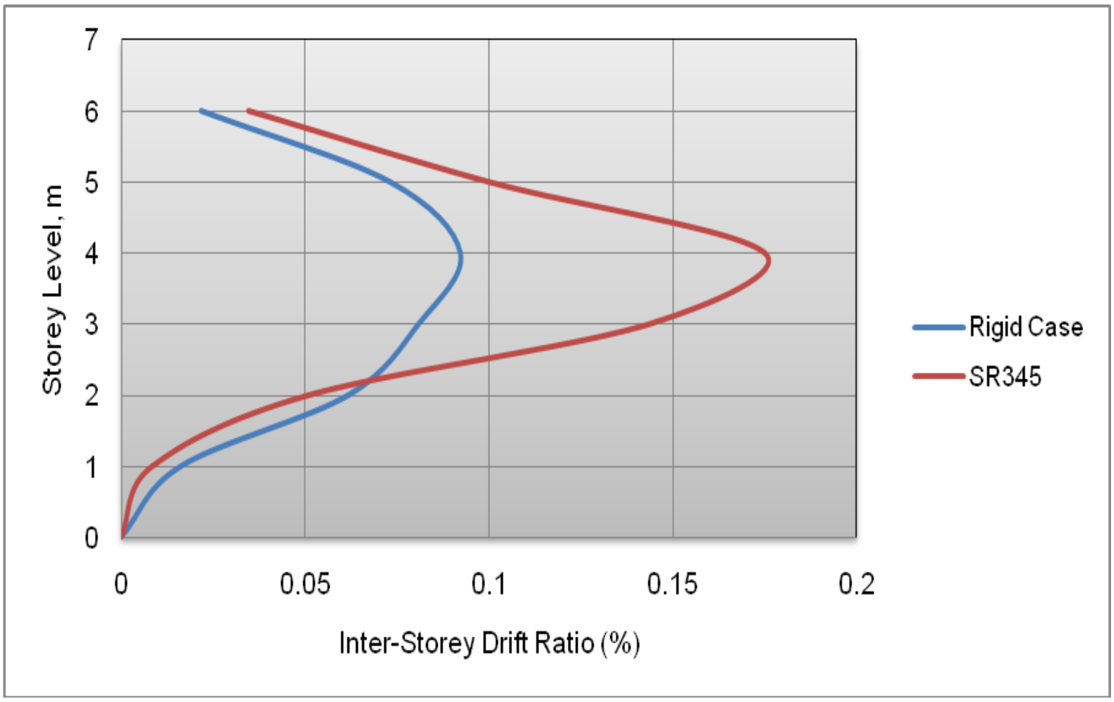


a)

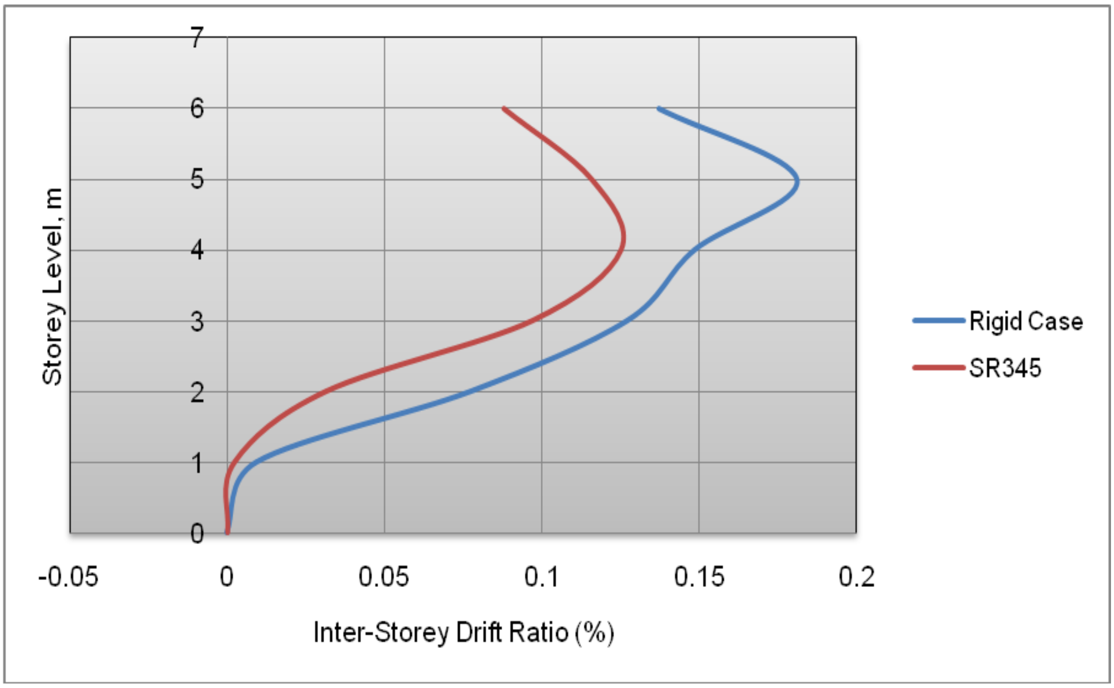


b)

Fig E12 Inter-storey drift ratio a) x-direction b) y-direction

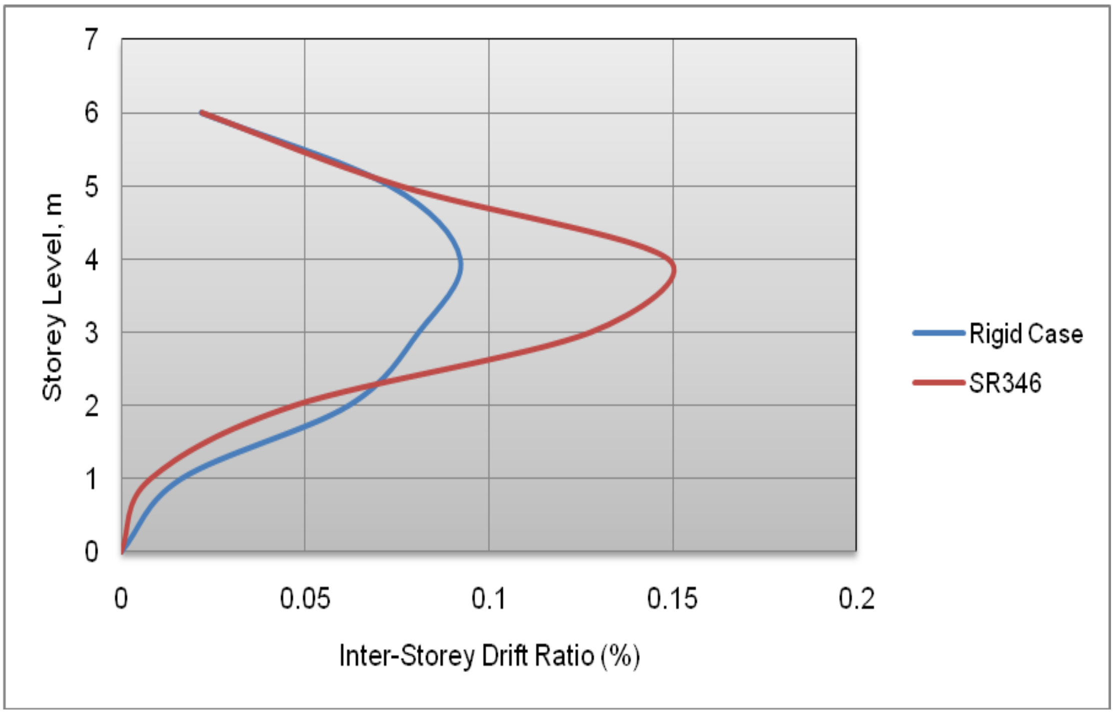


a)

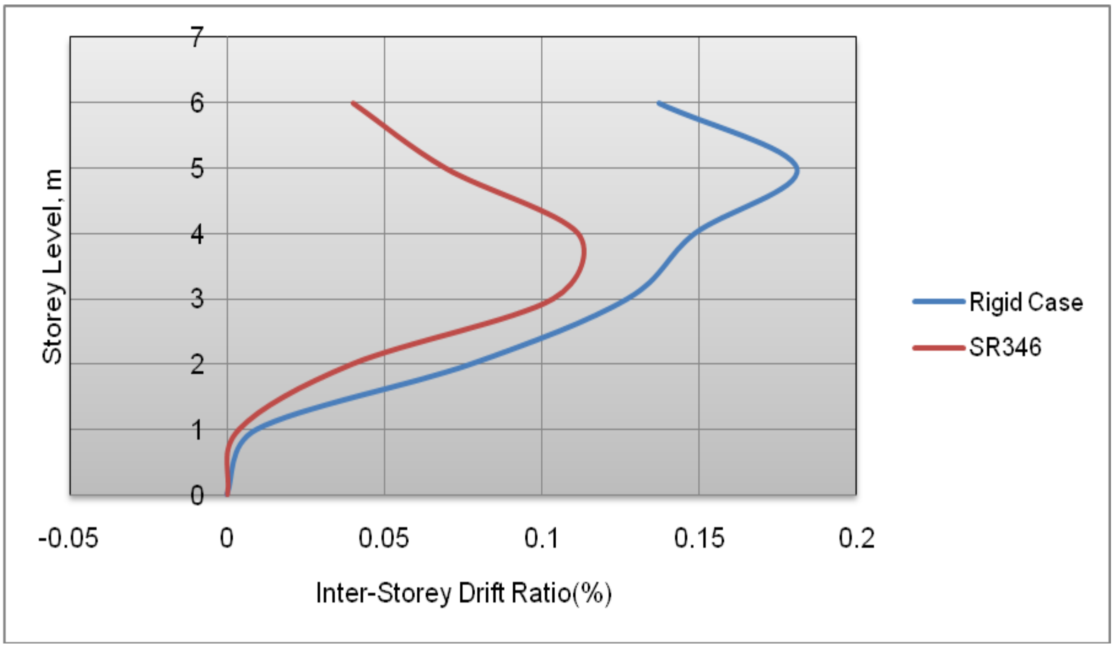


b)

Fig E13 Inter-storey drift ratio a) x-direction b) y-direction

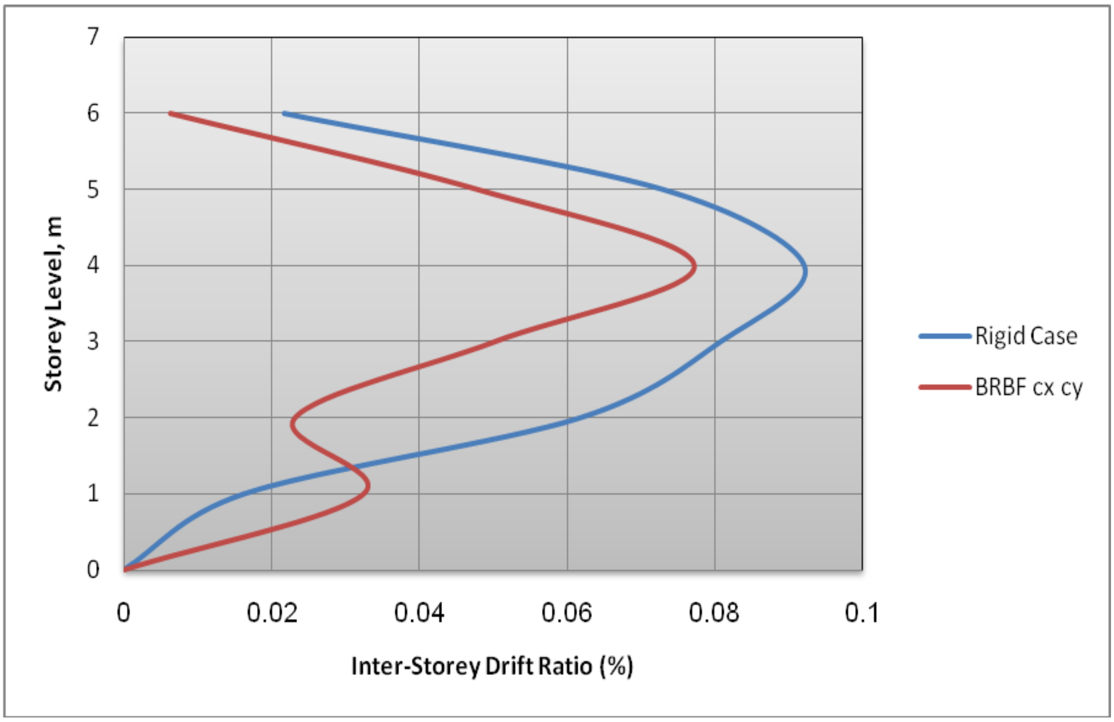


a)

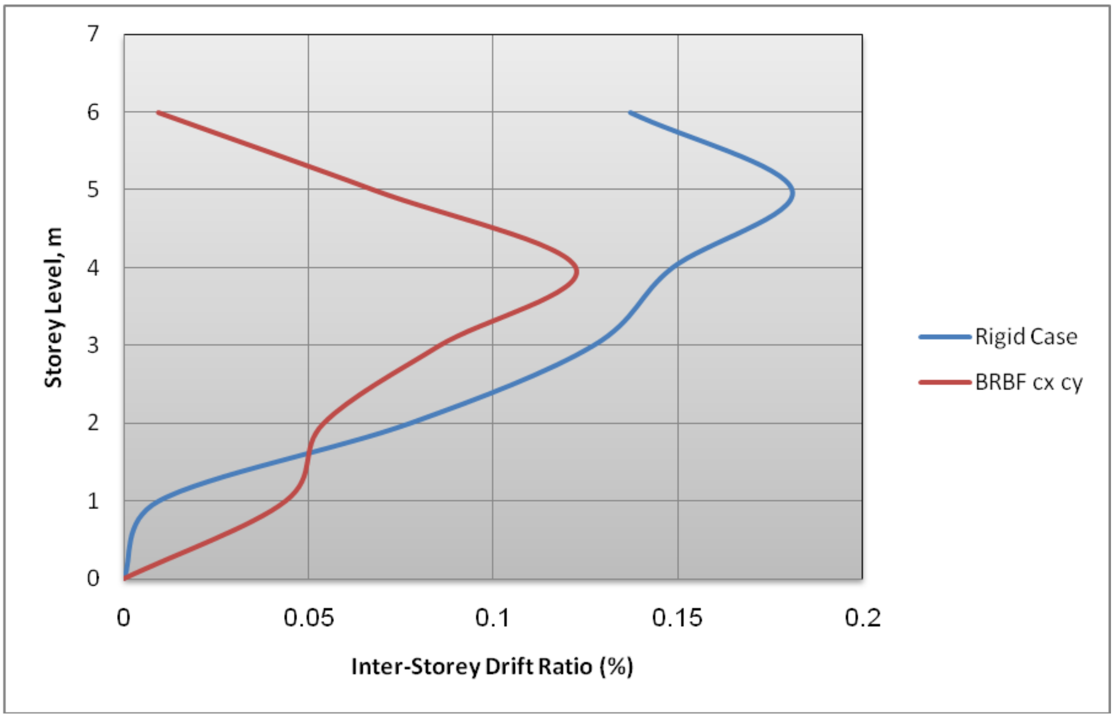


b)

Fig E14 Inter-storey drift ratio a) x-direction b) y-direction

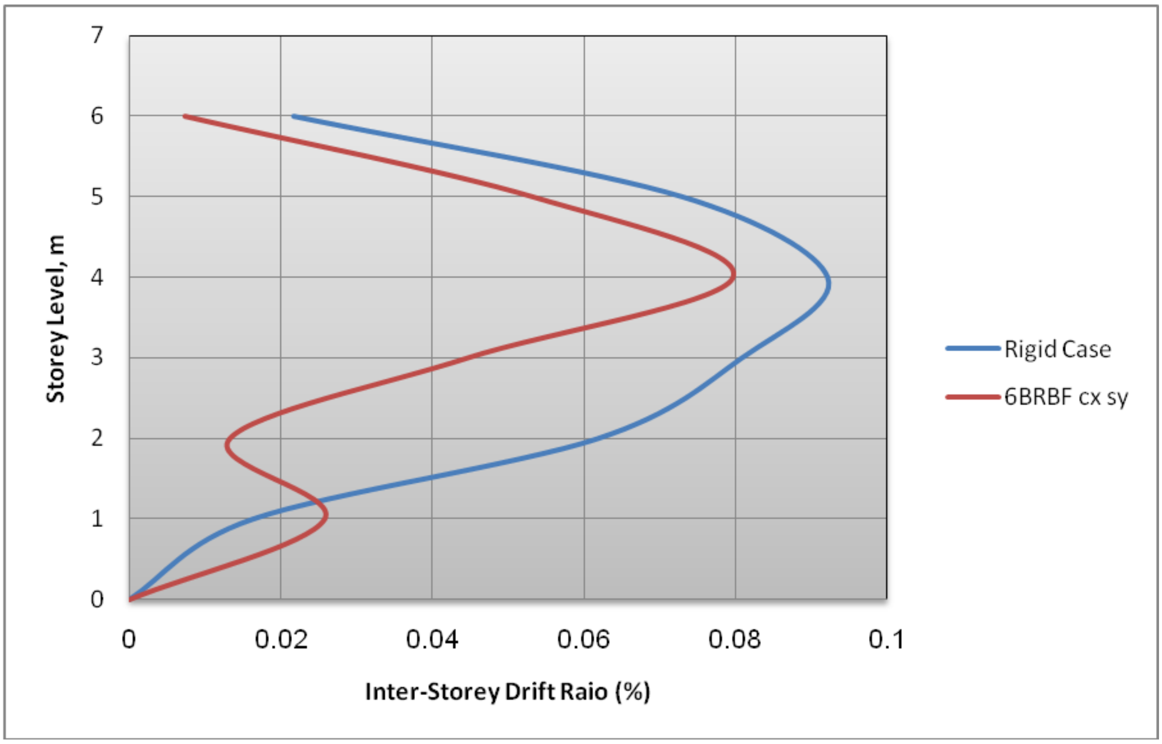


a)

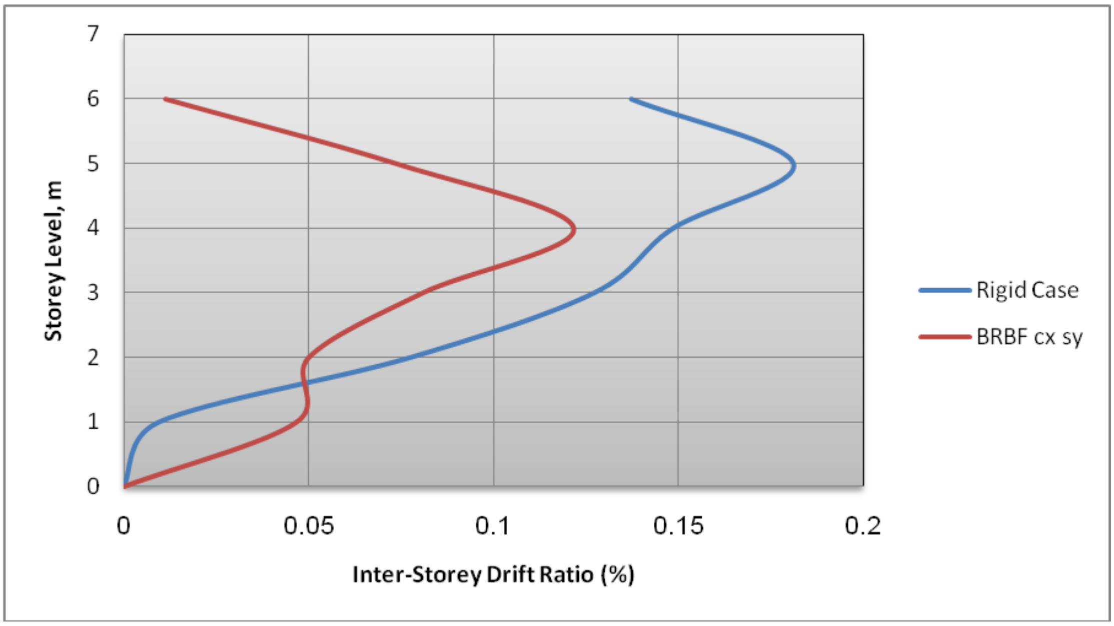


b)

Fig E15 Inter-storey drift ratio a) x-direction b) y-direction

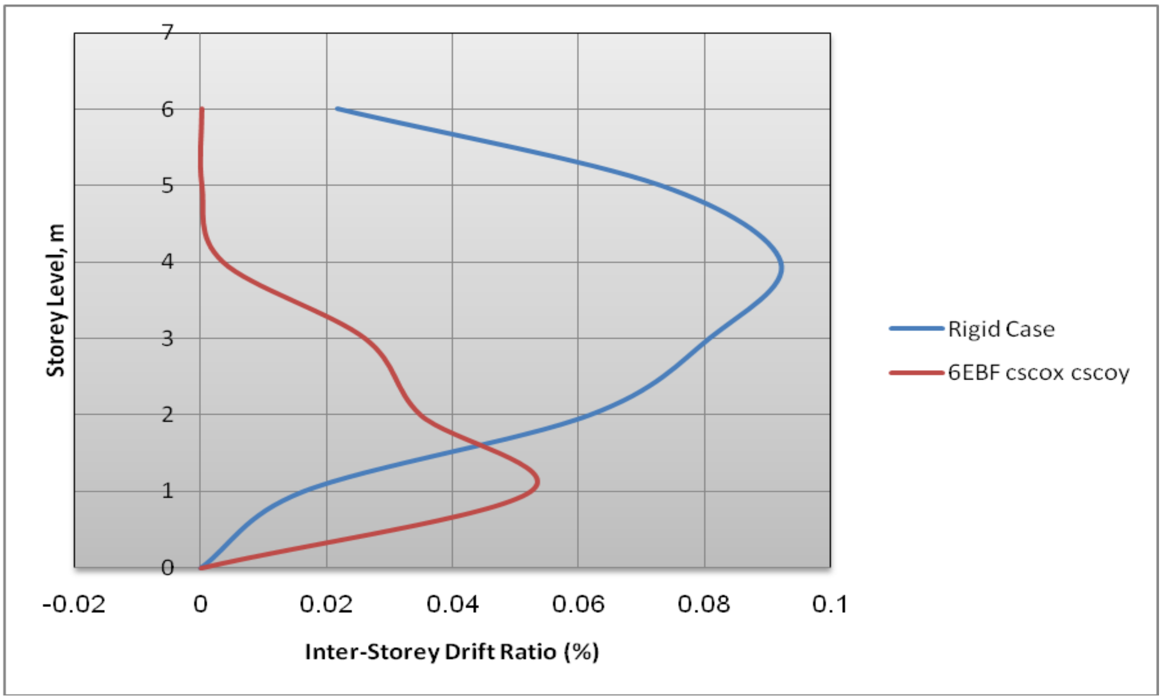


a)

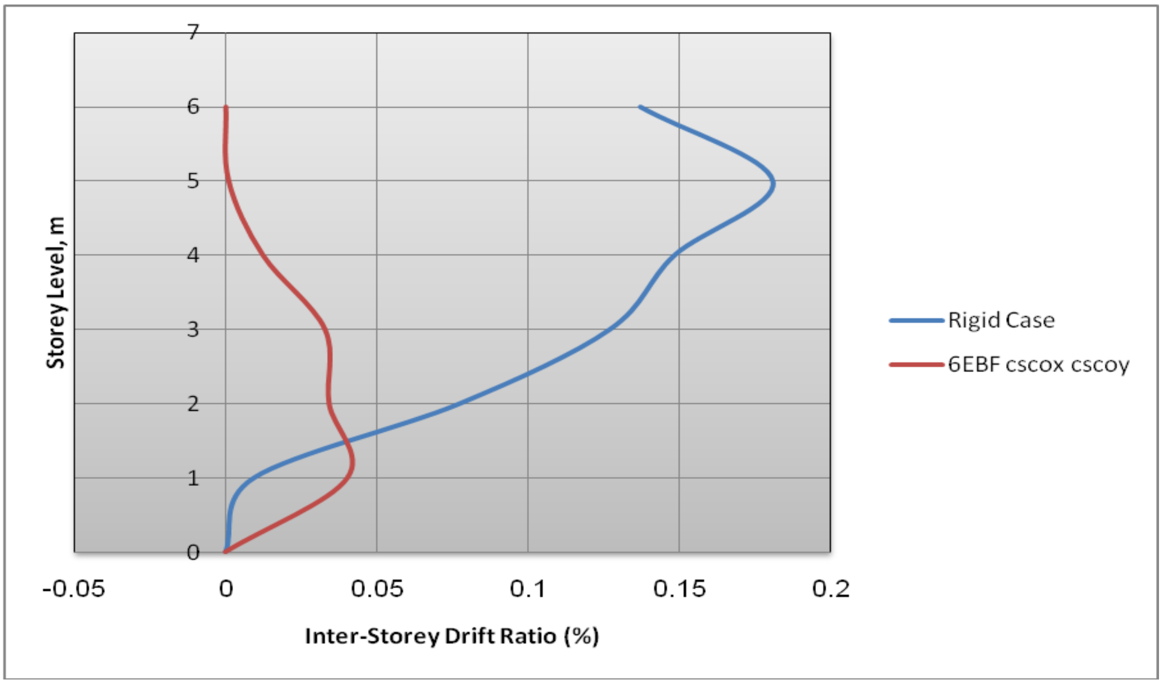


b)

Fig E16 Inter-storey drift ratio a) x-direction b) y-direction



a)

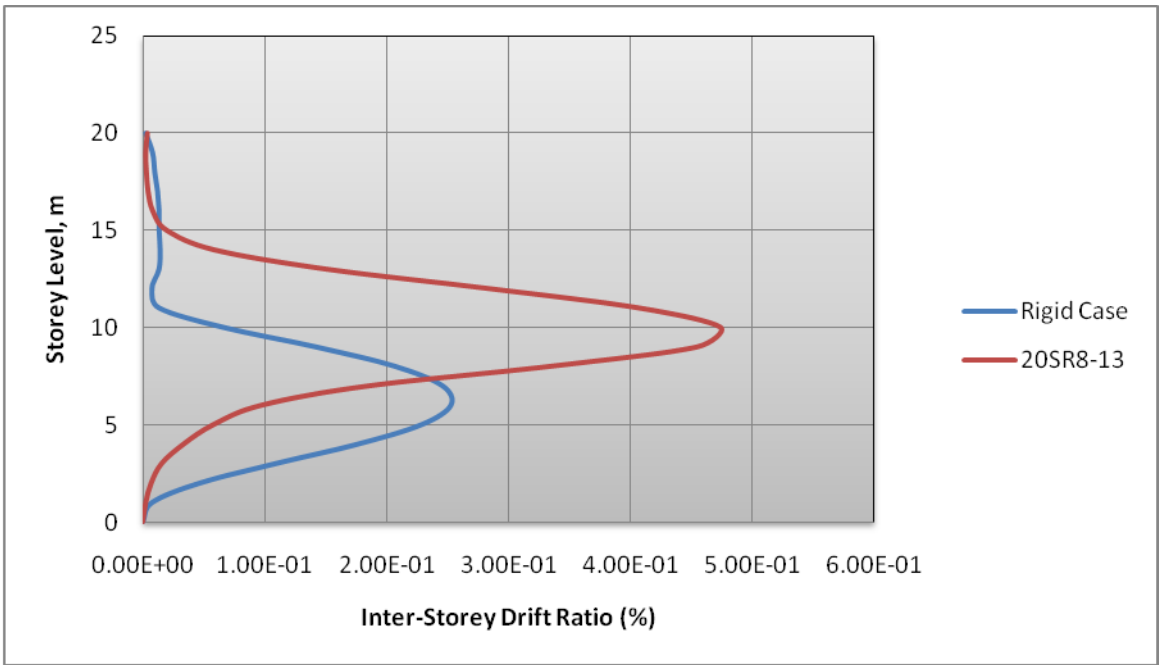


b)

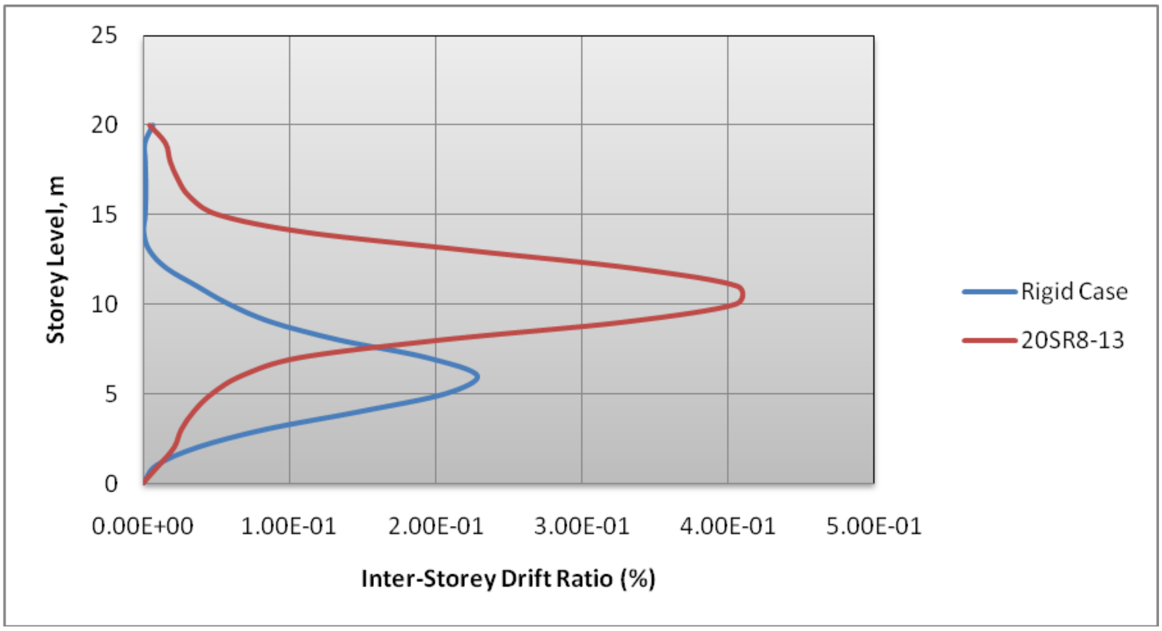
Fig E16 Inter-storey drift ratio a) x-direction b) y-direction

APPENDIX F

20-STOREY SYSTEMS INTER-STOREY DRIFT RATIO

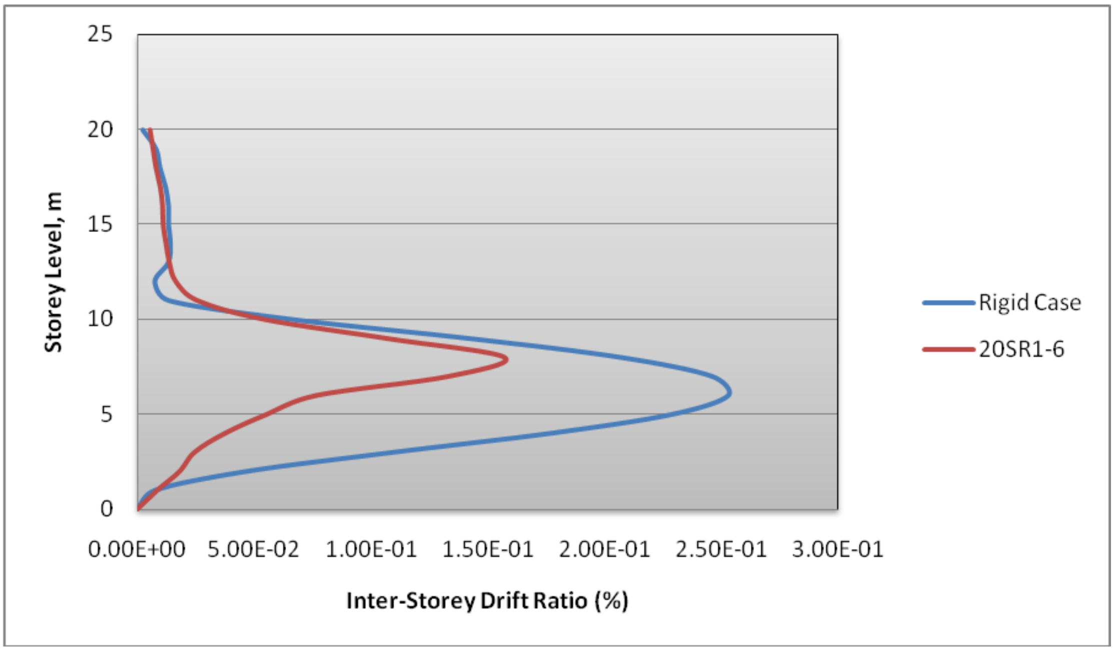


a)

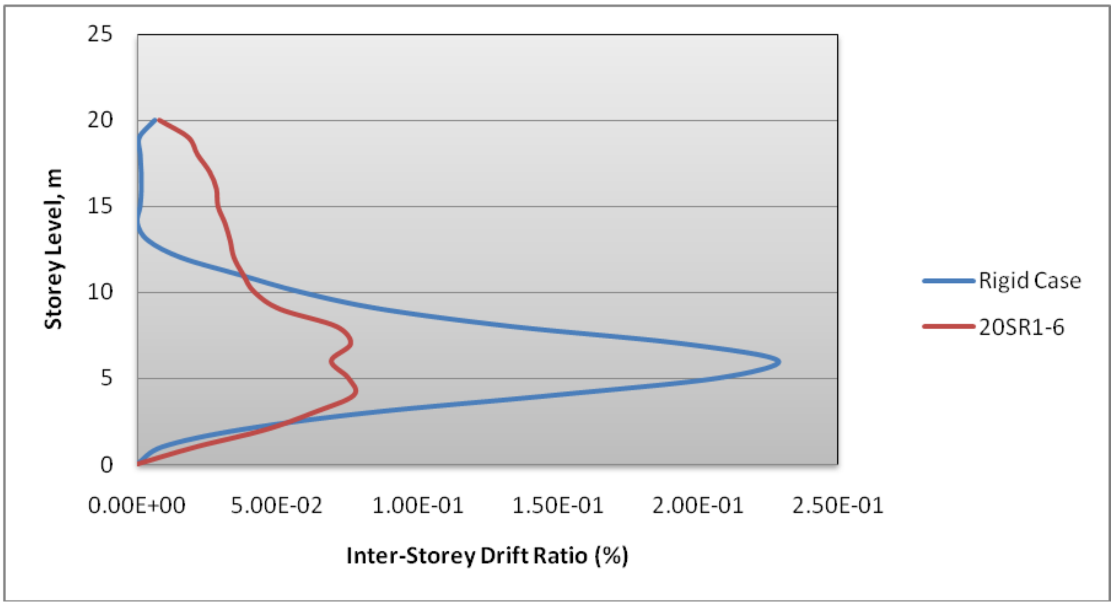


b)

Fig F1 Inter-storey drift ratio a) x-direction b) y-direction

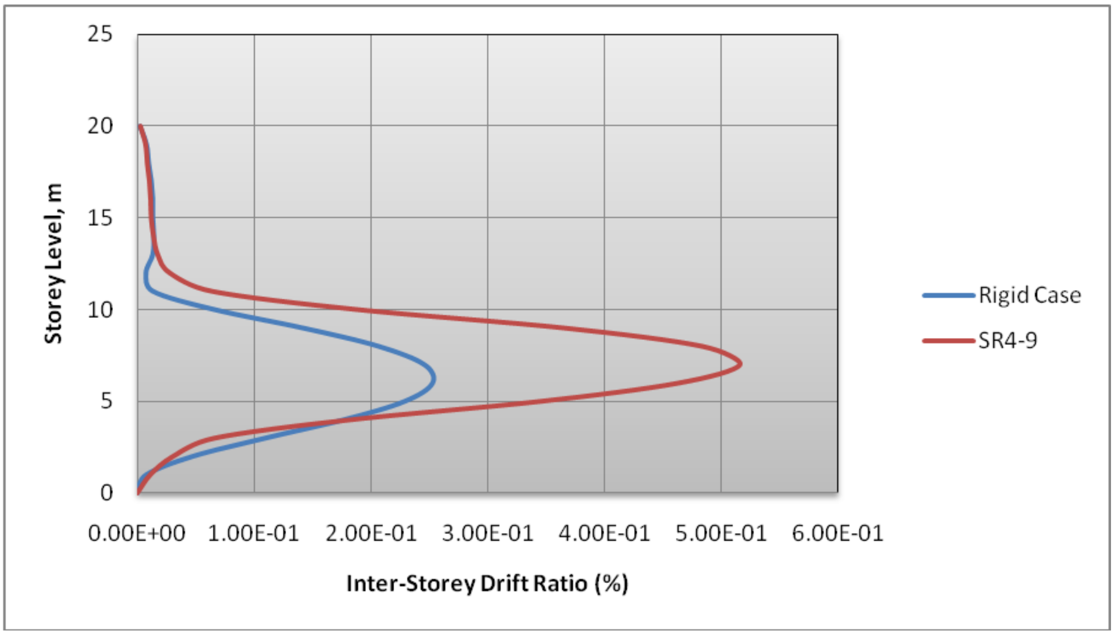


a)

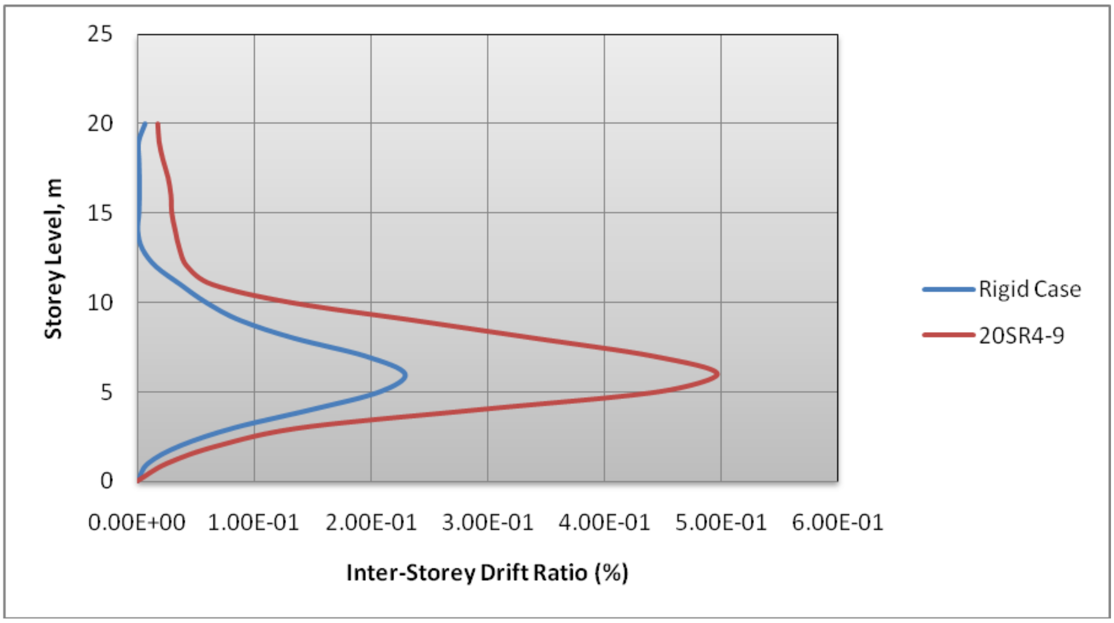


b)

Fig F2 Inter-storey drift ratio a) x-direction b) y-direction

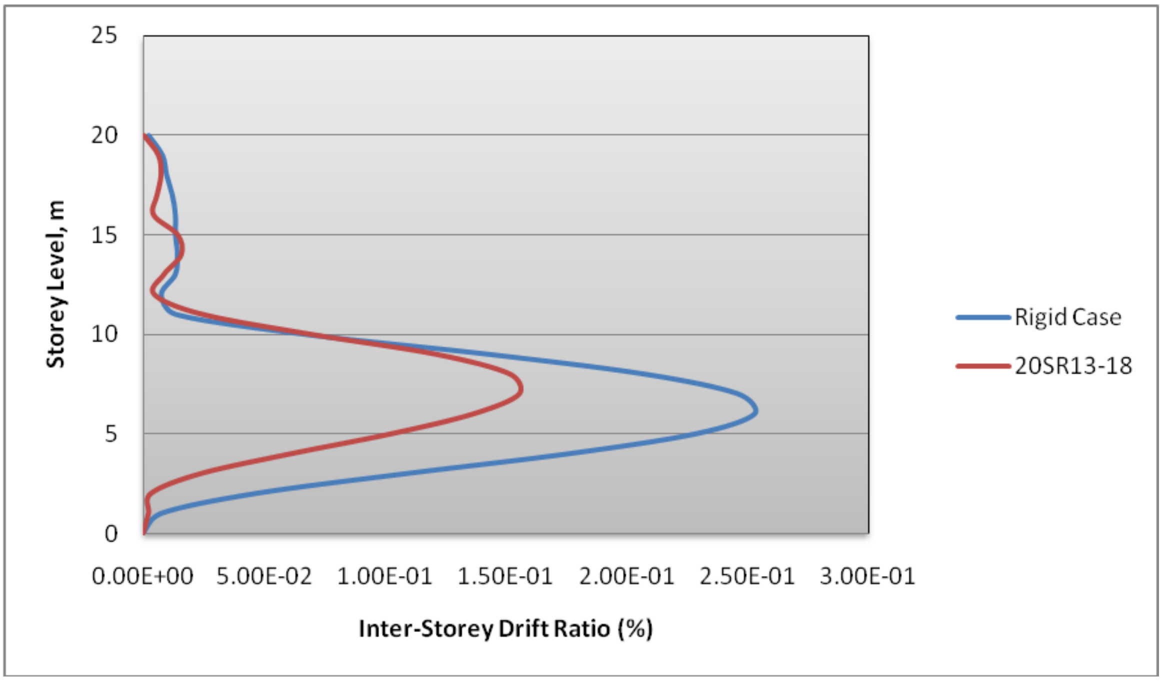


a)

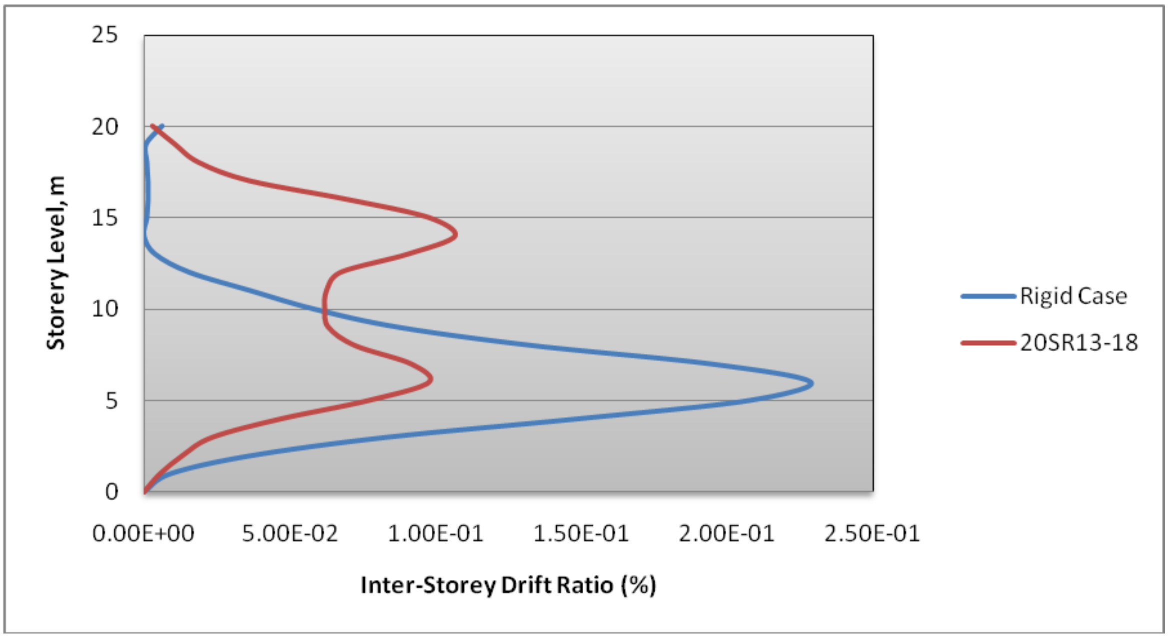


b)

Fig F3 Inter-storey drift ratio a) x-direction b) y-direction

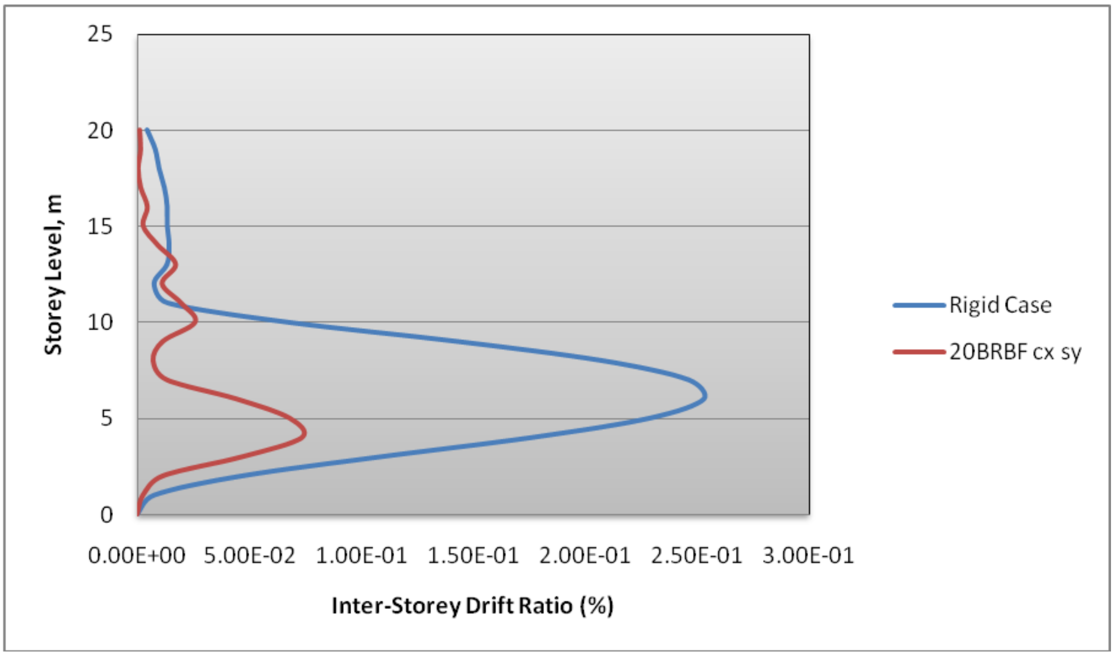


a)

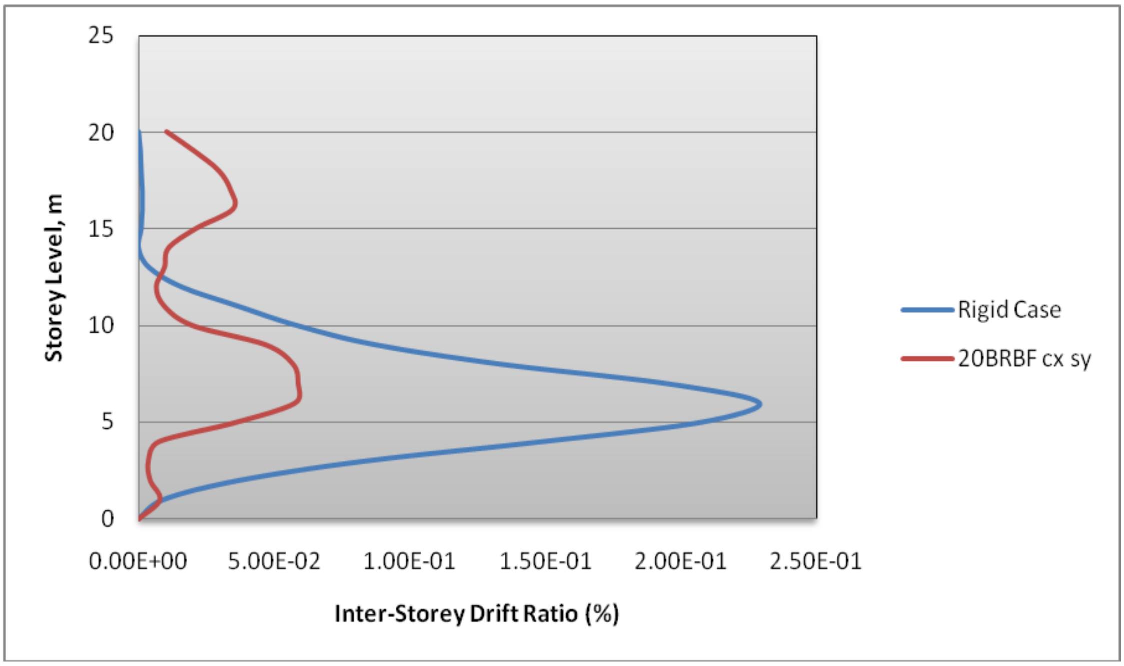


b)

Fig F4 Inter-storey drift ratio a) x-direction b) y-direction

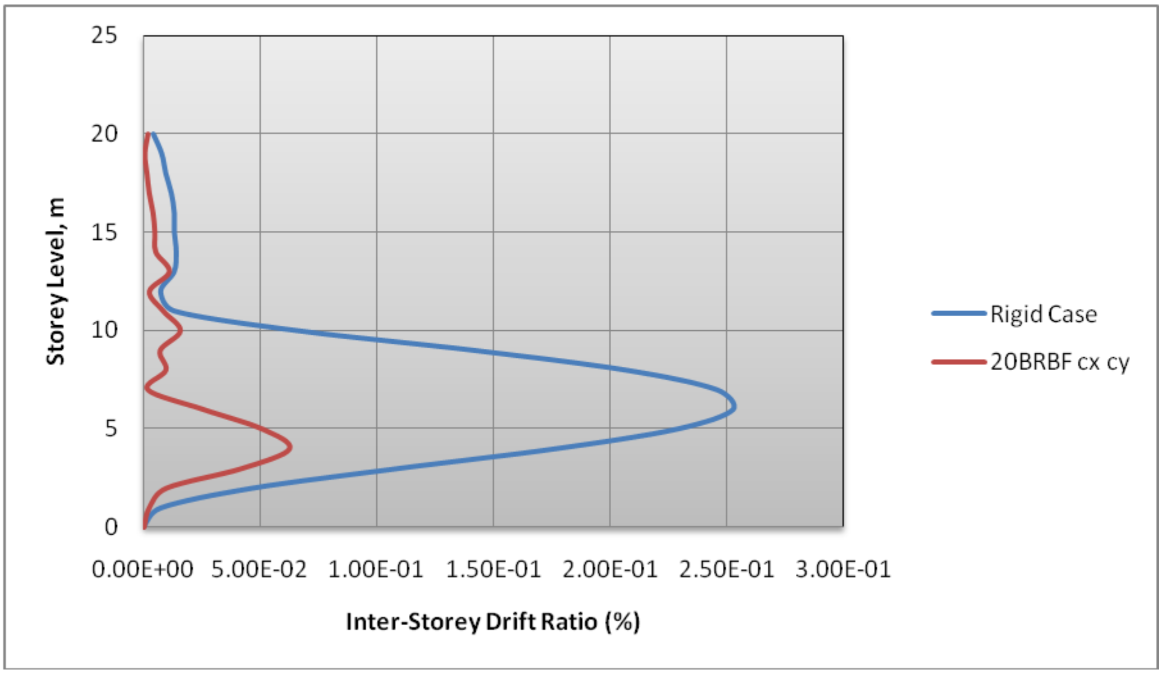


a)

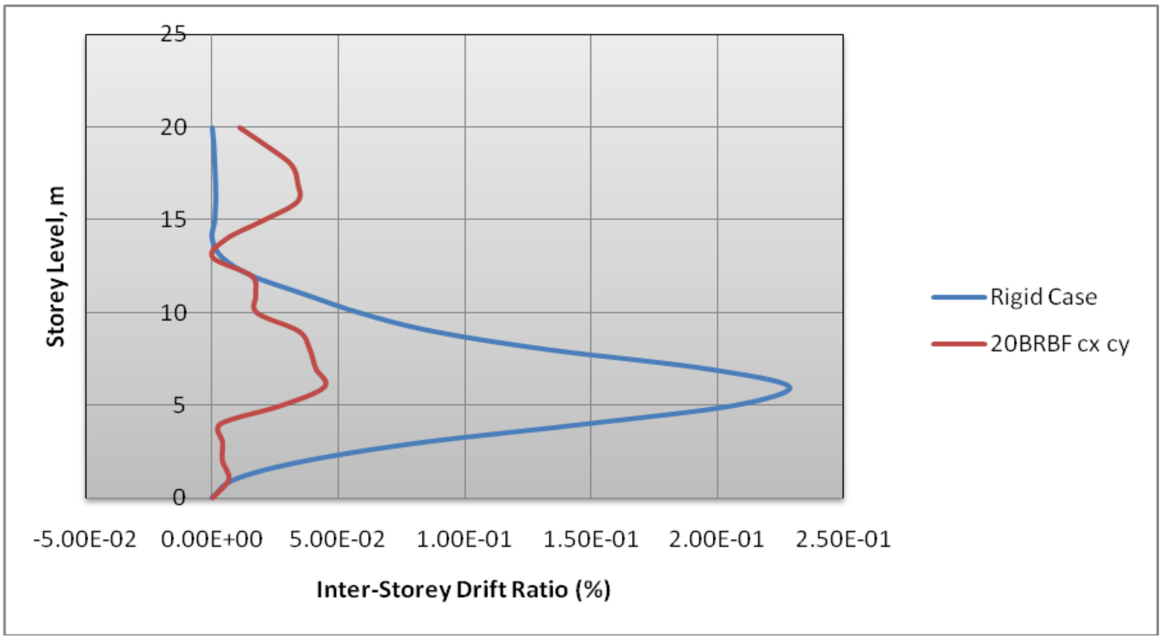


b)

Fig F5 Inter-storey drift ratio a) x-direction b) y-direction

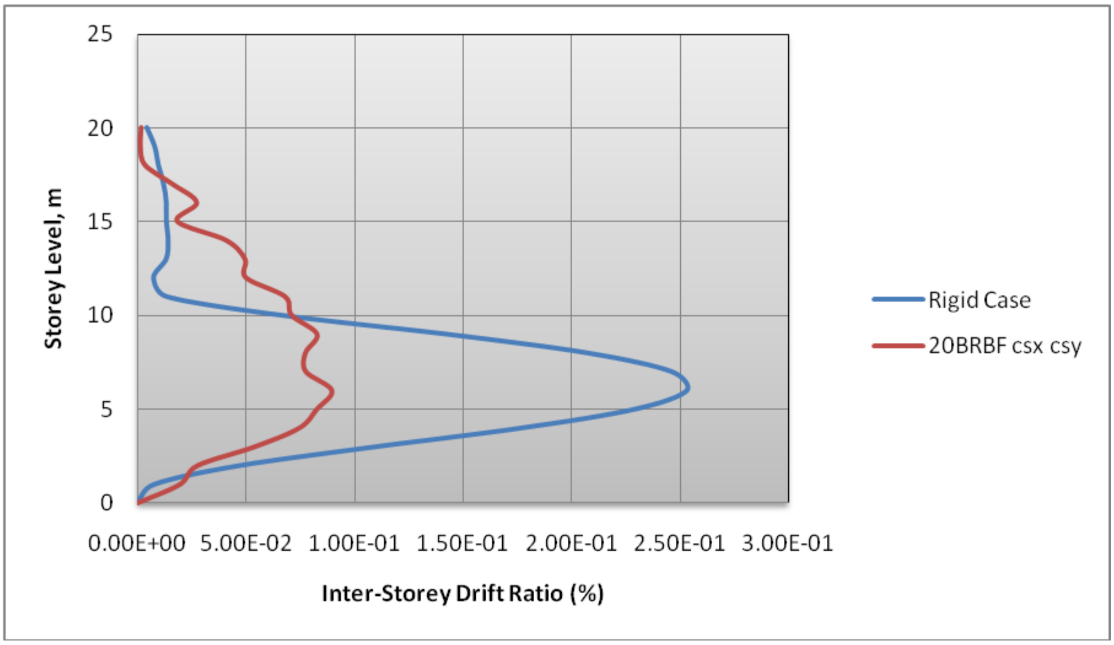


a)

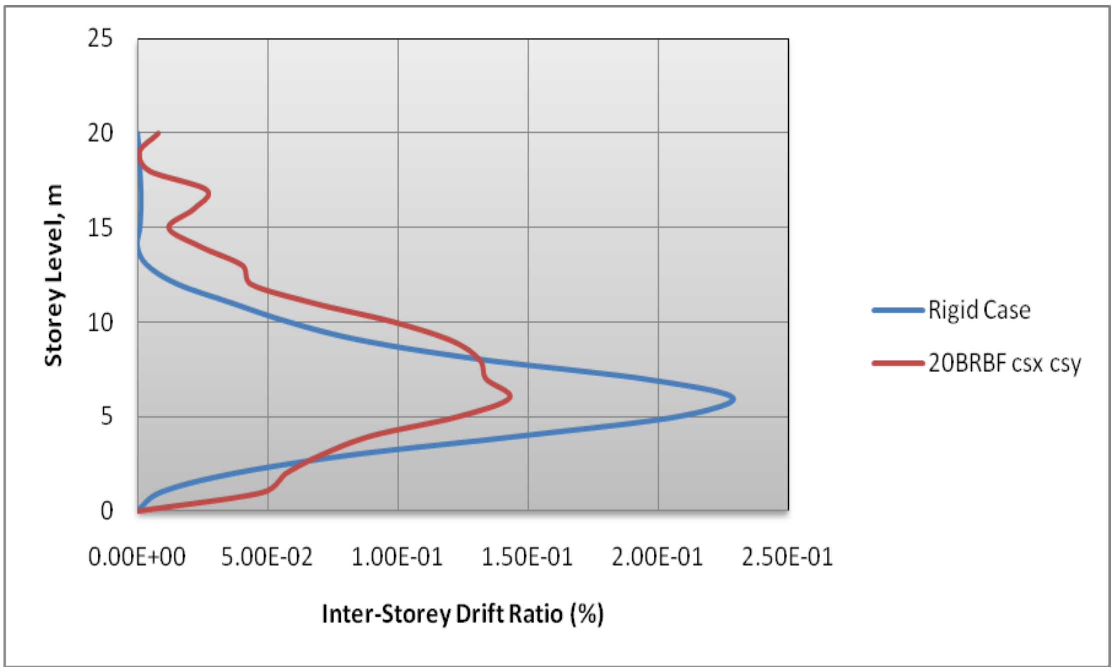


b)

Fig F6 Inter-storey drift ratio a) x-direction b) y-direction



a)

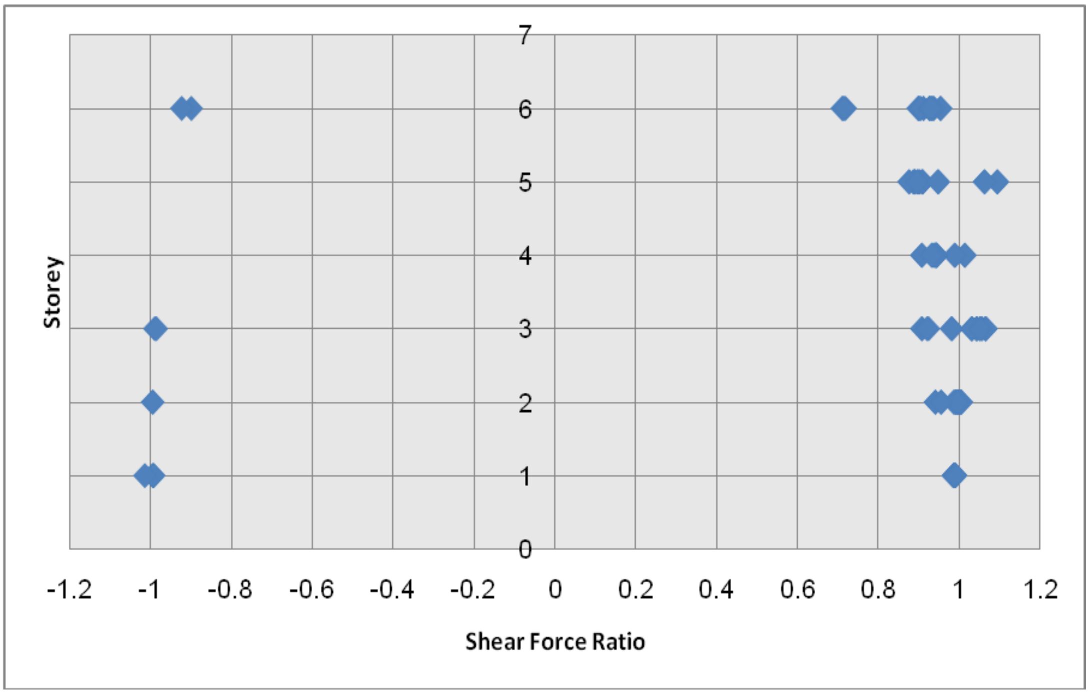


b)

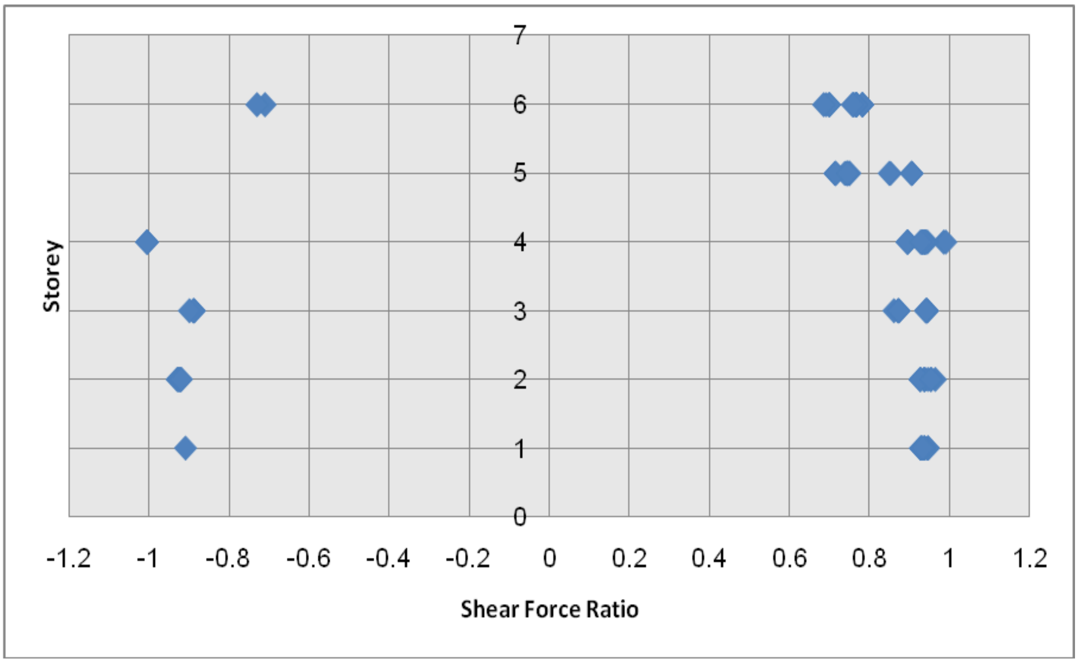
Fig F7 Inter-storey drift ratio a) x-direction b) y-direction

APPENDIX G

FORCE DISTRIBUTION IN 6PRMRF MEMBERS

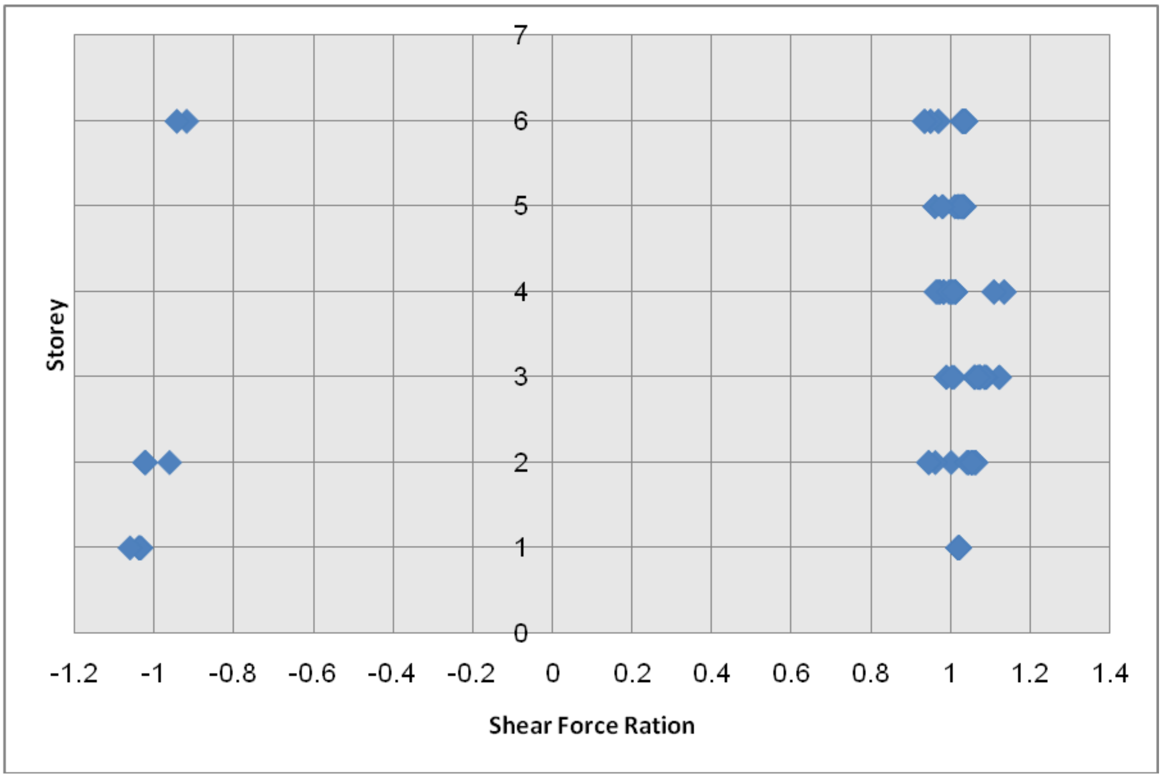


a)

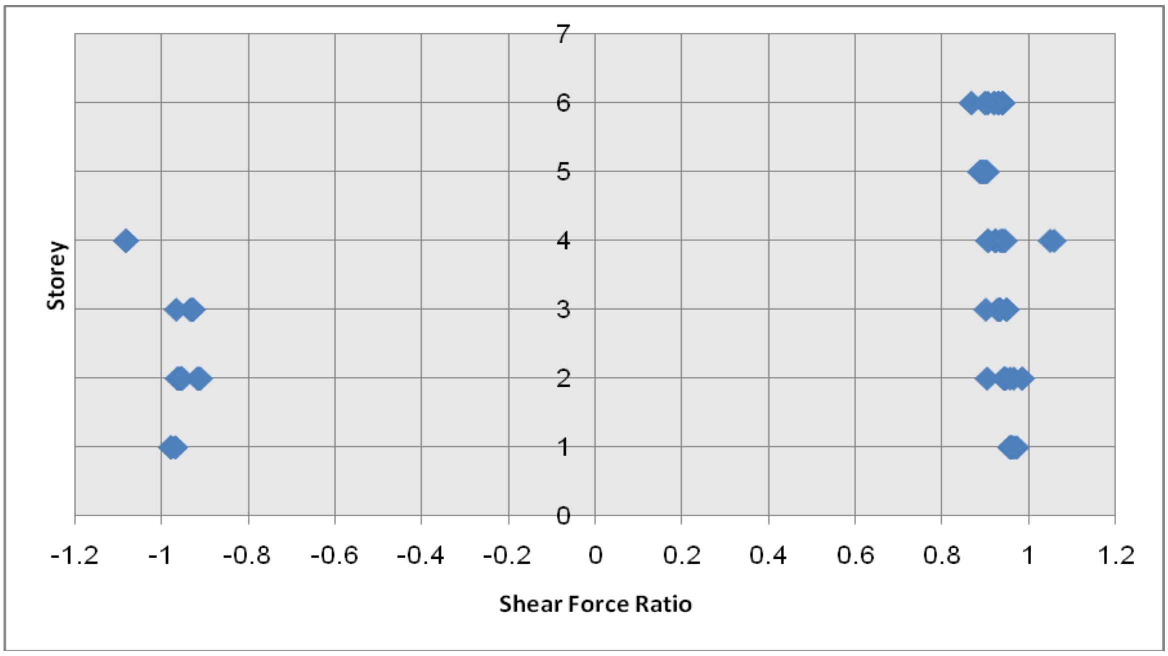


b)

Fig G1 shear force ratio in column for 6SR45 a) x-direction b) y-direction

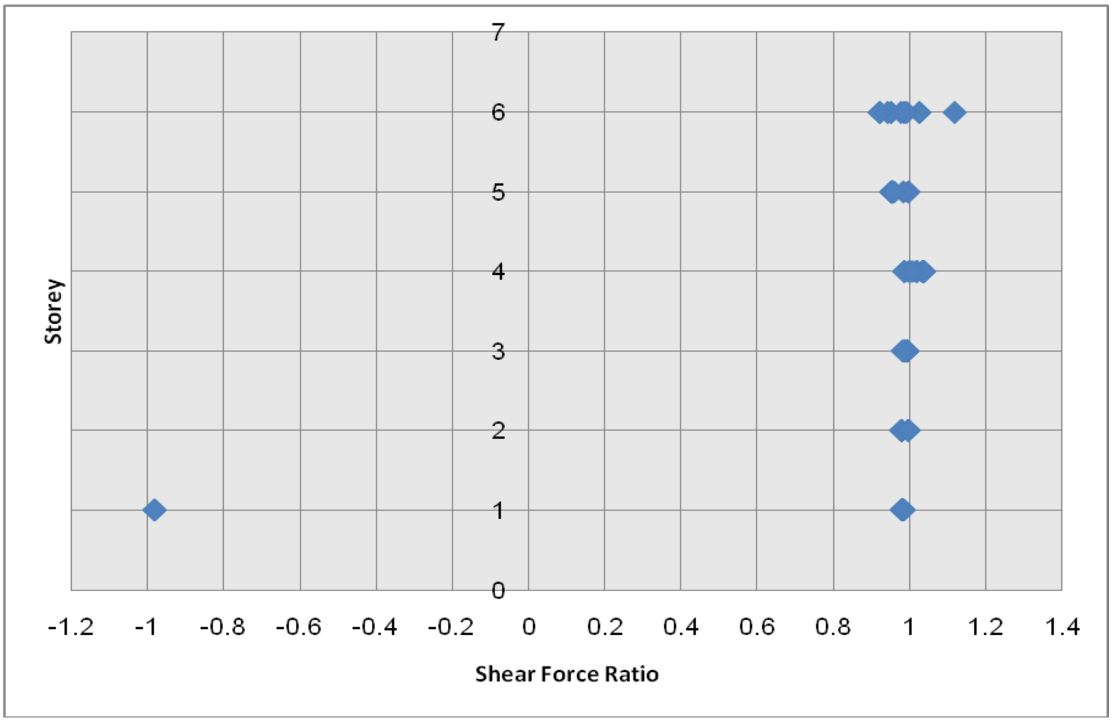


a)

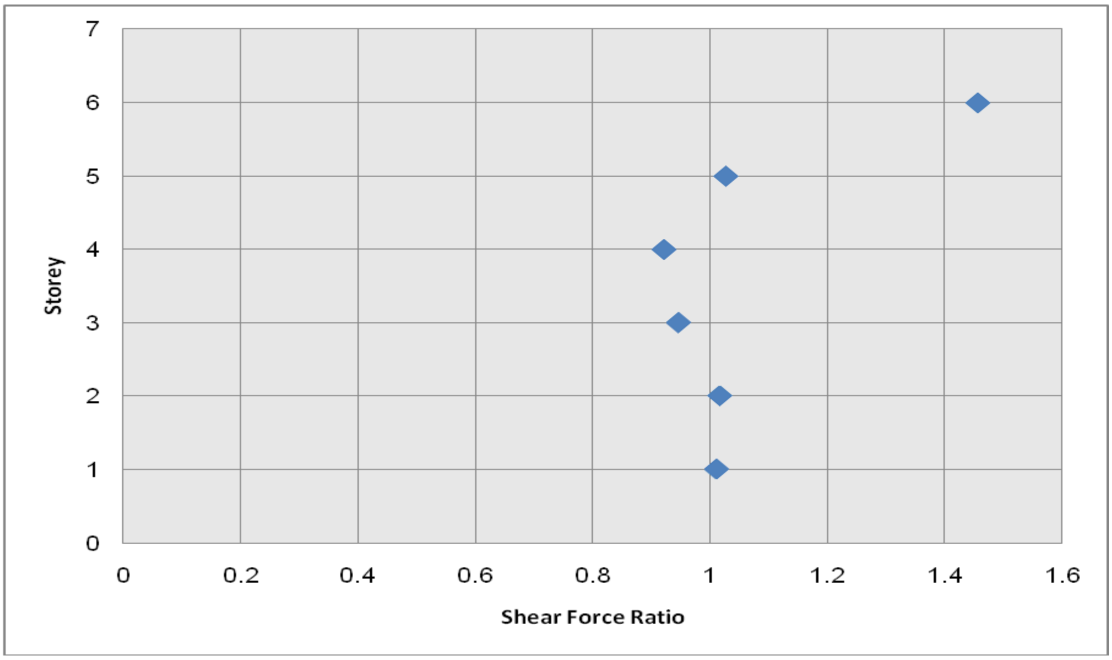


b)

Fig G2 shear force ratio in column for 6SR34 a) x-direction b) y-direction

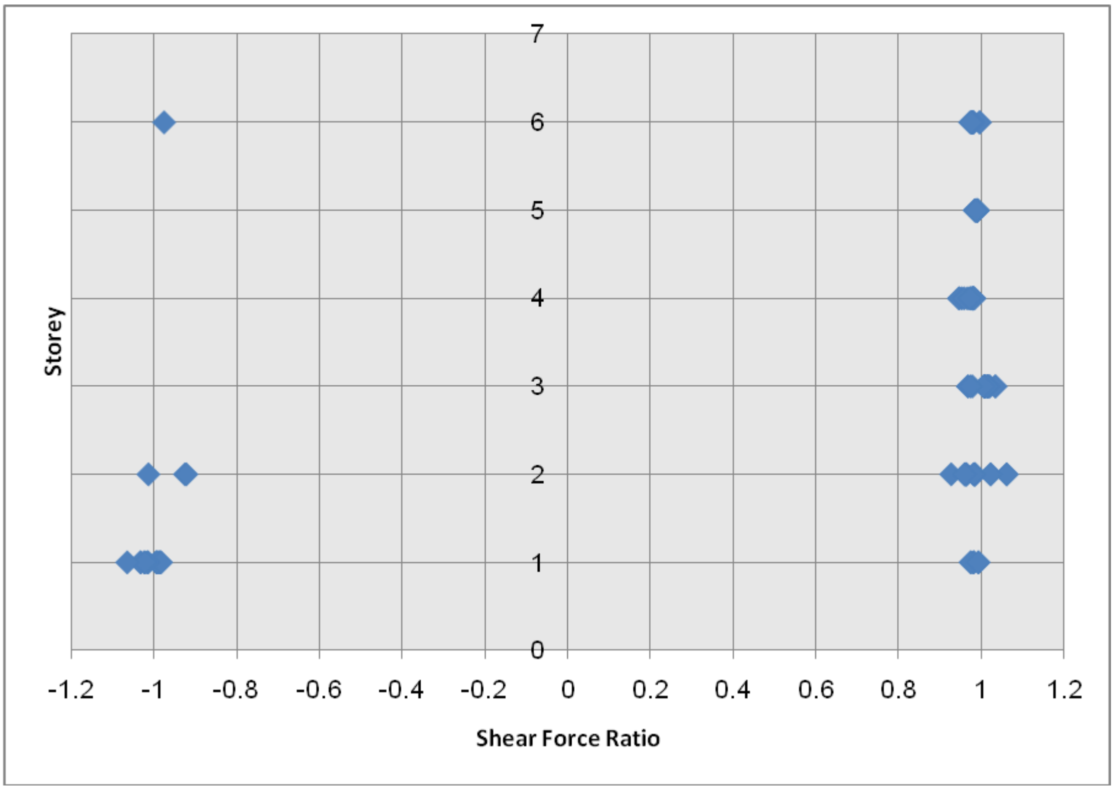


a)

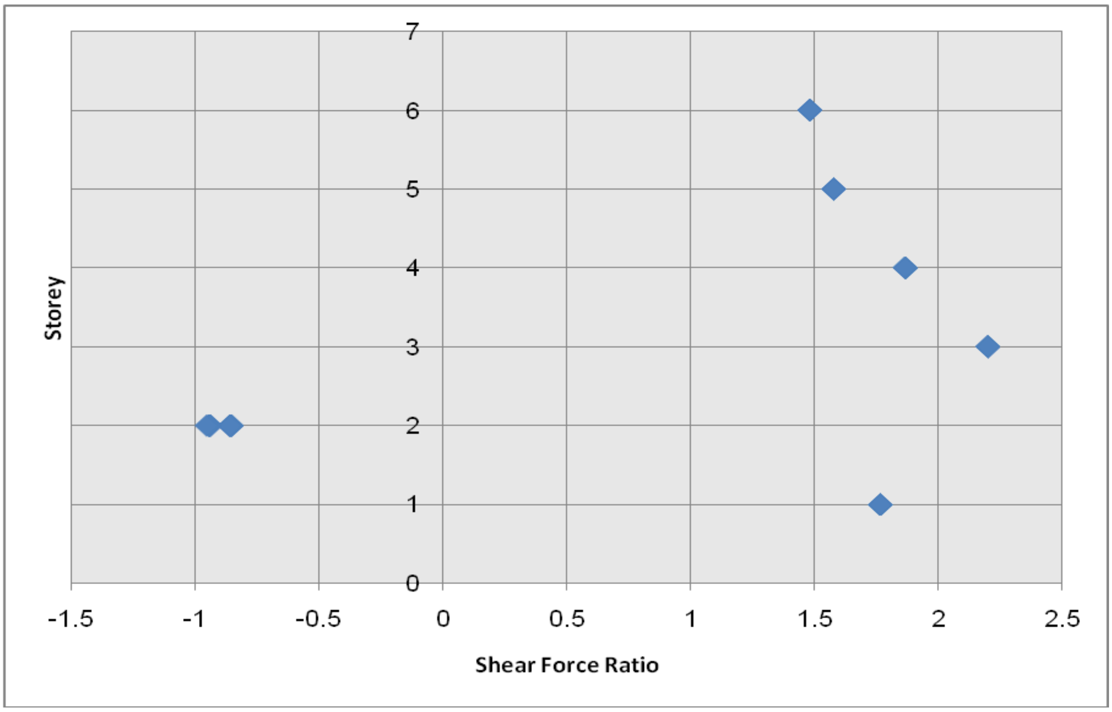


b)

Fig G3 shear force ratio in column for 6SR56 a) x-direction b) y-direction

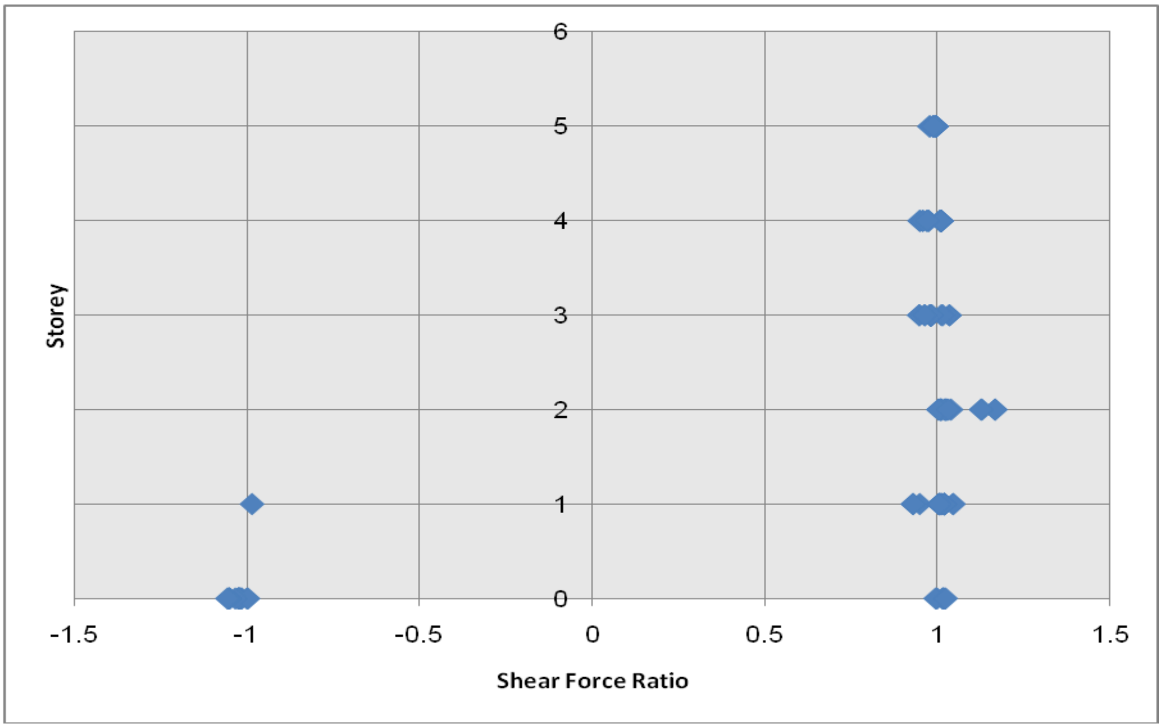


a)

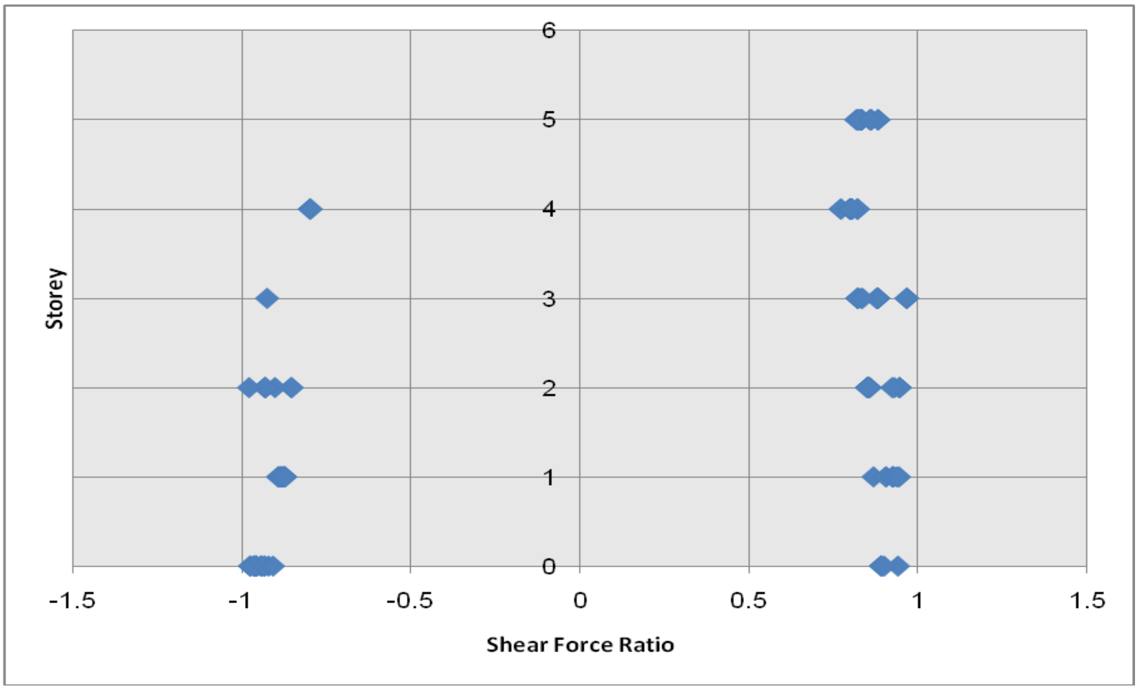


b)

Fig G4 shear force ratio in column for 6SR12 a)x-direction b) y-direction



a)



b)

Fig G5 shear force ratio in column for 6SR23 a) x-direction b) y-direction

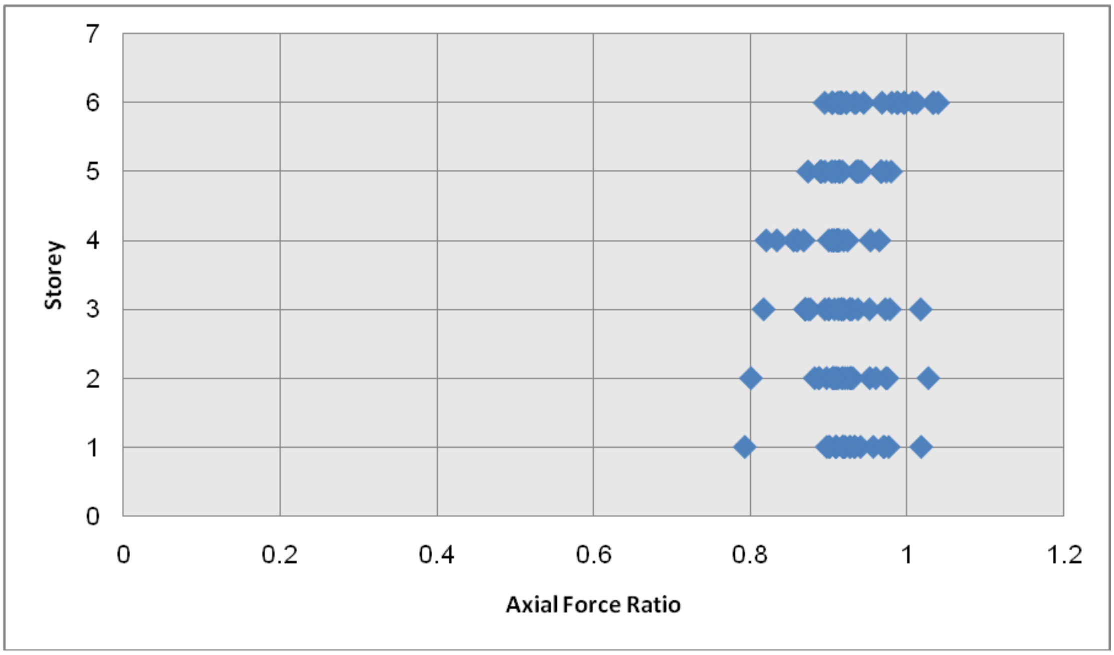


Fig G6 axial force ratio in columns for 6SR45

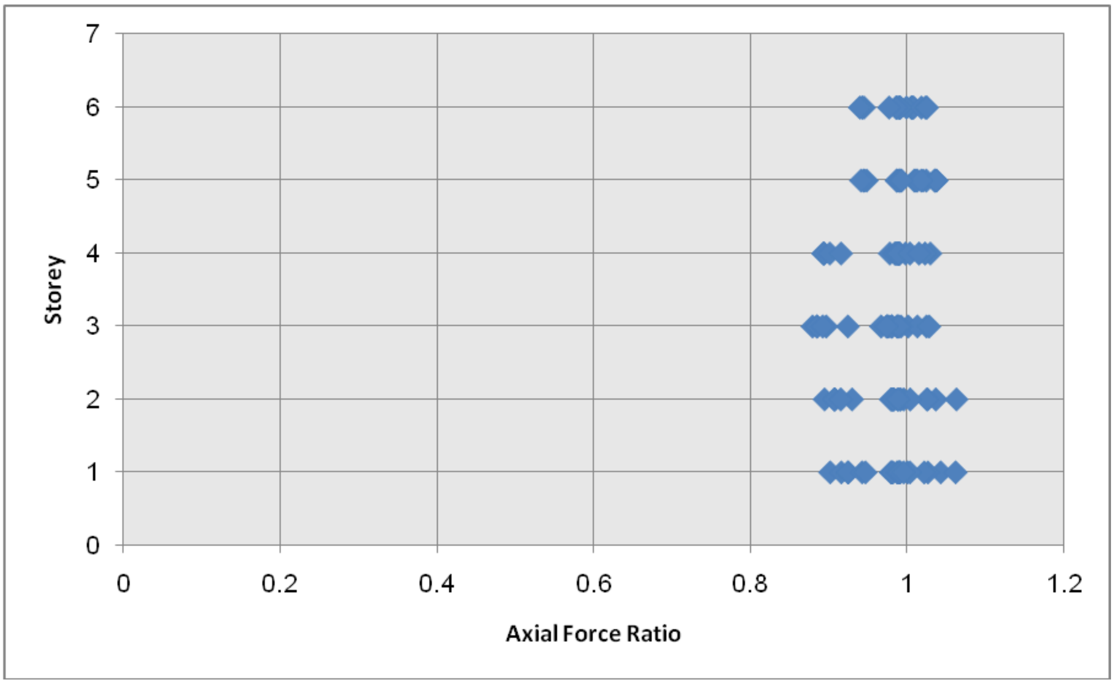


Fig G7 axial force ratio in columns for 6SR34

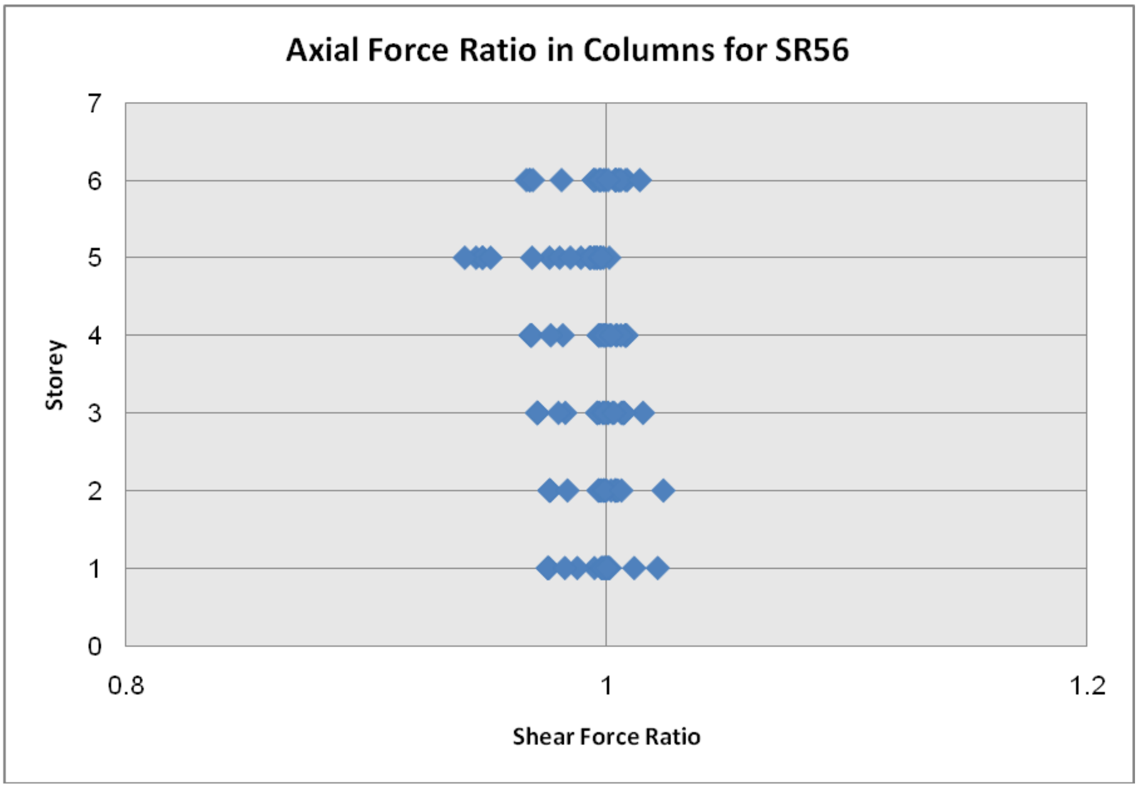


Fig G8 axial force ratio in columns for 6SR56

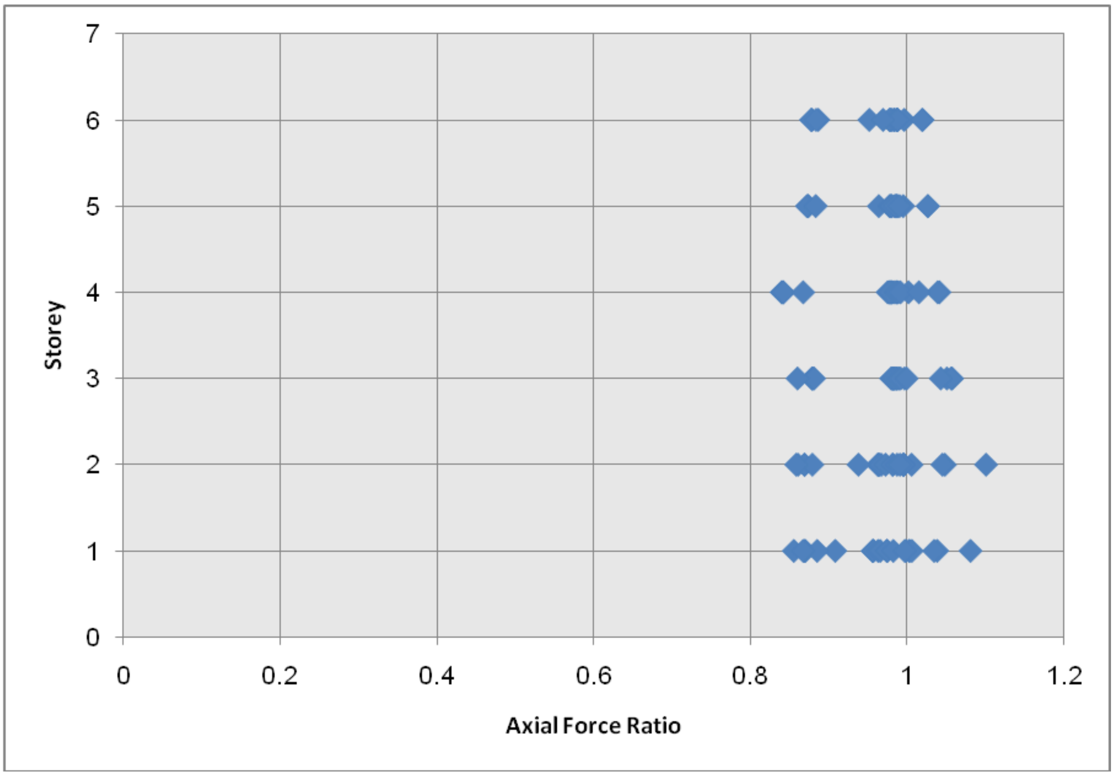


Fig G9 axial force ratio in columns for 6SR12

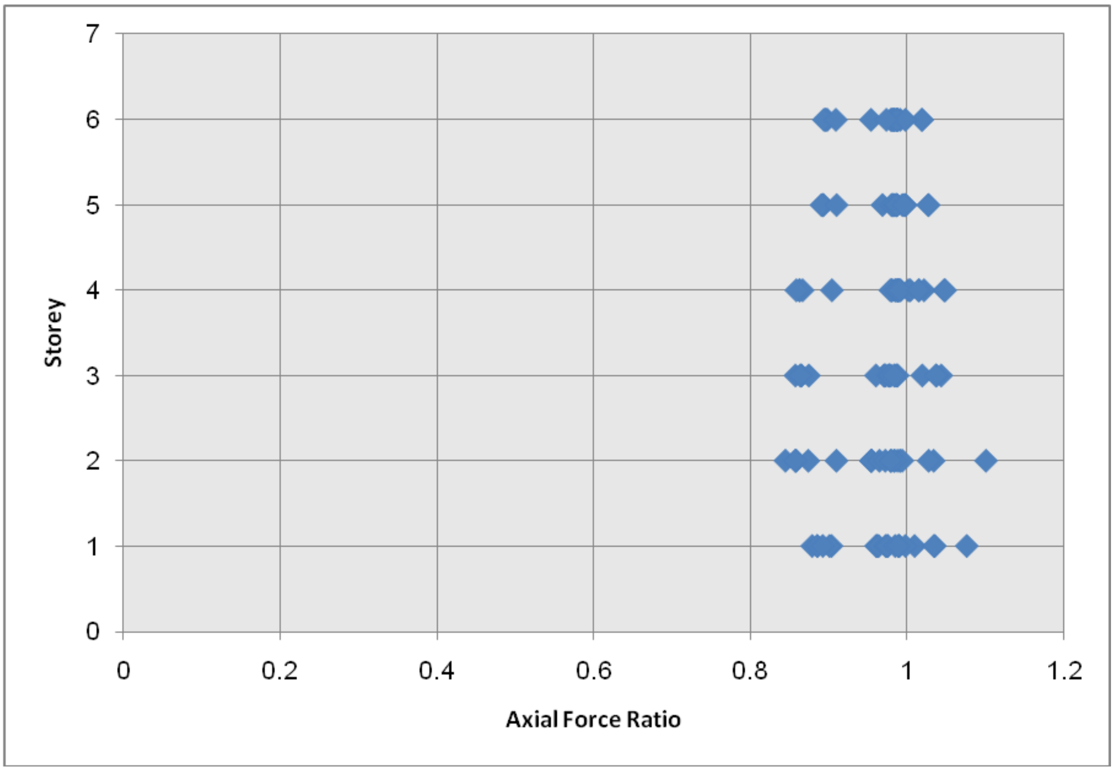
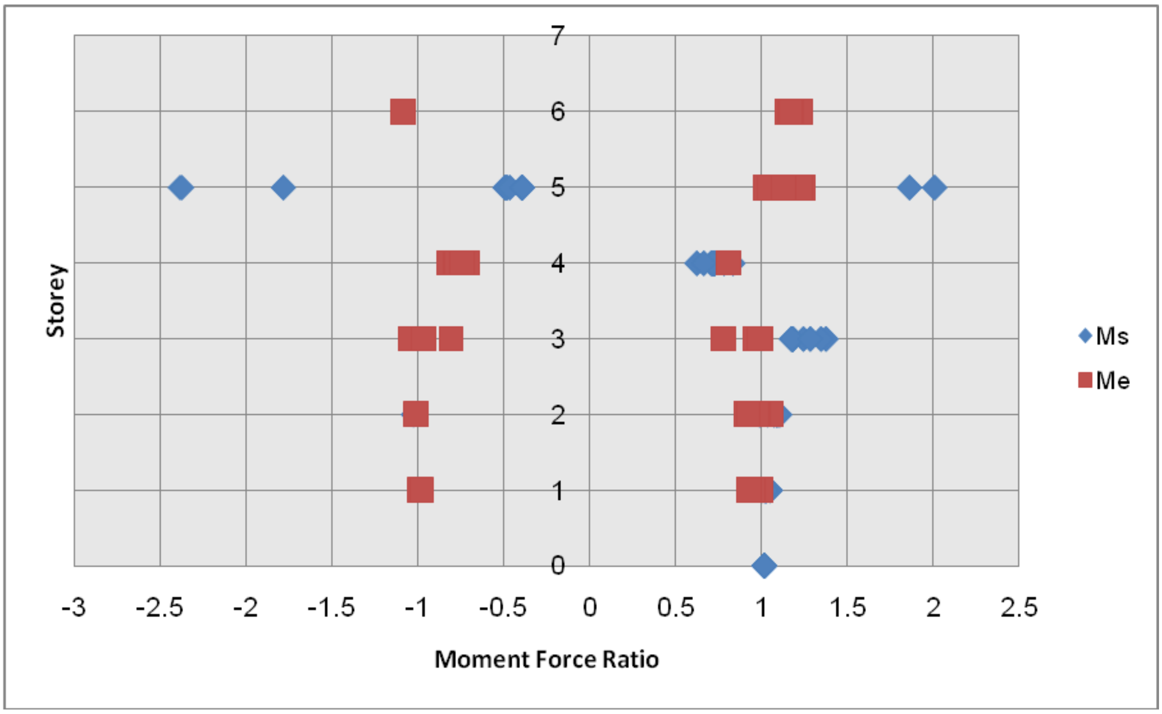
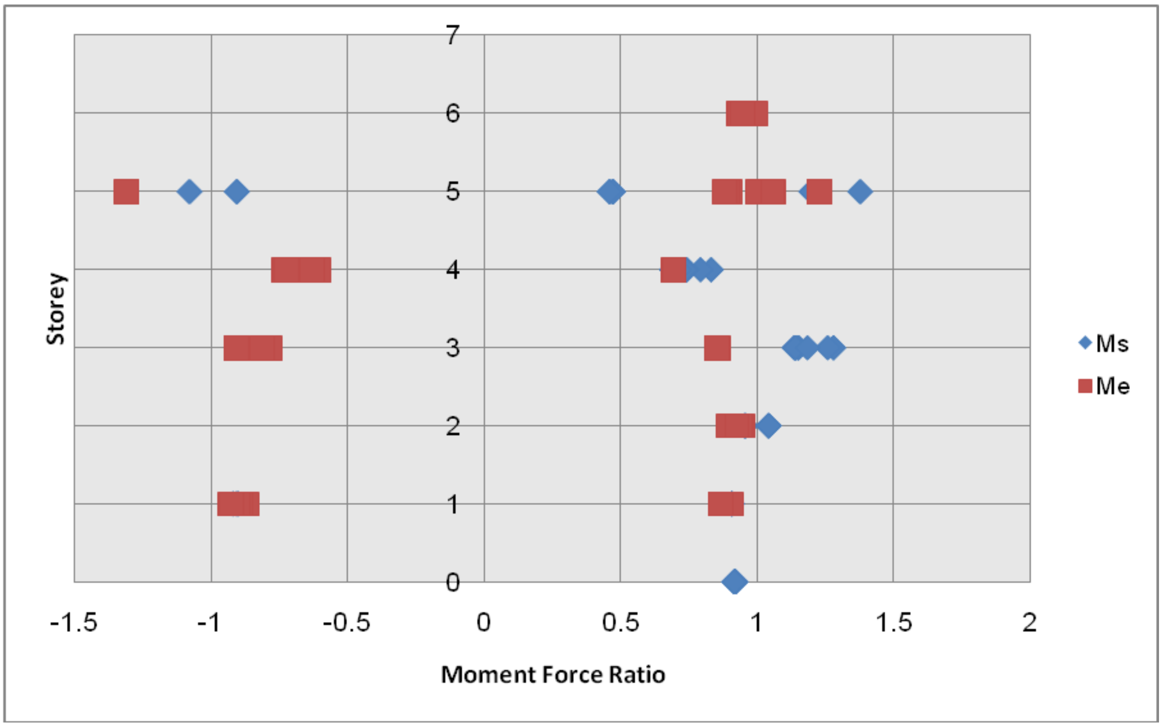


Fig G10 axial force ratio in columns for 6SR23

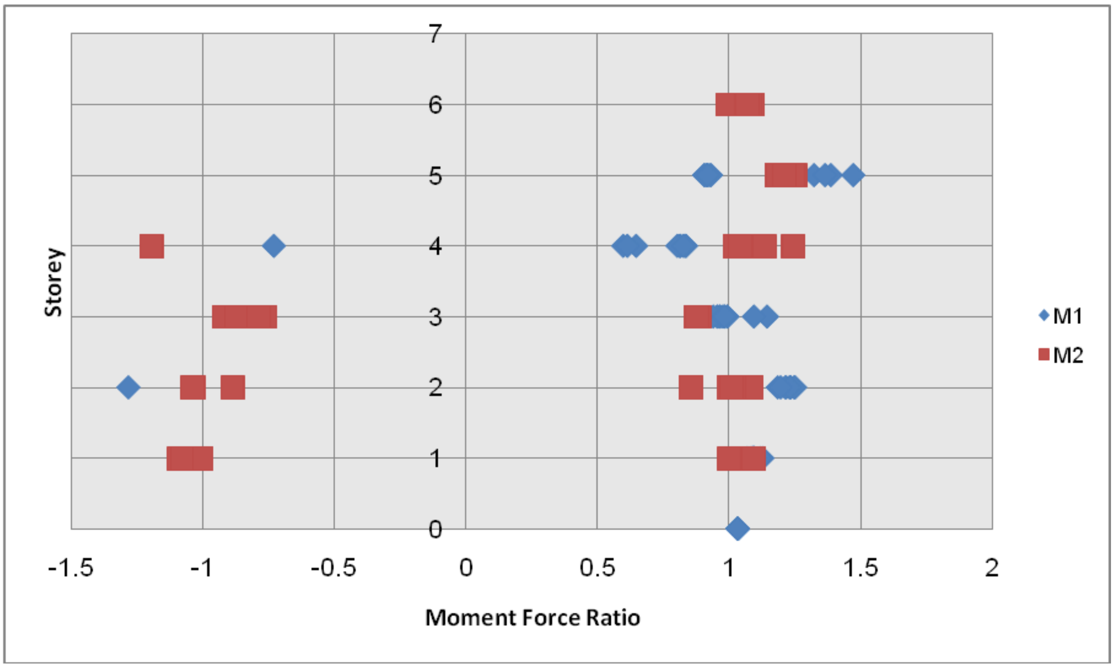


a)

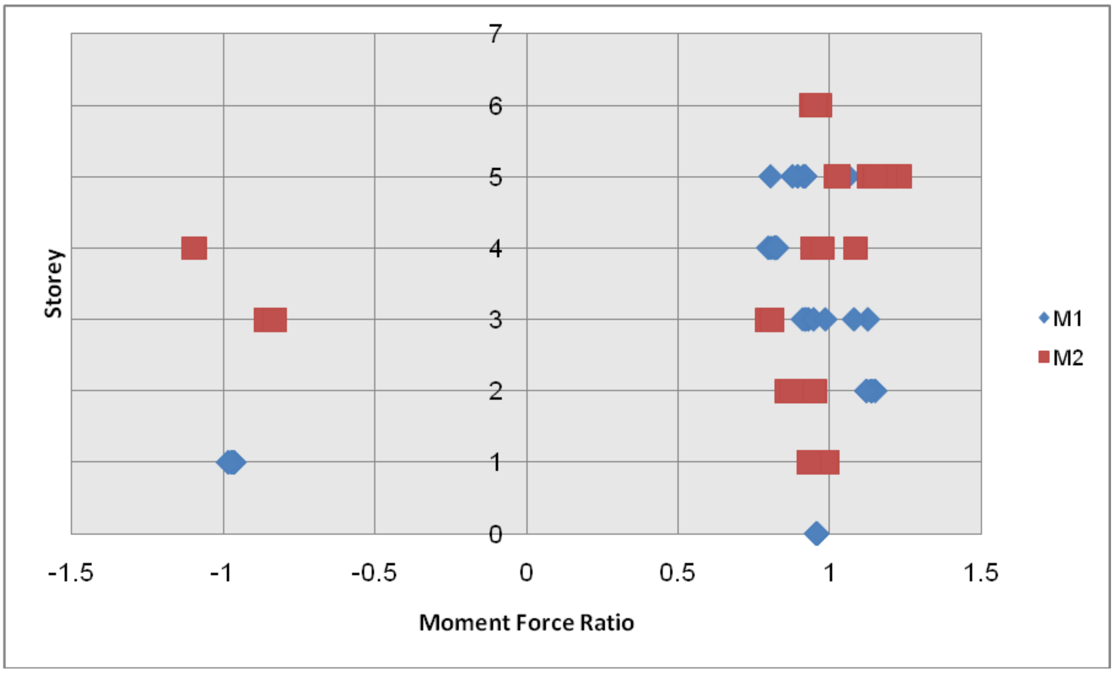


b)

Fig G11 moment force ratio in columns for 6SR45 a) x-direction b) y-direction

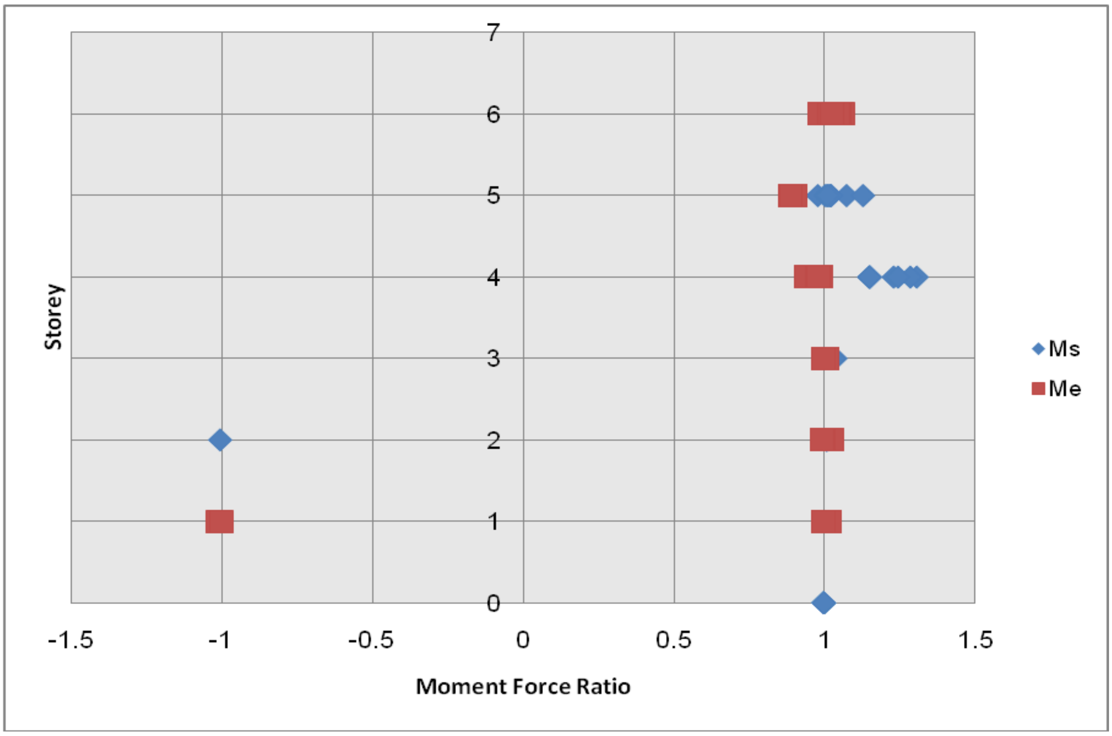


a)

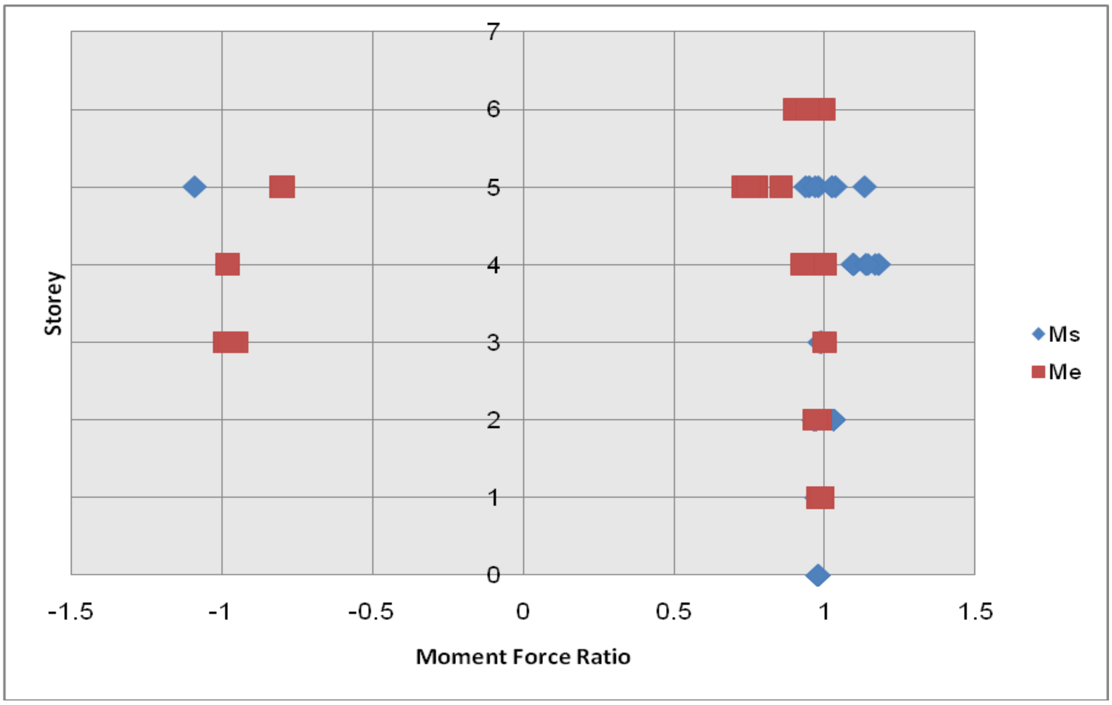


b)

Fig G12 moment force ratio in columns for 6SR34 a) x-direction b) y-direction

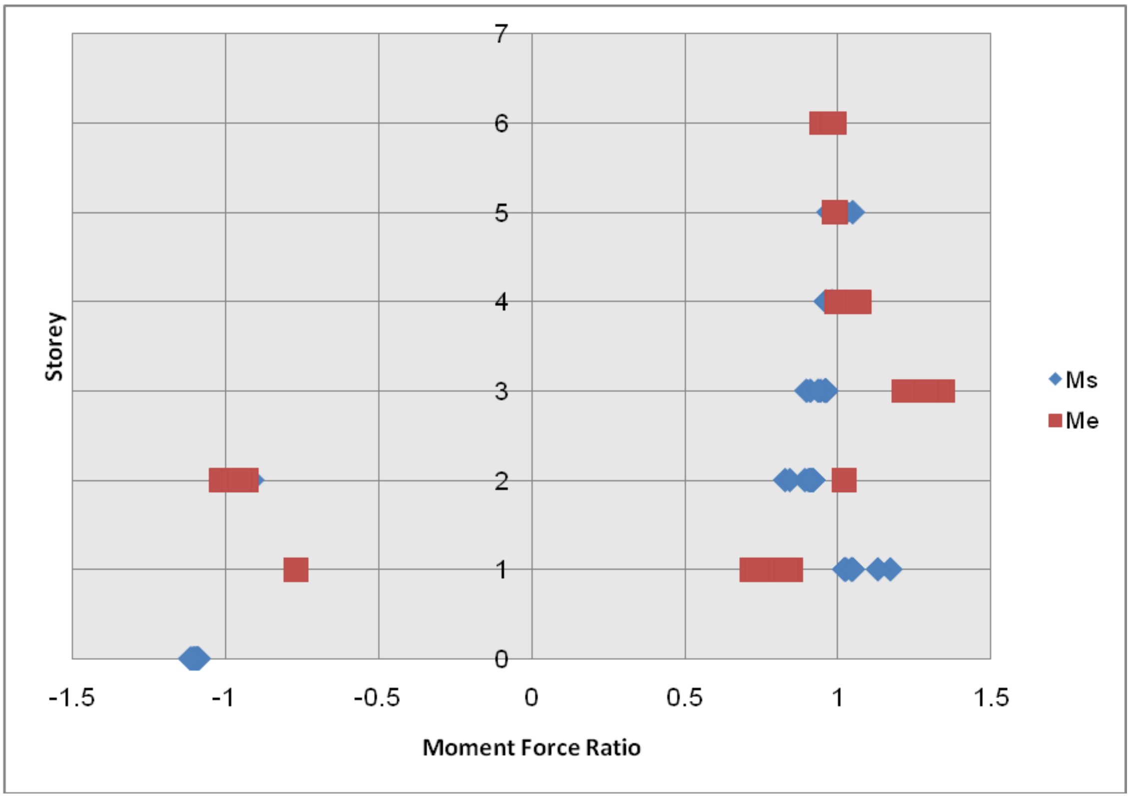


a)

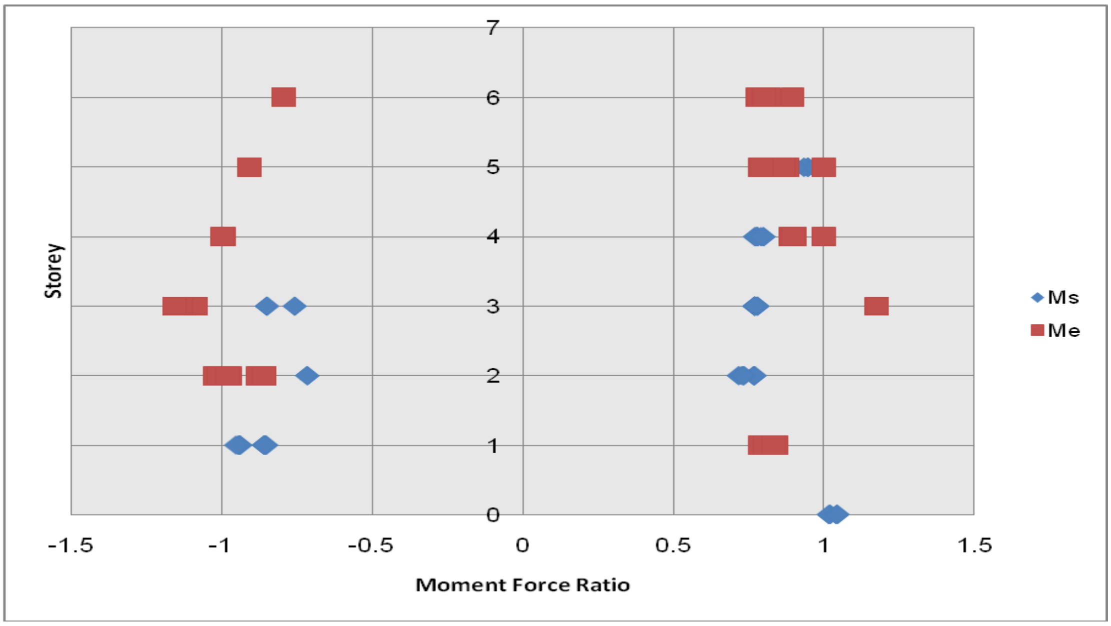


b)

Fig G13 moment force ratio in columns for 6SR56 a) x-direction b) y-direction

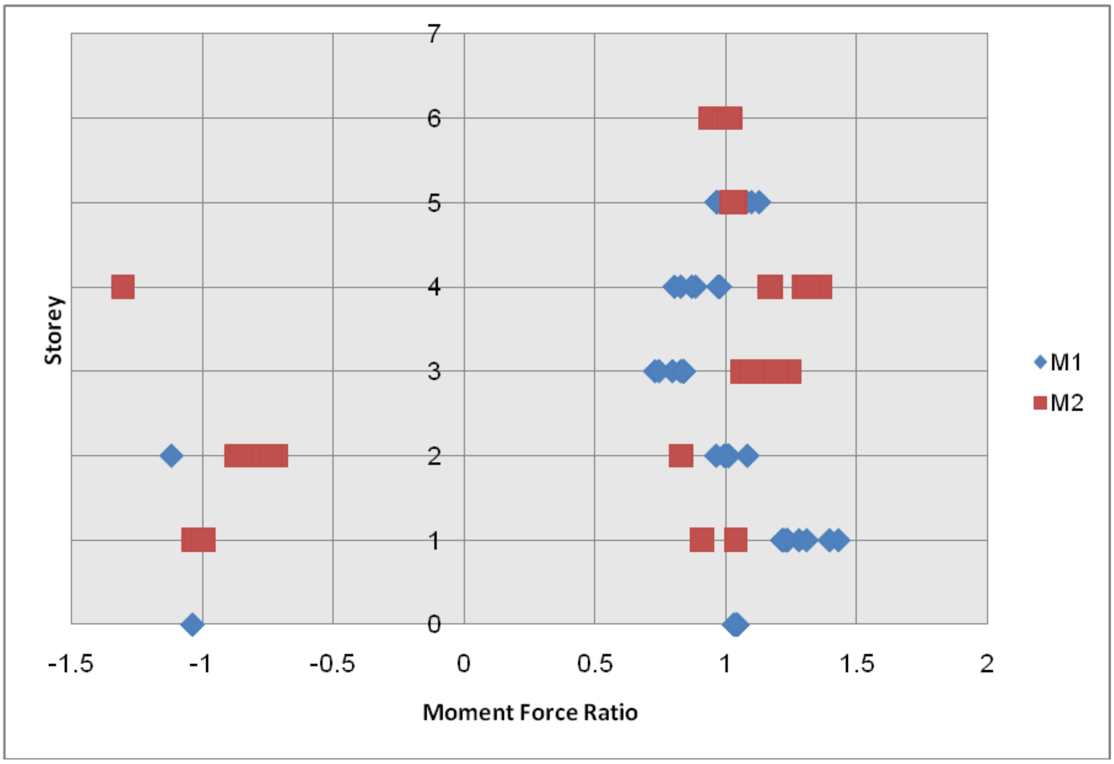


a)

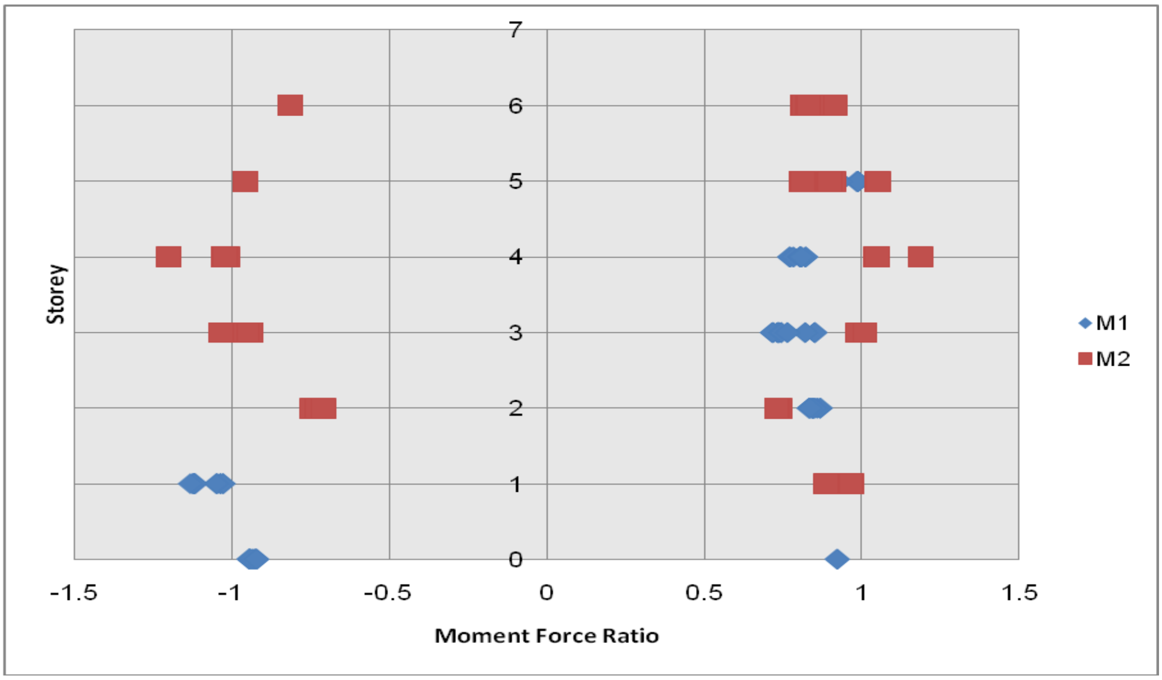


b)

Fig G14 moment force ratio in columns for 6SR12 a) x-direction b) y-direction

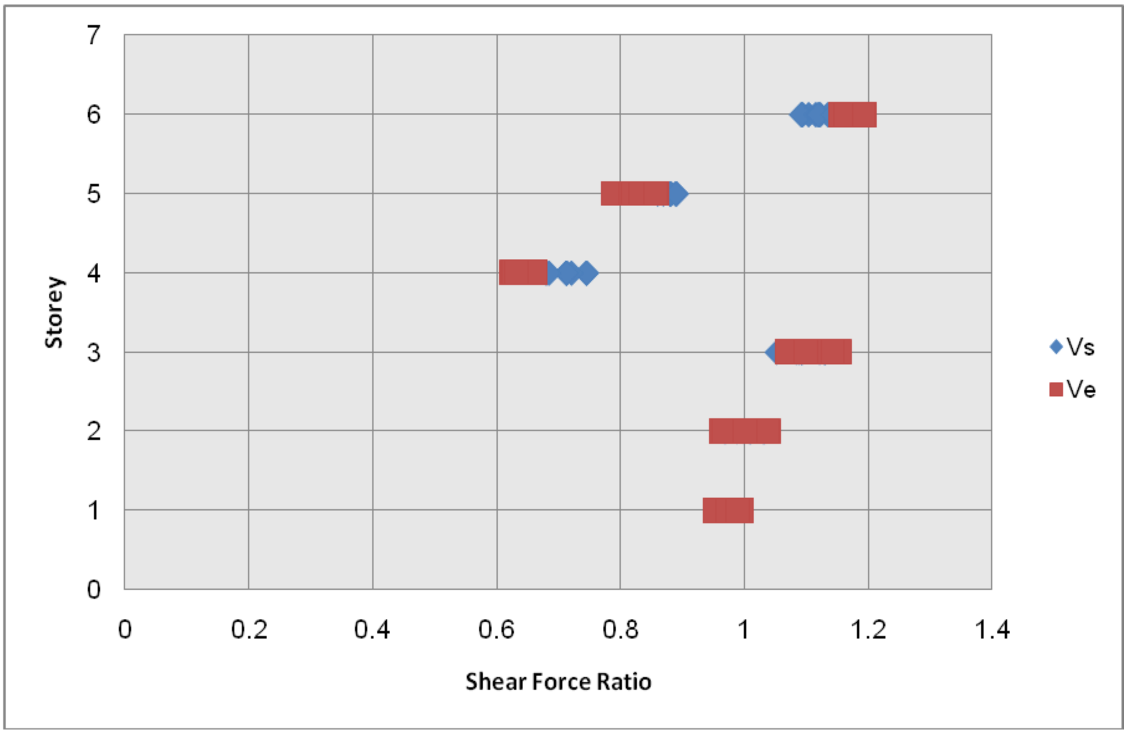


a)

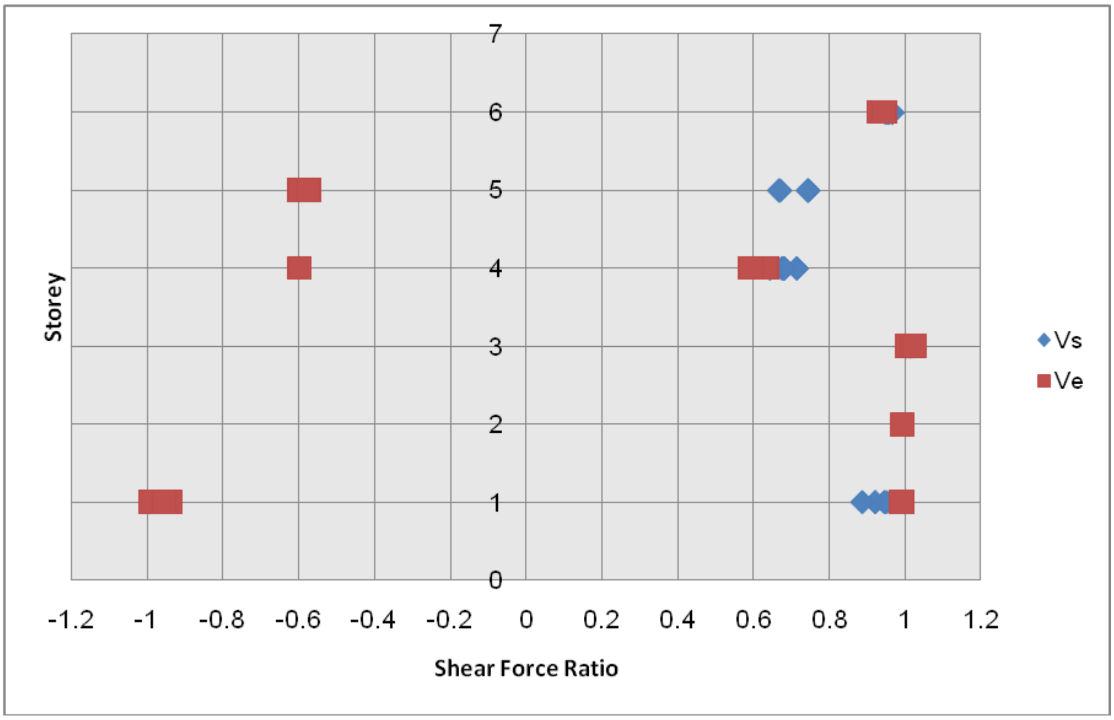


b)

Fig G15 moment force ratio in columns for 6SR23 a) x-direction b) y-direction

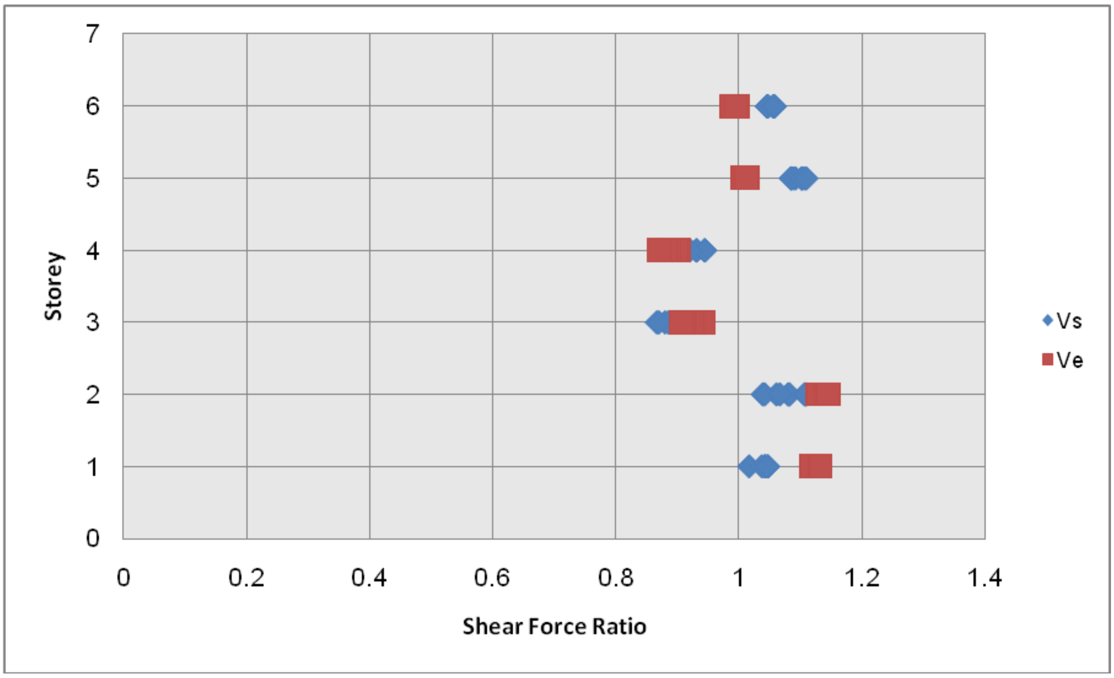


a)

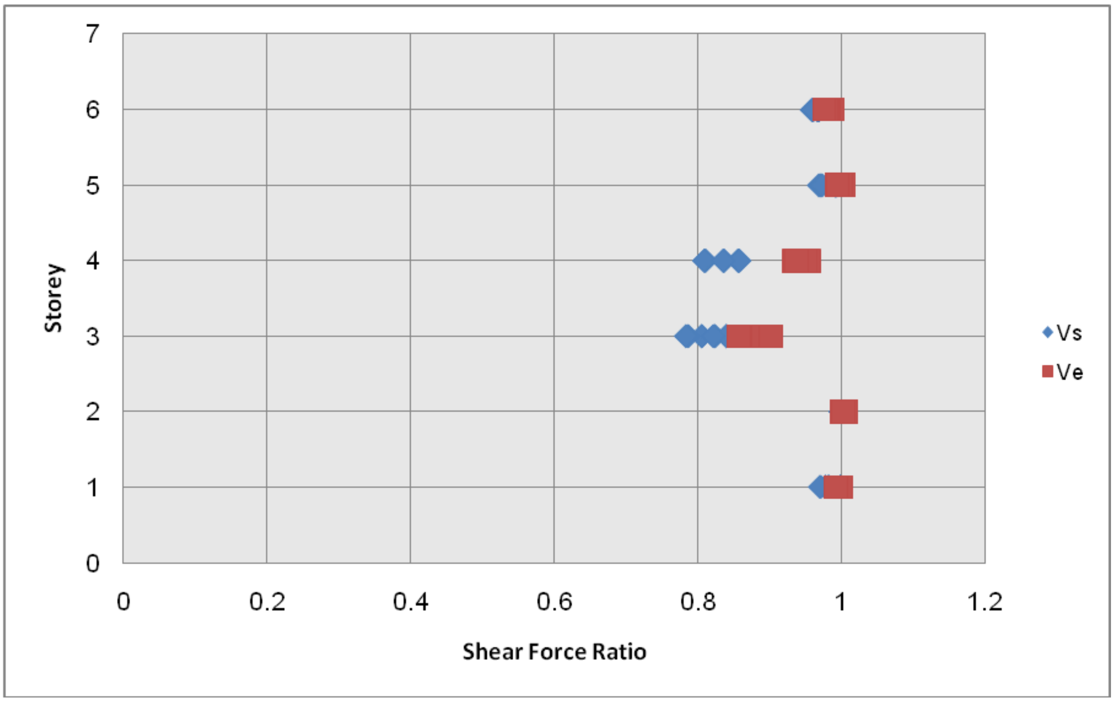


b)

Fig G16 shear force ratio in beams for 6SR45 a) x-direction b) y-direction

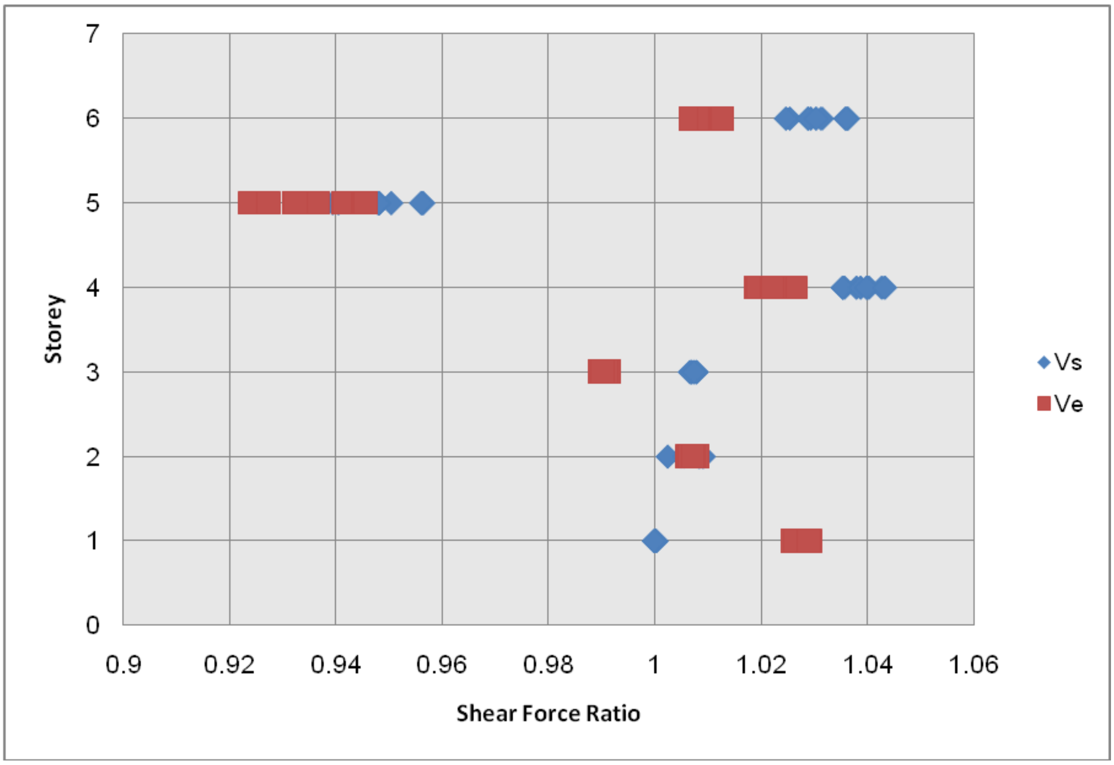


a)

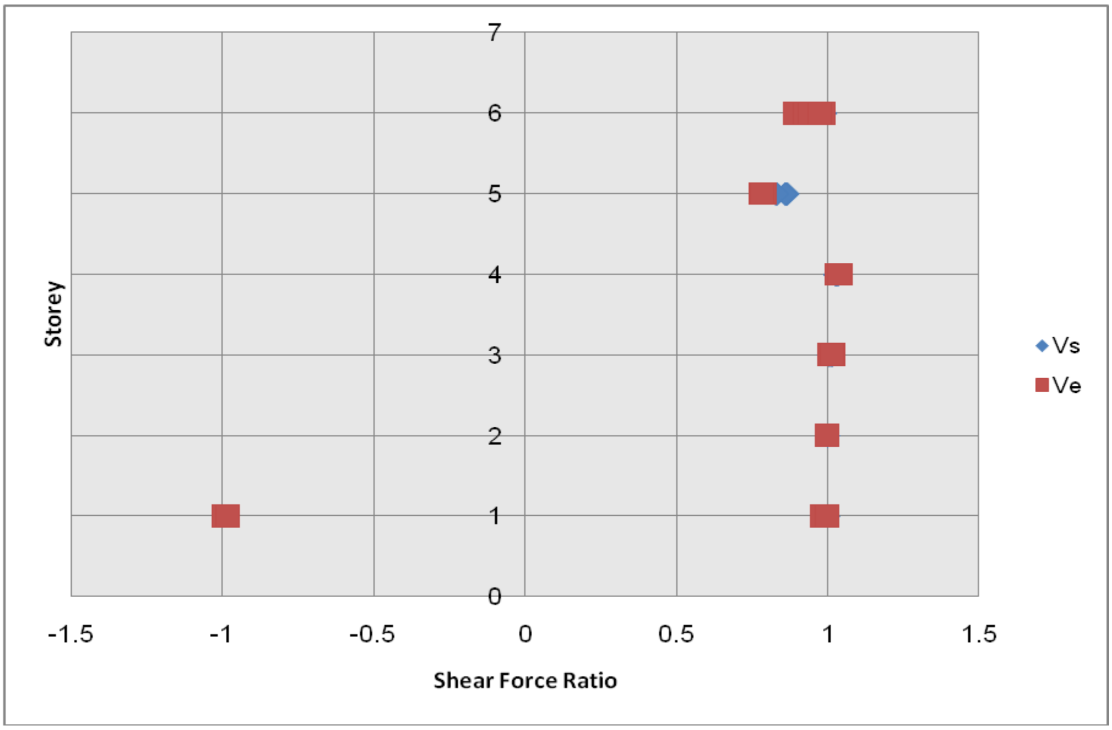


b)

Fig G17 shear force ratio in beams for 6SR34 a) x-direction b) y-direction

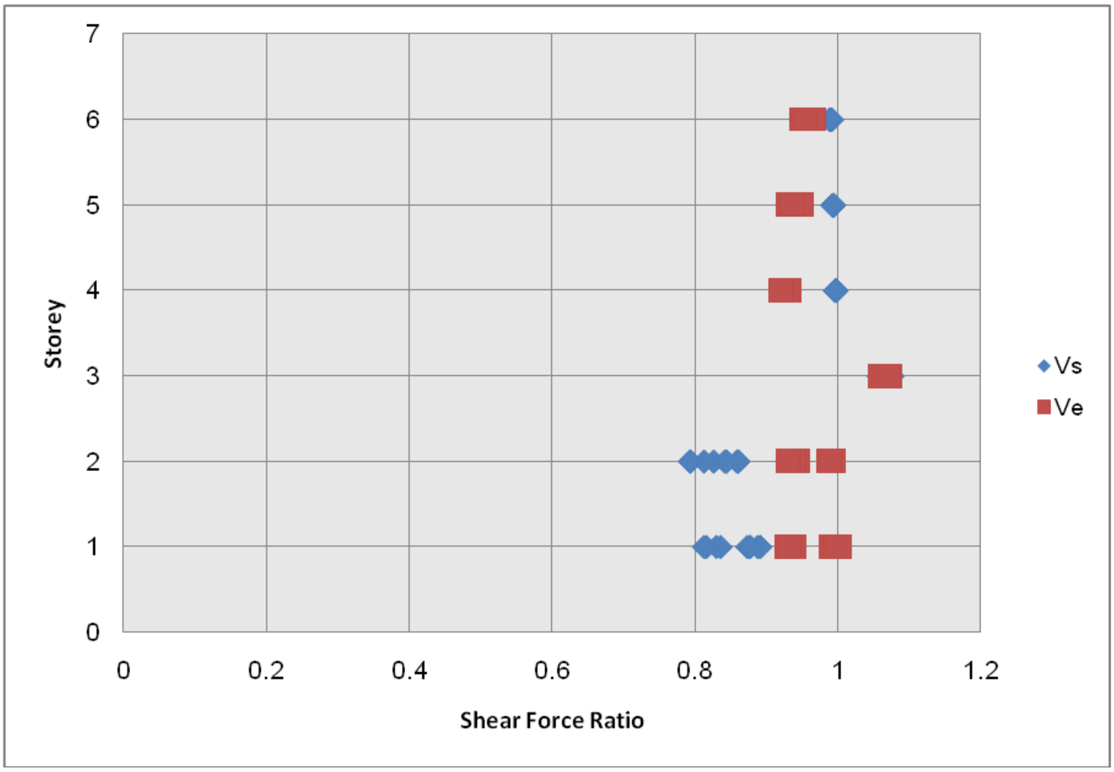


a)

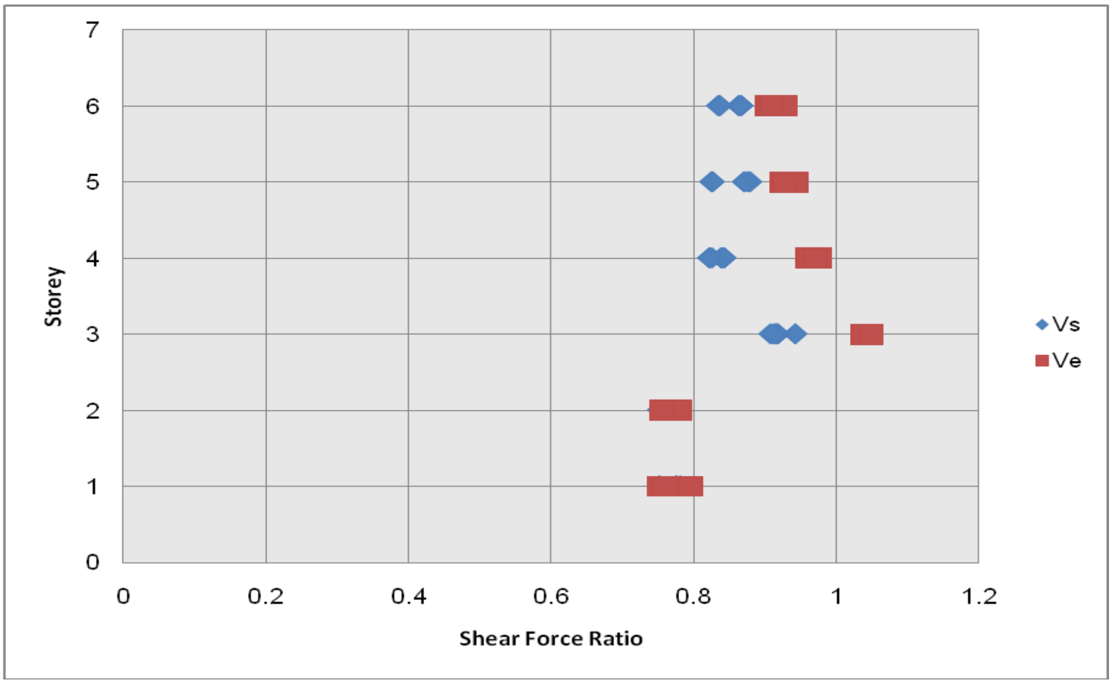


b)

Fig G18 shear force ratio in beams for 6SR56 a) x-direction b) y-direction

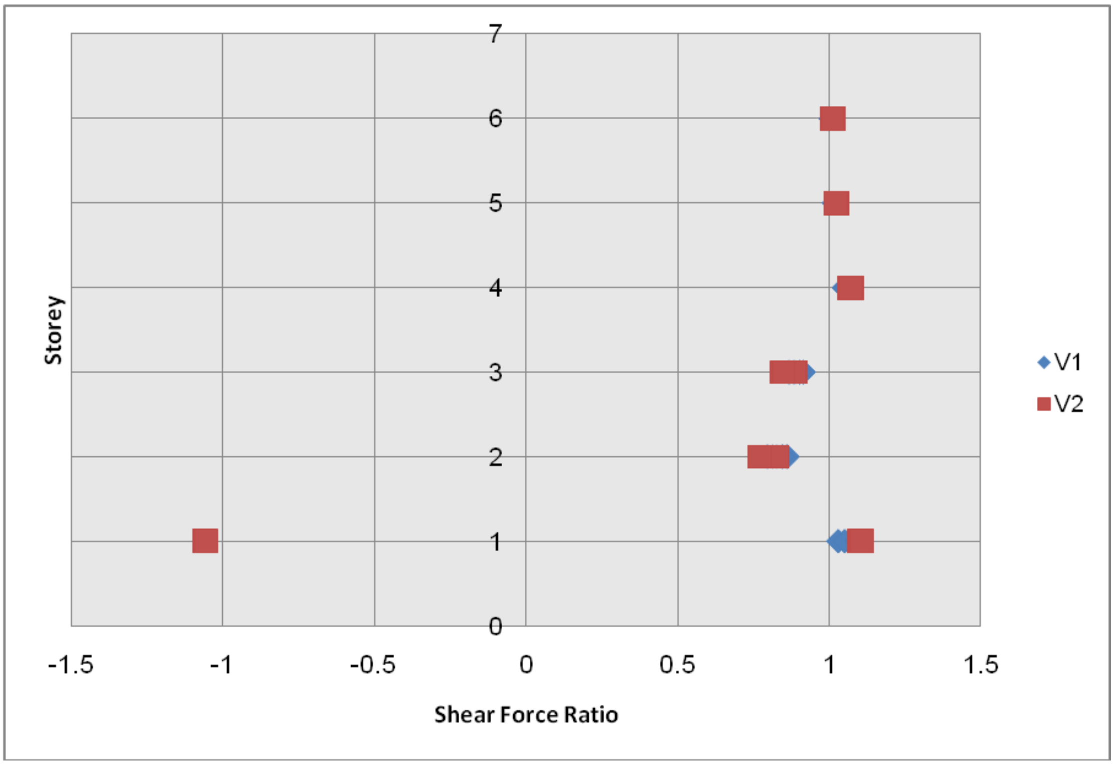


a)

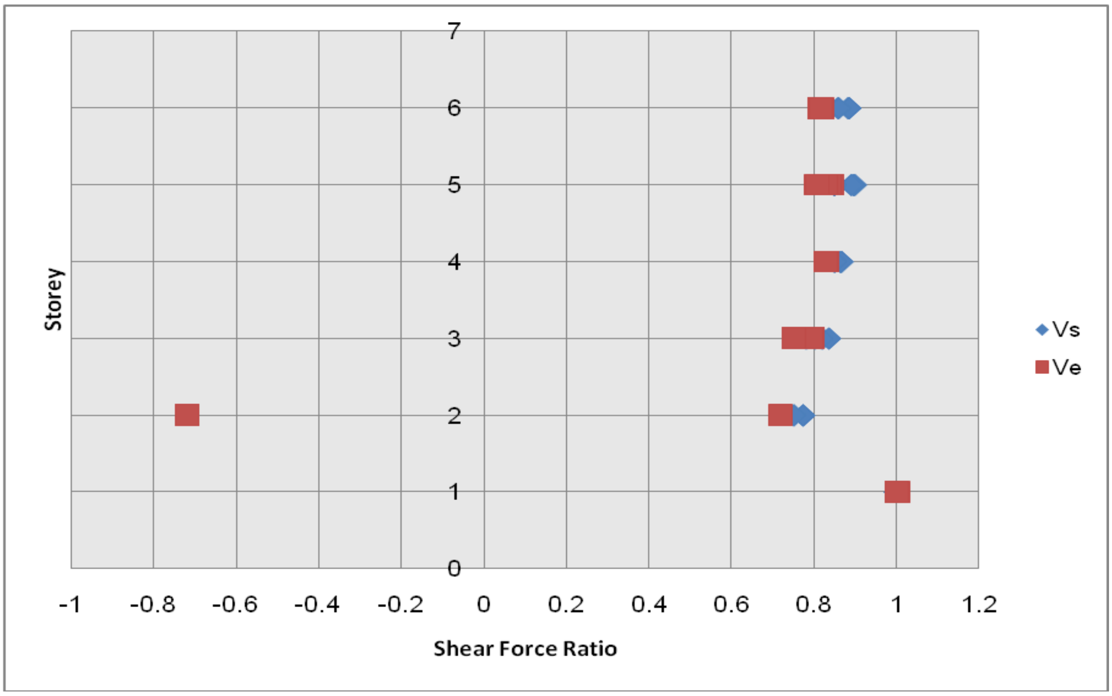


b)

Fig G19 shear force ratio in beams for 6SR12 a) x-direction b) y-direction

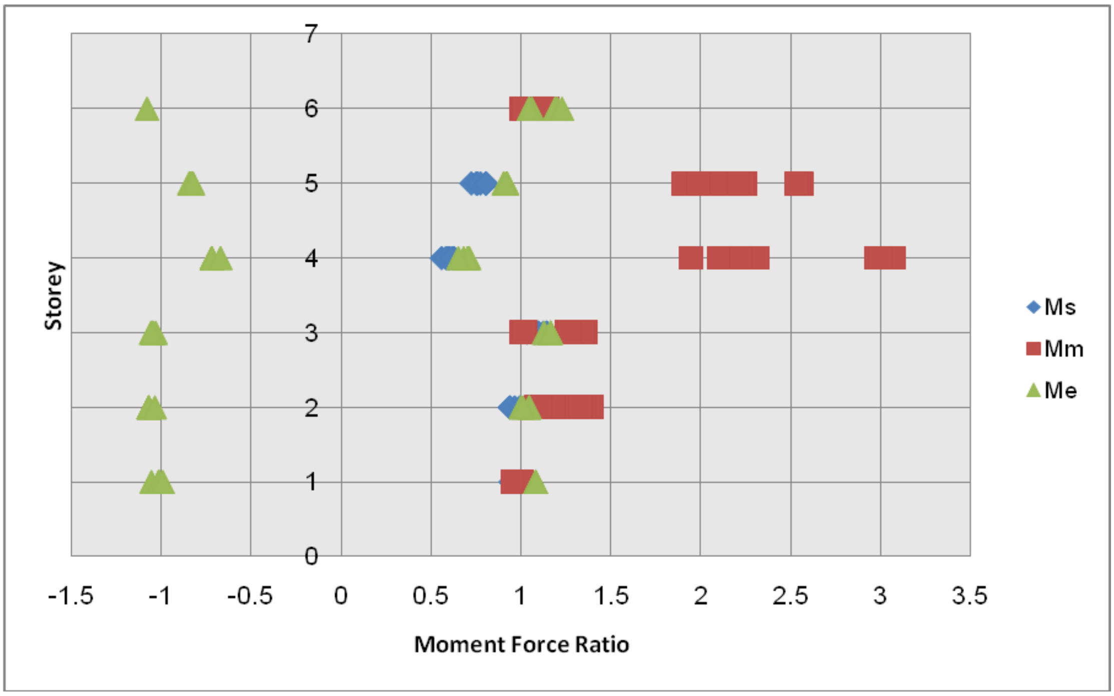


a)

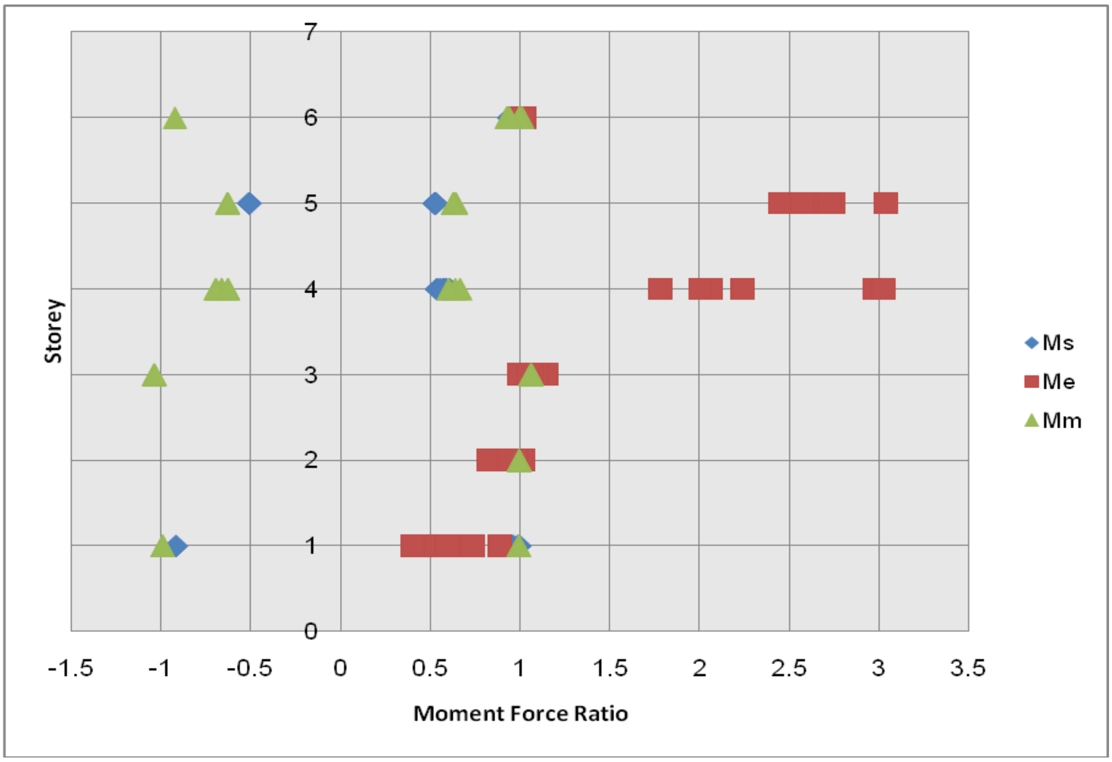


b)

Fig G20 shear force ratio in beams for 6SR23 a) x-direction b) y-direction

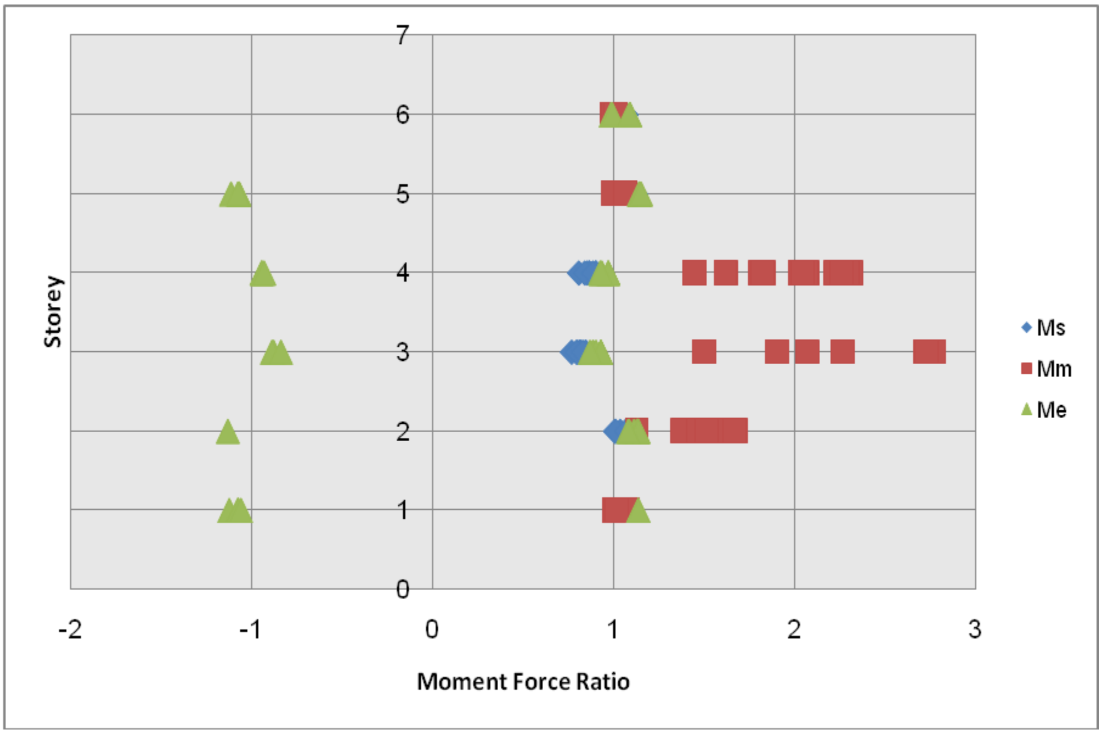


a)

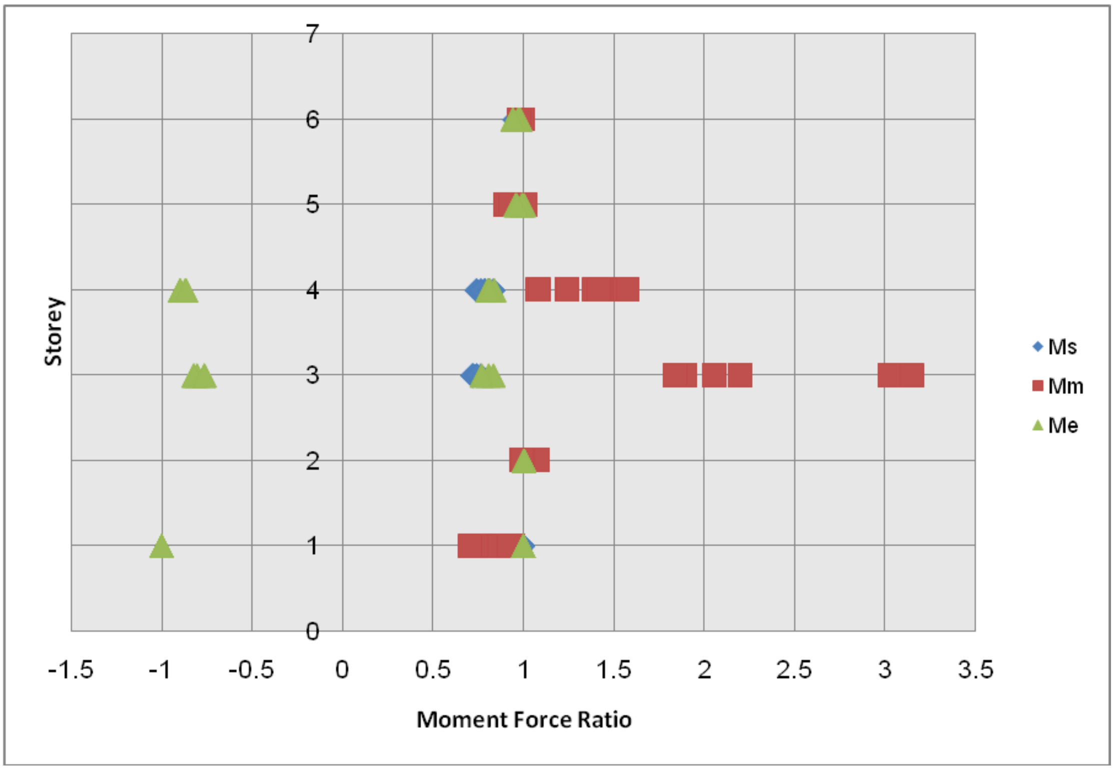


b)

Fig G21 Moment force ratio in beams for 6SR45 a) x-direction b) y-direction

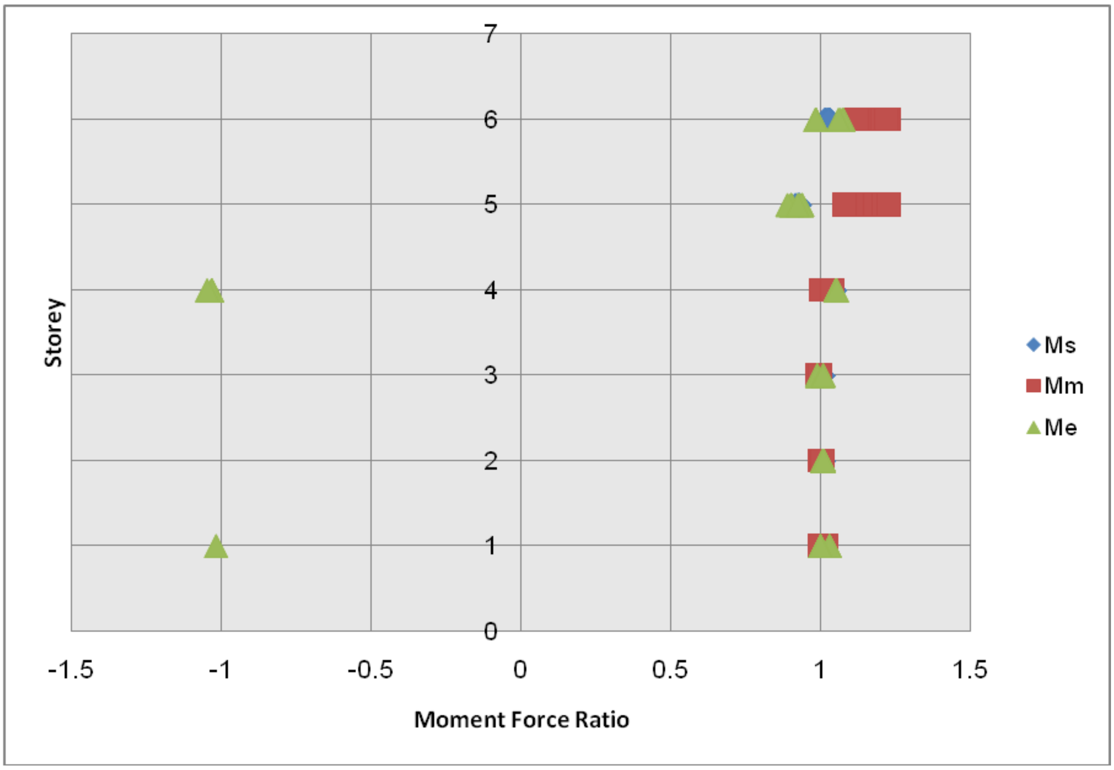


a)

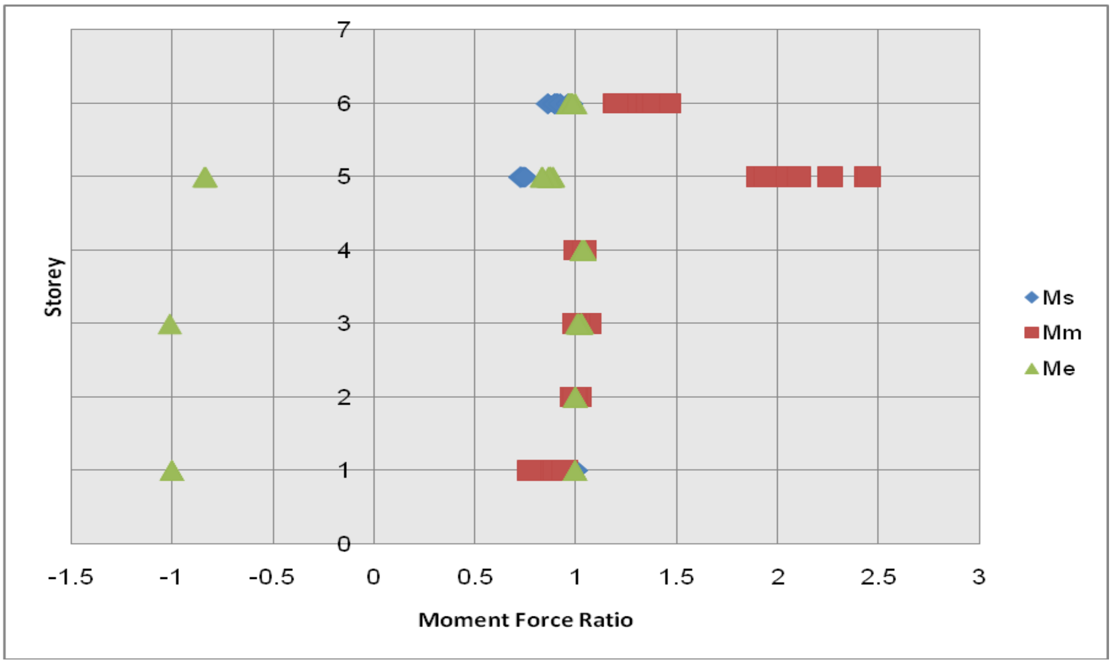


b)

Fig G22 Moment force ratio in beams for 6SR34 a) x-direction b) y-direction

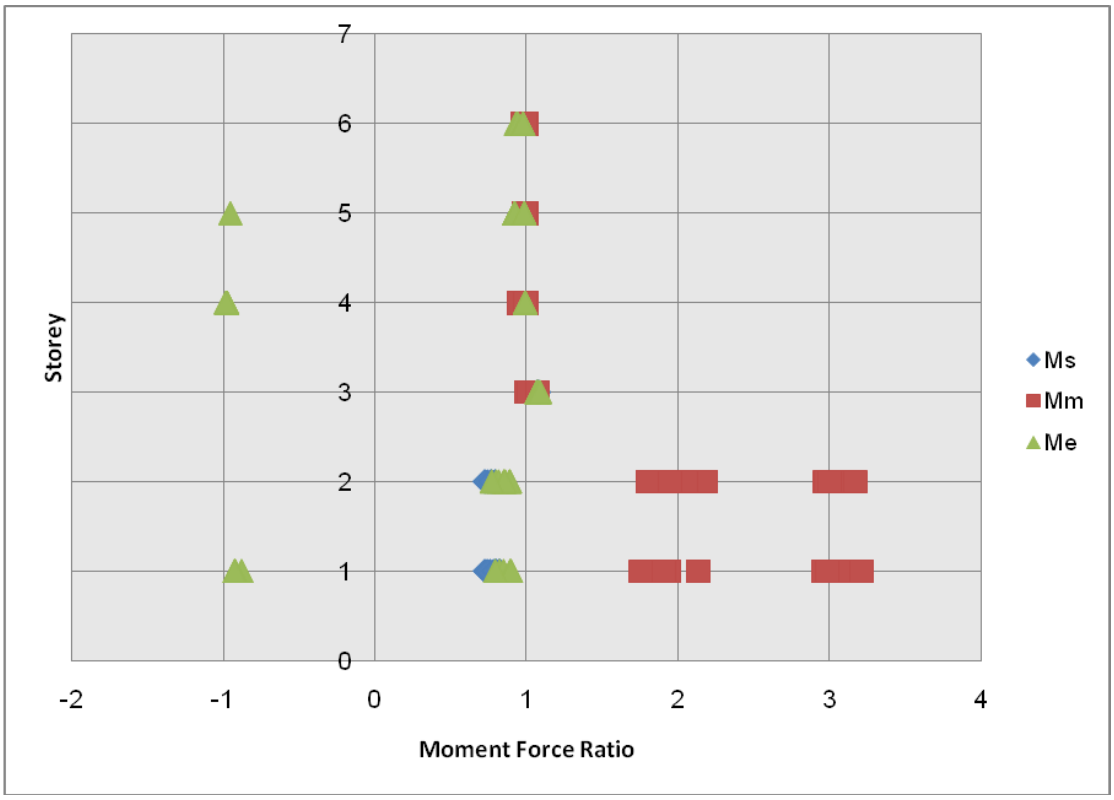


a)

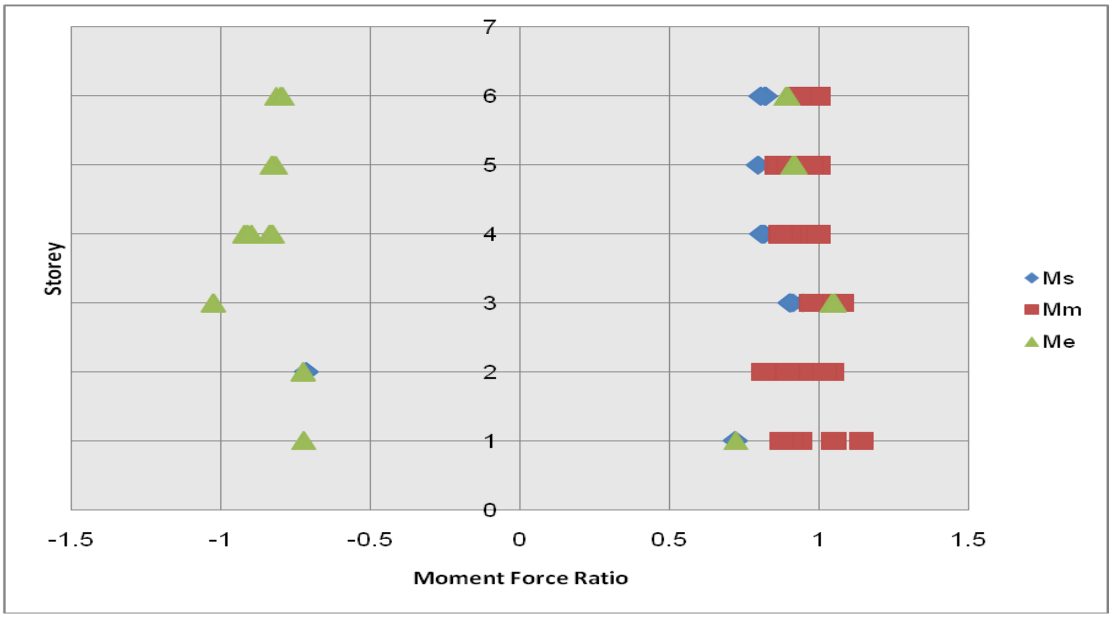


b)

Fig G23 Moment force ratio in beams for 6SR56 a) x-direction b) y-direction

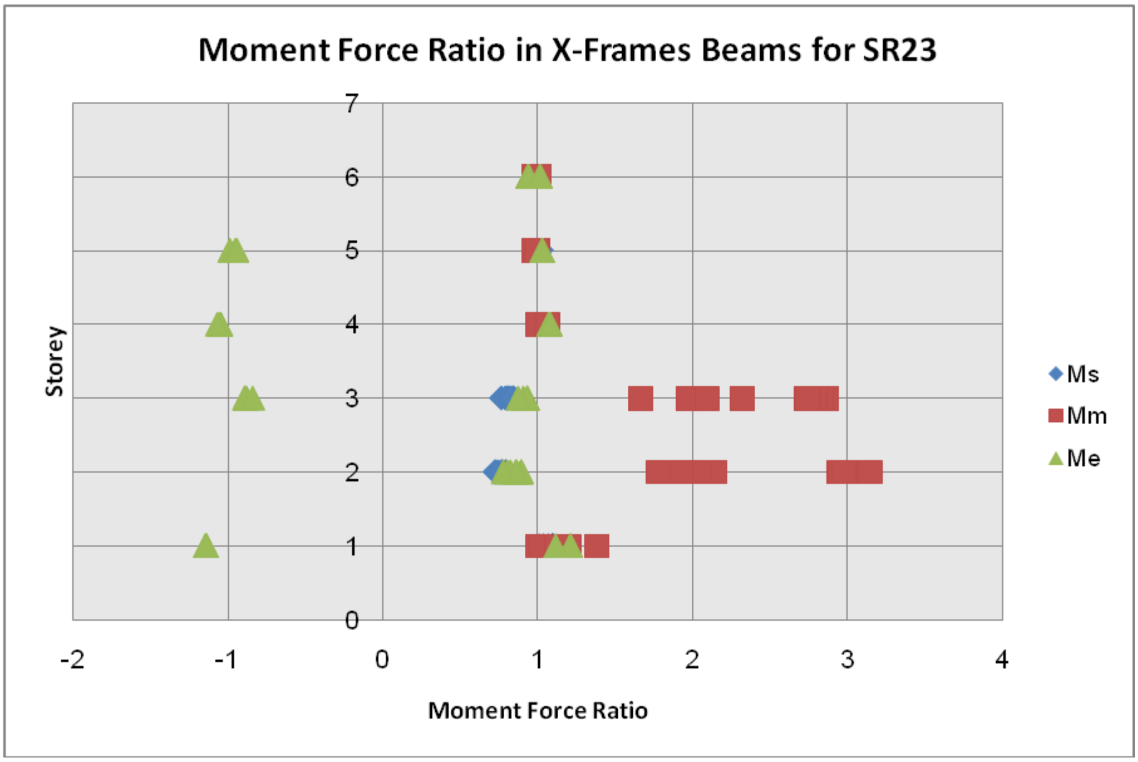


a)

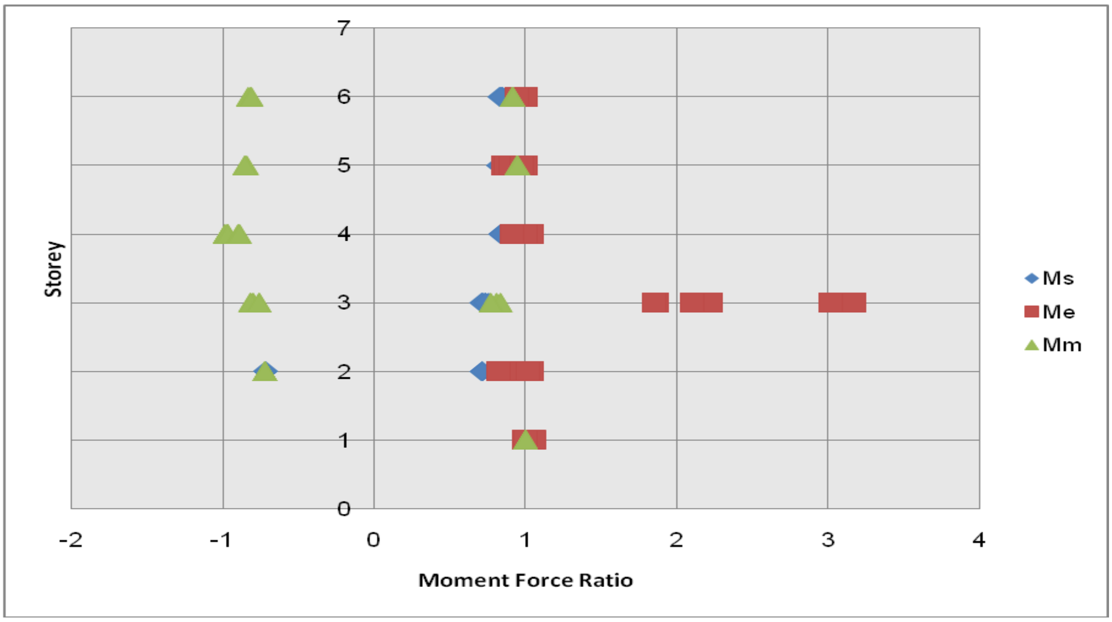


b)

Fig G24 Moment force ratio in beams for 6SR12 a) x-direction b) y-direction



a)

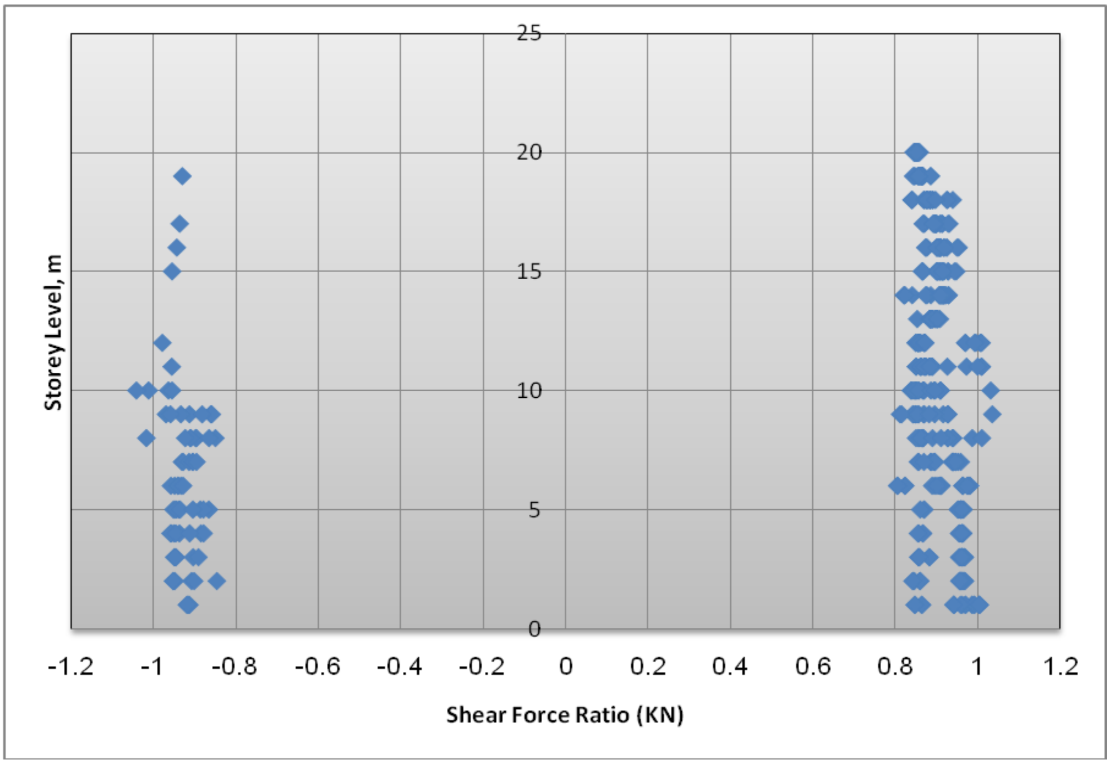


b)

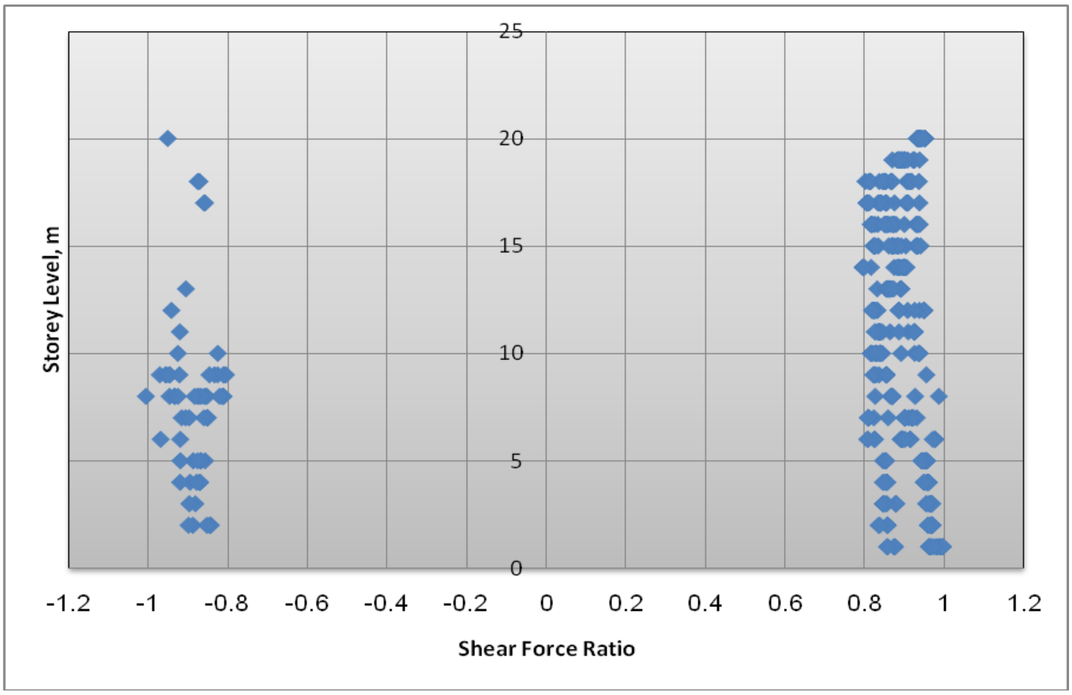
Fig G25 Moment force ratio in beams for 6SR23 a) x-direction b) y-direction

APPENDIX H

FORCE DISTRIBUTION IN 20PRMRF MEMBERS

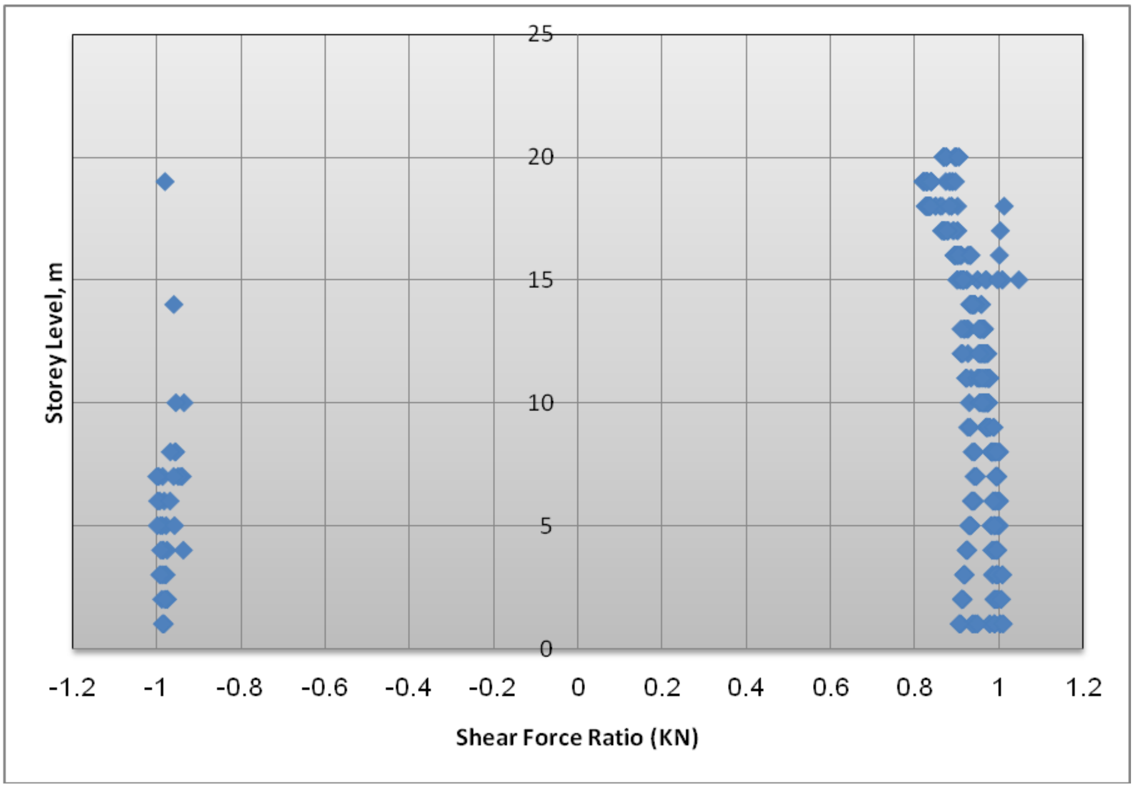


a)

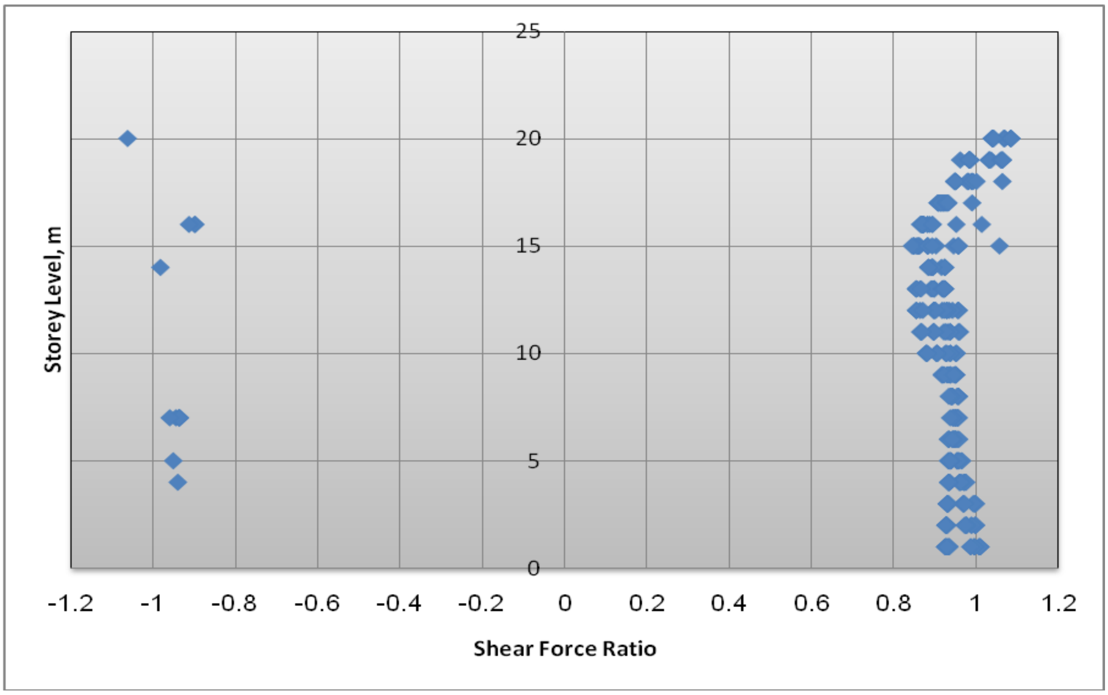


b)

Fig H1 Shear Force ratio in columns for 20SR8-13 a) x-direction b) y-direction

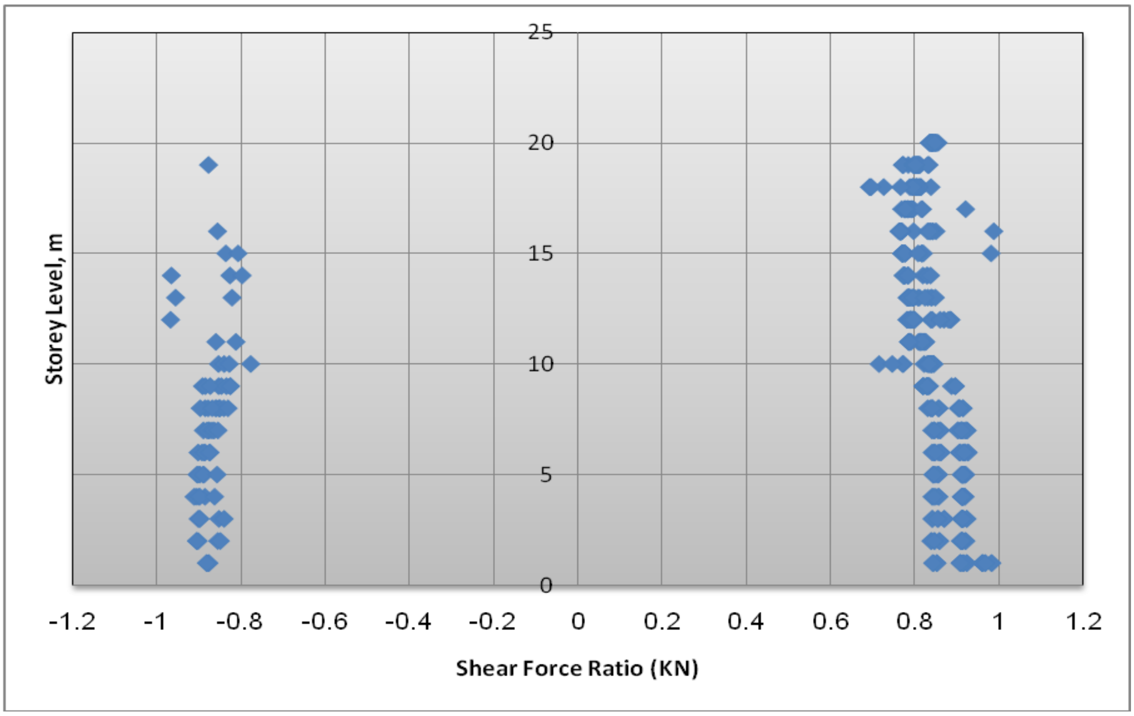


a)

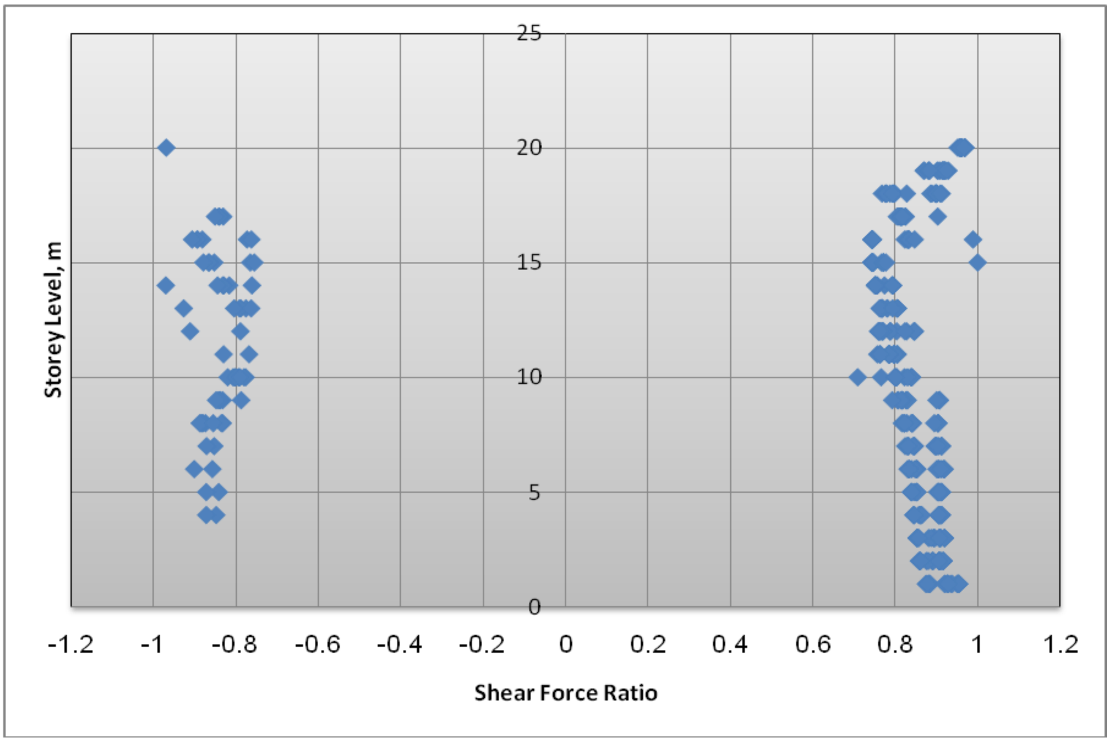


b)

Fig H2 Shear Force ratio in columns for 20SR1-6 a) x-direction b) y-direction

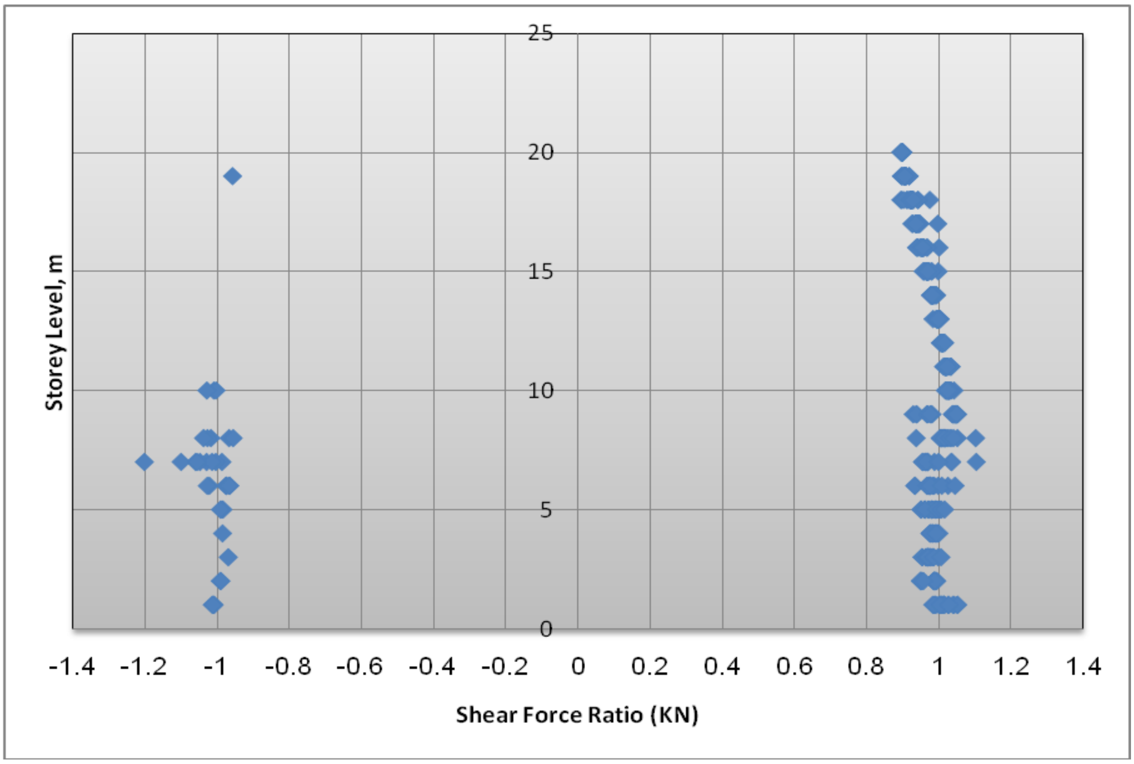


a)

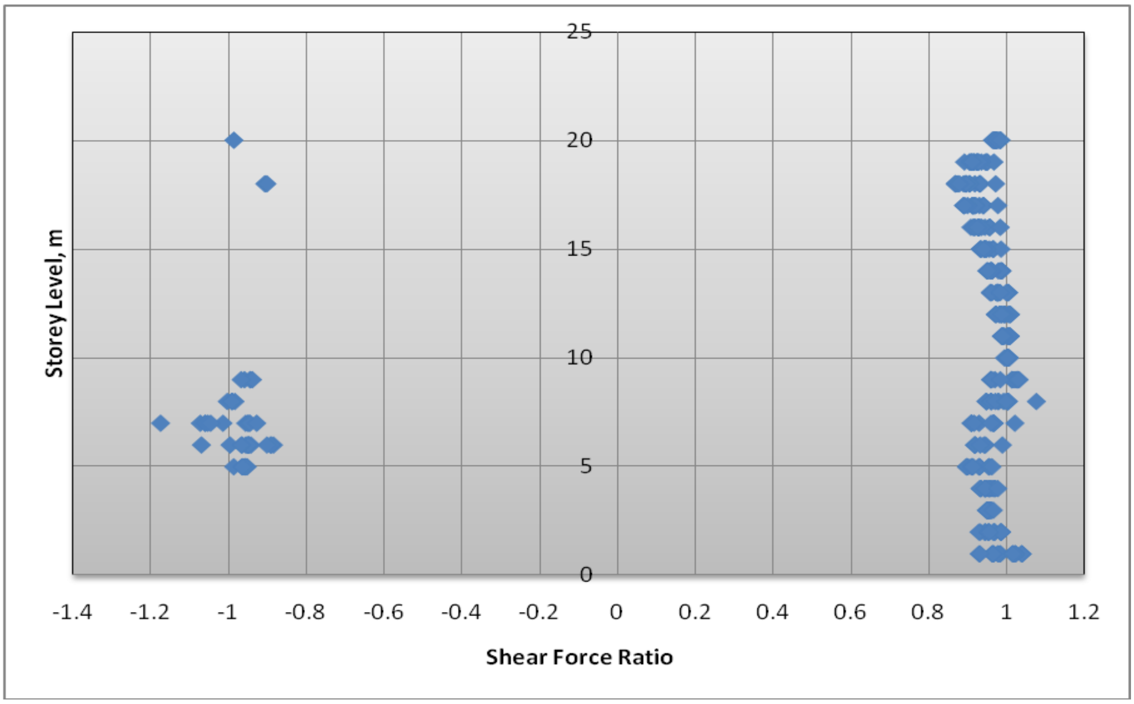


b)

Fig H3 Shear Force ratio in columns for 20SR4-9 a) x-direction b) y-direction



a)



b)

Fig H4 Shear Force ratio in columns for 20SR13-18 a) x-direction b) y-direction

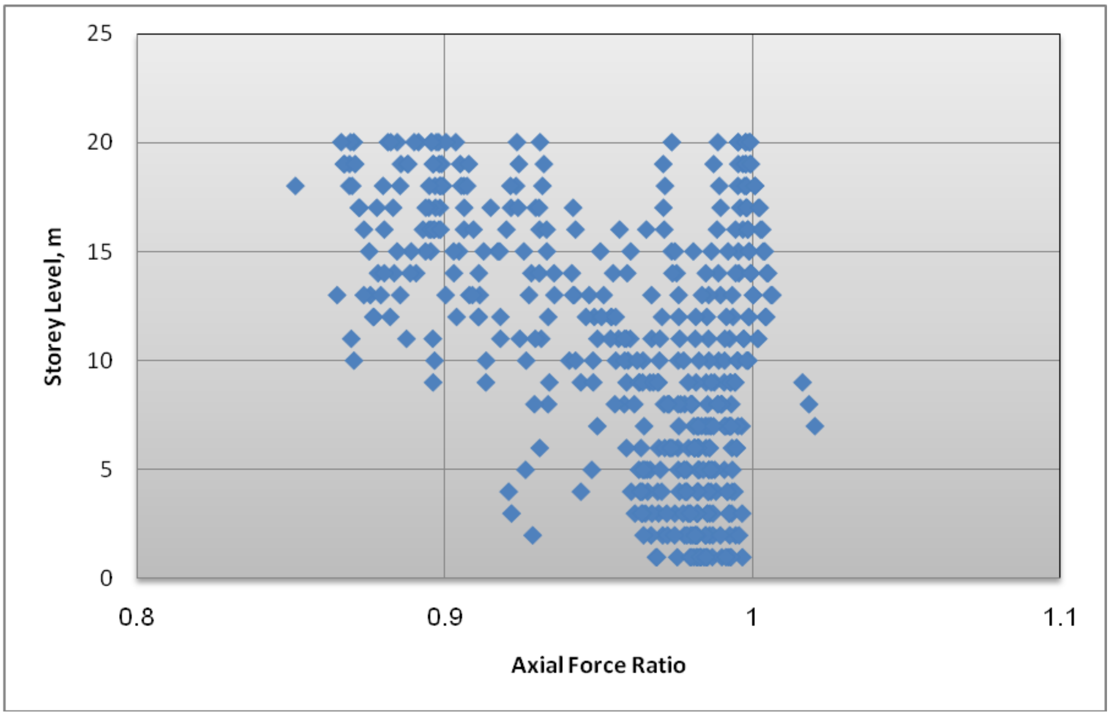
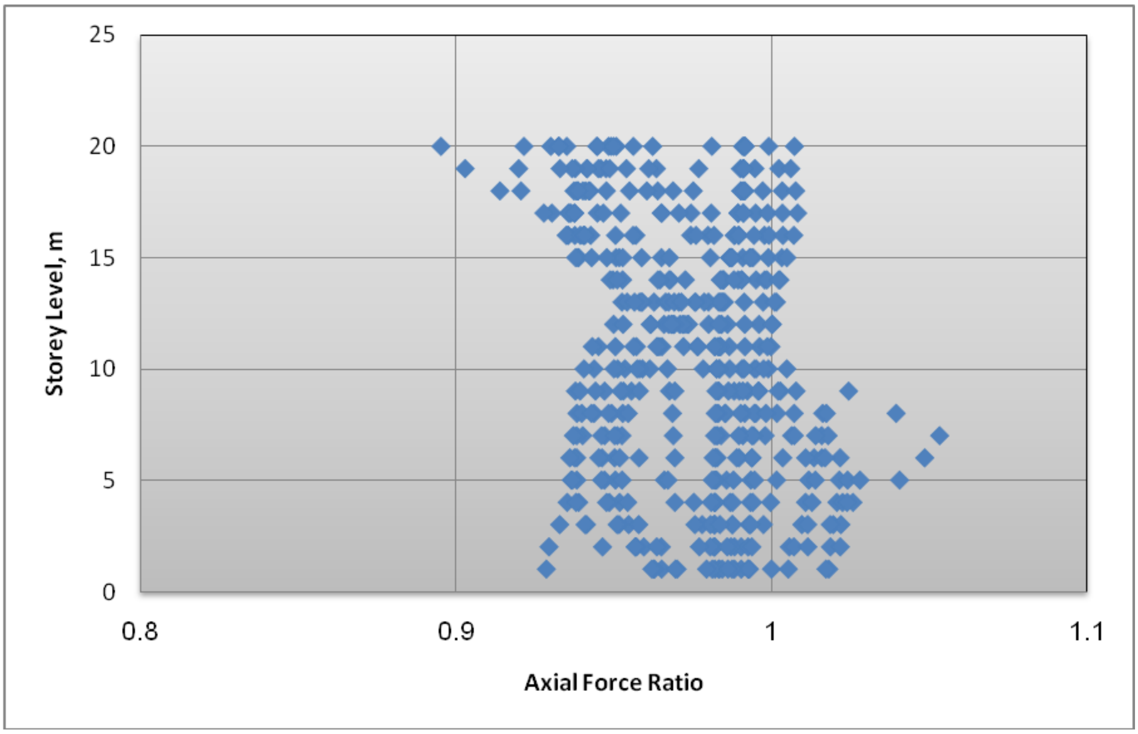


Fig H5 axial Force ratio in columns for 20SR8-13



b)

Fig H6 axial Force ratio in columns for 20SR1-6

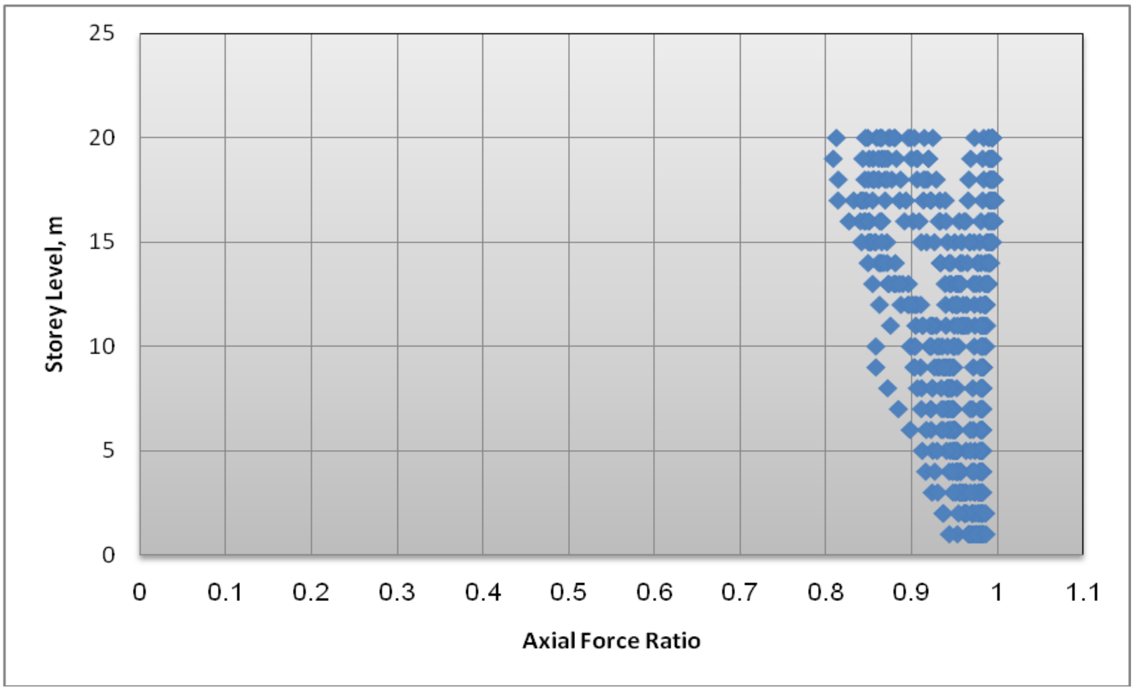


Fig H7 axial Force ratio in columns for 20SR4-9

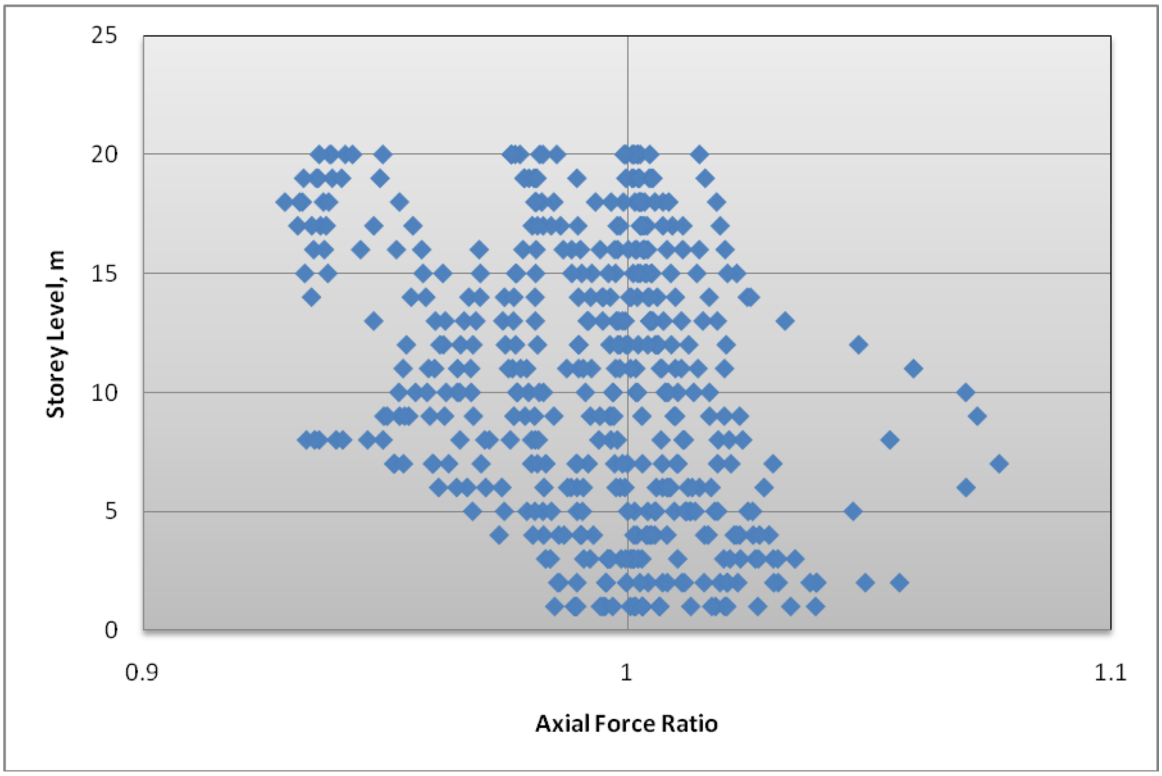
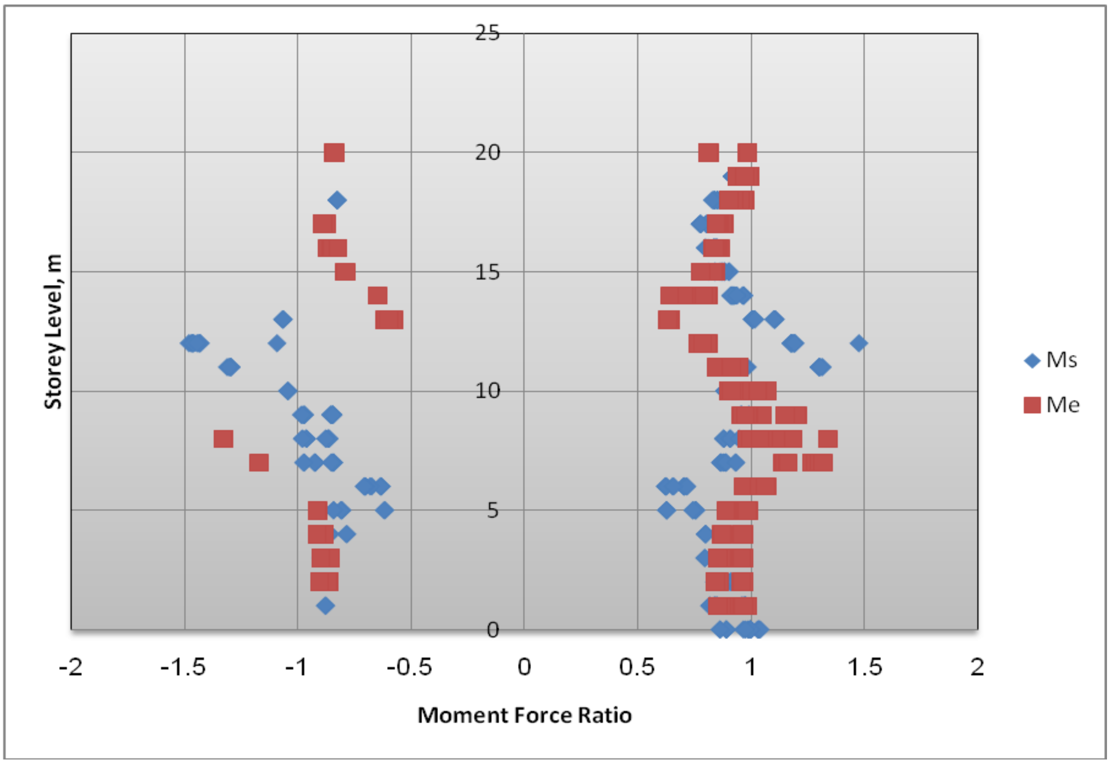
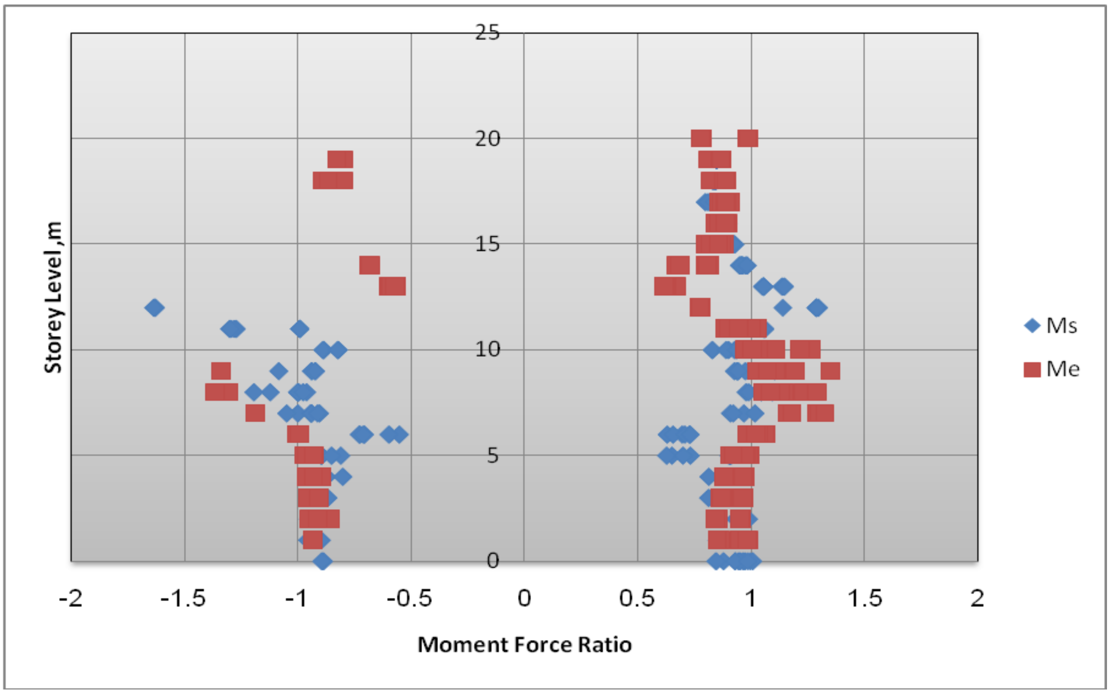


Fig H8 axial Force ratio in columns for 20SR13-18

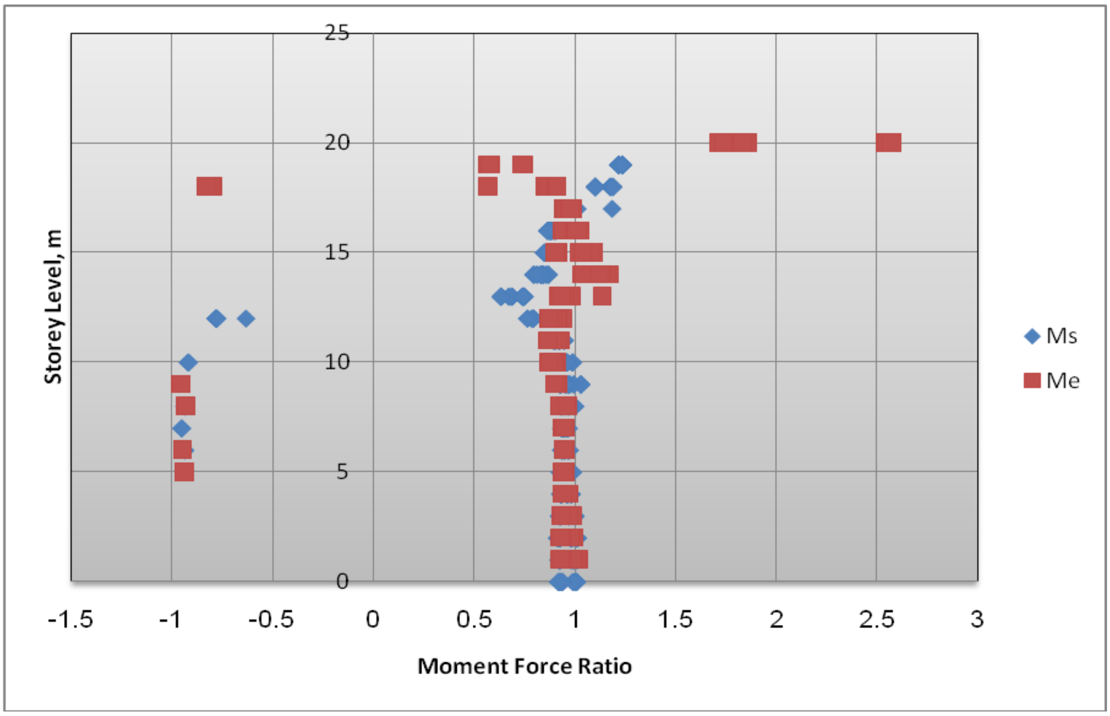


a)

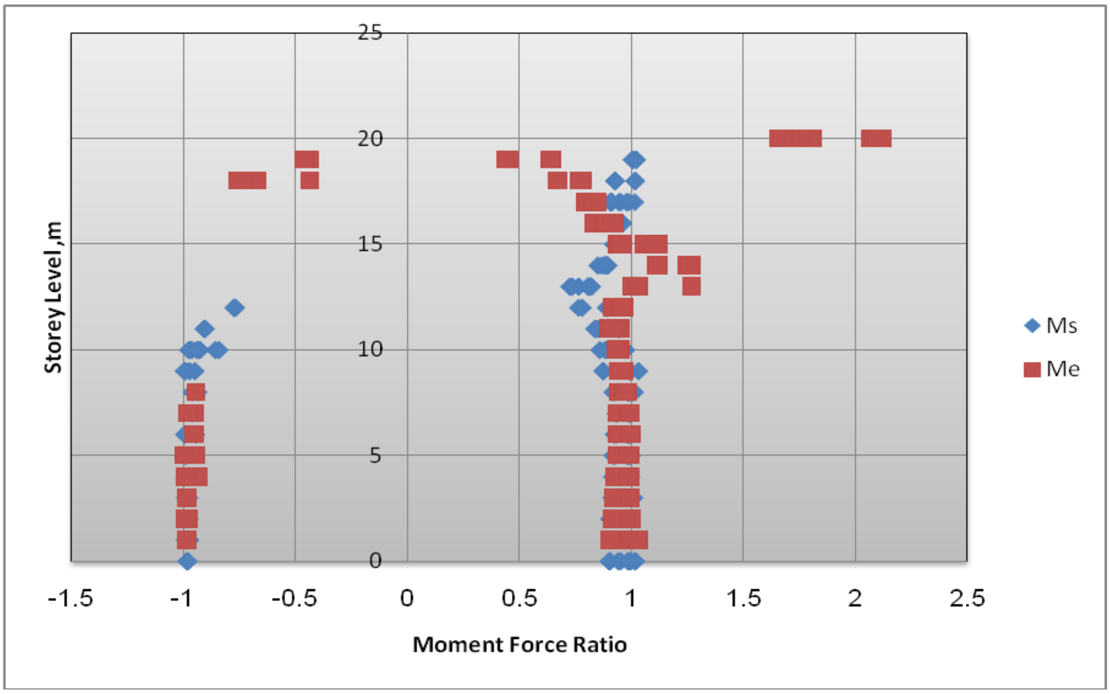


b)

Fig H7 Moment Force ratio in columns for 20SR8-13 a) x-direction b) y-direction

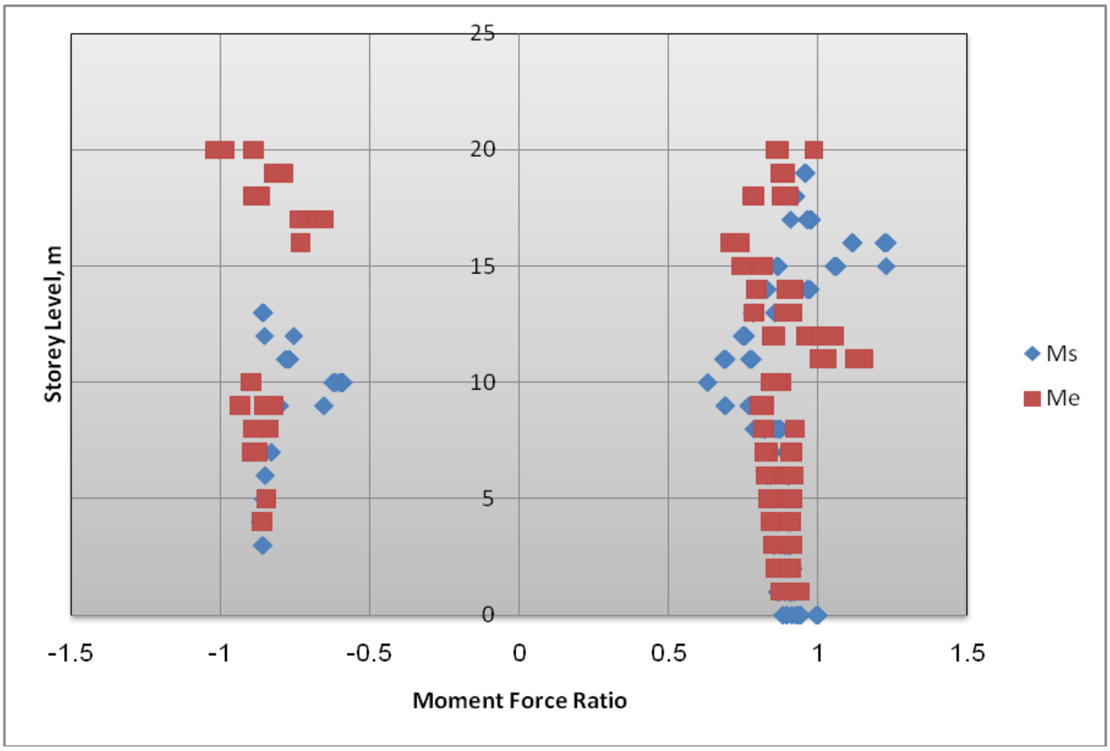


a)

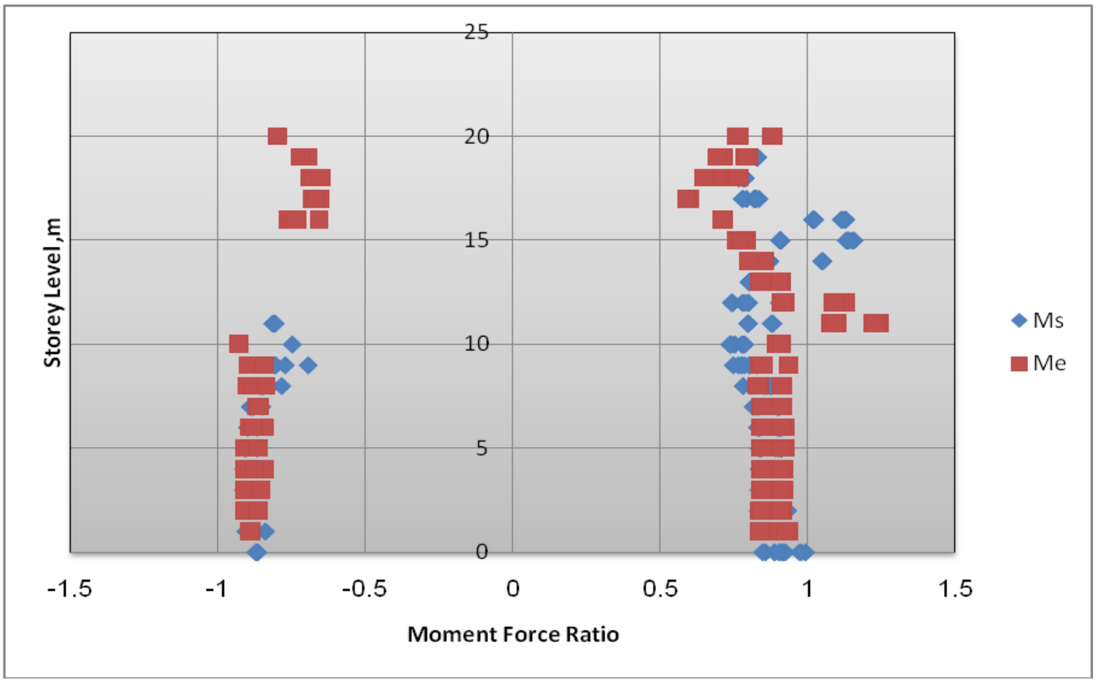


b)

Fig H8 Moment Force ratio in columns for 20SR1-6 a) x-direction b) y-direction

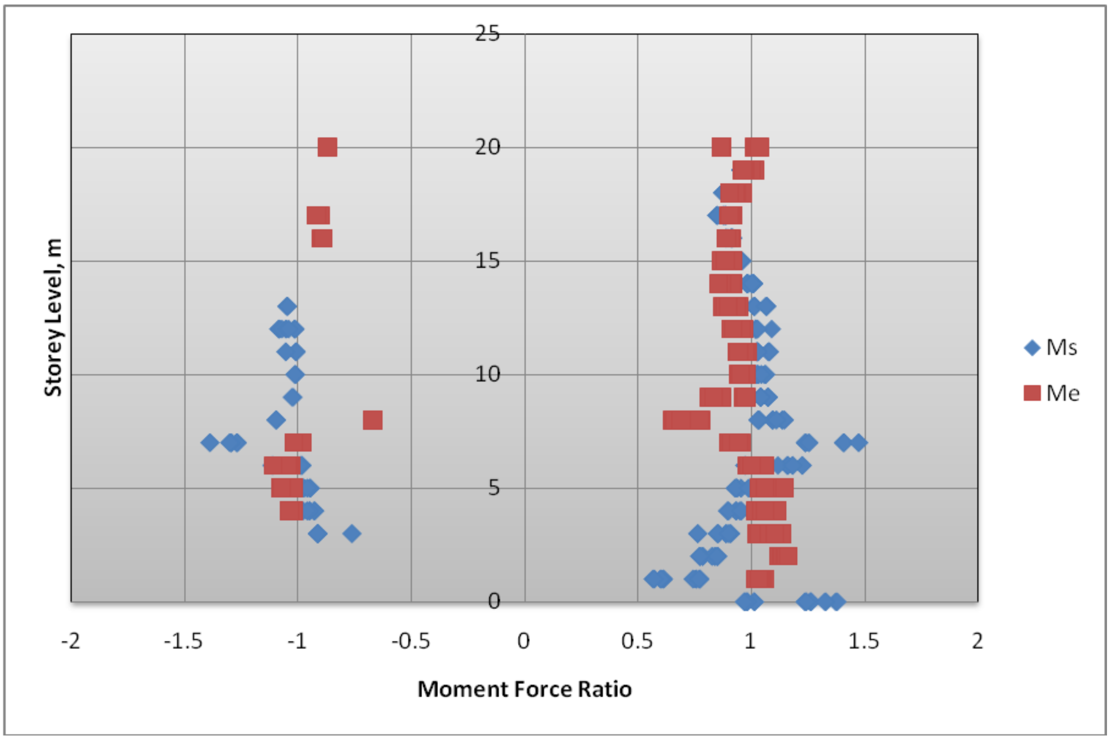


a)

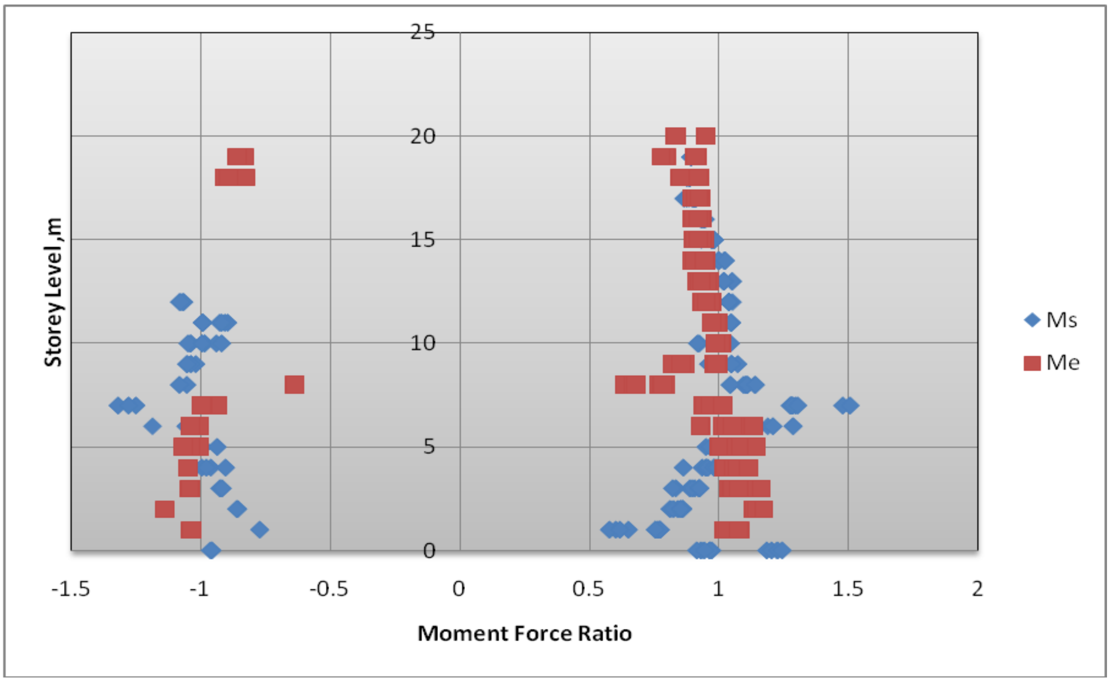


b)

Fig H9 Moment Force ratio in columns for 20SR4-9 a) x-direction b) y-direction

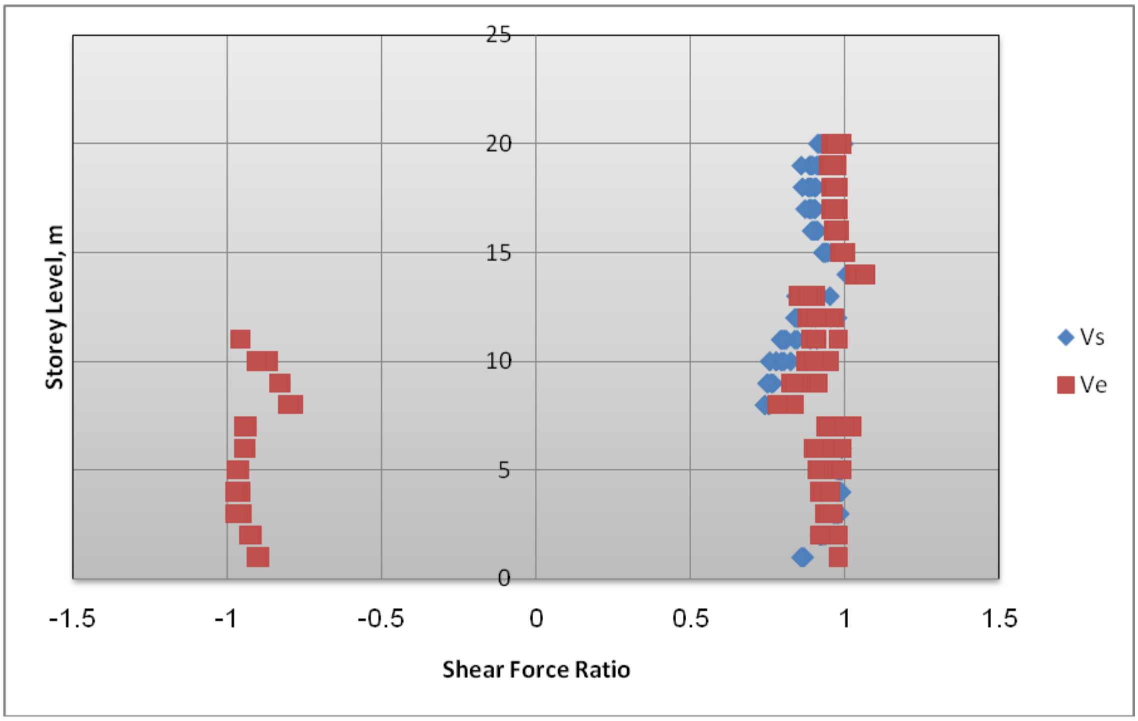


a)

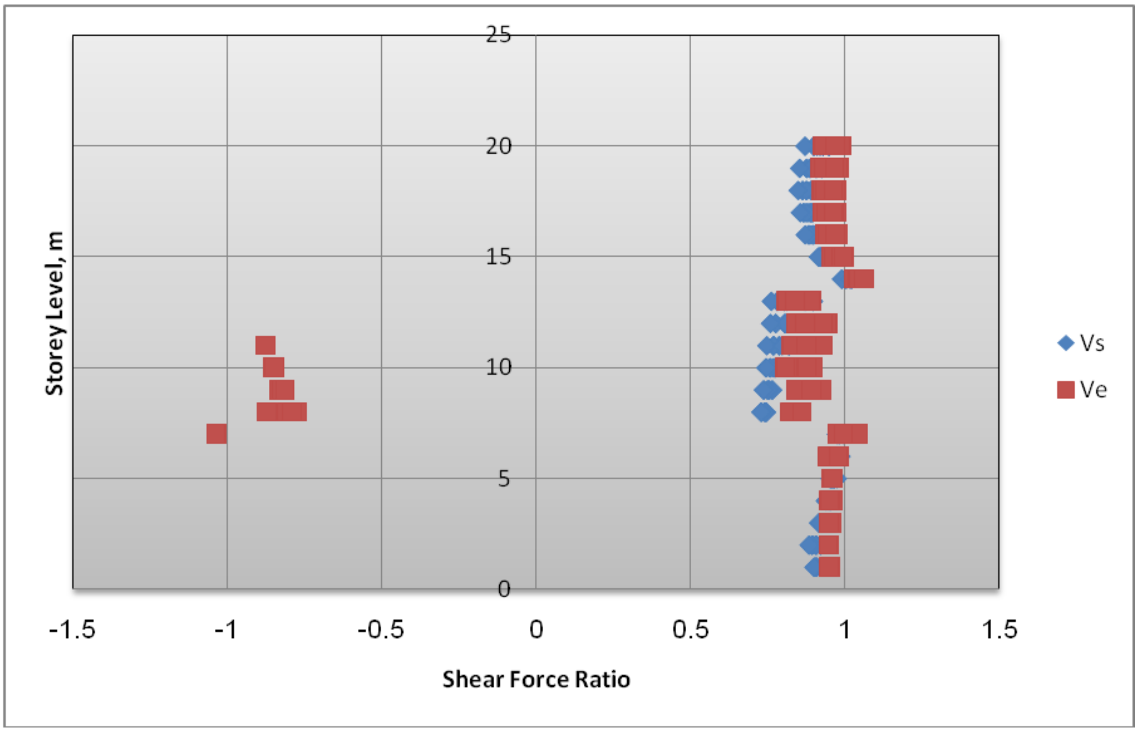


b)

Fig H10 Moment Force ratio in columns for 20SR13-18 a) x-direction b) y-direction

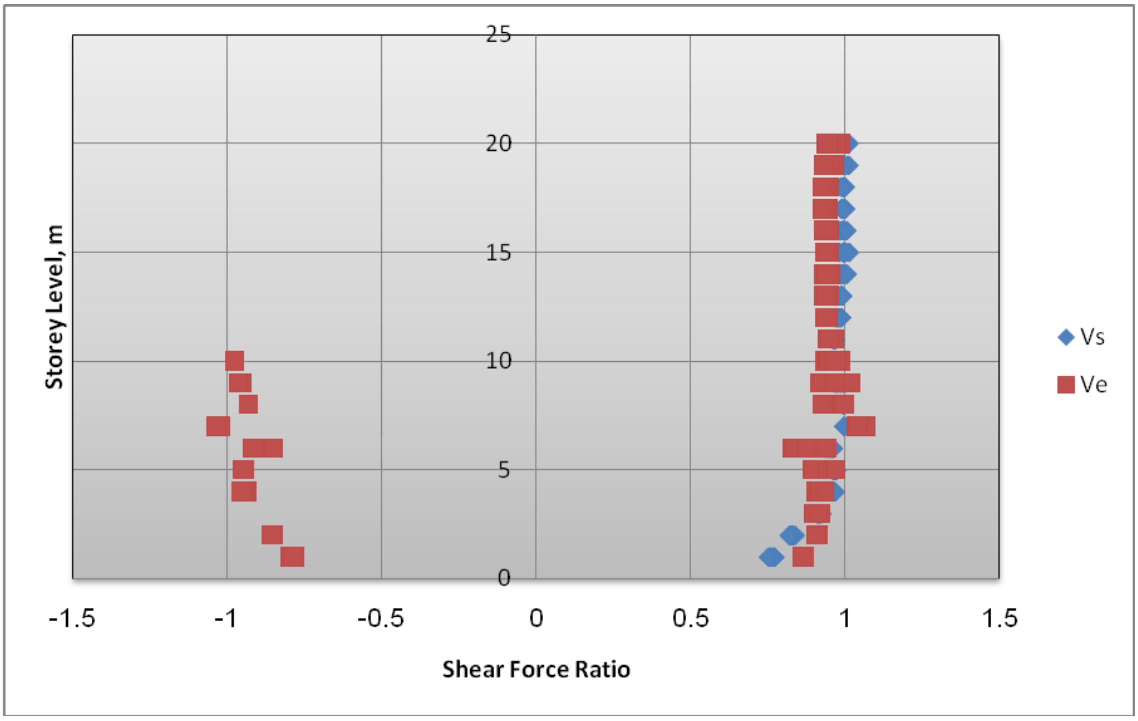


a)

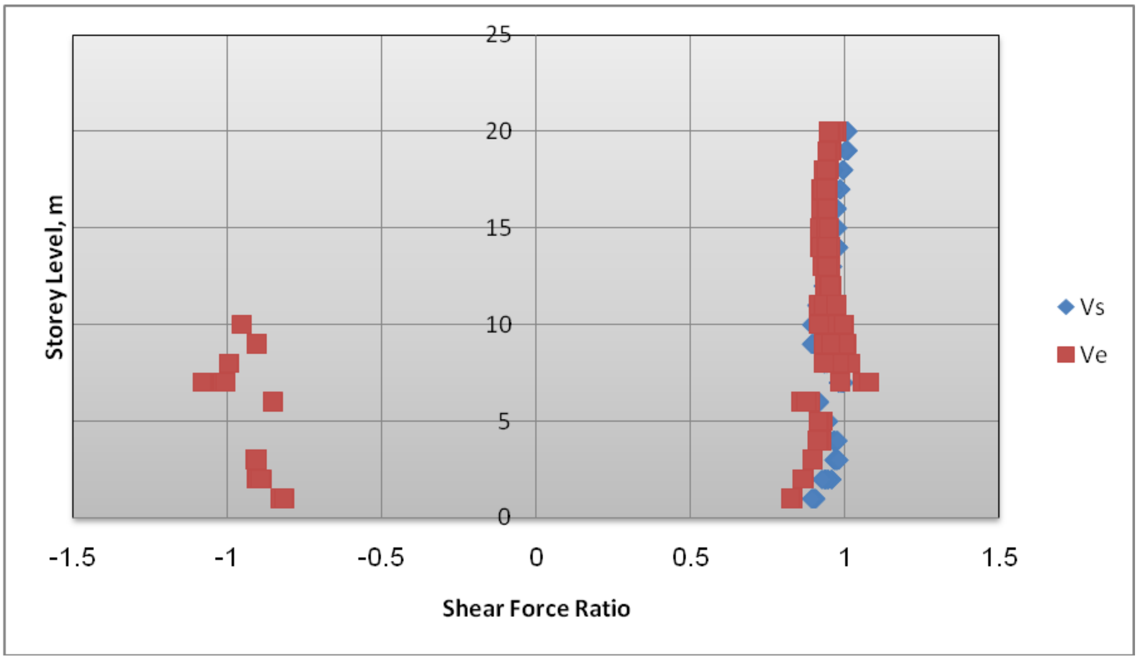


b)

Fig H11 Shear Force ratio in Beams for 20SR8-13 a) x-direction b) y-direction

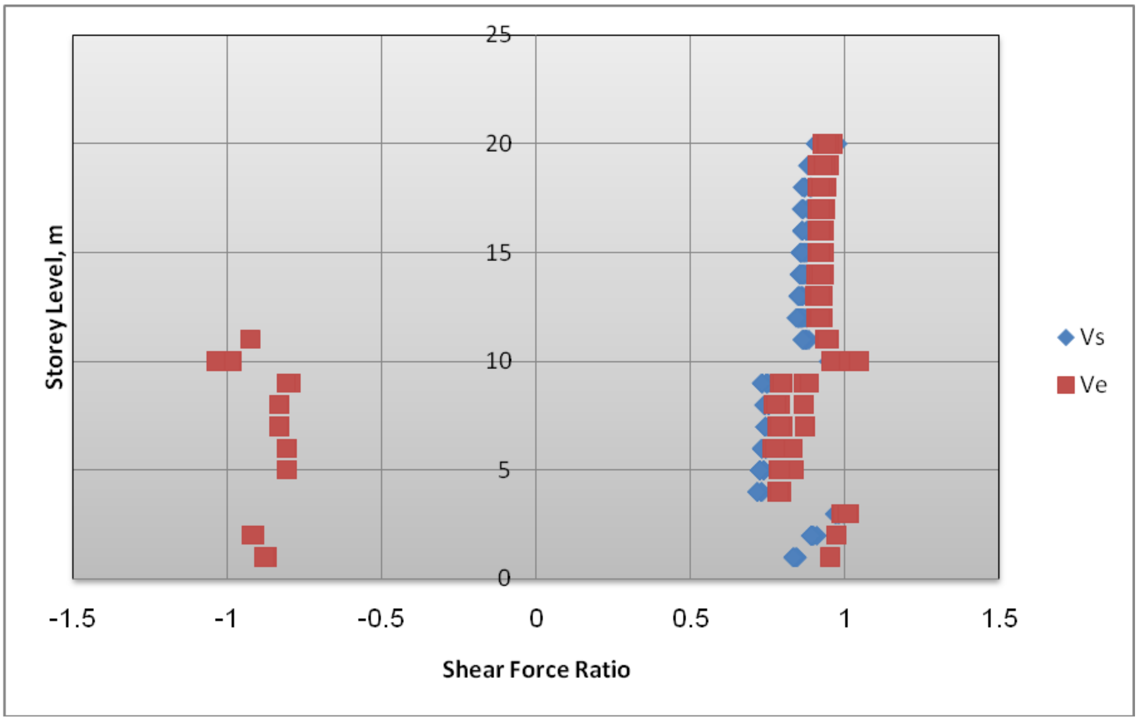


a)

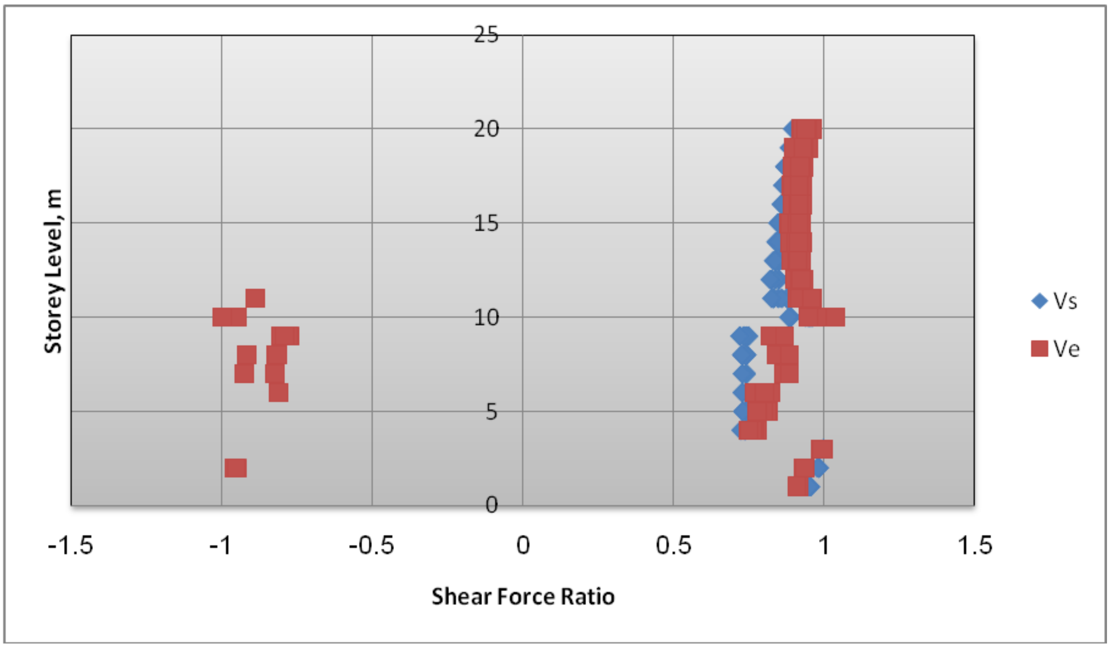


b)

Fig H12 Shear Force ratio in Beams for 20SR1-6 a) x-direction b) y-direction

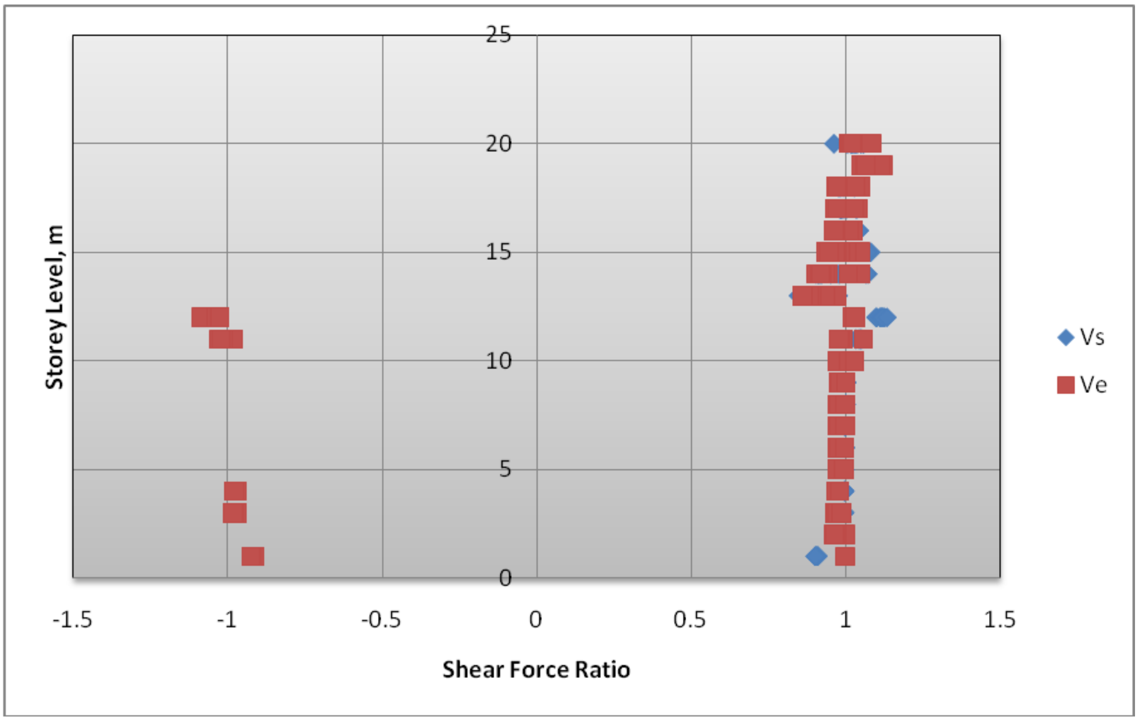


a)

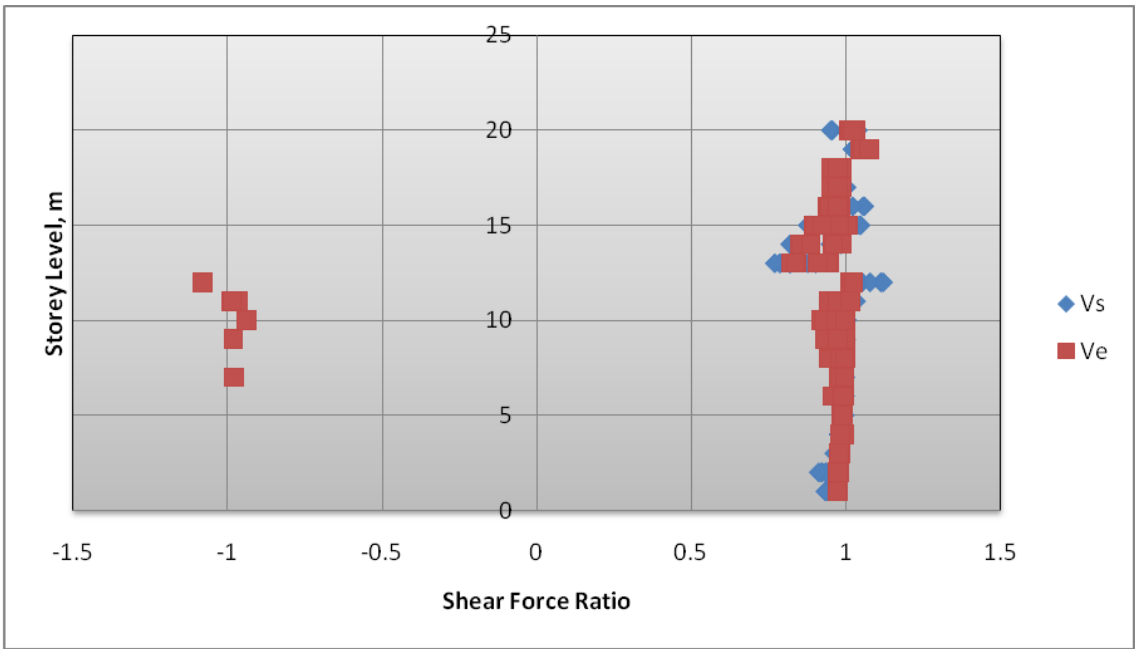


b)

Fig H13 Shear Force ratio in Beams for 20SR4-9 a) x-direction b) y-direction

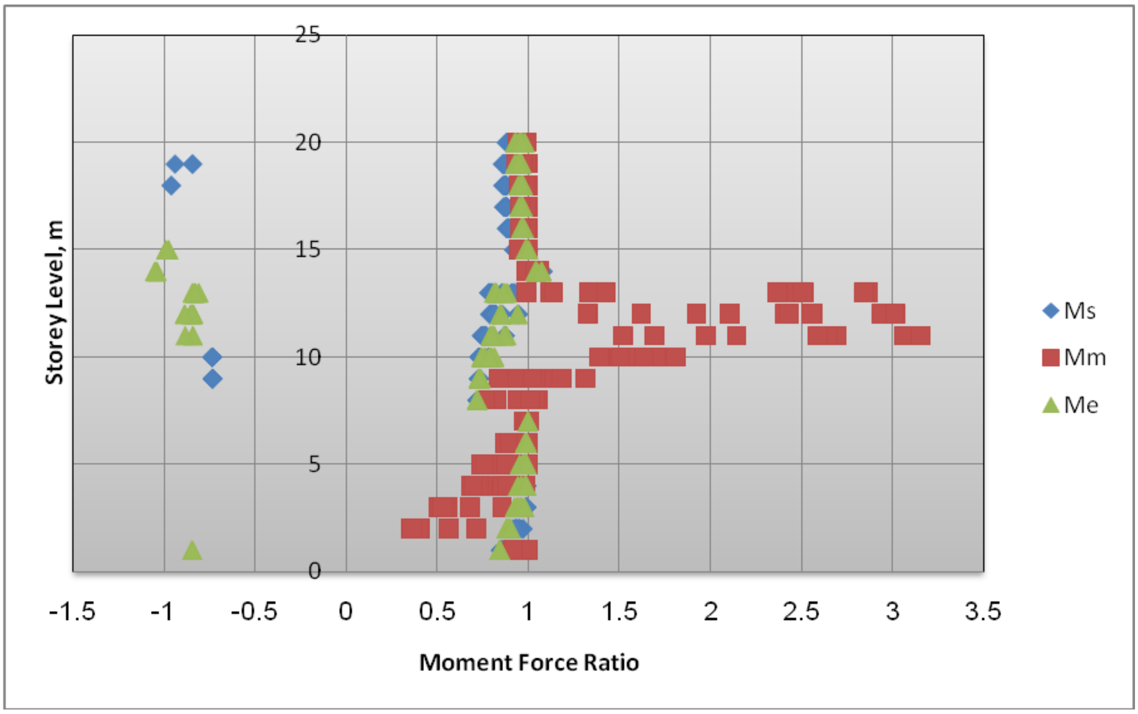


a)

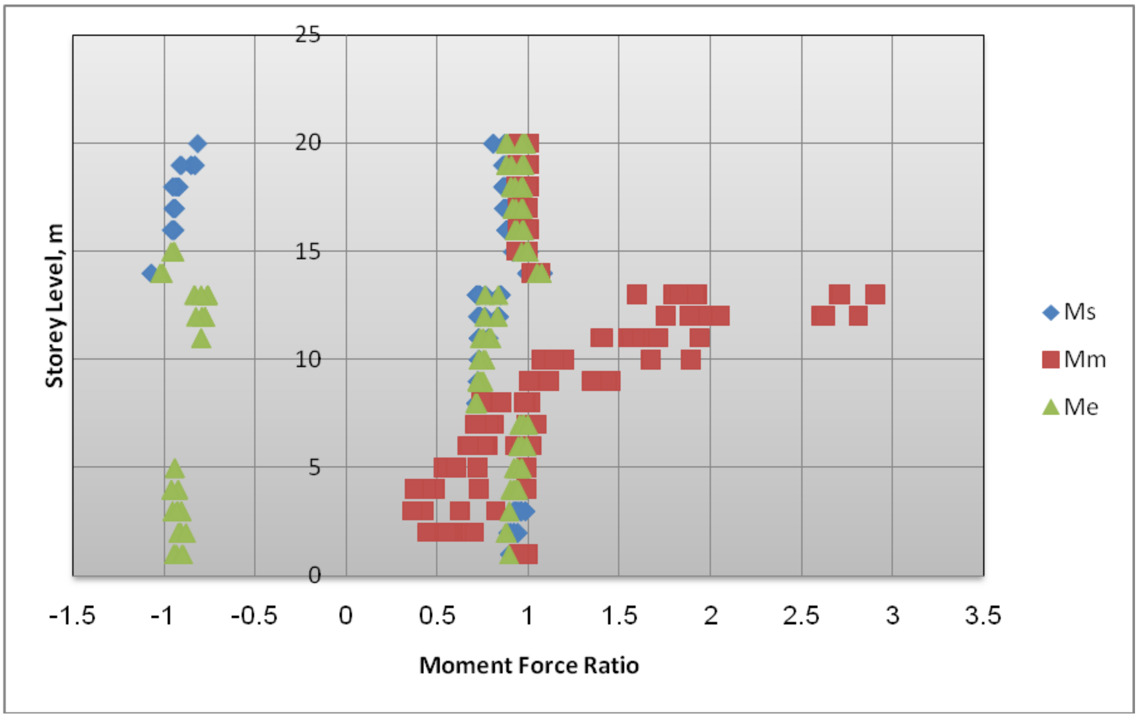


b)

Fig H14 Shear Force ratio in Beams for 20SR13-18 a) x-direction b) y-direction

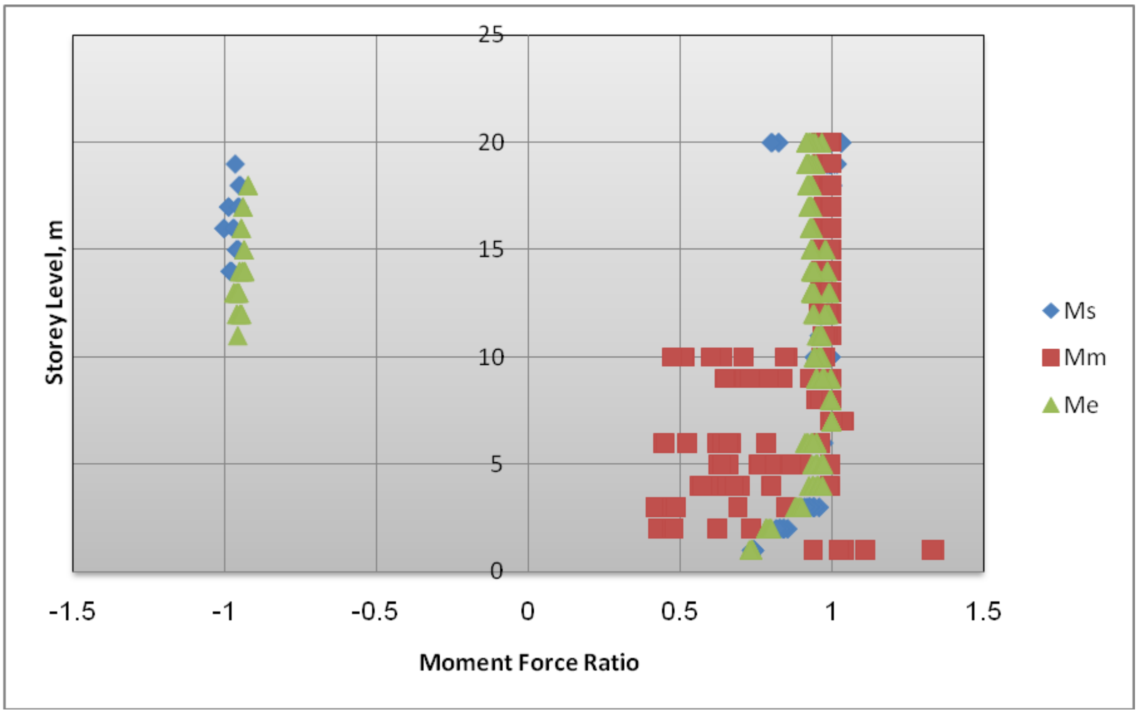


a)

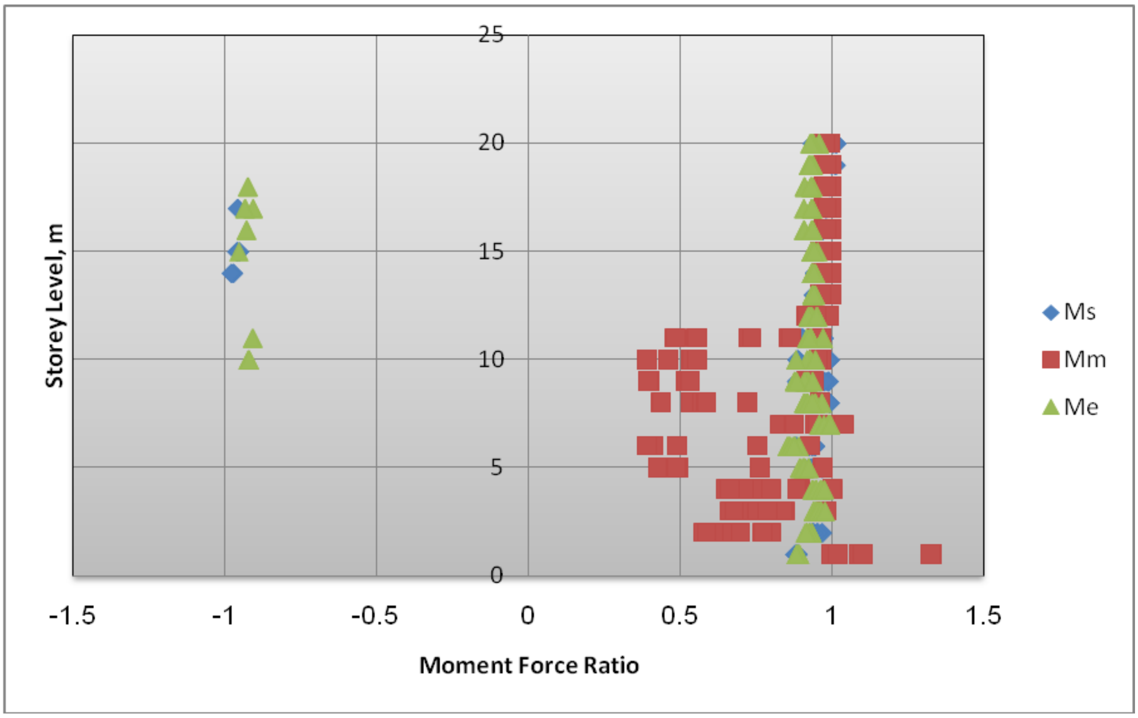


b)

Fig H15 Moment Force ratio in Beams for 20SR8-13 a) x-direction b) y-direction

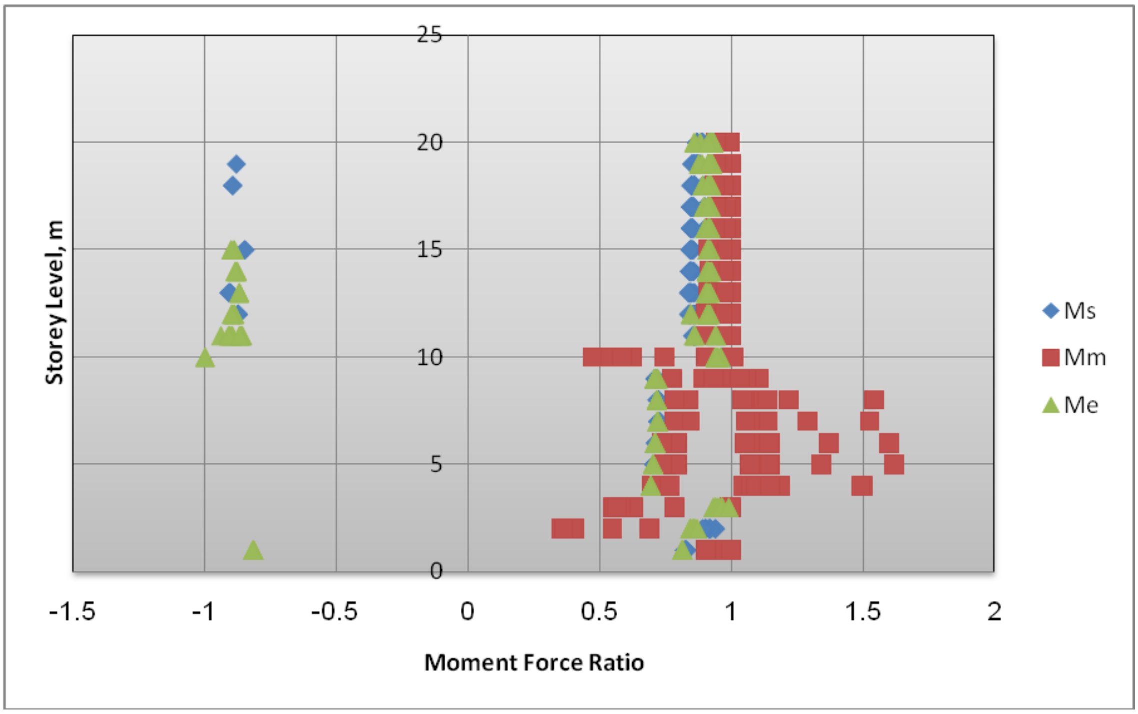


a)

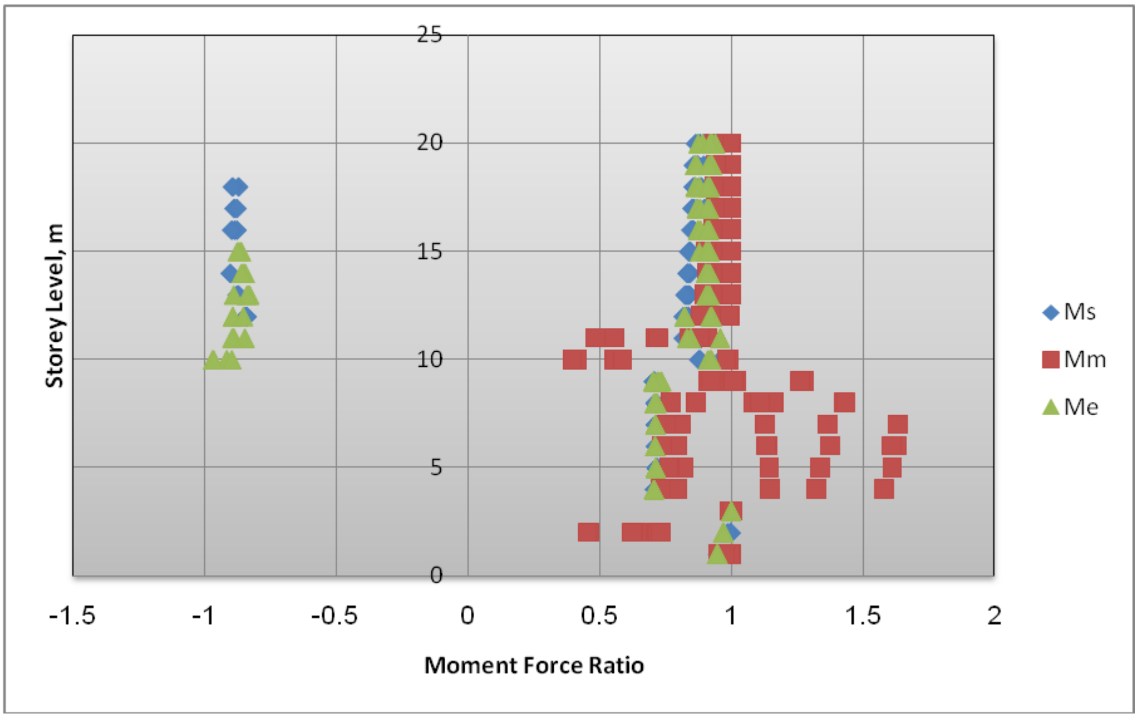


b)

Fig H16 Moment Force ratio in Beams for 20SR1-6 a) x-direction b) y-direction

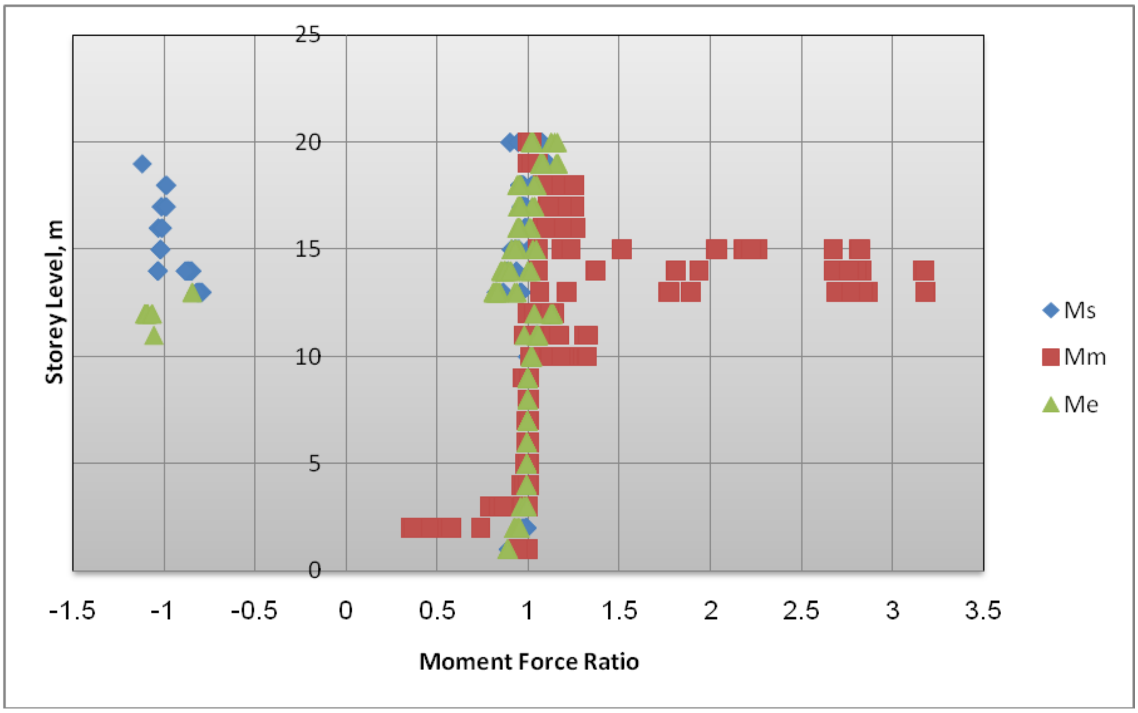


a)

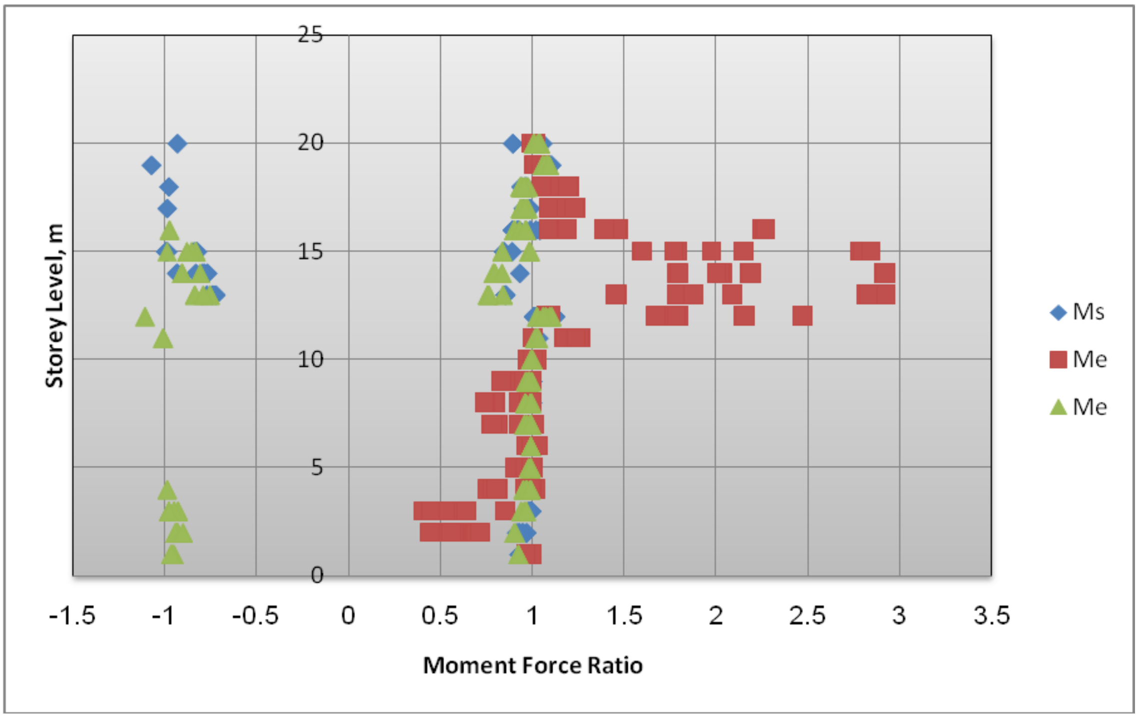


b)

Fig H17 Moment Force ratio in Beams for 20SR4-9 a) x-direction b) y-direction



a)

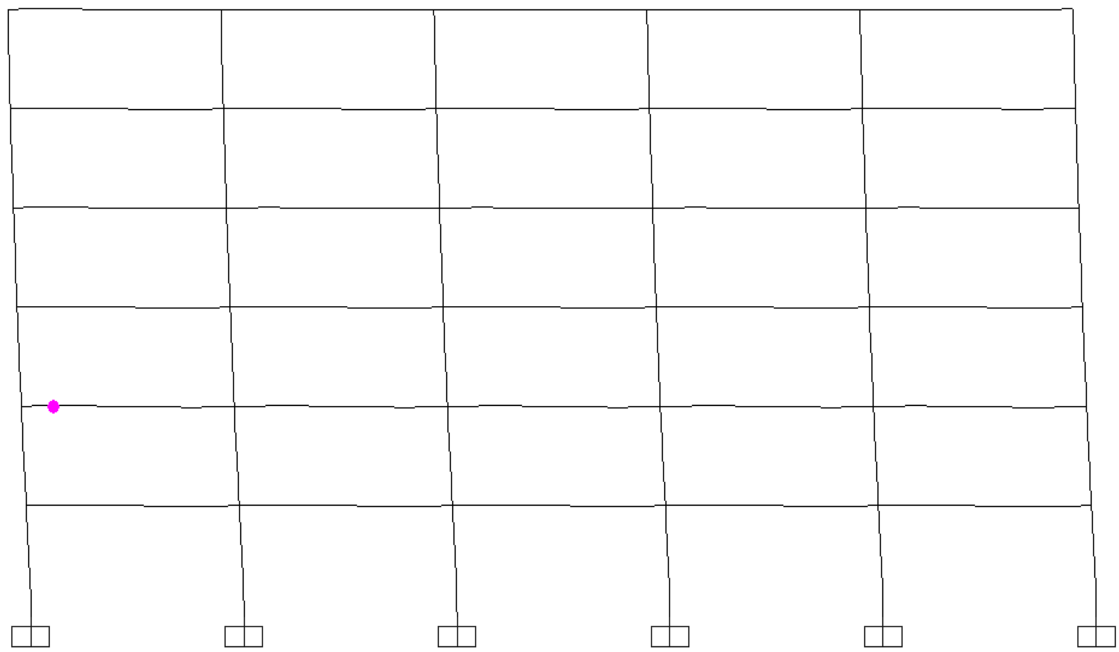


b)

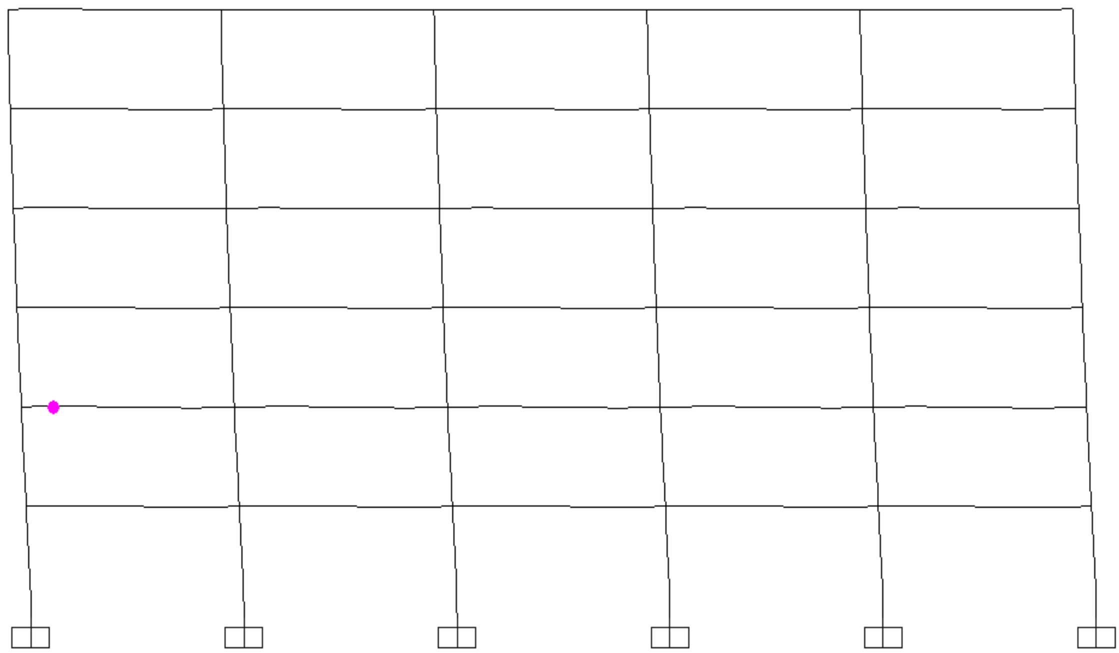
Fig H18 Moment Force ratio in Beams for 20SR13-18 a) x-direction b) y-direction

APPENDIX I

PLASTIC HINGE FORMATION FOR 6PRMRF SYSTEM UNDER TABAS EARTHQUAKE



a)



b)

Fig I1 flexural Hinge location for 6FRMRF in the x-direction a) first plastic hinge location b) Plastic hinge location at the end of analysis

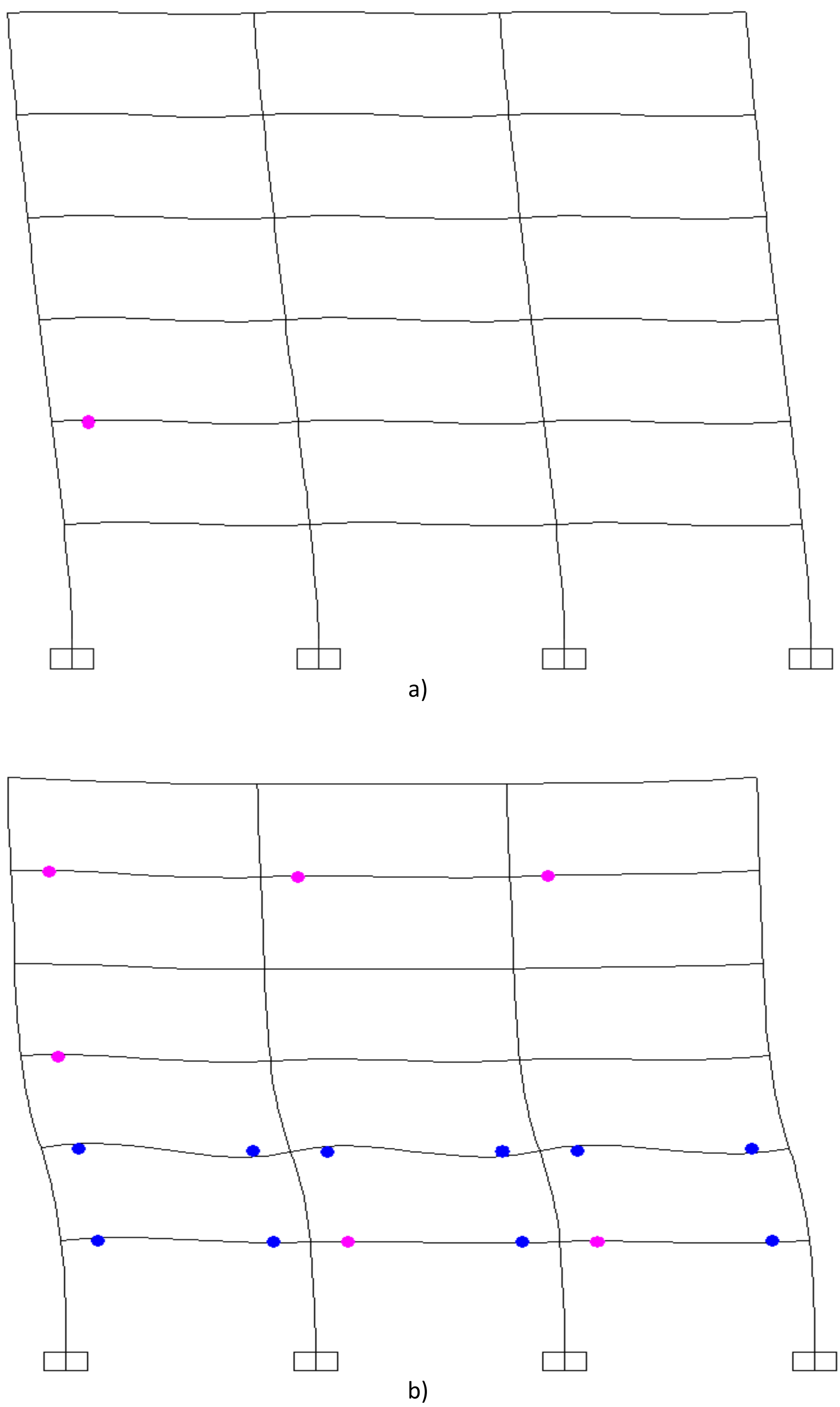
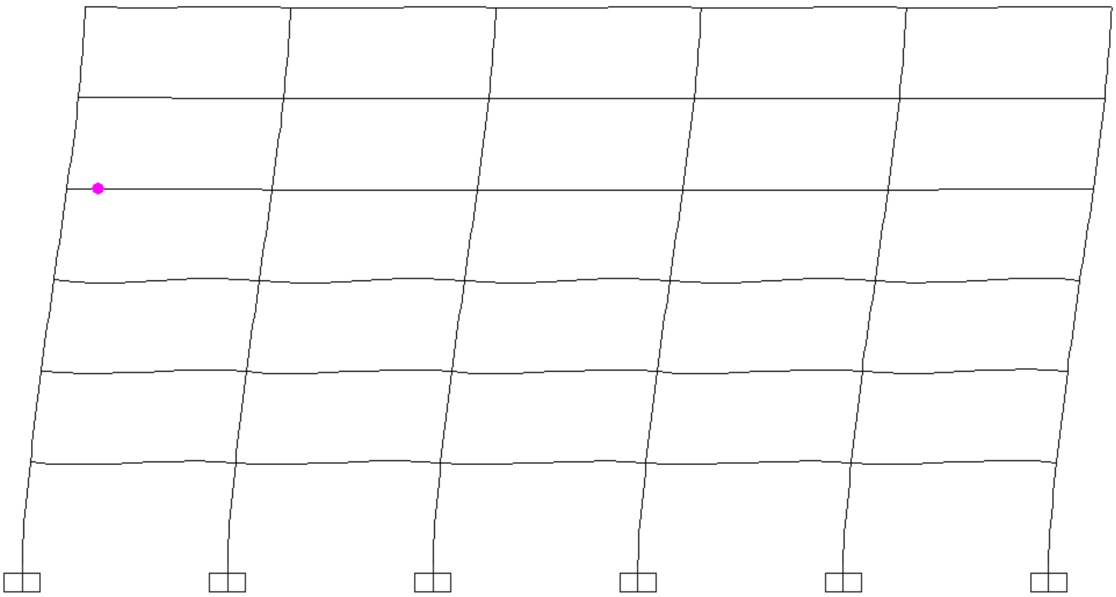
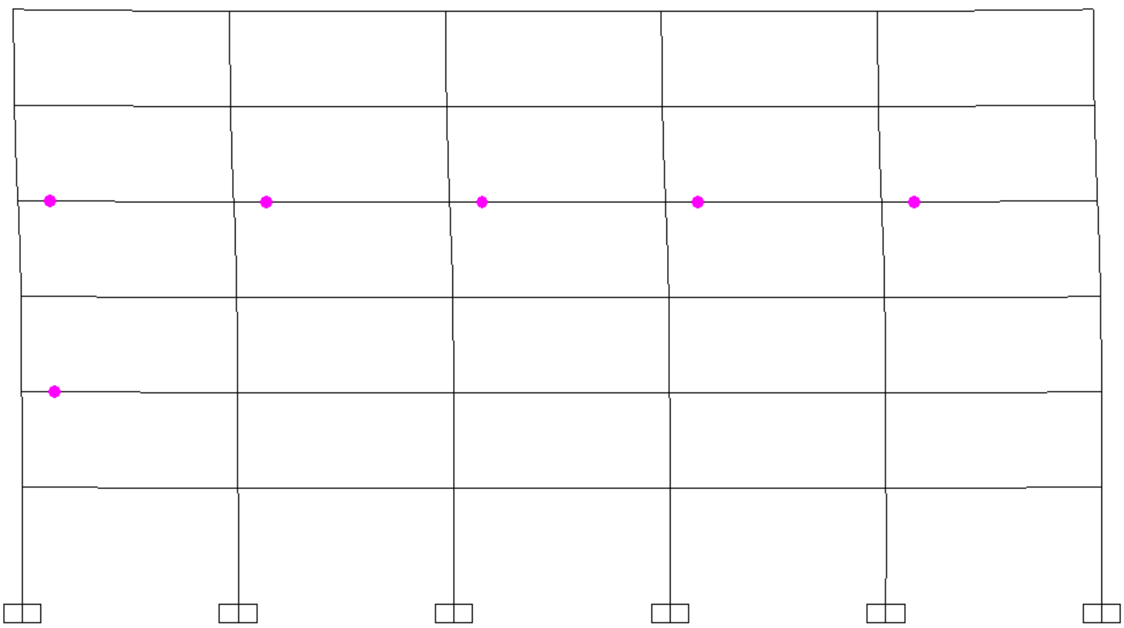


Fig I2 flexural Hinge location for 6FRMRF in the y-direction a) first plastic hinge location b) Plastic hinge location at the end of analysis

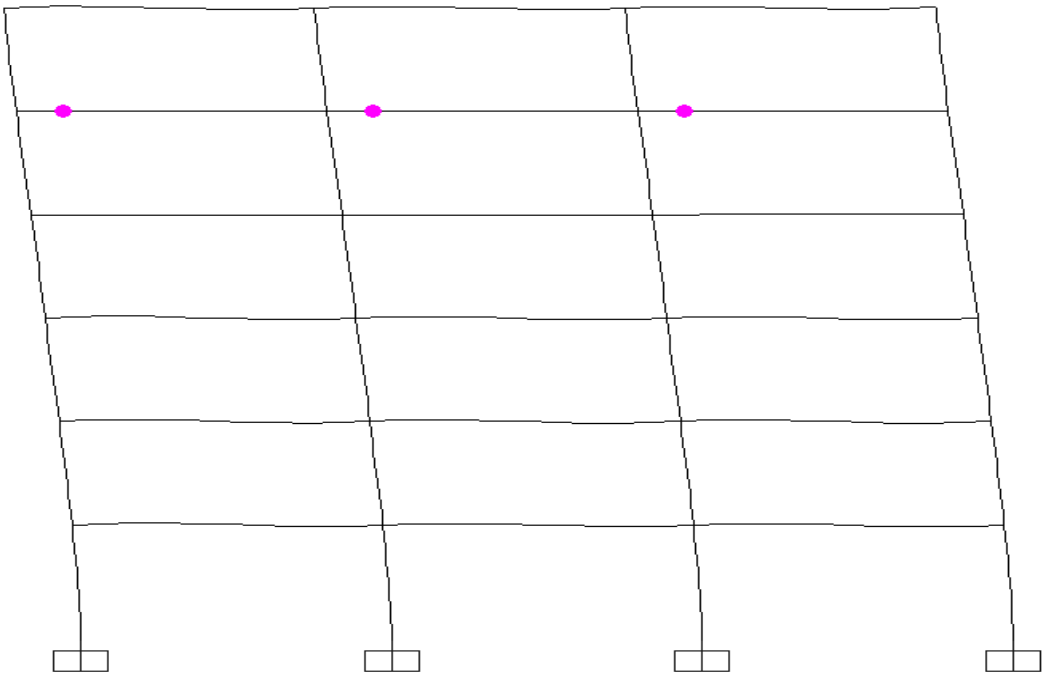


a)

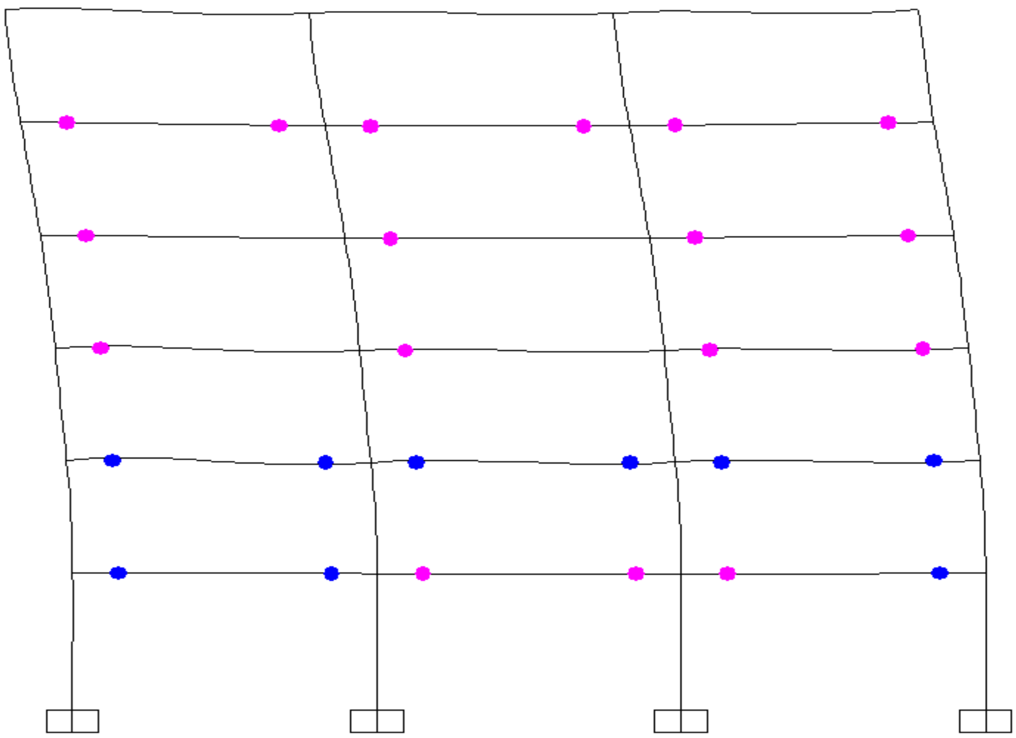


b)

Fig I3 flexural Hinge location for 6SR45 in the x-direction a) first plastic hinge location
b) Plastic hinge location at the end of analysis

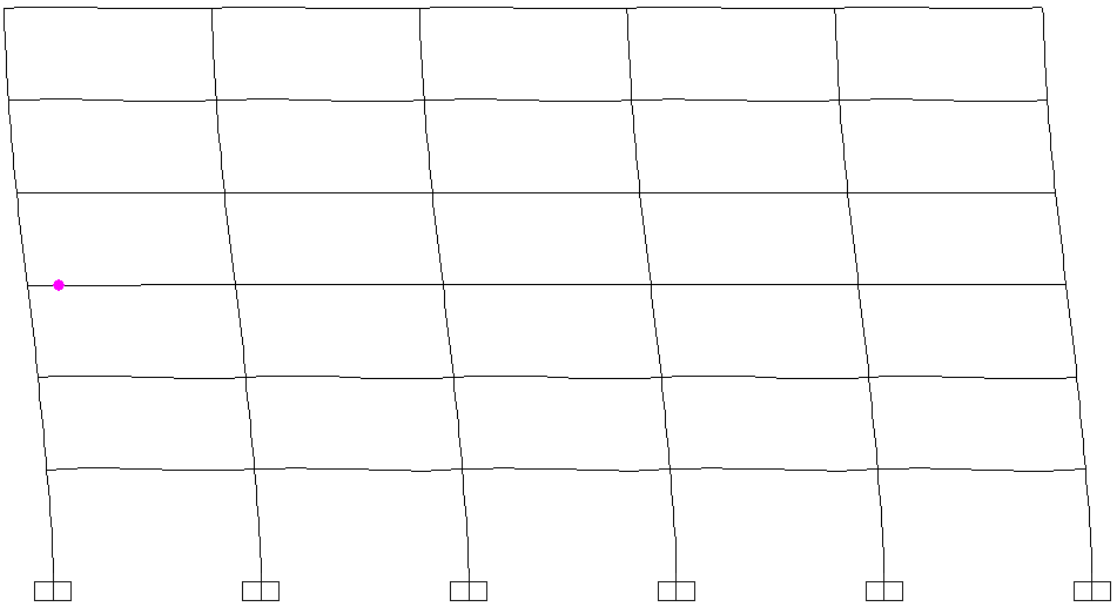


a)

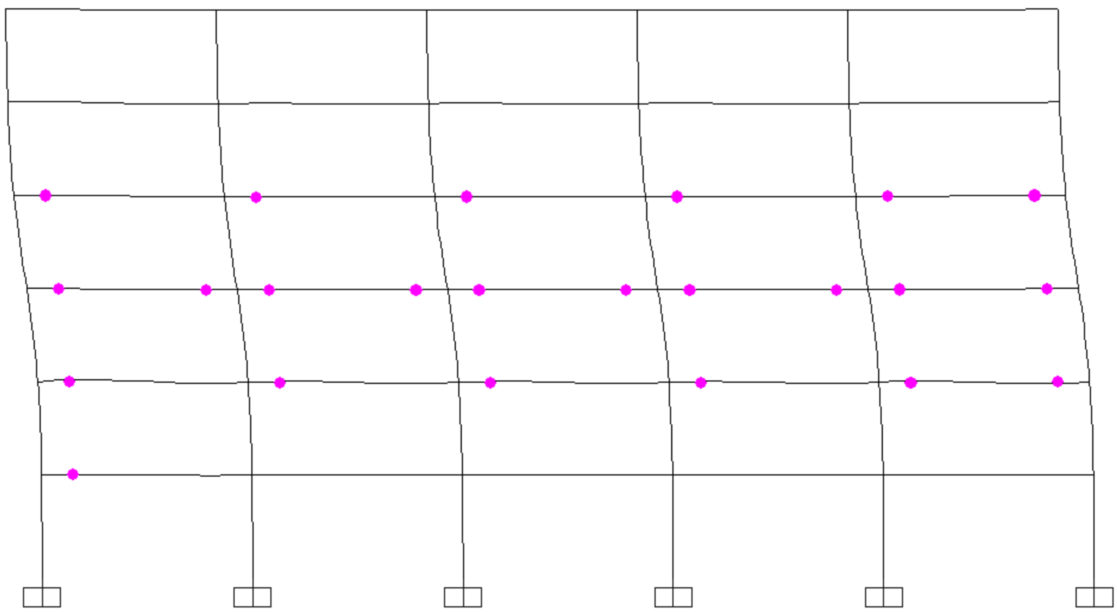


b)

Fig I4 flexural Hinge location for 6SR45 in the y-direction a) first plastic hinge location b) Plastic hinge location at the end of analysis

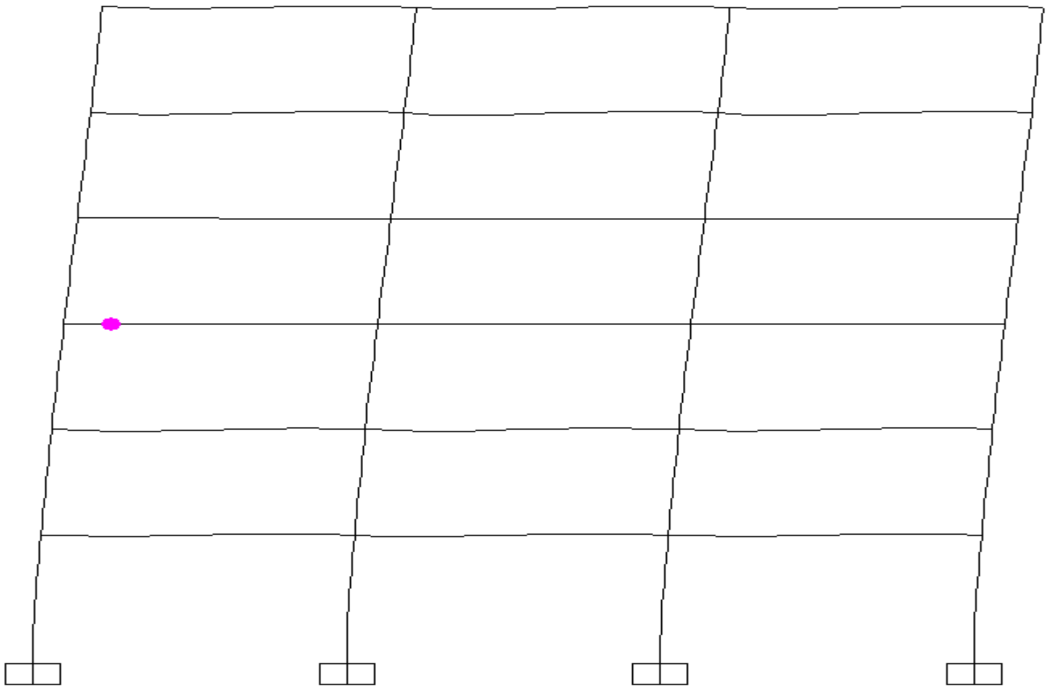


a)

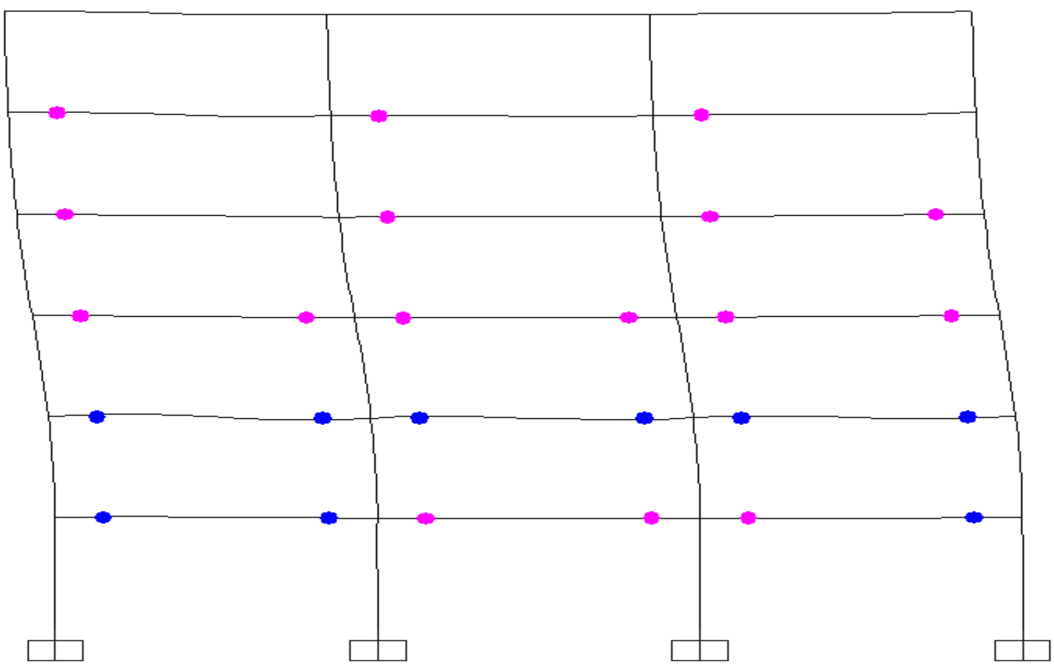


b)

Fig I5 flexural Hinge location for 6SR34 in the x-direction a) first plastic hinge location
b) Plastic hinge location at the end of analysis

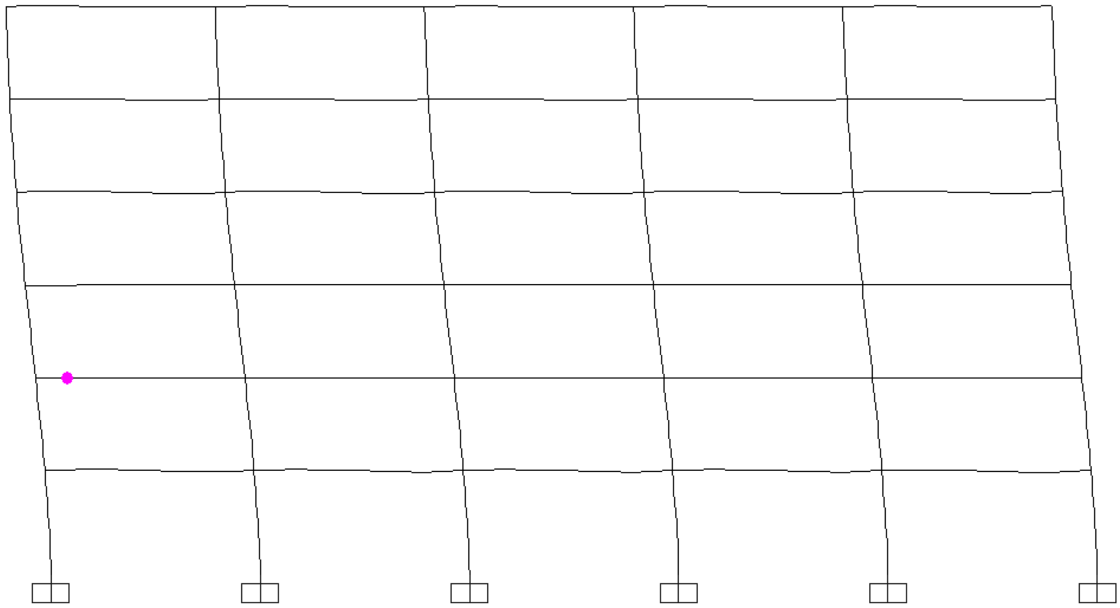


a)

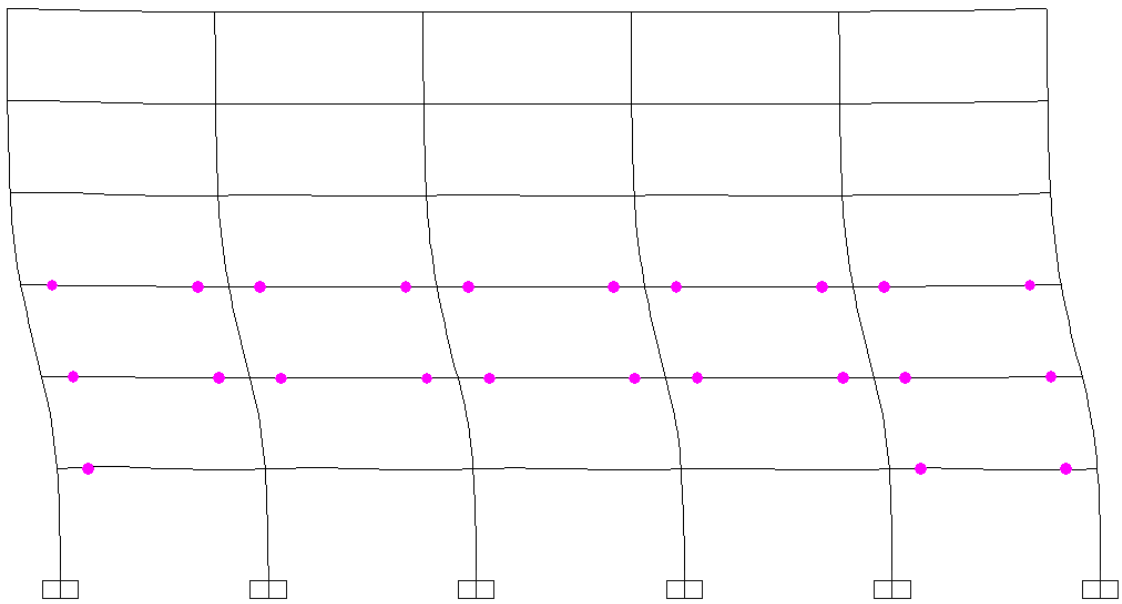


b)

Fig I6 flexural Hinge location for 6SR34 in the y-direction a) first plastic hinge location b) Plastic hinge location at the end of analysis

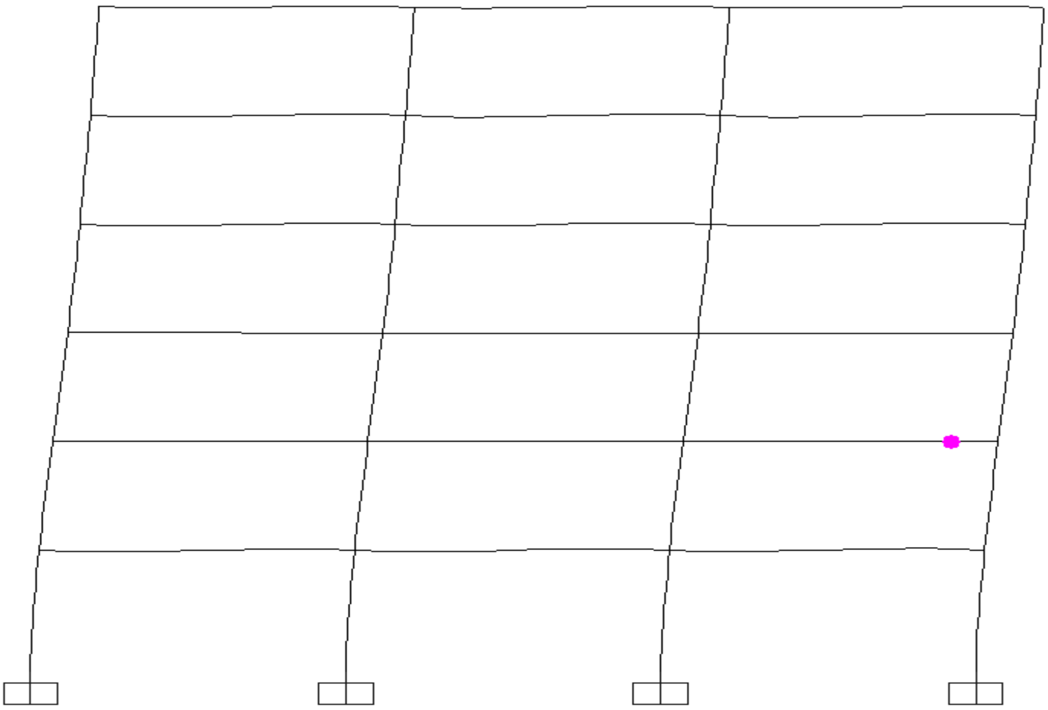


a)

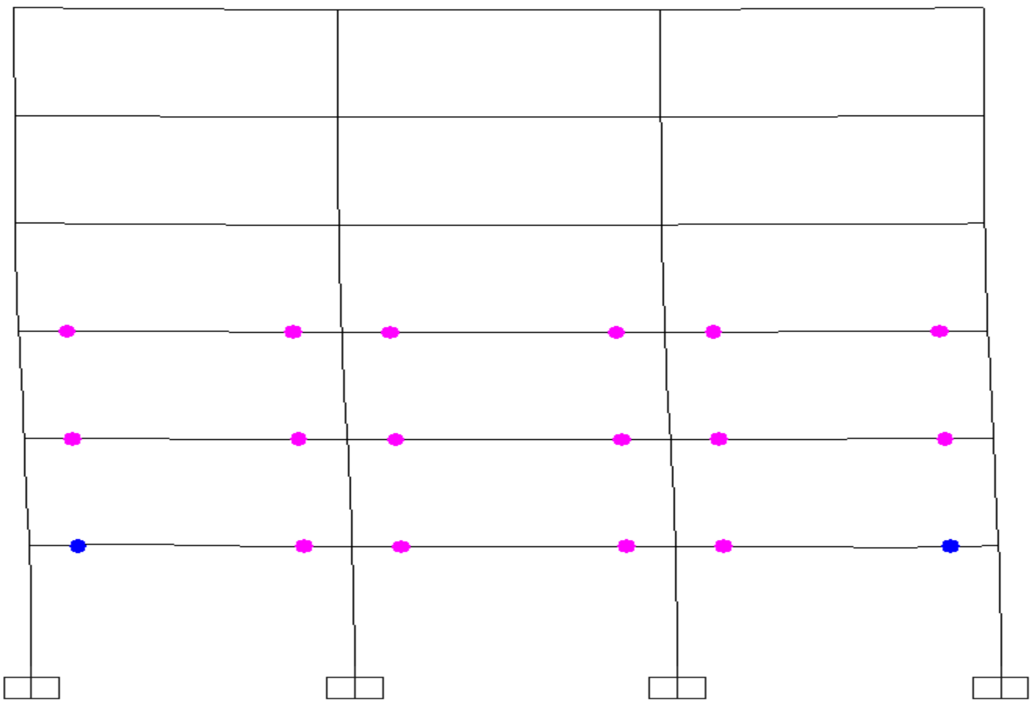


b)

Fig I7 flexural Hinge location for 6SR23 in the x-direction a) first plastic hinge location b) Plastic hinge location at the end of analysis

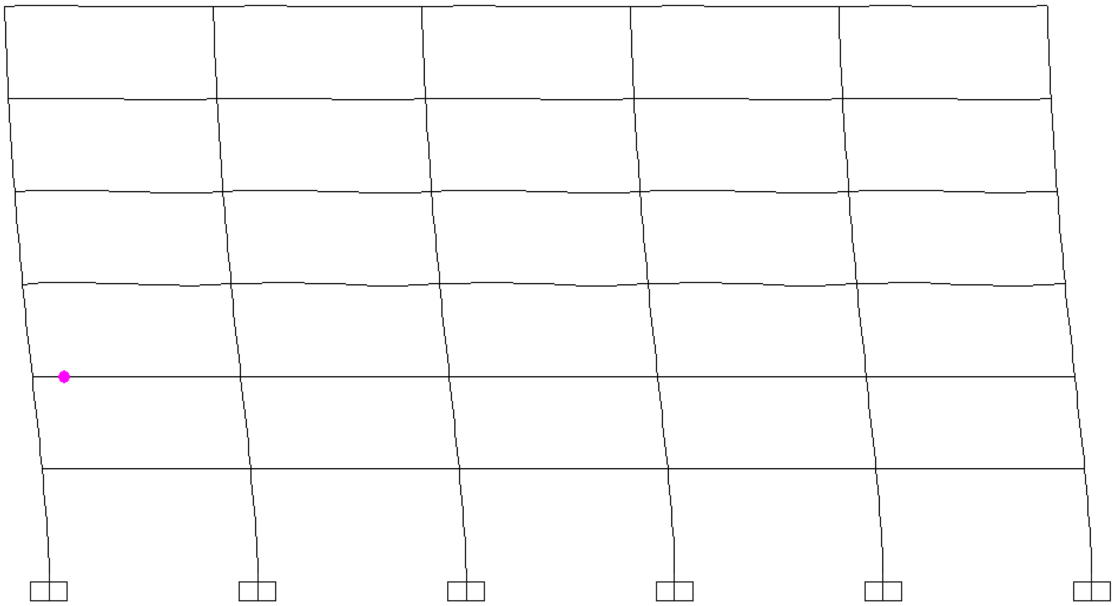


a)

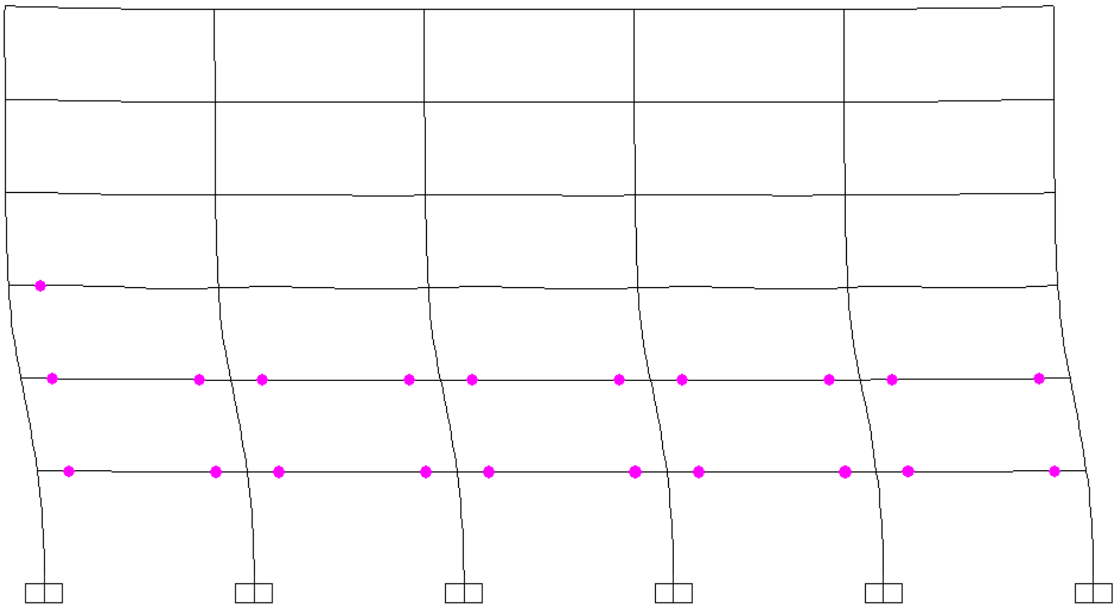


b)

Fig I8 flexural Hinge location for 6SR23 in the y-direction a) first plastic hinge location b) Plastic hinge location at the end of analysis

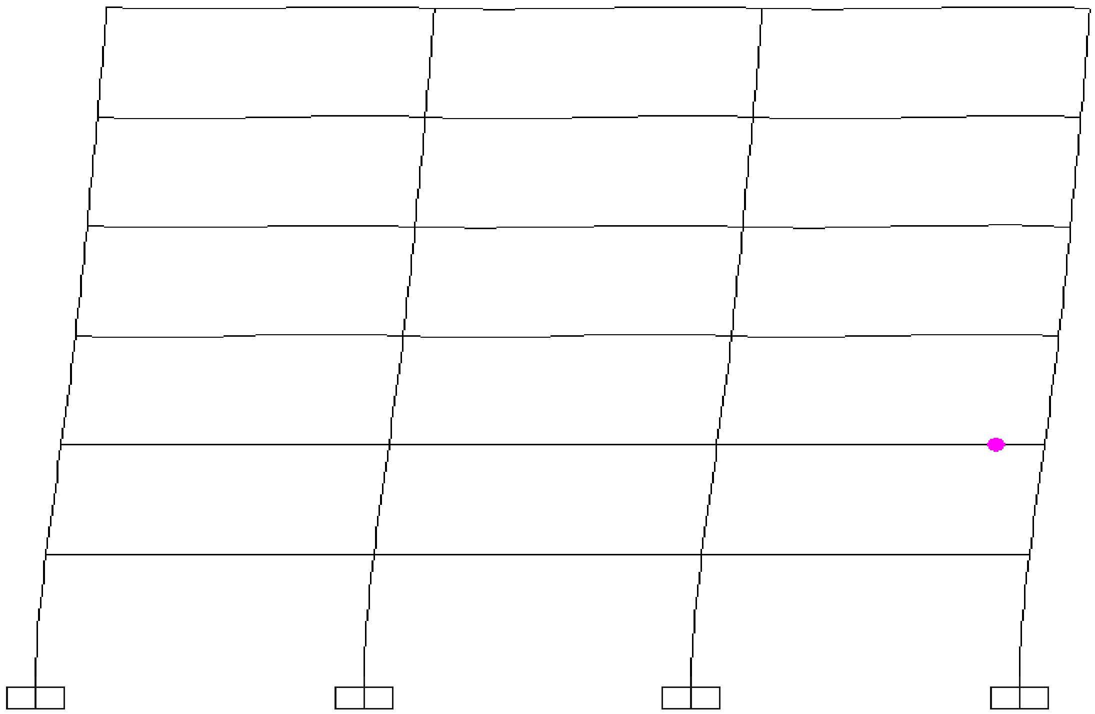


a)

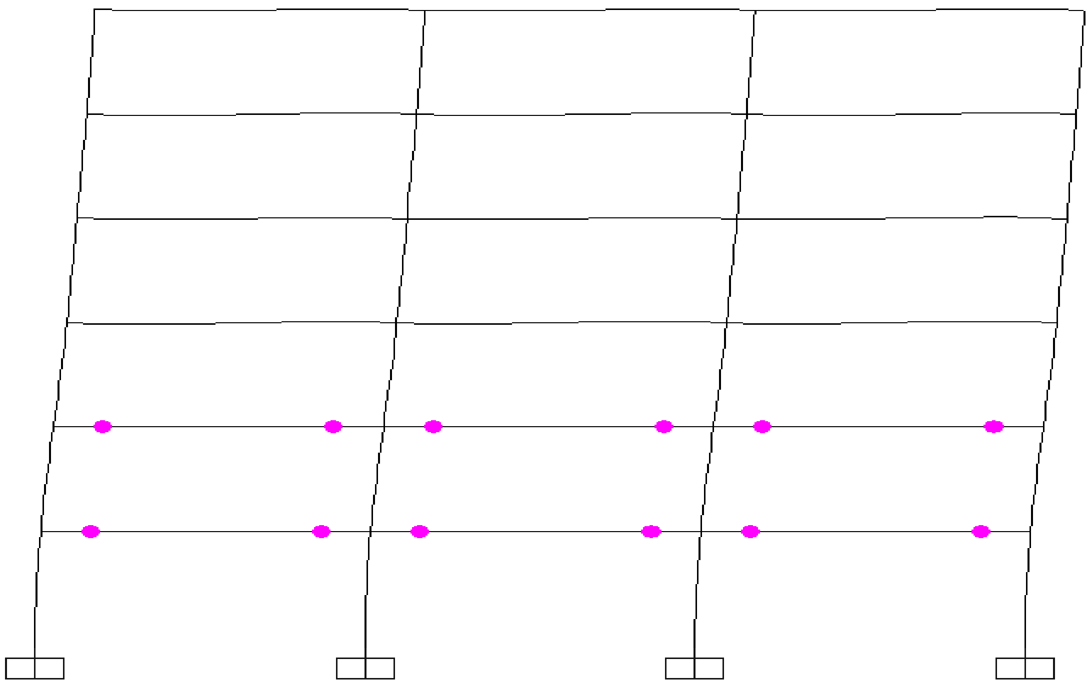


b)

Fig I9 flexural Hinge location for 6SR12 in the x-direction a) first plastic hinge location b) Plastic hinge location at the end of analysis

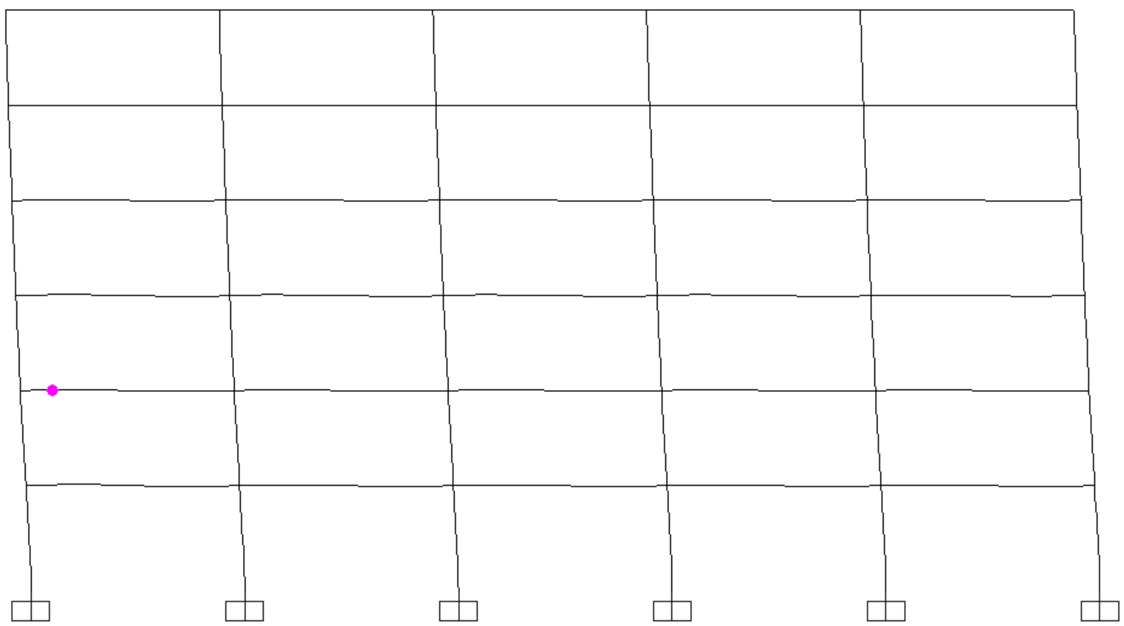


a)

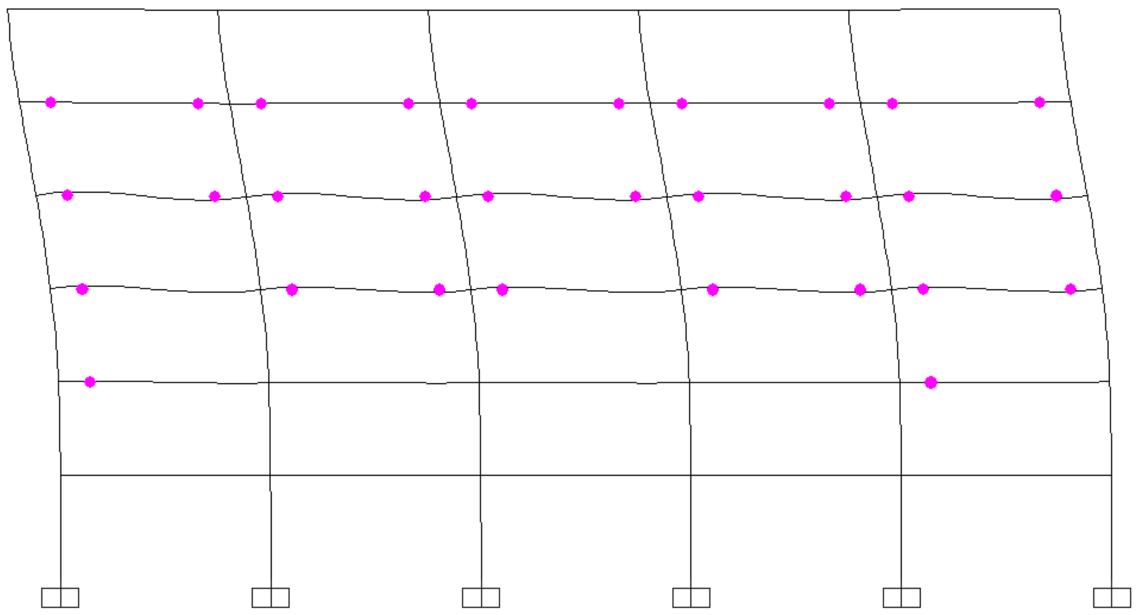


b)

Fig I10 flexural Hinge location for 6SR12 in the y-direction a) first plastic hinge location b) Plastic hinge location at the end of analysis

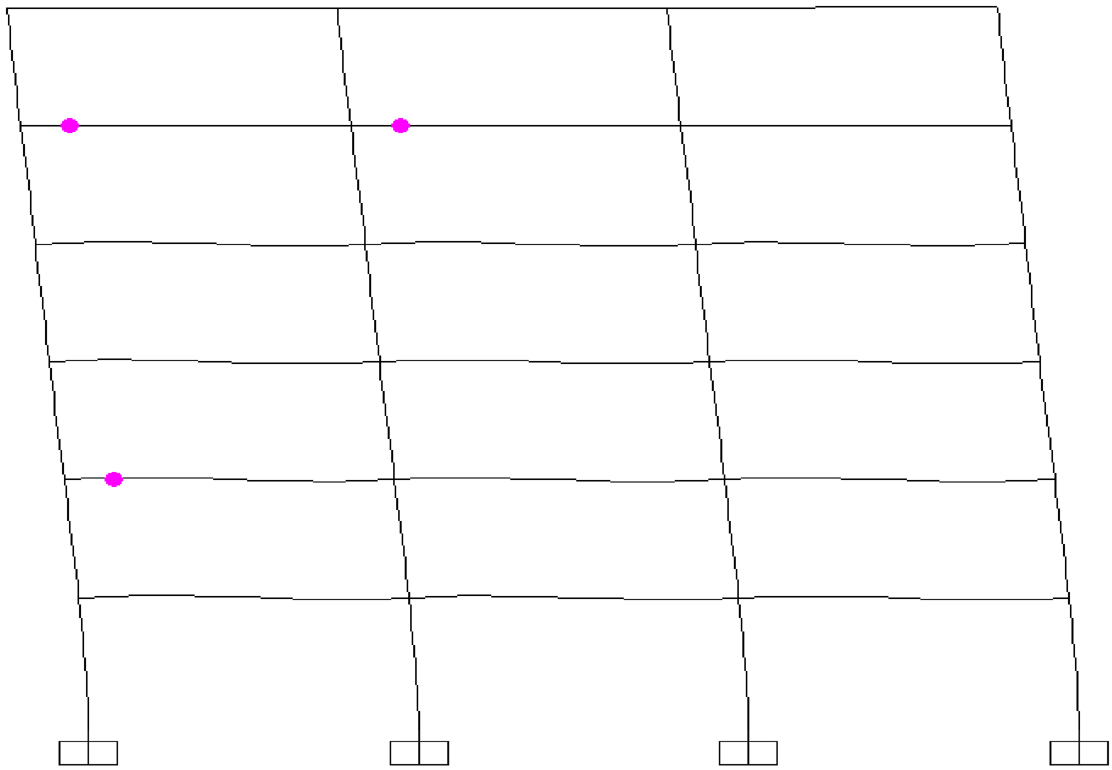


a)

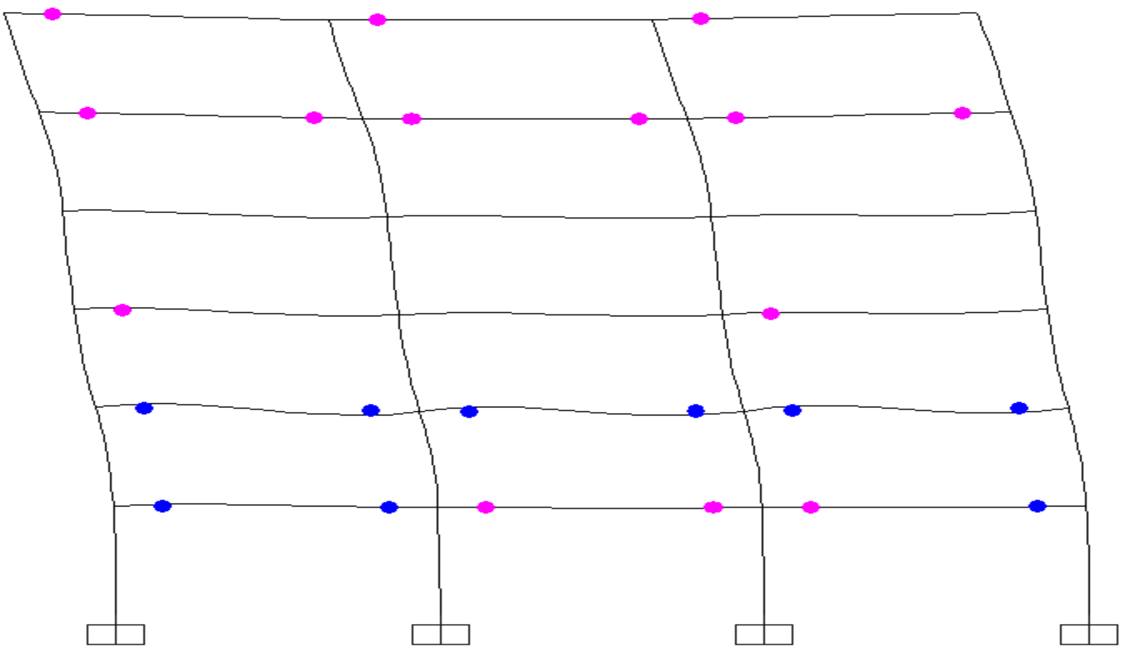


b)

Fig I11 flexural Hinge location for 6SR56 in the x-direction a) first plastic hinge location
b) Plastic hinge location at the end of analysis

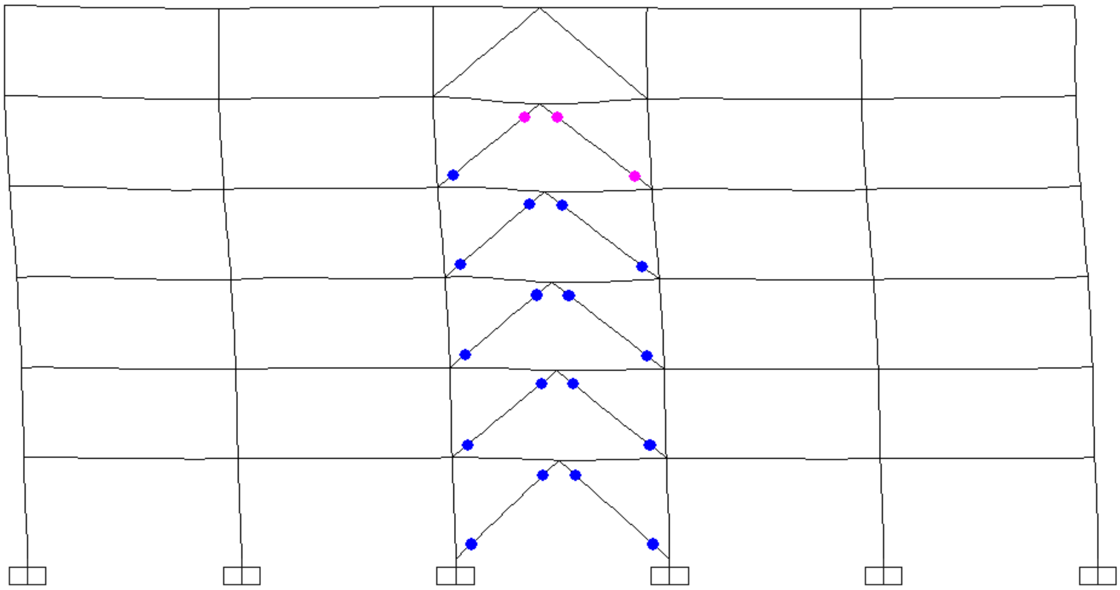


a)

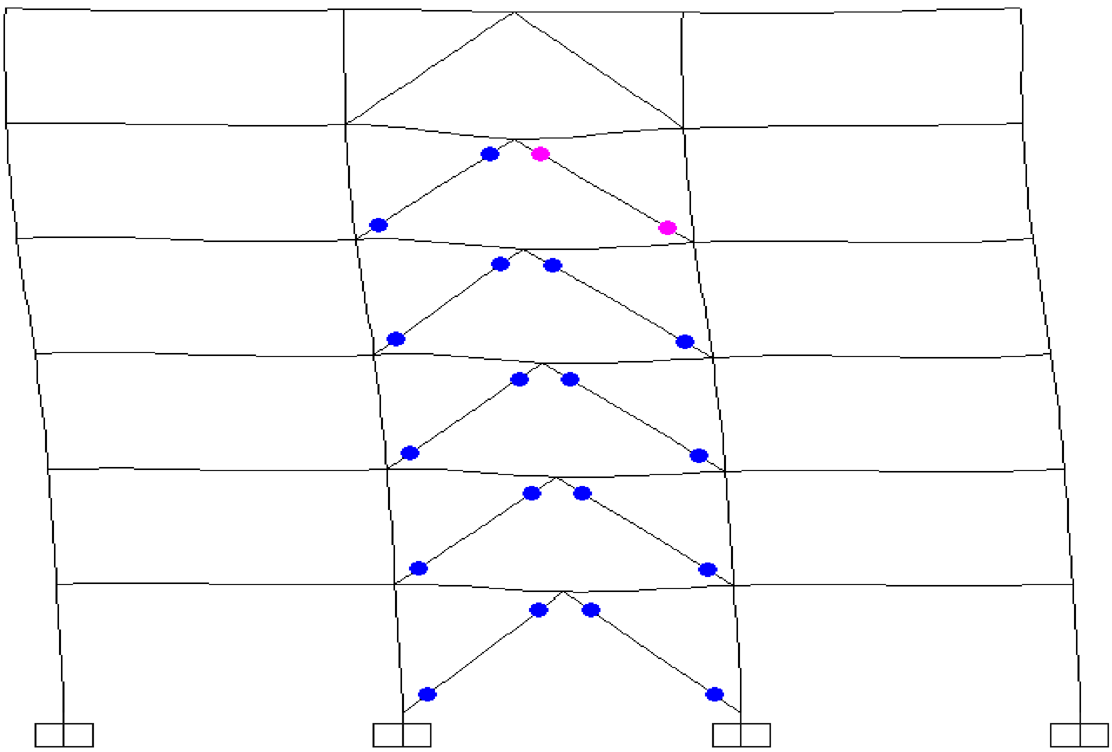


b)

Fig I12 flexural Hinge location for 6SR56 in the y-direction a) first plastic hinge location
b) Plastic hinge location at the end of analysis

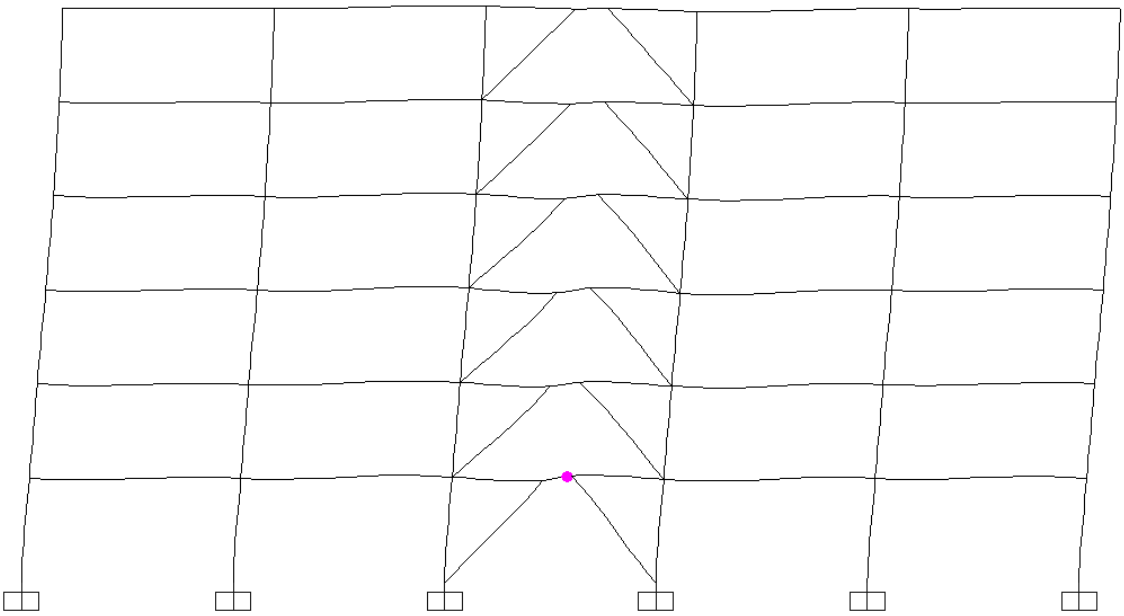


a)

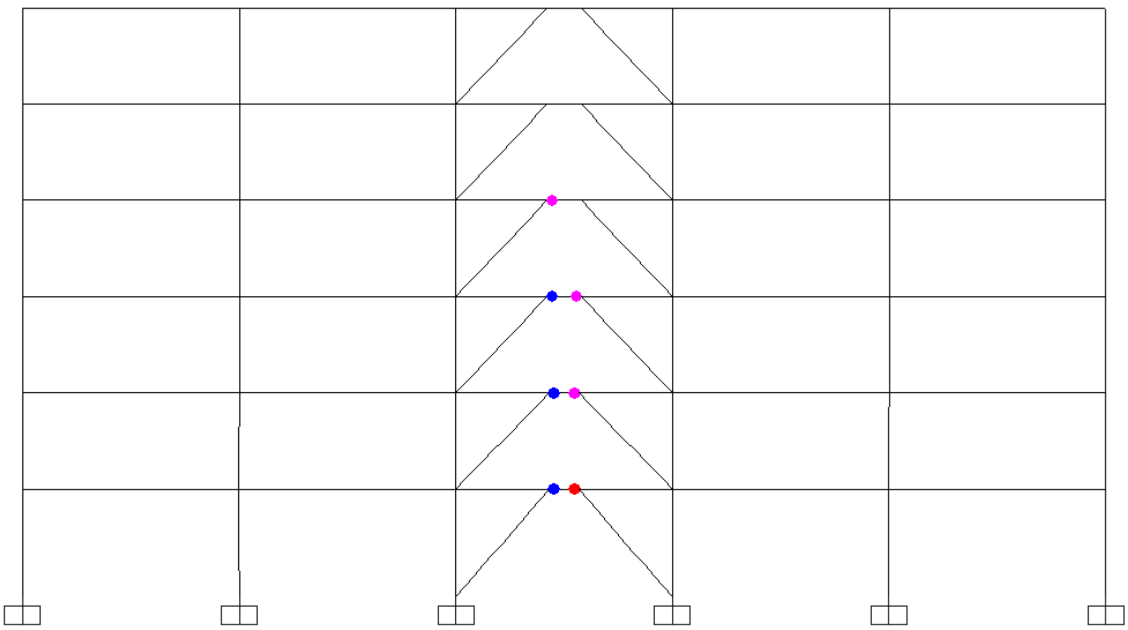


b)

Fig I13 flexural Hinge location for 6BRBF system a) x-direction frames b) y-direction frames

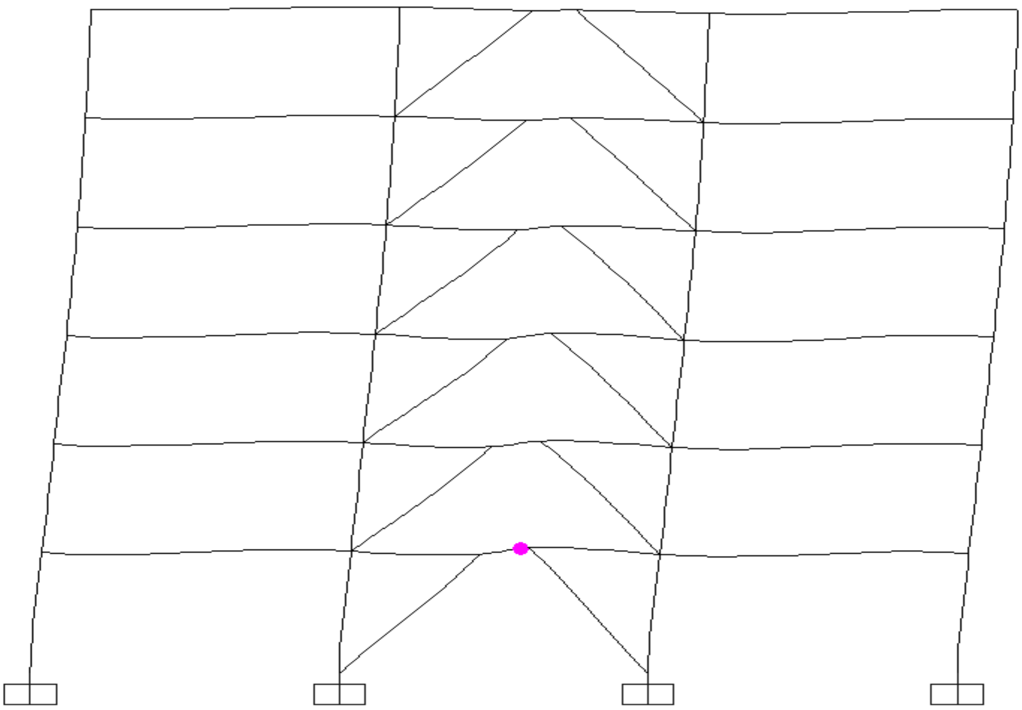


a)

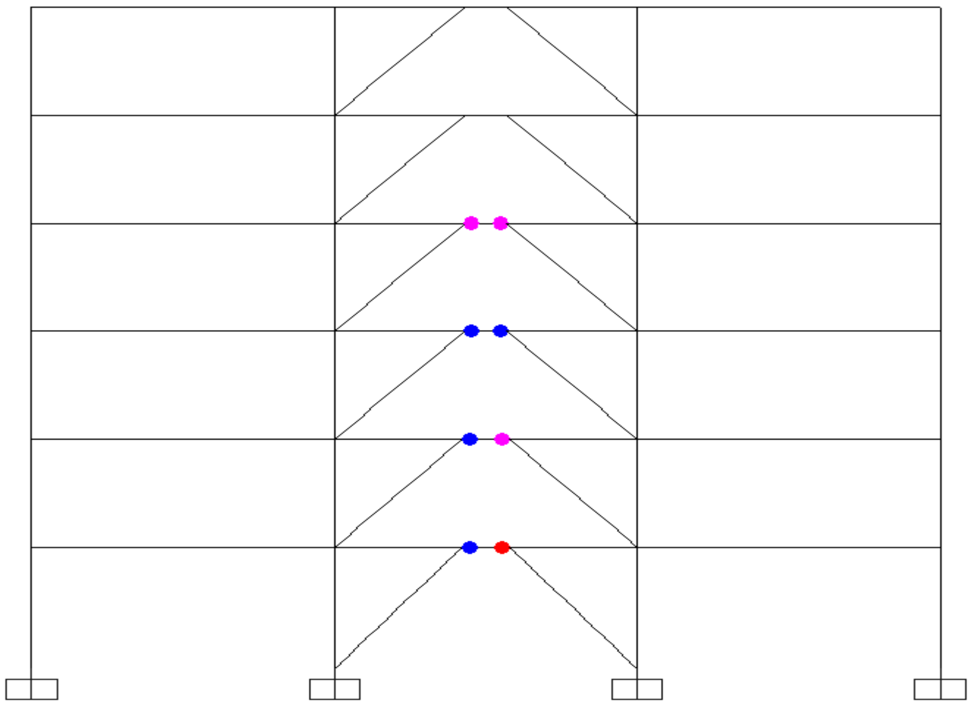


b)

Fig I14 shear Hinge location in x-direction frames for 6EBF1 csx csy a) first plastic hinge location b) failure mechanism

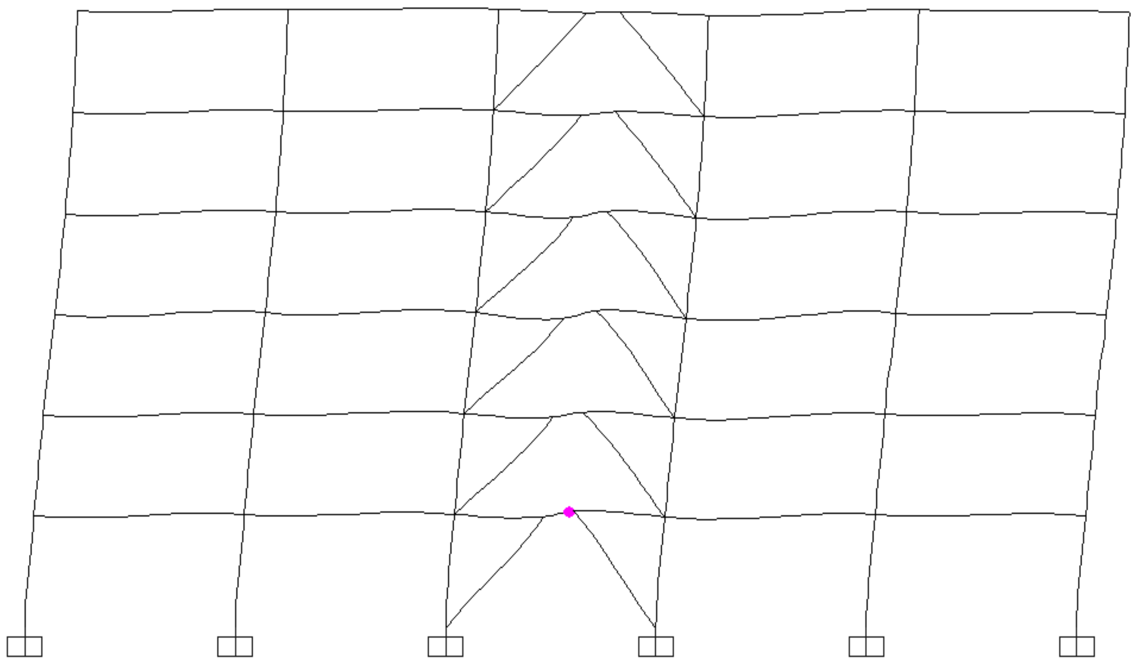


a)

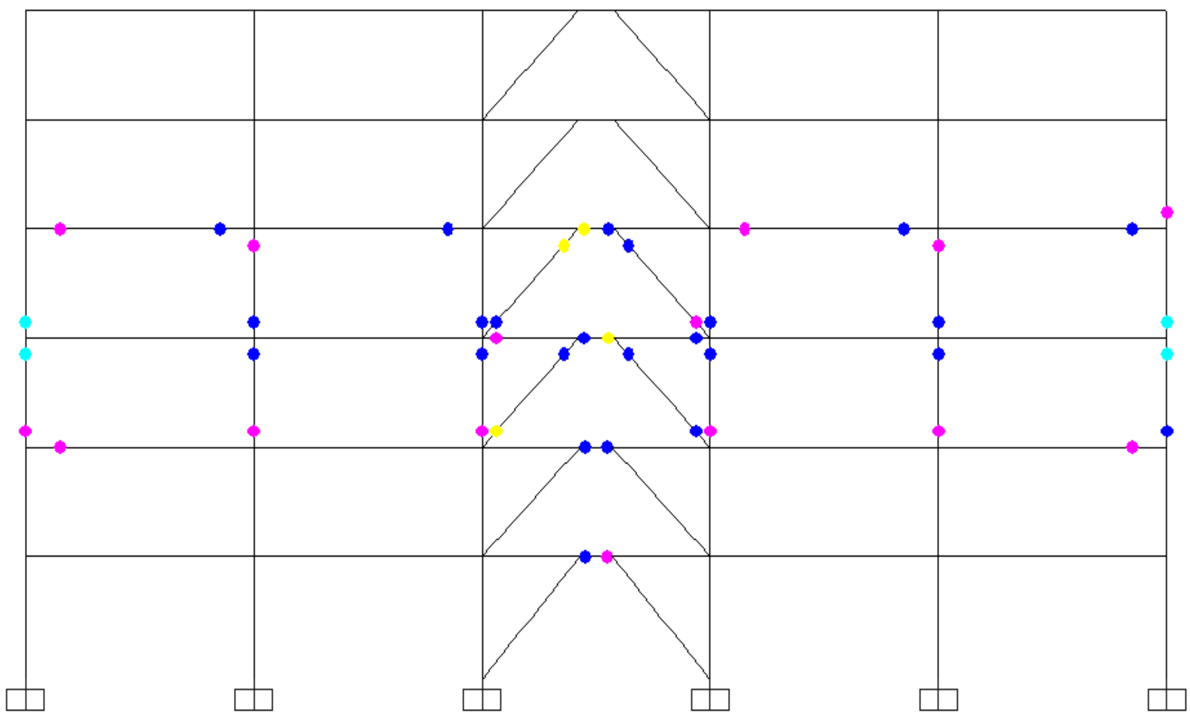


b)

Fig I15 shear Hinge location in y-direction frames for 6EBF1 csx csy a) first plastic hinge location b) failure mechanism

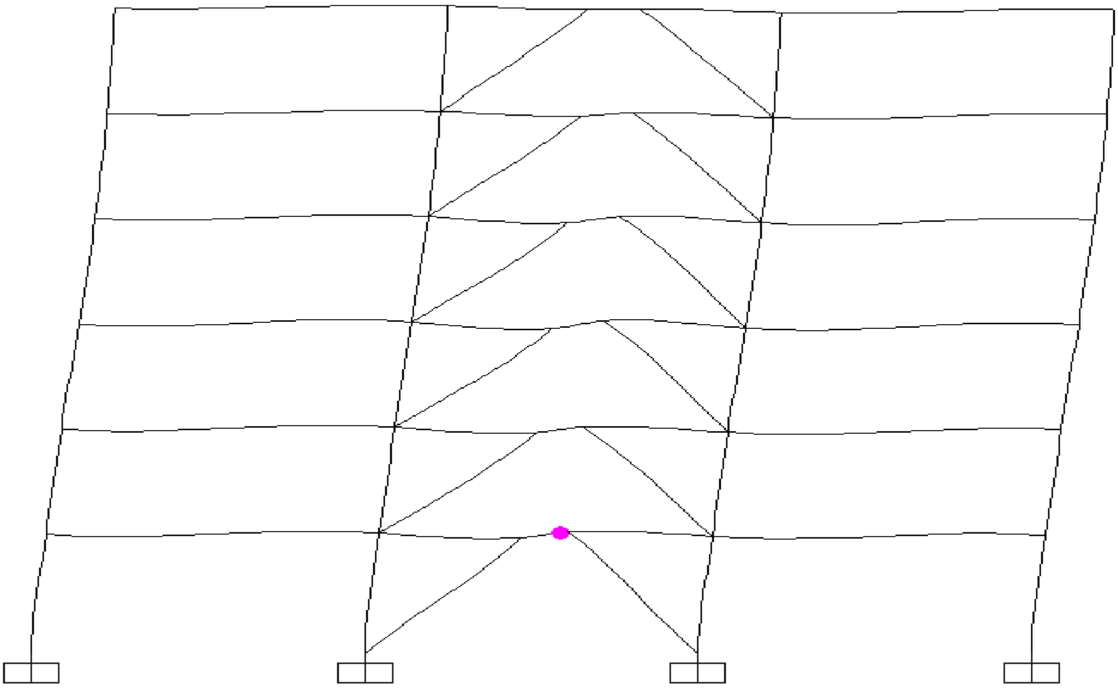


a)

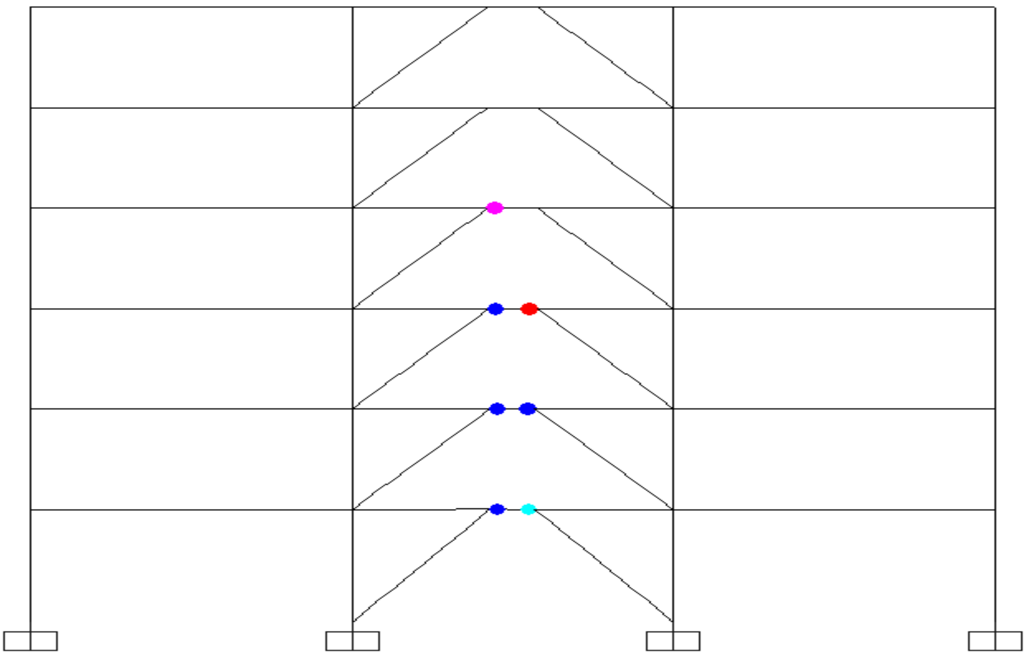


b)

Fig I16 shear Hinge location in x-direction frames for 6EBF2 csx csy a) first plastic hinge location b) failure mechanism

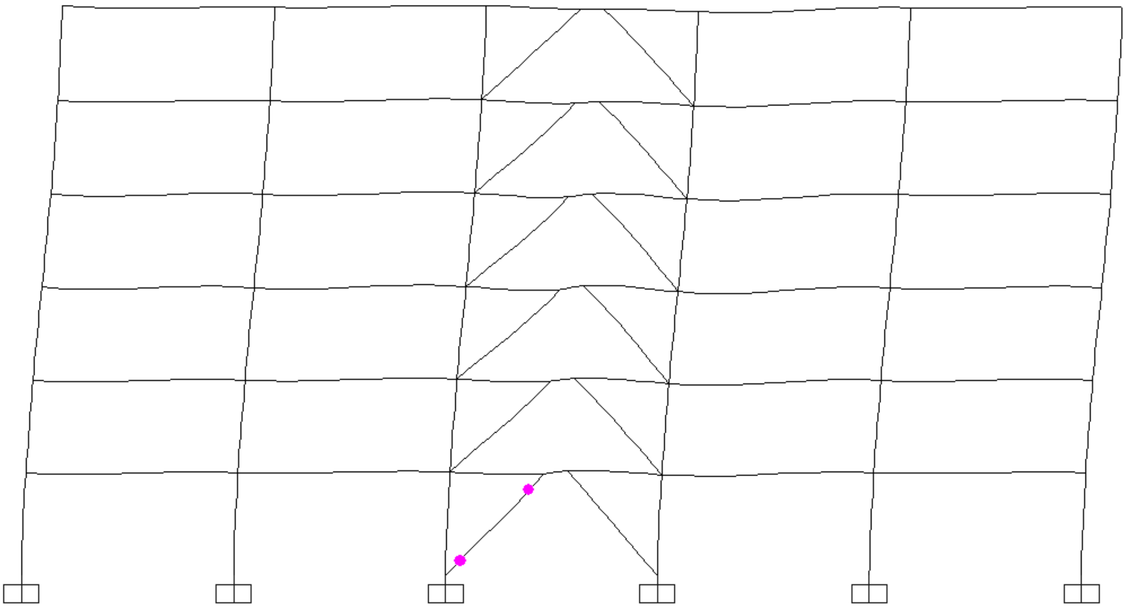


a)

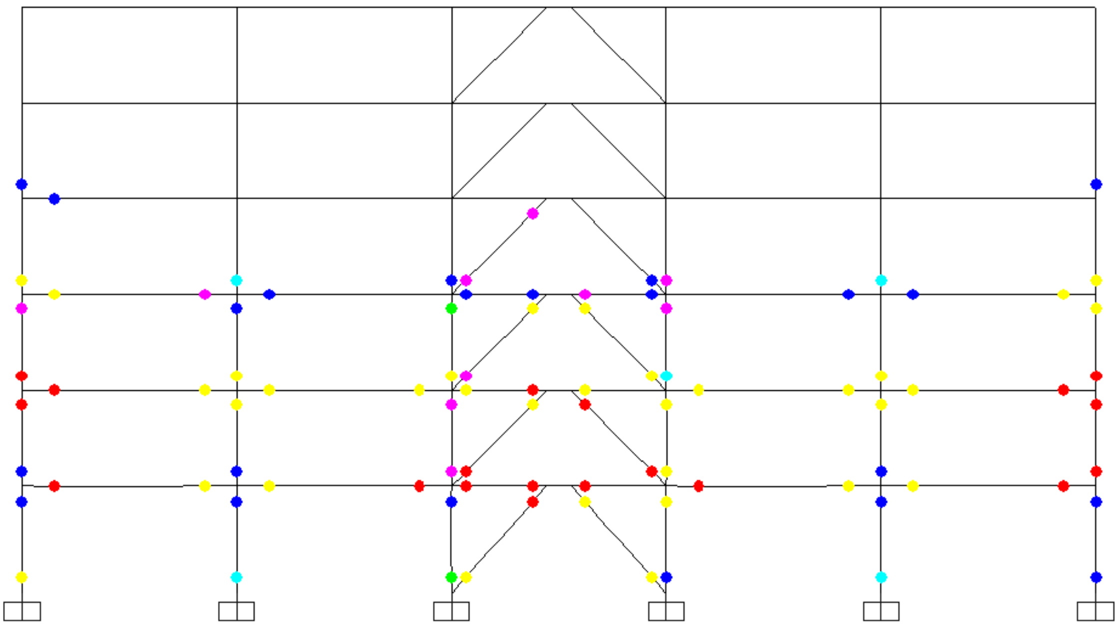


b)

Fig I17 shear Hinge location in y-direction frames for 6EBF2 csx csy a) first plastic hinge location b) failure mechanism

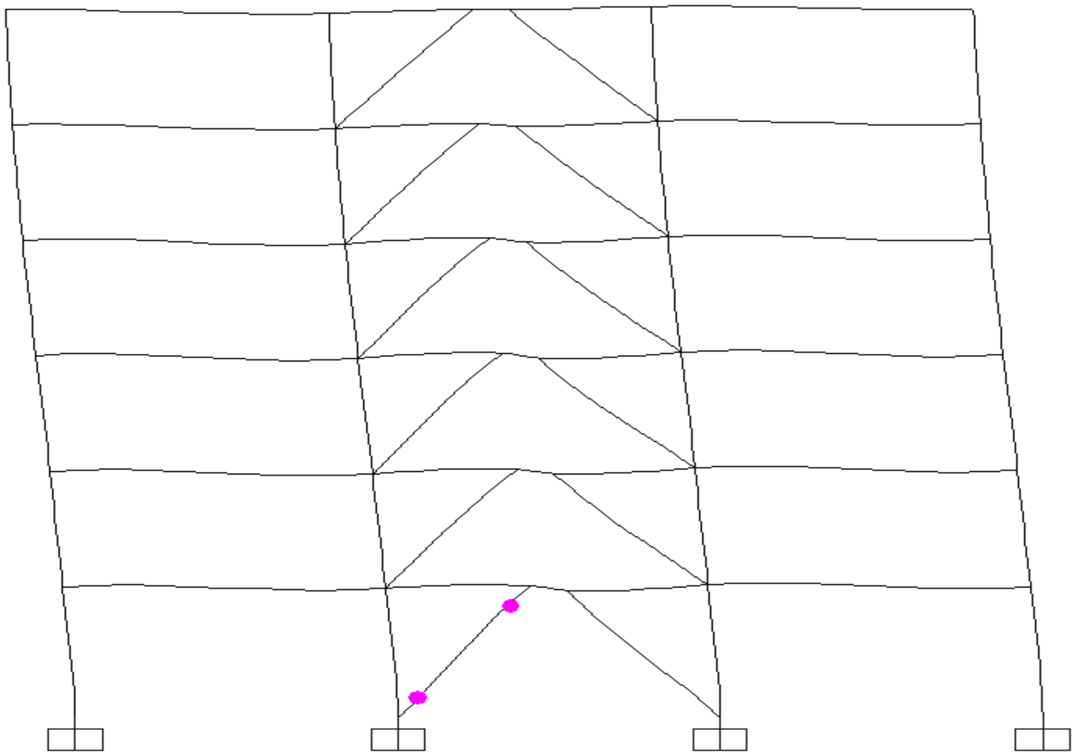


a)

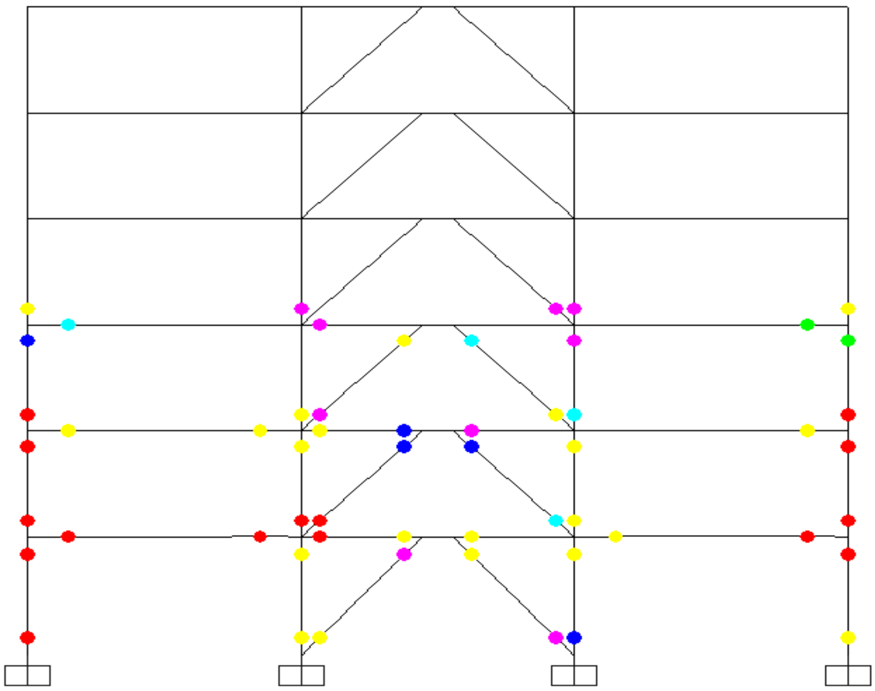


b)

Fig I18 shear Hinge location in x-direction frames for 6EBF3 csx csy a) first plastic hinge location b) failure mechanism

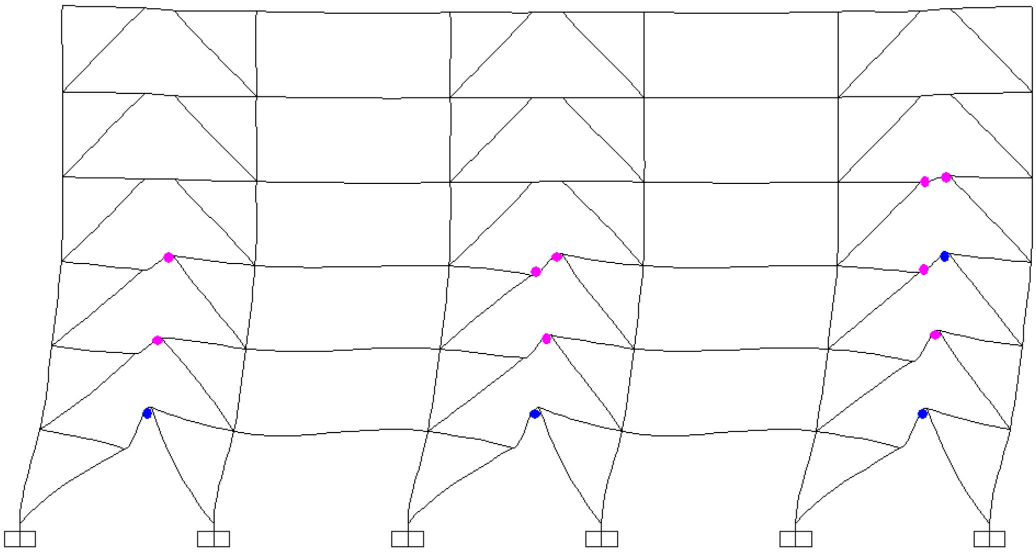


a)

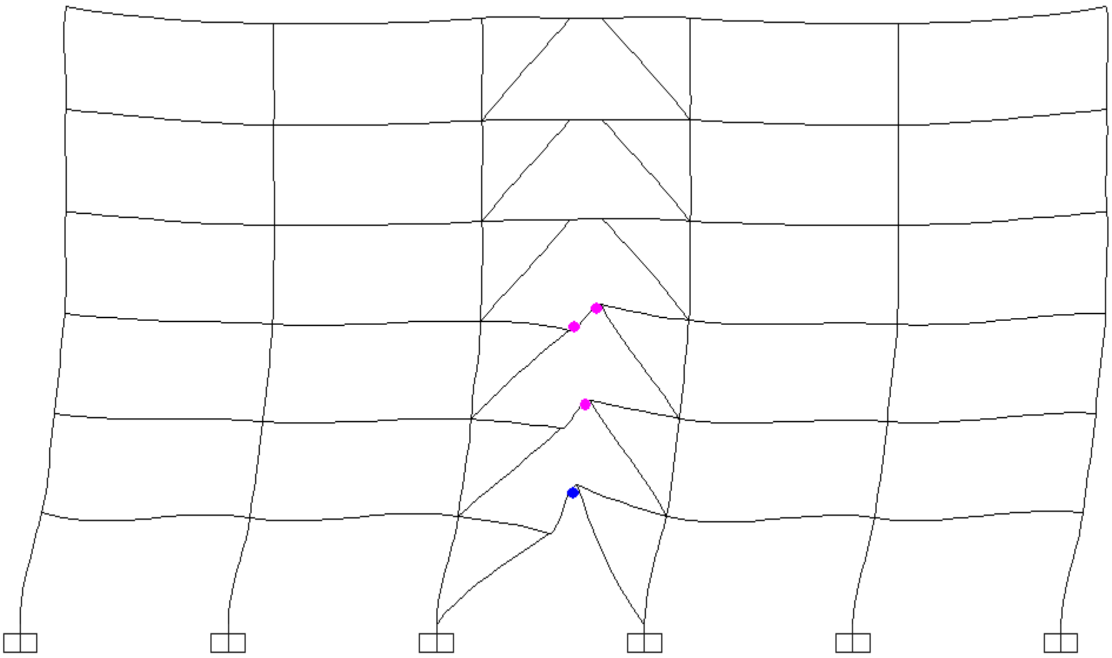


b)

Fig I19 shear Hinge location in x-direction frames for 6EBF3 csx csy a) first plastic hinge location b) failure mechanism

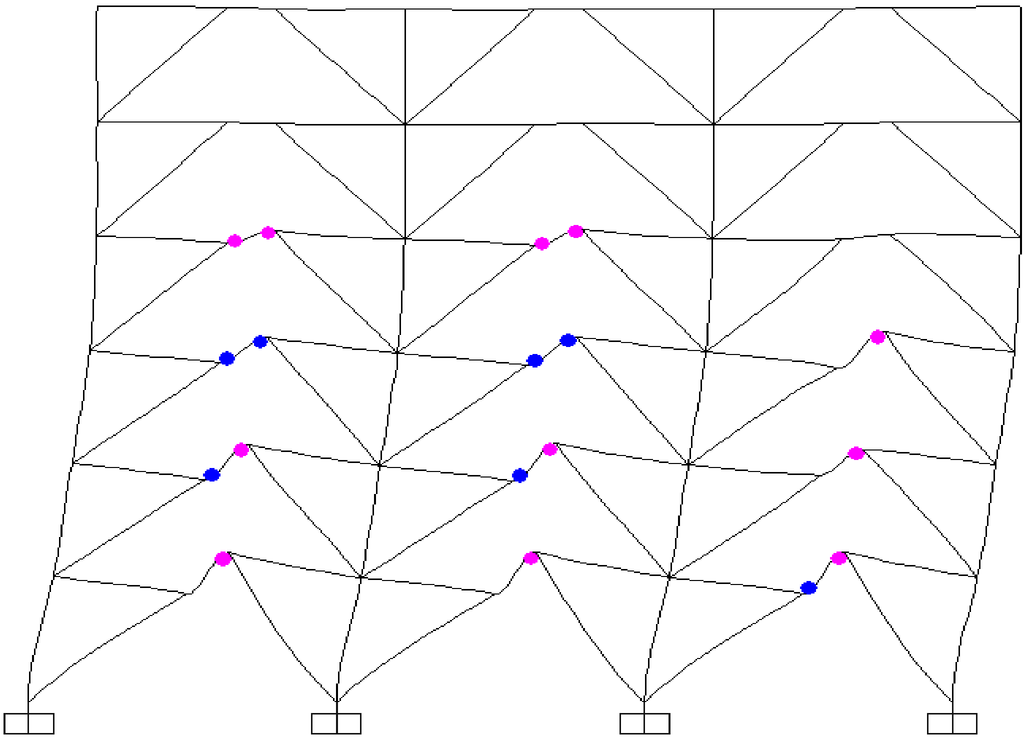


a)

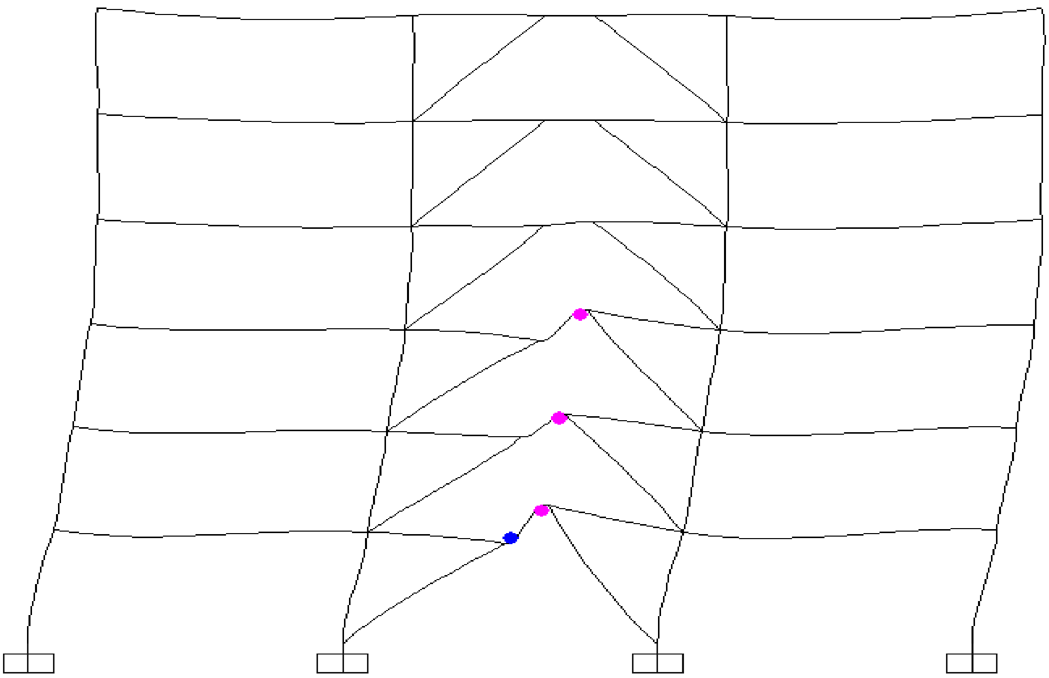


b)

Fig I20 shear Hinge location in x-direction frames for 6EBF cscox cscoy a) failure mechanism at the outer frames b) failure mechanism at the core frames



a)

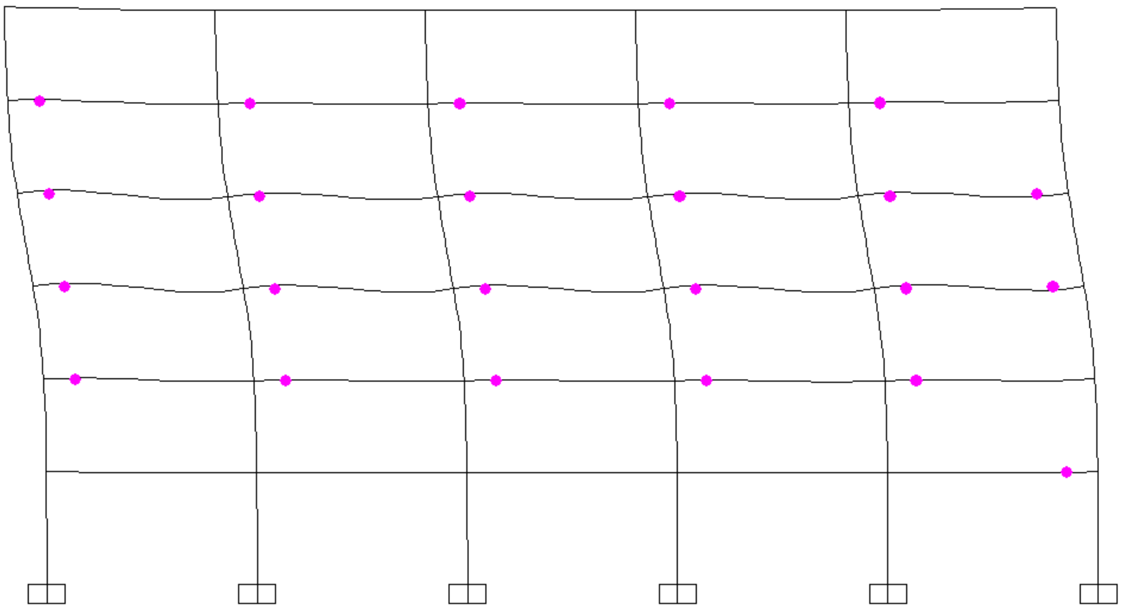


b)

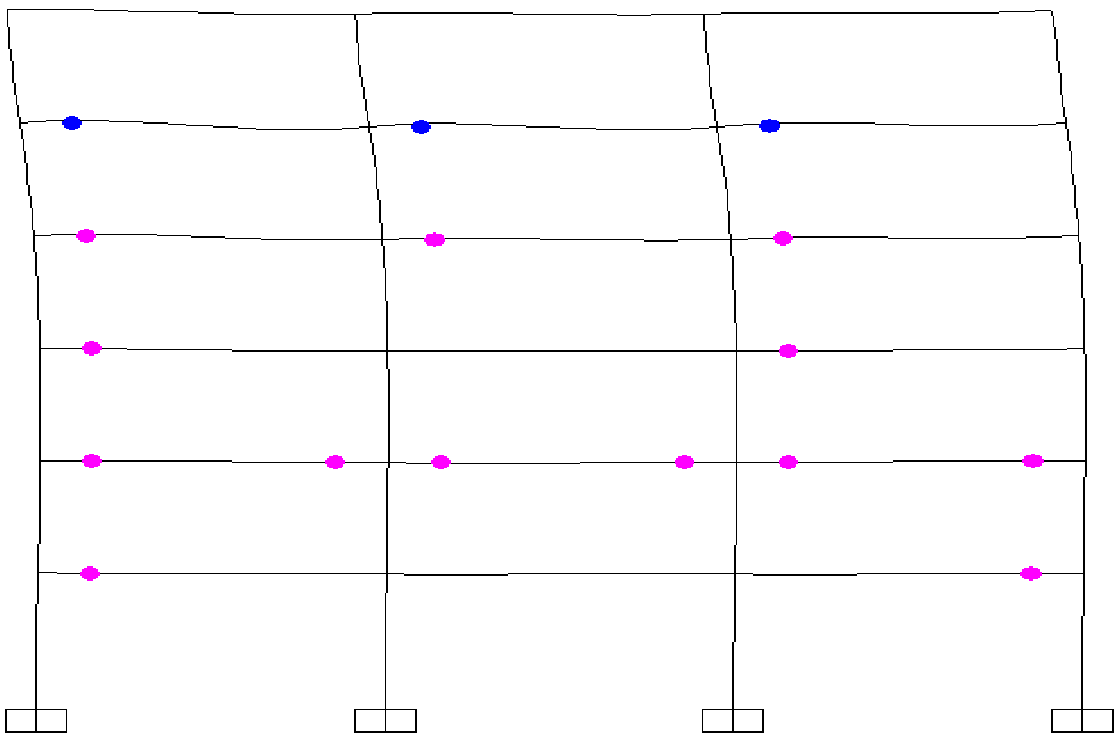
Fig I21 shear Hinge location in y-direction frames for 6EBF cscox cscoy a) failure mechanism at the outer frames b) failure mechanism at the core frames

APPENDIX J

PLASTIC HINGE FORMATION FOR 6PRMRF SYSTEM UNDER NORTHRIDGE EARTHQUAKE

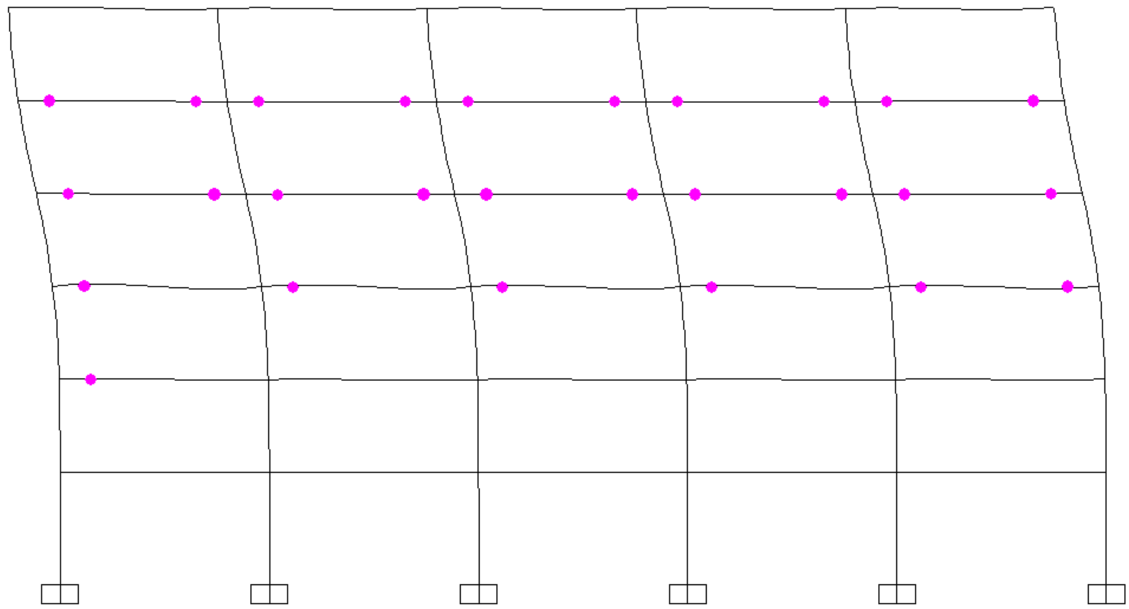


a)

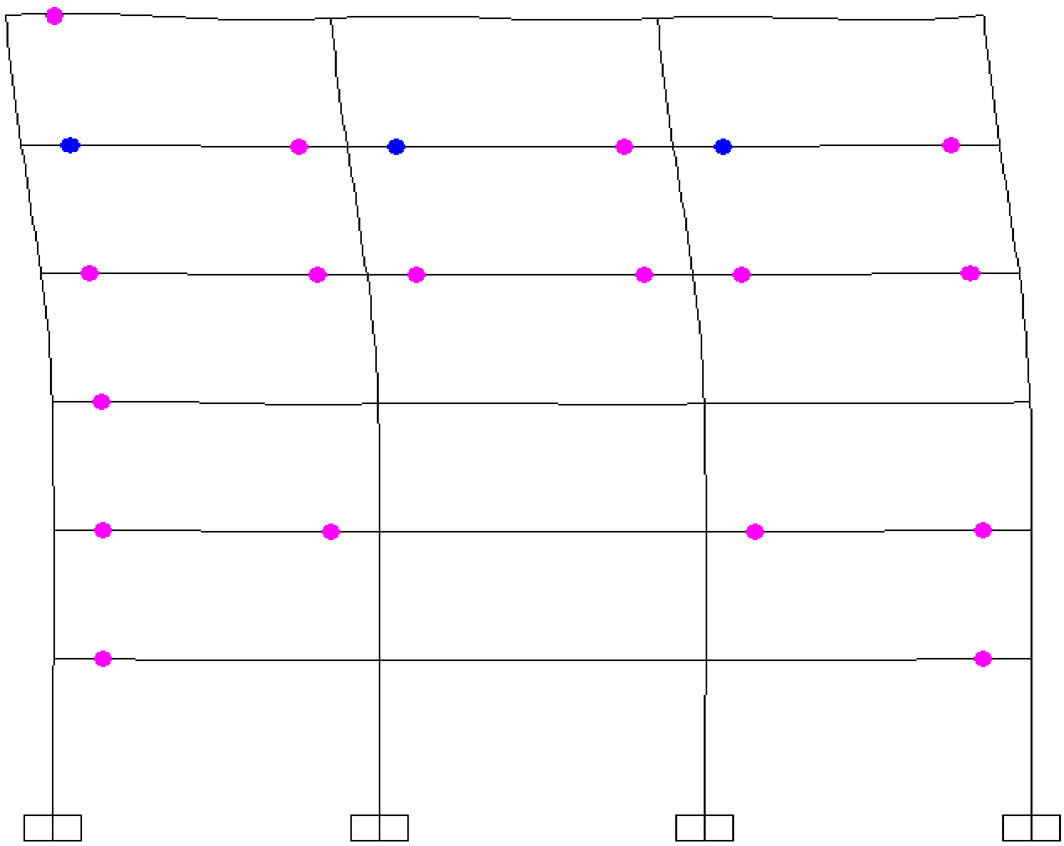


b)

Fig J1 flexural Hinge location for 6FRMRF a) Plastic hinge location for X-frame
b) Plastic hinge location for y-frame

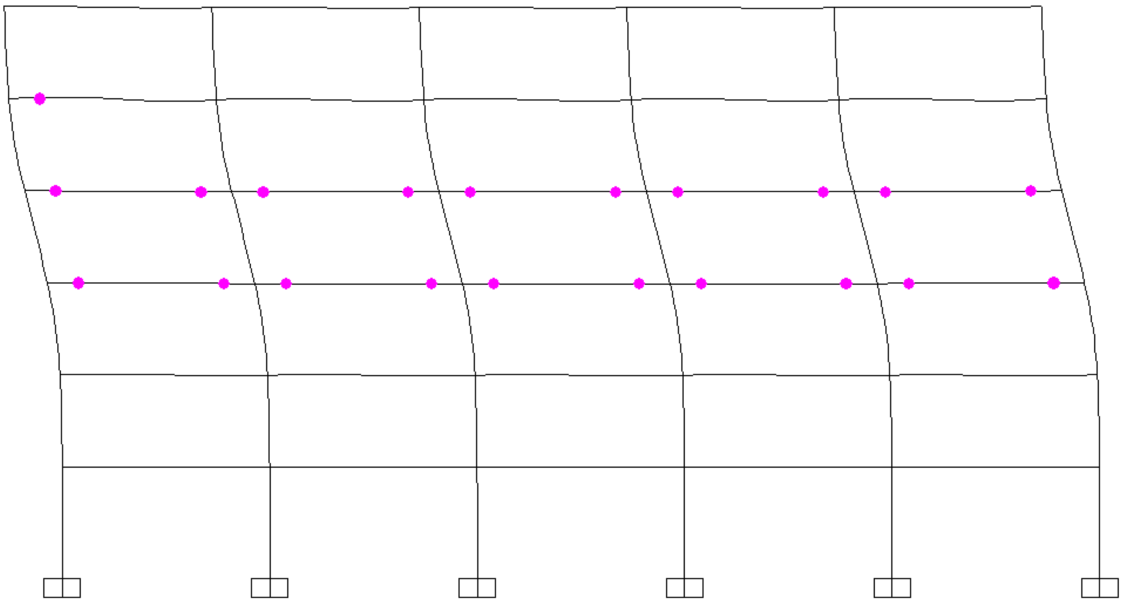


a)

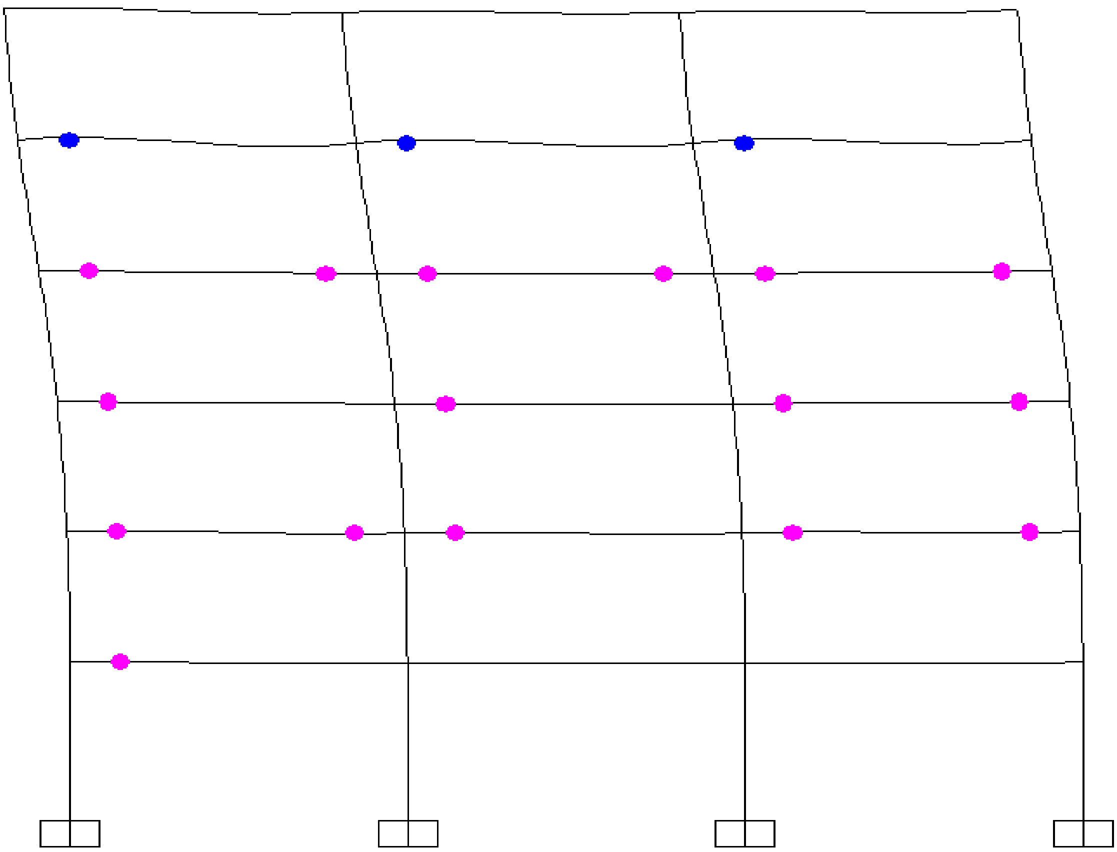


b)

Fig J2 flexural Hinge location for 6SR45 a) Plastic hinge location for X-frame
b) Plastic hinge location for y-frame

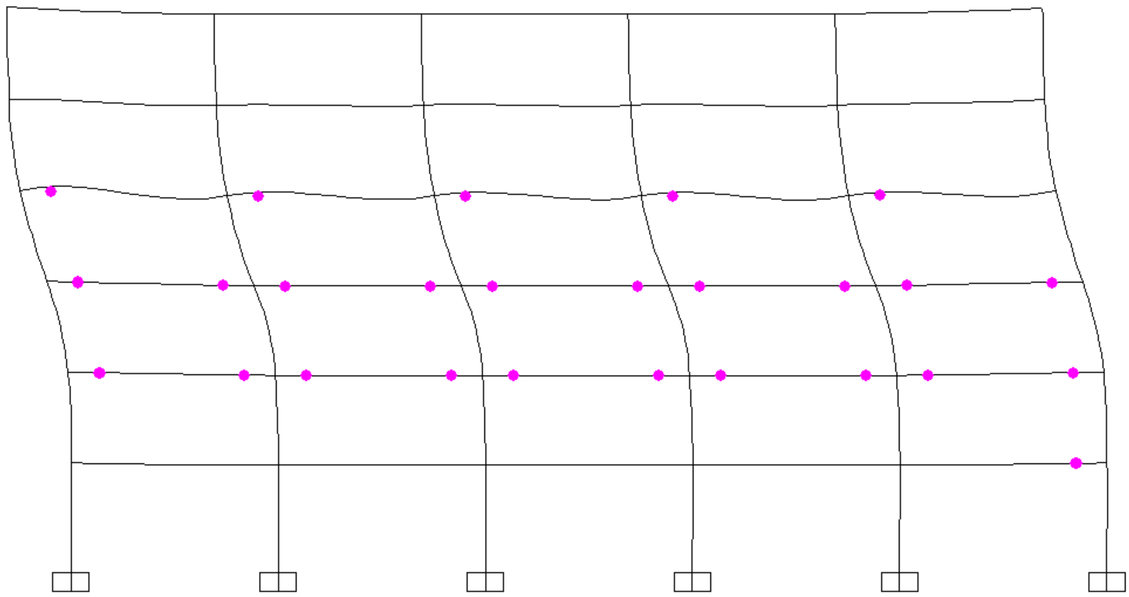


a)

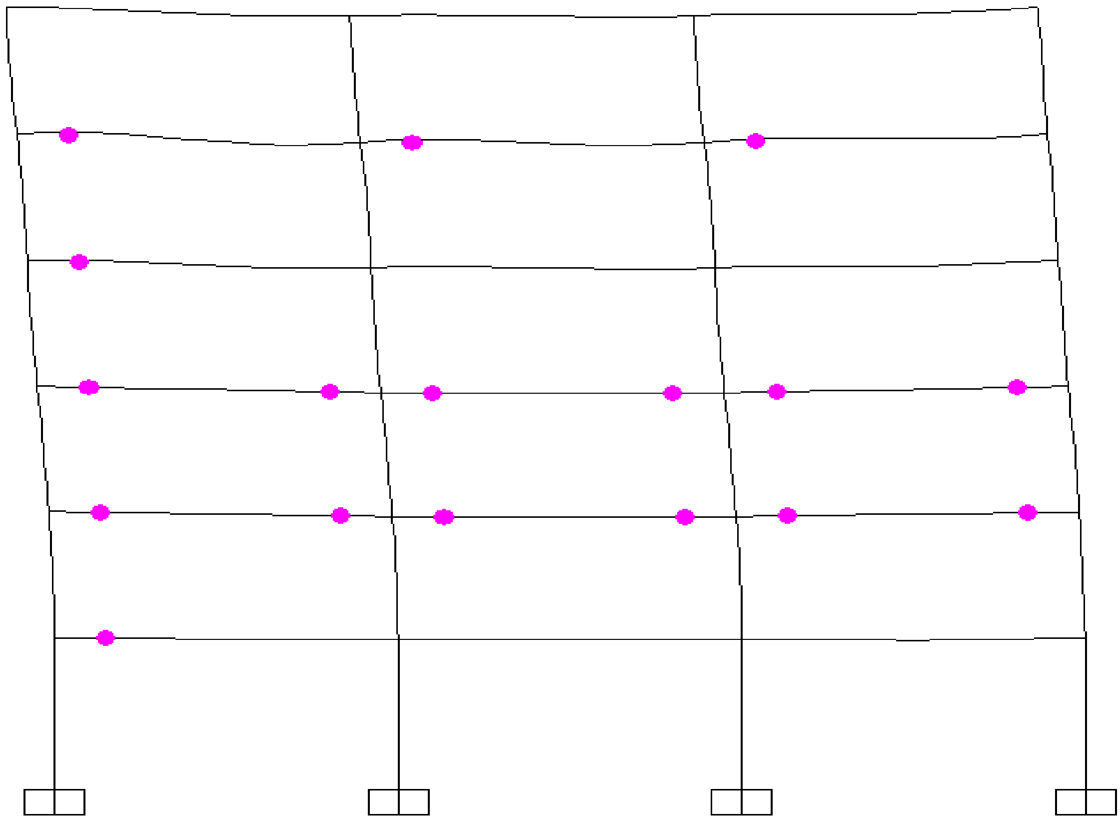


b)

Fig J3 flexural Hinge location for 6SR34 a) Plastic hinge location for X-frame
b) Plastic hinge location for y-frame

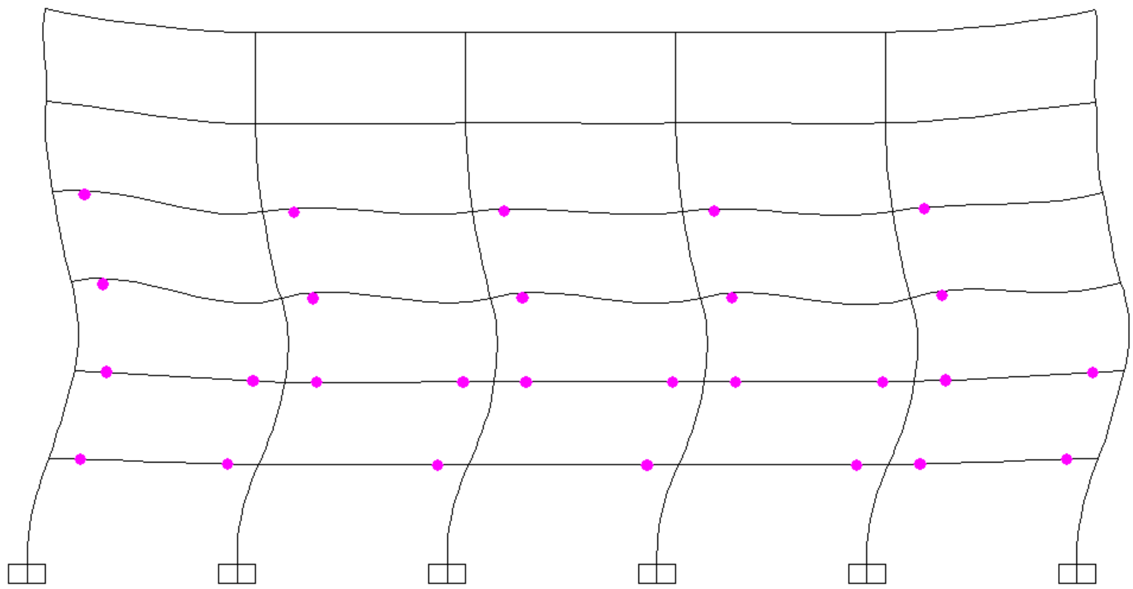


a)

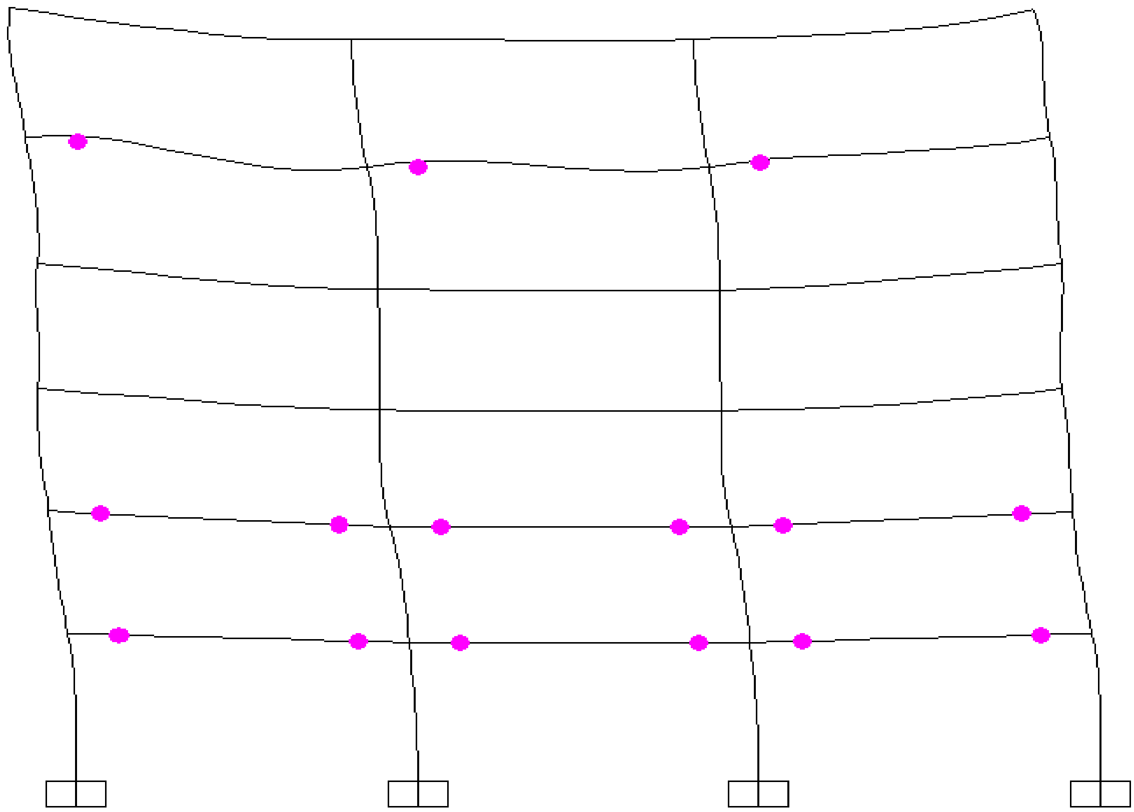


b)

Fig J4 flexural Hinge location for 6SR23 a) Plastic hinge location for X-frame
b) Plastic hinge location for y-frame

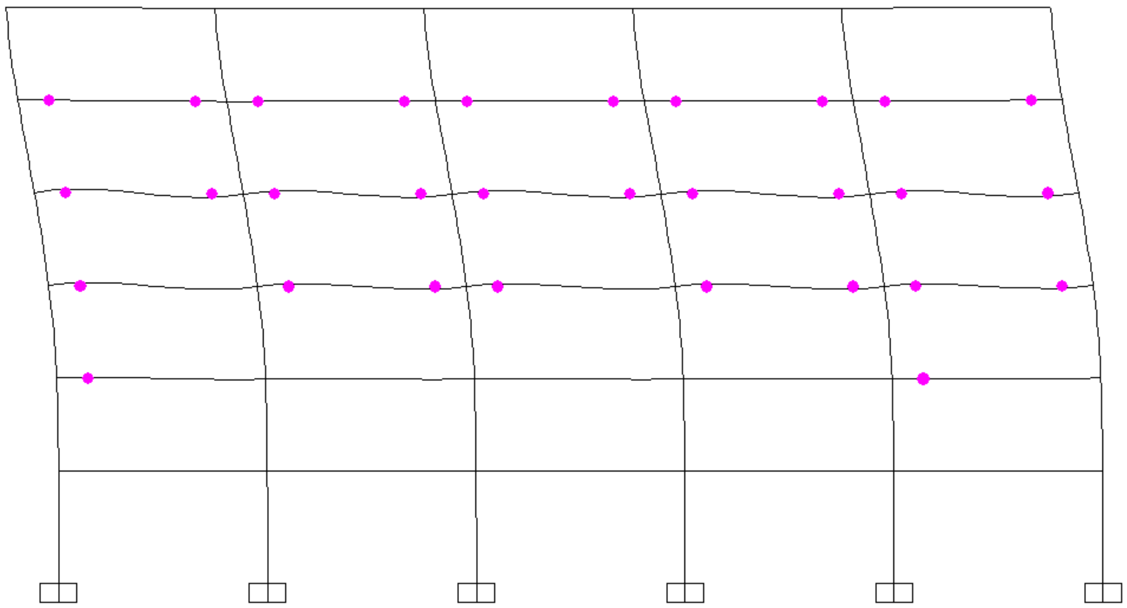


a)

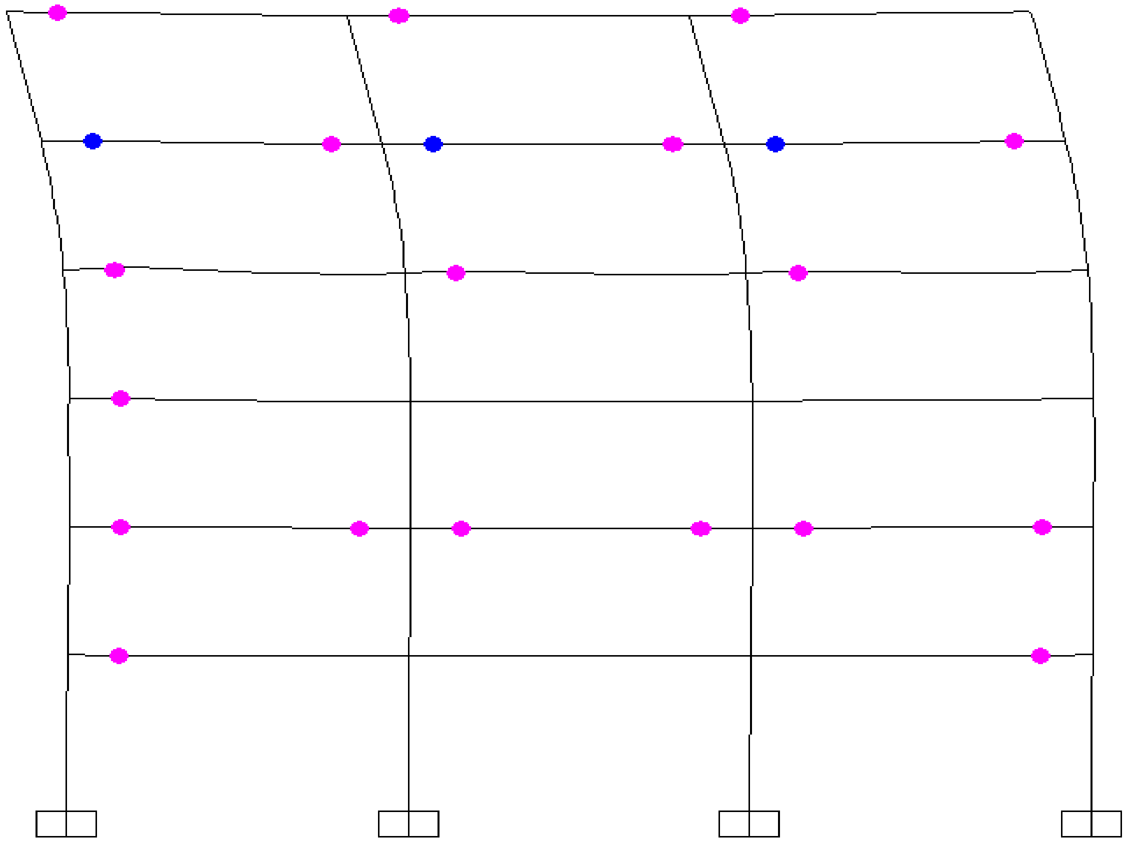


b)

Fig J5 flexural Hinge location for 6SR12 a) Plastic hinge location for X-frame
b) Plastic hinge location for y-frame



a)



b)

Fig J5 flexural Hinge location for 6SR56 a) Plastic hinge location for X-frame
b) Plastic hinge location for y-frame

APPENDIX K

PLASTIC HINGE FORMATION FOR 20-STOREY SYSTEM

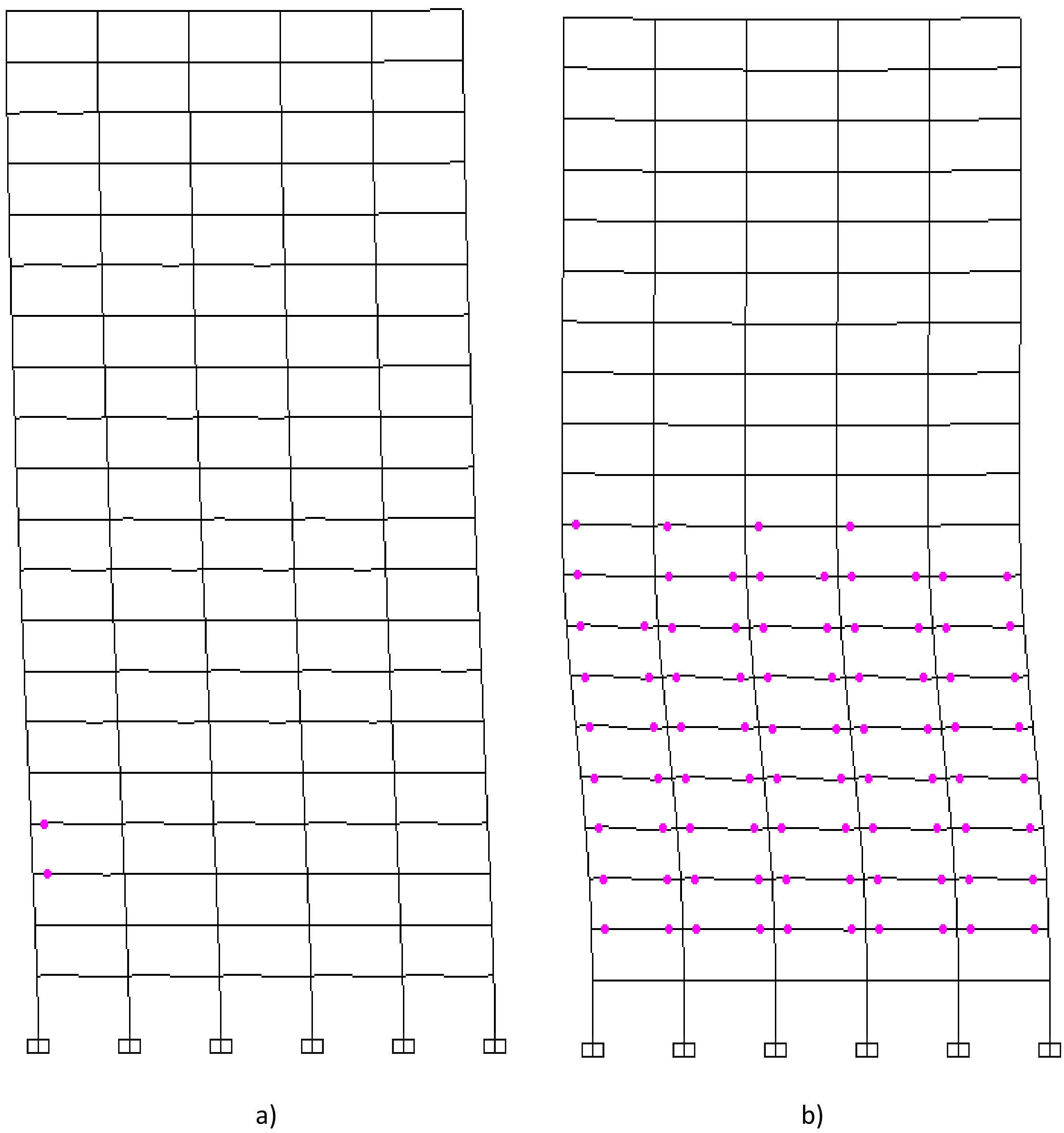


Fig K1 Flexure Hinge location in x-direction frames for 20FRMRF a) first plastic hinge location b) failure mechanism

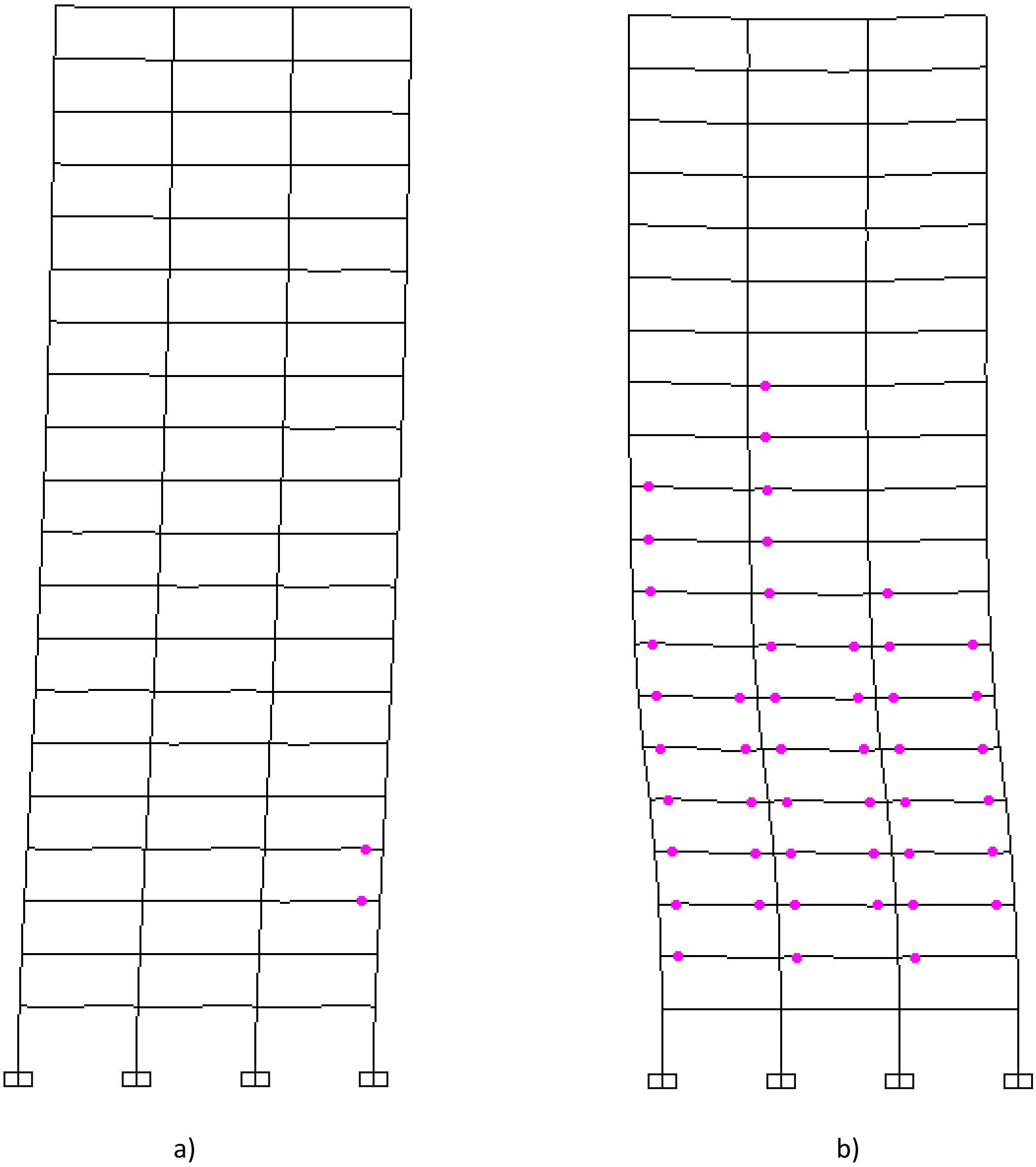
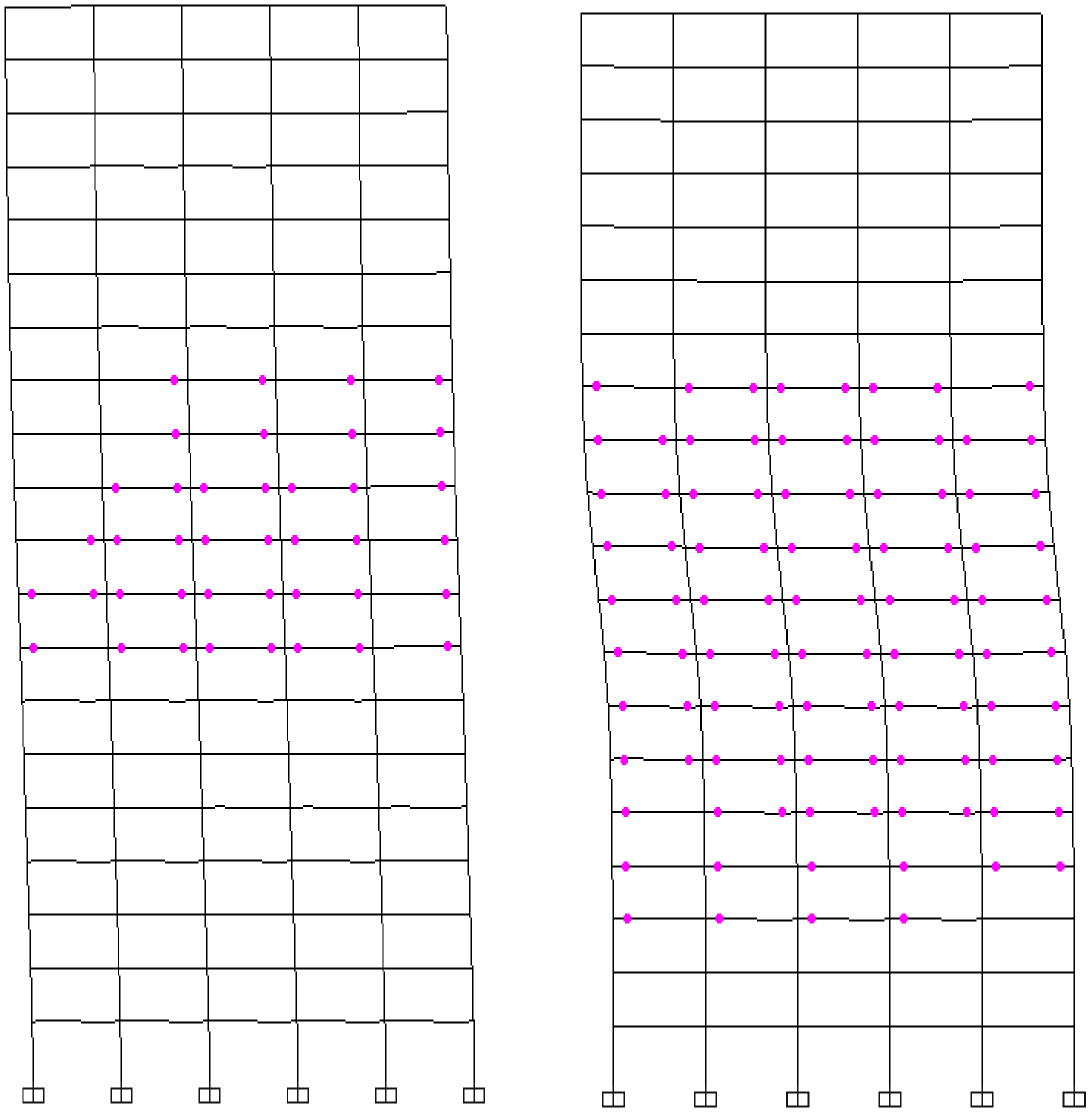


Fig K2 Flexure Hinge location in y-direction frames for 20FRMRF a) first plastic hinge location b) failure mechanism



a) b)

Fig K3 Flexure Hinge location in x-direction frames for 20SR8-13 a) first plastic hinge location b) failure mechanism

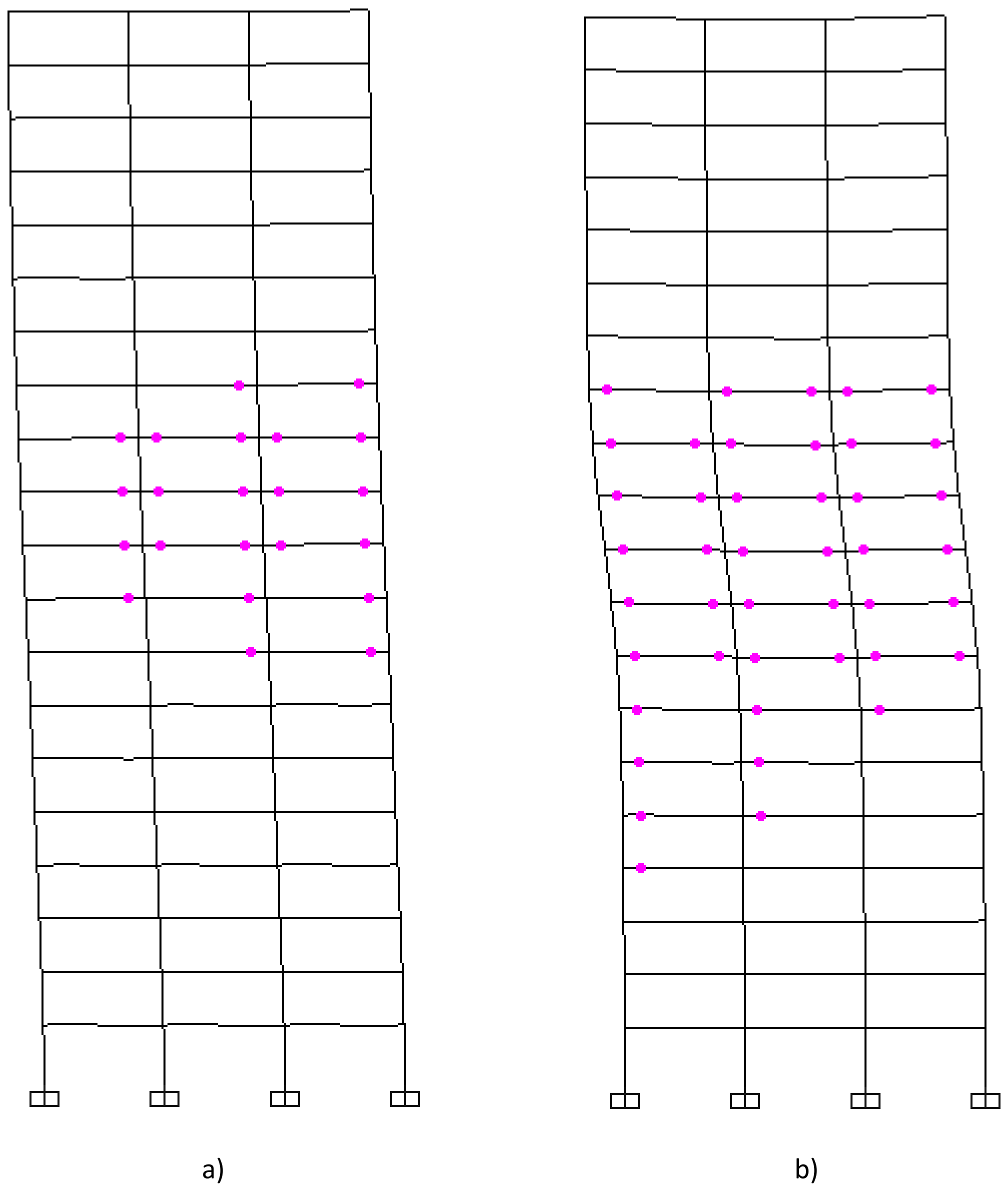
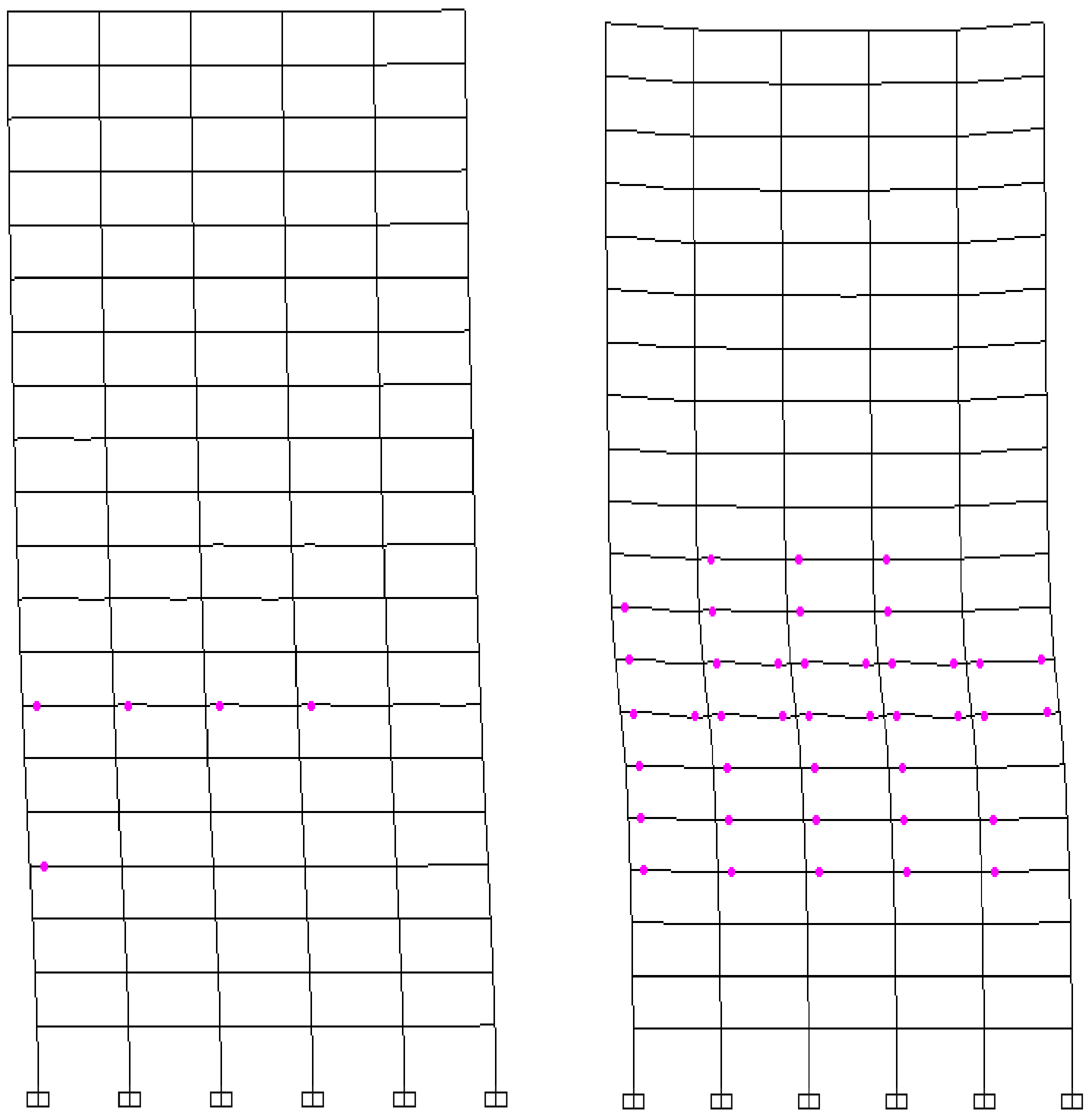
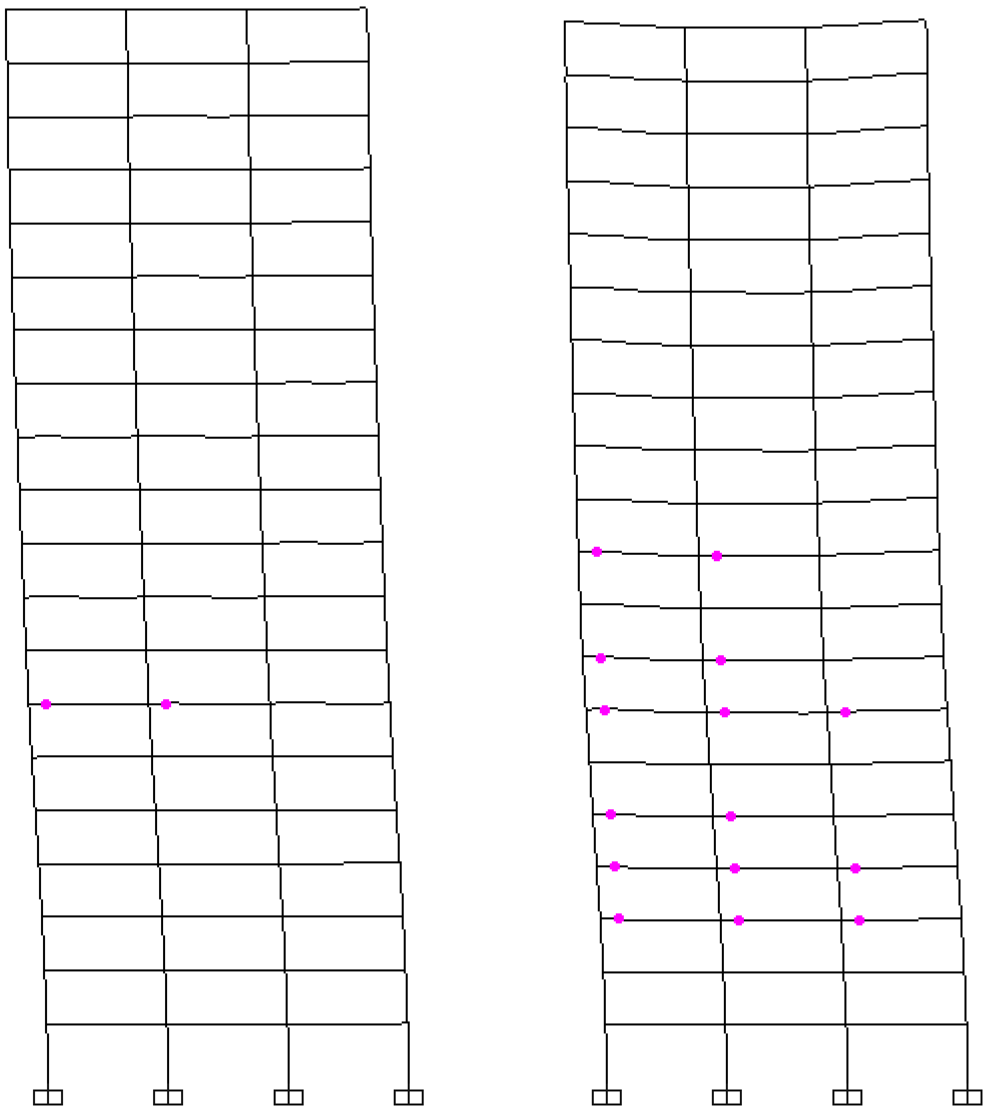


Fig K4 Flexure Hinge location in x-direction frames for 20SR8-13 a) first plastic hinge location b) failure mechanism



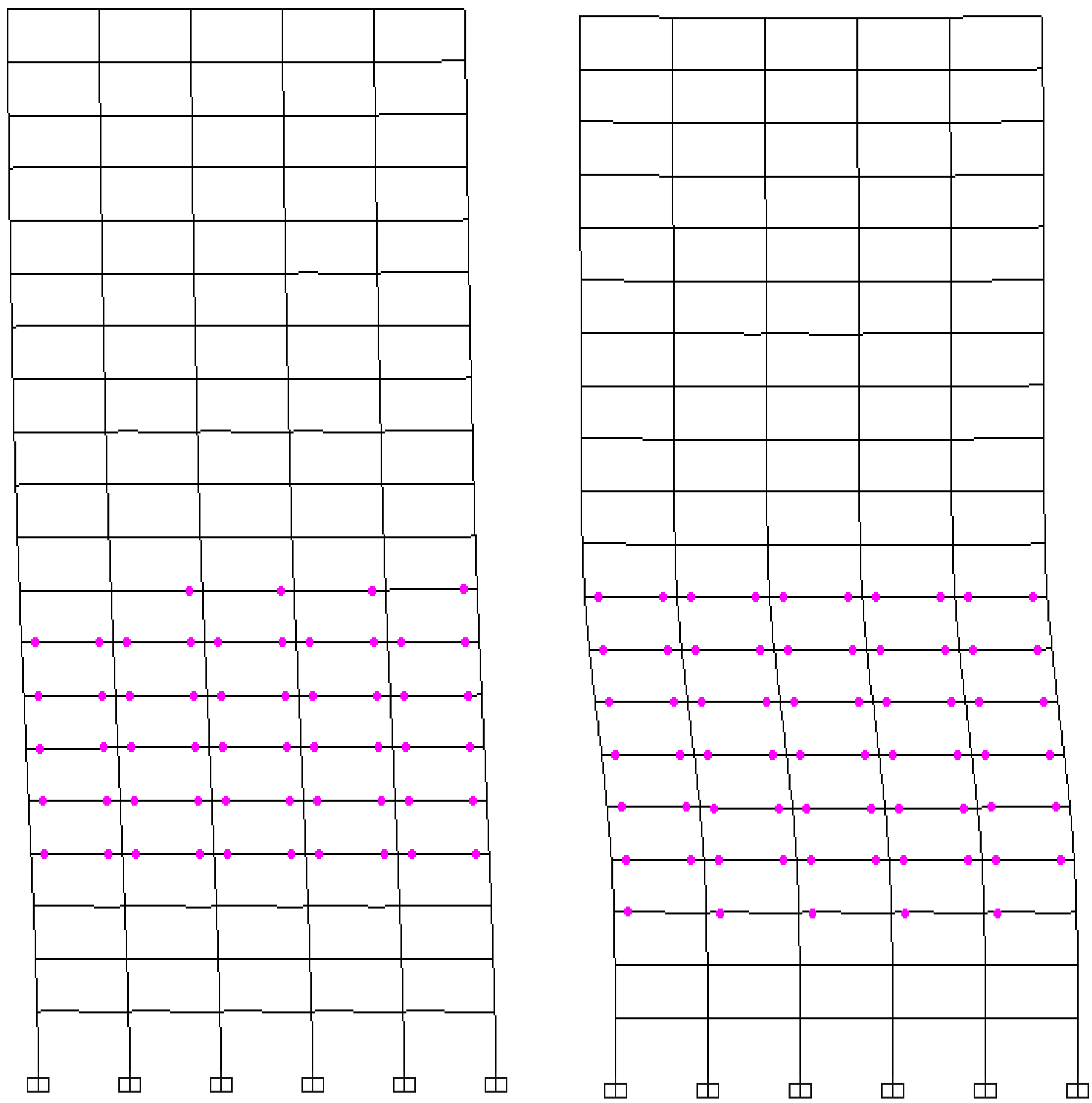
a) b)

Fig K5 Flexure Hinge location in x-direction frames for 20SR1-6 a) first plastic hinge location b) failure mechanism



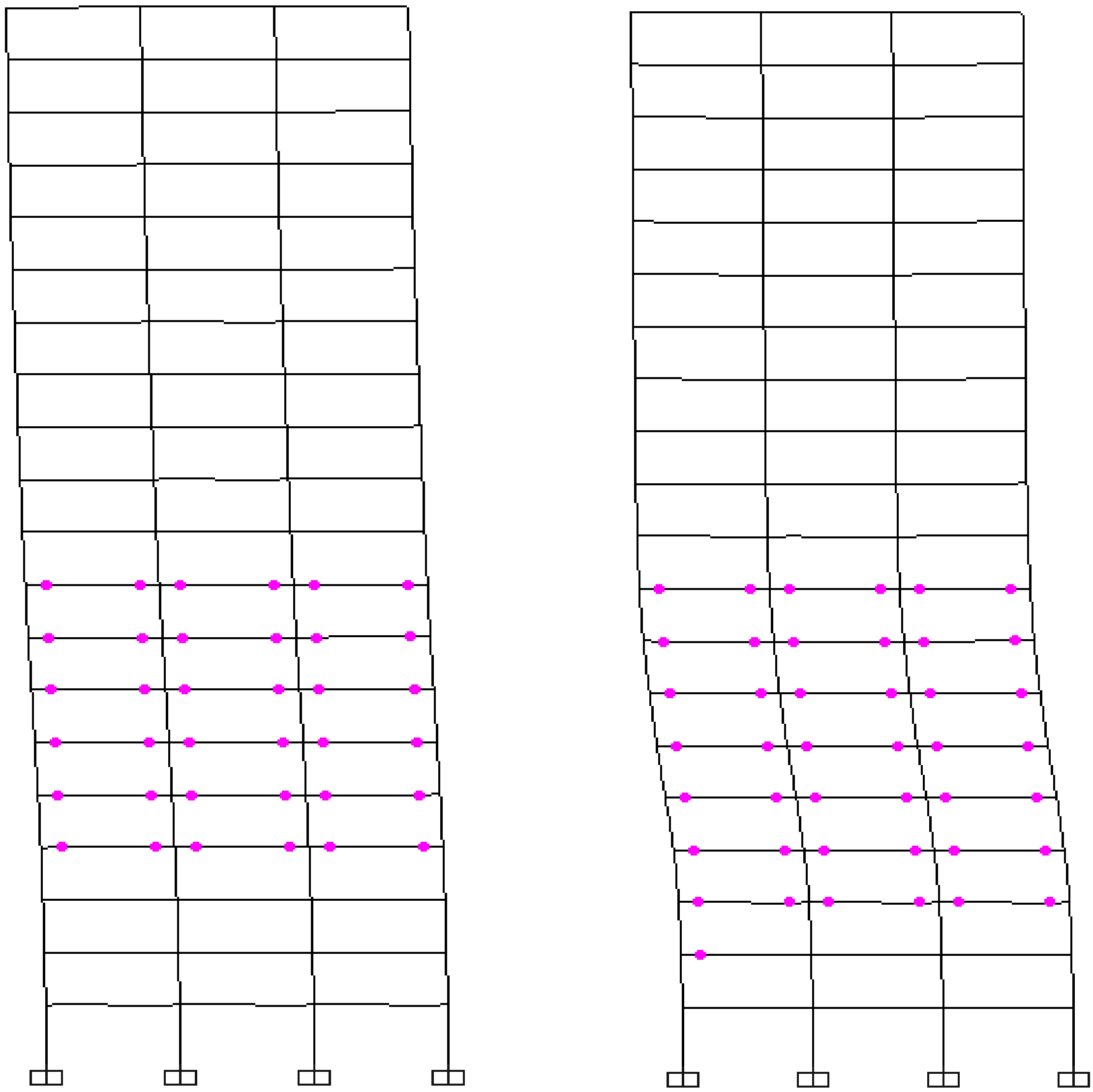
a) b)

Fig K6 Flexure Hinge location in y-direction frames for 20SR1-6 a) first plastic hinge location b) failure mechanism



a) b)

Fig K7 Flexure Hinge location in x-direction frames for 20SR4-9 a) first plastic hinge location b) failure mechanism



a) b)

Fig K8 Flexure Hinge location in y-direction frames for 20SR4-9
a) First plastic hinge location b) failure mechanism

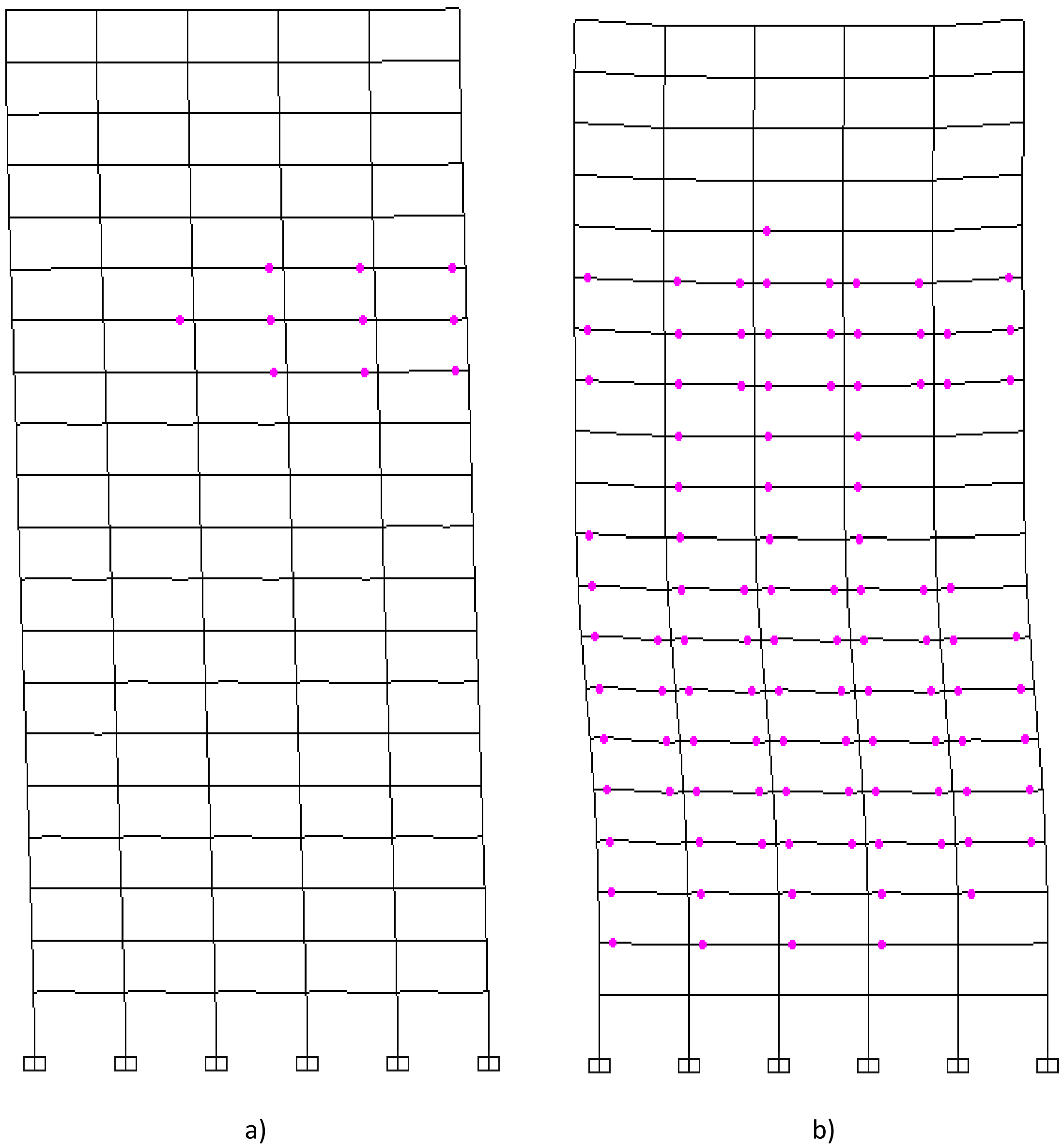
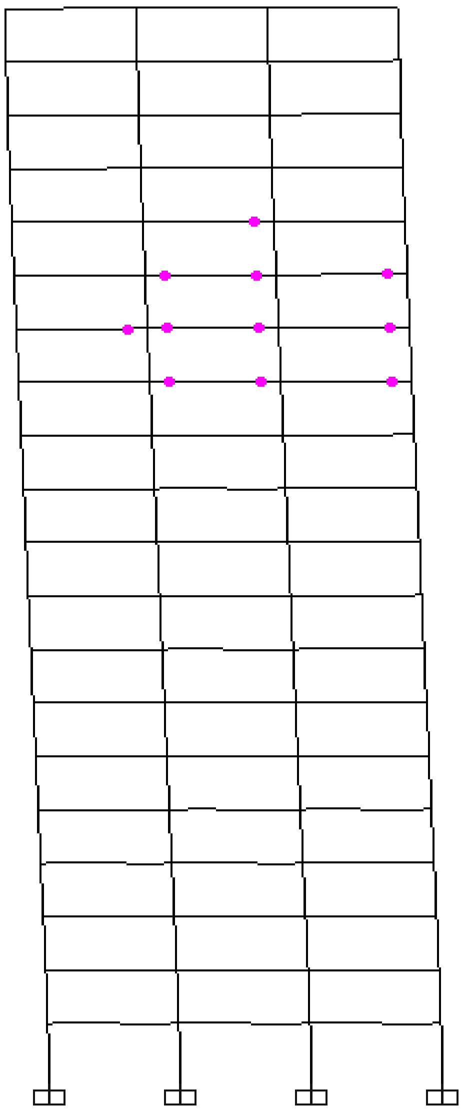
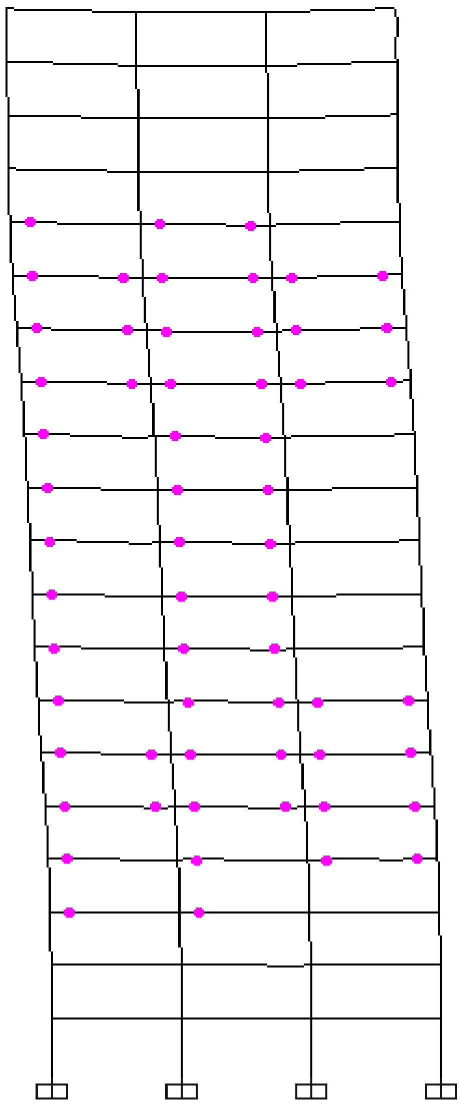


Fig K9 Flexure Hinge location in x-direction frames for 20SR13-18
a) First plastic hinge location b) failure mechanism



a)



b)

Fig K10 Flexure Hinge location in y-direction frames for 20SR13-18
a) First plastic hinge location b) failure mechanism

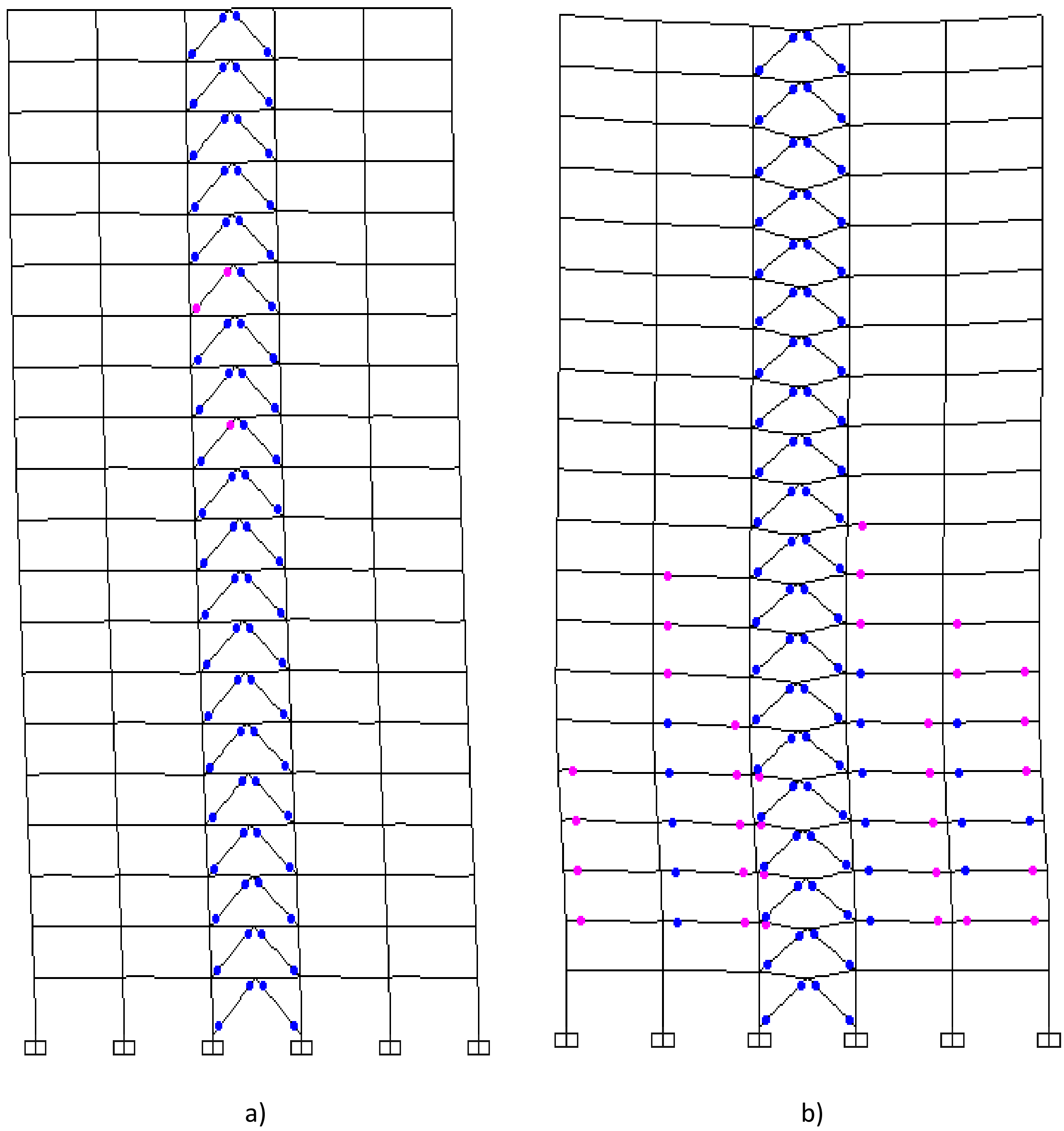
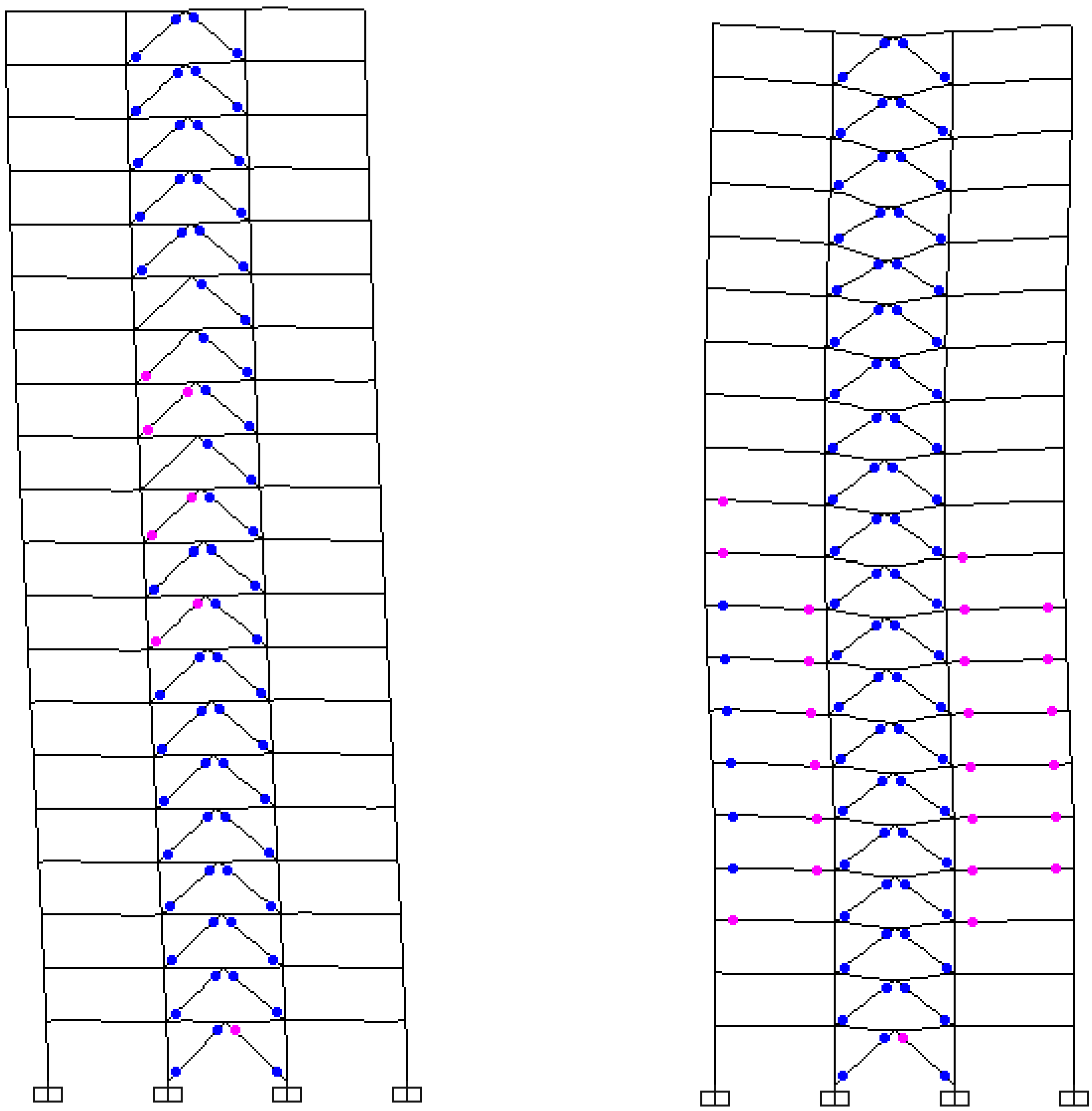
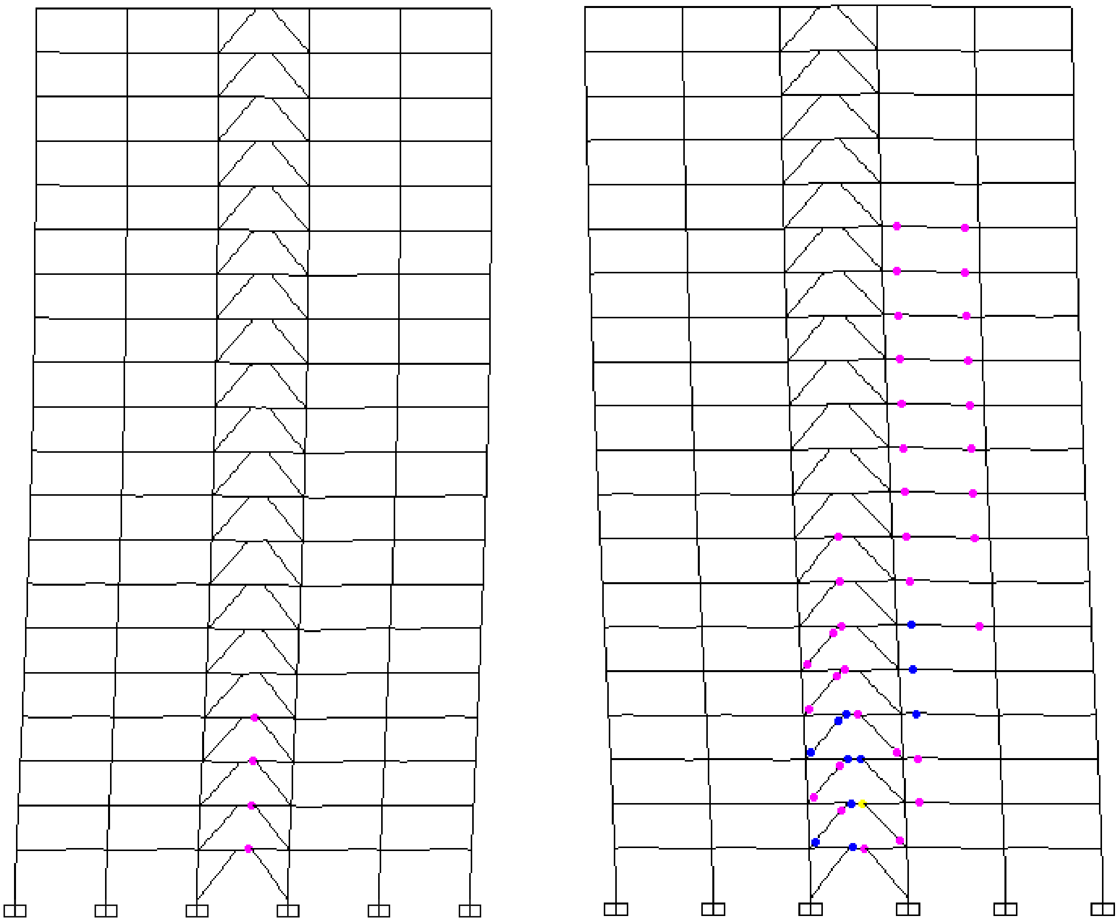


Fig K11 Flexure Hinge location in y-direction frames for 20SR13-18
a) First plastic hinge location b) failure mechanism



a) b)

Fig K12 Flexure Hinge location in y-direction frames for 20BRBF a) first plastic hinge location b) failure mechanism



a) b)

Fig K13 Flexure Hinge location in y-direction frames for 20EBF cx cy
a) First plastic hinge location b) failure mechanism

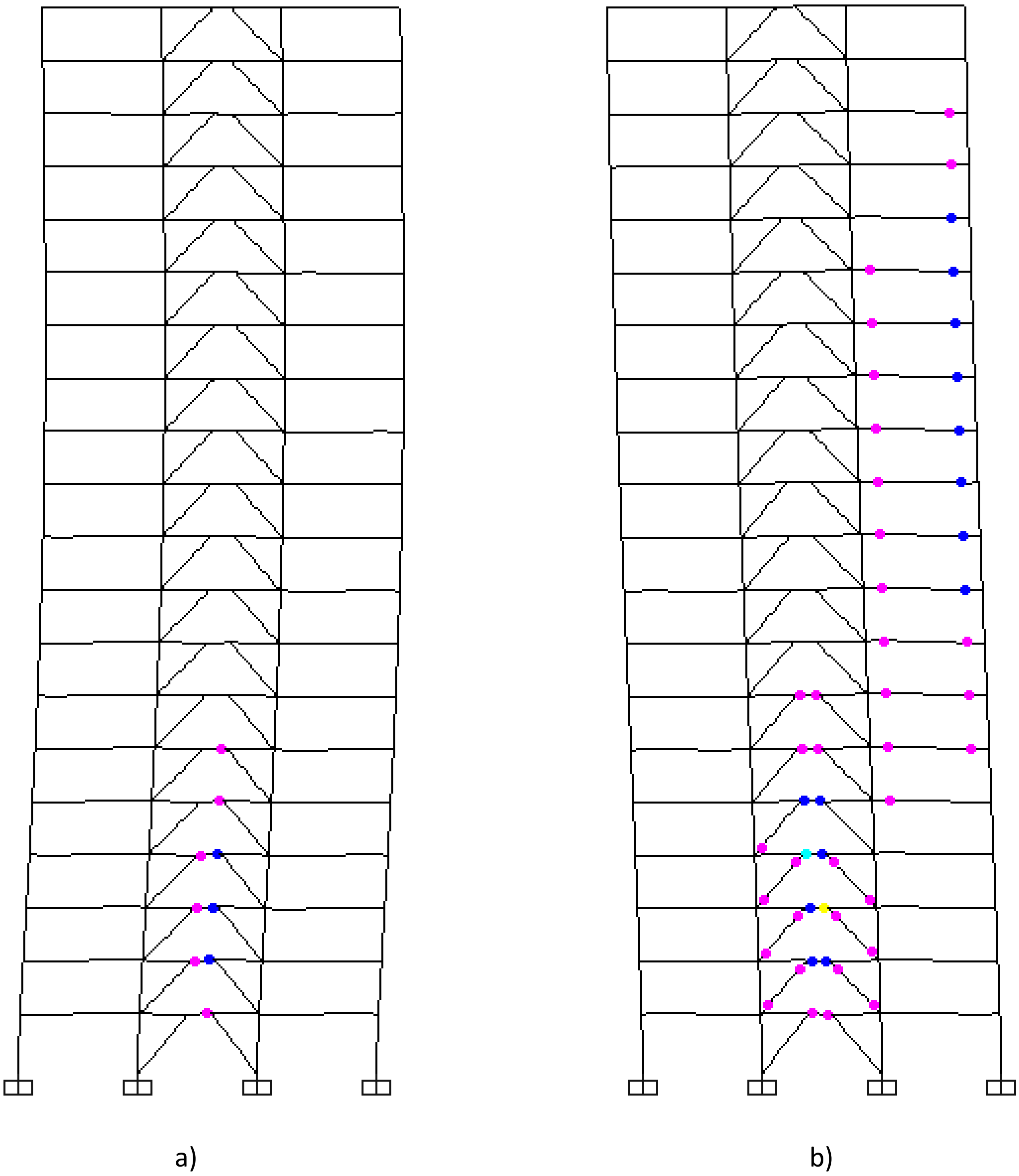
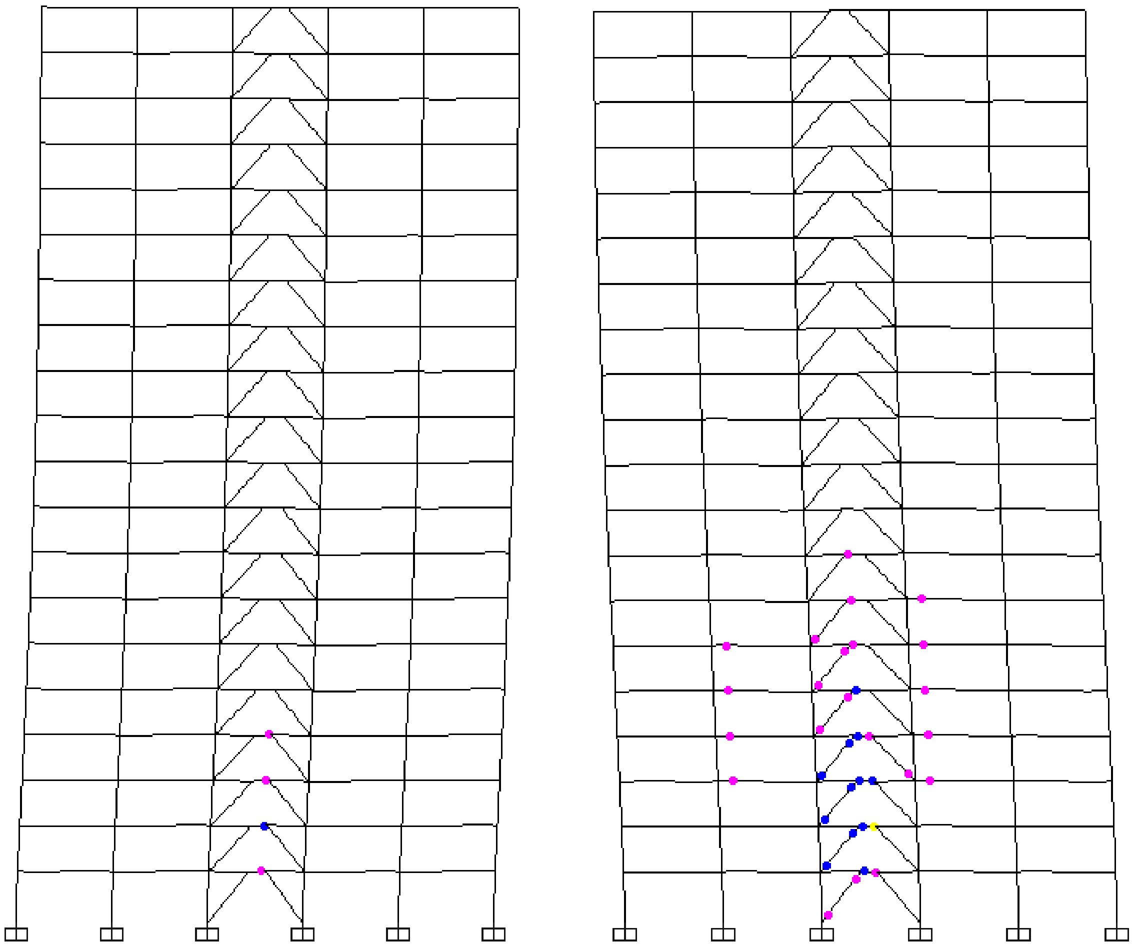


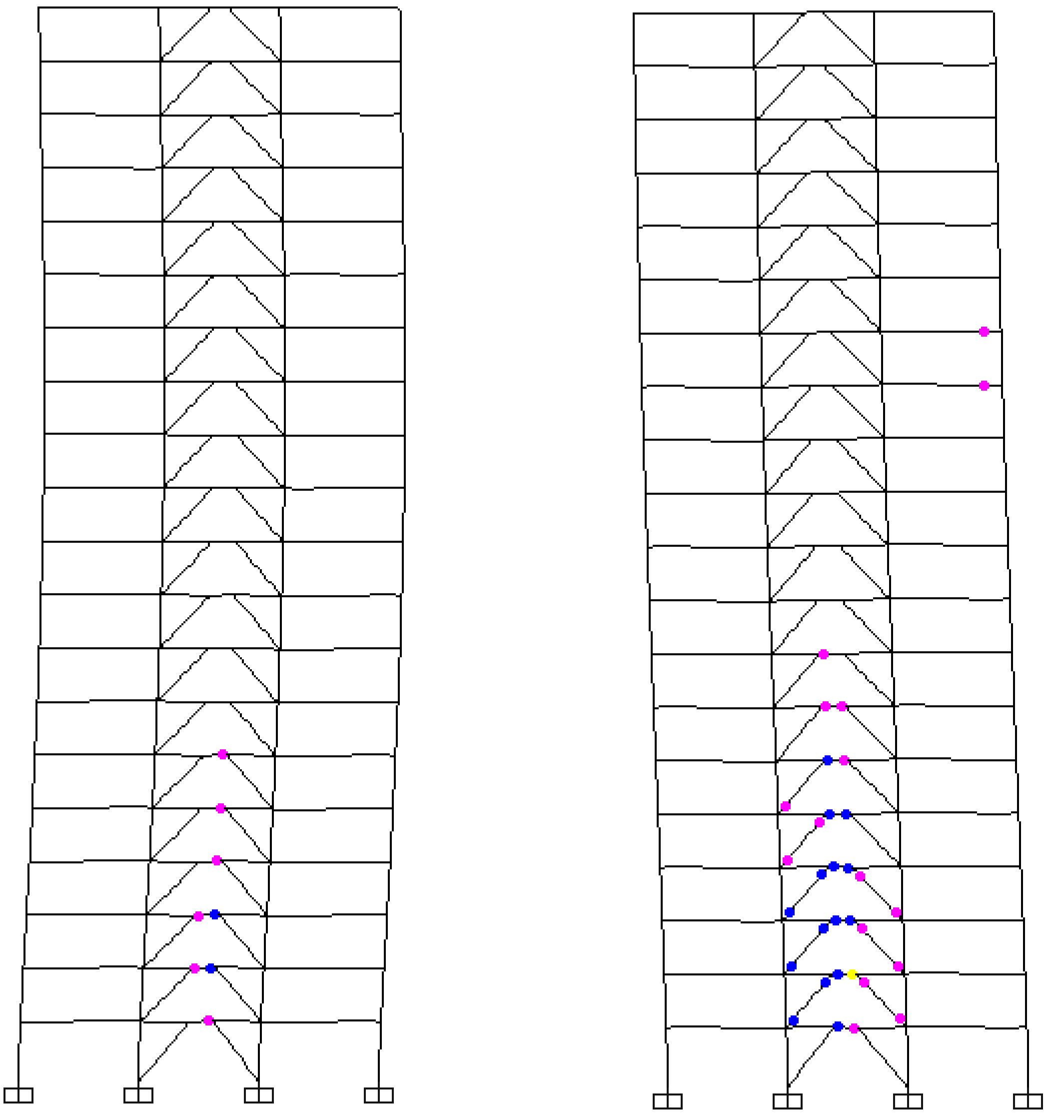
Fig K14 Flexure Hinge location in y-direction frames for 20EBF cx sy
a) first plastic hinge location b) failure mechanism



a)

b)

Fig K15 Flexure Hinge location in y-direction frames for 20EBF1 cx sy
a) First plastic hinge location   b) failure mechanism



a) b)

Fig K16 Flexure Hinge location in y-direction frames for 20EBF1 cx sy
a) First plastic hinge location b) failure mechanism

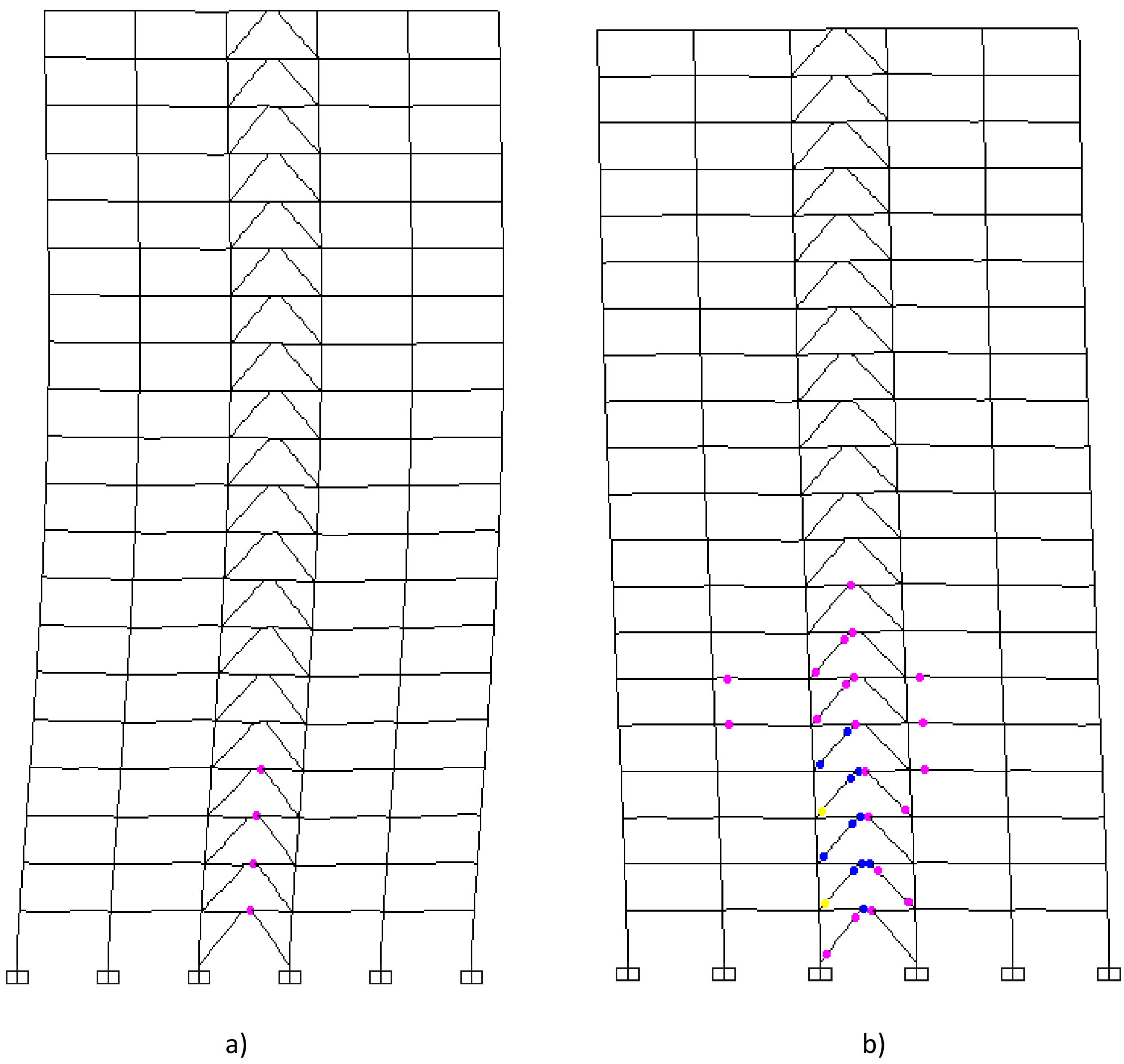
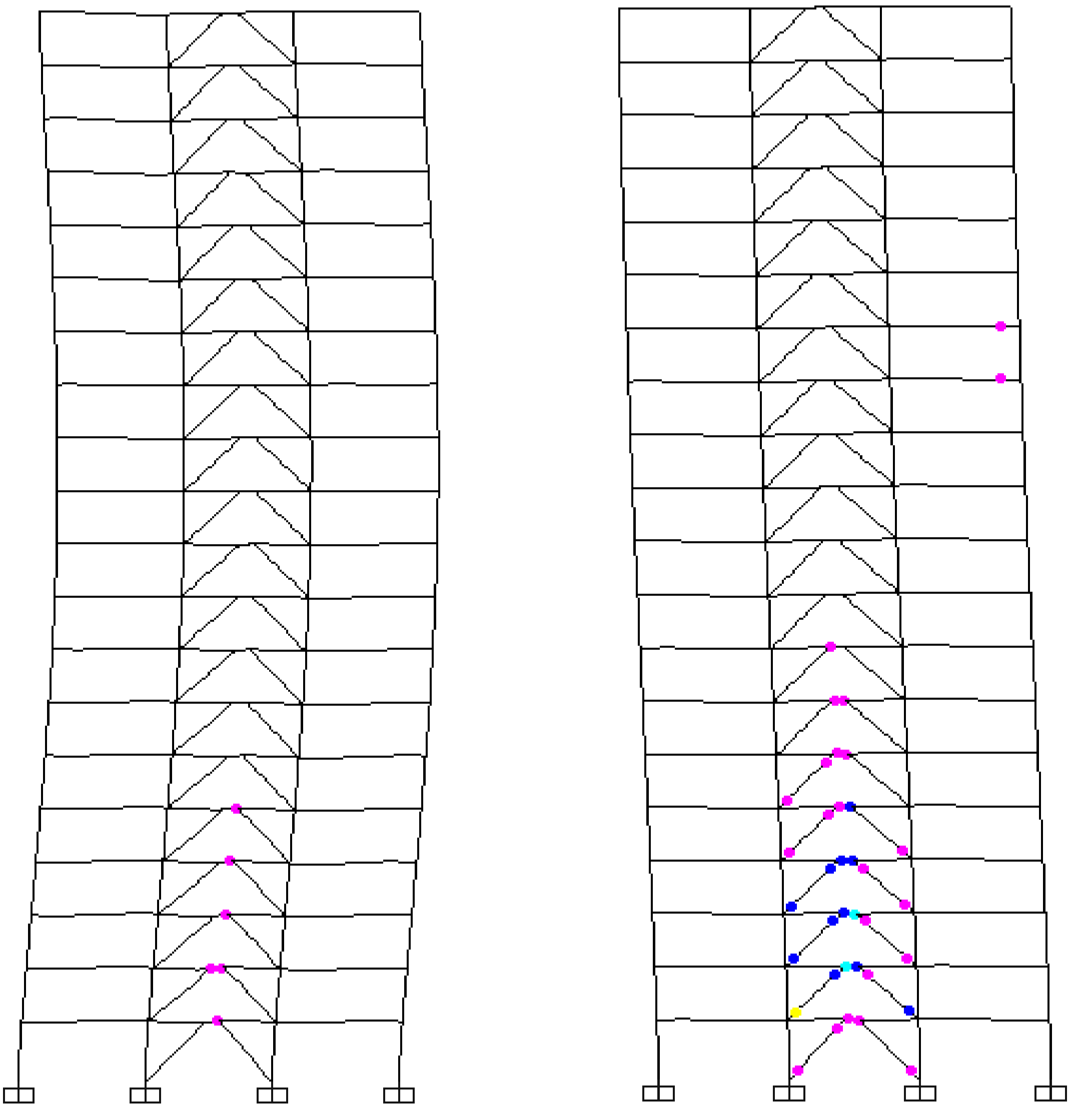


Fig K17 Flexure Hinge location in y-direction frames for 20EBF2 cx sy
a) First plastic hinge location b) failure mechanism



a) b)

Fig K18 Flexure Hinge location in y-direction frames for 20EBF2 cx sy
a) First plastic hinge location b) failure mechanism

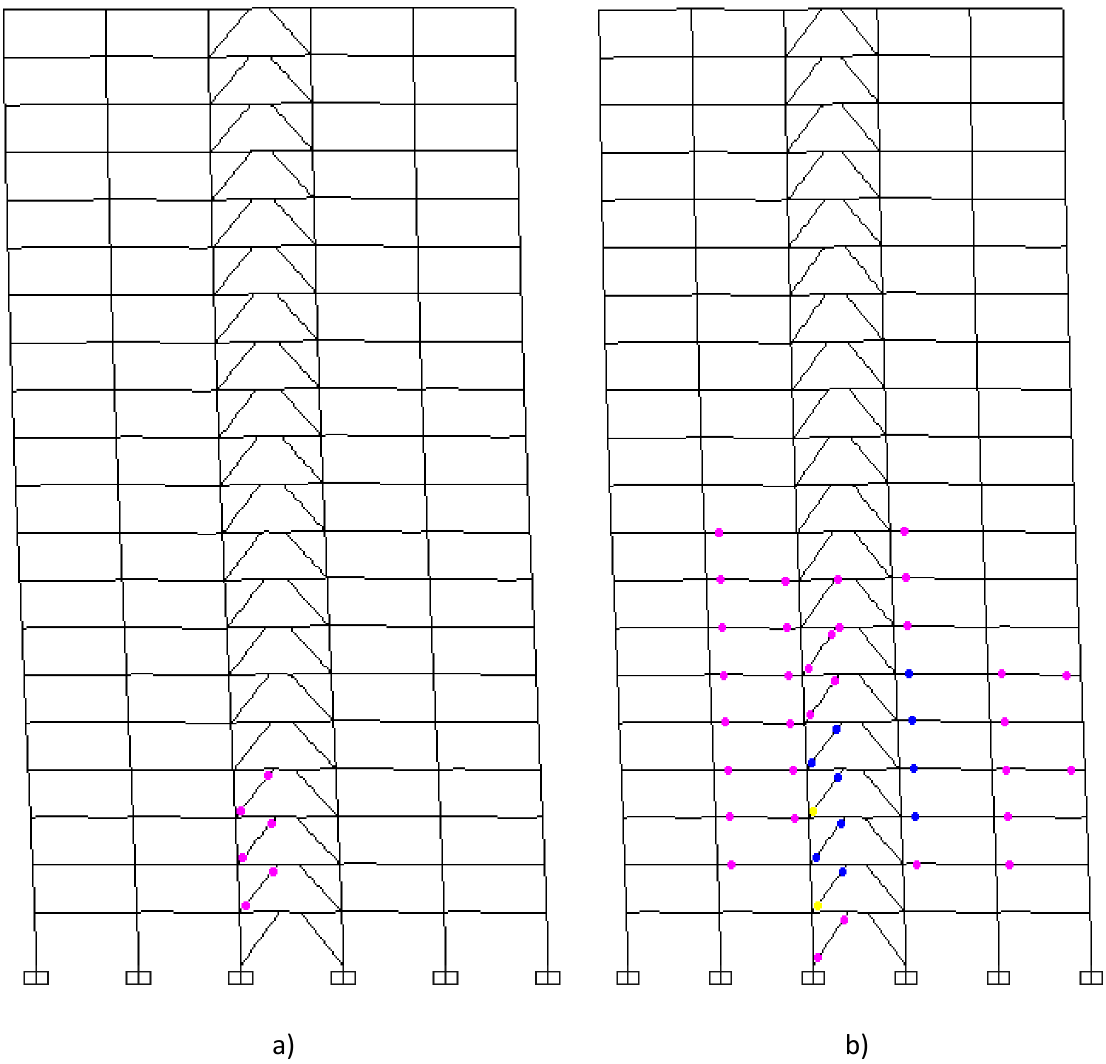


Fig K19 Flexure Hinge location in y-direction frames for 20EBF3 cx sy
a) First plastic hinge location b) failure mechanism

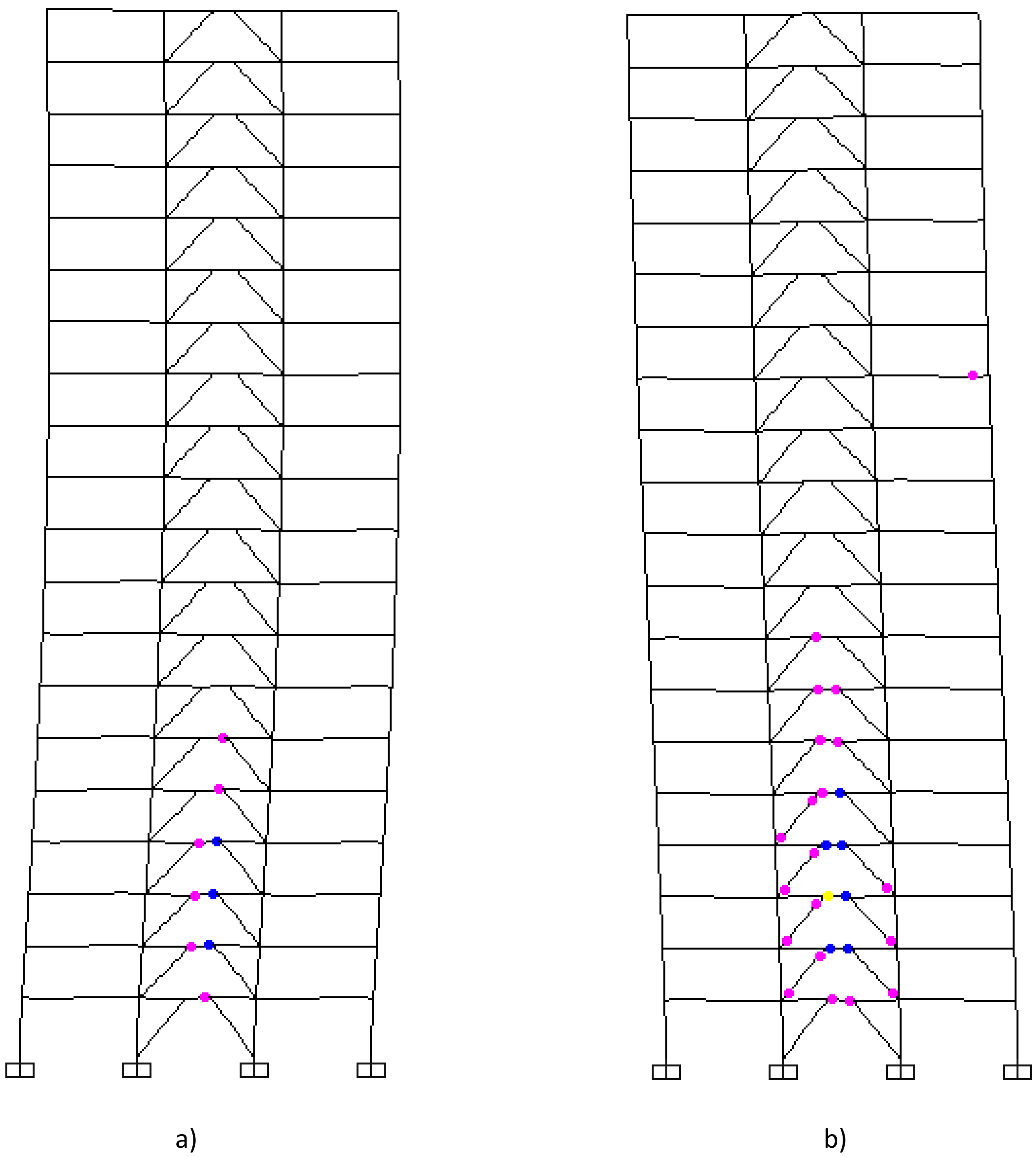
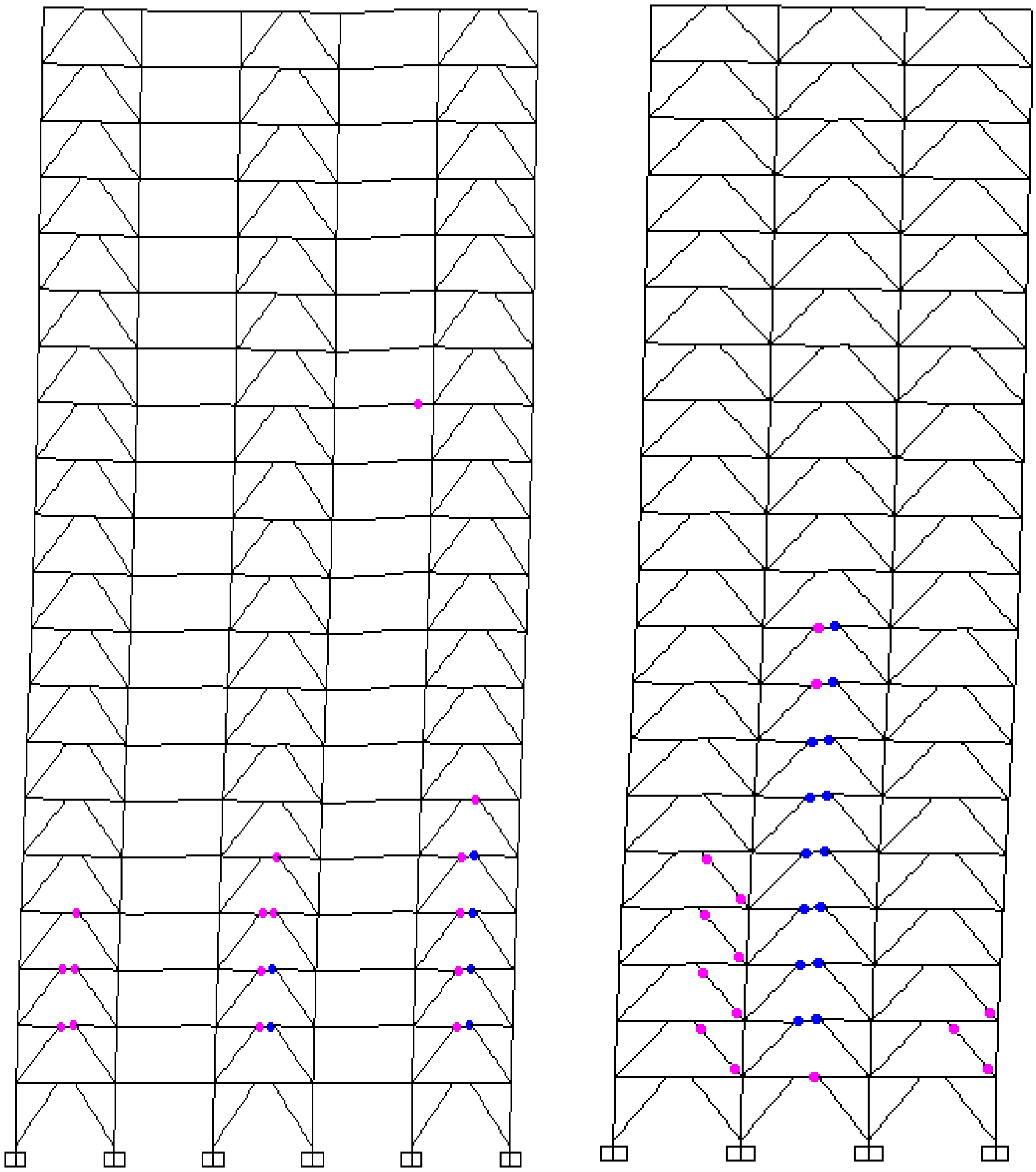


Fig K20 Flexure Hinge location in y-direction frames for 20EBF3 cx sy
a) First plastic hinge location b) failure mechanism



a) b)

Fig K21 Flexure Hinge location in for 20EBF3 cscox cscoy a) Failure mechanism for X-frame

b) Failure mechanism for Y-frame

التحليل اللاخطي الزلزالي للعمارات العالية مع روابط شبه جامدة

اعداد
احمد غازي الطرابشة

المشرف
الدكتور ياسر الحنيطي

المشرف المشارك
الدكتور غازي ابو فرسخ

ملخص

في هذا البحث، اربعة انظمة فولاذية وهي النظام المقاوم للانحناء مع روابط جامدة، النظام المقاوم للانحناء مع روابط شبه جامدة، النظام مع روابط ممنوعه من الانحناء، والنظام مع الروابط التي لا تلتقي بنقطة واحدة، هذه الانظمة سوف تعرض لمجموعة من التحاليل اللاخطية الزلزالية ثلاثية الابعاد، والتحاليل اللاخطية الساكنة، والهدف من ذلك هو تقييم الاداء الزلزالي لهذه الانظمة، واقتراح نظام مع روابط شبه جامدة بحيث يمتلك هذا النظام قدرة افضل على تبديد الطاقة، والقدرة على العودة الى وضعه الطبيعي قبل الزلزال، وهذ عن طريق ايجاد طريقه لوضع الروابط شبه الجامدة بحيث تعطي التصرف الزلزالي المرغوب به.
عمارتان مختلفتان بالخصائص سوف تدرسان في هذا البحث، العمارة الاولى تحتوي على ستة طوابق بحيث تمثل العمارات متوسطة الارتفاع والعمارة الثانية تحتوي على عشرين طابق وتمثل العمارات العالية، الخواص التي سوف تدرس لهذه الانظمة هي القدرة على تبديد الطاقة، القدرة على العودة الى الوضع الاصلي بعد انتهاء الزلزال، القدرة على الذهاب لمسافة كبيرة تحت الزلزال من غير تأثير على قوة احتمالها، في البداية عدة اقتراحات لمواقع الروابط غير الجامدة سوف تدرس من خلال مقارنة الخصائص التي سبق ذكرها ثم بعد ذلك النظام الذي يمتلك افضل الخصائص سوف يقارن مع الانظمة الاخرى.
النتائج النهائية اظهرت ان النظام مع الروابط شبه الجامدة اظهر افضل النتائج فيما يتعلق بالعمارات العالية، بينما النظام مع الروابط الممنوعة من الانحناء اظهر افضل النتائج للعمارات متوسطة الارتفاع اما النظام مع الروابط التي لا تلتقي بنقطة واحدة فيقترح استخدامه في الابنية المنخفضة الارتفاع وذلك في المناطق الزلزالية.